IDENTIFICATION OF VEHICLE PARAMETERS FROM BRIDGE DYNAMIC RESPONSE

A Thesis Submitted in
Partial Fulfillment of the Requirements
for the Degree of

DOCTOR OF PHILOSOPHY

By

R. Lalthlamuana

CIVIL ENGINEERING DEPARTMENT
INDIAN INSTITUTE OF TECHNOLOGY GUWAHATI
GUWAHATI-781039, INDIA

APRIL, 2015

IDENTIFICATION OF VEHICLE PARAMETERS FROM BRIDGE DYNAMIC RESPONSE

A Thesis Submitted in
Partial Fulfillment of the Requirements
for the Degree of

DOCTOR OF PHILOSOPHY

By

R. Lalthlamuana

CIVIL ENGINEERING DEPARTMENT
INDIAN INSTITUTE OF TECHNOLOGY GUWAHATI
GUWAHATI-781039, INDIA
APRIL, 2015

DEDICATION

To my beloved grandfather C. Thandanga.
His words of inspiration and encouragement
in pursuit of excellence, still linger on.

CERTIFICATE

It is certified that the work contained in the thesis entitled "**Identification of Vehicle Parameters from Bridge Dynamic Response**", by **R. Lalthlamuana** (Roll No: 11610402) a student of the Department of Civil Engineering, Indian Institute of Technology, Guwahati, submitted for the award of the degree of Doctor of Philosophy, has been carried out under my supervision and that this work has not been submitted elsewhere for a degree.

Dr. S. Talukdar
Professor
Department of Civil Engineering
Indian Institute of Technology
Guwahati, Assam, India

April, 2015

ACKNOWLEDGEMENT

Foremost, I would like to express my sincere gratitude to my advisor Prof. S. Talukdar for his continuous support to my Ph.D study and research, for his patience, motivation, enthusiasm, and immense knowledge. His guidance helped me in all the time of my works.

Besides my advisor, I would like to thank the rest of my Doctoral committee members: Prof. A. Dutta, Prof. S. K. Dwivedy, and Dr. A. Chakraborty, for their encouragement and fruitful suggestions.

I would like to thank Prof. A. Dutta, Dean of Institute Works, IIT Guwahati and Prof A. K. Sarma, Head of Civil Engineering Department for allowing me to conduct field experiment on bridge located near IIT Guwahati main gate and providing financial grant. My sincere thanks also go to Dr. Arun Ch. Borsaikia, Mr. Biswajit Debnath and Mr. Mrinal Sarma for helping me to conduct the test.

I am also thankful to my friends, Mr. Palash Dey, Mr. Mahendra Reddy and Mr. Ravi Bayyavarapu for their co-operation and help while carrying out my research works.

Special thanks go to my family members. Words cannot express how grateful I am to my mother and father for all of the sacrifices that they have made for my research study. Their prayer for me was what sustained me so far.

R. Lalthlamuana

April, 2015

ABSTRACT

Every bridge has certain restriction for the vehicle load and length. When the limit exceeds, permit has to be sought from the competent authority to pass the vehicle through the bridge. Weigh bridges are installed at important sections of highways to restrict the overloaded vehicles to enter the bridge. Presently, weigh-in-motion system in use can estimate the axle loads. But it incurs high cost of installation and maintenance. Accuracy is also affected by the speed of the vehicle and unevenness of the pavement. For given structural configuration, construction materials and road surface condition, the physical parameters of vehicle also play a significant role in bridge dynamic behavior. Traditionally, the bridge design load is calculated by magnifying static live load with impact factor. Days are not far when complete moving load time history would be necessary to check the design of long span bridges. Recognizing the practical significance of the research on moving load identification, attempts have been made in this thesis to carry out theoretical and experimental study for the estimation of vehicle parameters from the bridge dynamic response.

In the present study, a conditional probability based approach known as "particle filtering technique" has been utilized to estimate the physical parameters of a passing vehicle from the measured dynamic response of the bridge. The particle filter technique requires a mathematical model of the system for the repeated generation of response samples, which is termed as "Forward Scheme". In the present work, a semi analytical method has been developed and interfaced with the particle filter method for generation of response samples. In the proposed semi-analytical method, the bridge has been modeled as Euler Bernouli beam with uniform cross sectional properties. Along with flexural vibration of bridge, the torsional motion of the bridge due to eccentric vehicle path has been considered in the study. Three vehicle models, viz, (i) Model-1: Quarter Car Model (ii) Model-2: Half Car Model with bending flexibility of the vehicle and (iii) Model-3 Full Car Model with bending and torsional flexibility of the vehicle has been incorporated in the semi-analytical formulation. The bridge deck surface roughness has been modelled as the realization of non-homogeneous process in spatial co-ordinates. The non homogeneity of pavement profile has been

incorporated by superimposing variable mean surface over random unevenness. The present study considers two types of mean profile-(i) pre-cambered bridge surface which is often adopted to compensate excessive vertical deflection of the bridge under live load and (ii) approach road settlement as a construction defect.

A dynamic field test has been conducted on an existing bridge with controlled movement of a loaded truck at different speed. The test bridge has been modeled in Finite Element software SAP 2000 in order to update the bridge physical parameters using a combined Response surface and Genetic algorithm approach. The acceleration of bridge deck has been recorded at five locations, which have been utilized in particle filter technique to estimate test truck parameters.

Dynamic behavior of three different bridge-vehicle models has been studied using proposed semi-analytical method to examine the effect of different bridge vehicle parameters on the bridge response statistics and on the dynamic amplification factor. The effect of vehicle flexibility on the bridge dynamic response has been also investigated. Identification of vehicle parameters of three models has been presented with the help of simulated results. The interaction force between vehicle and bridge has been reconstructed using the identified parameters and the states of the system. Effects of measurement location, artificial noise level, vehicle speed and pavement roughness conditions on the accuracy of identified vehicle parameters have been studied.

Lastly, field test results have been utilized in particle filter method to estimate the parameters of the test truck. Different model options in Forward scheme of the particle filtering method have been studied with the help field data. The study reveals that vehicle flexibility has noticeable effect on the bridge dynamic response for long and slender vehicle body. The proposed semi-analytical method of bridge-vehicle interaction dynamics when combined with particle filter method has shown remarkable performance in terms of saving of computational time and improving the accuracy of the estimate of vehicle parameters.

CONTENTS

CERTIFICATE i

ACKNOWLEDGEMENT ii

ABSTRACT iii

CONTENTS v

LIST OF TABLES xii

LIST OF FIGURES xvi

NOMENCLATURES xxxiii

1 INTRODUCTION 1

1.1 Overview 1

1.2 Literature Review 3

1.2.1 Vehicle Parameter Identification 3

1.2.1.1 Method of identification 3

1.2.1.2 Parameters identification using probabilistic approach 8

1.2.2 Vehicle Bridge Interaction 10

1.2.2.1 Vehicle model for the dynamic analysis of bridge 10

1.2.2.2 Modeling of bridge deck unevenness 15

1.2.2.3 Bridge model 17

1.2.2.4 Method of solution for bridge vehicle interaction problem 21

1.2.2.5 Bridge dynamic test 31

1.3 Gaps in Literature 32

1.4 Scope and Objectives of the Present Work 33

1.5 Organization of Thesis 34

2 VEHICLE PARAMETER IDENTIFICATION 35

2.1 Overview 35

2.2 Methods of Moving Load Identification 35

2.2.1 Direct Inverse Method 36

2.2.1.1 Time domain method 36
2.2.1.2 Frequency domain method 37
2.2.2. Indirect Inverse Method 38
2.2.2.1 Optimization based indirect inverse scheme 38
2.2.2.2 Probabilistic based indirect inverse scheme 39
2.3 General Theory of Particle Filtering Method 40
2.3.1 Bayesian Inference to Dynamic State Estimation 40
2.3.2 Monte Carlo Integration and Importance Sampling 42
2.3.3 Bootstrap Particle Filtering 44
2.3.4 Resampling 47
2.4 Application of Bootstrap Particle Filtering Method for Vehicle Parameter Identification 49
2.5 Closure 54

3 BRIDGE-VEHICLE INTERACTION MODEL 55

3.1 Overview 55
3.2 Idealization of Bridge 55
3.3 Deck Roughness 56
3.3.1 Mean surface profile 56
3.3.2 Random unevenness 58
3.4 Coupled System Equations 62
3.4.1. Bridge-vehicle equations of motion for Model-1 63
3.4.2. Bridge-vehicle equations of motion for Model-2 65
3.4.3. Bridge-vehicle equations of motion for Model-3 67
3.5 Closure 69

4 DEVELOPMENT OF A SEMI-ANALYTICAL METHOD IN FORWARD SCHEME 71

4.1 Overview 71
4.2 Discretization of Partial Differential Equations 72
4.2.1 Discretization of flexible vehicle equation of motions 72
4.2.1.1 Transverse vibration of vehicle body 72
4.2.1.2 Torsional Vibration of Vehicle body 75

4.2.2 Discretization of bridge equations of motions 77
4.2.2.1 Bending Vibration of bridge 77
4.2.2.2 Torsional Vibration of bridge 79
4.3 Response Statistics 82
4.4 Dynamic Amplification Factor 87
4.5 Closure 88

5 FIELD TESTING AND FINITE ELEMENT MODEL UPDATING 89

5.1 Overview 89
5.2 Test Bridge 89
5.3 Test Vehicle 91
5.4 Deck Roughness Measurement 92
5.5 Instrumentation of Test Bridge 94
5.5.1 Accelerometer and Data Acquisition System 94
5.5.2 Test Truck Speed Measurement 95
5.6 Finite Element Modeling of the Bridge 96
5.7 Finite Element Model Updating 97
5.7.1 Response Surface Method (RSM) 98
5.7.1.1 Design of Experiments (DoE) 98
5.7.1.2 Construction of Response Surface Function 101
5.7.1.3 Development of Objective Function 102
5.7.2 Genetic Algorithm 102
5.8 Procedure of Response Surface based FE model updating of Test Bridge 103
5.9 Closure 106

6 RESULT AND DISCUSSION- PART-I: DYNAMIC BEHAVIOUR OF THEORETICAL MODELS 105

6.1 Overview 107
6.2 System parameters 107
6.2.1 Bridge parameters 108
6.2.2 Vehicle parameters 108
6.2.2.1 Quarter Car Model (Model-1) 109
6.2.2.2 Half Car Model (Model-2) 109

6.2.2.3 Full Car Model (Model-3) 109
6.3 Response Statistics for Model-1 109
6.3.1 Vehicle response statistics 110
6.3.2 Bridge response 112
6.3.2.1 Effect of vehicle speed 112
6.3.2.2 Effect of eccentricity of vehicle path 114
6.3.2.3 Effect of approach road settlement 115
6.4 Dynamic Amplification Factor for Model-1 116
6.4.1 Effect of bridge surface roughness and vehicle speed 116
6.4.2 Effect of bridge span and velocity 117
6.4.3 Effect of vehicle mass and approach settlement 118
6.5 Response Statistics for Model-2 119
6.5.1 Vehicle Response 119
6.5.2 Bridge Response 123
6.5.2.1 Effect of vehicle speed 123
6.5.2.2 Effect of eccentricity of vehicle path 125
6.5.2.3 Effect of approach road settlement 125
6.5.2.4 Effect of vehicle bending modes 126
6.6 Dynamic Amplification Factor for Model-2 128
6.6.1 Effect of bridge surface roughness and vehicle speed 128
6.6.2 Effect of bridge span and velocity 129
6.6.3 Effect of vehicle axle spacing and approach settlement on DAF 130
6.6.4 Effect of vehicle mass and approach settlement 131
6.7 Response Statistics for Model-3 132
6.7.1 Vehicle Response 133
6.7.2 Bridge Response 139
6.7.2.1 Effect of vehicle speed 140
6.7.2.2 Effect of eccentricity of vehicle path 141
6.7.2.3 Effect of approach road settlement 142
6.7.2.4 Effect of vehicle structural modes 143
6.8 Dynamic Amplification Factor for Model-3 143
6.8.1 Effect of bridge surface roughness and vehicle speed 144
6.8.2 Effect of bridge span and velocity 145
6.8.3 Effect of vehicle axle spacing and approach settlement on DAF 145

6.8.4 Effect of vehicle mass and approach settlement 146
6.9 Comparison of Different Models Behaviour 148
6.9.1. Bridge response with pre-cambered profile 148
6.9.2. Bridge Response with approach road settlement 148
6.10 Closure 149

7 RESULT AND DISCUSSION- PART-II: VEHICLE PARAMETER IDENTIFICATION FROM SIMULATED BRIDGE RESPONSE 151

7.1 Overview 151
7.2 Comparison of Vehicle Load Estimation with Published Results 151
7.2.1 Comparison with the results of numerical study 152
7.2.2 Comparison with the results of experimental study 153
7.3 Influence of Various Factors on Vehicle Parameter Identification in Model-1 154
7.3.1 Effect of bridge response measurement location 155
7.3.2 Effect of artificial noise level 159
7.3.3 Effect of initial vehicle parameters for construction of prior PDF 159
7.3.4 Effect of different vehicle velocity 161
7.3.5 Effect of different deck surface roughness condition 162
7.3.6 Effect of approach road settlement 163
7.4 Influence of Various Factors on Vehicle Parameter Identification in Model-2 164
7.4.1 Effect of bridge response measurement location 164
7.4.2 Effect of artificial noise level 172
7.4.3 Effect of initial vehicle parameters for construction of prior PDF 173
7.4.4 Effect of different vehicle velocity 175
7.4.5 Effect of different deck surface roughness condition 176
7.4.6 Effect of approach road settlement 177
7.5 Influence of Various Factors on Vehicle Parameter Identification in Model-3 179
7.5.1 Effect of bridge response measurement location 180
7.5.2 Effect of artificial noise level 193

7.5.3 Effect of initial vehicle parameters for construction of prior PDF 194
7.5.4 Effect of different vehicle velocity 198
7.5.5 Effect of different deck surface roughness condition 198
7.5.6 Effect of approach road settlement 198
7.6 Comparison of CPU processing time for estimation of vehicle parameters with numerically generated samples 203
7.7 Closure 208

8 RESULTS AND DISCUSSION- PART-III: VEHICLE PARAMETER IDENTIFICATION FROM FIELD MEASUREMENT 209

8.1 Overview 209
8.2 Field test data 209
8.2.1 Bridge deck surface 209
8.2.2 Bridge dynamic test results 210
8.2.3 Estimation of bridge natural frequency and damping 213
8.3 Finite Element Updating of Bridge Parameters 214
8.4 Identification of Vehicle Parameters from Measured Response 219
8.4.1 Identification of vehicle gross mass 220
8.4.2 Identification of vehicle suspension stiffness and damping 221
8.4.3 Identification of vehicle body flexural and torsional rigidity 227
8.5 Comparison of Reconstructed Acceleration with Experiment Value 228
8.6 Effect of Multiple Sensor Data on Identification of Parameters 229
8.6.1 Identification of vehicle gross mass 229
8.6.2 Identification of vehicle suspension stiffness and damping 232
8.7 Closure 237

9 CONCLUSIONS AND FUTURE SCOPE OF THE WORK 239

9.1 Overview 239
9.2 Conclusions 239
9.2.1 Dynamic behaviour of theoretical models 239
9.2.2 Vehicle parameter identification from simulated results 242
9.2.3 Vehicle parameter identification from field test results 244
9.3 Future Scope of the Study 248

9.4 Closure 248
APPENDIX A 249
APPENDIX B 255
APPENDIX C 266
APPENDIX D 285
REFERENCES 287
LIST OF PUBLICATIONS 308

LIST OF TABLES

Table 3.1	Road classification based on roughness magnitude coefficient (ISO 8608: 1995)	62
Table 4.1	Matrix size for different model	83
Table 5.1	Location of sensors	94
Table 5.2	Central Composite Design for different number of factors (Deng and Cai, 2009)	99
Table 5.3	Three factor Central Composite Design (Mayers *et.al,* 1989)	101
Table 7.1	Comparison of the estimate of gross vehicle weight with published results (Law *et al,* 2004)	153
Table 7.2	Effect of response measurement location on indentified vehicle parameters	158
Table 7.3	Effect of different noise level on the estimated vehicle parameters	159
Table 7.4	Range of Mass of vehicle and wheel Mass to construct prior *PDF*	160
Table 7.5	Range of Suspension stiffness and Tyre stiffness to construct prior *PDF*	160
Table 7.6	Range of Suspension damping and Tyre damping to construct prior *PDF*	161
Table 7.7	Effect of initial range of parameters on the estimated vehicle parameters	161
Table 7.8	Performance of the algorithm at different vehicle speed (V)	162
Table 7.9	Effect of bridge deck surface condition on the estimated vehicle parameters	162
Table 7.10	Effect of approach settlement on identified vehicle parameters	163
Table 7.11	Identification of parameters with different bridge response measurement location	171

Table 7.12	Identification of parameters with different percentage of noise	173
Table 7.13	Range of vehicle mass, flexural rigidity and wheel mass to construct prior *PDF*	174
Table 7.14	Range of Suspension stiffness and Tyre stiffness to construct prior *PDF*	174
Table 7.15	Range of Suspension damping and Tyre damping to construct prior *PDF*	174
Table 7.16	Effect of initial range of parameters on the estimated vehicle parameters	174
Table 7.17	Effect of vehicle speed on the estimated vehicle parameters	176
Table 7.18	Effect of bridge deck surface condition on the estimated vehicle parameters	177
Table 7.19	Effect of approach settlement on identified vehicle parameters	178
Table 7.20	Effect of response measurement location on identified vehicle parameters	193
Table 7.21	Effect of artificial noise level on identified vehicle parameters	194
Table 7.22	Range of mass of vehicle, flexural rigidity and torsional rigidity to construct prior *PDF*	195
Table 7.23	Range of suspension stiffness, tyre stiffness and wheel mass to construct prior *PDF*	195
Table 7.24	Range of suspension damping and tyre damping to construct prior *PDF*	195
Table 7.25	Effect of initial range of parameters on identified vehicle parameters	196
Table 7.26	Effect of different vehicle velocity on identified vehicle parameters	199
Table 7.27	Effect of different deck surface roughness condition on identified vehicle parameters	200

Table 7.28	Effect of approach slab settlement on identified vehicle parameters	201
Table 7.29	Comparison of computer processing time for estimation of Model-1 vehicle parameters	204
Table 7.30	Comparison of computer processing time for estimation of Model-2 vehicle parameters	205
Table 7.31	Comparison of computer processing time for estimation of vehicle body parameters of Model-3	206
Table 7.32	Comparison of computer processing time for estimation of wheel parameters of Model-3	207
Table 8.1	Peak acceleration at different sensors	213
Table 8.2	Base line value, unit change and range of bridge parameters	214
Table 8.3	Experimental design values for the three bridge parameters	215
Table 8.4	Results of simulation for the responses	216
Table 8.5	Updated results for bridge parameters	218
Table 8.6	Comparison of updated natural frequencies with experiment results	218
Table 8.7	Identification of vehicle mass with different model	221
Table 8.8	Vehicle suspension damping for different vehicle speed	222
Table 8.9	Identification of vehicle suspension parameters using Model-1	223
Table 8.10	Identification of vehicle suspension parameters using Model-3	226
Table 8.11	Identification of vehicle body flexural and torsional rigidity	228
Table 8.12	Identification of vehicle mass with different sets of sensor location using moving mass model	231
Table 8.13	Identification of vehicle mass with different sets of sensor location using Model-1	231

Table 8.14	Identification of vehicle mass with different sets of sensor location using Model-3	232
Table 8.15	Identification of vehicle mass with different sets of sensor location using FE Model	232
Table 8.16	Identification of vehicle suspension parameters with different sets of sensor location using Model-1	236
Table 8.17	Identification of vehicle suspension parameters with different sets of sensor location using Model-3	237

LIST OF FIGURES

Fig. 2.1	Estimate of the filtering posterior distribution at time instant *l*	47
Fig. 2.3	Resampling processing for different steps of iteration	48
Fig.2.3	Flow chart for Bootstrap Particle Filtering method for identification of vehicle parameters	53
Fig. 3.1	Deterministic mean surface profile in the form of shallow parabolic	57
Fig. 3.2	Deterministic mean surface profile in the form of approach slab settlement	58
Fig. 3.3	Discretized one-sided power spectral density function	61
Fig. 3.4	Bridge subjected to Quarter Car vehicle Model	63
Fig. 3.5	Bridge subjected to Half Car vehicle Model	65
Fig. 3.6	Bridge subjected to Full Car vehicle Model	68
Fig. 5.1	Photograph of the tested bridge	90
Fig. 5.2	Elevation of the tested bridge	91
Fig. 5.3	Cross section of tested bridge middle span	91
Fig. 5.4	Photograph of test truck TATA 1616	92
Fig. 5.5	Test truck wheel configuration	92
Fig. 5.6	Cross section of test truck frame	92
Fig. 5.7	Measurement of bridge deck surface profile	93
Fig.5.8.	Layout of bridge instrumentation	94

Fig.5.9	(a) Kinemetrics Epi-Sensor ES-U2 force balanced uniaxial accelerometer, (b) B0554 MGC Data Acquisition System	95
Fig. 5.10	Accelerometer glued to deck surface with data cable	95
Fig. 5.11	Genesis Handheld Directional Radar gun	96
Fig. 5.12	Truck speed measurement using radar gun	96
Fig. 5.13	Finite element model of bridge (top isometric view)	97
Fig. 5.14	Two factor Central Composite Design	100
Fig. 5.15	Three factor Central Composite Design (Mayers *et.al,* 1989)	100
Fig. 5.16	Flow chart of Genetic Algorithm	104
Fig. 5.17	Flow chart of response surface based Finite Element model updating	105
Fig.6.1	Cross section of T-beam Bridge	108
Fig.6.2	Sprung mass displacement	110
Fig.6.3	Sprung mass velocity	110
Fig.6.4	Sprung mass acceleration	111
Fig.6.5	Unsprung mass displacement	111
Fig.6.6	Unsprung mass velocity	112
Fig.6.7	Unsprung mass acceleration	112
Fig.6.8	Bridge vertical displacement at mid-span	113
Fig.6.9	Bridge vertical velocity at mid-span	114
Fig.6.10	Bridge vertical acceleration of at mid-span	114

Fig.6.11	Bridge mid-span displacement due to different eccentricity of vehicle path (e_x), (A) e_x=0.5 m, (B) e_x =1 m, (C) e_x =1.5 m	115
Fig.6.12	Bridge mid span deflection for different settlement	116
Fig.6.13	Dynamic amplification factor with vehicle speed and bridge surface roughness coefficient	117
Fig.6.14	Dynamic amplification factor with change in bridge span and vehicle speed	118
Fig.6.15	Dynamic amplification factor for different vehicle mass and approach road settlement	119
Fig.6.16	Mean displacement of vehicle C.G	120
Fig.6.17	Mean Velocity of vehicle at C.G	120
Fig.6.18	Mean acceleration of vehicle at C.G	120
Fig.6.19	Front wheel displacement	121
Fig.6.20	Front wheel velocity	121
Fig.6.21	Front wheel acceleration	122
Fig.6.22	Rear wheel displacement	122
Fig.6.23	Rear wheel velocity	123
Fig.6.24	Rear wheel acceleration	123
Fig.6.25	Bridge displacement at mid span	124
Fig.6.26	Bridge velocity at mid span	124
Fig.6.27	Bridge acceleration at mid span	125
Fig.6.28	Bridge mid-span displacement due to different eccentricity of vehicle path (e_x), (A) e_x=0.5 m, (B) e_x =1 m, (C) e_x =1.5 m	125

Fig.6.29	Bridge mid span deflection for different settlement	127
Fig.6.30	Effect of flexibility on bridge displacement response, (A) E_vI_v=5.3x10^6 N-m^2, (B) E_vI_v=6.4x10^7 N-m^2, (C) E_vI_v=8.2x10^{10} N-m^2	127
Fig.6.31	Comparison of front wheel interaction force, (A) Only rigid modes of vehicle body (B) vehicle body rigid modes with first five structural bending modes	127
Fig.6.32	Comparison of rear wheel interaction force, (A) Only rigid modes of vehicle body (B) vehicle body rigid modes with first five structural bending modes	127
Fig.6.33	Maximum displacement of bridge at mid span (A) Only rigid modes of vehicle body (B) vehicle body rigid modes with first elastic mode (C) vehicle body rigid modes with first three structural modes (D) vehicle body rigid modes with first five structural modes	128
Fig.6.34	Dynamic amplification factor with vehicle speed and bridge surface roughness coefficient	129
Fig.6.35	Dynamic amplification factor with bridge span and vehicle speed	130
Fig.6.36	Dynamic amplification factor for different axle spacing and approach settlement	131
Fig.6.37	Dynamic amplification factor for different vehicle mass and approach road settlement	132
Fig.6.38	Vertical displacement of vehicle at C.G	133
Fig.6.39	Vertical velocity of vehicle at C.G	134
Fig.6.40	Vertical acceleration of vehicle at C.G	134

Fig.6.41	Torsional rotation of vehicle at C.G	134
Fig.6.42	Torsional velocity of vehicle at C.G	135
Fig.6.43	Torsional acceleration of vehicle at C.G	135
Fig.6.44	Displacement of front wheel in right side of the vehicle	136
Fig.6.45	Velocity of front wheel in right side of the vehicle	136
Fig.6.46	Acceleration of front wheel in right side of the vehicle	136
Fig.6.47	Displacement of front wheel in left side of the vehicle	137
Fig.6.48	Velocity of front wheel in left side of the vehicle	137
Fig.6.49	Acceleration of front wheel in left side of the vehicle	137
Fig.6.50	Displacement of rear wheel in right side of the vehicle	138
Fig.6.51	Velocity of rear wheel right in side of the vehicle	138
Fig.6.52	Acceleration of rear wheel in right side of the vehicle	138
Fig.6.53	Displacement of rear wheel in left side of the vehicle	139
Fig.6.54	Velocity of rear wheel in left side of the vehicle	139
Fig.6.55	Acceleration of rear wheel in left side of the vehicle	139
Fig.6.56	Bridge displacement at mid span	140
Fig.6.57	Bridge velocity at mid span	141
Fig.6.58	Bridge acceleration at mid span	141
Fig.6.59	Bridge mid-span displacement due to different eccentricity of vehicle path (e_x), (A) e_x=0.5 m, (B) e_x =1 m, (C) e_x =1.5 m	142
Fig.6.60	Bridge mid span deflection for different settlement	142

Fig.6.61	Maximum displacement of bridge at mid span (A) Only rigid modes of vehicle body, (B) Three rigid modes along with first elastic mode in both bending and torsion (C) Three rigid modes along with first three structural modes in bending and torsion (D) Three rigid modes along with first five structural modes bending and torsion	143
Fig.6.62	Dynamic amplification factor with vehicle speed and bridge surface roughness coefficient	144
Fig.6.63	Dynamic amplification factor with vehicle speed and bridge span	145
Fig.6.64	Dynamic amplification factor for different axle spacing and approach settlement	146
Fig.6.65	Dynamic amplification factor for different vehicle mass and approach settlement	147
Fig.6.66	Bridge displacement at mid-span	148
Fig.6.67	Bridge displacement at mid-span	149
Fig.7.1	Comparison of reconstructed dynamic axle load with published result (Law *et al,* 2004)	153
Fig.7.2	Progressive estimate of model car mass using experimental data (Law *et al,* 1997) and its comparison with true value	154
Fig.7.3	Bridge acceleration at mid-span and quarter span for vehicle speed 60 km/h	155
Fig.7.4	Progressive estimate of vehicle mass m_v from acceleration data at different locations	155
Fig.7.5	Progressive estimate of wheel mass m_w from acceleration data at different locations	156

Fig.7.6	Progressive estimate of vehicle suspension stiffness k_v from acceleration data at different locations.	156
Fig.7.7	Progressive estimate of vehicle suspension damping c_v from acceleration data at different locations	156
Fig.7.8	Progressive estimate of tyre stiffness k_t from acceleration data at different locations	157
Fig.7.9	Progressive estimate of tyre damping c_t from acceleration data at different locations	157
Fig.7.10	Evolution of PDF for measurement at mid span (a) mass of vehicle and (b) mass of wheel	157
Fig.7.11	Evolution of PDF for measurement at mid span (a) suspension stiffness and (b) suspension damping	158
Fig.7.12	Evolution of PDF for measurement at mid span (a) tyre stiffness and (b) tyre damping	158
Fig.7.13	Comparison of interaction force based on identification from acceleration data at two locations	159
Fig.7.14	Comparison of reconstructed interaction force based on identification from different range of values used to construct prior PDF $p(\Phi_0)$	161
Fig.7.15	Progressive estimate of vehicle mass m_v from acceleration data with consideration of 20 mm approach settlement and without settlement	163
Fig.7.16	Progressive estimate of wheel mass m_w from acceleration data with consideration of 20 mm approach settlement and without settlement	164

Fig.7.17	Bridge acceleration at mid-span and quarter span for vehicle speed 60 km/h	164
Fig.7.18	Progressive estimate of vehicle mass m_v from acceleration data at different locations	165
Fig.7.19	Progressive estimate of front wheel mass m_{w1} from acceleration data at different locations	165
Fig.7.20	Progressive estimate of rear wheel mass m_{w2} from acceleration data at different locations	166
Fig.7.21	Progressive estimate of front vehicle suspension stiffness k_{v1} from acceleration data at different locations	166
Fig.7.22	Progressive estimate of rear vehicle suspension stiffness k_{v2} from acceleration data at different locations	166
Fig.7.23	Progressive estimate of front vehicle suspension damping c_{v1} from acceleration data at different locations	167
Fig.7.24	Progressive estimate of rear vehicle suspension damping c_{v2} from acceleration data at different locations	167
Fig.7.25	Progressive estimate of front tyre stiffness k_{t1} from acceleration data at different locations	167
Fig.7.26	Progressive estimate of rear tyre stiffness k_{t2} acceleration data at different locations	168
Fig.7.27	Progressive estimate of front tyre damping c_{t1} from acceleration data at different locations	168
Fig.7.28	Progressive estimate of rear tyre damping c_{t2} from acceleration data at different locations	168

Fig.7.29	Progressive estimate of vehicle flexural rigidity EI_v from acceleration data at different locations	169
Fig.7.30	Evolution vehicle mass PDF for measurement at mid span	169
Fig.7.31	Evolution of PDF for measurement at mid span (a) mass of front wheel and (b) mass of rear wheel	169
Fig.7.32	Evolution of PDF for measurement at mid span (a) front suspension stiffness and (b) rear suspension stiffness	170
Fig.7.33	Evolution of PDF for measurement at mid span (a) front suspension damping and (b) rear suspension damping	170
Fig.7.34	Evolution of PDF for measurement at mid span (a) front tyre stiffness and (b) rear tyre stiffness	170
Fig.7.35	Evolution of PDF for measurement at mid span (a) front tyre damping and (b) rear tyre damping	171
Fig.7.36	Evolution of PDF of vehicle flexural rigidity for measurement at mid span	171
Fig.7.37	Comparison of reconstructed front wheel interaction force based on identification from measured bridge acceleration data at different bridge span location	172
Fig.7.38	Comparison of reconstructed rear wheel interaction force based on identification from measured bridge acceleration data at different bridge span location	172
Fig.7.39	Comparison of reconstructed front axle interaction force based on identification from different range of values used to construct prior PDF $p(\Phi_0)$	175

Fig.7.40	Comparison of reconstructed rear axle interaction force based on identification from different range of values used to construct prior PDF $p(\Phi_0)$	175
Fig.7.41	Progressive estimate of vehicle mass m_v from bridge acceleration with and without approach settlement	178
Fig.7.42	Progressive estimate of front wheel mass m_{w1} from bridge acceleration with and without approach settlement	178
Fig.7.43	Progressive estimate of rear wheel mass m_{w2} from bridge acceleration with and without approach road settlement	179
Fig.7.44	Bridge acceleration at mid span and quarter span	179
Fig.7.45	Progressive estimate of vehicle mass m_v from acceleration data at different locations	180
Fig.7.46	Progressive estimate of mass moment of inertia I_{mv} from acceleration data at different locations.	181
Fig.7.47	Progressive estimate of front-right side wheel mass m_{w11} from acceleration data at different locations	181
Fig.7.48	Progressive estimate of front-left wheel mass m_{w21} from acceleration data at different locations	181
Fig.7.49	Progressive estimate of rear-right wheel mass m_{w12} from acceleration data at different locations	182
Fig.7.50	Progressive estimate of rear-left wheel mass m_{w22} from acceleration data at different locations	182
Fig.7.51	Progressive estimate of front-right vehicle suspension stiffness k_{v11} from acceleration data at different locations	182

Fig.7.52	Progressive estimate of front-left vehicle suspension stiffness k_{v21} from acceleration data at different locations	183
Fig.7.53	Progressive estimate of rear-right vehicle suspension stiffness k_{v12} from acceleration data at different locations	183
Fig.7.54	Progressive estimate of rear-left vehicle suspension stiffness k_{v22} from acceleration data at different locations	183
Fig.7.55	Progressive estimate of front-right vehicle suspension damping c_{v11} from acceleration data at different locations	184
Fig.7.56	Progressive estimate of front-left vehicle suspension damping c_{v21} from acceleration data at different locations	184
Fig.7.57	Progressive estimate of rear right vehicle suspension damping c_{v12} from acceleration data at different locations	184
Fig.7.58	Progressive estimate of rear-left vehicle suspension damping c_{v22} from acceleration data at different locations	185
Fig.7.59	Progressive estimate of front-right tyre stiffness k_{t11} from acceleration data at different locations	185
Fig.7.60	Progressive estimate of front-left tyre stiffness k_{t21} from acceleration data at different locations	185
Fig.7.61	Progressive estimate of rear-right side tyre stiffness k_{t12} from acceleration data at different locations	186
Fig.7.62	Progressive estimate of rear-left side tyre stiffness k_{t22} from acceleration data at different locations	186
Fig.7.63	Progressive estimate of front-right side tyre damping c_{t11} from acceleration data at different locations	186

Fig.7.64	Progressive estimate of front-left side tyre damping c_{t21} from acceleration data at different locations	187
Fig.7.65	Progressive estimate of rear-right side tyre damping c_{t12} from acceleration data at different locations	187
Fig.7.66	Progressive estimate of rear-left side tyre damping c_{t22} from acceleration data at different locations	187
Fig.7.67	Progressive estimate of vehicle body flexural rigidity EI_v from acceleration data at different locations	188
Fig.7.68	Progressive estimate of vehicle body torsional rigidity GJ_v from acceleration data at different locations	188
Fig.7.69	Evolution of PDF of vehicle mass for measurement at mid span	188
Fig.7.70	Evolution of PDF for measurement at mid span (a) front-right (b) front-left wheel mass	189
Fig.7.71	Evolution of PDF for measurement at mid span (a) rear-right (a) rear-left wheel mass	189
Fig.7.72	Evolution of PDF for measurement at mid span (a) front-right (b) front-left suspension stiffness	189
Fig.7.73	Evolution of PDF for measurement at mid span (a) front-right (b) front-left suspension damping	190
Fig.7.74	Evolution of PDF for (a) front-right (b) front-left side of vehicle tyre stiffness	190
Fig.7.75	Evolution of PDF for (a) front-right (b) front-left tyre damping	190

Fig.7.76	Evolution of PDF for (a) vehicle body flexural rigidity and (b) vehicle body torsional rigidity	191
Fig.7.77	Comparison of reconstructed interaction force imposed by front-right wheel with Reference force	191
Fig.7.78	Comparison of reconstructed interaction force imposed by front-left wheel with Reference force	191
Fig.7.79	Comparison of reconstructed interaction force imposed by rear-right wheel with Reference force	192
Fig.7.80	Comparison of reconstructed interaction force imposed by rear-left wheel with Reference force	192
Fig.7.81	Comparison of mean of identified and true dynamic interaction force (a) front-right (b) rear-right wheel using different prior distribution	192
Fig.7.82	Comparison of mean of identified and true dynamic interaction force (a) front-left (b) rear-left wheel using different prior distribution	196
Fig.7.83	Comparison of standard deviation of identified and true dynamic interaction force (a) front-right (b) rear-right wheel using different prior distribution	197
Fig.7.84	Comparison of standard deviation of identified and true dynamic interaction force (a) front-left (b) rear-left wheel using different prior distribution	197
Fig.7.85	Progressive estimate of vehicle mass m_v from acceleration data with consideration of 20 mm approach settlement and without settlement	197

Fig.7.86	Progressive estimate of front-right wheel mass m_{w11} from acceleration data with consideration of 20 mm approach settlement and without settlement	201
Fig.7.87	Progressive estimate of front-left wheel mass m_{w21} from acceleration data with consideration of 20 mm approach settlement and without settlement	202
Fig.7.88	Progressive estimate of rear-right wheel mass m_{w12} from acceleration data with consideration of 20 mm approach settlement and without settlement	202
Fig.7.89	Progressive estimate of rear-left wheel mass m_{w22} from acceleration data with consideration of 20 mm approach settlement and without settlement	202
Fig.8.1	Measured bridge deck surface profile	203
Fig.8.2	Classification of deck surface profile based on ISO specification (ISO 8608: 1995)	210
Fig.8.3	Measured bridge acceleration at sensor-1 for vehicle speed 21 km/h	211
Fig.8.4	FFT of bridge acceleration at sensor-1 for vehicle speed 21 km/h	211
Fig.8.5	Measured bridge acceleration at sensor-1 for vehicle speed 43 km/h	211
Fig.8.6	FFT of bridge acceleration at sensor-1 for vehicle speed 43 km/h	212
Fig.8.7	Measured bridge acceleration at sensor-4 for vehicle speed 21 km/h	212

Fig.8.8	FFT of bridge acceleration at sensor-4 for vehicle speed 21 km/h	212
Fig.8.9	Measured bridge acceleration at sensor-4 for vehicle speed 43 km/h	212
Fig.8.10	FFT of bridge acceleration at sensor-4 for vehicle speed 43 km/h	213
Fig.8.11	Mode shape of updated Finite Element bridge model	218
Fig.8.12	Peak acceleration response of bridge at different sensor location (V=43 km/h)	219
Fig.8.13	Progressive estimate of vehicle mass based on bridge acceleration from sensor-1	220
Fig.8.14	PDF of vehicle mass estimate at different stage of iterations	221
Fig.8.15	Progressive estimate of vehicle suspension stiffness k_v from measured acceleration data considering Model-1	223
Fig.8.16	Progressive estimate of vehicle suspension damping c_v from measured acceleration data considering Model-1	223
Fig.8.17	Progressive estimate of front-right suspension stiffness k_{v11} from measured acceleration data considering Model-3	224
Fig.8.18	Progressive estimate of front-left suspension stiffness k_{v21} from measured acceleration data considering Model-3	224
Fig.8.19	Progressive estimate of rear-right side suspension stiffness k_{v12} from measured acceleration data considering Model-3	224
Fig.8.20	Progressive estimate of rear-left side suspension stiffness k_{v22} from measured acceleration data considering Model-3	225

Fig.8.21	Progressive estimate of front-right vehicle suspension damping c_{v11} from measured acceleration data considering Model-3	225
Fig.8.22	Progressive estimate of front-left vehicle suspension damping c_{v21} from measured acceleration data considering Model-3	225
Fig.8.23	Progressive estimate of rear-right vehicle suspension damping c_{v12} from measured acceleration data considering Model-3	226
Fig.8.24	Progressive estimate of rear-left vehicle suspension damping c_{v22} from measured acceleration data considering Model-3	227
Fig.8.25	Progressive estimate of vehicle body flexural rigidity EI_v from measured acceleration data	228
Fig.8.26	Progressive estimate of vehicle body torsional rigidity GJ_v from measured acceleration data	227
Fig.8.27(a)	Comparison of reconstructed bridge acceleration response at sensor-1 with field test result	228
Fig.8.27(b)	Comparison of peak acceleration at different sensor locations obtained in different models with field test result	229
Fig.8.28	Progressive estimate of vehicle mass for multiple sensor data using moving mass model	230
Fig.8.29	Progressive estimate of vehicle mass for multiple sensor data using Model-1	230
Fig.8.30	Progressive estimate of vehicle mass for multiple sensor data using Model-3	231

Fig.8.31	Progressive estimate of vehicle mass for multiple sensor data using FE Model	231
Fig.8.32	Progressive estimate of vehicle suspension stiffness k_v for different sets of sensors considering Model-1	233
Fig.8.33	Progressive estimate of vehicle suspension damping c_v from measured acceleration data considering Model-1	233
Fig.8.34	Progressive estimate of front-right suspension stiffness k_{v11} from measured acceleration data considering Model-3	233
Fig.8.35	Progressive estimate of front-left suspension stiffness k_{v21} from measured acceleration data considering Model-3	234
Fig.8.36	Progressive estimate of rear-right side suspension stiffness k_{v12} from measured acceleration data considering Model-3	234
Fig.8.37	Progressive estimate of rear-left side suspension stiffness k_{v22} from measured acceleration data considering Model-3	234
Fig.8.38	Progressive estimate of front-right vehicle suspension damping c_{v11} from measured acceleration data considering Model-3	235
Fig.8.39	Progressive estimate of front-left vehicle suspension damping c_{v21} from measured acceleration data considering Model-3	235
Fig.8.40	Progressive estimate of rear-right vehicle suspension damping c_{v12} from measured acceleration data considering Model-3	235
Fig.8.41	Progressive estimate of rear-left vehicle suspension damping c_{v22} from measured acceleration data considering Model-3	236

NOMENCLATURES

$[A]$	System coefficient matrix
$[A]^+$	Pseudo inverse of the matrix $[A]$
$[A(t)]$	State matrix of coupled vehicle-bridge system
$[A(\omega)]$	System matrix in frequency domain
A_s	Amplitude of cosine wave
b_i	Distance of ith wheel from centre line of vehicle body
$\{b\}$	Time series vector of measured response of bridge deck
$\{b(\omega)\}$	Frequency domain function of the measured bridge response at selected station
c_v	Suspension damping of Model-1
c_{v1}	Front suspension damping of Model-2
c_{v2}	Rear suspension damping of Model-2
c_{v11}	Front-right suspension damping of Model-3
c_{v21}	Front-left suspension damping of Model-3
c_{v12}	Rear-right suspension damping of Model-3
c_{v22}	Rear-left suspension damping of Model-3
c_t	Tyre damping of Model-1
c_{t1}	Tyre damping of Model-2
c_{t2}	Rear tyre damping of Model-2
c_{t11}	Front-right tyre damping of Model-3
c_{t21}	Front-left tyre damping of Model-3
c_{t12}	Rear-right tyre damping of Model-3
c_{t22}	Rear-left tyre damping of Model-3
C_b	Viscous damping per unit length of bridge
C_{br}	Rotational damping per unit length of bridge
C_v	Viscous damping per unit length of the vehicle body
C_{vT}	Rotational viscous damping per unit length of the vehicle body
$[C(t)]$	Time dependent damping matrix of coupled vehicle-bridge system
D_1	Vehicle centroid distance from the leading edge of the vehicle body
D_2	Vehicle centroid distance from the trailing edge of the vehicle body
e_x	Load eccentricity

E_bI_b	Flexural rigidity of the bridge
$E_k(x_k,t_k)$	Standard error of the mean (SEM)
E_vI_v	Flexural rigidity of flexible vehicle body
f_1(t)	Moving load function for front axle
f_2(t)	Moving load function for rear axle
$f_l(.)$	Non linear function that relates the measurements to the system state
$\{f(\omega)\}$	Frequency variation of moving force
$f_b(x,t)$	Impressed vertical force on the bridge due to vehicle interaction
$f_T(x,t)$	Imposed torque on the bridge due to vehicle interaction
$F(t)$	Input excitation
F_{obj}	Objective function for optimization based indirect inverse scheme
$\{F(t)\}$	Generalized stochastic force vector for coupled vehicle-bridge system
$\{F(\omega)\}$	Fourier transform of the input excitation
$g_l(.)$	System transition function
$g_0(t)$	Gaussian stochastic process
G_bJ_b	Torsional rigidity of bridge
G_vJ_v	Torsional rigidity of the vehicle cross section
$h(x)$	Bridge deck profile
h_0	Central rise of mean parabolic surface
h_1	Magnitude of approach road settlement
$h_m(x)$	Deterministic mean surface profile
$h_r(x)$	Random road surface unevenness
$h(t)$	Impulse response function
$[H(\omega)]$	Frequency Response Function
$H_j(\omega,t)$	Transient frequency response function
I_{mv}	Polar moment of inertia per unit length of vehicle body cross section
I_{mb}	Polar moment of inertia per unit length of bridge cross section
$[I]$	Identity matrix
k_v	Suspension stiffness of Model-1
k_{v1}	Front suspension stiffness of Model-2
k_{v2}	Rear suspension stiffness of Model-2
k_{v11}	Front-right suspension stiffness of Model-3
k_{v21}	Front-left suspension stiffness of Model-3

k_{v12}	Rear-right suspension stiffness of Model-3
k_{v22}	Rear-left suspension stiffness of Model-3
k_t	Tyre stiffness of Model-1
k_{t1}	Tyre stiffness of Model-2
k_{t2}	Rear tyre stiffness of Model-2
k_{t11}	Front-right tyre stiffness of Model-3
k_{t21}	Front-left tyre stiffness of Model-3
k_{t12}	Rear-right tyre stiffness of Model-3
k_{t22}	Rear-left tyre stiffness of Model-3
$[K(t)]$	Time dependent stiffness matrix of coupled vehicle-bridge system
l_v	Length of vehicle body
L	Bridge span
L_r	Ramp length
$L(.)$	Likelihood function
m	Roughness shape coefficient
m_b	Mass per unit length of bridge
m_{qv}	Sprung mass of Model-1
m_v	Mass per unit length of flexible vehicle body
m_w	Unsprung mass of Model-1
m_{w1}	Front wheel mass of Model-2
m_{w2}	Rear wheel mass of Model-2
m_{w11}	Front-right wheel mass of Model-3
m_{w21}	Front-left wheel mass of Model-3
m_{w12}	Rear-right wheel mass of Model-3
m_{w22}	Rear-left wheel mass of Model-3
$[M]$	Mass matrix of coupled vehicle-bridge system
M_{vk}	Generalized mass of vehicle body in bending
$\overline{M}_{vk}$	Generalized mass of vehicle body in bending
n	Sizes of the coupled vehicle-bridge system matrix
N	Number of terms used to build up the road surface roughness
N_l	Total number of time step
N_p	Random samples of vehicle parameters
N_t	Number of time instants considered

N_s	Number of time history samples inside the ensemble output set
$p(.)$	Probability density function
$\{p(t)\}$	State vector of coupled vehicle-bridge system
P_{iden}	Identified vehicle parameters
P_{true}	True vehicle parameters
$\{P(t)\}$	Augmented load vector in state-space equation
$Q_{bk}(t)$	Generalized force in the k^{th} mode of bridge in flexure
$Q_{vk}(t)$	Generalized force in the k^{th} mode of transverse vibration of vehicle body
r_m	Measured response time histories
r_s	Simulated response time histories
$\{r(t)\}$	Response vector of coupled vehicle-bridge system
$r_{Pm}(t)$	Particular integral of the coupled vehicle-bridge system differential equation
$R_{g0g0}(\tau)$	Autocorrelation function
$S_{g0g0}(\omega)$	Temporal power spectral density function
$S_{g0g0}(\Omega)$	Two-sided power spectral density function in space domain
$S_{GG}(\Omega)$	One sided spectral density
$u_j(t)$	Time dependent Eigenvector of coupled vehicle-bridge system state matrix
$[U(t)]$	Modal matrix of coupled vehicle-bridge system
V	Vehicle speed
w_s	Normalized weight of particle
$W(.)$	Importance weights
$\{x(t)\}$	Time series vector
$\{X(\omega)\}$	Fourier transform of the vector of response co-ordinates
X_{0j}	Constants of integration to be determined from the initial conditions
$y(t)$	Measured output at different stations
$y(x,t)$	Bridge deflection measured at location x from the reference point at time instant t
$Y_{dynamic}$	Maximum response due to fluctuating load imposed on the bridge due to vibratory motion of the vehicle excited by road unevenness

Y_{static}	Response of the bridge at the mid span location for adverse position of static wheel loads
z_1	Heave motion of sprung mass
z_2	Vertical motion of un-sprung mass
$z(u,t)$	Vertical deflection of the vehicle body measured at location u from the reference point at time instant t
Z_l	Bridge response measurement
$\alpha_j(t)$	Time dependent eigenvalues of coupled vehicle-bridge system state matrix
$\delta(.)$	Dirac-delta function
$\Delta\Omega$	Spatial frequency bands width
$\eta_{bk}(t)$	Time dependent generalized coordinate of bridge in bending
$\eta_{Tk}(t)$	Time dependent generalized coordinate of bridge in torsion
$\eta_{vk}(t)$	Time dependent generalized coordinate of vehicle body in bending
$\Gamma_{identified\ value}$	Identified vehicle parameters value
$\Gamma_{reference\ value}$	True vehicle parameters value
Γ_L	Lower bound of the vehicle parameters for construction of prior PDF
Γ_U	Upper bound of the vehicle parameters for construction of prior PDF
λ	Wavelength of road unevenness
$\mu(.)$	Mean value of identified vehicle parameters
μ_F	Mean of bridge vehicle interaction force
$\mu_Y(t_k)$	Mean of the output samples
$\mu_k(x_k,t_k)$	Mean response of bridge
$\gamma_l\ (t)$	Time dependent generalized coordinate of vehicle body in torsion
$\sigma_Y(t_k)$	Standard deviation of the output samples
$\phi_b(x)$	Bridge mode shapes in bending
$\phi_{vk}(u)$	Vehicle mode shapes in bending
$\bar{\phi}_{vk}(u)$	Vehicle mode shapes in torsion
$\{\Phi\}$	System parameters
$\pi(.)$	Probability density function
ξ_{bk}	Modal damping ratio of bridge in bending
ξ_{vk}	Modal damping ratio of vehicle body in bending

ξ_{vTk}	Modal damping ratio of vehicle body in torsion
ξ_{Tl}	Modal damping ratio of bridge in torsion
$\psi_{vk}(t)$	Time dependent generalized coordinate used to describe torsional motion
$\sigma(.)$	Standard deviation of identified vehicle parameters
σ_F	Standard deviation of bridge vehicle interaction force
θ_s	Random phase angle
$\theta_{Tb}(u)$	Bridge mode shapes in torsion
ω	Temporal frequency
ω_b	Bridge natural frequency in bending
ω_T	Bridge natural frequency in torsion
ω_{vk}	Vehicle body natural frequency in bending
$\overline{\omega}_{vk}$	Vehicle body natural frequency in torsion
Ω	Wave number / spatial frequency
Ω_0	Discontinuity frequency of road
Ω_s	Road spatial frequency
Ω_L	Lower cut-off frequencies of spatial unevenness
Ω_U	Upper cut-off frequencies of spatial unevenness

1

INTRODUCTION

1.1 Overview

The passage of vehicles over the bridge induces its self-weight in addition to dynamic tyre force resulted from the vibration of vehicles. Vehicles are complex structural systems with combinations of wheels and body connected by suspension elements. Vehicle receives input through its moving wheels due to deflected surface of bridge and pavement unevenness. The shock and vibration caused by surface unevenness are transmitted from wheels to the super structure of vehicle through the suspension system. The vertical irregularities of surface in longitudinal and transverse directions induce heave, pitch, roll, yaw and axial motions in the vehicle.

The vibration of moving vehicle is transmitted as oscillatory load on the bridge which varies both in space and time. It may be noted that vehicle and bridge are integral parts of transportation system. The performance of one is affected by the performance of other and vice versa. For given structural configuration, construction materials and road surface condition, the physical parameters of vehicle also play a significant role in bridge dynamic behavior. Traditionally, the bridge design load is calculated by magnifying static live load with impact factor. Days are not far when complete moving load time history would be necessary to check the design of long span bridges.

Due to rapid growth of traffic in modern times, there is necessity of construction of new roads in which several bridges over the streams or railway tracks may be required. The bridges are now-a-days subject to vehicular loading of different pattern than that found in design codes. The estimation of dynamic vehicular load is significant for finding dynamic load factor for bridge design, to determine fatigue life and for structural health monitoring of bridge structures. It may be mentioned that dynamic component of the load causes rapid degradation of pavement structure showing spatial repeatability which is of concern to bridge management.

The vehicles are likely to come across bridges at different locations of highways and load they carry has important bearing on the performance of the bridges. The weight of the vehicle is

key parameter which governs the design of bridge. Overloaded vehicles moving along the bridge may shorten the life span of the bridge. A traditional way of controlling overloading on highway bridges is to measure the gross weight of the vehicle in static condition. This is generally obtained by "weigh-bridge" system installed on the sides of highways and also in factories to monitor loading on highway pavement and bridge. The distribution of load to different axles is, however, not known from weigh bridge record. It is to be mentioned that knowledge of suspension parameters is also essential along with the gross weight of the vehicle to know the complete moving load time history.

Recently lot of emphasis is placed on "road friendly suspensions" such that less dynamic load is induced on the pavement of a road or bridge. The vehicles with "road friendly suspensions" are even permitted to carry extra load over and above the allowable load (National Code of Practice Vehicle Standards Bulletine 11, 2004). At present, due to development of sensor technology, it has become possible to know axle weight of the vehicle in a highway bridge. However, determination of suspension parameters along with weight is not possible by the existing method. The moving vehicles and the bridge are two sub systems coupled with each other having a common interface. Such coupled system gives rise to challenging problems in modeling of the vehicle and bridge. The bridge surface irregularity is the main source of excitation to moving wheels. The surface roughness is caused by continuous degradation of pavement due to imposition of vehicle load which varies in random manner. In addition to that construction features such as expansion joint, pre-cambering of longitudinal profile and various defects in construction are met in practice. This triggers the vehicle vibration and as a result, bridge pavement also experiences high dynamic load.

Determination of moving load time history from the measured bridge response falls under a class of "inverse problem". The solution of the inverse problems is always associated with some challenges. However, the use of modern high speed computers, sophisticated sensors and data acquisition systems have offered various advantages to carry out research on inverse problems in vehicle-bridge interaction. The present thesis is an endeavor to contribute to this challenging area using theoretical and experimental investigation.

1.2 Literature Review

1.2.1 Vehicle Parameter Identification

Several methods have been reported using different techniques on vehicle static and dynamic load identification based on simulation and experimental observation. Some of the important works which earned various degrees of success are described in brief in this section.

1.2.1.1 Method of Identification

Information about the actual truck loads on highway bridges were used to obtain from truck surveys where the trucks were stopped for measurement and weighing on static weighing scales, known as "weigh bridges". Marshal and Murphy (2003) reported influence of various factors affecting the accuracy of weigh bridge system.

However, during the past few decades information about truck loads have been collected using the weight-in-motion (WIM) scales installed in the pavement while the truck moves at normal speeds. The first WIM of vehicle was developed by Norman and Hopkins (1952). The most common WIM sensor for data collection purpose is the piezoelectric sensor. There is one more variety of WIM system which uses bending plate scale. Bending plate technology incorporates a steel plate with strain gauges attached to its underside (Koniditsiotis and Peters, 2008). Using this technique only vehicle static weight can be obtained and installation cost is high.

In other WIM systems, a highway bridge has been used for weighing truck, referred to as bridge weight-in-motion (B-WIM) system. Measurement of vehicle weight using bridge response was proposed by Moses (1979) and many improvements of the system have taken place over the years (Znidaric *et al.,* 2002; Cheng *et al.,* 2007 and Helmi *et al.,* 2014). Similar to conventional WIM system, this method is failed to determine actual dynamic load induced in the bridge due to passing vehicle.

O'Connor and Chan (1988) employed least square method to estimate equivalent static load and their dynamic variation with time based on bridge response measurement. Vehicle bridge interaction was ignored in the system model. It was found that the use of measured bending moments gives better results than measured deflections. Although acceptable results have been found, it is believed that difficulties may arise in using accelerometer data as input to

the algorithm because of the possible occurrence of high frequency noise in these records, leading to error in computed deflection and consequent larger errors in the load estimate.

Law *et al.* (1997) developed a method to indentify the force in time domain on the basis of the modal superposition principle, and assuming the force as a step function in a small time interval. Least square method was used to estimate the unknown moving force. Computer simulation and laboratory tests shows the method was effective and acceptable results could be obtained by combining the use of bending moment and acceleration measurement. The proposed method is beneficial to the identification of vehicles with only a limited number of axles, since each additional moving force adds another set of equation which must be solved; a much greater computational cost may involved. Due to ignorance of vehicle suspension system, bridge deck surface condition could not be included in the identification algorithm which may lead to significant error in the estimation of moving load. Combination of bending moment and acceleration measurements were used in the identification of moving force.

Chan *et al.* (1999) proposed a method for identification of moving load called interpretive method. On which the bridge displacement at various locations are transformed to modal values. The bridge displacements were numerically differentiated to obtain the corresponding modal velocity and modal acceleration. And then the values of axle load at any instant were obtained using least squares method. Although vehicle suspension is included in the model, road surface condition is not taken into account. As mentioned in the study, the proposed identification method could estimate moving load with minimum error only at certain ratio of bridge span to axle spacing.

Chan *et al.* (2000) made comparative studies on the four existing moving force identification theory using laboratory vehicle-bridge model set up. The bending moment and acceleration responses of model bridge were simultaneously measured when the vehicle moves across the bridge at different speeds. Although all four methods gave acceptable results to some extent, time domain method was strongly recommended. Similar to the earlier study, vehicle structure interaction were not considered in all the comparisons of different method.

Zhu and Law (2000) employed “Tikhonov regularization” technique to provide bounds to the ill-conditioned results in the identification problem. The improved algorithm was then used to study the effect of different parameters on the identification results through single-force and multi-force identification. Timoshenko beam model was found to be better than Euler-Bernoulli beam model in the identification of moving force. The dynamic behavior of the

bridge deck under moving loads was analyzed using the orthotropic plate theory and modal superposition principle, and Tikhonov regularization procedure was applied to provide estimate of identified forces in the time domain.

Zhu and Law (2000) have conducted computer simulation and laboratory study on the effectiveness of the proposed method in identifying forces travelling along the central line or at an eccentric path on the bridge deck. It was found that when the lower modes of the bridge deck are dominated by vibrational modes along the longitudinal axis, a beam model instead of a plate mode may be conveniently used in the identification process.

Two methods have been reported by Zhu and Law (2003) to identify moving loads on the top of a bridge deck. One is based on the exact solution (ESM) and the other is based on the finite element formulation (FEM). In the study bridge was modeled as an orthotropic plate subjected to point load without consideration of surface roughness. Their experimental studies reveal that both the exact solution method and the finite element method could identify moving loads with small eccentricity, but the finite element method requires greater number of measured information to have the same accuracy as the exact solution method.

Jiang *et al.* (2004) identified vehicle parameters moving on multi-span continuous bridge taking into account the bridge deck surface roughness. Vehicle was modeled as two degrees of freedom system. Newmark-β method was employed to solve the governing differential equation. The identification has been realized through robust multi-stage optimization scheme based on genetic algorithm, which searches for the best estimates of parameters by minimizing the errors between the measured accelerations and the reconstructed accelerations from the identified parameters. The identified parameters were also used to estimate the time varying contact forces between the vehicle and the bridge.

Zhu and Law (2006) developed a method based on modal superposition and regularization technique to identify moving load on an elastically supported multi-span continuous bridge deck. They found that measured acceleration gives better results than those from strains. Also it was concluded that the number of bridge vibrational modes considered in the identification should cover the frequency range of excitation forces for an accurate identification. Accuracy of the estimate was found to be dependent on stiffness ratio of the bearing to the deck slab.

Chatterjee *et.al* (2006) presented a wavelet based approach of strain signals to identify axle passage in a bridge. In this study, conventional axle detector on bridge surface was not used;

instead, strain transducer was fitted underneath the bridge deck. Experimental data were collected from a two lane short culvert due to passage of muliaxles wagon. Numerical simulations were carried with heave-pitch model of vehicle over a beam model representing bridge. Strain data obtained numerically and experimentally were processed using reverse biorthogonal wavelet transform. Study reported that error may increase if peaks are located at wrong locations.

The past researches adopted Least-squares solution in combination with conventional regularization for identification of moving load on the bridge. It has been found that accuracy of the identified results greatly depend on an assigned regularization parameter, which is very sensitive to the vehicle-bridge properties such as the speed of the vehicle or the roughness amplitude of the bridge surface. To overcome this problem, regularization scheme using the updated static component (USC) technique was proposed by Pinkaew (2006). The technique extracts the static components of the identified axle loads and leaves only the associated dynamic components to be identified. Then an iterative method has been implemented to improve the accuracy of the identified results. Although improvements in accuracy and computational time have been achieved, still the algorithm was found to be highly dependent on the sampling frequency of bridge measurement. Furthermore, numerical solution has been employed for forward solution of the bridge vehicle model. The mismatching of the measurement and the forward solution sampling rate may leads to higher identification error of the moving load.

Researchers (Liljencrantz *et. al.,* 2007) have also paid attention to apply weigh-in-motion technology on railways to detect railway traffic load. Study conducted on an instrumented bridge has shown that it is possible to detect axle load, spacing and speed of the passing train over the bridge. First they attempted to identify the peak strain in two sensors and then knowing the time difference between two peaks, an initial guess of the speed was obtained. However, presence of noise in field data the estimate of speed was not satisfactory, which was improved subsequently by minimizing the phase difference of signals in two sensors. No attempt, however, has been made to estimate suspension parameters of train and no consideration was given to track irregularity in simulated results.

Zhu *et al.* (2009) formulated moving load identification method in state space with the application of regularization on the solution. The bridge was represented as an orthotropic rectangular plate, and the loads were modeled as a group of loads moving on top of the bridge

at a fixed distance and at a constant speed. The Hamilton principle and the modal superposition principle were employed in the formulation. They found that identification based on bridge acceleration response gives better estimate of moving load than the bridge strain response. Significant effect of measurement noise on moving load estimation was found, the estimation error was in the range of 18% to 32% for 10% level of noise.

Multiple vehicle dynamic axle loads on multi-span continuous bridge was identified by Asnachinda *et al* (2008) using least squares regularization optimization. The updated static component was employed to improve the accuracy and workability of the inverse solution. Finite element method was adopted for the forward scheme. The proposed algorithm was validated with laboratory experiment. Accuracy of the identified axle load was found to be dependent on the vehicle mass and speed. Furthermore, effect of noise presented in the measured bridge response was not included in the study.

A stochastic force identification algorithm was proposed by Wu and Law (2011) in which the statistics of dynamic interaction forces between bridge and vehicle were obtained from a set of sample of the random bridge responses. Theoretical formulation on vehicle bridge model was done by considering four degrees of freedom vehicle system moving on simply supported Euler Bernoulli beam. Bridge deck surface profile was modeled as Gaussian random process by the Karhunen- Loeve expansion. Effect of the number of the samples used and the different road surface profiles on the accuracy of the proposed algorithm were investigated.

Measurement of suspension parameters is an important aspect of inverse procedure in vehicle dynamics to determine "road friendliness" of the vehicle. Thite *et. al.* (2011) outlined a procedure to estimate suspension parameters of a vehicle in the frequency domain. This method has taken measurement noise into account. They have found that use of frequency content in combination with a frequency response function estimator can reduce the effect of measurement noise. The method was based on an indirect matrix inversion method. The procedure has been illustrated using lump parameter half car model. This method does not consider any stochastic environment in which vehicle are expected to work.

Lu and Liu (2013) proposed identification method for physical parameters of coupled bridge vehicle system. Governing equation of the bridge idealized as a beam model was established from finite element analysis. Passing vehicle has been represented by quarter car model. The

dynamic responses of the system were obtained from direct integration method. Inverse problem was solved using Least squares method. In order to provide bounds to the solution, the damped least-squares method (DLS), which is also the well-known Tikhonov regularization, was used in the pseudo-inverse calculation. Although satisfactory results were obtained from the model, but stochastic road profile and higher degrees of freedom vehicle model has been ignored in their study.

1.2.1.2 Parameter identification using probabilistic approach

Development of Bayesian state estimation methodologies has added a new dimension in system identification involving various uncertainties. Recursive Bayesian estimation, also known as a Bayes filter, is a general probabilistic approach for estimating an unknown probability density function recursively over time using incoming measurements and a mathematical process model. Several researchers adopted this estimation technique in different field of engineering.

Bayesian theory was originally discovered by the British researcher Thomas Bayes in 1763, and is also referred to as Bayes' law or Bayes' rule (Bayes and Price, 1763). Bayes' theorem shows the relation between two conditional probabilities that are the reverse of each other. However, Bayesian theory has not gained its deserved attention in the early days until its modern form was rediscovered by the French mathematician Pierre-Simon de Laplace in 1812 as reported by Bayes and Price (1763). Bayesian inference (Bernardo and Smith, 1998; Robert, 2001) has become one of the important branches in statistics, and has been applied successfully in statistical decision, detection and estimation, pattern recognition, and machine learning.

Different methods have been proposed to utilize Bayesian inference. Kalman (1960) computes the posterior distribution exactly for linear Gaussian systems by updating finite-dimensional statistics recursively. This theorem is named after Kalman, and is also referred to as Kalman Filter. However, this filter is limited to linear and Gaussian system only.

For nonlinear, non-Gaussian models, the Kalman Filter algorithm can be applied to a linearized model with Gaussian noise with the same first- and second-order moments. This approach is commonly referred to as the extended Kalman filter (Smith and Schmidt, 1962). This may work well but without any guarantees for mildly nonlinear systems where the true posterior is unimodal i.e., only one peak and essentially symmetric. Arasaratnam *et al*. (2007)

proposed Gaussian sum Kalman filters by representing the posterior distribution with a Gaussian mixture distribution. Filters in this class can handle multimodal posteriors.

The Monte Carlo techniques behind particle Filters have existed since the 1950s (Hammersley and Morton, 1954) but a lack of computational power at that time and problems with degeneracy have kept these methods generally overlooked. Gordon *et al*., (1993) proposed an algorithm for implementing recursive Bayesian filters, called as bootstrap particle filter. The required density of the state vector was represented as a set of random samples, which were updated and propagated by the algorithm. This method is not restricted by assumptions of linearity or Gaussian noise. The proposed method was tested for tracking problem, performance of the bootstrap filter was found to be greatly superior to the standard extended Kalman filter.

Arulampalam *et al*. (2002) investigated performance of particle filter method for non-linear and non-Gaussian dynamic state estimation. Several case studies have been conducted for different Bayesian filter such as Kalman filter (KF), sampling importance resampling (SIR) filter, auxiliary sampling importance resampling (ASIR) filter and regularized particle filter (RPF). It has been found that for a particular problem, if the assumptions of the Kalman filter hold, then no other algorithm can outperform them. However, in a variety of real scenarios, the assumptions do not hold, and approximate techniques must be employed.

Ristic *et al.* (2004) utilized particle filter method for different tracking problems including ballistic target, bearings only , range only, bistatic radar and terrain aided tracking including robotics. In realistic environment and complicated tracking process such as false detections and multiple targets, particle filter method was found to be much superior to the other stochastic filtering technique.

In view of reliability and accuracy of performance, Particle filter method attracted many researchers in the field of communication engineering, image processing and ecology to estimate state of the system and hidden parameters from noisy signal data (Qian *et al.,* 2003 and Ying *et al.,* 2010). This technique has been employed not only in engineering problems, but also in economics (Kim *et al*., 1998; Johannes *et al*., 2009), neuroscience (Salimpour and Soltanian-Zadeh, 2009) and biochemical networks (Djuric and Bugallo, 2009) to name a few.

Davidson *et al.* (2010) employed particle filter method for vehicle positioning using road maps. Theoretical simulations and experiments were conducted. Since particle filters have no

restrictions on the type of models and noise distribution, modeling error of velocity and heading measurement was found to be more accurate than other methods.

Bootstrap particle filter method has also been employed in the field of water resource engineering (Shi and Chen, 2011). The test results demonstrate that the bootstrap filter tracking method is superior to the Kalman filter tracking and the Super-PIV methods for measuring low density, high velocity gradient flows.

Nasrellah and Manohar (2011) developed parameters identification procedure by combining bootstrap particle filter with finite element method for structural modeling. Performance of the proposed method was examined by theoretical simulation, laboratory and field test results. Although satisfactory results were obtained, but computational cost was found to be significantly high.

In application of Particle filter technique to identify vehicle parameters, it is necessary to adopt a suitable mathematical model for repeated generation of response samples. The next section of the literature review focuses on the various studies conducted on bridge vehicle interaction dynamics.

1.2.2 Vehicle Bridge Interaction

The dynamic interaction between a bridge and the moving vehicles represents a special discipline within the broad area of structural dynamics. Theoretically, the two subsystems, the bridge and moving vehicle, can be simulated as two elastic structures having a common interface. Each is characterized by some frequencies of vibration. The two subsystems interact with each other through the contact forces. A large number of authors contributed to this area on modeling of vehicle, bridge structures and pavement unevenness as well as on the various techniques of solutions.

1.2.2.1 Vehicle model for the dynamic analysis of bridge

Articles on bridge vibration due to vehicle movement dates back to the middle of nineteenth century in the works of Willis (1849) and Stokes (1849), for investigation of the collapse of the Chaster Rail Bridge in England in 1847, the first case for collapse of a railway bridge in history. The contribution of Stoke and Willis is considered historical, since they are among the first to bring the problem of vehicle impacts to the design desks of bridge engineers. In their study, a passing vehicle has been idealized as a moving load at constant velocity. It has

been found that dynamic responses of bridge due to moving vehicle are significantly higher than those observed for the static case.

Timoshenko (1922) derived approximate solution to the problem of simple beam subjected to moving loads ignoring its inertia effect. It has been observed that this model could capture essential dynamic characteristics of the bridge caused by the vehicle moving action with a significant degree of accuracy.

The moving load model was adopted by Ayre *et al.* (1950) and Ayre and Jacobsen (1950) for investigating the dynamic responses of two-span beam and later by Vellozzi (1967) to study the vibration of suspension bridges. Chen (1978) adopted moving load model in analyzing the dynamic response of continuous beams.

The moving load model is the simplest model which has been frequently adopted by researchers to examine dynamic behavior of bridges subjected to moving vehicle (Tan and Shore, 1968a; Fryba, 1968; Festis, 1973; Sridharan and Malik, 1978; Wu and Dai, 1987; Waever *et al.*, 1990; Galdos *et al.,* 1993; Gbadeyan and Oni, 1995; Wang, 1997; Zheng *et al.,* 1998; Rao, 2000; Chen and Li, 2000 and Dugush and Eisenberger, 2002). However, the effect of interaction between the bridge and the vehicle was ignored in those type of vehicle model. Due to this reason, the moving load model is appropriate only for the case where the mass of the vehicle is small relative to that of bridge, and only when the vehicle response is not of interest.

Jeffcott (1929) improved moving load model by considering inertia effect in the vehicle model. This model has been found to be appropriate when vehicle mass is comparatively large to bridge mass. Vehicle inertia effect on bridge dynamic response has been carried out by a number of researchers. Employing Fourier series expansion, Stanisic and Hardin (1969) determined the response of a simple beam under an arbitrary number of moving masses. By the use of Green's function, algorithms for dealing with the moving mass problem has been studied by Ting *et al*. (1974) and Sadiku and Leipholz (1987).

Stanisic (1985) derived a closed form solution for a simple beam carrying a single moving mass by means of expansion of the eigen functions in a series. Using a semi analytical approach, the same model was adopted by Akin and Mofid (1989) in their study of the dynamic response of beams with various boundary conditions. The drawback of moving mass

model is that it excludes the bouncing motion of vehicle relative to the bridge. As a result of which bridge deck surface roughness cannot be incorporated with this model.

The vehicle model can still be enhanced through consideration of the elastic and damping effects of the suspension systems. The simplest model in this case is a moving mass supported by a spring-dash pot unit, the so-called *sprung mass* model. Biggs (1964) presented semi-analytical solution to the problem of a simple beam traversed by a sprung mass. Comparison with the experimental result shows that sprung mass model gives more realistic results than the moving load model.

Chatterjee *et al.* (1994) and Chatterjee *et al.* (1994) studied effect of moving vehicle on multi span continuous and suspension bridge. The bridge response was obtained in time domain by using an iterative procedure employed at each time step to take into account the non-linearity of the pavement-vehicle interactive force.

Similar vehicle model has been utilized by Pesterev *et al.* (2001) to examine the response of an elastic continuum to multiple moving oscillators. Series expansion technique was employed to obtain system response.

Pesterev *et al*. (2003) studied the asymptotic nature of the solution of the moving oscillator problem and found that in the limiting case the moving oscillator problem and the moving mass problem for a simply supported beam are equivalent in terms of the beam displacements, but not in terms of the beam stresses. Also, it was shown that for small values of spring stiffness, the moving oscillator problem is equivalent to the moving load problem.

Sprung mass vehicle model has been improved by considering vehicle as two degrees of freedom system taking account of the tyre elastic properties and wheel mass. This type of model was called *quarter car model*. This model has been adopted by several researches such as Fryba (1972), Genin *et al.* (1975), Genin and Chung (1979) and Green and Cebon (1994). The bouncing mode of vehicle is particularly important because it is often within the range of the first natural frequency of most highway bridges.

Wen (1960) incorporated vehicle pitching motion in the model which has been called as *half car model.* Using this model, a multiple-axle truck or tractor-trailer can be represented as a number of discrete masses each supported by a set of spring and dashpot (Veletsos and Huang (1970), Tan *et al*. (1998). In a study by Yang *et al*. (1999), a railroad car was

simulated as a rigid beam supported by two sets of spring-dashpot unit each resting on a wheel mass. The effect of vehicle roll on bridge dynamics cannot be considered with this model, and the analysis is confined only in the pitching plane only.

Yadav and Upadhyay (1993) used a *heave-pitch-roll model* or *full car model*, for an analysis of the response characteristics evaluation of a vehicle moving over a flexible track. A lumped mass model of the vehicle was constructed over two axles with two wheels (right and left) at each axle, giving a four-wheel configuration. The shock absorber for each wheel consists of two tiers of linear springs and dampers. The sprung mass has three degrees of freedom-heave, pitch and roll. The truck, linkage and the wheel masses were lumped as an un-sprung mass in between the tyre of the shock absorbers. The un-sprung masses were assumed to have only heave motion. This results in a vehicle model with total of seven degrees of freedom.

Vehicle models with seven and twelve degrees of freedom were developed by Wang *et al.* (1993) according to H20-44 and HS20-44 which are major design vehicles in the American Association of State Highway and Transportation Officials (AASHTO). For the modeling of H20-44 vehicle, three rigid masses represent the truck, front wheel set, and rear wheel set, respectively. The truck was assigned three degrees of freedom, corresponding to the vertical displacement (y), rotation about the transverse axis (pitch or θ), and rotation about the longitudinal axis (roll or φ), each wheel set is provided with two degrees of freedom in vertical and roll directions. The total degrees of freedom in the model were seven. Similarly, another vehicle model with twelve degrees of freedom was developed to represent an HS20-44 truck. The equations of motion of the system were derived using Lagrange's formulation method. Assumptions were made to simplify the complex physical truck model as, constant speed of vehicle, each tire contacts the road at a single point, and force inputs were limited to vertical direction. Provision was made in the vehicle model for wheel lift which improves the earlier vehicle model where the assumption of vehicle is always in contact with a bridge element. Under this condition, the vertical stiffness was taken as zero.

Some researchers (Zeng and Dai, 1994) have been motivated to use bond graph theory originally proposed by Paynter (1961) to study heavy axle-train bridge interaction. It may be mentioned that concept of bond graph has been used in modeling two subsystems-vehicle and bridge. Multiple rigid body model and Euler Bernouli beam assumptions have been used in modeling two subsystems. Main emphasis was given to investigate wheel-rail impact forces based on energy flow.

In order to study the train–rails–bridge interaction, a train composed of a sequence of identical cars was considered by Wu *et al*. (2001), in which each car was assumed to consist of a car body, assumed to be rigid, resting on the front and rear bogies, each of which in turn is supported by two wheel sets. A total of five degrees of freedom were assigned to the car body and also to each bogie, to account for the vertical, lateral, rolling, yawing, and pitching motions. In contrast, only three degrees of freedom are assigned to each wheel set, which relate to the vertical, lateral and rolling motions.

The emergence of high speed train in rapid transportation system has attracted many researchers (Wiriyachai *et.al*, 1982; Nielsen and Abrahamsson, 1992) to carry out investigation on modeling aspects of train-track-bridge interaction. In a more recent study conducted by Ziyaeifar (2005), an improvement of vehicle model was noted considering three elements Maxwell model in suspension mechanism. The unique feature of Maxwell model is that a second spring is connected in series with dashpot in addition to a parallel spring. Choosing a proper stiffness for the serial spring, study has shown that it becomes possible to suppress large velocity dependent suspension force due to track irregularity. However, in the study, vehicle has been considered as rigid body and track irregularity assumed to be of deterministic form.

Law and Zhu (2005) investigated effect of deck surface roughness and vehicle braking on bridge dynamic responses considering seven degrees of vehicle model. It has been found that braking of the vehicle generates excitation forces covering a wide range of frequencies and this requires a large number of bridge vibration modes for an accurate prediction of the responses.

A full car vehicle model has been employed by Deng and Cai (2009) for estimation of vehicle parameters from measured bridge response. Gonzalez *et al*. (2011) utilized full car vehicle model to represent five axle articulated truck. Shear stress increment in the bridge due to heavy vehicles crossing a highway bridge has been investigated. Both the authors employed numerical solution to obtain the system responses.

Growing interest on vehicle modeling has significantly contributed to vehicle-infrastructure interaction studies. Cantero *et. al.* (2010) devoted completely on the derivation of equation of motions of general road vehicle. The equations could be finally transformed to second order system of ordinary differential equations. Such type of formulation facilitates modeling of

multi axles in the tractor and/or trailor in planar and three dimensional vehicle-infrastructure problems. However, they ignored elastic strain in the vehicle elements which may be of concern to long vehicle and its effect on bridge.

Chang *et al.* (2011) modeled wheel of the vehicle moving on the bridge as a rigid disk with a finite radius which has been called as rigid disk model. Since the adoption of a point model for the wheels implies that the wheels can faithfully move over the profile of rough surfaces with steep valleys. This is certainly not true, as a wheel of finite size can never touch the bottom of a steep, narrow valley. However, this model considered only the geometry of the wheel without any emphasis on its material properties. In addition to this, determination of contact inference between wheel and road surface may require huge amount of iteration. This may significantly increase the computational cost when higher degrees of freedom vehicle model is considered.

1.2.2.2 Modeling of Bridge Deck unevenness

The bridge deck unevenness causes moving vehicles to pick up dynamic excitation, which in turn imposes oscillatory loads on the deck. The analyst needs to choose an appropriate model for the deck roughness. Attempts have been made to model the roughness in terms of statistical parameters form profile measurements of a large number of road or bridge surfaces. Shinozuka (1971) has presented an efficient and practical method of simulating multivariate and multidimensional process with specific cross-spectral density. When the cross-spectral density matrix of an *n*-variate process was specified, its component process can be simulated as the sum of cosine function with random frequencies and random phase angle. A homogeneous multidimensional process can also be simulated in terms of the sum of the cosine functions with random frequencies and random phase angle.

Dodds and Robson (1973) have shown that typical road surfaces might be considered as realization of homogeneous and isotropic two dimensional Gaussian random processes. The complete description of the roughness is provided by single auto correlation function evaluated from longitudinal profile.

Honda *et al.* (1982) has shown that Power Spectral Density (PSD) was related to parameters called roughness and waviness index. These parameters can shift the roughness level up and down and thus a guideline for classification of roads in terms of roughness has been framed.

The effect of time dependent forces on bridges was studied by Coussy et *al.* (1988). The authors analyzed the influence of surface irregularities on the dynamic response of bridges under suspended moving loads. They idealized the bridge as an elastic beam and the surface irregularities are modeled by PSD for frequency domain analysis.

Marcondes *et al.* (1991) proposed a model of relationship between pavement PSD and parameter called International Roughness Index (IRI). In order to establish the relationship, spectral analysis of different measured profiles was carried out whereas IRI was computed using mathematical model of quarter car simulation.

Road surface roughness is the excitation source for the dynamic response of a moving vehicle system. Xu and Yong (1993) proposed an autocorrelation function model for road roughness to specify the road surface random characteristics. Power spectral density for road roughness and driver absorbed power level was considered to define road quality index.

The power spectral density (PSD) is a useful tool to analyze the periodically modulated random processes. Huang and Wang (1991) employed periodically modulated random process to describe road surface. The random numbers which have approximate white noise properties were generated first. Then, these random numbers were passed through the first order recursive filter. Finally, the output function was considered as the road surface roughness.

Henchi *et al.* (1998) described the randomness of the bridge surface roughness by a periodically modulated random process. The power spectral density (PSD) proposed by Dodds and Robson (1973) was utilized to specify the random road profile. From the PSD, deck surface profile was generated using the FFT algorithm with the Monte Carlo simulation.

Sun *et al.* (2001) compared two widely accepted PSD functions describing road surface roughness proposed by Dodds and Robson (1973) and the other by Honda *et al.* (1982). It has been found that Dodds and Robson's PSD has higher values for the frequencies above $1/2\pi$ cycle/m. Since the available PSD functions only represents the characteristics of road surface roughness along the longitudinal direction. Liu *et al* (2002) utilized auto-regressive and moving average (ARMA) for simulation of road surface profile in transverse direction. Dynamic behavior of multi-girder bridges under heavy trucks was investigated incorporating proposed correlated road surface roughness.

Imine *et. al.* (2005) has carried out studies to evaluate road roughness using longitudinal profile analyser and robotic approach based on sliding mode observer in control theory. The study reveals that road profile can be accurately estimated if vertical displacement of wheels and vehicle body bounce and rotations are obtained correctly. The practical use of the study is to estimate wheel load on the vehicle.

Some researchers attempted to find road roughness based on acceleration records of a vehicle travelling over a road (Gonzalez *et.al*, 2011). In their work, accelerometers have been fitted to the axles to acquire the time history of the acceleration while driving the vehicle over a section of road at constant speed. Power spectral density (PSD) function of vehicle acceleration has been obtained and then PSD of road roughness has been found using transfer function of the vehicle. In practice, transfer function is to be obtained experimentally by driving the vehicle over a measured road profile. Once the PSD of the road is identified, it is possible to classify the road as being very good, good, poor etc.

Road surface irregularity has been found to be an important parameter for fatigue damage assessment of heavy vehicle (Bogsjo *et.al*, 2012). Actual road profile contains short segments with above average irregularity and such irregularities cause most of the fatigue damage. In their study, three new road roughness models such as homogeneous Laplace Moving average (LMA) model, non-homogeneous Laplace process and a hybrid model that combines Gaussian and Laplace process have been developed. It has been found that LMA model works very well for smaller road sections in which homogeneous Gaussian model is an approximation. However, the homogenous Gaussian model has been found to underestimate fatigue damage of vehicle components.

1.2.2.3 Bridge model

Dynamic behavior of bridge due to passing vehicle attracted several researchers. Different models have been adopted for the bridge depending on type and support condition.

In the study of vehicle induced bridge vibration, a simply supported beam at both ends is the most popularly adopted model by earlier researchers (Willis, 1849; Stokes, 1849; Timoshenko, 1922; Ayre *et al.* 1950; Biggs, 1964; Fryba, 1972; Sridharan and Mallik, 1979; Green and Cebon, 1994; Tan *et al.*, 1998). Beam model was found to be appropriate since most of the bridge length to width ratio is more than two. Modal superposition method with

contribution from odd number modes has been used to obtain the beam dynamic stresses. However, random deck surface roughness was ignored in all their theoretical studies.

Various types of bridges have been considered in study of the vehicle-induced vibrations. Chu *et al*. (1979) and Wiriyachai *et al*. (1982) conducted case studies on truss bridges by considering simple beam model with equivalent cross sectional properties of the full truss section. Impact factors in the bridge due to passing vehicle were investigated. However, damping of the bridge and vehicle was ignored in their study.

Chattejee *et al.* (1993) modeled truss bridge by considering multi-degrees of freedom with lumped mass system. The effect of bending action was incorporated in their model by taking sufficient number of nodes along the deck between two joints of the truss. Dynamic response of the truss bridge was also investigated by continuum approach. The stiffness of the truss corresponding to the vertical degrees of freedom at the deck level joints was provided by the stiffness of an interconnected spring system. Different types of truss pattern including Pratt truss, Warren truss with no verticals and Warren truss with inclined upper chord were considered in the study. Although credible results were obtained but interaction between vehicle and bridge was ignored in the models.

Chatterjee and Datta (1995) idealized truss arch bridge as equivalent continuum model. The effect of the struts was considered by replacing them by a number of interconnected springs located at the deck-strut joints. Inertia effect of the struts and the arch along with the deck has been taken in the modeling. The mass of the struts and the appropriate portion of the mass of the arch were lumped at the beam joints. In order to utilize the continuum theory, these lumped masses at the nodes were distributed over small length, and then continuum analysis was performed. However, this technique increases the number of dynamic degrees of freedom since the number of spans to be considered in the continuum analysis increases, and requires more computational time.

Finite element model was employed for investigation of steel arch bridge dynamic characteristic subjected to moving vehicle (Ju and Lin, 2003; Nam *et al.,* 2008; Costley *et al.,* 2015). The difficulties arising from the use of traditional node to linear algorithms have been overcome by adopting a moving wheel element which has the cubic interpolation function. Criteria to predict bridge-vehicle resonance effect was proposed. Although, bridge vehicle interaction was considered, but bridge deck surface unevenness was ignored in their study.

Ballasted pre-stressed concrete single track railway bridges, consisting of several box girders were studied by Chu *et al.* (1986). On which each girder assumed to share equal loads was treated as a beam. The moment of inertia of the bridge was taken to be the number of girders times the moment of inertia of each girder. Similar procedures were used to obtain lateral moment of inertia and torsional constant. The procedure is considered to be conservative as the amount of post tension in the transverse direction is not large enough to make the girder act as single unit. Rail irregularities are modeled using power spectral density function.

In the study of impact factor for simple and multi-span beam, Yang *et al.* (1995) represented actual box girder bridge as series of beam element with appropriate sectional properties. Vehicle is modeled as lump masses supported by suspension spring and dash pot. All the degrees of freedom associated with the car bodies were first condensed with dynamic condensation method. The condensed elements, as well as the element that were not in directly contact with the vehicle were assembled using direct stiffness method to form the equation of motion for the entire bridge vehicle interaction system.

Kou and De-Wolf (1997) studied the vibrational behavior of continuous span highway bridge. Their approach was based on using the finite-elements method for the three dimensional dynamic bridge analyses. The bridge structure was discretized into elements, with girder and floor beams modeled as beam elements (it has six degrees of freedom) and the concrete deck was modeled as plate elements (four node quadrilateral isotropic elements with six degrees of freedom at each node). The bridge riding surface roughness was based on Fourier series finite wavelength profile.

Based on the Lagrangian approach Cheung *et al.* (1999) analyzed the vibration of a multi-span non-uniform bridge subjected to a moving vehicle by using modified beam vibration functions as the assumed modes which is a summation of prismatic beam vibration mode and augmenting cubic spline expressions so that the former term will satisfy the boundary conditions. In their study different multiple span continuous box girder bridges were modeled as beam element.

Marchesiello *et al.* (1999) studied the interaction of multi-span continuous bridges modeled by isotropic plates with multi degrees of freedom vehicles moving at constant speed. Road surface roughness was modeled as stationary random process. It was concluded that the

theoretical modes, defined by means of the Rayleigh Ritz approach, have been found to be in good agreement with an FE model, thus giving confidence to the analytical results.

Huang *et al.* (1992) analyzed the impact of three span continuous steel beam bridge with six different span lengths due to vehicle moving over different classes of road with various speed. The bridge was treated as grillage beam system. Dynamic response of the bridge was analyzed with finite element method.

Wang (1992) studied the dynamic behavior of multi girder bridges due to vehicle moving across rough bridge decks. The girder bridge was treated as grillage system. Dynamic response of the bridge was analyzed with finite element method. The bridge was divided into grillage elements. The rigidities of longitudinal element included those of girders and deck slabs, while the stiffness of transverse element includes slabs and diaphragms. Road profile was represented by power spectral density function.

Galdos *et al.* (1993) proposed a method for determining dynamic impact factor for horizontally curved steel box girder-bridge under vehicle loadings. The bridge structure was analyzed as two dimensional grids with load applied normal to the plane of the grid surface. The box was represented as curved line elements with three degrees of freedom, two rotations and one translation.

Yang *et al.* (2001) developed analytical solutions for a simply supported horizontal curved beam subjected to vertical and horizontal moving loads regarded as centrifugal force due to movement of vehicle along the curved path has been considered in their analysis. All the deformations were assumed to be small so that the linear theory applies. The bridge girder was made of constant, bi-symmetric cross section with negligible warping resistance. The two ends of the curved beam are assumed to be simply supported, in the sense that the flexural displacements and twisting rotation of the beam are restrained at the supports.

Kawatani and Kim (2001) simulated dynamic wheel load moving on the bridge. Finite element method and modal analysis were adopted to develop equation of motion for the bridge. Girder system and lateral bracing have been idealized as beam element with 6 DOF at each node and the deck slab was idealized as four noded plate element with Lagrange polynomials. The lumped mass system and Rayleigh damping were adopted to form mass and damping matrices of the bridge model, respectively. Full car vehicle model with random deck

surface roughness has been considered in their model. Parametric study has been conducted on steel plate girder and prestressed concrete bridge.

1.2.2.4 Method of Solution for Bridge Vehicle Interaction Problem

A beam that is simply supported at both ends is the most popular structure that has ever been adopted in the study of vehicle-induced vibrations. Except for the research works that rely exclusively on analytical approaches, there is basically no restriction on the type of structures considered in vehicle bridge dynamics interaction problems, as the structures can always be represented by finite elements of various forms; the only difference being that a simpler bridge model requires less preparation and computation efforts. However, simpler beam model provides bench mark solution and at the same, it is possible to obtain physical reason of structural behaviour very easily with the help of simple model.

Timoshenko (1922) recognized that imperfect balance of locomotive driving wheels produces impact effect on long span bridges. The induced forced vibration was obtained by considering the bridge as beam of constant cross section with simply supported ends. Differential equation of motion of the beam under the action of a single harmonically varying force that moves along the span at constant speed was obtained using energy principles and solved for the given boundary conditions taking contribution of fundamental mode. Damping was ignored in the formulation.

A method based on successive approximation has been developed by Jeffcott (1929) to address the problems of vibration in railway bridges under the action of moving and fluctuating load. The effect of damping force and inertia effect of moving mass on the deflection of beam has been investigated.

Inglish (1934), in his classic book, addressed the vibration problems in Railway Bridge using analytical techniques and pointed out many interesting facts that are applicable in field. The harmonic series method of analysis adopted by him showed that load with shorter wavelength rapidly decreases beam deflection. He commented further that damped oscillation in railway bridge is due to lack of elasticity in track and ballast and friction at the end bearings. The "residual oscillation" after vehicle leaves the bridge persists for greater duration in case of long span bridges.

Fryba (1972) gave a comprehensive treatment for the various vehicle models, i.e., the moving load, moving mass, and moving sprung mass, concerning primarily to the dynamic response of the structures traversed by the vehicles. The analytical solutions as well as numerical solutions for some of the problems were obtained.

Radhey and Traill- Nash (1980) gave a systematic and comprehensive study to determine the effects of vehicle braking response. The researcher's study was made with the bridge represented by beam as well as with more realistic representation by an orthotropic plate. The effect of bridge tranverse flexibility is firstly considered by including an additional torsional degree of freedom in simple beam representation. Newmark β scheme was used for the numerical integration of the bridge vehicle coupled system equations.

The effect of time dependent forces on bridges was studied by Coussy et *al.* (1988). The authors analyzed the influence of surface irregularities on the dynamic response of bridges under suspended moving loads. They idealized the bridge as an elastic beam and the surface irregularities are modeled by PSD for frequency domain analysis. Numerical technique was used to solve the coupled differential equation. It was found that surface condition considerably affect the Dynamic Amplification Factor.

Chan and O'Connor (1990) suggested a simple vehicle model in which each axle load consists of constant load plus constant sinusoidal varying components that may be used to estimate impact in the highway bridge. The magnitude of this varying load has been set here arbitrarily as ± 10 % about the mean. Maximum bending moments in a simple girder are determined using span, static axle loads, and the relative magnitude of the dynamic load component. Impact values are predicted for a range of spans with a dynamic load component equal to 10% of the static load.

Dynamic load is an important factor in bridge design and evaluation. Hwang and Nowak (1991) analyzed dynamic load on bridge. Road profiles were simulated using stationary PSD of the stochastic process. Vehicle has been idealized as a full car vehicle model and bridge was represented by prismatic beam. Monte Carlo method was employed to simulate the traffic on the bridge. Newmark- β method was used for solving system equations of motion. Calculations were carried out for steel and prestressed concrete girder bridge. Influence of vehicle and bridge parameters on dynamic load factor was investigated.

Vibration behavior of simple-span highway girder bridges induced by heavy truck load was studied by Chang (1994). The surface unevenness was considered as the main source of bridge vibration under moving load. The dynamic characteristics of bridge response have been investigated in the time and frequency domains. Their studies concluded that impact factor used in current design codes was underestimated with rough deck profiles. Impact factor formulae were suggested based on span length, surface roughness and vehicle speed.

Green *et al.* (1995) investigated the effect of heavy vehicle leaf spring and air spring suspension on dynamics of highway bridges. Four axles articulated vehicle idealized as half car model was considered and the bridge was represented by a simple beam model with first natural frequency. The bridge dynamic responses were obtained by modeling bridge and vehicle separately and combining the models with iterative procedures. The proposed method of solution was validated by field test results. Effect of vehicle suspension on the bridge response was studied in terms of dynamic response increment. It has been found that air suspended vehicle causes lower dynamic response in the bridge than steel suspended vehicle. Based on their theoretical results, it was suggested that air-sprung vehicle could be allowed to carry more load than vehicle with leaf spring suspension.

Michaltsos *et al.* (1996) studied linear dynamics response of simply supported uniform beam under a moving load of constant magnitude and velocity by including the effects of its mass. The individual and coupling effects of the mass of moving load, its velocity and of other parameters have been studied. Newmark β scheme was used for the numerical integration of the bridge vehicle coupled system equations. They found that bridge deflection increases at higher velocity with increase in the ratio of vehicle mass to bridge mass.

A study to investigate braking effect of vehicle has been carried out by Kishan and Traill-Nash (1997) on bridge idealized as beam and concluded that braking force affects the response considerably. Initial bounce of a vehicle on its suspension was recognized as a major source of bridge loading and it was found that braking of a vehicle on a bridge could induce significant dynamic loads. Newmark scheme was used for the numerical integration of the bridge vehicle coupled system equations.

Dynamic response of bridge girders with elastic bearing to moving train load has been studied analytically by Yau *et al.* (1997). It was found that the insertion of elastic bearings at

the supports of the beam for the purpose of isolating the earthquake forces may adversely amplify the dynamic response of the beam to moving train loads.

Henchi *et al.* (1998) proposed an explicit algorithm technique to solve the coupled dynamic system using a modal superposition method for the bridge structure and the physical components for the vehicles using Lagrange's formulation. Bridge has been represented by beam and plate model using finite element approach. Dynamic behavior of bridge subjected to multiple vehicles at different location has been studied using a coupled iterative scheme. However, authors stated that when high frequencies of bridge participate in motion, the iterative scheme did not show good performance.

Dynamic behavior of pre-stress concrete bridge subjected to moving vehicle was studied by Chan *et al.* (1999). Bridge was modeled as a beam of constant cross-section with constant mass per unit length, having linear, viscous proportional damping. Small deflection theory has been used neglecting the effects of shear deformation and rotary inertia. Vehicle was idealized as a moving load with constant speed. Newmark-β scheme was used for the evaluation of dynamic response of bridge due to vehicle-induced vibration.

Rao (2000) employed mode superposition method to study dynamic response of an Euler-Bernoulli beam under moving loads. The inertial effects of the moving load were included in the analysis. The time-dependent equations of motion in modal space have been solved by the method of multiple scales. Resonance condition of the system was found to be solely depending on the ratio of the moving load mass to the beam mass.

Ichikawa *et al.* (2000) studied the effects of inertia and the moving velocity on the dynamic behavior of multi span continuous beam subjected to a moving mass at constant velocity. The bridge was idealized as a multiple supported continuous Euler-Bernoulli's beam simply supported at both the ends. Beam equation of motion was discretized using modal superposition technique. Numerical integration scheme has been adopted to obtain the system response. They concluded that the inertia of the moving mass has greater influences on the second and the successive spans than the first span.

Zhu and Law (2003) studied dynamic behavior of the bridge deck under moving loads using orthotropic plate theory and modal superposition principle. Analytical solution was obtained to get the bridge responses at different locations. Simply supported beam slab type bridge deck with the aspect ratio less than two was considered for parametric studies. It has been

concluded that equivalent beam model of the bridge deck could give an estimate on the impact factor along the centerline of the deck, but it would underestimate the dynamic responses at the edge of the structure.

Yang *et al.* (2004) analyzed vehicle bridge interaction using condensation method. To resolve the coupling problem, the sprung mass equation is first discretized using Newmark's finite difference formula and then condensed to that of bridge element in contact. The similar results have been found when it compared with the analytical solution.

Cai and Chen (2004) analyzed coupled three dimensional vehicle-bridge system under strong winds. Vehicle was modeled as a combination of several rigid bodies, axle mass blocks, and dampers, considering wind and roughness induced loads. The dynamic properties of long span bridge were obtained using different kinds of finite elements such as beam elements and truss elements. System equation of motion was solved using Ranga-Kutta method.

Law and Zhu (2005) studied the dynamic behavior of a multi-span non-uniform continuous bridge under a moving vehicle considering the effects of the interaction between the structures, the road roughness and the vehicle. A ramp function was assumed for braking force based on the test result on highway vehicle conducted by the *Transport and Road Research Laboratory*, England. It was concluded that the vehicle braking significantly affect the dynamic response of bridge.

In the study of vehicle-track-bridge interaction considering vehicle's pitching effect, Lou (2005) applied finite element method. The moving vehicle was modeled as a two axle mass spring damper system having four degrees of freedom. The rail was modeled as an upper beam while deck as a lower beam of finite length. The upper beam rests on closely spaced sleepers which were idealized as series of springs and dampers. The equations of the system were derived by means of Hamilton principle. These equations were solved by means of step by step integration method. It was observed that if track irregularity is neglected, vehicle pitching effect has little influence on vehicle and bridge response.

Effect of approach span conditions on a bridge dynamic response induced by moving vehicle has been investigated by several researchers (Shi *et al.,* 2008 and Cai *et al.,* 2009). Finite element technique has been adopted to bridge vehicle coupled system model. For computational efficiency generalized modal coordinates were used for bridge and physical co-ordinates were used for truck. Stochastic road surface including approach span condition

were incorporated in the model. Equations of motion were solved in time domain by using Runge-Kutta method. Several parametric studies on the effect of approach span condition in terms of impact factor were conducted. It was found that AASHTO specification under estimate impact effect for the bridge with larger faulting condition.

Lu *et al.* (2009) adopted pseudo-excitation method (PEM) for non-stationary random vibration of vehicle-bridge systems. Bridge vehicle interaction model element was adopted to reduce computational effort. 10 DOF vehicle model moving on simply supported and three span continuous bridges were considered for case study. In comparison with conventional Monte Carlo method for estimating statistical response, PEM was found to reduce computational time. However, contribution of vehicle structural mode was ignored although long and slender vehicle 14m axle spacing was considered in the vehicle model.

Xua *et al.* (2010) proposed a general procedure for stress and acceleration response analysis of coupled vehicle and long-span bridge systems using the mode superposition method. The resonance conditions of simple and continuous beams under a sequence of equidistant moving loads of identical weights were determined. Number of vibration modes required in the stress analysis was also discussed. Results obtained by the proposed method were validated with the field test results conducted on long span suspension bridge.

Yin *et al.* (2010) studied non-stationary random vibration of bridge under vehicles with variable speed using the covariance equivalent technique. This method transfers non-stationary white noise process to stationary white noise process. Simple beam model subjected to haft car vehicle model was taken for parametric studies. The numerical results show that factors such as different road surface roughness coefficients, initial speeds, vehicle accelerations, and vehicle braking conditions have very significant influence on the impact factors under non-stationary random inputs.

Yin *et al.* (2011) studied the vibration of a bridge-vehicle coupled system considering significance of high-pier bridges lateral vibrations induced by the moving vehicular loads. Their study was focused on establishing a new methodology considering the bridge's lateral vibration induced by moving vehicles. Comparison of the theoretical simulations and field measurements shows that the proposed method can be applied to study the bridge lateral vibration induced by moving vehicles with good accuracy. It was found that both the lateral

and longitudinal vibrations of the high-pier bridge can significantly affect the riders' comforts and be of concern to the passengers.

Ju (2011) idealized bridge as three dimensional Timoshenko beam. The equation of motion was developed by continuum approach. Passing vehicle has been modeled as a rigid body with two wheel axles. Each wheel axle was connected to two spring-dampers in vertical and longitudinal directions. Road surface roughness, eccentricities of vehicle location and variable vehicle speed were considered in the study. Coupled dynamic response was obtained using Newmark integration method. Obtained results were compared with finite element results. It has been found that interpolation function in the FEM model causes errors at the high-frequency vibration, and the generation of a fine mesh of the bridge can overcome this problem for the finite-element method. However, the computer time required for the finite-element method was found to be significantly increased.

Ouyang (2011) compared analytical formulation and finite element method for a moving load problem. Various moving load problems such as vehicle-bridge, vehicle-ground, train-track interactions were included in the study. He concluded that a big advantage of using an analytical formulation for a moving-load problem was that when a load moves in the spatial domain its location always corresponds to a continuous coordinate. This allows easy enforcement of displacement continuity and force equilibrium of the moving and stationary bodies at the moving coordinate. In contrast, in a finite element formulation, the moving load is located in different element domains at different time, hence it is difficult to track its location constantly and in particular relate its motion to that of the FE nodal displacement vector as it traverses different element domains. Apparently, the numerical procedure for a moving-load problem using the finite element method is more complicated and less accurate than using an analytical method.

Bridge-vehicle dynamic interaction with simple model has attracted some researchers to find a new way for health monitoring of bridge (Carden and Fanning, 2004; Lin and Yang, 2009; Yang *et al*., 2012). In this work, authors have shown by means of analytical solution that bridge frequency become visible in vehicle acceleration for certain condition of vehicle/bridge mass ratio and pavement roughness. Practical implementation of this work has been reported by Cantero and O'Brien (2013).

Dynamic behaviors of steel arch bridge with side-by-side multiple vehicles loading moving over a rough deck was investigated by Huang (2012). Full car vehicle model was considered and the equations of motion were constructed using Lagrange's formulation. Road surface roughness was considered to be realization of a stationary Gaussian random process. Bridge equations of motion were built up using finite element method, and then Newmark integration scheme was employed to obtain the bridge responses. Effect of vehicle speed on the bridge response was represented in terms of impact factor and found to be significantly increased with vehicle speed. However, it has been reported that computational cost is very high and requires higher random access memory.

Effect of sudden deceleration of vehicle on the bridge dynamic response was investigated by Azimi *et al.* (2013). Vehicle bridge interaction element model was proposed. The effect of deceleration was considered as external load acting on each part of the vehicle masses. Although finite element approach was employed, but simple beam subjected to half car model was considered in the case study. In addition to this, vehicle body structural mode and deck surface roughness were ignored in the study. Bridge response was found to be increased with higher vehicle speed and significant increment in the bridge response was found when rate of deceleration is high.

Kozar and Malik (2013) developed a technique for application of spectral method in bridge vehicle interaction problem. Spectral method was formulated in terms of matrix operators capable of discretizing and combining Kirchhoff-Love plates and Bernoulli beams. The boundary conditions have been imposed using Lagrange multipliers so that combinations of Dirichlet and Neumann conditions could be dealt with. The proposed method allowed a bridge to be represented as a 3D structure with realistic cross-section. The proposed method has been tried on a real example of a bridge loaded with a moving vehicle.

A closed-form solution for evaluating the dynamic behavior of a multi-span bridge has been derived by Johansson *et al.* (2013). Boundary conditions of the bridge were assigned to the characteristic function of a beam to obtain its natural frequencies of vibration and corresponding mode shapes. A Laplace transformation was applied to the governing differential equation which was then solved for each normal mode in the frequency domain.
The proposed method has been successfully used in a parametric study with the data of several existing bridges. However, simplest vehicle model moving with a constant speed has

been considered and torsional motion of bridge due to eccentric loading was ignored in the model formulation.

Lau and Au (2013) outlined finite element formulation for calculating internal forces, bending moment and shear force of Euler-Bernoulli beams under moving vehicles. Internal forces were derived based on dynamic equilibrium conditions. Bridge responses were obtained using Wilson-θ method. Internal dynamic forces in simply supported and continuous beam due to moving load have been investigated. A case study on dynamic amplification factor of the bridge for different vehicle speed has been conducted.

Zhang and Shepard (2014) examined response of simply supported beam subjected to arbitrary transient moving load using analytical solution and also verified by a finite element method. The response using analytical method was found to be agreed very well with the response obtained from FEM solution approach. Based on these results, it was concluded that the analytical method used for the initial configuration study is accurate. Furthermore, the FE method seems suitable for use in future research where more complex configurations and alternative support conditions might be considered.

Zhang *et al.* (2014) estimated fatigue life of bridge due to vehicle induced vibration and non-stationary hurricane wind. Three axle vehicle and cabled stayed multiple span bridge have been modelled using finite element approach. The long undulations in the roadway pavement have been modeled as a zero-mean stationary Gaussian random process and the road surface profile was generated through an inverse Fourier transformation. Runge - Kutta method was employed to solve equations of motions in time domain.

Fu (2015) investigated effect of cracks on vibration of a continuous bridge subjected moving vehicle. Lagrange's equations were employed to develop the modal superposition analysis of a continuous beam with switching cracks subjected to a moving vehicle. Vehicle has been idealized as a half car model moving with a constant speed. It has been mentioned that vehicle location is changing with time. As a result, the generalized matrices vary with time, which resulted in differential equation with time dependent coefficient. Houbolt step by step method was employed to obtain bridge response.

Zeng *et al.* (2015) utilized multi body dynamic model to develop equations of motion for vehicle body and Finite Element method for continuous girder bridge model. Seven span continuous girder bridges were considered for parametric studies. Both track induced and

ground shaking were considered. The track irregularities have been treated as deterministic function while ground motion as random. Bridge responses under these actions have been obtained by the pseudo- excitation method (PEM). Simulated results were compared with Newmark-β method and Wilson-θ method. Both of which were found to be inefficient than the adopted method. However, bridge torsional mode which may be triggered by vehicle eccentric loading as well as ground motion was ignored in their bridge model.

Since bridge deck surface roughness is a random process, vibration of bridge due to passing vehicle becomes random process. Zhibin-Jin *et al.* (2015) studied vehicle-bridge coupled vibration by implementing a random vibration and reliability based approach. System dynamic equation was derived using the principle of virtual work utilizing a linearized wheel-rail contact equation. Explicit linearization method was employed to avoid iterative solution at each time step of the integration. The proposed method of solution was validated with the results obtained from Monte Carlo simulation. Comparing with the traditional methods, significant reduction in the computational time was found using the proposed method of solution

Bridge foundation settlement was incorporated in the vehicle bridge interaction problem by Ahmari *et al.* (2015). Vehicle was idealized as a rigid full car model and bridge as continuous plate. The governing equations of motion were derived using Hamilton principle and solved by Newmark integration scheme. It was found that dynamic load allowance increases depending on the support location where settlement occurs. In addition, mode of settlement, magnitude of the foundation settlement and length of the bridge span also affect dynamic load factor.

Zhong *et al* (2015) studied dynamic behavior of prestressed continuous bridge due to moving vehicle. The bridge was modeled as a continuous beam with eccentric prestress and the vehicle was represented by half car model. Governing equations of motion for both the sub-system were constructed using virtual work principle and solved by Newmark integration method. Abaqus FE model was utilized to validate their results. Several parametric studies including prestress amplitude, eccentric load and span length were conducted. Bridge dynamic response was found to be decreased when amplitude of prestress increase. However, effect of deck surface roughness and vehicle body structural modes are ignored in their study.

1.2.2.5 Bridge Dynamic Test

Full scale bridge dynamic test is a most reliable method to determine true dynamic properties like mode shapes, natural frequencies and damping ratios of bridge. These parameters can be used as a basis for validating or updating of analytical model so that the models represent the actual bridge properties and boundary conditions. In addition to this, measured bridge response can also be utilized to identify passing vehicle parameters as well as induced dynamic load in the bridge. Bridge test results are reported in many literatures. Among these, some of the literatures relevant to the present bridge test programme have been reviewed.

Several instruments or sensors and loading condition have been used for existing bridge vibration test. Lee *et al.* (1987) carried out both static and dynamic test on an old concrete bridge. Vibration of bridge subjected to light truck weighing 2.2 tonnes moving at various speed was measured with seismographs and accelerometers placed at the middle of the central of span.

Cunha *et al.* (2001) used a nonconventional testing system for a test of cable stayed bridge ambient vibration. Bridge deck vibration was measured using six independent triaxial accelerographs which are permanently installed at different locations. Vibration of stay cables which were not directly accessible from the bridge deck also have been measured using laser Doppler velocimeter. Static and dynamic bridge deflection under various vehicle speeds was measured by Hou *et al.* (2005) by installing inclinometer on the bridge deck.

Meng *et al.* (2007) used Global Positioning System (GPS) and triaxial accelerometer in the field test to record dynamic response-displacement and acceleration of suspension footbridge. Potisuk and Higgins (2007) performed dynamic test on concrete deck girder bridge subjected to moving truck loading using strain gauges and displacement transducers placed at critical section of the bridge.

Three spans, two lane concrete bridge loaded with five axle truck was tested by Li *et al.* (2008) using strain gauge, displacement transducer and accelerometer. Two dynamic field test- forced and ambient vibration test were conducted by Conte *et al.* (2008) on suspension bridge with an orthotropic steel deck. Four different controlled traffic load patterns and seven different vehicle-induced impact load configurations were used in the forced vibration tests. The dynamic response of the bridge was measured by force-balanced accelerometers deployed along a whole length of the bridge.

Two lane post tensioned reinforced concrete bridge was tested by Morassi and Tonon (2008). Uniaxial piezoelectric accelerometers were used to measure the bridge's vertical response to the induced excitation. The vertical dynamic motions of the deck structure were produced by means of a vibration generator consisting of a closed-loop electro-mechanic actuator mounted in a vertical direction. Model updating was carried out using field test results. Not only updated models but also the dynamic characteristics obtained from measured response are essential for vibration-based structural health monitoring (Doebling *et al.,* 1996 and Sohn *et al.,* 2003).

Casas and Aparicio (1994) attempted to identify bridge stiffness characteristics with an aim to detect damage in bridge components using mode shapes and natural frequencies obtained from bridge dynamics test. Bridge dynamic test results were used by Brownjohn (2003) for assessment of highway bridge upgrading and finite element model updating. Sokol and Flesch (2005) determined soil stiffness properties from bridge dynamic test. Brencich and Sabia (2007) studied efficiency of masonry bridge element from measured bridge dynamic response.

Siringgoringo *et al.* (2013) utilized full scale dynamic test for damage detection and to observe dynamic characteristics of post tensioned concrete bridge. Furthermore, full scale bridge test result has been used for assessment of induced dynamic force on the bridge and to determine dynamic load allowance factor (Szurgott *el at,* 2011).

Kwasniewski *et al.* (2006) investigated actual contribution of bridge surface condition in the bridge dynamic response subjected to moving vehicle. They also updated the finite element model of bridge from the experimental results. Vehicle parameters moving on the bridge were identified by Deng and Cai (2009) based on bridge dynamic test result. Nasrellah and Manohar (2011) utilized measured dynamic response of multi-span masonry arch bridge for structural system identification. Railway wagon was considered for vehicle loading. Bridge structure material properties such as Young's modulus and Poisson's ratio were considered to be identified based on measured bridge responses.

1.3 Gaps in Literature

Literatures available on the identification of moving load parameters on bridges using particle filter technique are scanty. Further researches are necessary to establish the popularity of the particle filter technique in vehicle-bridge coupled dynamics in presence of stochasticity of

contact forces. It was realized by researchers that particle filtering technique is computationally expensive, as large number of response samples are required to obtain converged results. Although particle filter technique may take care of model inaccuracies, forward solution of mathematical model of the dynamic system with iterative or numerical schemes require more computational time. Numerical instability may arise due to mismatch between the instrument sampling frequency and numerical scheme. In view of this fact, it would be advantageous if an idealized but quite accurate physical model is evolved which enables a closed form solutions to be interfaced with the iterative process of the particle filtering technique.

Literature survey has revealed that in identification of vehicle induced moving load over bridge, rigid vehicle model has been adopted in all studies reported so far in literatures. In modern times, it is worth mentioning that vehicles have become longer to carry larger payload. Such vehicles are prone to elastic deformation caused by road excitation. The vehicle model considering flexibility has not been addressed in bridge-vehicle interaction studies.

1.4 Scope and Objective of the Present Work

From literature survey it is found that Particle Filtering Technique for moving force identification has not been gained popularity in case of complicated vehicle model in stochastic environment because of intensive computational work involved. It was also felt that investigation should be carried out to incorporate vehicle flexibility in the vehicle model to represent long slender vehicle of lighter material that are frequently travelling with heavy pay load. Non homogeneity of the surface roughness of the bridge deck due to various constructional features or defects require to be included in solving inverse problems in bridge-vehicle dynamics. Thus, the objectives of present thesis are listed below:

- To identify parameters of a passing vehicle from simulated dynamic response of bridge using particle filter method.
- To develop bridge vehicle interaction model considering vehicle flexibility and non-homogeneous road unevenness.
- To develop a semi-analytical method for generation of response samples required in forward scheme of particle filtering technique with an aim to enhance the performance of the inverse method.

- To conduct field dynamic test on an existing bridge under controlled movement of a loaded truck and to update finite element model of the test bridge.
- To utilize field measured data to estimate truck parameters using the approach developed in the present study.

1.5 Organization of Thesis

In the present thesis, nine chapters have been included. **Chapter-1** gives introduction, literature review, identifies gaps in the previous studies and gives the scope and objectives of the present work. **Chapter-2** discusses basic principles of moving load identification with detail procedure and flowchart of the particle filtering process that has been implemented for identification of vehicle parameters in the present study. **Chapter-3** describes formulation of three bridge-vehicle coupled system models to be used for solving forward problem in particle filter method. The system models are: Model-1 (Bridge-Quarter Car vehicle model), Model-2 (Bridge-Half Car vehicle model) and Model-3 (Bridge-Full Car vehicle model). Model-2 considers vehicle body to be flexible in bending while in model-3, both bending and torsional flexibility are incorporated. **Chapter-4** presents a semi-analytical method developed in the present study to find the response statistics of bridge-vehicle system and to use this approach in forward scheme of particle filter technique. **Chapter-5** gives detail of instrumentation and procedure of dynamic test conducted on an existing bridge with the controlled movement of a loaded truck along the bridge. Finite Element Modelling of test bridge in SAP2000 and updating process based on response surface and genetic algorithm have also been included in this chapter. For the clarity in reading, results and discussions of the thesis have been split up into three chapters. **Chapter-6** presents the theoretical results obtained by a proposed semi-analytical method to reveal the influence of various bridge-vehicle parameters on system dynamic behavior. This, in fact, gives a pilot study to judge the sensitivity of different parameters to be used in inverse problem. **Chapter-7** discusses the results of vehicle parameter identification based on simulated bridge response from three different bridge-vehicle models. **Chapter-8** presents field test results, finite element model updating of the test bridge and results of test truck parameters identification utilizing field measured data in particle filter method. **Chapter-9** provides general conclusions arrived in the present study. Appendices A, B and C follow the Chapter-4 while Appendix D follows Chapter-7. References and list of publication from the present works are given at the end.

2

VEHICLE PARAMETER IDENTIFICATION

2.1 Overview

The estimation of system parameters of structures plays a significant role in structural condition assessment and health monitoring. The moving vehicle and bridge are two sub systems interconnected with each other. They exhibits coupled dynamic behavior due to forces at contact points. Moving force estimation from the dynamic response of the bridge falls in a class of 'inverse problem'. In this chapter, a general theory of moving load identification has been discussed pointing out the difficulties encountered in implementing the existing scheme. The present study aims to identify vehicle parameters from measured bridge dynamic response implementing a conditional probability based approach known as "Bootstrap Particle filter". In this report, sometimes the word "particle filter" is also used to mean bootstrap particle filter method. Measured bridge response has been considered as observable variable while passing vehicle parameters as hidden variables. Semi-analytical method has been proposed to relate hidden and observable variables used in "Forward Scheme" of the particle filter method. Mean of the hidden parameters are estimated from constructed posterior density of the passing vehicle parameters given measured dynamic response of the bridge. The identified vehicle parameters have been utilized to reconstruct the interaction force between the bridge and wheels of the vehicle. Step by step procedure has been discussed along with necessary equations. Lastly, a Flow chart of the method has been presented for implementing the procedure in Computer Programme in MATLAB environment.

2.2 Methods of Moving Load Identification

Direct measurement of vehicle load time history over the bridges is not feasible at all. However, measurements of structural response under moving load may be utilized to estimate the vehicle load in indirect way that has motivated many researchers to develop analytical, numerical and computational techniques to find load time history registered by a passing vehicle. This area of research falls under the class commonly called as "inverse engineering" which are commonly used for state or parameters estimation of the dynamic

system. Concept of solving such inverse problem is to determine the system inputs if the system outputs are known. In this regard, the inverse solution method can be grouped into two major heads such as *direct inverse method* and *indirect inverse method*.

2.2.1 Direct Inverse Method

Time history of moving load is found directly from measured bridge response. Strain gauge and accelerometers are common transducers used in acquiring response time history of bridge at several locations. In this category, there are two distinct approaches, one is time domain and another is frequency domain method. Frequency domain, however, is restricted to linear problems.

2.2.1.1 Time domain method

In linear dynamics, the system output to an arbitrary excitation can be written adopting Duhamel integral (Inman, 2001) as

$$y(t) = \int_0^t h(t-\tau)F(\tau)d\tau \tag{2.1}$$

where $h(t)$ is the impulse response function and $F(t)$ is the input excitation. The aim is to find $F(t)$ from the measured output $y(t)$ at different stations. Careful reading of existing literatures in time domain method of moving load identification (Law *et al*, 1997; Chan *et al*, 1998; Zhu and Law, 2003) reveals that identification problem finally could be transformed to a linear algebraic equation of the form

$$[A]\{x(t)\} = \{b\} \tag{2.2}$$

where $\{x(t)\} \in \mathrm{R}^n$ is a time series vector of unknown force $F(t)$, $\{b\} \in \mathrm{R}^k$ is the time series vector of measured response of bridge deck. The system coefficient matrix $\mathrm{A} \in \mathrm{R}^{n \times k}$ is associated with bridge-vehicle system. In general number of measured stations (k) is not equal to the number of unknown time dependent force. Such type of situation occurring in moving load identification is falling into class of ill-posed problem (Uhl, 2007). For this, unique solution does not exist and there is no globally defined solution on the given data. But when $n>k$, the equation have a solution given in the least square sense as

$$\{x(t)\} = [A]^{+}\{b\} \tag{2.3}$$

where $[A]^+$ denotes pseudo inverse of the matrix $[A]$, defined by

$$[A]^+ = \{[A]^T[A]\}^{-1}[A]^T \tag{2.4}$$

Some authors (Yu and Chan 2003, Jankawshi 2013) recommended using singular value decomposition (SVD) instead of pseudo-inverse solution (PI). Stevens (1987) suggested regularization method to overcome the difficulties of ill-conditioned matrix. Regularization process is the technique to transform ill-posed problem to well posed problem. Popular regularization method is Tikhonov method (Tiknonov and Arsenin, 1977) which has been successfully applied in moving load identification problem.

2.2.1.2 Frequency domain method

In linear dynamics, output and input is related in frequency domain as

$$\{X(\omega)\} = [H(\omega)]\{F(\omega)\} \tag{2.5}$$

In which $\{X(\omega)\}$ is the Fourier transform of the vector of response co-ordinates, $\{F(\omega)\}$ is the Fourier transform of the input excitation and $[H(\omega)]$ is a complex matrix called "Frequency Response Function", which depends on inertia, stiffness and damping properties of the system. The expression for $[H(\omega)]$ is given below

$$[H(\omega)] = \{-\omega^2[M] + i\omega[C] + [K]\}^{-1} \tag{2.6}$$

With the knowledge of bridge-vehicle system model, frequency domain representation of moving force estimation can be expressed as before in time domain method,

$$[A(\omega)]\{f(\omega)\} = \{b(\omega)\} \tag{2.7}$$

Where $[A(\omega)]$ is the system matrix in frequency domain, $\{f(\omega)\}$ is frequency variation of moving force and $\{b(\omega)\}$ is the frequency domain function of the measured bridge response at selected station. The number of unknown forces is usually less than the number of stations at which response is measured. Under such circumstances, the system is over determined and usually pseudo inverse of the matrix $[A(\omega)]^+$ post-multiplied by $\{b(\omega)\}$ yields the Fourier transform of unknown moving forces. If matrix $[A(\omega)]$ is square, then $[A(\omega)]^+=[A(\omega)]^{-1}$, in which case unknown force vector can be directly found from Eq.(2.7). If matrix $[A(\omega)]$ is singular, then problem is ill-posed. A regularization technique as in time

domain method was tried by various authors (Zhu and Law, 2002; Yu and Chan, 2003). Such problems in inverse techniques demands tremendous efforts in obtaining correct estimates. Finally the moving load time history is to be obtained by inverse Fourier Transformation process.

2.2.2. Indirect Inverse Method

In this inverse method, first vehicle parameters are identified from measured bridge response signal. The response may be strain, displacement or acceleration picked up by the sensors while the vehicle is in motion. On obtaining an estimate of system parameters, mathematical model of the coupled system is solved to reconstruct axle load time history

Following indirect inverse schemes have been used for estimating vehicle parameters from bridge dynamic response

2.2.2.1 Optimization based indirect inverse scheme

In an optimization based indirect inverse scheme, an objective function was constructed based on the residual between the measured and simulated bridge response using Least square method given by Deng and Cai (2009).

$$F_{obj} = \sqrt{\sum_{i=1}^{n} \{r_m(i) - r_s(i)\}^2} \tag{2.8}$$

where i and n are the time-point number and total number of time points in the response time history respectively; r_m and r_s are the measured and simulated response time histories, respectively.

Vehicle axle load could be reconstructed from the identified vehicle parameters using stochastic global search technique, called Genetic Algorithm (GA) based on the mechanics of natural genetics.

Setting proper upper bound and lower bound as well as a proper set of initial values for the parameters to be identified in the GA program, the objective function (F_{obj}) can then be optimized. The identified error can be calculated as

$$Identified\ \ Error = \left| \frac{P_{iden} - P_{true}}{P_{true}} \right| \times 100\% \tag{2.9}$$

where P_{iden} and P_{true} are the identified parameter and the true parameter, respectively.

2.2.2.2 Probabilistic based indirect inverse scheme

Another technique adopted in direct inverse scheme was based on Bayesian inference, called particle filter method (Nasrellah and Manohar, 2010). Noisy measured bridge response had been utilized for vehicle parameters estimation so that axle load time history can be re-constructed. Probabilistic based indirect inverse scheme is elaborated in the next section.

In the light of past research works, more realistic vehicle model has been found to be needed for better estimation of vehicle parameters and axle load identification. When bridge idealization is concerned, a beam model instead of a plate mode had been found to be accurate enough in the identification when the lower modes of the bridge deck are dominated by vibrational modes along the longitudinal axis (Zhu and Law, 2000). Also, it has been found that Finite element beam model requires a lot more of the measured information to have the same accuracy as the modeling of bridge as a continuous system (Zhu and Law, 2003). Identification using Direct inverse scheme is limited to simple forward scheme due to ill condition comes into picture. Even though regularization method had been employed to overcome this deficiency, significant identification error have been reported when bridge random surface profile was taken into consideration for forward scheme. In view of these, probabilistic based indirect inverse method has been adopted for identification of vehicle parameters as well as axle load estimation in the present study which has capability to incorporate uncertainties present in the forward scheme. Uncertainties may be related to modelling error of the physical system, measurement noise, vehicle path eccentricity and variation of vehicle speed during bridge responses measurement. The Particle filter method involves large number of iteration. In order to overcome this drawback, a closed form solution has been proposed for the sample generations in forward scheme.

For the purpose of vehicle load identification, the modeling of vehicle - bridge coupled system and determination of dynamic response has been referred to as a "*Forward scheme*". In the present work, three different vehicle models such as Quarter Car model, Flexible Half Car model and Flexible Full Car model have been considered in bridge-vehicle interaction dynamics. Bridge has been idealized as simply supported Euler Bernoulli's beam incorporating flexural and torsional vibration mode. In addition to this, bridge deck surface has been considered as non homogeneous random process in space

domain. Detail formulation and method of solution have been given in Chapter-3 and Chapter-4.

2.3 General Theory of Particle Filtering Method

Particle filtering is a nonlinear filtering whose output is not a linear function of its input. The Monte Carlo techniques behind the particle filters have existed since the 1950s (Hammersley and Morton, 1954) but a lack of computational power at that time rendered these methods unpopular. Since the introduction of the bootstrap filter (Gordon *et al*., 1993) and more general resampling schemes, there has been a large increase in research in this area.

2.3.1 Bayesian Inference to Dynamic State Estimation

In order to analyze and make inference about a dynamic system, at least two models are required in a probabilistic form: first, a system dynamic model which will describe the evolution of state with time, and second, measurement model relating the noisy measurements to the state. The dynamic model formulation in probabilistic form and the the updating of information on receipt of new measurements are ideally suited for the Bayesian approach of state estimation. A recursive filtering is a convenient solution when an estimate of dynamic state is required every time a measurement is received. A recursive filtering approach means that received data can be processed sequentially than as a batch, so that it is not necessary to store the complete data set or to process existing data if a new measurement becomes available. Such a filter consists of two essential stages: prediction and update. In the prediction stage system model is employed to predict the state one step ahead of the measurement. Since the state is contaminated by model noise, prediction generally translates, deforms and broadens the state probability density function. The updated operation uses the latest measurement to modify the prediction. This is achieved using Bayes theorem, which is the mechanism for updating knowledge about the target state in the light of extra information from new data.

The dynamic state evolves according to the following discrete-time stochastic model:

$$x_{l+1} = \Psi_l(x_l, \eta_l) \quad ; \qquad l=0,1,2,3.... N_t \tag{2.10}$$

where $x_l \in \mathbf{R}^{nx}$, nx is the dimension of state vector; $\mathbf{R}$ is a set of real numbers; $l \in N_t$ is the time index and N_t is te set of natural numbers. Ψ_l is a transition function of the state; x_l and η_l are referred as the process noise sequences. The measurements are related to the system state via measurement equation:

$$y_l = \Theta_l(y_l, \zeta_l) \quad ; \qquad l=0,1,2,3.... N_t \tag{2.11}$$

where $y_l \in \mathbf{R}^{ny}$, ny is the dimension of measurement vector; Θ_l is a transition function of the state; y_l and ζ_l are referred as the measurement noise sequence. Model noise and measurement noise are assumed to be independent and identically distributed random variables which are independent of past and current state and whose probability density functions are assumed to be known.

A filter estimates dynamic state x_l based on the sequence of all available measurements denoted as $Y_l = \{y_1, y_2, y_3...., y_l\}$ up to time l. The objective of the filter is to estimate the current state of the system x_l from available measurements Y_l. Since both x_l and Y_l are contaminated by noise n_x and ζ_l, complete information of the state is possible if we can construct the PDF of x_l, denoted as $p(x_l \mid Y_l)$, conditioned on available measurements Y_l ; Before starting the iteration, measured response is not available. In that case only state has to be guessed whose probability density can be approximated as $p(x_0) \equiv p(x_0|y_0)$, y_0 being the initial record of response which practically does not exist before starting the iteration.

Suppose that the required $p(x_{l-1}| Y_{l-1})$ at time l-1 is available. The prediction density of the system state at time l can be expressed using Chapman-Kolmogorov equation (Gordon *et al*., 1993) as

$$p(x_l \mid Y_{l-1}) = \int p(x_l \mid x_{l-1}) p(x_{l-1} \mid Y_{l-1}) dx_{l-1} \tag{2.12}$$

The evolution of probability of the state $p(x_l|x_{l-1})$ is defined by system equation (2.12) and known statistics of model noise η_l. Using conditional densities it can be expressed as

$$p(x_l \mid x_{l-1}) = \int p(x_l \mid x_{l-1}, \eta_{l-1}) p(\eta_{l-1} \mid x_{l-1}) d\eta_{l-1} \tag{2.13}$$

Also, it is assumed that η_l to be independent of the state. Hence one has

$$p(\eta_{l-1} \mid x_{l-1}) \equiv p(\eta_{l-1}) \tag{2.14}$$

From the system equation, Eq. (2.10), it follows that if x_{l-1} and η_{l-1} are known, then deterministically x_l can be expressed in terms of x_{l-1} and η_{l-1}. Mathematically, the $p(x_l|x_{l-1}, \eta_{l-1})$ can be written as

$$p(x_l \mid x_{l-1}, \eta_{l-1}) \equiv \delta\{x_l - \Psi(x_{l-1}, \eta_{l-1})\} \tag{2.15}$$

where, δ(.) is the Dirac-delta function. Substituting Eqs (2.14) and (2.15) in Eq. (2.13), we have

$$p(x_l \mid x_{l-1}) = \int \delta\{x_l - \Psi(x_{l-1}, \eta_{l-1})\} p(\eta_{l-1}) d\eta_{l-1} \tag{2.16}$$

This can be substituted in the prediction equation (2.13). At time step l when the measurement y_l becomes available, the updating is carried out. This involves an update of the prediction (or prior) using Bayesian relation

$$p(x_l \mid Y_l) = \frac{p(y_l \mid x_l) p(x_l \mid Y_{l-1})}{\int p(y_l \mid x_l) p(x_l \mid Y_{l-1}) dx_l} \tag{2.17}$$

The dynamic state estimation equations in (2.10)-(2.17) can no longer be solved in closed form as the functions are nonlinear. The basic premise of particle filter method is to approximately evaluate the multi-dimensional integrals using Monte Carlo simulations. A large number of samples are simulated in the computer and are passed through the system equation to predict a priori state of the system. Once the measurements are available, application of a criterion for minimization of the error leads to a posteriori estimate of the state. Thus, Particle Filtering is essentially a predictor-corrector algorithm.

2.3.2 Monte Carlo Integration and Importance Sampling

Monte Carlo method is a numerical technique which relies on random sampling to approximate their results and it applies this process to the numerical estimation of integrals. Other algorithms usually evaluate the integrand at a regular grid while Monte Carlo randomly chooses a point at which the integrand is evaluated. This method is particularly useful for higher-dimensional integrals (Caflisch, 1998).

Suppose it is required to evaluate numerically a multidimensional integral, given as (Ristic *et. al.,* 2004)

$$I = \int h(\eta) d\eta \tag{2.18}$$

where $\eta \in \mathbf{R}^n$. Monte Carlo integration method factorize $h(\eta)=g(\eta)\cdot\pi(\eta)$ in such a way that $\pi(\eta)$ is interpreted as a probability density satisfying $\pi(\eta) \geq 0$ and $\int \pi(\eta)d\eta=1$. Assuming that it is possible to draw a samples $\{\eta^i; i=1, 2,..., N_p\}$ distributed according to $\pi(\eta)$. The mean estimate of the integral $\int g(\eta)\cdot\pi(\eta)\, d\eta$ using Monte Carlo integration method can be written as

$$I_N = \frac{1}{N}\sum_{i=1}^{N} g(\eta^i) \tag{2.19}$$

where N is a number of samples drawn from the probability density $\pi(\eta)$. The variance of $g(\eta)$ can be given as

$$\sigma_N^2 = \frac{1}{N-1}\sum_{i=1}^{N}\{g(\eta^i) - I_N\}^2 \tag{2.20}$$

In the context of Bayesian estimation, probability density $\pi(\eta)$ is the posterior density. However, usually it is not possible to sample effectively from the posterior density, being multivariate and nonstandard (Ristic *et. al.,* 2004). Application of importance sampling method is the only way to overcome this problem.

Importance sampling forms the basis for the sequential Monte Carlo methods to solve the recursive equation given in Eq. (2.17). Continuing the same integral (Eq. 2.18), suppose it is only possible to generate samples from a density $f(\eta)$, referred to as importance or proposal density (Ristic *et. al.,* 2004), being similar to $\pi(\eta)$. Monte Carlo estimate becomes possible if there exist a correct weighting of the sample. Due to similarity of the probability densities $\pi(\eta)$ and $f(\eta)$, any integral of the form $\int g(\eta)\cdot\pi(\eta)\, d\eta$ can be written as

$$I = \int g(\eta)\pi(\eta)\, d\eta = \int g(\eta)\frac{\pi(\eta)}{f(\eta)} f(\eta) d\eta \tag{2.21}$$

Now, Eq. (2.21) can be integrated using Monte Carlo estimate by generating $N_p >> 1$ independent samples $\{\eta^i; i=1, 2,..., N_p\}$ distributed according to $f(\eta)$ and forming the weighted sum, given as

$$I_N = \frac{1}{N}\sum_{i=1}^{N} g(\eta^i) W(\eta^i) \tag{2.22}$$

where, $W(\eta^i)= \pi(\eta^i)/ f(\eta^i)$ are the importance weights.

In more general, even if the information about the normalizing factor of the desired density $\pi(\eta)$ is not available, Monte Carlo estimate of the integral can be written as,

$$I_N = \frac{\frac{1}{N}\sum_{i=1}^{N} g(\eta^i)W(\eta^i)}{\frac{1}{N}\sum_{i=1}^{N} W(\eta^i)} \tag{2.23}$$

2.3.3 Bootstrap Particle Filtering

The Bayesian inference given in Eq. (2.17) can then be solved by Monte Carlo integration method with sequentially updating a distribution using importance sampling techniques. This sequential Monte Carlo approach is known as Bootstrap Particle Filtering proposed by Gordon *et. al* (1993). A detail implementation of sequential Monte Carlo method can be shown as follows,

Let the sequence of all target states up to time l be given as $X_l = \{x_j, j=0,1,2\ldots, l\}$ and the joint posterior probability density at time l be denoted as $p(X_l \mid Y_l)$, and its marginal density be $p(x_l \mid Y_l)$. The joint posterior density at l can be approximate as, (Doucet *et. al.,* 2000)

$$p(X_l \mid Y_l) \approx \sum_{i=1}^{N} W_l^i \delta(X_l - X_l^i) \tag{2.24}$$

where, X_l^i, (i=0,1,2…, N) is a set of support points of posterior density $p(X_l \mid Y_l)$ with associated weight W_l^i, (i=0,1,2…, N_p) and N_p is a number of samples.

Now, we have a discrete weighted approximation of the true posterior density, $p(X_l \mid Y_l)$. Employing the principle of importance sampling described in Section 2.3.2, the normalized weights X_l^i are chosen. If the samples X_l^i were drawn from an importance density $f(X_l \mid Y_l)$, the normalized weight can be written as

$$W_l^i = \frac{p(X_l^i \mid Y_l)}{f(X_l^i \mid Y_l)} \tag{2.25}$$

Suppose at time step l-1, a samples constituting an approximation to $p(X_{l-1}|Y_{l-1})$ is available. It will be required to approximate the density $p(X_l|Y_l)$ when measurement y_l at time l is available. If the importance density is chosen to factorize such that (Ristic *et. al.* 2004)

$$f(X_l \mid Y_l) \equiv f(x_l \mid X_{l-1}, Y_l)\ f(x_l \mid Y_{l-1}) \tag{2.26}$$

then, a samples $X_l^i \sim f(X_l \mid Y_l)$ can be obtained by augmenting each of the existing samples $X_{l-1}^i \sim f(X_{l-1} \mid Y_{l-1})$ with the new state $x_l^i \sim f(x_l \mid Y_{l-1}, Y_l)$. In order to obtain the weight update equation, the PDF $p(X_l \mid Y_l)$ has to be first expressed in terms of $p(X_{l-1} \mid Y_{l-1})$, $p(y_l \mid x_l)$ and $p(x_l \mid x_{l-1})$ as follows

$$p(X_l \mid Y_l) = \frac{p(x_l \mid X_l, Y_{l-1})\ p(X_l \mid Y_{l-1})}{p(y_l \mid Y_{l-1})} \tag{2.27}$$

$$= \frac{p(x_l \mid X_l, Y_{l-1})\ p(x_l \mid X_{l-1}, Y_{l-1})\, p(X_{l-1} \mid Y_{l-1})}{p(y_l \mid Y_{l-1})} \tag{2.28}$$

$$= \frac{p(y_l \mid x_l)\ p(x_l \mid x_{l-1})}{p(y_l \mid Y_{l-1})}\, p(X_{l-1} \mid Y_{l-1}) \tag{2.29}$$

$$\alpha \quad p(y_l \mid x_l)\ p(x_l \mid x_{l-1})\, p(X_{l-1} \mid Y_{l-1}) \tag{2.30}$$

Substituting Eq. (2.26) and Eq. (2.30) in Eq. (2.25), the weight update equation can be expressed as

$$W_l^i = W_{l-1}^i \frac{p(y_l \mid x_l^i)\ p(x_l^i \mid x_{l-1}^i)}{q(x_l^i \mid x_{l-1}^i, y_l)} \tag{2.31}$$

where, $$W_{l-1}^i = \frac{p(X_{l-1}^i \mid Y_{l-1})}{q(X_{l-1}^i \mid Y_{l-1})} \tag{2.32}$$

Candy (2009) mentioned that, $q(x_l^i \mid x_{l-1}^i, y_l) \rightarrow p(x_l^i \mid x_{l-1}^i)$. Hence updated weight can be written as

$$W_l^i = W_{l-1}^i \times L(y_l \mid x_l^i) \tag{2.33}$$

where, $L(y_l \mid x_l^i)$ is a measurement likelihood and i=1,2,3…. N_p. As mentioned earlier, if the normalizing factor of the desired density is unknown, then it is required to perform normalization of the importance weights (Ristic *et. al.,* 2004). Normalized important weight can be written as

$$w_l^i = \frac{W_l^i}{\sum_{i=1}^{N} W_l^i} \tag{2.34}$$

The posterior filter density $p(x_l \mid Y_l)$ can be approximated as

$$p(x_l \mid Y_l) \approx \sum_{i=1}^{N_p} w_l^i \delta(x_l - x_l^i) \tag{2.35}$$

Thus, in a Bootstrap Particle Filtering, weights become simple and only depend on the likelihood; therefore, it is not even necessary to perform a sequential updating (Candy, 2009). In this filtering technique, continuous distributions are approximated by discrete random measures composed of these weight particles where the particles are samples of the unknown or hidden states from the system model and the weights are the probability masses which are estimated using Bayesian recursions. An estimate of the filtering posterior distribution at time instant l is shown in Fig. 2.1 in terms of weight (probabilities) and particles (samples). In the figure, square box represents locations of particles and their corresponding weights. It can be seen that the particles need not be equally spaced or conform to a uniform grid and that they tend to coalesce in high probability region.

Filtering algorithm can be summarized as follows (Gordon *et. al,* 1993; Arulampalam *et. al,* 2002)

(i) Initial stage: Generate the initial state, x_0^i and model noise η_0^i from known PDF, i=1,2,3…N_p on which N_p is a number of particles.

(ii) Prediction: Determine state of the system (particle) x_l^i at l=1 based on initial state of the system.

(iii) Update: Calculate the likelihood $L(y_l \mid x_l^i)$ using the current particle and measurements.

(iv) Resampling: Resample the set of particles retaining and replicate those of highest weight (probability), $\hat{x}_l^i \Rightarrow x_l^i$. Then generate the new set of particles. Set l=l+1 and if $l < N_l$ (N_l is the total number of time steps), then go to step (ii) and repeat other steps.

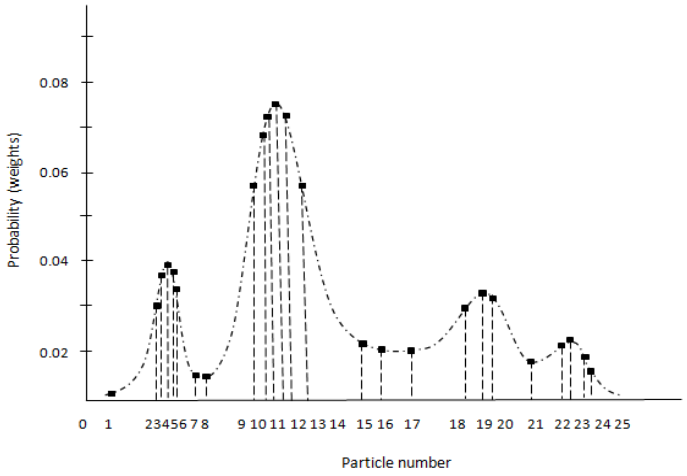

Fig. 2.1 Estimate of the filtering posterior distribution at time instant l is shown

2.3.4 Resampling

In this section 'resampleing" procedure adopted in the filtering process has been explained in detail. Resampling has been performed by regenerating N_p number of particles drawn from the current population of particles by means of the normalized weights, given in Eq. (2.39), as selection probabilities. Particles of low probability (small weights) are removed and those of high probability (large weights) are retained and replicated, apparently analogous to genetic algorithm. The resampling process is conceptually illustrated in Fig. 2.2. In this figure, particles location and weight is represented by rhombus of pale dark colour with different sizes, indicating weight and size direct relationship. It can be seen that more particles has been regenerated from the particles under higher weight, that is, larger the rhombus size and the peaks of the estimated posterior densities approaching more and more the target PDF in successive iterations.

Resampling, therefore, can be thought of as a realization of enhanced particles, $\hat{x}_l^i$, extracted from the original samples, x_l^i based on their acceptance probability (or normalized weight of particles) w_l^i at time l, Statistically, we have

$$p(\hat{x}_l^i = x_l^i) = w_l^i \qquad for\ i = 1,2,3,..., N_p \tag{2.36}$$

or it can be written symbolically as

$$\hat{x}_l^i \Rightarrow x_l^i \tag{2.37}$$

where, '$\Rightarrow$' stands for the Resampling operator generating a set of new particles $\{\hat{x}_l^i\}$, replacing the old set of particles $\{x_l^i\}$.

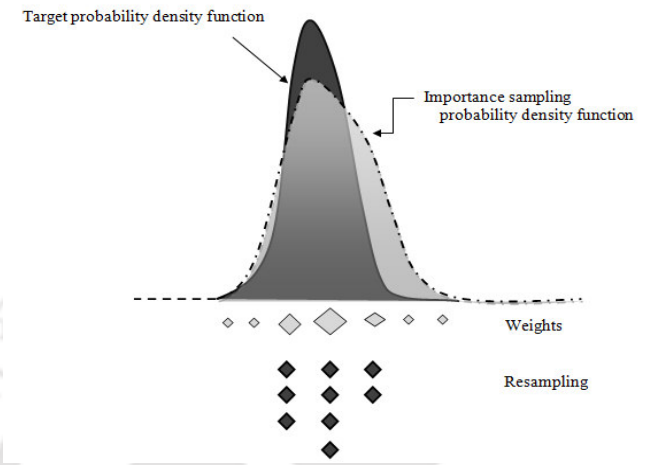

Fig. 2.2 Resampling processing for different steps of iteration

Different resampling methods are available to implement the resampling of particles (Candy, 2009). Multinomial resampling algorithms employed in present Particle Filtering is discussed below.

Multinomial resampling approach is to resample with replacement, since the probability of each particle x_l^i is given by the normalized weight w_l^i. Following are the steps:

(i) Let a set of particles and weight at time l be represented as $\{x_l^i, w_l^i\}$, where $i = 1,2\ldots,N_p$.

(ii) Generate uniformly distributed random number, $v_k \rightarrow U(0,1)$, where $i = 1,2\ldots,N_p$.

(iii) Determine the index, $i_k : i_k = k$ for cumulative probability function $\Pr(x_l^{ik} = x_l^k) = v^k$.

(iv) Select a new sample, $\hat{x}_l^{ik} \Rightarrow x_l^i$ and weight $\hat{w}_l^{ik} = 1/N_p$ based on the new sample index, i_k.

(v) Then, generate a new particles: $\{\hat{x}_l^{ik}, \hat{w}_l^i\}$ for $k = 1,2,\ldots N_p$.

Here, index notation i_k represents original i^{th} particle and the new k^{th} particle using inverse cumulative probability function method. This sampling technique is equivalent to drawing, i_k; $k = 1, 2,\ldots N_p$ samples from multinomial distribution $M(N_{ik}, w_l^{ik})$.

The main idea of this resampling technique is to first construct the cumulative distribution function (CDF) from original random particles $\{x_l^{ik}, w_l^i\}$, as it is given by

$$\Pr(X_l \le x_l^i) \approx \sum_{i=1}^{Np} w_l^i \mu(x_l - x_l^i) \tag{2.38}$$

where $\mu(.)$ is the unit step function.

Uniform random samples v_k are drawn from the interval [0,1] and projected onto the inverse cumulative distribution function corresponding to the associated probability and identifying the particular new samples index, i_k, and corresponding replacement particle. The particles with highest weights will be selected more frequently, thereby, replacing particles with lower weights and therefore the new random measure is created. Selection of new particles $\hat{x}_{ik}$ according to the multinomial distribution can be expressed as

$$\hat{v}_{ik} = x(F^{-1}(v_k)) \quad for \sum_{s=1}^{i-1} w_s \le v_k < \sum_{s=1}^{i} w_s \tag{2.39}$$

where, i=1,2,3…N, w_s is a normalized weight of particle at time step l. F^{-1} denotes the generalized inverse of cumulative distribution of normalized particle weights.

2.4 Application of Bootstrap Particle Filtering Method for Vehicle Parameter Identification

The main objective of the present thesis is to use "bootstrap particle filter" or simply "particle filter method" in identification of vehicle parameters from measured bridge response and to conduct various parametric studies to examine the efficiency of the inverse method, which has very limited application in solving inverse problems related to bridge-vehicle dynamics in the past. The vehicle parameters to be identified include vehicle masses, wheel masses, suspension stiffness and damping, tyre stiffness and damping. In case of flexible model of vehicles incorporated in the present study, flexural and torsional rigidities are to be included in the list.

Let the parameters to be identified be represented by a vector $\{\Phi\}$. Bridge parameters (span, cross section, support conditions, material properties) and the velocity with which vehicle traverse the bridge are taken to be known. However, the proposed scheme can also

include those additional parameters. The system states r_l are assumed to propagate according to system equation

$$r_{l+1} = g_l(r_l; \Phi_l, \eta_l) \quad ; \quad l=0,1,2,3.... N_t \tag{2.40}$$

in which, l represents discretized time dimension and N_t is the number of time instants considered. $\Phi_l \in \mathbf{R}^d$ is a d-dimensional vehicle parameters vector which is considered as constant for small interval of time, $r_l \in \mathbf{R}^n$ is a n-dimensional vector denoting the state of the system, a model noise $\eta_l \in \mathbf{R}^m$ is the discretized m-dimensional vector of a sequence of independent and identically distributed random variables which are independent of past and current state and whose probability density function are assumed to be known. $g_l(.)$ is a system transition function.

When the system measurements become available, the system states are related to these measurements via the observation equation.

$$Z_l = f_l(r_l; \Phi_l, \zeta_l); \quad l=0, 1, 2, 3.... N_t \tag{2.41}$$

where $Z_l \in R^p$ is a p-dimensional bridge response measurement vector, a measurement noise $\zeta_l \in R^s$ is a s-dimensional vector of a sequence of independent and identically distributed random variables and $f_l(.)$ is a non linear function that relates the measurements to the system state

Since, state of the system is dependent on system parameters $\{\Phi\}$, observation equation can be rewritten as

$$Z_l = f_l(\Phi_l, \zeta_l) \quad ; \quad l=0, 1, 2, 3.... N_t \tag{2.42}$$

Vehicle parameters identification problem can now be considered as being equivalent to the determination of the posterior probability density function $p(\Phi_l \mid Z_l)$. According to Bayesian theorem $p(\Phi_l \mid Z_l)$ can be written as (Ristic et. al. 2004)

$$p(\Phi_l \mid Z_l) = \lambda\, p(Z_l \mid \Phi_l)\, p(\Phi_l) \tag{2.43}$$

where, $p(\Phi_l \mid Z_l)$ is the posterior PDF, $p(Z_l \mid \Phi_l)$ is the likelihood of individual parameters, $p(\Phi)$ is the prior probability density function and λ is the normalizing parameter evaluated as

$$\lambda = [\int p(\Phi_l \mid Z_l)\, p(\Phi_l) d\phi_l]^{-1} \tag{2.44}$$

Thus knowing posterior PDF $p(\Phi_l \mid Z_l)$, first few moments of the vehicle parameters Φ_l, conditioned on bridge response measurement Z_l, at each time step can be determined.

The main steps of the particle filtering algorithm for identifying vehicle parameters has been stated in a sequential manner for implementation in computer program in MATLAB environment as follows:

(i) Initial stage: Draw N_p random samples of vehicle parameters $\{\Phi_{0j}\}_{j=1}^{Np}$ from the assumed PDF $\{p(\Phi_{0j})\}_{j=1}^{Np}$

(ii) Prediction: Determine bridge response using available vehicle parameters and employing forward solution at time step l. If N_p is sufficiently large, these estimates are approximately distributed as $\{p(f_l^m[\Phi_{lj}] \mid Z_l^m)\}_{j=1}^{Np}$.

where, m=1,2,3…N_m is number of response measurement locations, Z_l^m denotes measured bridge response at location m and $f_l^m[\Phi_{lj}]$ represents simulated bridge response at location m using generated particles.

It may be noted here that present study proposes a semi-analytical scheme to generate response samples in prediction stage with an aim to enhance the performance of the particle filter method. The proposed method of response sample generations has been given in Chapter-3 and Chapter-4.

(iii) Update: Once the measurements are available for different measurement location m (m=1,2,3….N_m) at time l, evaluate the likelihood corresponding to all the samples which depends on the nature of measurement noise probability distribution. Normalized weight for each particle can be obtained as

$$w_j = \frac{\prod_{m=1}^{Nm} L(Z_l^m \mid f_l^m[\Phi_{lj}])}{\sum_{j=1}^{N_p} \left\{ \prod_{m=1}^{Nm} L(Z_l^m \mid f_l^m[\Phi_{lj}]) \right\}} \tag{2.45}$$

in which, $\prod_{m=1}^{Nm} L(Z_l^m \mid f_l^m[\Phi_{lj}])$ represents likelihood of measured bridge response given measured bridge response for each particle j at time l for different measurement locations m. The discrete mass probability function for the next iteration is defined as

$$P(\Phi_{lj} = f_l^m[\Phi_{lj}]) = w_j \tag{2.46}$$

(iv) Resample: From the discrete mass distribution function, a new set of N_p samples of Φ_{lj} are generated. This constitutes the posterior estimates of Φ_{lj}. The mean of estimates are obtained by averaging across the ensemble, and is expressed as

$$\mu_{l|l} = \frac{1}{N_p}\sum_{j=1}^{N_p}\Phi_{lj} \tag{2.47}$$

The corresponding standard deviation of the estimate is calculated as

$$\sigma_{l|l} = \sqrt{\frac{1}{N_p - 1}\sum_{j=1}^{N_p}(\Phi_{lj} - \mu_{l|l})^2} \tag{2.48}$$

Set l=l+1 and if $l < N_t$ then go to step (ii) and repeat other steps, otherwise stop. In this way, the filtering is carried out for the entire available time history of measurements.

A flow diagram of the Bootstrap Particle Filtering algorithm is shown in Fig 2.3 where the procedures of vehicle parameters identification based on measured bridge response are again illustrated.

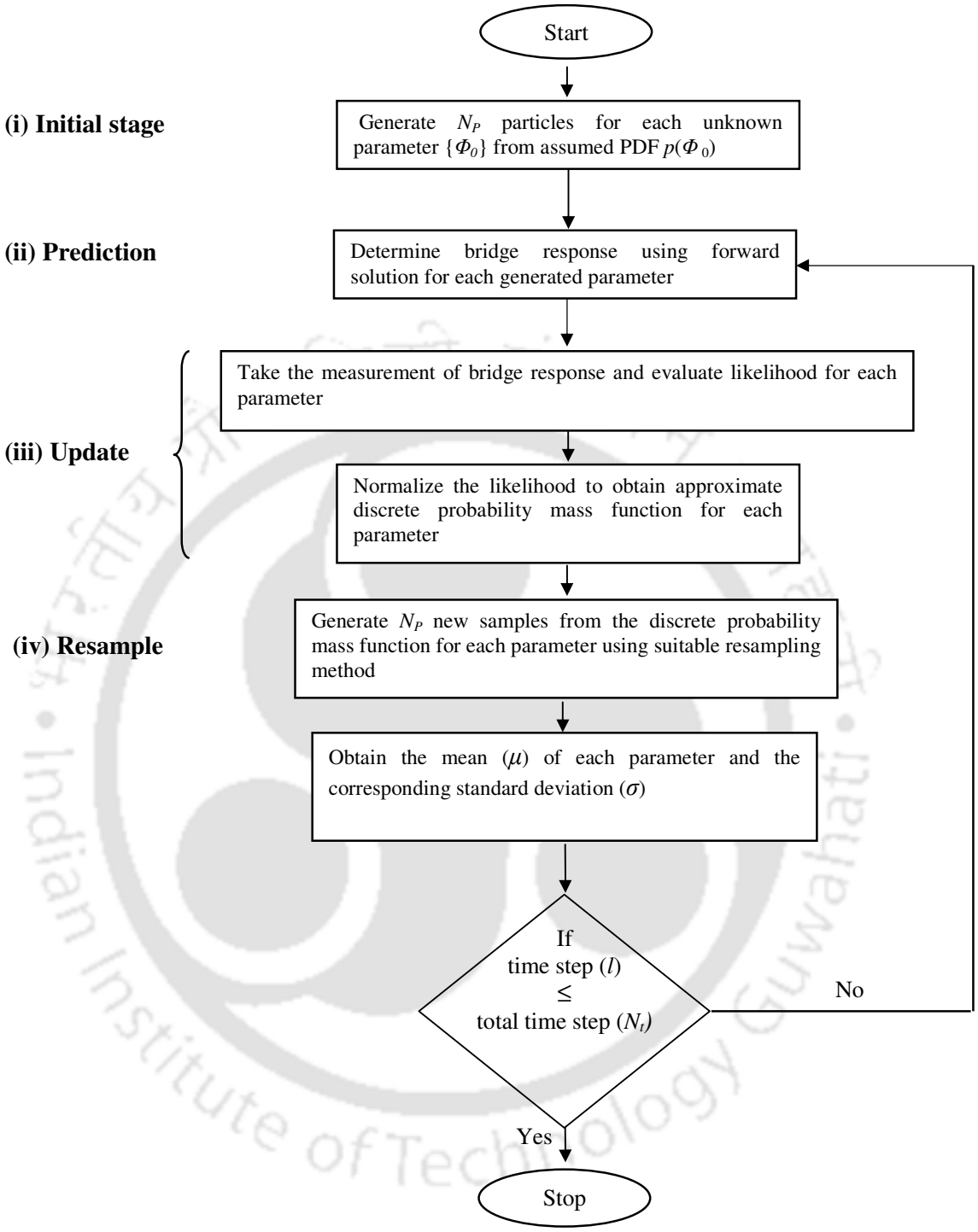

Fig.2.3 Flow chart for Bootstrap Particle Filtering method for identification of vehicle parameters

2.5 Closure

The present chapter describes different approaches of inverse problem which have been applied for moving load identification as well as passing vehicle parameters estimation based on measured bridge response. The inverse solution methods have been grouped into two major heads such as direct inverse method and indirect inverse method. Methods which can directly estimate bridge dynamic load are termed here as direct inverse method. On the other hand, the indirect inverse methods extract vehicle parameters from measured bridge response first, and then bridge dynamic loads are reconstructed using identified vehicle parameters and states of the system. Present thesis focuses on the indirect inverse scheme based on conditional probability. The method can be viewed as combined application of Monte Carlo integration and importance sampling technique to Bayesian inference, called as Bootstrap Particle Filter. The Bootstrap Particle Filter has been applied to the problem of vehicle parameters identification in the present thesis. Step by step procedure of the particle filter method along with Flow chart for the extraction of hidden vehicle parameters from noisy signals has been developed. The particle filter method is computationally expensive. In the present study, we have attempted to overcome this drawback by combining a semi-analytical solution for the bridge vehicle interaction problem in particle filter method. Bridge-vehicle models and the proposed semi-analytical method for the forward scheme have been presented in Chapter-3 and Chapter-4.

.

3

BRIDGE-VEHICLE INTERACTION MODELS

3.1General

Development of bridge vehicle model is essential in the proposed method of vehicle parameters identification based on available dynamic response of the bridge. In the present study, these models and methods of solution have been grouped under “forward scheme” as stated in Chapter-2. Depending on the desired accuracy and quantum of information required, three models of vehicles in increasing order of complexity have been employed in the forward scheme. The present research is not only confined to the vehicle parameters identification but also aims to provide information on the dynamic behavior of a bridge in presence of several variations of bridge -vehicle parameters. This would judge the sensitivity of models for change of different vehicle parameters. Conventionally, the moving vehicles have frequently been idealized as a number of moving loads as long as finding of the bridge response is only concerned. But this idealization is incapable to judge the influence of key parameters such as bridge deck surface irregularity, speed of the vehicle, suspension and tyre characteristics. In order to incorporate all these parameters, the bridge and moving vehicles are idealized as two sub systems interconnected to each other at wheel contact. The present research has paid attention on the effect of vehicle flexibility on the bridge dynamic response which was mostly ignored in earlier research. But its necessity is felt in modeling procedure considering the evolution of longer vehicles with slender body made of advanced lighter materials.

3.2 Idealization of bridge

In particle filtering technique, it is necessary that forward problem of the model has to be solved, for which the analyst has the option of choosing an appropriate model of the system. The choice of model depends on the purpose of analysis, computational cost and desired accuracy. Usually, transverse dimension of bridge deck is small compared to its span and therefore, a simplified beam model is suitable option to establish a clear connection between bridge response and vehicle parameters (Fryba, 1996), especially in case of implementing a computationally intensive method for the estimation of system parameters. The simpler

model when tuned to fundamental natural frequency of the real bridge is expected to predict dynamic behavior similar to real structure. In the present study, a single span bridge has been idealized as Euler Bernoulli beam of uniform cross section and damping properties. Both bending and torsional motion of the bridge have been incorporated in the model.

3.3 Deck roughness

Vehicle traversing over the bridge is excited by the roadway conditions at the contact points. The deviation of a pavement surface from a true planner surface is termed as surface unevenness. These conditions can be characterized by deterministic mean surface profile superimposed over randomly undulating pavement. Deterministic mean surface profile may represent construction defects, pot holes, approach road settlement, expansion joints, development of corrugation, pre-cambering of deck surface, etc. The random unevenness of the pavement profile is assumed to be of Gaussian nature and homogeneous in space (Shinozuka, 1971). In temporal domain, this remains stationary excitation process as long as vehicle velocity is constant. However, it may be noted that the process becomes non-homogeneous in space in presence of a variable mean profile even the vehicle velocity is constant (Yadav and Nigam, 1978).

The vertical height of the bridge deck profile along the longitudinal axis measured with respect to flat datum at a point x from the reference station can be represented by

$$h(x) = h_m(x) + h_r(x) \tag{3.1}$$

where $h(x)$ is bridge deck profile which is composed of two parts. The first part $h_m(x)$ is a deterministic mean surface profile and $h_r(x)$ is a road surface unevenness.

3.3.1 Mean surface profile

In the present study, two types of deterministic mean profile - (i) pre-cambering of bridge in the form of shallow parabolic curve (ii) approach settlement as ramp function have been considered. The analytical form of representing deterministic mean profile are given below

Case (i): Pre-cambering of bridge

The advances in design, construction materials and method of construction enables today's engineer to build long span bridges. One problem that is faced by the engineer in long span bridges is to control deflection limit in order to achieve better serviceability. It is to be noted

that in some cases of bridge design, deck deflection under dead load and live load may cross serviceability limit. As a measure of safety, upward pre-cambering of deck surface is recommended to compensate for additional vertical deflection (Detailed Project Report, Public Works Department, Govt. of Arunachal Pradesh, India, 2012). The pre-cambered profile is generally adopted as a shallow parabola, central rise being made equal to the additional maximum vertical deflection that bridge would undergo due to dead load and live load in service.

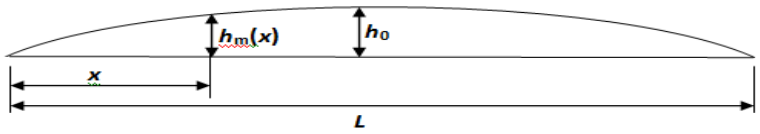

Fig. 3.1 Deterministic mean surface profile in the form of shallow parabolic

In the present study, we incorporate pre-cambering of bridge deck in the form of shallow parabola (Fig.3.1), the equation of which with reference to origin at the left hand support is given by

$$h_m(x) = \frac{4h_0}{L^2} x(L-x) \quad , \; 0 \le x \le L \tag{3.2}$$

where $h_m(x)$ is a mean deck surface profile at a distance x from the left support, h_0 is the central rise of mean parabolic surface, and L is the bridge span.

Case (ii): Approach road settlement

Very often, the transition from road to bridge is not smooth. This is because the bridge approach experiences settlement relative to the bridge deck. As a result of this, there is an abrupt change in road level. The settlement may be caused due to inadequate compaction of sub-grade soil, poor drainage or other faulty construction issues. The settlement is often referred as “bump at the end”. The vehicle experiences a sudden dynamic load at the entry/exit depending on the severity of the settlement. Due to increased vibration of vehicle, bridge pavement experiences higher dynamic load. The settlement also affects ride quality, vehicle controllability and fatigue life of vehicle.

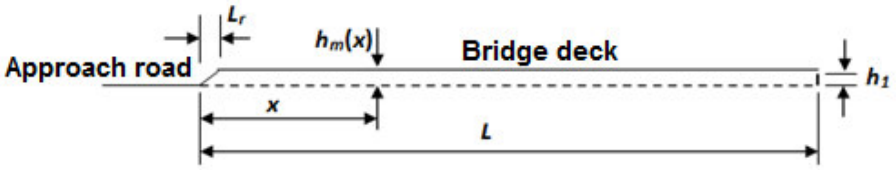

Fig. 3.2 Deterministic mean surface profile in the form of approach road settlement

In the present study, the model of approach settlement (Fig. 3.2) has been given by following equations

$$h_m(x) = \begin{cases} \dfrac{h_1}{L_r} x & if \quad 0 \le x \le L_r \\ h_1 & if \quad x \ge L \end{cases} \tag{3.3}$$

where, h_1 represents approach settlement , L_r is the ramp length and L is the bridge span.

3.3.2 Random unevenness

The road surface roughness in Bridge-Vehicle interaction dynamics can be described as a stationary Gaussian random field characterized by its power spectral density (PSD) function (Schiehlen, 2009; Lombaert and Conte, 2011; ISO 8608: 1995). Therefore, this subsection includes a general introduction to random Gaussian processes with their stochastic characteristics, a description of roadway profiles as a random process, as well as an illustration of models for the realizations of roadway profiles.

In general, for a Gaussian stochastic process $g_0(t)$ with an autocorrelation function $R_{g0g0}(\tau)$ and a two-sided power spectral density function $S_{g0g0}(\Omega)$, the following relations hold (Shinozuka and Deodatis, 1991)

$$E[g_0(t)]=0 \tag{3.4}$$

$$E[g_0(t+\tau)g_0(t)]=R_{g_0g_0}(\tau) \tag{3.5}$$

$$S_{g_0g_0}(\omega) = \frac{1}{2\pi}\int_{-\infty}^{\infty} R_{g_0g_0}(\tau)\,\exp(-i\omega\tau)d\tau \tag{3.6}$$

$$R_{g_0g_0}(\tau) = \int_{-\infty}^{\infty} S_{g_0g_0}(\omega)\,\exp(-i\omega\tau)d\kappa \tag{3.7}$$

where ω denotes the temporal frequency

Dodds and Robson (1973) suggested a simplified way of describing the road surfaces to avoid a laborious procedure which is often obtained by measuring existing roadways. In the present research, road unevenness has been treated as a realization of a stationary Gaussian homogeneous random process described by its power spectral density function in the space domain $S_{g0g0}(\Omega)$ with Ω as the wave number / spatial frequency. However, the dynamic analysis has been performed in the time domain, hence, a description of the road unevenness in the time domain is needed. Therefore, the temporal power spectral density function $S_{g0g0}(\omega)$ is to be computed. Assuming a constant speed for the vehicle V, the relationship between $S_{g0g0}(\omega)$ and $S_{g0g0}(\Omega)$ can be derived as follows:

(i) Since the vehicle is traveling at a constant speed of V, any instant of the travel time 'τ' can be expressed in terms of the distance travelled 'x' as

$$\tau = \frac{x}{V} \tag{3.8}$$

(ii) A cycle of wavelength $\lambda = 2\pi/\Omega$ is covered in period T as

$$T = \frac{\lambda}{V} \tag{3.9}$$

Therefore, the temporal frequency can be written as

$$\omega = \frac{2\pi}{T} = \frac{2\pi V}{\lambda} = V\Omega \tag{3.10}$$

(iii) Substituting the above Eqs. (3.8), (3.9) and (3.10) in Eq. (3.6), we get

$$S_{g_0g_0}(\omega = V\Omega) = \frac{1}{V}\{\frac{1}{2\pi}\int_{-\infty}^{\infty} R_{g_0g_0}(x)\exp(-i\Omega x)dx\} \tag{3.11}$$

$$= \frac{1}{V} S_{g_0g_0}(\Omega) \tag{3.12}$$

Using the relationship given in Eq. (3.12) the temporal spectral density function $S_{g0g0}(\omega)$ can be obtained from the spatial spectral density function $S_{g0g0}(\Omega)$. When performing the analysis in the time domain, one can deduce that the excitation of the vehicle due to road unevenness can be described as non-stationary when the vehicle speed is time dependent (Schiehlen, 2009).

In most of the engineering applications, the one-sided spectral density function is derived from measurements for which the following relation holds

$$S_{GG}(\Omega) = 2S_{gg}(\Omega) \tag{3.13}$$

in which S_{GG} (Ω) is one sided spectral density. Based on the work of past researchers (Rice,1954; Shinozuka and Deodatis, 1991), there are two main models for generating realizations of random processes. One consists of a series of sines and cosines with random amplitudes and the other consists of a series of cosine terms having random phase angles with a specified probability density function. In regard to Vehicle-Bridge interaction dynamics analysis, the latter is often adopted for the realization of road profiles (Olivia *et. al.,* 2013), as shown below

$$h_r(x) = \sum_{s=1}^{N} A_s \cos(2\pi\, \Omega_s x + \theta_s) \tag{3.14}$$

where $h_r(x)$ is the deck surface random unevenness which is a Gaussian process (Shinozuka, 1971) with an independent random phase angle θ_s uniformly distributed from 0 to 2π. N is the number of terms used to build up the road surface roughness, .A_s is the amplitude of cosine wave, Ω_s is the spatial frequency (c/m) within the interval [Ω_L , Ω_U] where Ω_L , Ω_U are lower and upper cut-off frequencies of spatial unevenness . The parameters A_s and Ω_s are computed as

$$A_s = \sqrt{S_{GG}(\Omega_s)\Delta\Omega} \tag{3.15}$$

$$\Omega_s = \Omega_L + \left(s - \frac{1}{2}\right)\Delta\Omega \tag{3.16}$$

where $S_{GG}(\Omega_s)$ is the one-sided spatial power spectral density function (m^2/c/m) of road surface unevenness as given in Eq. (3.13).

The above equations shows that the power spectral density can be discretized into spatial frequency bands of a width of ΔΩ, and the corresponding discretized frequencies are used in the realization of the process as shown in Fig. 3.3. However, the entire frequency domain of the power spectral density cannot be used in the realization due to mathematical and physical reasons (Shinozuka, 1971). Cut-off frequencies are needed for the realizations of road surfaces. The discretizing frequency band is defined as:

$$\Delta\Omega = \frac{(\Omega_U - \Omega_L)}{N} \tag{3.17}$$

As mentioned earlier Ω_L, Ω_U are lower and upper cut-off frequencies respectively and N is the number of terms used to build up the road surface roughness.

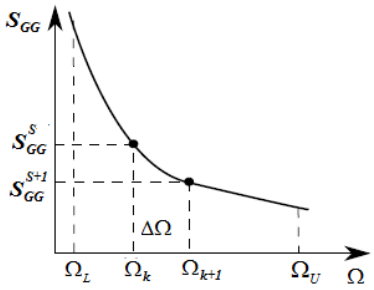

Fig. 3.3 Discretized one-sided power spectral density function

The long wavelength irregularities correspond to low frequency components and short wavelength irregularities correspond to high frequency components (Newland, 1993). The different wavelengths and their corresponding frequencies excite different vibrational modes of the heavy vehicle. The bouncing mode of the sprung mass is more of low frequency mode while the axle hop and pitching modes are of higher frequencies (Cebon, 1999). Furthermore, when the wavelengths of the irregularities are too small compared with the dimensions of the contact patch between the tire and the roadway, the tyre absorbs these irregularities due to its flexibility. This phenomenon is referred to as "tyre envelopment", which reduces the excitations of the axle of the vehicle. Therefore, filtering or smoothing algorithms are recommended (Newland 1986) depending on the dimension of the contact patch. Often a moving averaging filter is used for such purposes (Sayers and Karamihas, 1996). However, the effects of tyre envelopment of short wavelengths irregularities can be neglected for normal highway speeds, whereas for low speeds tyre envelopment becomes important and more detailed models for the contact patches may be significant (Captain *et. al.* 1979; Cebon, 1999).

The power spectral density function $S_{GG}(\Omega_s)$ (m^2/c/m) of road surface unevenness can be expressed as (Huang and Wang, 1992)

$$S_{GG}(\Omega_s) = S_{GG}(\Omega_0) \times \left(\frac{\Omega_s}{\Omega_0}\right)^{-m} \tag{3.18}$$

where Ω_0 is referred as discontinuity frequency and is taken as $1/2\pi$ (c/m). m and $S_{GG}(\Omega_0)$, are the roughness magnitude coefficient and the roughness shape coefficient respectively. They are indicators of roughness intensity. The ISO suggested that for m=2, lower cut off frequency Ω_L=0.1 c/m and upper cutoff frequency Ω_U = 2.0 c/m (Sun and Kennedy, 2002)

may be considered to determine dynamic load on the wheel induced by pavement unevenness.

On examination of the Eq. (3.18), it is revealed that at very low spatial frequency ($\Omega_s \rightarrow 0$), the power spectral density becomes unbounded, i.e., $S_{GG}(\Omega_s) \rightarrow \infty$. In view of this, Yin *et al* (Yin *et. al*. 2010) suggested an improved equation as follows,

$$S_{GG}(\Omega_s) = S_{GG}(\Omega_0) \times \frac{\Omega_0^2}{\Omega_s^2 + \Omega_L^2} \tag{3.19}$$

The PSD function given by Eq.(3.19) has been adopted in the present study. Using the relationship given in Eq. (3.12), the temporal spectral density function $S_{GG}(\omega_s)$ has been obtained from the spatial spectral density function $S_{GG}(\Omega_s)$ given in Eq. (3.19). ISO classified road into five classes, depending on different road surface conditions. Table 3.1 gives ISO specified values for this classification (ISO 8608: 1995).

Table 3.1 Road classification based on roughness magnitude coefficient (ISO 8608: 1995)

Road class	Road roughness coefficient $S_{GG}(\Omega_0)$ (10^{-6} m^2/c/m)
A (very good)	$2 < S_{GG}(\Omega_0) \leq 8$
B (good)	$8 < S_{GG}(\Omega_0) \leq 32$
C (average)	$32 < S_{GG}(\Omega_0) \leq 128$
D (poor)	$128 < S_{GG}(\Omega_0) \leq 512$
E (very poor)	$512 < S_{GG}(\Omega_0) \leq 2028$

3.4 Coupled System Equations

In the present section, theoretical models of bridge-vehicle system, required in the forward scheme of particle filtering method have been discussed. Different vehicle models in order of increasing complexity that have been considered to simulate bridge response are

(i) Bridge-Quarter Car Vehicle Model (Model-1)

(ii) Bridge-Half Car Vehicle Model with bending flexibility (Model-2)

(iii) Bridge-Full Car Vehicle Model with bending and torsional flexibility (Model-3).

3.4.1. Bridge-vehicle equations of motion for Model-1

In the present study, first a generic vehicle model known as "Quarter Car Model" has been adopted to implement the identification scheme. In this model, vehicle mass is considered to be lumped at the centroid of the vehicle. It is called as sprung mass and is denoted by symbol m_{qv}. The mass of wheel, tire and part of the suspension is referred to as the un-sprung mass m_w. The wheel contact is at one point only, and therefore, sometimes it is called as "single input model". Moreover, all motions are in vertical direction, and therefore it is also termed as "heave model". The characteristics of the vehicle suspension system have been assumed to be linear. The bridge-vehicle model has been shown in Fig. 3.4.

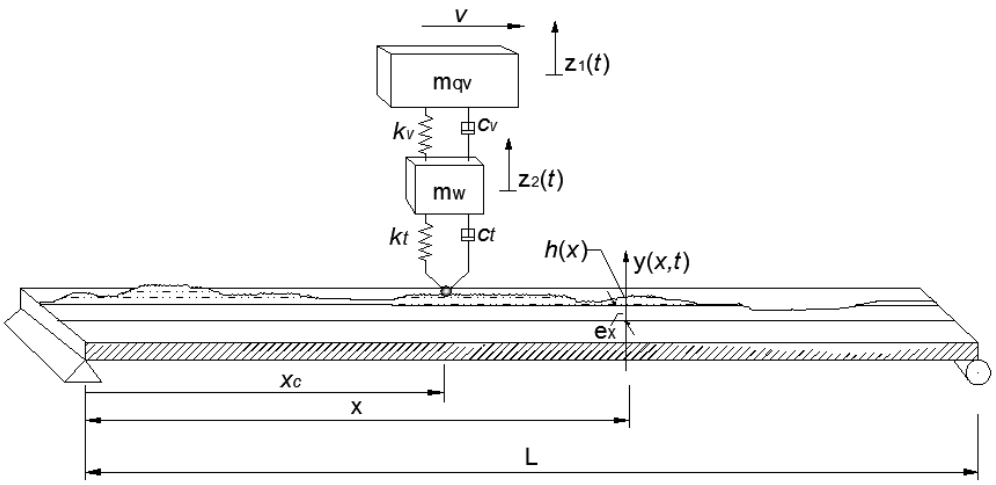

Fig. 3.4 Bridge subjected to Quarter Car vehicle Model

All translatory motions are assumed to be positive in upward direction. The sprung mass m_{qv} is subjected to heave motion z_1 in vertical direction. The vertical displacement of un-sprung mass m_w is z_2. The vehicle body and the un-sprung mass are connected by suspension system comprising spring element of stiffness k_v and dashpot with damping constant c_v respectively. Tyre stiffness and damping are k_t and c_t respectively. It may be noted that the vertical degrees of freedom z_1, z_2 and bridge deflection $y(x,t)$ are measured with reference to their respective static equilibrium position at any instant of time t. The equation of motion for the vehicle is coupled with the bridge equation of motion through the interaction force existing at the contact point of the two systems.

The governing differential equations of motion of the two lumped masses can be written as

$$m_{qv}\ddot{z}_1(t) + c_v\{\dot{z}_1(t) - \dot{z}_2(t)\} + k_v\{z_1(t) - z_2(t)\} = 0 \tag{3.20}$$

$$\begin{aligned} &m_w\ddot{z}_2(t) + k_t[z_2(t) - \{y(x_c,t) + h(x_c)\}] \\ &+ k_v\{z_2(t) - z_1(t)\} + c_v\{\dot{z}_2(t) - \dot{z}_1(t)\} + c_t[\dot{z}_2(t) - \{\dot{y}(x_c,t) + \dot{h}(x_c)\}] = 0 \end{aligned} \tag{3.21}$$

where $h(x)$ is the pavement roughness at a distance x from the reference station, x_c denotes the location of wheel contact form the same reference station. $h'(x) = \frac{dh}{dx}$, $\dot{h}(x) = \frac{dh}{dt} = V\frac{dh}{dx}$ and V is the speed of vehicle.

The vehicle may travel along the bridge in eccentric path. This gives rise to torsional motion in the bridge. The most of the bridge cross section is symmetrical about the vertical axis and therefore, bending and torsion can be analyzed independently when the eccentric vertical loading is transferred at the centre-line of the bridge as a combination of vertical load and torsional couple (Chatterjee *et.al*, 1994).

The governing differential equation of motion of the bridge in flexure and torsion can be expressed as

$$E_bI_b\frac{\partial^4 y(x,t)}{\partial x^4} + C_b\frac{\partial y(x,t)}{\partial t} + m_b\frac{\partial^2 y(x,t)}{\partial t^2} = f_b(x,t) \tag{3.22}$$

in which m_b *is* the mass per unit length, C_b is viscous damping per unit length whereas E_bI_b represents flexural rigidity of the bridge. The imposed vertical force $f_b(x,t)$ on the bridge due to vehicle interaction is given by

$$\begin{aligned} f_b(x,t) = -[&k_t\{z_2(t) - y(x,t) - h(x)\} + c_t\{\dot{z}_2(t) - y(x,t) - h(x)\}]\delta(x - x_c) \\ &-\{m_w + m_{qv}\}g\delta(x - x_c) \end{aligned} \tag{3.23}$$

The governing differential equation of torsional vibration of bridge can be written as

$$G_bJ_b\frac{\partial^2\gamma(x,t)}{\partial x^2} - C_{bT}\frac{\partial\gamma(x,t)}{\partial t} - I_{mb}\frac{\partial^2\gamma(x,t)}{\partial t^2} = f_T(x,t) \tag{3.24}$$

in which I_{mb}, represents the polar moment of inertia per unit length of bridge cross section, G_bJ_b is the torsional rigidity and C_{br} is the rotational damping per unit length of bridge respectively. The distributed torque due to eccentricity can be expressed as

$$f_T(x,t) = -[k_t\{z\ (t) - y(x,t) - h(x)\} + c_t\{\dot{z}\ (t) - y(x,t) - h(x)\}]e_x\delta(x - x_c) \\ -\{m_w + m_v\}g\, e_x\, \delta(x - x_c) \tag{3.25}$$

In the Eqs. (3.23) and (3.25), $\delta(.)$ is Dirac delta function. The function has the following property

$$\int_{-\infty}^{\infty} f(x)\,\delta(x - x_c)dx = f(x_c) \tag{3.26}$$

3.4.2. Bridge-vehicle equations of motion for Model-2

In the second model, vehicle body with two axles (front and rear) have been considered and named as "Half Car Model". However, the model has been improved considering bending of the vehicle body. The full vehicle body along the length has been represented as Euler-Bernoulli beam with bending flexibility. The length of the vehicle is l_v. The analysis is limited to the linear suspension characteristics. The bridge-vehicle model has been shown in Fig. 3.5.

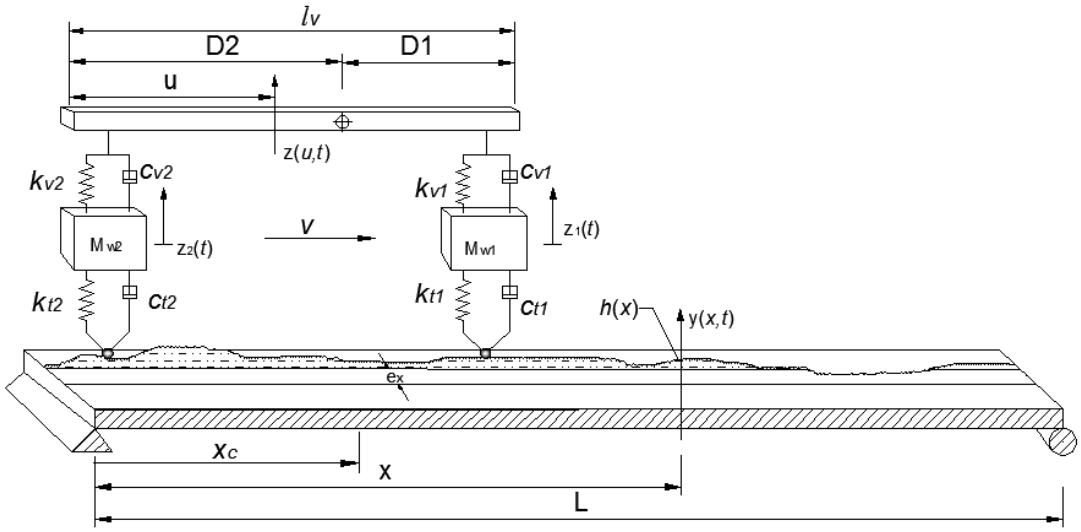

Fig. 3.5 Bridge subjected to Half Car vehicle Model

Vehicle centroid is located by the distance D_1 and D_2 measured from the trailing and leading edge of the vehicle body respectively. The governing differential equation of motion of the vehicle vertical deflection can be expressed as

$$E_v I_v \frac{\partial^4 z(u,t)}{\partial u^4} + C_v \frac{\partial z(u,t)}{\partial t} + m_v \frac{\partial^2 z(u,t)}{\partial t^2} = f_v(u,t) \tag{3.27}$$

in which m_v denotes the mass per unit length, , $E_v I_v$ is the flexural rigidity and C_v is viscous damping per unit length of the vehicle body, $z(u,t)$ represents vertical deflection of the vehicle body measured at location u from the reference point (taken at the left end of the vehicle) at time instant t. The vertical force imposed on the vehicle body is given by

$$f_{vF}(u,t) = \sum_{j=1}^{2} [k_{vj}\{z(u,t) - z_j(t)\} + c_{vj}\{\dot{z}(u,t) - \dot{z}_j(t)\}]\delta(u - u_j) \tag{3.28}$$

u_j represent the location of the attachment point of suspension from the reference point, $z_j(t)$ denote the vertical displacement of wheel, k_{vj} are the vehicle suspension stiffness, c_{vj} are the vehicle suspension damping. The subscript j=1, 2 represents the suspension location, for example j=1 denotes all quantities related to front suspension and j=2 for rear suspension.

The equations of motion for two un-sprung masses are given by

$$\begin{aligned} m_j \ddot{z}_j(t) + k_{tj}\{z_j(t) - y(x_j,t) - h(x_j)\} + k_{vj}\{z_j(t) - z(u_j,t)\} \\ + c_{tj}\{\dot{z}_j(t) - \dot{y}(x_j,t) - \dot{h}_i(x_j)\} + c_{vj}\{\dot{z}_j(t) - \dot{z}(u_j,t)\} = 0 \end{aligned} \quad (j=1, 2) \tag{3.29}$$

The governing differential equations of motion of the beam in bending and torsion are same as Eqs.(3.22) and (3.24). However, due two wheel inputs, time varying force and torque imposed on the bridge in Eqs.(3.22) and (3.24) has to be replaced by

$$\begin{aligned} f_b(x,t) = -\sum_{j=1}^{2} [k_{tj}\{z_j(t) - y(x,t) - h(x_j)\} + c_{tj}\{\dot{z}_j(t) - \dot{y}(x,t) - h(x)\}]\delta(x - x_j) \\ - \sum_{j=1}^{2} \{m_{wj} + \frac{1}{2} m_v l_v\} g\, \delta(x - x_j) \end{aligned} \tag{3.30}$$

$$\begin{aligned} f_T(x,t) = -\sum_{j=1}^{2} [k_{tj}\{z_j(t) - y(x,t) - h(x\ )\} + c_{tj}\{\dot{z}_j(t) - \dot{y}(x,t) - h(x)\}]e_x\, \delta(x - x_j) \\ - \sum_{j=1}^{2} \{m_{wj} + \frac{1}{2} m_v l_v\} g\, e_x \delta(x - x_j) \end{aligned} \tag{3.31}$$

In which $f_b(x,t)$ is the imposed vertical force and $f_T(x,t)$ is imposed torque on the bridge. k_{tj} and c_{tj} represent tyre stiffness and tyre damping at front axle (j=1) and rear axle (j=2) locations respectively.

3.4.3. Bridge-vehicle equations of motion for Model-3

A more realistic model of vehicle is a "Full Car Model", in which vertical motion (heave), rotation about the transverse axis (pitch) and rotation about longitudinal axis (roll) can be included. In vehicle dynamics, these motions are generally considered as rigid body modes. Since in the present study, one objective was to incorporate flexible modes of vehicle body, we idealized vehicle body as slender beam undergoing elastic bending and torsion in addition to rigid body modes. In Model-2, bending flexibility is already included. The Model-3 is the extension of Model-2 incorporating torsional mode of the vehicle. The bridge-vehicle model has been shown in Fig. 3.6. The vehicle undergoes rolling due to variation of transverse profile of deck. The bridge structure is subject to four point input which varies both in space and time.

The partial differential equations of motion of flexible vehicle body in bending and torsion are given by

$$E_v I_v \frac{\partial^4 z(u,t)}{\partial u^4} + C_v \frac{\partial z(u,t)}{\partial t} + m_v \frac{\partial^2 z(u,t)}{\partial t^2} = f_v(u,t) \tag{3.32}$$

$$GJ_v \frac{\partial^2 \theta_{vT}(u,t)}{\partial u^2} - C_{vT} \frac{\partial \theta_{vT}(u,t)}{\partial t} - I_{mv} \frac{\partial^2 \theta_{vT}(u,t)}{\partial t^2} = f_{vT}(u,t) \tag{3.33}$$

The symbols appearing in Eq.(3.32) have already been defined in section 3.4.2. In torsional vibration of vehicle body given by Eq.(3.33), the term G_vJ_v denotes torsional rigidity of the vehicle cross section, I_{mv} is mass moment of inertia about the centroid of vehicle body, C_{vT} is the rotational viscous damping per unit length of the vehicle body.

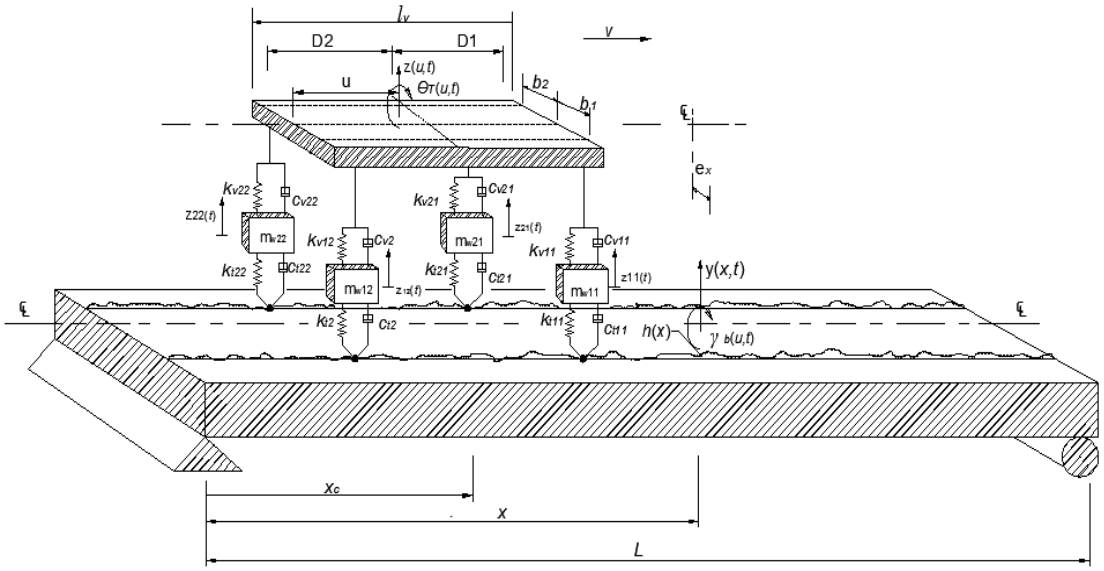

Fig. 3.6 Bridge subjected to Full Car vehicle Model

The imposed vertical force on the vehicle body is given by

$$f_{vF}(u,t) = \sum_{j=1}^{2}\sum_{i=1}^{2}[k_{vij}\{z(u,t)-z_{ij}(t)\}+c_{vij}\{\dot{z}(u,t)-\dot{z}_{ij}(t)\}]\delta(u-u_j) \qquad (3.34)$$

where index i=1,2 denotes right and left wheel on each axle, j=1,2 denotes front and rear axle of vehicle body. u_j represent the location of the attachment point of vehicle suspension from the reference point, z_{ij} denote the vertical displacement of wheel, k_{vij} are the vehicle suspension stiffness, c_{vij} are the vehicle suspension damping; $\delta(.)$ is Dirac delta function.

The imposed torque on the vehicle body is given by

$$f_{vT}(u,t) = \sum_{j=1}^{2}\sum_{i=1}^{2}(-1)^{1+i}[k_{vij}\{z(u,t)-z_{ij}(t)\}+c_{vij}\{\dot{z}(u,t)-\dot{z}_{ij}(t)\}]\, b_i\, \delta(u-u_j) \qquad (3.35)$$

where, b_i is the transverse distance of the particular wheel from the vehicle longitudinal axis. Index i=1, 2 denotes right and left wheel on each axle.

In this model, the vertical translation of four lumped un-sprung masses are governed by following equations

$$m_{wij}\ddot{z}_{ij}(t)+k_{tij}\{z_{ij}(t)-y_i(x_j,t)-h_i(x_j)\}+k_{vij}\{z_{ij}(t)-z(u_j,t)\}$$
$$+c_{tij}\{\dot{z}_{ij}(t)-\dot{y}_i(x_j,t)-\dot{h}_i(x_j)\}+c_{vij}\{\dot{z}_{ij}(t)-\dot{z}(u_j,t)\}=0 \quad (3.36)$$

(i=1,2; j=1,2)

In the above equation m_{wij} represents unsprung masses, where index i=1, 2 denotes right and left wheel on each axle, j=1, 2 denotes front and rear axle of vehicle body.

The governing equations of motion of the bridge remain same as in Model-1, with the exception that force and torque input over the bridge have to modified on account of four wheel contacts as

$$f_b(x,t)=-\sum_{j=1}^{2}\sum_{i=1}^{2}[k_{tij}\{z_{ij}(t)-y(x,t)-h_i(x_j)\}+c_{tij}\{\dot{z}_{ij}(t)-\dot{y}(x,t)-\dot{h}_i(x_j)\}]\delta(x-x_j)$$
$$-\sum_{j=1}^{2}\sum_{i=1}^{2}\{m_{wij}+\frac{1}{4}m_v l_v\}g\delta(x-x_j) \quad (3.37)$$

$$f_T(x,t)=\sum_{j=1}^{2}\sum_{i=1}^{2}(-1)^i[k_{tij}\{z_{ij}(t)-y(x,t)-h_i(x_j)\}$$
$$+c_{tij}\{\dot{z}_{ij}(t)-\dot{y}(x,t)-\dot{h}_i(x_j)\}]\times\{b_i-(-1)^i e_x\delta(x-x_j)\} \quad (3.38)$$
$$+\sum_{j=1}^{2}\sum_{i=1}^{2}(-1)^i\{m_{wij}+\frac{1}{4}m_v l_v\}g\times\{b_i-(-1)^i e_x\delta(x-x_j)\}$$

k_{tij} are the vehicle suspension stiffness, c_{tij} are the tyre stiffness and damping respectively. i=1, 2 is used for right and left wheel on each axle whereas subscript j=1,2 is for front and rear axle of vehicle body. The other symbols appearing in the Eqs.(3.37) and (3.38) have been already explained whenever they first appeared.

3.5 Closure

In this chapter, bridge-vehicle dynamic models have been developed using both continuous and lumped parameters approach. The bridge and vehicle in the model are coupled due to interaction force at the contact points. The mathematical model of the bridge has been represented by partial differential equations using both space and time variable in bending and torsional motion. Vehicle models have been developed in increasing order of complexity in order to use those in inverse solution and to compare their efficiency when field data would be used to identify the vehicle parameters. The flexibility of vehicle both in bending and torsion has been included in the present study. This aspect presented in the thesis is thought to be a new investigation in vehicle-bridge interaction dynamics as it has become

necessary due to evolution of long and slender vehicle in modern days. The non homogeneous pavement roughness in presence of variable mean has been incorporated in addition to Gaussian random profile represented by the power spectral density function. This is also practically significant due to development of localized defects in the pavement or due to special provisions in the constructions, which are not covered in classifying road conditions by ISO 8608 (1995).

4

DEVELOPMENT OF A SEMI-ANALYTICAL METHOD IN FORWARD SCHEME

4.1 Overview

The present method of moving load identification is based on Bootstrap Particle Filtering approach. This is an indirect inverse scheme which necessarily requires a forward solution. The "forward solution" is understood as the development of mathematical model of the system and its solution using analytical or numerical method. The process of parameter estimation involves huge amount of iterations in which one requires to repetitively generate response samples. In view of this computational cost and to avoid numerical instability, a semi analytical method has been proposed. The problems of numerical instability may arise due to mismatch of theoretical time step and sampling frequency of the data acquisition system. By use of the proposed method, any sampling frequency in theoretical calculation can be chosen in respect of measured data to improve accuracy of the parameter estimation. Moreover, the method does not require a smooth function of power spectral density function of random unevenness. In fact, the response integral are formulated taking into consideration of any form of power spectral density function that can be found from actual measured profile of the bridge pavement.

In the present section, a generalized procedure has been outlined to handle a combination of continuous and lumped parameter system used to model bridge-vehicle interaction dynamics. First, the partial differential equations (PDE) are discretized into ordinary differential equations (ODE) in generalized time dependent coordinates using mode superposition techniques. The uncoupled ODE along with lumped parameter equations of the model are then recast into state space form and again decoupled using time dependent complex eigen modes. A closed form solution of response integral has been derived corresponding to each input sample which was modeled as non-homogeneous process. In this way, response samples are generated to form 'ensemble' of the response process. Thereafter, Monte Carlo technique has been used to find the response statistics. This offers a great advantage to vehicle parameters identification using Bootstrap Particle Filtering method because of faster

generation of large number of samples. The proposed method of solution has also been utilized for studying the dynamic behavior of bridge-vehicle coupled system to examine the influence of various bridge-vehicle parameters on the response statistics.

4.2 Discretization of Partial Differential Equations

Three bridge-vehicle system models adopted in the present study as given in the previous chapter, consists of flexible vehicle body in Model-2 and Model-3. These are modeled by Partial Differential equations (PDE). The bridge model considered in the study is also a continuous system and therefore, represented mathematically by PDE. The equations of motion of the continuous systems have been discretized into normal coordinates using modal superposition technique (Inman 2001). For this, one needs to know natural frequencies and corresponding mode shapes of the continuous system.

4.2.1 Discretization of flexible vehicle equation of motions

Model-2 considers vehicle body as flexible in bending whereas Model-3 takes both elastic bending and torsion into account. The vehicle has been idealized as free-free beam. In Model-2, there are two rigid body modes (vertical bounce and pitch) in addition to modes in bending vibration. The Model-3 takes account of rigid body heave, pitch and rolling in addition to elastic bending and torsional modes.

4.2.1.1 Transverse vibration of vehicle body

Two rigid modes in transverse vibration of vehicle body can be written as

$$\begin{aligned} \phi_{-1} &= 1, \\ \phi_0 &= u - D_2 \end{aligned} \tag{4.1}$$

D_2 is the distance of vehicle centre of gravity from the trailing edge of the vehicle (refer Fig. 3.5 in Chapter-3), u represents distance along the vehicle body at time instant t from its trailing edge.

The elastic bending modes are obtained by solving the equation of motion (3.22) in absence of external force and damping. The solution for the elastic bending mode of the beam is given by (Inman, 2001)

$$\phi_{vk}(u) = A_1 \cosh(\beta_k u) + A_2 \cos(\beta_k u) + A_3 \sinh(\beta_k u) + A_4 \sin(\beta_k u) \tag{4.2}$$

where, $\beta_{vk} = \left(\frac{\omega_{vk}^{\ 2} m_v}{E_v I_v} \right)^{0.25}$ (4.3)

in which, index v represents vehicle, E_vI_v is the vehicle body flexural rigidity, $\phi_{vk}(u)$ is the k^{th} mode function of vehicle body in flexure corresponding to natural frequency ω_{vk}, A_i (i=1,2,…4) are the constants of integration to be determined from the boundary conditions.

The boundary conditions of the free-free beam can be written as

$$E_v I_v \frac{\partial^2 z(0,t)}{\partial u^2} = E_v I_v \frac{\partial^2 z(l_v,t)}{\partial u^2} = 0 \quad (4.4)$$

$$E_v I_v \frac{\partial^3 z(0,t)}{\partial u^3} = E_v I_v \frac{\partial^3 z(l_v,t)}{\partial u^3} = 0 \quad (4.5)$$

Application of boundary conditions in Eq. (4.2), a characteristic equation is obtained as below

$$\cosh(\beta_{vk} l_v)\cos(\beta_{vk} l_v) - 1 = 0 \quad (4.6)$$

The transcendental Eq.(4.6) can be solved for multiple values of β_{vk} , l_v and hence natural frequencies in elastic mode can be obtained from Eq.(4.3). Corresponding to each natural frequency, a mode shape function can be obtained from Eq.(4.2) as

$$\phi_{vk} = \sin(\alpha_k u) + \sinh(\alpha_k u) + \lambda_k[\cos(\alpha_k u) + \cosh(\alpha_k u)] \quad (4.7)$$

where,

$$\lambda_k = \frac{\cos(\alpha_k l_v) + \cosh(\alpha_k l_v)}{\sin(\alpha_k l_v) + \sinh(\alpha_k l_v)} \quad (4.8)$$

The displacement of the vehicle body at any location u measured from the trailing end of the vehicle now can be written using modal superposition theory of linear system as

$$z(u,t) = \sum_{k=-1}^{\infty} \phi_{vk}(u)\eta_{vk}(t) \quad (4.9)$$

where $\phi_{vk}(u)$ is the vehicle mode shapes, $\eta_{vk}(t)$ is the time dependent generalized coordinate, k is the mode number; k= -1, 0 are for two rigid body translatory and pitching mode, k=1,2,3…∞ represent elastic mode sequence of free-free beam. Although theoretically,

infinite number of elastic modes exists, for all practical purpose the modes are to be truncated to a finite size n_v.

Substituting Eq. (4.9) in Eq. (3.22) of Chapter-3, and multiplying both sides of the equation by $\phi_{vj}(u)$ and then integrating with respect to u from 0 to l_v, one has

$$\sum_{k=1}^{\infty}\int_0^{lv}\{E_vI_v\frac{d^4\phi_{vk}}{dz^4}\eta_{vk}(t)+C_v\phi_{vk}(u)\dot{\eta}_k(t)+m_v\phi_{vk}(u)\ddot{\eta}_{vk}(t)\}\phi_{vk}(u)du=\int_0^{lv}f_v(u,t)\phi_{vk}(u)du \quad (4.10)$$

Based on the assumption of proportional damping in the beam and employing orthogonality conditions of the modes (Inman, 2001), the equation of motion for transverse vibration of beam can be discretized as

$$\ddot{\eta}_{vk}(t)+2\xi_{vk}\omega_{vk}\dot{\eta}_{vk}(t)+\omega_{vk}^2\eta_{vk}(t)=Q_{vk}(t) \quad (4.11)$$

$$(k=-1,0,1,2,\ldots)$$

where ξ_{vk} is the modal damping ratio. The generalized force Q_{vk} is given by

$$Q_{vk}(t)=\frac{1}{M_{vk}}\int_0^{l_v}f_v(u,t)\phi_{vk}(u)du \quad (4.12)$$

Making use of the property of Dirac Delta function, generalized force $Q_{vk}(t)$ in the k^{th} mode of transverse vibration of vehicle body can be expressed as,

$$\begin{aligned}Q_{vk}=\frac{1}{M_{vk}}[&k_{v1}\{z_1(t)-\sum_{k=-1}^{n_v}\phi_{vk}(u_1)\eta_{vk}(t)\}\phi_{vk}(u_1)+c_{v1}\{\dot{z}_1(t)-\sum_{k=-1}^{n_v}\phi_{vk}(u_1)\dot{\eta}_{vk}(t)\}\phi_{vk}(u_1)\\&k_{v2}\{z_2(t)-\sum_{k=-1}^{n_v}\phi_{vk}(u_2)\eta_{vk}(t)\}\phi_{vk}(u_2)+c_{v2}\{\dot{z}_2(t)-\sum_{k=-1}^{n_v}\phi_{vk}(u_2)\dot{\eta}_{vk}(t)\}\phi_{vk}(u_2)]\end{aligned} \quad (4.13)$$

The term M_{vk} appearing in the above equations is the generalized mass in k^{th} mode and is given by

$$M_{vk}=\int_0^{l_v}m_v\phi_{vk}^2(u)du \quad (4.14)$$

Substituting Eq.(4.1) and Eq.(4.7) in Eq.(4.14) and performing the integration in the domain of the bridge, generalized mass can be expressed as

$$M_{v_{-1}}=m_vl_v \quad (4.15)$$

$$M_{v_O}=D_2^2l_vm_v-D_2l_v^2m_v+\frac{1}{3}l_v^3m_v \quad (4.16)$$

$$M_{vk} = \frac{1}{4\alpha_k} m_v [4\lambda_k \{\sin(\alpha_k l_v) + \sinh(\alpha_k l_v)\}^2 + \lambda_k^2 \{4\alpha_k l_v + \sin(2\alpha_k l_v) + \sinh(2\alpha_k l_v) + 4\cos(\alpha_k l_v)\sinh(\alpha_k l_v) + 4\sin(\alpha_k l_v)\cosh(\alpha_k l_v)\} - \sin(2\alpha_k l_v) + \sinh(2\alpha_k l_v) - 4\cos(\alpha_k l_v)\sinh(\alpha_k l_v) + 4\sin(\alpha_k l_v)\cosh(\alpha_k l_v)] \quad (4.17)$$

(k=1,2,3…)

4.2.1.2 Torsional Vibration of Vehicle body

The Model-3 is an improved version of Model-2 wherein the torsion of vehicle body in addition to bending has been considered. The equation of motion of flexible vehicle body in torsion can be discretized in a similar fashion once the natural frequencies in torsion and corresponding modes are known. The vehicle being free at the ends, elastic torsional modes will be accompanied by rigid rolling.

Thus one rigid mode can be written as

$$\bar{\phi}_{v0}(u) = 1 \quad (4.18)$$

The elastic torsional modes are obtained by solving the homogeneous part of the equation of motion (3.24) neglecting damping. The solution for the elastic torsional mode of the beam is given by (Inman 2001)

$$\bar{\phi}_{vk}(u) = \bar{A}_1 \cos(\bar{\gamma}_k u) + \bar{A}_2 \sin(\bar{\gamma}_k u) \quad (4.19)$$

(k=1,2,3….)

where, $\bar{\gamma}_k = \bar{\omega}_{vk} \sqrt{\frac{I_{mv}}{G_v J_v}}$ (4.20)

in which, G_vJ_v is a vehicle body torsional rigidity, I_{mv} is a mass moment of inertia, $\bar{\phi}_{vk}(u)$ is the k^{th} mode function of vehicle body in torsion corresponding to natural frequency $\bar{\omega}_{vk}$, $\bar{A}_i$ (i=1,2) are the constants of integration to be determined from the boundary conditions. The end conditions of the free-free beam in twisting can be expressed as,

$$G_v J_v \frac{\partial \theta_{Tv}(0,t)}{\partial u} = 0 \quad (4.21)$$

$$G_v J_v \frac{\partial \theta_{Tv}(l_v,t)}{\partial u} = 0 \quad (4.22)$$

Applying these conditions in Eq.(4.19), a characteristic equation is obtained as below

$$\sin \bar{\gamma}_k l_v = 0 \tag{4.23}$$

The Eq. (4.23) is satisfied by multiple roots, such as

$$\bar{\gamma}_k l_v = \pi, 2\pi, \ldots \tag{4.24}$$

Hence natural frequencies in elastic torsional mode can be obtained from Eq. (4.20). Corresponding to each natural frequency, a mode shape function for elastic torsion can be obtained from Eq. (4.19) utilizing the end conditions in Eq.(4.21) and (4.22) as

$$\bar{\phi}_{vk}(u) = \cos\left(\frac{k\pi u}{l_v}\right) \quad ; (k=1,2,3\ldots.) \tag{4.25}$$

Once, natural frequencies and corresponding modes are obtained, one can use mode summation principle to express the twist distribution along the length of the vehicle as

$$\theta_{Tv}(u,t) = \sum_{k=0}^{\infty} \bar{\phi}_{vk}(u)\, \bar{\psi}_{vk}(t) \tag{4.26}$$

where, $\bar{\phi}_{vk}(u)$ is the k^{th} mode function of vehicle body in torsion corresponding to natural frequency $\bar{\omega}_{vk}$, $\psi_{vk}(t)$ represents corresponding time dependent generalized coordinate used to describe torsional motion. k= 0 is taken to denote rigid body rolling mode, k=1,2,3…∞ are for elastic torsional modes. For practical applications only first n_{vT} torsional modes has to be taken into account.

Substituting Eq. (4.26) in Eq. (3.24) of Chapter-3 and following steps similar to the ones stated in case of discretization of bending equation of motion of the vehicle body, one obtains the uncoupled equation of motions for torsion as

$$\ddot{\bar{\psi}}_{vk}(t) + 2\bar{\xi}_{vk}\bar{\omega}_{vk}\dot{\bar{\psi}}_{vk}(t) + \bar{\omega}_{vk}^2\bar{\psi}_{vk}(t) = \frac{1}{\bar{M}_{vk}}\sum_{j=1}^{2}\sum_{i=1}^{2}(-1)^{1+i}[k_{vij}\{\sum_{k=0}^{n_{Tv}}\bar{\phi}_{vk}(u_j)\,\bar{\psi}_{vk}(t) - z_{ij}(t)\} + c_{vij}\{\sum_{k=0}^{n_{Tv}}\bar{\phi}_{vk}(u_j)\,\dot{\bar{\psi}}_{vk}(t) - \dot{z}_{ij}(t)\}]\, b_i\, \bar{\phi}_{vk}(u_j) \tag{4.27}$$

in which generalized mass $\bar{M}_{vk}$ in the k^{th} mode is given by

$$\bar{M}_{vk} = \int_0^{l_v} I_{mv}\bar{\phi}_{vk}^2(u)du \tag{4.28}$$

$$\overline{M}_{v0} = I_{mv} l_v \quad (k=0) \tag{4.29}$$

$$\overline{M}_{vk} = \frac{I_{mv} l_v}{4k\pi}\{2k\pi + \sin(2k\pi)\} \quad \text{for } k=1,2,3\ldots n_{vT} \tag{4.30}$$

4.2.2 Discretization of bridge equations of motions

4.2.2.1 Bending Vibration of bridge

The ends of the bridge are assumed to be simply supported, for which following conditions for vertical displacement and bending moments at the boundaries must be satisfied

$$y(0,t) = y(L,t) = 0 \tag{4.31}$$

$$E_b I_b \frac{\partial^2 y(0,t)}{\partial x^2} = E_b I_b \frac{\partial^2 y(L,t)}{\partial x^2} = 0 \tag{4.32}$$

Solution of free vibration of bridge yields the natural frequency of the beam in bending mode as

$$\omega_{bk} = (k\pi)^2 \sqrt{\frac{E_b I_b}{m_b L^4}} \tag{4.33}$$

in which k=1,2,…. denotes number of bending modes

The k^{th} mode of transverse vibration of beam can be obtained as

$$\phi_{bk}(x) = \sin \frac{k\pi x}{L} \tag{4.34}$$

where L is the length of the beam.

Using principle of mode superposition, one can write the transverse displacement of bridge at a location x as

$$y(x,t) = \sum_{k=1}^{\infty} \phi_{bk}(x)\eta_{bk}(t) \tag{4.35}$$

It is now possible to discretize partial differential equations of motion of the beam making use of the orthogonality conditions. The discretized equation of bending vibration of beam now can be written as

$$\ddot{\eta}_{bk}(t) + 2\xi_{bk}\omega_{bk}\dot{\eta}_{bk}(t) + \omega_{bk}^2 \ddot{\eta}_{bk}(t) = Q_{bk}(t) \tag{4.36}$$

where k=*1,2,3…….*n_b

The generalized force $Q_{bk}(t)$ in the k^{th} mode of bridge in flexure is given as,

$$Q_{bk}(t) = \frac{1}{M_{bk}} \int_0^L f_b(x,t)\phi_{bk}(x)dx \tag{4.37}$$

in which generalized mass M_{bk} in the k^{th} mode is given by

$$\begin{aligned} M_{bk} &= \int_0^L m_b \phi_{bk}^2(x)dx \\ &= \frac{m_b L}{4k\pi}\{2k\pi - \sin(2k\pi)\} \end{aligned} \tag{4.38}$$

Once the expression for vertically imposed forcing function over the beam for different vehicle models are known in Chapter-3 (Eqs 3.23, 3.28 and 3.34), it is now possible to find the expression for the generalized forces in transverse motion of the bridge for each model using Eq.(4.37).

Model-1

The generalized force for Model-1 is derived as

$$\begin{aligned} Q_{bk}(t) = \frac{1}{M_{bk}}\Big(& [k_t\{z_2(t) - \sum_{k=1}^{n_b}\phi_{bk}(x_j)\eta_{bk}(t) - h(x)\} + c_t\{\dot{z}_2(t) \\ & - \sum_{k=1}^{n_b}\phi_{bk}(x_j)\dot{\eta}_{bk}(t) - h(x)\}]\phi_{bk}(x_c) - \{m_w + m_{qv}\}g\phi_{bk}(x_c)\Big) \end{aligned} \tag{4.39}$$

In the above equation, Q_{bk} is the generalized force in k^{th} mode of the beam, M_{bk} stands for generalized mass of the beam in the k^{th} mode, k_t, c_t are the tyre stiffness and damping of the beam, $\phi_{bk}(x)$ is the mode shape function at a spatial coordinate x. Other symbols appearing in Eq.(4.39) have been already defined whenever they first appeared.

Model-2

The generalized force for Model-2 is expressed as

$$\begin{aligned} Q_{bk}(t) = \frac{1}{M_{bk}}\Big(& \sum_{j=1}^{2}[k_{tj}\{z_j(t) - \sum_{k=1}^{n_b}\phi_{bk}(x_j)\eta_{bk}(t) - h(x_j)\} \\ & + c_{tj}\{\dot{z}_j(t) - \sum_{k=1}^{n_b}\phi_{bk}(x_j)\dot{\eta}_{bk}(t) - \dot{h}(x_j)\}]\phi_{bk}(x_j) - \frac{1}{M_{bk}}\sum_{j=1}^{2}\{m_{wj} + \frac{1}{2}m_v l_v\}g\ \phi_{bk}(x_j)\Big) \end{aligned} \tag{4.40}$$

In this equation, impressed force over the bridge acts at two locations, x_j (j=1,2) due to two wheels on the vehicle. Accordingly, in Eq.(4.40), one has to refer the quantities at two wheel location, the parameters are subscripted by a location index j, in which we denote j=1 for front suspension and front tyre where as j=2 refers to rear suspension and rear tyre. Other parameters have been already introduced while formulating the equation of motions of the Model-2.

Model-3

In Model-3, the generalized force has been expressed as

$$Q_{bk}(t) = \frac{1}{M_{bk}}\Big(\sum_{j=1}^{2}\sum_{i=1}^{2}[k_{tij}\{z_{ij}(t) - \sum_{k=1}^{n_b}\phi_{bk}(x_j)\eta_{bk}(t) - h_i(x_j)\} + c_{tij}\{\dot{z}_{ij}(t) - \sum_{k=1}^{n_b}\phi_{bk}(x_j)\dot{\eta}_{bk}(t) - \dot{h}_i(x_j)\}]\phi_{bk}(x_j) - \frac{1}{M_{bk}}\sum_{j=1}^{2}\sum_{i=1}^{2}\{m_{wij} + \frac{1}{4}m_v l_v\} g\ \phi_{bk}(x_j)\ \Big) \quad (4.41)$$

Due to four wheel contacts, imposed forces are acting at four locations. The location of wheels are specified by two *location* subscripts i, j (i=1,2; j=1,2). The first subscript i take the value of 1 for right and 2 for left locations. As explained earlier, second subscript j=1 is used for front and j=2 is used for rear locations. Thus it is possible to recognize the contribution of each wheel to transfer the moving load over the bridge. Moreover, the wheels are likely to sense unequal pavement profile at their location in real situation, which makes the vehicle to exhibit, translatory motion in vertical direction coupled with rotational motion about longitudinal and transverse axis. Other symbols not defined in this paragraph, convey similar meanings as stated in case of Model-1 and Model-2.

4.2.2.2 Torsional Vibration of bridge

It has been mentioned earlier that present method of analytical solution considers eccentricity of vehicle path. As a result, torsion is caused on the bridge cross section. It is assumed that ends of the bridge is prevented from rotation (Chatterjee *et al*,1994) and hence following end conditions should be taken into the account for solving partial differential equation of torsional of motion of the bridge

$$\theta_{Tb}(0,t) = 0 \quad (4.42)$$

$$\theta_{Tb}(L,t) = 0 \tag{4.43}$$

The solution for the elastic torsional mode of the beam is given by (Inman 2001)

$$\phi_{Tl}(x) = \overline{C}_1 \cos(\vartheta_l x) + \overline{C}_2 \sin(\vartheta_l x) \tag{4.44}$$

(l=1,2,3….)

$\overline{C}_i$ (i=1, 2) are the constants of integration to be determined from the boundary conditions.

Application of boundary conditions Eqs.(4.42) and (4.43) in Eq. (4.44), yields following expression for natural frequency and corresponding modes

$$\omega_{Tl} = \frac{l\pi}{L}\sqrt{\frac{G_b J_b}{I_{mb}}} \tag{4.45}$$

$$\phi_{Tl}(x) = \sin(\frac{l\pi}{L}x) \tag{4.46}$$

in which, G_bJ_b is a bridge torsional rigidity, I_{mb} is a mass moment of inertia of bridge, $\phi_{Tl}(x)$ is the l^{th} mode function of vehicle body in torsion corresponding to natural frequency ω_{Tl}, Now one can express the twist of the bridge cross section due to load caused by eccentric vehicle path as

$$\theta_{Tb}(x,t) = \sum_{l=1}^{\infty} \phi_{Tl}(x_j)\gamma_l(t) \tag{4.47}$$

where, $\phi_{Tl}(x)$ is the l^{th} mode function of bridge in torsion corresponding to natural frequency, ω_{Tl} ,$\gamma_l(t)$ represents time dependent generalized coordinate. l=1,2,3…n_T represent elastic mode sequence of fixed-fixed beam and n_{vT} is the number of significant modes of flexible vehicle body in torsion.

Following similar procedure for discretization of torsional equation as outlined earlier in case of vehicle body, the decoupled equations of motion in torsional vibration of bridge can be written as

$$\ddot{\gamma}_l(t) + 2\xi_{Tl}\omega_{Tl}\dot{\gamma}_l(t) + \omega_{Tl}^2\gamma_l(t) = Q_{Tl}(t), \qquad (l=1, 2, 3\ldots n_T) \tag{4.48}$$

where n_T represents number of bridge torsional modes, ω_{Tl} and ξ_{Tl} are the natural frequency and modal damping coefficient of the l^{th} mode in torsion respectively. The generalized torque in the l^{th} mode is given by,

$$Q_{Tl}(t) = \frac{1}{M_{Tl}} \int_0^L f_T(x,t)\phi_{Tl}(x)dx \tag{4.49}$$

The torsional natural frequency ω_{Tl} and corresponding to mode ϕ_{Tl} for the given simply supported boundary conditions with no warping restraints have been taken from reference (Inman 2001). The generalized mass moment of inertia M_{Tl} in the l^{th} mode is given by,

$$M_{Tl} = \int_0^L I_{mb}\phi_{Tl}^2(x)dx \tag{4.50}$$

$$M_{Tl} = \frac{I_{mb}L}{4l\pi}\{2l\pi + \sin(2l\pi)\} \tag{4.51}$$

Due to change of number of wheel input over the bridge in different bridge-vehicle interaction model, one can now find the generalized torque for different model chosen in the present study. For each model, the imposed torque is now given below.

Model-1

The generalized torque expression in Model-1 can be written as

$$\begin{aligned} Q_{Tl} = \frac{1}{M_{Tl}}[k_t\{z(t) - \sum_{l=1}^{n_T}\phi_{Tl}(x_j)\gamma_l(t) - h(x)\} + c_t\{\dot{z}(t) - \sum_{l=1}^{n_T}\phi_{Tl}(x_j)\dot{\gamma}_l(t) - h(x)\}]e_x\phi_{Tl}(x_c) \\ - \frac{1}{M_{Tl}}\{m_w + m_{qv}\}g\, e_x\, \phi_{Tl}(x_c) \end{aligned} \tag{4.52}$$

in which Q_{Tl} is generalized torque in the l^{th} mode generated due to eccentricity of the vehicle path. It may be noted that when the vehicle follow centerline of the bridge, e_x=0 and therefore only bending vibration of the bridge is relevant.

Model-2

In Model-2, one can express the generalized torque as

$$Q_{Tl} = \frac{1}{M_{Tl}} \sum_{j=1}^{2} [k_{t\,j} \{ \sum_{l=1}^{n_T} \phi_{Tl}(x_j) \gamma_l(t) - z_j(t) - h(x_j) \}$$
$$+ c_{t\,j} \{ \sum_{l=1}^{n_T} \phi_{Tl}(x_j) \dot{\gamma}_l(t) - \dot{z}_j(t) - \dot{h}(x_j) \}] \, e_x \phi_{Tl}(x_j) \; - \frac{1}{M_{T\,l}} \sum_{j=1}^{2} \{ m_{w\,j} + \frac{1}{2} m_v l_v \} \, g \, e_x \, \phi_{Tl}(x_j) \tag{4.53}$$

Here again modal contribution on the impressed torque over the bridge is coming from two axle loads, whose locations are specified by the index *j*. As before, *j*=1 is taken to denote front wheel and *j*=2 for rear wheel. Meaning of other symbols has been defined earlier.

Model-3

The expression for the generalized torque on the bridge causing torsion can be derived as

$$Q_{Tl} = \frac{1}{M_{Tl}} \sum_{j=1}^{2} \sum_{i=1}^{2} (-1)^i [k_{t\,i\,j} \{ \sum_{l=1}^{n_T} \phi_{Tl}(x_j) \gamma_l(t) - z_{i\,j}(t) - h_i(x_j) \}$$
$$+ c_{t\,i\,j} \{ \sum_{l=1}^{n_T} \phi_{Tl}(x_j) \dot{\gamma}_l(t) - \dot{z}_{i\,j}(t) - \dot{h}_i(x_j) \}] \times \{ b_i - (-1)^i e_x \} \phi_{Tl}(x_j) \tag{4.54}$$
$$- \frac{1}{M_{T\,l}} \sum_{j=1}^{2} \sum_{i=1}^{2} \{ m_{wi\,j} + \frac{1}{4} m_v l_v \} g \times \{ b_i - (-1)^i e_x \} \phi_{Tl}(x_j)$$

where location of wheels are specified by two location subscripts *i*, *j* (*i*=1,2; *j*=1,2). Subscript *i* take the value of 1 for right and 2 for left locations. Similar to Model-2, second subscript *j*=1 is used for front and *j*=2 is used for rear locations. b_i is the transverse distance of the particular wheel (left or right) from the vehicle longitudinal axis and e_x is the distance of particular wheel from the bridge centerline.

4.3 Response Statistics

The system equations for each model are coupled second order ordinary differential equations which can be expressed in matrix notation as

$$[M]\{\ddot{r}(t)\} + [C(t)]\{\dot{r}(t)\} + [K(t)]\{r(t)\} = \{F(t)\} \tag{4.55}$$

where, $\{r\,(t)\}$ is the response vector, $\{F(t)\}$ is the generalized stochastic force vector. $[M]$, $[C(t)]$ and $[K\,(t)]$ are system mass, damping and stiffness matrix respectively. It may be noted that the effect of coupling of the bridge-vehicle motion has been reflected in the time dependent damping and stiffness matrices because of change in wheel position with time. Sizes of the system matrix (n) are different for each vehicle model, as shown in Table 4.1.

Table 4.1 Matrix size for different model

Model No	Matrix size (n)
1	$(2+n_b+n_T)\times(2+n_b+n_T)$
2	$(n_v+2+n_b+n_T)\times(n_v+2+n_b+n_T)$
3	$(n_v+n_{vT}+4+n_b+n_T)\times(n_v+n_{vT}+4+n_b+n_T)$

State-space representation of system equations is suitable for bridge-vehicle interaction problems, since suspension damping is not small and diagonalization of damping matrix as in case of Rayleigh's damping in configuration space may not be fully convincing. Second order coupled system equations can be converted to $2n$ dimensional first order differential equation as follows (Juang, 1994)

Multiplying both sides of equation (4.55) by $[M]^{-1}$, we have

$$[M]^{-1}[M]\{\ddot{r}(t)\}+[M]^{-1}[C(t)]\{\dot{r}(t)\}+[M]^{-1}[K(t)]\{r(t)\}=[M]^{-1}\{F(t)\} \tag{4.56}$$

or $$[I]\{\ddot{r}(t)\}+[M]^{-1}[C(t)]\{\dot{r}(t)\}+[M]^{-1}[K(t)]\{r(t)\}=[M]^{-1}\{F(t)\} \tag{4.57}$$

where $[I]$ is an identity matrix

Introducing an identity

$$\{\dot{r}(t)\}-\{\dot{r}(t)\}=\{0\} \tag{4.58}$$

The above equation (4.57) and (4.58) can be augmented to $2n$ size as

$$\begin{Bmatrix}\{\ddot{r}(t)\}\\ \{\dot{r}(t)\}\end{Bmatrix}+\begin{bmatrix}[M]^{-1}[C(t)] & [M]^{-1}[K(t)]\\ -[I] & [0]\end{bmatrix}\begin{Bmatrix}\{\dot{r}(t)\}\\ \{r(t)\}\end{Bmatrix}=\begin{Bmatrix}[M]^{-1}\{F(t)\}\\ \{0\}\end{Bmatrix} \tag{4.59}$$

Let $\{p(t)\}$ be a $2n$ dimensional vector defined by

$$\{p(t)\}=\begin{Bmatrix}\{\dot{r}(t)\}\\ \{r(t)\}\end{Bmatrix} \tag{4.60}$$

The vector $\{p(t)\}$ that contains the displacements and velocities is termed as the state vector (Juang, 1994). Similarly, state matrix $[A(t)]$ and state load vector $\{P(t)\}$ can be expresse as

$$[A(t)] = \begin{bmatrix} [M]^{-1}[C(t)] & [M]^{-1}[K(t)] \\ -[I] & [0] \end{bmatrix} \tag{4.61}$$

$$\{P(t)\} = \begin{Bmatrix} [M]^{-1}\{F(t)\} \\ \{0\} \end{Bmatrix} \tag{4.62}$$

Using Eqs. (4.60), (4.61) and (4.62), system equation of motion (4.59) can be rewritten as

$$\{\dot{p}(t)\} + [A(t)]\{p(t)\} = \{P(t)\} \tag{4.63}$$

Let the eigenvalues of the state matrix $[A(t)]$ be $\alpha_1(t)$, $\alpha_2(t)$, $\alpha_3(t)$,..... $\alpha_{2n}(t)$ and the corresponding complex conjugate eigenvectors be $\{u(t)\}^1$, $\{u(t)\}^2$, $\{u(t)\}^3 \ldots \{u(t)\}^{2n}$.

Let the modal matrix $[U(t)]$ be formed with eigenvectors arranged in column and then using linear transformation $\{p(t)\}=[U(t)]\{v(t)\}$ in Eq.(4.63), along with orthogonality condition of the complex eigen vectors, the decoupled first order system is given below (Nigam, 1983)

$$\dot{v}_j(t) + \alpha_j v_j(t) = R_j(t), \qquad j = 1,2,3....2n \tag{4.64}$$

where

$$R_j = \sum_{k=1}^{n} u'_{js} \sum_{s=1}^{n} m'_{sk} F_k(t) \tag{4.65}$$

u'_{js} denotes elements in the inverse of the matrix $[U(t)]$ and m'_{sk} the elements in the inverse of matrix $[M]$.

The general solution of Eq. (4.64) in Stieltjes integral (Nigam, 1983) form may be expressed as

$$v_j(t) = X_{0j} \exp(-\alpha_j t) + \int_{-\infty}^{\infty} H_j(\omega, t) dS[R_k(\omega)] \tag{4.66}$$

where X_{0j} are constants of integration to be determined from the initial conditions. $H_j(\omega,t)$ is the transient frequency response function given by (Nigam 1983)

$$H_j(\omega, t) = \frac{1}{i\omega - \alpha_j}[\exp(-i\omega t) - \exp\{-\alpha_j(t - t_0)\}] \tag{4.67}$$

Here i is the imaginary unit. It can be seen that as $t_0 \rightarrow -\infty$, for the positive real part of α_j, $H_j(\omega,t)$ approaches the limiting value $[1/(-i\omega+\alpha_j)]\exp(-i\omega t)$. Eq. (4.67) can be rewritten as

$$H_j(\omega,t) = \frac{1}{-i\omega + \alpha_j}\{\exp(-i\omega t)\} \tag{4.68}$$

This is the characteristics of stable dynamic system. Using Eqs. (4.60) and (4.65) in Eq. (4.66), the original response vector $\{r(t)\}$ may be recovered as

$$r_m(t) = \sum_{j=1}^{2n} u_{m+n,j} X_{0j} \exp(-\alpha_j t) + \sum_{j=1}^{2n} u_{m+n,j} \sum_{s=1}^{n} u'_{js} \sum_{k=1}^{n} m'_{sk} \int_{-\infty}^{\infty} H_j(\omega,t) dS(F_k(\omega)) \tag{4.69}$$
$$m = 1,2,3.....n$$

The first term of Eq. (4.69) represents homogeneous solution of the system equation due to initial conditions where the second term of the equation is the contribution of forcing vector. Using the limiting value of transient frequency response function $H_j(\omega,t)$ as described by Nigam (1983), one can express the non homogeneous solution of Eq.(4.69) as,

$$r_{Pm}(t) = \sum_{j=1}^{2n} u_{m+n,j} \sum_{s=1}^{n} u'_{js} \sum_{k=1}^{n} m'_{sk} \int_{-\infty}^{\infty} \frac{\exp(i\omega t)}{-i\omega + \alpha_j} F_k(\omega) d\omega \tag{4.70}$$

in which $r_{Pm}(t)$ is the particular integral of the differential equation (4.69). $F_k(\omega)$ is the Fourier integral of $F_k(t)$, given as

$$F_k(\omega) = \frac{1}{2\pi} \int_{-\infty}^{\infty} F_k(\tau) \exp(-i\omega\tau) d\omega \tag{4.71}$$

Using Eq.(4.71) in Eq.(4.70) and changing the order of integration, Eq. (4.70) can be written as

$$r_{Pm}(t) = \sum_{j=1}^{2n} u_{m+n,j} \sum_{s=1}^{n} u'_{js} \sum_{k=1}^{n} m'_{sk} \int_{-\infty}^{\infty} F_k(\tau) \left[\frac{1}{2\pi} \int_{-\infty}^{\infty} \frac{\exp[i\omega(\tau - t)]}{-i\omega + \alpha_j} d\omega \right] d\tau \tag{4.72}$$

The improper integral inside the parenthesis can now be evaluated using Cauchy's Residue theorem (Jeffrey, 2004). Now, mapping ω to z for evaluating the integral one can write

$$\int_{-\infty}^{\infty} f(z) dz = -2\pi i \sum_{k=1}^{n} \text{Re}\, sidue[f(z); z_k] \tag{4.73}$$

$$\text{where} \quad f(z) = \frac{\exp[i z(\tau - t)]}{-i z + \alpha_j} \tag{4.74}$$

z_k are pole of the analytic function $f(z)$. In this case only one pole z_1=-iα_j in lower half of the Argand plane exists, hence Residue of the function $f(z)$ can be obtained as

$$\text{Re}\,sidue\,[f(z);z_1] = -\frac{1}{i}\exp\{\alpha_j(\tau - t)\} \tag{4.75}$$

Using Eq.(4.75) in Eq.(4.73) and thereafter substituting the resulting expression in Eq.(4.72), particular solution of the decoupled system equation can be expressed in a compact form.

$$r_{Pm}(t) = \sum_{j=1}^{2n} u_{m+n,j} \sum_{s=1}^{n} u'_{js} \sum_{k=1}^{n} m'_{sk} I_{jk} \tag{4.76}$$

where,

$$I_{jk} = \int_0^t \exp[\alpha_j(\tau - t)] F_k(\tau) d\tau \tag{4.77}$$

in which t is the bridge loading time defined as $t=x/V$ where x is the distance traversed by the vehicle at instant t, V is the constant speed of the vehicle. When the vehicle is at the point of exit, then $t=L/V$ where L is the span of the bridge. The index j=1,2,3….,2n is size of state vector and k=1,2,3…,n represents size of coupled system response vector.

Using Eq. (4.76), the general solution Eq. (4.69) now can be expressed in compact form

$$r_m(t) = \sum_{j=1}^{2n} u_{m+n,j} X_{0j} \exp(-\alpha_j t) + \sum_{j=1}^{2n} u_{m+n,j} \sum_{s=1}^{n} u'_{js} \sum_{k=1}^{n} m'_{sk} I_{jk} \tag{4.78}$$

Since, $F_k(t)$ is a random function in time variable due to moving wheel experiencing unevenness of bridge deck, the integral in most of the studies have been found by numerical method after digitally simulating roughness profile. In the present study, closed form expressions for the components of the above integral which generates each of the response samples have been developed for all the models and given in Appendix-A, B and C separately for easy referral. Thus response time history sample (sample output) corresponding to each sample of surface roughness (sample input) can be developed. Collecting all such output samples, the ensemble of random process is formed as

$$\{Y(t)\} = \{y_1(t), y_2(t), ..., y_n(t)\} \tag{4.79}$$

where $y_j(t)$ is the j^{th} sample time history in the ensemble set. At each time step t_k, $y_j(t_k)$ is the j^{th} realization of random process $Y(t_k)$. Thus one can find the mean $\mu_Y(t_k)$ and standard deviation $\sigma_Y(t_k)$ of the random process $Y(t)$ at any time step t_k, using the principle of statistics (Nigam, 1983) as

$$\mu_Y(t_k) = \frac{1}{N_s} \sum_{j}^{Ns} y_j(t_k) \tag{4.80}$$

$$\sigma_Y(t_k) = \sqrt{\frac{1}{N_s - 1}\sum_{j=1}^{Ns}\{y_j(t_k) - \mu_Y(t_k)\}^2} \tag{4.81}$$

in which N_s represents number of time history samples inside the ensemble set $\{Y(t)\}$.

4.4 Dynamic Amplification Factor

The dynamic effects resulting from the passage of vehicles is an important problem generally encountered in the bridge design. These effects need further attention as they may produce an unacceptable stresses in the bridge structures beyond the permissible limit due to repetitive action of vehicle. Traditionally, these dynamic effects have been taken into account by multiplying the static bridge response with a dynamic amplification factor. However, dynamic analysis is necessary when ideal conditions are not met.

Dynamic Amplification Factor from response statistics has been calculated in the present study taking contribution of mean and standard deviation as discussed below:

Considering any response variable Y as random process, and assuming 95% confidence interval which extends the sample distribution approximately two times the standard error of the mean (SEM) in each direction from the mean, the maximum dynamic response can be written as

$$Y_{dynamic} = \left|\mu_Y(x_k, t_k) + \mathrm{E}_Y(x_k, t_k)\right| \tag{4.82}$$

where $Y_{dynamic}$ denotes the maximum response due to fluctuating load imposed on the bridge due to vibratory motion of the vehicle, $\mu_k(x_k,t_k)$ is the mean response and $\mathrm{E}_k(x_k,t_k)$ is a standard error of the mean (SEM) defined as (DeCoursey, 2003)

$$\mathrm{E}_Y(x_k, t_k) = \frac{\sigma_Y(x_k, t_k)}{\sqrt{N_s/4}} \tag{4.83}$$

in which $\sigma_Y(x_k, t_k)$ is a standard deviation of bridge response and N_s is a number of samples.

Thus, Dynamic Amplification Factor (DAF) in this study is defined as

$$DAF = \frac{Y_{static} + Y_{dynamic}}{Y_{static}} = 1 + \frac{Y_{dynamic}}{Y_{static}} = 1 + DI \tag{4.84}$$

where, Y_{static} refers to the maximum static response of the bridge for adverse position of the wheel loads, DI represents dynamic increment.

4.5 Closure

In this chapter, semi-analytical solutions for three different coupled system models have been developed. Flexibility of vehicle body in bending and torsion has been included. Mode superposition technique has been employed to discretize partial differential equations (PDE) into ordinary differential equations (ODE) in generalized time dependent coordinates for the continuous systems. The uncoupled ODE along with lumped parameter equations of the model are then recast into state space form and again decoupled using time dependent complex eigen modes. Corresponding to each input sample, modeled as non-homogeneous process, a closed form solution of response integral has been derived. Thus 'ensemble' of the response process has been formed and processed to obtain response statistics using Monte Carlo technique. Due to faster generation of large number of samples, the proposed method of solution is expected to offer a great advantage to vehicle parameters identification using Bootstrap Particle Filtering method. In addition to this, the present solution has also been utilized to examine the influence of various bridge-vehicle parameters on the dynamic behavior of bridge-vehicle coupled system.

5

FIELD TESTING AND FINITE ELEMENT MODEL UPDATING

5.1 Overview

Full scale bridge dynamic test is the most reliable method to determine true dynamic properties such as, natural frequencies, mode shapes and damping ratios of bridge which can be used as a basis for validating or updating a theoretical model so that the model represents the actual bridge properties and boundary conditions. Bridge dynamic behavior obtained from field test is also used to assess the condition of the bridge and to estimate fatigue life of the bridge. In the present work, dynamic test on an existing bridge has been conducted with a loaded truck moving over the bridge. The main purpose of conducting field test and to acquire bridge acceleration record is to estimate the loaded truck weight and suspension parameters by solving an inverse problem. The particle filter algorithm has been employed utilizing measured response. This information is very valuable to judge the vehicle fitness also. The present chapter describes the detail of instrumentation used, procedure for test and data acquisition during field test. The finite element model of Test Bridge has been developed in commercially available software SAP 2000. The field data also serves the purpose of updating of physical properties of the theoretical Bridge Models to be used in forward scheme of particle filtering method.

5.2 Test Bridge

The test bridge has been selected considering some important issues such as obstruction to traffic flow, difficulties in instrumentation, structural behavior and span to width ratio. After careful thoughts, a concrete bridge located at approach road to Indian Institute of Technology Guwahati from NH-31 near Agyathuri Railway station, around 16 km from Guwahati Railway Junction, has been selected in the present study. The bridge serves the purpose of railway over bridge (ROB) to facilitate uninterrupted road traffic during passing of trains under the bridge. A photograph of the test bridge is shown in Fig. 5.1. The test bridge is of three spans and of double lane. The total length of bridge is 89 m, with middle span 39 m (clear) and both approach span 23 m (clear). The total lane width is 7.5 m. Each lane is independent and separated by divider (Fig.5.2 and Fig. 5.3). The divider walls are constructed

with 0.2m×0.2 m×0.5 m concrete blocks. A gap of 1.5m between two side walls is filled with soil. The test bridge construction started in the year 2003 and after completion it was opened for traffic in the year 2006. Since then there is a noticeable vibration of structures when moving load passes. Even this is felt by pedestrian on the other lane. As per the design drawings, M35 grade of concrete and Fe 415 steel was used in the construction. The bridge has four post tensioned cast in situ pre-stressed concrete girders at 2.4 m spacing and six middle cross girders. Rocker and roller type bearing has been used for the supports at the ends of each span. Bridge deck was cast with 200 mm thick RC slab over which asphalt concrete of thickness 150 mm was laid. Middle span is instrumented for dynamic test.

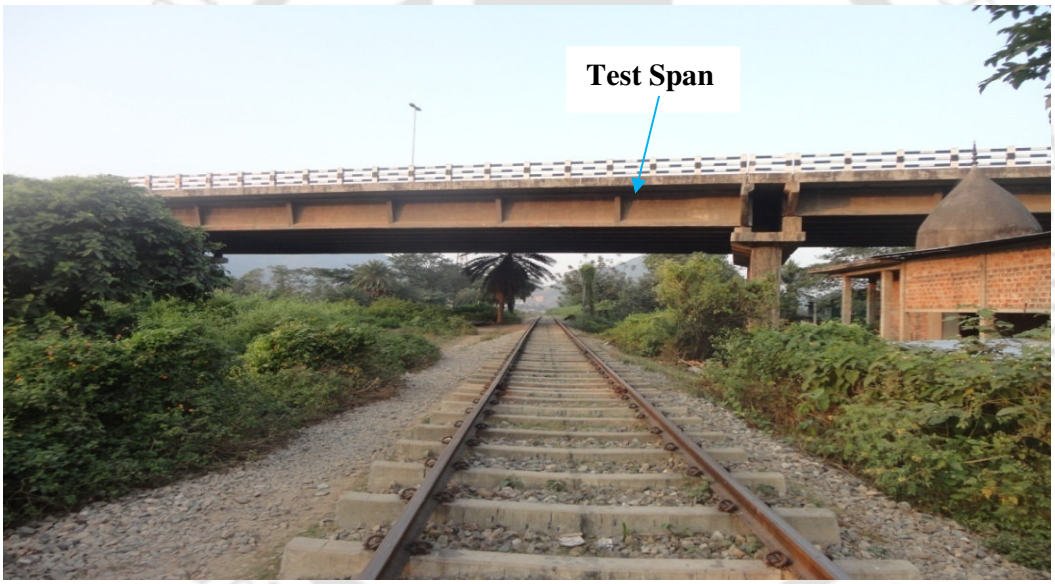

Fig. 5.1 Photograph of the tested bridge

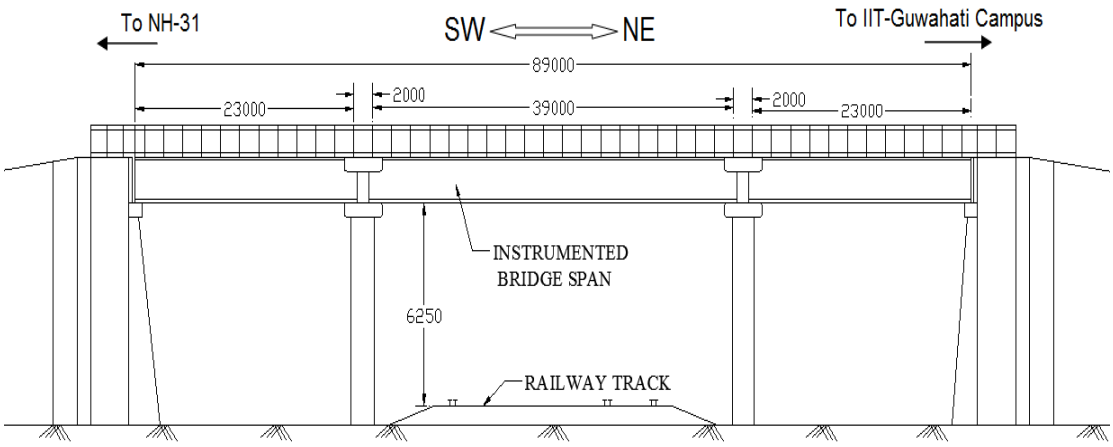

Fig. 5.2 Elevation of the tested bridge (All dimensions are in mm)

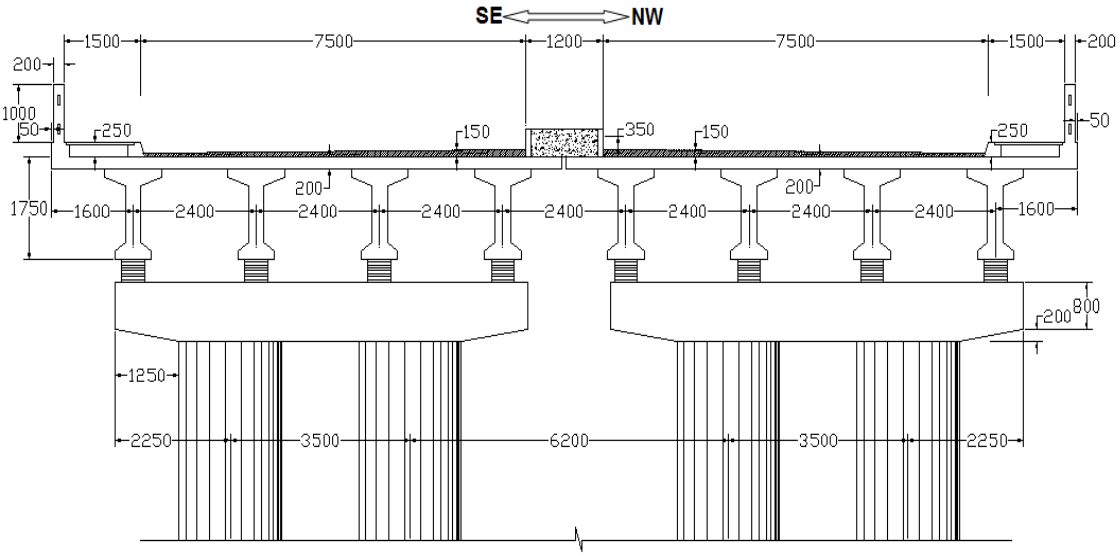

Fig. 5.3 Cross section of tested bridge middle span (All dimensions are in mm)

5.3 Test Vehicle

Dynamic test was performed using a single two axles TATA 1616 truck, which are used to carry heavy load. The truck was loaded with earth for the test. Fig. 5.4 shows that the truck was running with loaded earth over the bridge during the test. Gross weight of the loaded vehicle was measured in a weighbridge located near test site and found to be 19.42 tonnes (192.4 kN). The total length of the vehicle is 6 m. Wheel base: 3.65 m. wheel tread is 2 m. The test truck wheel configuration is shown in Fig. 5.5. Suspension is of semi-elliptical leaf spring type. Axles are made of heavy duty forged I beam. The truck has ladder type heavy duty frame with bolted cross members. Side members are of channel section, depth: 223 mm,

flange width 60 mm, thickness 7 mm, frame width 900 mm. The cross section is shown in Fig.5.6. Three vehicle speeds in the range of 20 km/h to 45 km/h and three runs for each speed were considered in the bridge test.

Fig. 5.4 Photograph of test truck TATA 1616

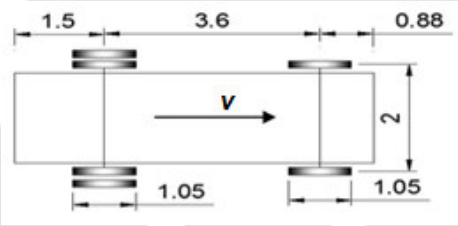

Fig.5.5 Test truck wheel configuration (All dimensions are in m)

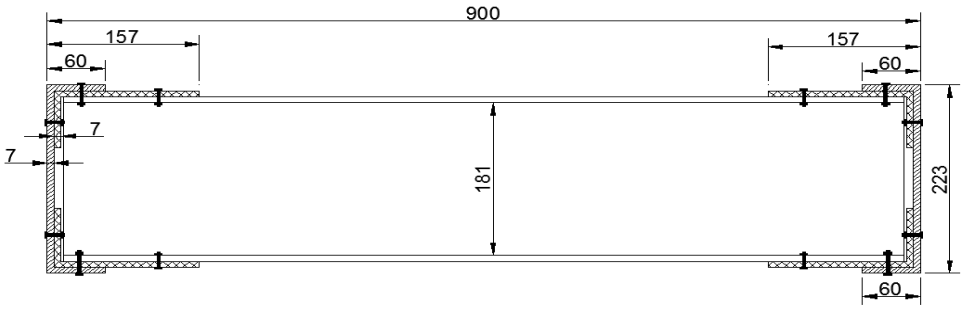

Fig.5.6 Cross section of test truck frame (All dimensions are in mm)

5.4 Deck Roughness Measurement

Surface profile of the bridge is one of the main sources of vehicle vibration in running condition which impose dynamic load over the bridge. Moreover, the deflection of a bridge modifies the surface profile and thus vehicle and bridge forms a coupled dynamic system. In

the present study, the bridge surface was first visually inspected. Deck surface appeared smooth. There were no potholes and other defects. However, at the exit and entry of the bridge, an approach road settlement of 25 mm has been noted during inspection of the bridge surface. There is a construction gap of about 10-15 mm size on both ends of the middle span. Before carrying out dynamic test with moving vehicle, longitudinal profile of the bridge deck has been surveyed using "Total station". Field survey conducted to determine the surface profile has been photographed and shown in Fig. 5.7. The total station is of make FOIF OTS635 having least count 0.1 mm. Vertical height of the bridge surface at the interval of 0.5 m along centerline of the span with reference to a datum has been measured. The datum is the horizontal plane passing through the first point of measurement. The total station is placed at a convenient place and leveled by adjusting tripod and the leveling screws. Thereafter, a pole fitted with prism was held at each point marked along the line. The pole was ensured vertical by adjusting a leveling bubble fitted in the pole. Telescope was directed towards the prism and the digitized reading has been noted down. Perpendicular offset, each of 1 m length was set out from the points over the centerline on either side by total station and poles are placed again on the tip of the offsets on either side of the centerline. Readings were then taken on the poles placed over the tip of the offset. The average relative height of the corresponding points along three longitudinal profiles was considered as the unevenness of the bridge in the experimental study. Bridge longitudinal profile and its Power Spectral density (PSD) function for road classification has been described in Chapter-8.

(a) (b)

Fig. 5.7 Measurement of bridge deck surface profile (a) Prism with pole placed over the points along the alignment (b) FOIF OTS635 Total Station

5.5 Instrumentation of Tested Bridge

The middle span of North-Western side was instrumented with five numbers of sensors which were glued to the deck as shown in Fig. 5.8. These sensors readings are digitalized using data acquisition system and stored in the computer. Exact straight line alignment for these sensors could not be maintained due to local degradation of deck surface. The location of sensors with their respective co-ordinates is given in Table 5.1.

Table 5.1 Location of sensors

Sensor number	Co-ordinates of sensor location(m)	
	X-axis	*Y*-axis
1	19.50	1.0
2	10.75	0.9
3	6.40	1.0
4	28.25	0.8
5	32.6	1.0

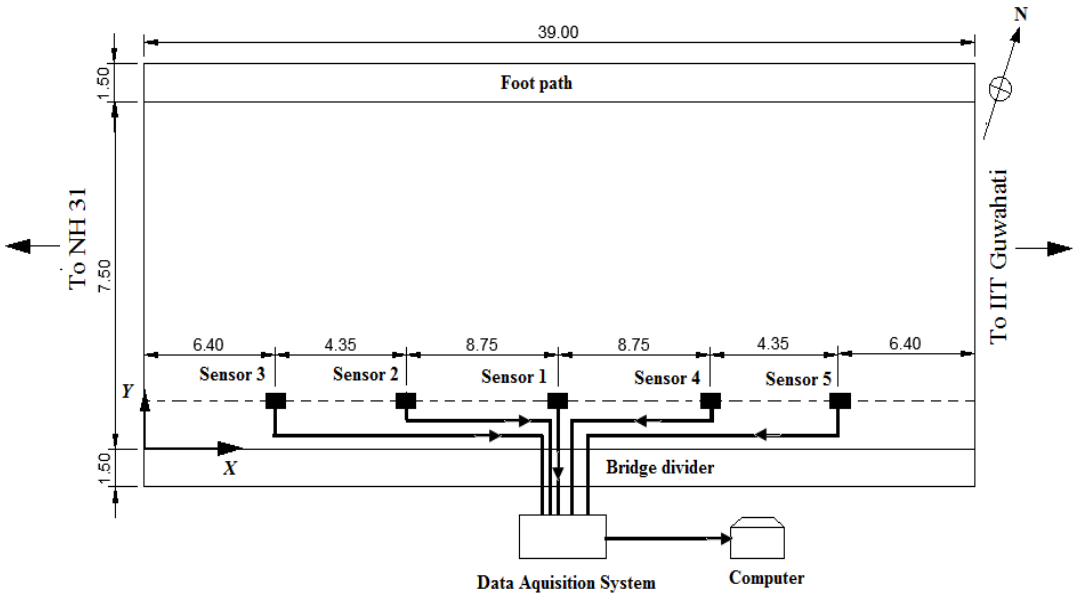

Fig.5.8. Layout of bridge instrumentation (All dimensions are in m)

5.5.1 Accelerometer and Data Acquisition System

The Kinemetrics Epi Sensor ES-U2 force-balanced uniaxial accelerometer possessing usable range of ± 0.25g to ± 0.4g was used in the bridge test shown in Fig. 5.9(a). Accelerometers readings were transmitted through data cable connected to Data acquisition system which was

kept inside a stationary car on the other lane. B0554 MGC plus HBM product data acquisition system with 0.003 m/s^2 accuracy, 16 channels and digital measure rate 19,200 values/second/channel was used for analog to digital converter. It is shown in Fig. 5.9(b). Power supply for the instruments was taken from electric pole located on the divider of the bridge. Photograph of accelerometer in position with data cable connected to Data Acquisition System is shown in Fig. 5.10.

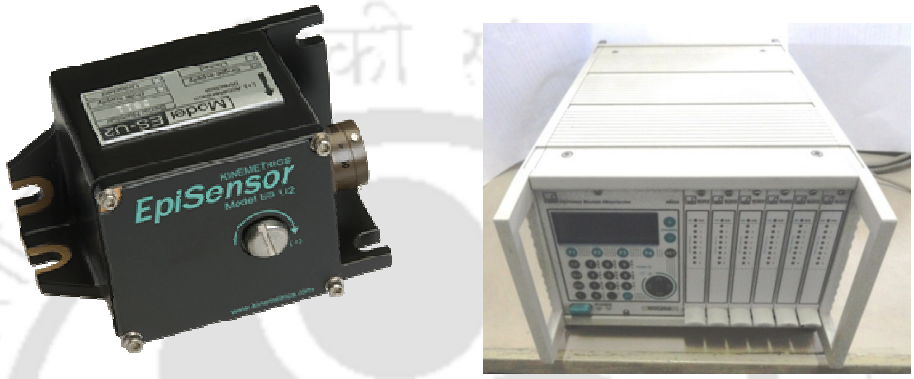

(a) (b)

Fig. 5.9 (a) Kinemetrics Epi-Sensor ES-U2 force balanced uniaxial accelerometer, (b) B0554 MGC Data Acquisition System

Fig. 5.10 Accelerometer glued to deck surface with data cable

5.5.1 Test Truck Speed Measurement

During dynamic test of bridge the test truck was allowed to move over the bridge at different velocities varying from 20 km/h-45 km/h. At each run truck speed was measured using

Genesis Handheld Directional Radar gun which has an accuracy of ± 1 km/h and sampling rate of 100 samples/sec. This is shown in Fig 5.11. Driver of the truck has been instructed to maintain the vehicle speed uniform without any acceleration and deceleration. Three average vehicle speed 20 km/h, 30 km/h and 40 km/h was considered as test truck speed. Actual truck speed during running condition was however confirmed by measurement using radar gun. Fig. 5.12 shows the measurement of truck speed using radar gun during the test.

Fig. 5.11 Genesis Handheld Directional Radar gun

Fig. 5.12 Truck speed measurement using radar gun

5.6 Finite Element Modeling of the Bridge

The tested bridge has been modeled using Finite element commercial software SAP 2000 shown in Fig. 5.13. Longitudinal and cross girders, given in Fig. 5.3, have been modeled as frame element while bridge deck as four noded shell element with 6 degrees of freedom at

each node. These elements are capable of simulating both the in plane and out of plane deformation (Hughes, 1987). In the present bridge model, support flexibility is neglected and simply supported boundary condition has been assumed for at each end. Vehicle load in the bridge has been considered as a point load *P* which is equivalent to gross weight of test truck, moving along the centre line of the bridge with a constant speed *v*.

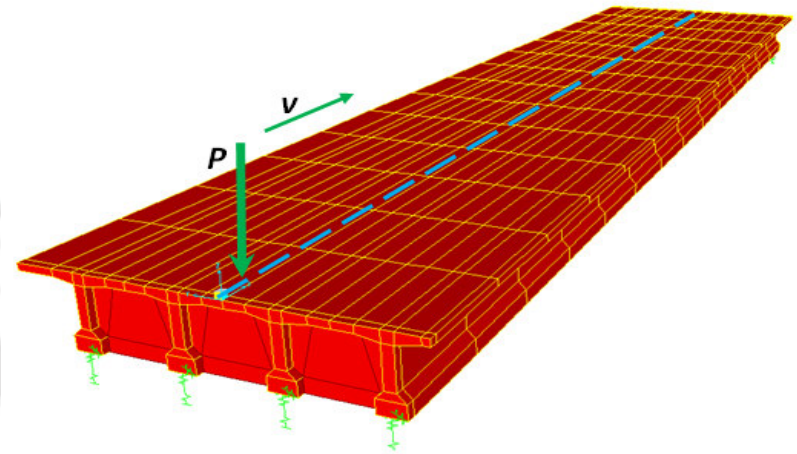

Fig. 5.13 Finite element model of bridge (top isometric view).

5.7 Finite Element Model Updating

In many Civil Engineering applications such as health monitoring, non-destructive damage detection and structural control, an accurate Finite Element model is considered because it can be used as a reference model to predict the performance of structures. Discrepancies between field test results and numerical results are always inevitable due to modeling error, simplified assumption made in the modeling process, uncertainties in material and geometric properties and boundary conditions. However, the model parameters can be modified to reduce this difference by a scientific method. This is called "model updating".

Several methods of finite element model updating have been proposed in the literatures (Mottershead and Friswell, 1993; Friswell and Mottershead, 1995; Maia and Silva, 1997). There are two approaches used in finite-element-model updating: direct methods (or non-iterative method) and iterative methods (Marwala, 2010). Non-iterative methods that directly update the elements of stiffness and mass matrices are one-step procedures (Baruch and Bar-Itzhack, 1978; Berman and Nagy, 1983). Iterative procedures use changes in physical parameters to update the finite element models and, thereby, generate models that are

equivalent to real structures (Esfandiari *et al*., 2012). No matter which method is used to update a FE model, the basic purpose of model updating is to modify the physical properties of the structure so as to minimize the difference between theoretical and experimental response.

However, if the structure of interest requires a large finite element model, a large number of computations involved can rule out many approaches due to the expensive computation in many runs. There are now many commercial finite element analysis packages available such as ANSYS, Abaqus and SAP2000 etc. The structural FE models are often constructed by using these packages. In all the iterative parameter updating methods, each iteration need to go back to run the finite element analysis package with any of the parameters updated, which limits the popular applications of structural FE model updating in practice.

In the present study a newly adopted method, called response surface based finite element updating, has been employed which is more practical and user-friendly especially when the structure of interest is modeled with commercial finite element analysis packages (Ren and Chen, 2010). This method utilizes the response surface for the best experimental design of the parameters to be updated, based on which numerical analysis can be performed to obtain explicit relationships between the structure responses and parameters from the simulation results. The parameters are then updated using the genetic algorithm (GA) by minimizing an objective function built up using the residuals between the measured structure responses and predicted responses from the obtained relationships.

5.7.1 Response Surface Method (RSM)

Response surface method (RSM) consists of a group of mathematical and statistical techniques used in the development of an adequate functional relationship between response of interest (output variable) and several independent variables which influence output of the system response (input variables). This method uses the response surface function (RSF) to approximate the actual state function, which is usually implicit and difficult to express. The basic steps involve in the response surface based finite element updating are discussed below:

5.7.1.1 Design of Experiments (DoE)

An important aspect of response surface method is the design of experiments (Box and Draper, 1987), usually abbreviated as DoE. These strategies were originally developed for the

model fitting in physical experiments, but can also be applied to numerical experiments. The objective of DoE is the selection of the points where the response should be evaluated. The term experiment herein refers to either physical experiments or computer experiments. DoE plays an important role in constructing a response surface. A detailed description of the design of experiments theory can be found in Box and Draper (1987), Myers and Montgomery (1995) and Montgomery (2000). There are many designs available for response surface function. The most popular method is the central composite design (CCD) introduced by Box and Wilson (1951). This design method gives most reliable response surface function especially for civil engineering structures (Ren and Chen, 2010).

The central composite design consists of factorial points, central points, and axial points. CCD was often developed through a sequential experimentation. The number of center points at the origin and the distance α of the axial runs from the design center are two parameters in the CCD design. The center runs contain information about the curvature of the surface. If the curvature is significant, the additional axial points allow ones to obtain an efficient estimation of the quadratic terms. There are many possible way of combining these three points depending on the number of factors; some of the combinations may be insignificant for a particular problem. In view of the practical aspect of bridge model updating, Deng and Cai (2009) listed out CCD for different number of factors given in Table 5.2. Two-factor factorial CCD is shown in Fig. 5.14. In the figure factorial points is represented as small circle, star represent axial points and a small circle located at the center denotes central point. X_1 and X_2 are the independent variables.

Table 5.2 Central Composite Design for different number of factors (Deng and Cai, 2009)

	Number of factors					
	2	3	4	5	6	7
Factorial points	2^2	2^3	2^4	2^{5-1}	2^{6-1}	2^{7-1}
Axial points	4	6	8	10	12	14
Center point	1	1	1	1	1	1
α	1.4141	1.6818	2.0	2.0	2.3784	2.8284
Total number of trials	12	18	28	30	48	82

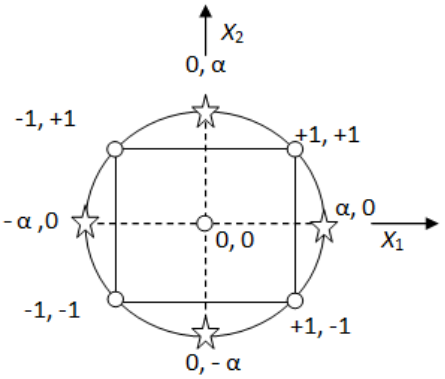

Fig. 5.14 Two factor Central Composite Design

A three-factor CCD adopted by Mayers *et.al* (1989) is shown in Fig 5.15 and their corresponding values are given in Table-5.3, which has been used in the present finite element model updating of the tested bridge. In the figure, X_1, X_2 and X_3 are independent variables. It should be noted that the given CCD design is a standard design form for a case with three factors. The center point is repeated four times since the information at the center point is more important to the response surface compared with the other points in the three factors central composite design. Here, α has been taken as 1.6818 (Mayers *et.al*, 1989).

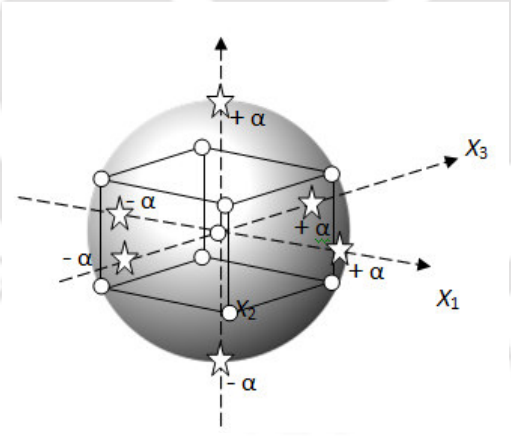

Fig. 5.15 Three factor Central Composite Design

Table 5.3 Three factor Central Composite Design (Mayers *et.al,* 1989)

Experimental trial	Factor Level Setting		
	X_1	X_2	X_3
1	-1	-1	-1
2	1	-1	-1
3	-1	1	-1
4	1	1	-1
5	-1	-1	1
6	1	-1	1
7	-1	1	1
8	1	1	0
9	$-\alpha$	0	0
10	α	0	0
11	0	$-\alpha$	0
12	0	α	$-\alpha$
13	0	0	α
14	0	0	0
15	0	0	0
16	0	0	0
17	0	0	0
18	0	0	0

5.7.1.2 Construction of Response Surface Function

In general, the low-order polynomial model is used to describe the response surface for conceptual as well as computational reasons. A polynomial model is usually a sufficient approximation in a small region of the response surface. Therefore, depending on the approximation of unknown function, either first-order or second-order models are employed. If the response can be defined by a linear function of independent variables, then the approximating function is a "first-order model". If there is a curvature in the response surface, then a higher degree polynomial should be used (Douglas, 2005). A two degree polynomial is termed as "second-order model". The two models can be given as

$$Y = \beta_0 + \sum_{j=1}^{n} \beta_j X_j \tag{5.1}$$

$$Y = \beta_0 + \sum_{j=1}^{n} \beta_j X_j + \sum_{j=1}^{n} \beta_{jj} X_j^2 + \sum_{i=1}^{n} \sum_{j=1}^{n} \beta_{ij} X_i X_j \tag{5.2}$$

Eqs. (5.1) and (5.2) represents first-order model and second-order model respectively. n is a number of independent variable. Y is the response and X denotes the independent variables or

system parameters to be updated, β_{0i}, β_j, β_{ij}, are the regression coefficient to be estimated from experimental design data. The Least squares method has been applied to estimate the coefficients β in the second order model.

The relationship between the response variable Y and independent variables X is usually unknown. Therefore, depending on the approximation of unknown function f, either first-order or second-order models are employed. The second-order model is flexible, because it can take a variety of functional forms and approximates the response surface locally Therefore, this model is usually a good estimation of the true response surface (Douglas, 2005). Due to this reason, second-order model has been adopted in the present study for the construction of response surface function.

5.7.1.3 Development of Objective Function

In a response surface based finite element updating method, a deviation between actual measured response and the virtual response obtained from the experimental trial using response surface function has to be minimized by means of any suitable optimization method. In the present study, a global search optimization method, called Genetic Algorithm has been employed for minimizing this deviation. The objective function can be written based on the least-squares method as shown below (Deng and Cai, 2009)

$$\varepsilon = \left[\sum_{k=1}^{n} (Y_k - Z_k)^2 \right]^{\frac{1}{2}} \tag{5.3}$$

where, ε is a deviation of measured and predicted response. Y_k is the predicted response from the response surface function whereas Z_k denotes measured response The number of system response considered for model updating is 'n'.

5.7.2 Genetic Algorithm

The Genetic Algorithm (GA) primarily formulated by (Goldberg, 1989) is a probabilistic global search and optimization method that mimics the metaphor of natural biological evolution. GA operates on a population of individuals (potential solutions), each of which is an encoded string (chromosome), containing the decision variables (genes). The structure of a GA is composed of an iterative procedure through the following five main steps:

(i) Generating random population $\{x_i\}_{i=1}^{n}$, each element of {x} is termed as chromosome.

(ii) Evaluation of the performance of each individual or chromosome x_i of the population, by minimizing a fitness function $f(x_i)$.

(iii) Application of genetic operators to obtain new offspring: Selection, Crossover and Mutation.

(iv) Re-evaluate fitness of each new offspring.

(v) Steps (iii) and (iv) are continued until a termination criterion is fulfilled.

5.8 Procedure of Response Surface based FE model updating of Test Bridge

A step by step procedure for the test bridge FE model updating using response surface technique has been described as follows:

(i) Let the bridge measured response be denoted as $\{Z\}$ which may include other derived parameters such as natural frequencies, damping etc.

(ii) Select the bridge dynamic parameters $\{X\}$ to be updated and then define a significance level for each selected parameters based on the design of experiments (DoE) method. Select numbers of experimental trial required on the basis of type of the experimental design.

(iii) Construct Finite Element model of the bridge using the generated bridge parameters from step (ii). Run Modal analysis and also determine time history of bridge response considering moving vehicle for each experimental trial.

(iv) Select a suitable quadratic polynomial function, given in Eq. (5.2), on the basis of structural parameters to be updated. Construct response surface function $\{Y\}$ using simulated results from step (iii) and Least Square method.

(v) Develop objective function using Eq. (5.2) and then minimize the objective function using GA until the stopping criterion is achieved.

The flow chart of Genetic Algorithm based global search optimization technique is presented first in Fig 5.16. A flow chart of response surface and GA based FE model updating technique implemented in the present study is then shown in Fig 5.17.

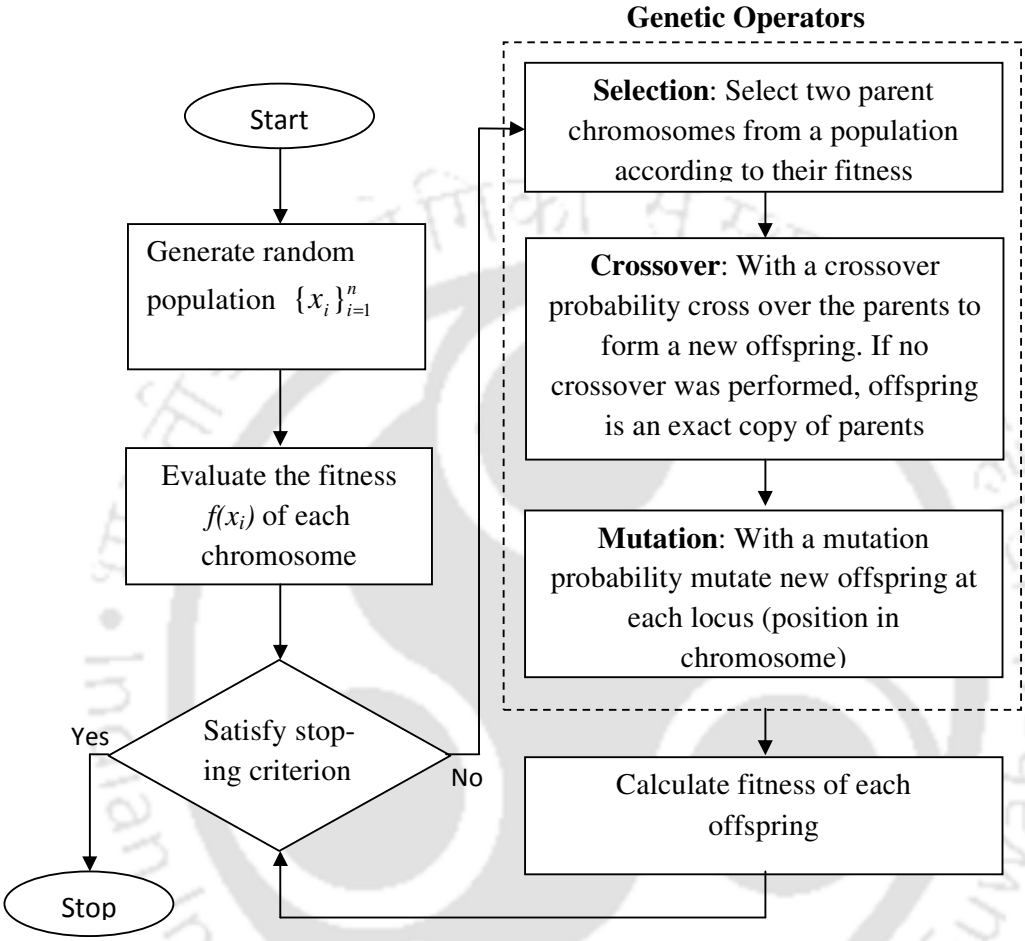

Fig. 5.16 Flow chart of Genetic Algorithm

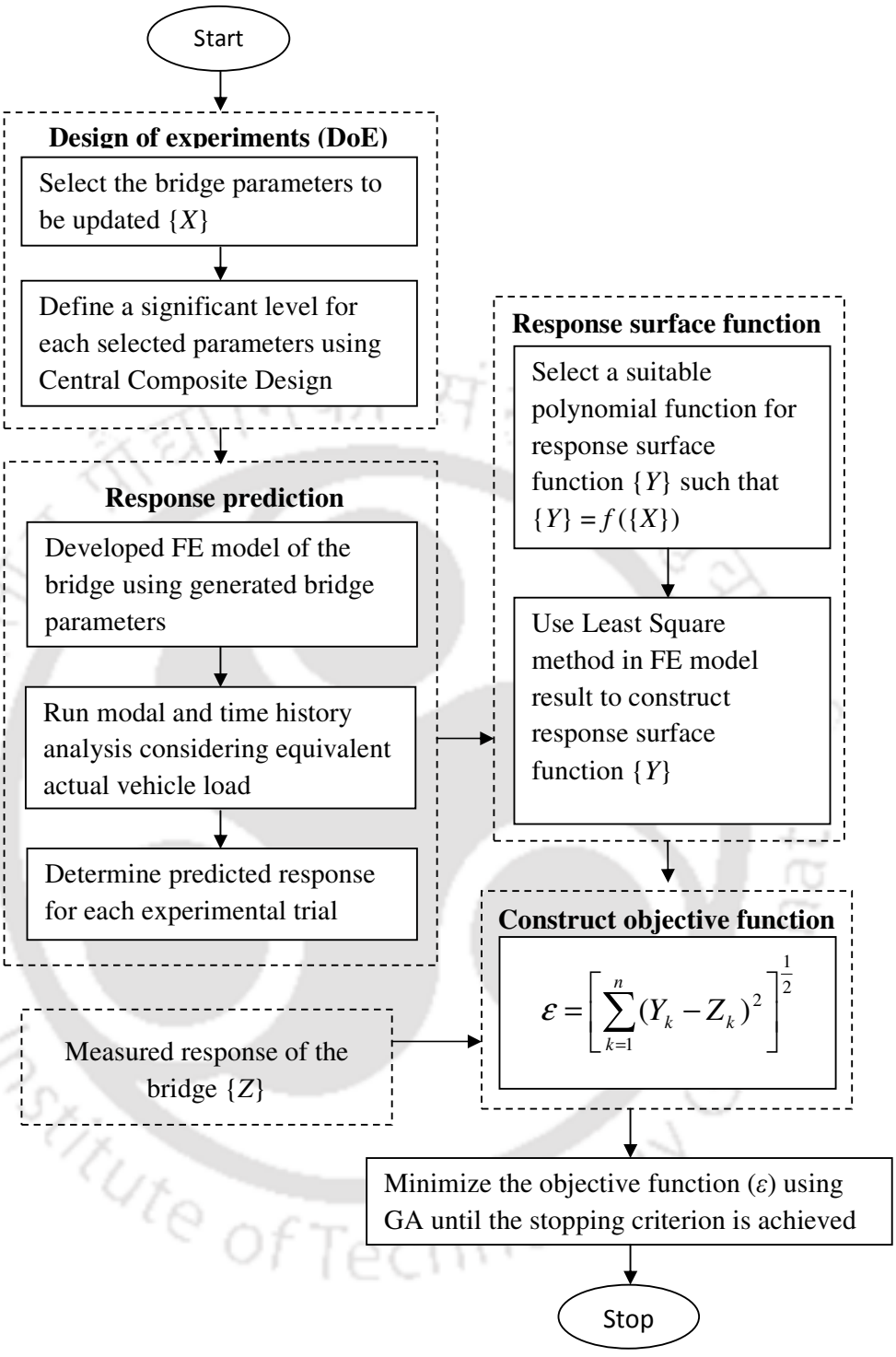

Fig. 5.17 Flow chart of response surface based Finite Element model updating

5.9. Closure

In the present chapter, procedure for the field testing of the bridge under moving load has been discussed with detail of Test Bridge, vehicle and instrumentation on the bridge. A three span bridge, each span being independently supported by rocker and roller bearings has been tested. Only middle span of the bridge has been instrumented. A controlled single truck movement has been considered to acquire the accelerations of bridge deck at five sensor locations. Truck loaded with earth has been allowed to run at three different speeds. Truck weight including earth load was determined in a weighbridge located near the test site. Actual truck speed was measured by radar gun. It may be noted the purpose of field test is to demonstrate implementation of particle filter method in identifying vehicle parameters using measured acceleration. FE model of the bridge has been created in SAP2000 commercial software which is later used as one of the preferred models in forward solution in the identification scheme. The purpose of the field test is also to update FE model, such that updated parameters of the bridge can be used in forward scheme. The updating of FE model parameters in the present study has been done using Response surface technique in combination with GA. The procedure has been described in the present chapters with the presentation of flow chart.

6

RESULT AND DISCUSSION- PART-I: DYNAMIC BEHAVIOUR OF THEORETICAL MODEL

6.1 Overview

In the present Chapter, dynamic response of bridge-vehicle coupled systems has been studied in order to give insight into to the physical behavior of semi-analytical models to be used in forward solution for parameter identification. The model sensitivity to change of bridge-vehicle parameters has been also examined with three different vehicle models interacting with a simply supported bridge. The non-homogeneous pavement input with variable mean profile such as (i) pre-cambering of deck surface and (ii) approach settlement has been included along with random unevenness to reflect different constructional features and defects met in practice. The mean and standard deviation of the vehicle and bridge mid span response quantities have been shown for three different coupled systems (Model-1, 2 and 3) considered in the present work. Further, the dynamic amplification factor of the bridge response has been obtained for variation of different bridge vehicle parameters and discussed to gain the understanding of various factors which need to be considered for design and maintenance of bridge.

6.2 System Parameters

The following system parameters have been adopted to generate numerical results and to conduct parametric study by numerical experiments.

6.2.1 Bridge parameters

The data of a RC slab –Girder type Bridge of span (L), 20m; three longitudinal girders and three cross girders one at mid span and other two at supports are adopted for theoretical study. The cross section of the bridge is shown in Fig 6.1. The lane width: 8.6 m, deck thickness: 200 mm, concrete characteristic strength 25 N/mm^2. The following physical parameters are assigned to the beam model in order to conduct parametric study: Mass (m_b): 11.15×10^3 kg/m, flexural rigidity (E_bI_b):3.7×10^{10} N-m^2, torsional rigidity (G_bJ_b): 1.695×10^{10}

N-m^2, mass moment of inertia (I_{mb}): 4.07×10^3 kg-m^2/m. It may be noted that cross section is symmetrical about the vertical axis through the centre of bridge and therefore, under vertical wheel load coupling of bending torsion vibration would not occur.

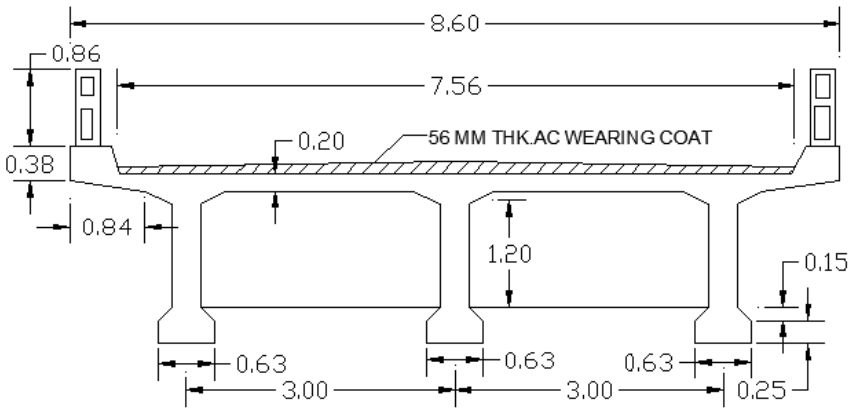

Fig.6.1 Cross section of T-beam Bridge (All dimensions are in m)

As mentioned in 6.1, a combination of deterministic variable mean and random surface roughness has been taken into account in the present study. Precambering has been assumed as a shallow parabola with central rise (h_0) as 0.01 m. Case studies using approach settlement, which is the relative difference between deck level and approach road (h_1) have been conducted with settlement value in the range of 0.01 m to 0.04 m. For modeling deck surface random roughness, the values of spectral roughness coefficient $S_{GG}(\Omega_0)$ have been taken as 2×10^{-6} to 180×10^{-6} m^2/(cycle/m) according to International Organization for Standardization (ISO 8608:1995) specifications for the class of different road conditions. As per ISO suggestion roughness shape coefficient m has been taken as 2, lower cut off frequency Ω_L=0.1 c/m and upper cutoff frequency Ω_U = 2.0 c/m (Sun and Kennedy, 2002).

6.2.2 Vehicle parameters

The data of a long and heavy commercial vehicle type TATA 3516C-EX has been chosen for the case studies. The following dimensions and physical parameters are used in computation in three different idealized models.

6.2.2.1. Quarter Car Model (*Model-1*)

This is a generic lumped mass model having single wheel contact. For this model, we take sprung mass (m_{qv}) = 18000 kg, unsprung mass (m_w) = 1600 kg, suspension stiffness (k_v) =

7.2×10^7 N/m, suspension damping (c_v) = 1.44×10^5 N-sec/m, tyre stiffness (k_t) = 1.8×10^6 N/m, tyre damping (c_t) = 1.5×10^4 N-sec/m.

6.2.2.2. Half Car Model (*Model-2*)

In Half Car Model vehicle body has been idealized as Euler-Bernoulli beam, which incorporates bending flexibility in the model. Following are the important physical parameters pertaining to vehicle: length (l_v): 12 m, axle spacing (wheel base): 9 m, flexural rigidity (E_vI_v): 5.3×10^6 N-m^2, Mass per unit length (m_v): 1500 kg/m, front and rear wheel masses (m_{w1},m_{w2}): 800 kg each, suspension stiffness front and rear (k_{v1}, k_{v2}): 3.6×10^7 N/m, suspension damping front and rear (c_{v1}, c_{v2}): 7.2×10^4 N-sec/m, front and rear tyre stiffness (k_{t1}, k_{t2}): 0.9×10^7 N/m, front and rear tyre damping (c_{t1}, c_{t2}): 0.7×10^4 N-sec/m. It may be noted that in continuous system infinite number of degrees of freedom are possible for which theoretically infinite number of natural frequencies exit. However, for practical solution, the number is truncated to a finite size. In this model, vehicle body undergoes rigid heave and pitch motion in addition to elastic bending modes.

6.2.2.3. Full Car Model (Model-3)

In addition to bending flexibility of vehicle body, torional flexibility has been incorporated in Full Car Model, Wheel masses (m_{w11},m_{w21}, m_{w12},m_{w22}): 400 kg each, suspension stiffness (k_{v11}, k_{v21}, k_{v12}, k_{v22}): 1.80×10^7 N/m, suspension damping (c_{v11}, c_{v21}, c_{v12}, c_{v22}): 3.60×10^4N-sec/m, front and rear tyre stiffness (k_{t11}, k_{t21}, k_{t12}, k_{t22}): $4.50\text{x}10^6$ N/m, front and rear tyre damping (c_{t11}, c_{t21}, c_{t12}, c_{t22}): 3.50×10^3 N-sec/m, torsional rigidity(G_vJ_v): 9.02×10^2N-m^2, mass moment of inertia (I_{mv}): 2.58×10^2kg-m^2/m. Wheel tread (transverse dimension between left and right wheel): 2 m. Vehicle body in Full Car Model has both bending and torsional flexible modes in addition to rigid body modes.

6.3 Response Statistics for Model-1

Dynamic responses of the coupled system are obtained using the presently developed semi-analytical formulations. The mean and standard deviation of response time histories have been presented. Vehicle response (sprung mass and unsprung mass) has been first shown for variation of its forward speed. After that, response statistics of the bridge at mid span locations have been presented for change of various parameters.

6.3.1 Vehicle Response

Mean and standard deviations of dynamic responses time history of the vehicle body (modeled as lumped sprung mass) for three different vehicle speeds are shown in Fig 6.2 to Fig. 6.4. For the case studies, poor condition of bridge deck surface as per ISO classification (ISO 8608:1995) and parabolic mean surface profile with central rise 0.01 m have been considered. In the figures μ_{dz1}, μ_{vz1} and μ_{az1} represents mean of sprung mass displacement, velocity and acceleration respectively while their corresponding standard deviations are denoted by σ with proper subscript. Mean displacement, velocity and acceleration of sprung mass and unsprung mass increase with increase in vehicle speed. Response pattern shows a single dominant frequency possibly induced from one of the pavement wavelengths present in random unevenness. Further, it is seen that peak of the responses shifts towards left as speed of vehicle increases indicating that temporal frequency of pavement excitation has been increased. Standard deviation does not show any definite pattern of variation in the vehicle sprung mass response history.

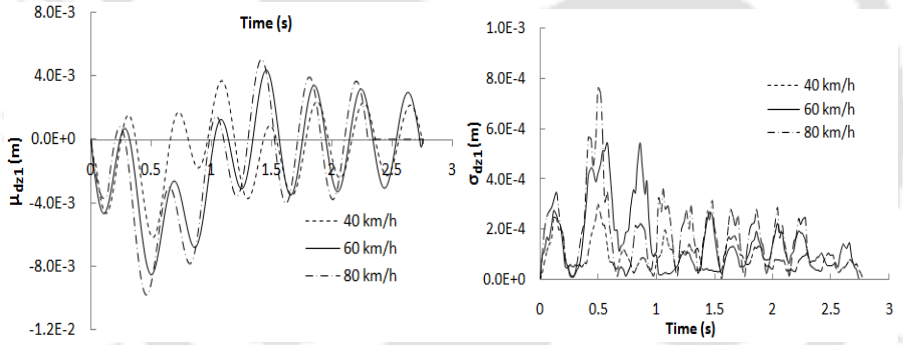

(a) Mean (b) Standard deviation

Fig.6.2. Sprung mass displacement

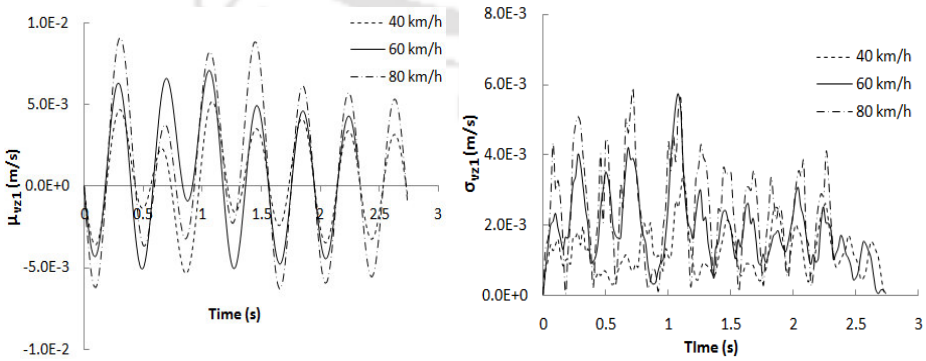

(a) Mean (b) Standard deviation

Fig.6.3. Sprung mass velocity

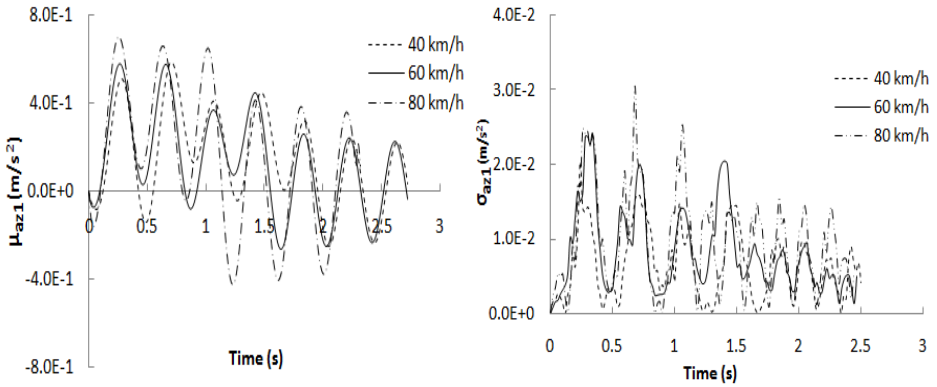

(a) Mean (b) Standard deviation

Fig.6.4. Sprung mass acceleration

The mean and standard deviation of displacement, velocity and acceleration of un-sprung mass have been shown in Fig. 6.5 to Fig. 6.7. It may be observed that unsprung mass response magnitude is higher than that of sprung mass quantities. This is expected as suspension system plays an important role to isolate vehicle body from road way disturbance. The standard deviations have no definite trend; however, at highest speed considered in the study, a sharp peak is noticed in displacement and acceleration whose magnitude is 2 to 4 times higher than that shown for lower speed. Coefficient of variation in peak magnitude of the response quantities are found to vary from 4% to 19%.

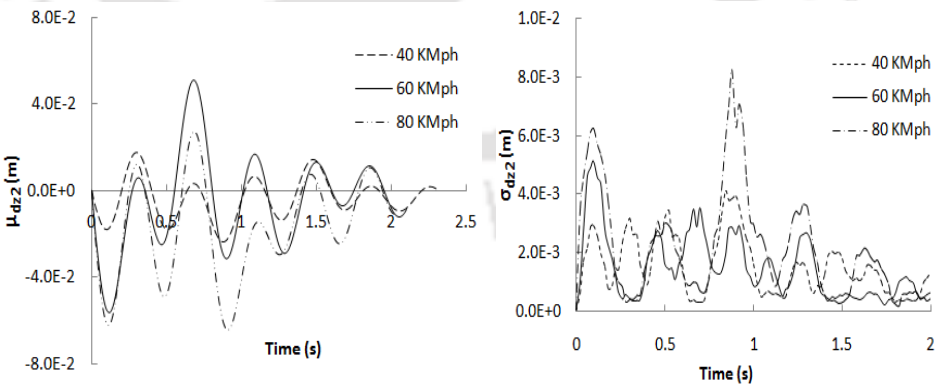

(a) Mean (b) Standard deviation

Fig.6.5. Unsprung mass displacement

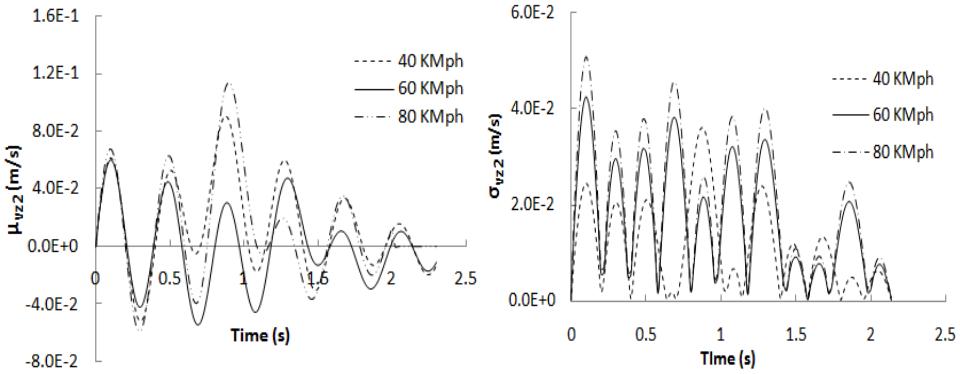

(a) Mean (b) Standard deviation

Fig.6.6 Unsprung mass velocity

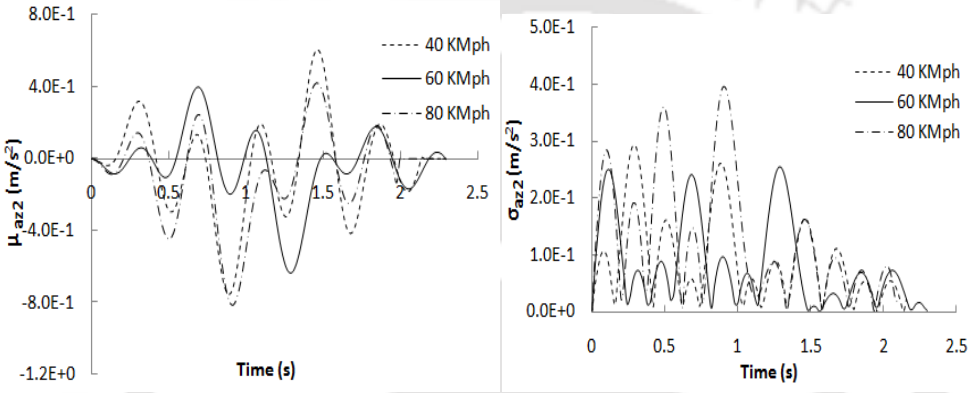

(a) Mean (b) Standard deviation

Fig.6.7. Unsprung mass acceleration

6.3.2 Bridge Response

In this subsection, the bridge dynamic response due to moving vehicle has been presented. Vehicle model-1, having two degrees of freedom has been considered. This model is a generic vehicle model which is first used in solving inverse problem in this study. Therefore, it has been felt necessary to study the bridge dynamic response using presently developed semi-analytical method with various bridge-vehicle parameters. The Bridge is subject to dynamic load at single contact point, the position of which changes with time along the span. Effect of speed, eccentricity of vehicle path, approach slab settlement on the mean and standard deviation of mid span response quantities has been studied.

6.3.2.1 Effect of vehicle speed

Response samples have been generated corresponding to the poor category of pavement as per ISO classification. Mean surface of deck is assumed as parabola. A roughness coefficient

$S_{GG}(\Omega_0)$ =160×10^{-6} m^2/cycle /m (ISO-8608: 1995) has been assumed to obtain the results. The mean responses (displacement -μ_{dy}, velocity- μ_{vy} and acceleration- μ_{ay}) along with the standard deviations (displacement-σ_{dz} , velocity -σ_{vz} and acceleration-σ_{az}) at mid span for three different vehicle speed 40 km/h (11.2 m/s), 60 km/h (16.8 m/s) and 80 km/h (22.4 m/s) have been shown in Fig. 6.8 to Fig. 6.10. It may be noted that as the vehicle leaves the bridge, the bridge is subject to free vibration with the initial conditions at the time when vehicle just crosses the bridge. This free vibration here is called as 'residual response' which is also captured and presented. The mean displacement of the bridge shows a single wave, exhibiting the peak at the instant when the load is near the mid span. It can be seen that there is about 38% increase in mean central deflection when vehicle speed changes from 40 km/h to 80 km/h. The peak of the mean central deflection distinctly shifts towards left when speed increases. This is expected as the input frequency is fashioned by the change of vehicle speed. Standard deviation of mean displacement shows multiple peaks, and thus it is significant to obtain second order statistics to reveal the interaction of different modes in a coupled system like the one being presented in the study. Multiple waves are visible in time derivatives of displacement. The magnitude of velocity and acceleration too has been found to increase with vehicle forward speed. Although, the magnitudes of standard deviation are insignificant for practical purpose, magnitude of the coefficient of variation of peak displacement, velocity and accelerations are found to be 0.165, 0.142 and 0.133 respectively.

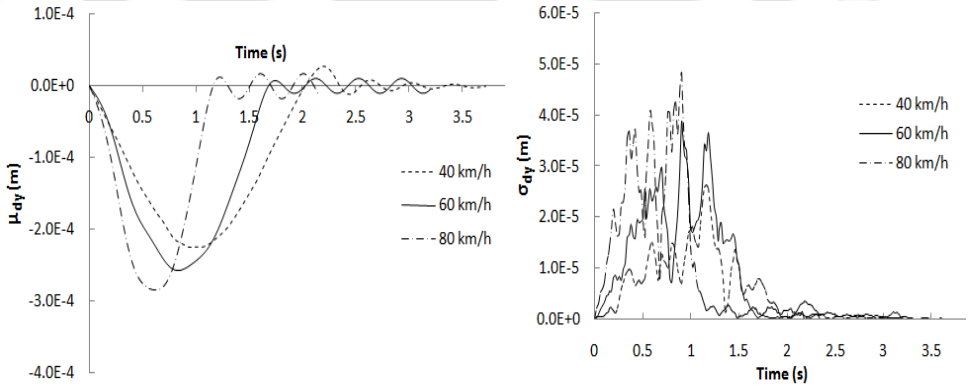

(a) Mean (b) Standard deviation

Fig.6.8. Bridge vertical displacement at mid-span

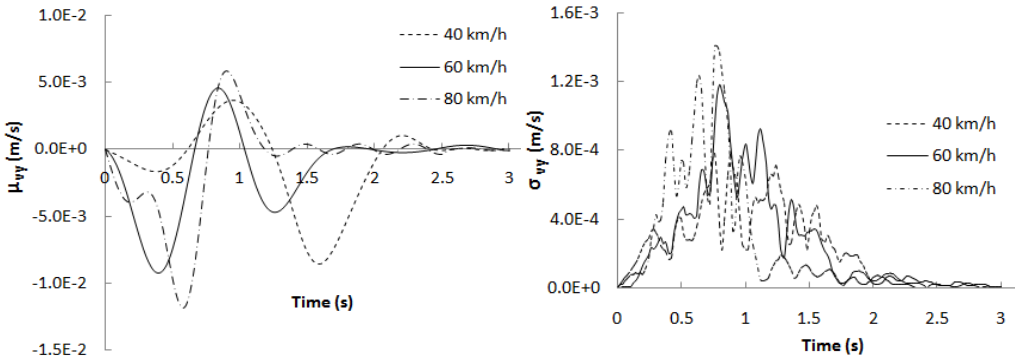

(a) Mean (b) Standard deviation

Fig.6.9. Bridge vertical velocity at mid-span

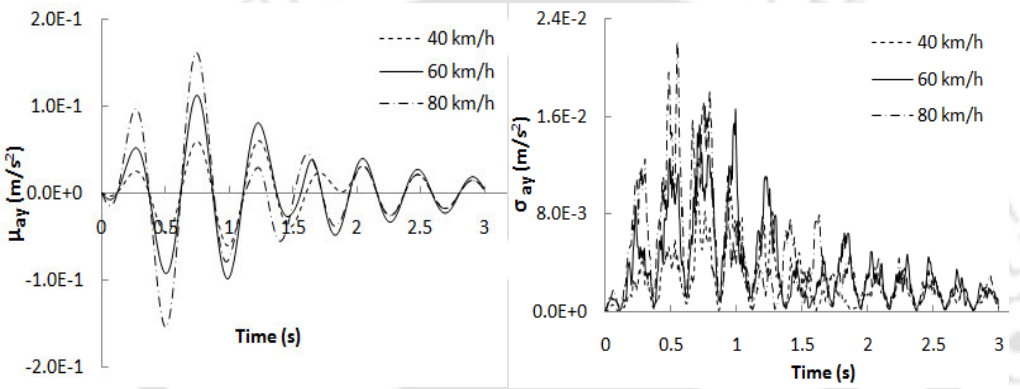

(a) Mean (b) Standard deviation

Fig.6.10. Bridge vertical acceleration of at mid-span

6.3.2.2 Effect of eccentricity of vehicle path

The vehicle always does not follow the centre line of the bridge. As a result, there is likely to be an eccentric loading and resulting torsional motion. In generating numerical results under this sub-section vehicle velocity is taken as 60 km/h. and pavement surface condition is assumed as poor. The contribution of torsional motion in mid span deflection of the bridge has been studied by varying wheel location from the centre line of the bridge deck. This is accomplished by changing the eccentricity of loading (e_x) from 0.5 m to 1.5 m. Mean of bridge mid span deflection for different load eccentricity and the corresponding standard deviation is shown in Fig. 6.11. An increase of mid span deflection in the range of 4% to 9% has been noticed for the eccentric vehicular load considered in this section.

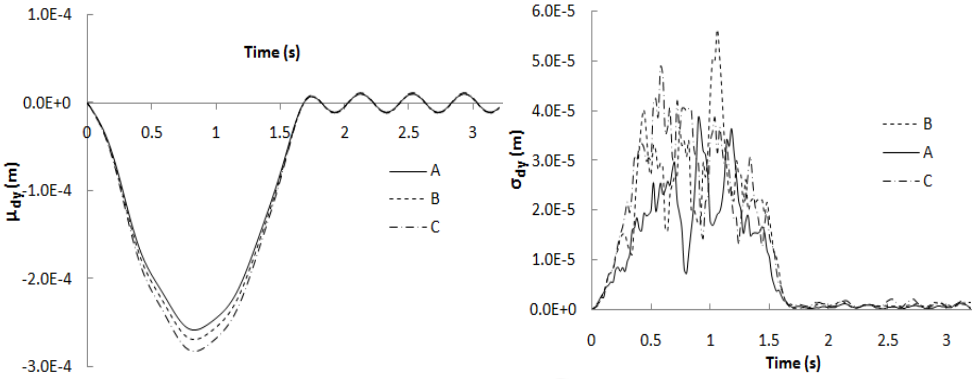

(a) Mean (b) Standard deviation

Fig.6.11. Bridge mid-span displacement due to different eccentricity of vehicle path (e_x), (A) e_x=0.5 m, (B) e_x =1 m, (C) e_x =1.5 m

6.3.2.3 Effect of approach road settlement

Approach settlement has been often found in many existing bridges. The field observation indicates that differential settlement between bridge deck and approach slab can be as much as 0.038 m (White *et al*., 2005). This causes a sudden change in relative difference between road level and bridge deck level. As a result, vehicle experiences a high transient input at entry even at low speed. The present study investigates the effect of approach settlement magnitudes on bridge dynamic response. In this case, solution has been obtained by changing the type of mean surface profile as detailed in section 3.3.1, whereas random unevenness corresponds to poor category of pavement. Mean and standard deviation of bridge mid span displacement for the vehicle speed 60 km/h vehicle speed are shown in Fig. 6.12. Only 1.2 % to 3.5 % increment in the bridge response has been found for approach settlement up to 15 mm. However, considerable increment of the response magnitude ranging from 12.5% to 21.74% has been observed when settlement increases from 25 mm to 40 mm. Standard deviations are found to be highly fluctuating, again reflecting the influence of transient input in second order statistics.

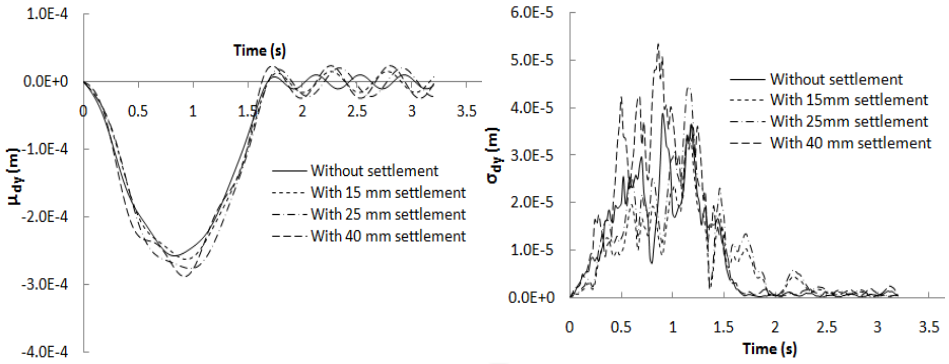

(a) Mean (b) Standard deviation

Fig.6.12 Bridge mid span deflection for different settlement

6.4. Dynamic Amplification Factor for Model-1

There are various key factors which affects the dynamic response of bridge. In this section dynamic amplification factor (DAF) has been studied for the variation of several bridge-vehicle parameters.

6.4.1 Effect of bridge surface roughness and vehicle speed

The surface roughness and speed of the vehicle are the two most influential factors that can cause increased DAF and rapid degradation of the bridge. Bridge dynamic amplification factor has been found by changing bridge surface roughness coefficient for good condition to poor condition as mentioned in ISO specification (ISO-8608: 1995) simultaneously along with the change in vehicle speed. DAF has been presented as surface plot and contour in Fig. 6.13. It may be noted that dynamic amplification increases with speed irrespective of pavement roughness up to a speed of 65 km/h, thereafter rate of increment seems to be slowed down. This may be attributed to the fact that the bridge interaction time with moving wheel is less. However, poor condition of pavement surface triggered by high speed of vehicle causes significant increase of DAF.

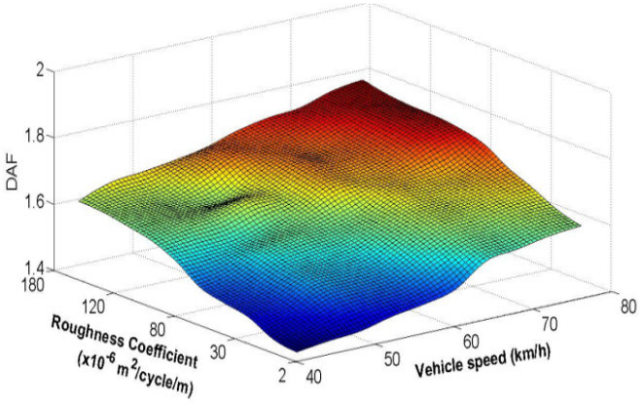

(a) Surface plot representation

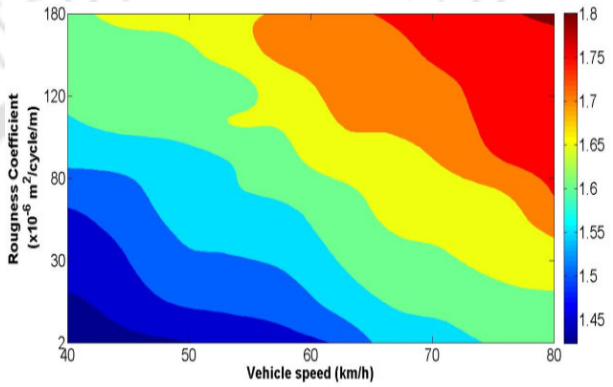

(b) Contour plot representation

Fig.6.13. Dynamic amplification factor with vehicle speed and bridge surface roughness coefficient

6.4.2 Effect of bridge span and velocity

The span of the bridge is an important factor which decides the impact factor in most of the bridge design codes. Combined effect of bridge span and speed of the vehicle on DAF is not fully known. Fig. 6.14 shows the DAF with variation of bridge span and velocity in the form of surface plot and contour. The contour plot can be helpful to select possible range of bridge span and satisfactory speed limit. The result shows that when the bridge span increases from 15m to 35m dynamic amplification factor decreases by an amount of 12% to 15 %, irrespective of increase in vehicle velocity. Although increasing span shows a decreasing trend in DAF as similar to the earlier studies (Hwang and Nowak, 1991) the increment found in the present case is not very significant for the range of span 15-35 m.

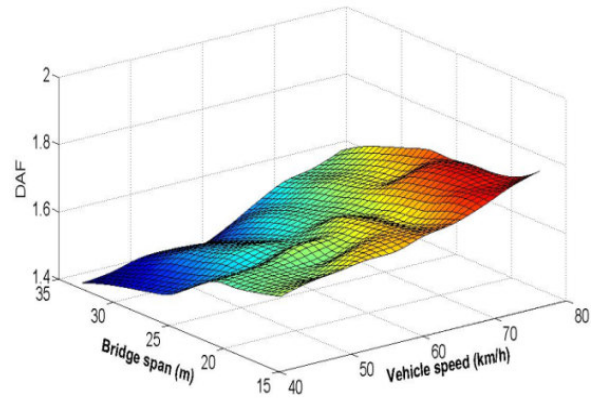

(a) Surface plot representation

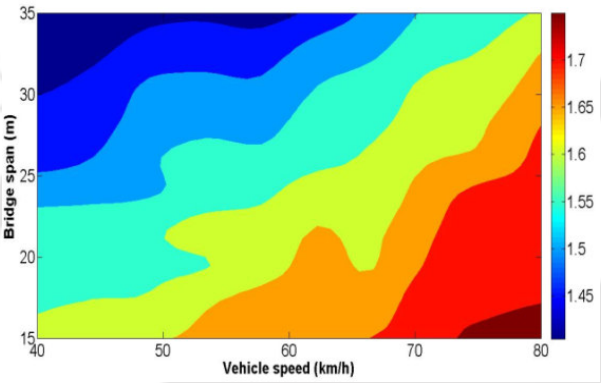

(b) Contour plot representation

Fig.6.14. Dynamic amplification factor with change in bridge span and vehicle speed

6.4.3 Effect of vehicle mass and approach settlement

The present study is intended to reveal the contribution of vehicle mass on the bridge response in presence of approach road settlement. The effect of vehicle mass as well as approach settlement on the DAF for a given vehicle speed 60 km/h has been studied and presented in the form of surface plot and contour in Fig. 6.15. It has been found that up to certain settlement of bridge approach, DAF decreases with increasing vehicle mass. This may be attributed to the reason that increase of vehicle weight increases maximum static deflection, which in turn causes the reduction of the non dimensional DAF. However, when approach road settlement increases from 20 mm to 30 mm, rapid increment of DAF from 3.14% to14.3% has been found even though the static response increases with increasing weight.

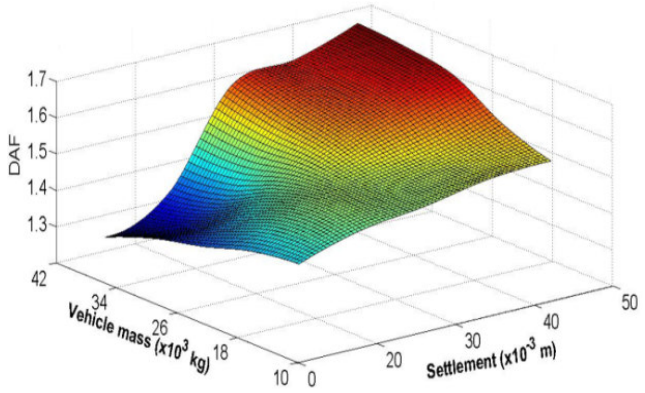

(a) Surface plot representation

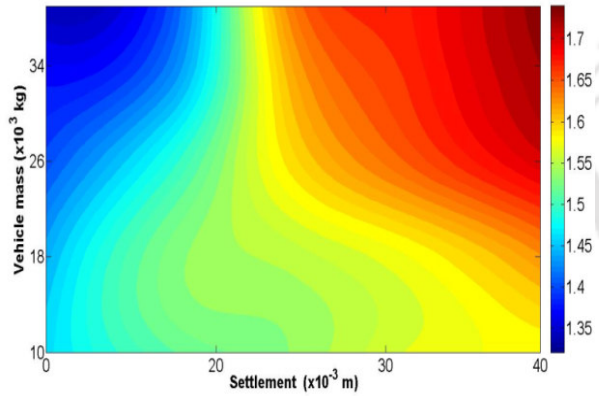

(b) Contour plot representation

Fig. 6.15 Dynamic amplification factor for different vehicle mass and approach road settlement

6.5 Response Statistics for Model-2

Model-2 incorporates vehicle body flexibility in bending which is an advanced version of a vehicle model and may realistically represents long slender vehicle body. Various parametric studies have been conducted in the present section to examine the contribution of vehicle body flexibility on the Bridge-Vehicle coupled dynamic behaviors.

6.5.1 Vehicle Response

The first and second order statistics of displacement, velocity and acceleration of vehicle centroid have been presented in Fig. 6.16 to Fig. 6.18. Similar characteristics of response pattern is reflected when different vehicle velocity considered in the present study. However, output frequency in case of vehicle response does not reveal notable change with variation of speed. It has also been observed that at highest speed considered in vehicle forward motion,

response magnitudes are lower in flexible vehicle model with two point input as compared to rigid lumped mass model with single point input. This may be due to the reason that a part of energy of coupled system is utilized for bending of vehicle body in flexible model and also due to action of input at two points instead of single point.

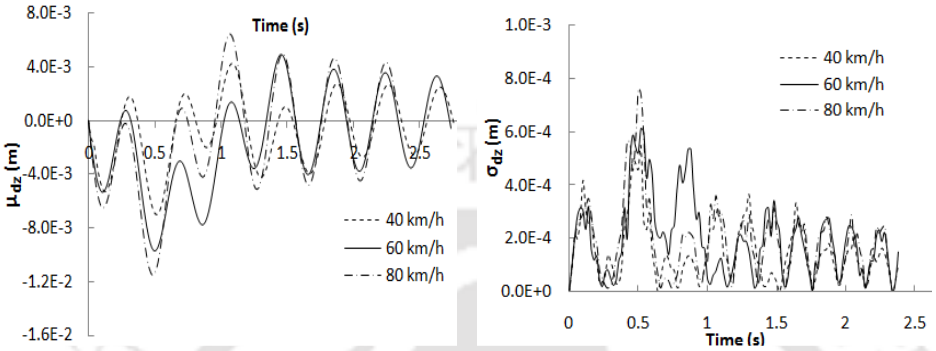

(a) Mean (b) Standard deviation

Fig.6.16. Mean displacement of vehicle C.G

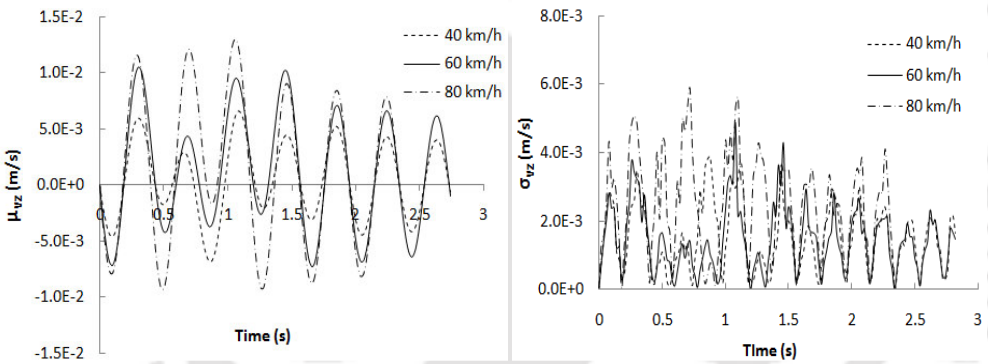

(a) Mean (b) Standard deviation

Fig.6.17. Mean Velocity of vehicle at C.G

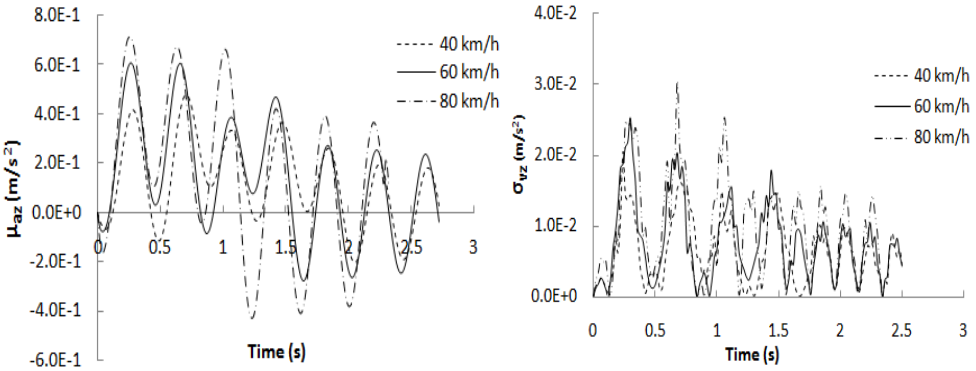

(a) Mean (b) Standard deviation

Fig.6.18. Mean acceleration of vehicle at C.G

The mean and standard deviation of front wheel displacement, velocity and acceleration time history have been shown in Fig.6.19 to Fig.6.21 and those for rear wheel have been presented in Fig.6.22 to Fig.6.24. The peak wheel response has been found to be lower in comparison with Quarter Car vehicle model. This becomes evident from the fact that interaction force is distributed at two points instead of concentrating at one point as in Quarter car model. Rear wheel has time delayed response and it experiences an already vibrating surface on entry. Due to this reason rear wheel responses are found to be higher than the front wheel dynamic response. Again, magnitude of peak responses appears higher with increased vehicle speed.

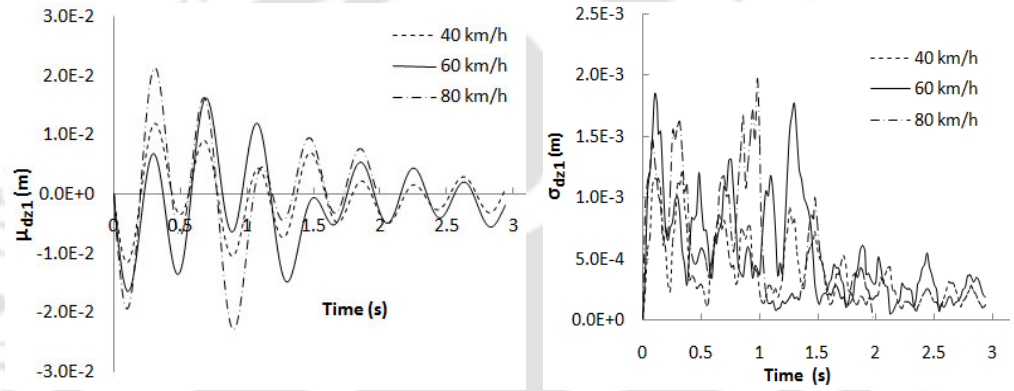

(a) Mean (b) Standard deviation

Fig.6.19. Front wheel displacement

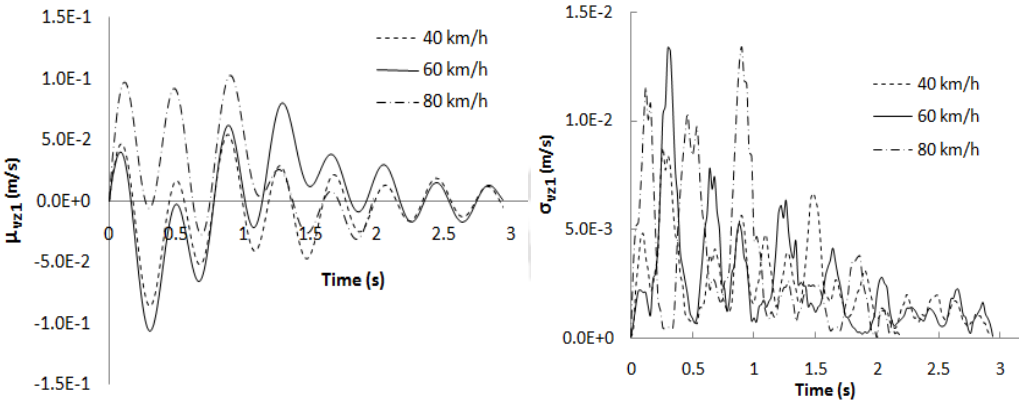

(a) Mean (b) Standard deviation

Fig.6.20. Front wheel velocity

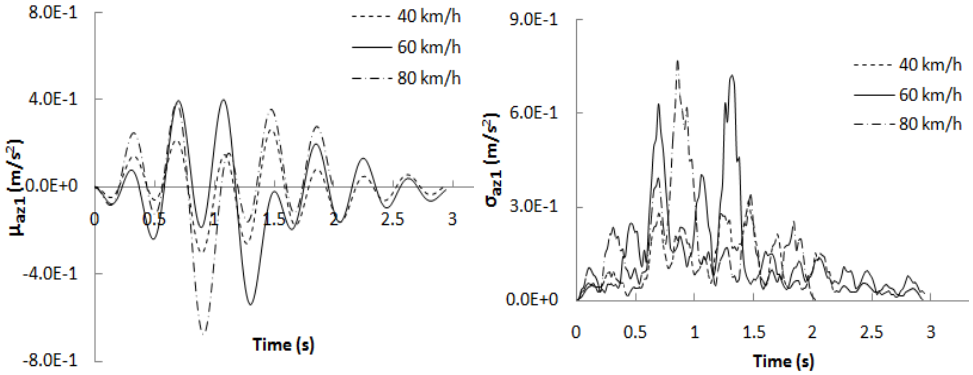

(a) Mean (b) Standard deviation

Fig.6.21. Front wheel acceleration

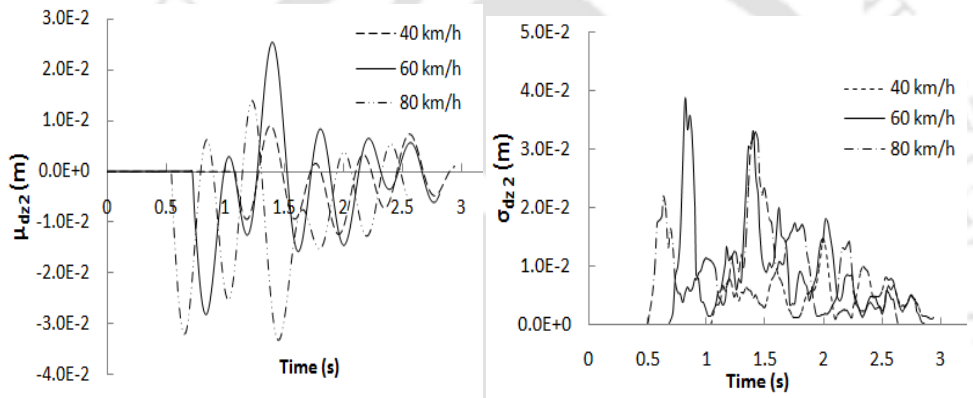

(a) Mean (b) Standard deviation

Fig.6.22. Rear wheel displacement

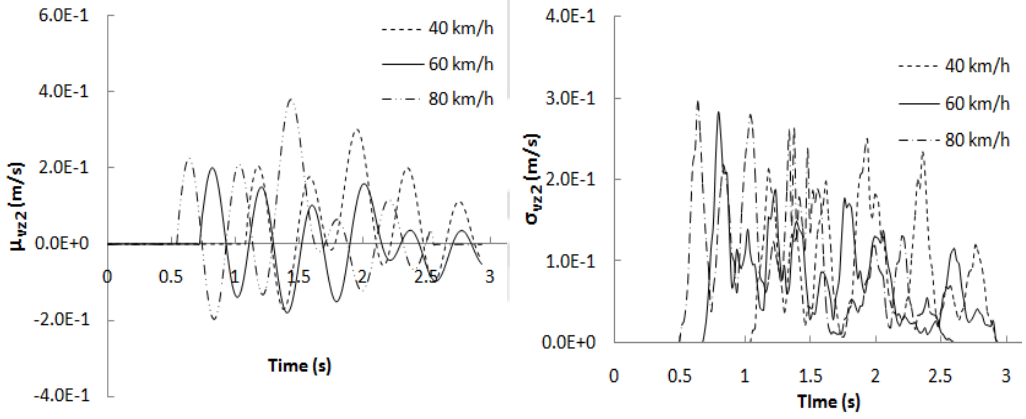

(a) Mean (b) Standard deviation

Fig.6.23. Rear wheel velocity

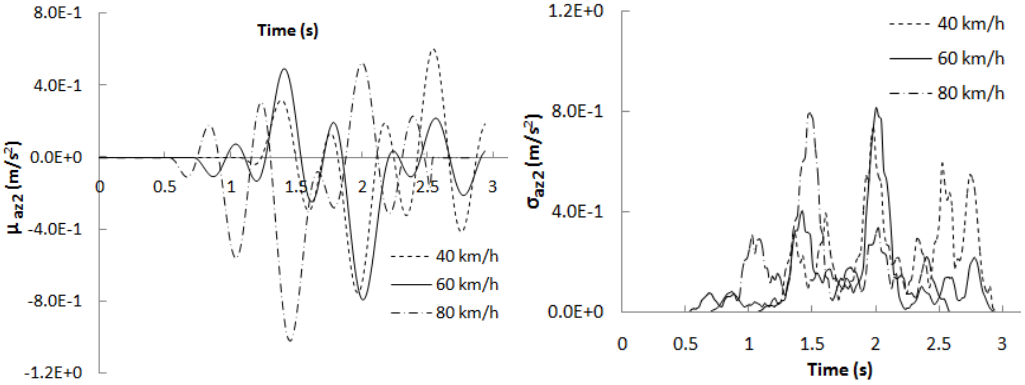

(a) Mean (b) Standard deviation

Fig.6.24. Rear wheel acceleration

6.5.2 Bridge Response

The mean and standard deviation of mid span displacement, velocity and acceleration of bridge when a Half car flexible model of vehicle interacts with the structure has been obtained and discussed in this section.

6.5.2.1 Effect of vehicle speed

Bridge mean responses at mid span –displacement, velocity and acceleration subjected to three vehicle speed and the corresponding standard deviation have been shown in Fig. 6.25 to Fig. 6.27. Similar to Model-1, mean of peak deflection is found to increase with the vehicle speed and shift of the peak occurs as velocity changes. This explains the fact that input dominant frequency gets modified as the vehicle speed changes. Second order statistics (standard deviation) of displacement and its derivatives clearly reflects presence of high frequency components in pavement unevenness, which is completely missed in first order statistics (mean). This is more evident in standard deviation of acceleration. The peak magnitude is clearly higher in case of vehicle travelling with higher velocity. No definite pattern is discernible in the standard deviation. The coefficient of variation of peak displacement, velocity and accelerations are found to be 0.11, 0.183 and 0.105 respectively. It may be mentioned that dynamic loads do not lead to major bridge damage, except in resonance but they contribute to continuous degradation of bridge increasing necessity of bridge maintenance.

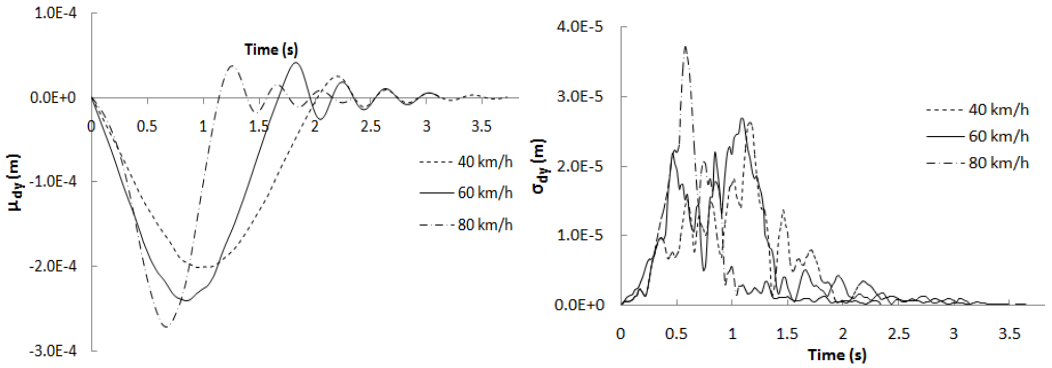

(a)Mean (b) Standard deviation

Fig. 6.25 Bridge displacement at mid span

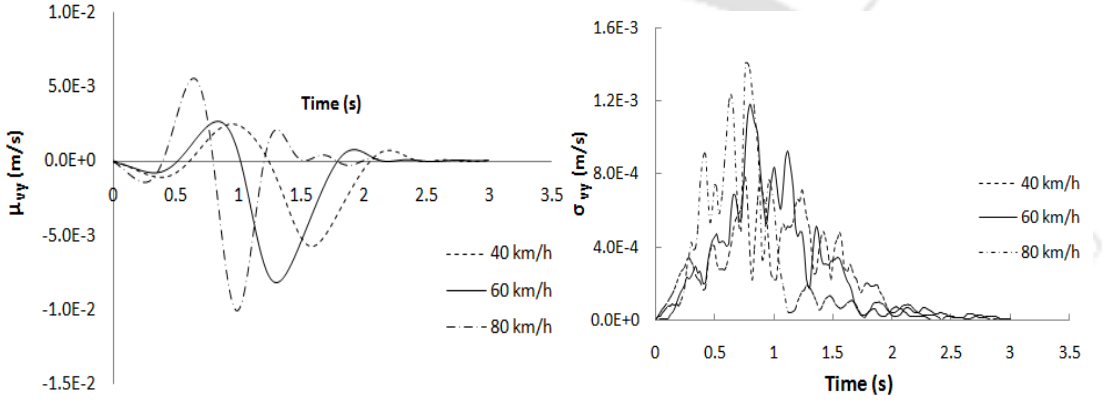

(a)Mean (b) Standard deviation

Fig. 6.26 Bridge velocity at mid span

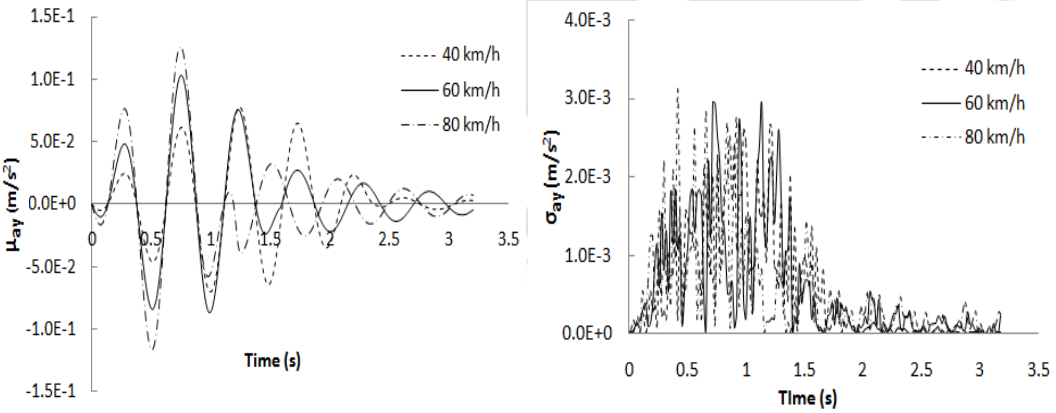

(a)Mean (b) Standard deviation

Fig. 6.27 Bridge acceleration at mid span

6.5.2.2 Effect of eccentricity of vehicle path

Different loading position from the centre of the bridge width has been considered to reflect the effect of eccentricity on the bridge response. The vehicle stiffness for comparing the results, shown in Fig. 6.28, is taken uniform (E_vI_v=5.3×10^6 N.m^2) with uniform vehicle velocity 60 km/h. The roughness of the bridge deck has been assumed to be of poor category as per ISO classification corresponding to roughness coefficient $S_{GG}(\Omega_0)$=160×10^{-6} m^2/cycle /m (ISO-8608: 1995). Result shows that 6% to 7% increment in the bridge peak displacement magnitude occurs as the eccentricity varies from 0.5 m to 1.5m.

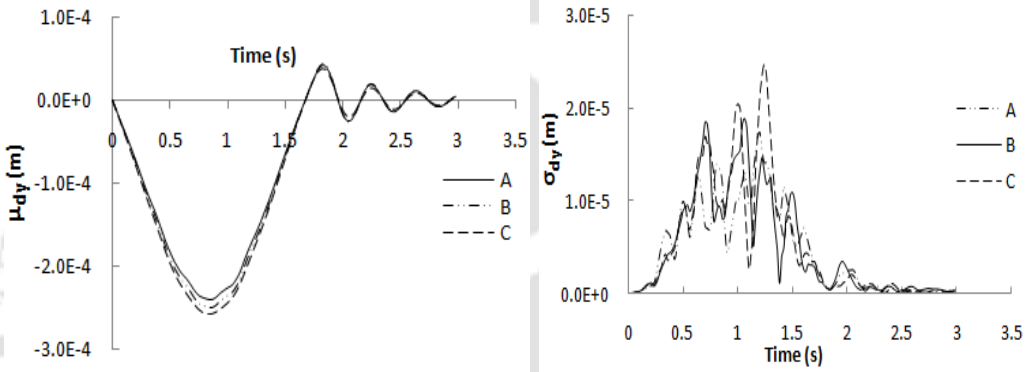

(a) Mean (b) Standard deviation

Fig.6.28. Bridge mid-span displacement due to different eccentricity of vehicle path (e_x), (A) e_x=0.5 m, (B) e_x =1 m, (C) e_x =1.5 m

6.5.2.3 Effect of approach road settlement

Approach settlement often present in existing bridges is a primary factor producing high vehicle impact to a bridge at entry. In the present study, effect of this factor on the bridge response has been examined for different settlement magnitudes. Bridge mid span displacements subject to vehicle of axle spacing 12 m travelling at 60 km/h speed are shown in Fig. 6.29. Increment in the bridge response has been found to be insignificant for approach settlement up to 15 mm which is also observed in discussing the behaviour of Model-1. However, the response magnitude increases considerably in the range of 12.5% to 31.3% when settlement is between 25 mm to 40 mm. Moreover, high frequency component of pavement unevenness is also captured in time history when high transient is set up as vehicle encounters a road level difference of 40 mm at entry.

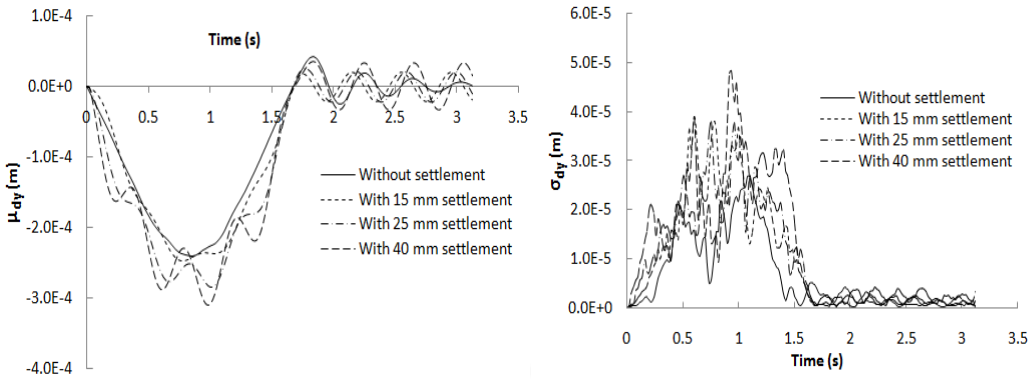

(a) Mean (b) Standard deviation

Fig.6.29. Bridge mid span deflection for different settlement

6.5.2.4 Effect of vehicle bending modes

The comparison of mean and standard deviation of bridge at mid span deflection with different values of vehicle flexural rigidity has been presented in Fig.6.30. It may be noted that as the vehicle becomes more flexible, the bridge mid span deflection is reduced. This is possibly due to the fact that substantial part of energy is utilized in bending vehicle body rather than transferring vibration energy to the pavement. In order to get clearer evidence of this fact, pavement interaction force time history for two wheels have been compared by taking separately only rigid modes and combination of rigid and first five bending modes of the vehicle. The comparison of mean and standard deviation of interaction force imposed by front wheel and rear wheel has been presented in Fig.6.31 and Fig. 6.32. The mean and standard deviation of force induced by flexible model of vehicle is found to be less compared with the vehicle having only rigid modes. The contribution of significant number of structural mode of vehicle on the bridge response has been examined in a bar diagram presented in Fig 6.33 (a) and Fig. 6.33 (b) by comparing maximum mean and standard deviation respectively. In generating numerical results under this section vehicle velocity is taken as 60 km/h. It may be seen that inclusion of bending modes of the vehicle reduces the response magnitude of the bridge. From the same figure it also reveals that when flexible modes of the vehicle are considered, summation of first five modes in modal super imposition procedure is adequate.

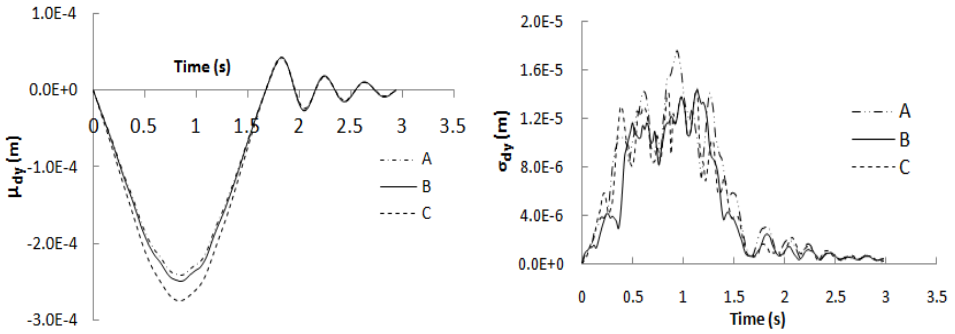

(a) Mean (b) Standard deviation

Fig.6.30. Effect of flexibility on bridge displacement response, (A) E_vI_v=5.3x10^6 N-m^2, (B) E_vI_v=6.4x10^7 N-m^2, (C) E_vI_v=8.2x10^{10} N-m^2

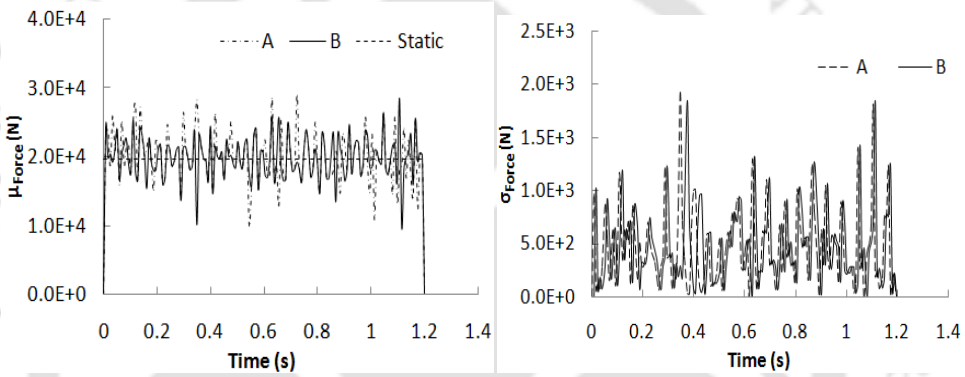

(a) Mean value (b) Standard deviation

Fig.6.31. Comparison of front wheel interaction force, (A) Only rigid modes of vehicle body (B) vehicle body rigid modes with first five structural bending modes

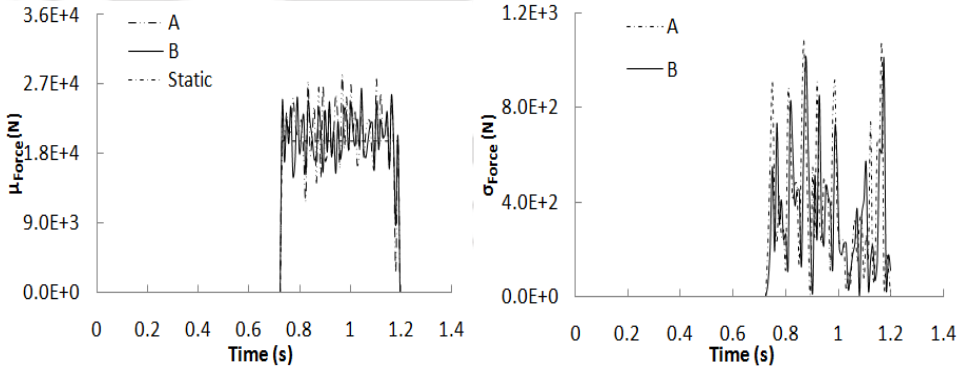

(a) Mean value (b) Standard deviation

Fig.6.32. Comparison of rear wheel interaction force, (A) Only rigid modes of vehicle body (B) vehicle body rigid modes with first five structural bending modes

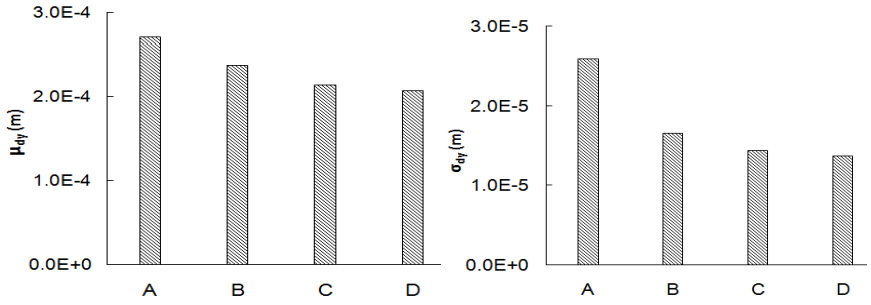

(a) Mean (b) Standard deviation

Fig.6.33. Maximum displacement of bridge at mid span (A) Only rigid modes of vehicle body (B) vehicle body rigid modes with first elastic mode (C) vehicle body rigid modes with first three structural modes (D) vehicle body rigid modes with first five structural modes

6.6. Dynamic Amplification Factor for Model-2

In the present day's scenario, vehicle configuration has greatly changed. This obviously has an impact on the dynamic amplification factor of bridge response. In the present section, a numerical study has been conducted to examine the effect of various important parameters on DAF, taking flexible vehicle model into consideration.

6.6.1 Effect of bridge surface roughness and vehicle speed

Experimental investigations report that bridge deck surface roughness and speed of the vehicle are prominent factors that can cause increased dynamic amplification factor leading to rapid degradation of the bridge (Huang *et al.,* 1992). Bridge dynamic amplification factor has been found by changing bridge surface roughness coefficient for very good condition to poor condition as mentioned in ISO specification (ISO 8608: 1995) simultaneously with change in vehicle speed. Hence, a surface plot and contour has been shown in Fig. 6.34. The results show that for the same vehicle load poor condition of road increases DAF by an amount of 12% to 17% when vehicle moves over it. Moreover simultaneous increase in vehicle speed leads to further amplification. This necessitates proper maintenance of bridge surface and speed restriction.

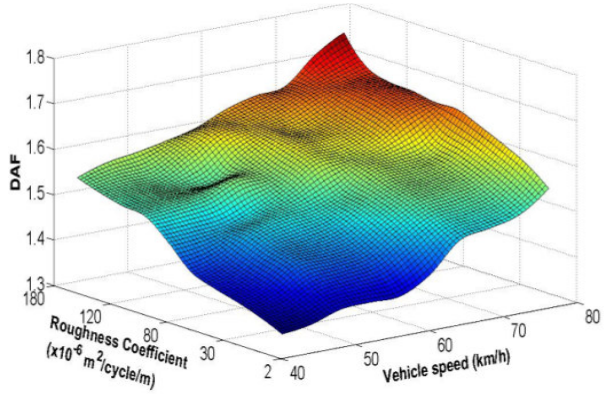

(a) Surface plot representation

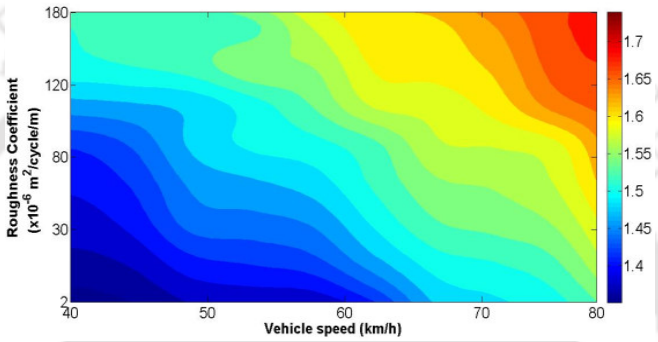

(b) Contour plot representation

Fig.6.34. Dynamic amplification factor with vehicle speed and bridge surface roughness coefficient

6.6.2 Effect of bridge span and velocity

In most of the bridge design codes span of the bridge decides the impact factor. Although some researchers (Hwang and Nawak, 1991; Paultre *et. al.,* 1992; Brady *et. al.,* 2006; Hossain and Amanat, 2011) have explored the combined effect of bridge span and velocity on Dynamic Amplification Factor, their study ignored vehicle flexibility. Fig. 6.35 shows the variation of DAF with the bridge span and velocity in the form of surface plot and contour. The sections of the plot along the span direction indicate that in a span range of 15m to 35m, dynamic amplification factors decrease by an amount of 5.4% to 8.1% while the sections along speed axis reveal that increase of speed from 40 km/h to 80 km/h results in 10% to 16% increment of DAF in the range of span considered in the study. This example may indicate that representation of impact factor only by bridge span is insufficient to incorporate vehicle induced dynamic load in the design of bridge.

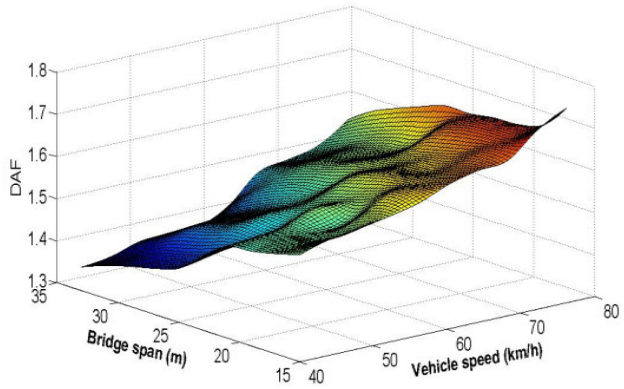

(a) Surface plot representation

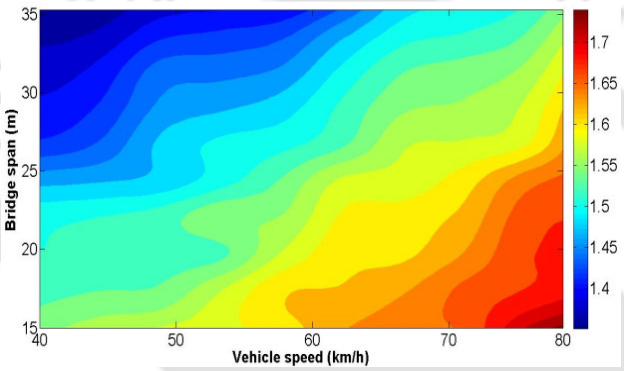

(b) Contour plot representation

Fig.6.35. Dynamic amplification factor with change in bridge span and vehicle speed

6.6.3 Effect of vehicle axle spacing and approach settlement on DAF

The effect of vehicle axle spacing as well as approach road settlement on the dynamic amplification factor (DAF) is shown in Fig. 6.36. Result shows that if approach slab settlement does not exist, DAF decreases with increase in vehicle axle spacing. This is expected as the increase of axle spacing causes bending modes to be more active than the rigid body modes. However, in presence of significant amount of bridge approach settlement (25 mm–40 mm), flexibility of vehicle would not give any advantage in terms of the reduction of DAF, rather DAF has been found to increase by 6% to 17%.

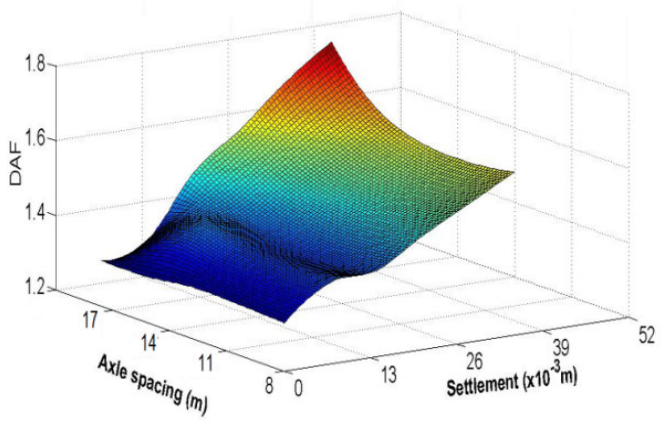

(a) Surface plot representation

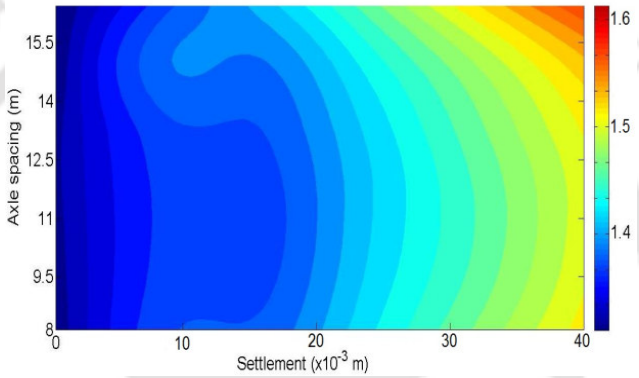

(b) Contour plot representation

Fig.6.36. Dynamic amplification factor for different axle spacing and approach settlement

6.6.4 Effect of vehicle mass and approach settlement

The contribution of distributed vehicle mass on the bridge response with different approach slab settlement magnitude has been presented. Fig. 6.37 shows combined effect of vehicle mass and approach road settlement on the dynamic amplification factor (DAF) as surface plot and contour. It has been found that up to certain settlement of approach road, DAF decreases with increasing vehicle mass. Hwang and Nowak (1991) observed the same effect on DAF of bridge for a rigid model of vehicle. It is obvious that increase in vehicle weight increases maximum static deflection as a result of which reduction of amplification factor occurs. The same trend has been observed even with the presence of approach settlement up to 15 mm. However, when approach settlement increases beyond it and goes up to maximum value chosen as 40 mm, DAF is found to increase by an amount of 9.2% to 18.5% even though the static response increases with increasing weight. Result shows that when vehicle experiences a smooth entry, an increase in its mass has not much significant effect on the bridge response,

but even small and sudden difference of road profile at the bridge entry can cause considerable amount of transient response. This calls for the proper inspection and maintenance of the bridge approach and expansion joints.

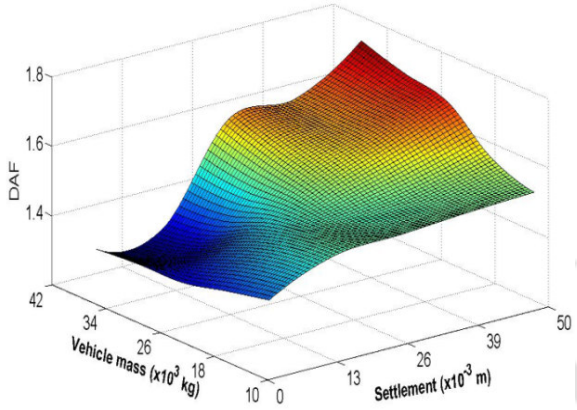

(a) Surface plot representation

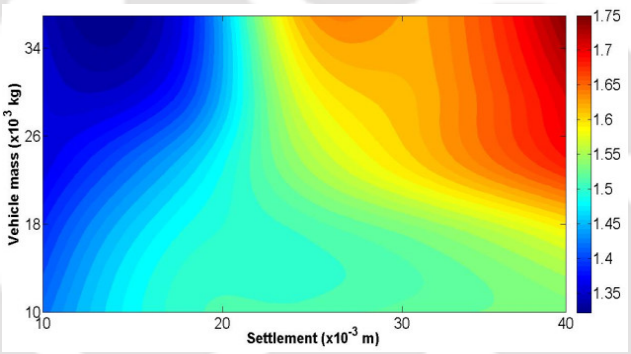

(b) Contour plot representation

Fig.6.37. Dynamic amplification factor for different vehicle mass and approach road settlement

6.7 Response Statistics for Model-3

In the present section, dynamic behavior of Bridge-Vehicle coupled system has been investigated idealizing vehicle as a Full Car Model which is expected to predict more realistic results then the previous vehicle models. In this model, vehicle is excited by pavement input at four wheel locations as described in Section 3.4.3 of Chapter 3. Since wheels experience different unevenness at each of the four locations, vehicle body undergoes bounce and rotation about longitudinal and transverse axis. This model is sometimes described as Heave-pitch-roll model. In the present study, we consider vehicle body as flexible in both bending

and torsion, therefore elastic bending and torsion modes are considered along with three rigid body modes (heave, pitch and roll). Results have been presented to observe the behavior of the model for the variation of different parameters.

6.7.1 Vehicle Response

The mean and standard deviation of displacement, velocity and acceleration at the centroid of vehicle body has been shown in Fig. 6.38 to Fig. 6.40. The vehicle body vertical displacement is influenced by both bending and twisting modes. The mean displacement shows interaction of various modes of vibration with appearance of higher frequency components as compared to that seen in other two models. More rapid fluctuation of peaks is observed in mean displacement, velocity and acceleration time history of vehicle centroid. Standard deviation of mean displacement at centroid of vehicle body displays a high peak when vehicle is nearer the mid span of the bridge. It may be noted that vehicle is excited by two sources-one is pavement unevenness and another is bridge deflection. Twist of the vehicle body is non uniform as the elastic torsional vibration takes place and varies along the length of the vehicle. The mean and standard deviation of torsional rotation, torsional velocity and torsional acceleration are depicted in Fig.6.41 to Fig.6.43.

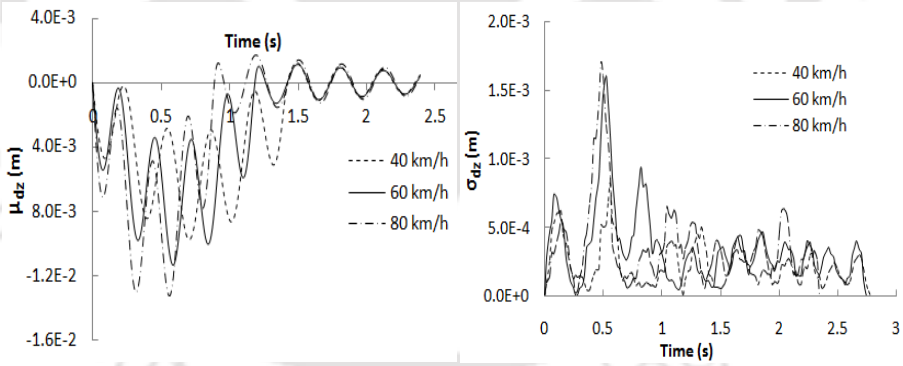

(a) Mean (b) Standard deviation

Fig.6.38. Vertical displacement of vehicle at C.G

The response mean shows that as long as vehicle is within the bridge, the output frequency is affected by the interaction of various modes in the coupled system showing high fluctuation of magnitudes of peak. In the analysis, no wheel input from bridge pavement is considered as soon as the vehicle completely crosses the bridge and therefore free vibration takes place at different frequency. This is more clearly visible in mean acceleration time history. In the standard deviation of transverse rotation, rolling velocity and acceleration, multiple peaks are

seen. The response magnitudes in translatory and rotational motion increase with the increase in vehicle forward velocity.

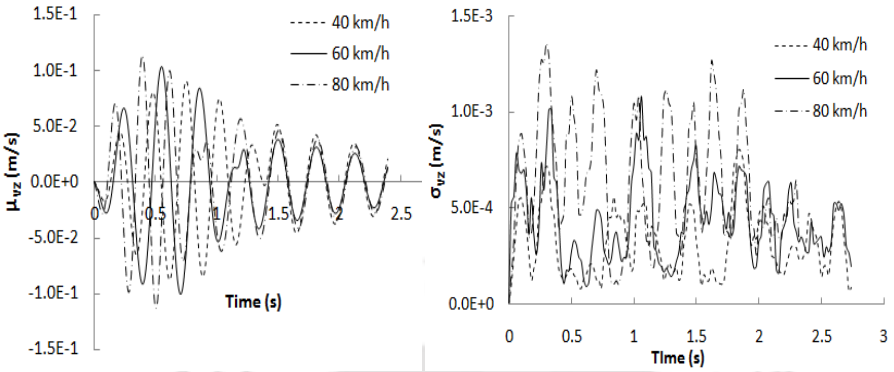

(a) Mean (b) Standard deviation

Fig.6.39. Vertical velocity of vehicle at C.G

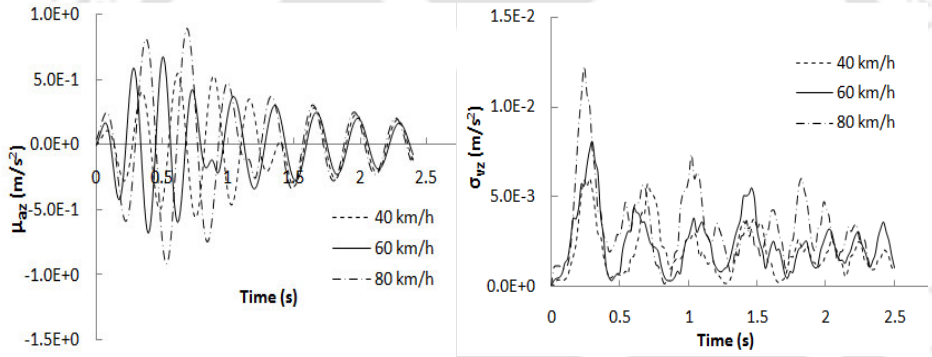

(a) Mean (b) Standard deviation

Fig.6.40. Vertical acceleration of vehicle at C.G

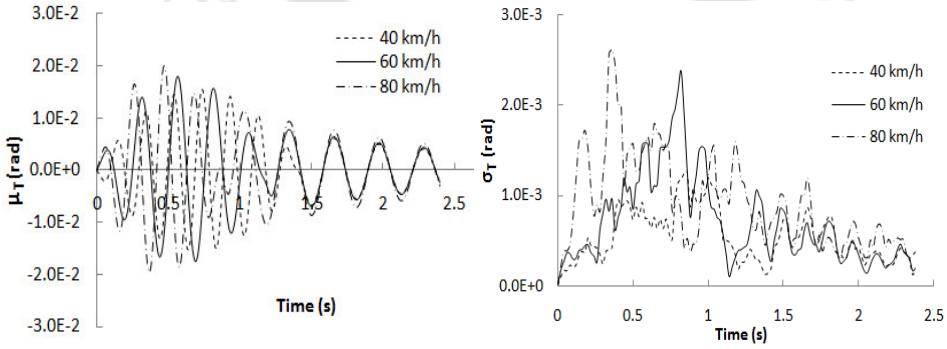

(a) Mean (b) Standard deviation

Fig.6.41. Torsional rotation of vehicle at C.G

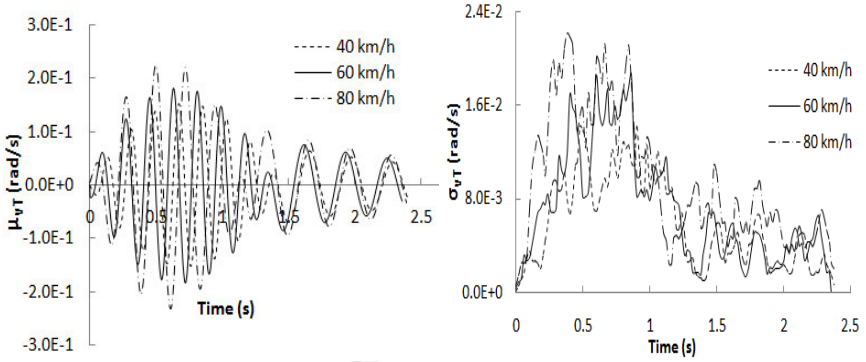

(a) Mean (b) Standard deviation

Fig.6.42. Torsional velocity of vehicle at C.G

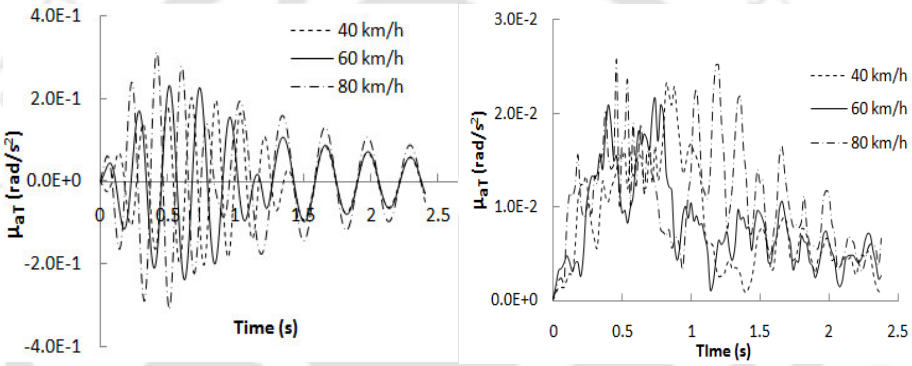

(a) Mean (b) Standard deviation

Fig.6.43. Torsional acceleration of vehicle at C.G

The mean and standard deviation of displacement, velocity and acceleration time history for each of the four unsprung masses have been shown in Fig.6.44 to Fig.6.55. It may be noted that as rear wheel enters into the bridge later, response time histories of rear unsprung masses have been shown with time delay. No remarkable influence of velocity on the magnitudes of wheel displacement is clearly reflected in the entire segment of the time history. However, it is seen that each wheel represents somewhat different features in terms of the location of peak and magnitude for each of vehicle speed considered. This may be due to rolling of vehicle as the wheel experiences different input from longitudinal and transverse bridge surface profile. The mean and standard deviation of wheel responses are found to be lower compared to the model where rolling of the vehicle body has been ignored.

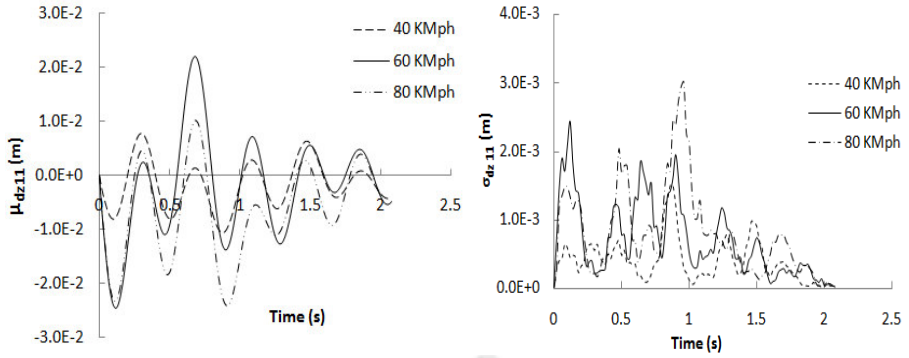

(a) Mean (b) Standard deviation

Fig.6.44. Displacement of front wheel in right side of the vehicle

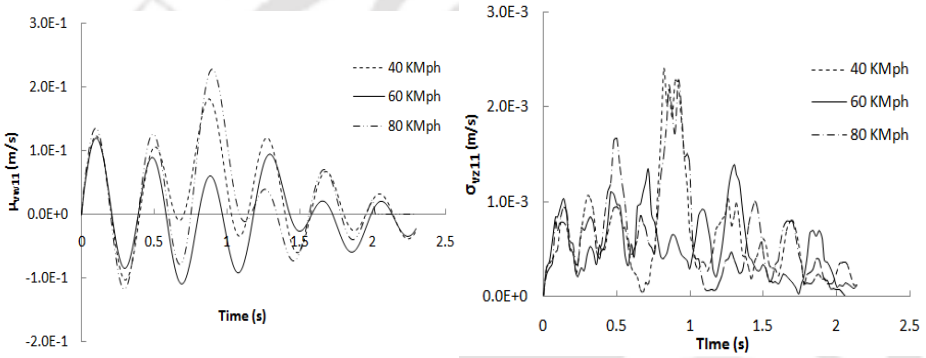

(a) Mean (b) Standard deviation

Fig.6.45. Velocity of front wheel in right side of the vehicle

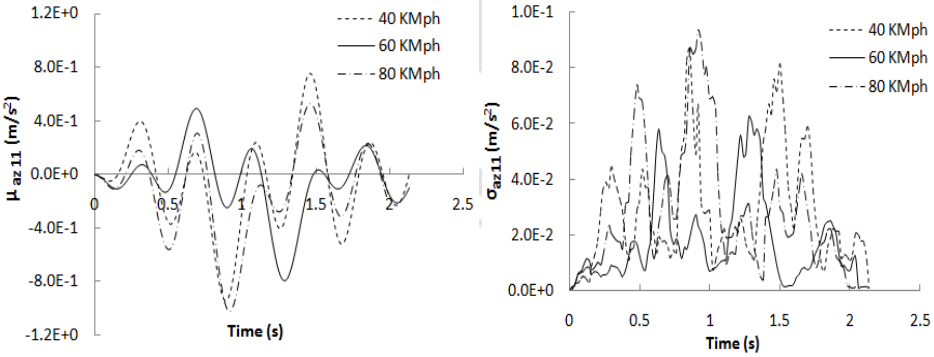

(a) Mean (b) Standard deviation

Fig.6.46. Acceleration of front wheel in right side of the vehicle

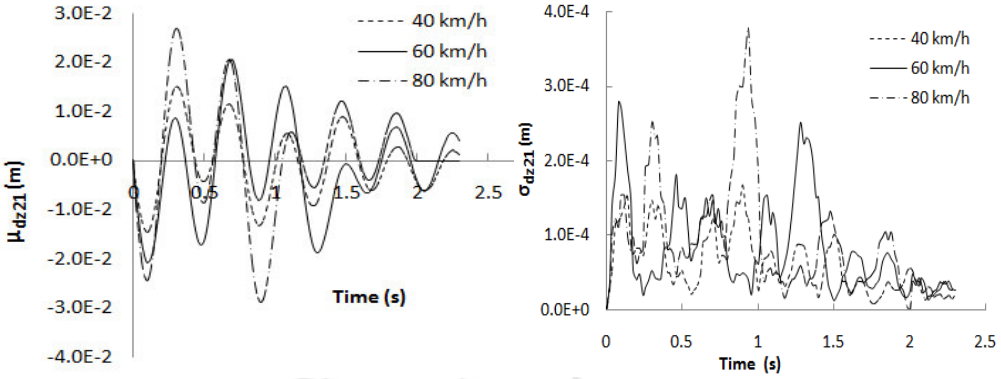

(a) Mean (b) Standard deviation

Fig.6.47. Displacement of front wheel in left side of the vehicle

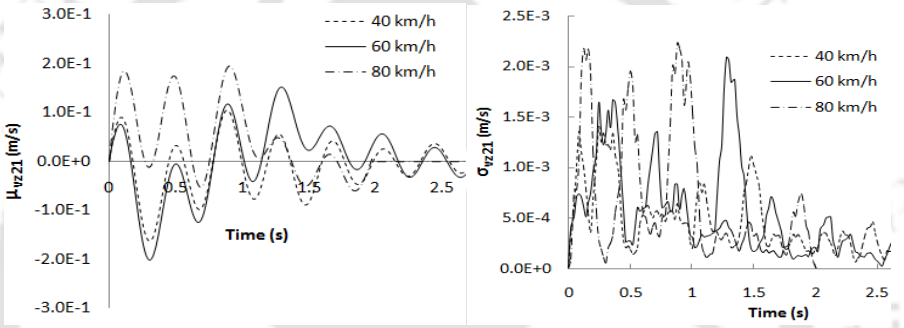

(a) Mean (b) Standard deviation

Fig.6.48. Velocity of front wheel in left side of the vehicle

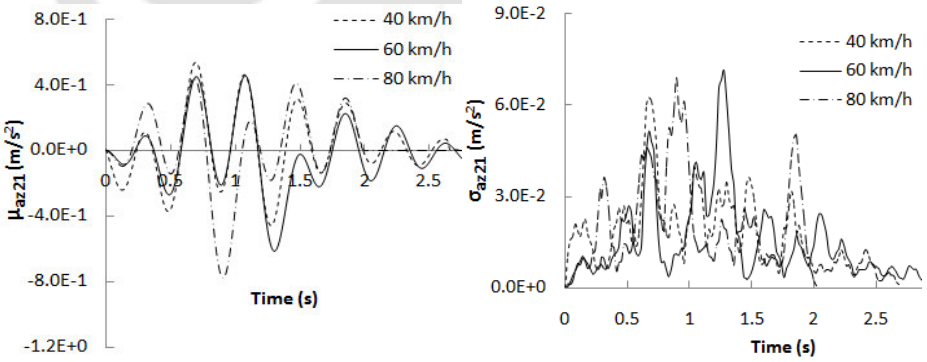

(a) Mean (b) Standard deviation

Fig.6.49. Acceleration of front wheel in left side of the vehicle

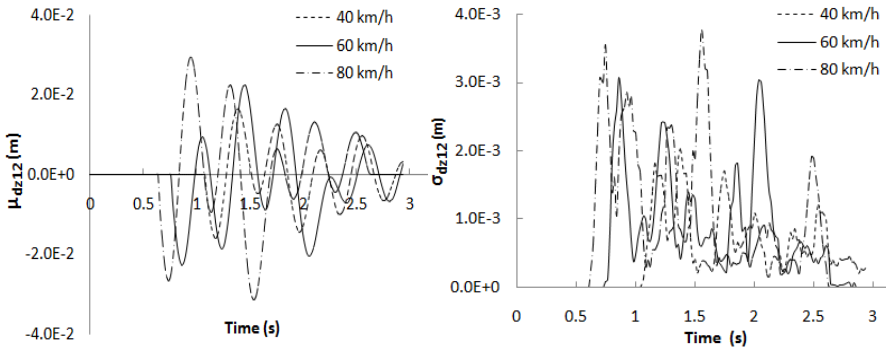

(a) Mean (b) Standard deviation

Fig.6.50. Displacement of rear wheel in right side of the vehicle

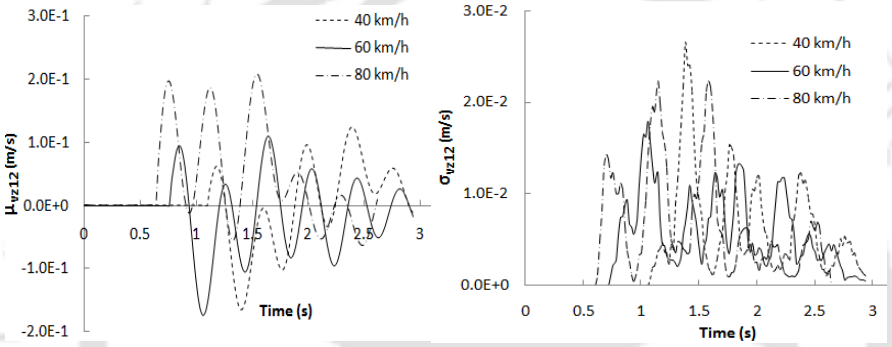

(a) Mean (b) Standard deviation

Fig.6.51. Velocity of rear wheel right in side of the vehicle

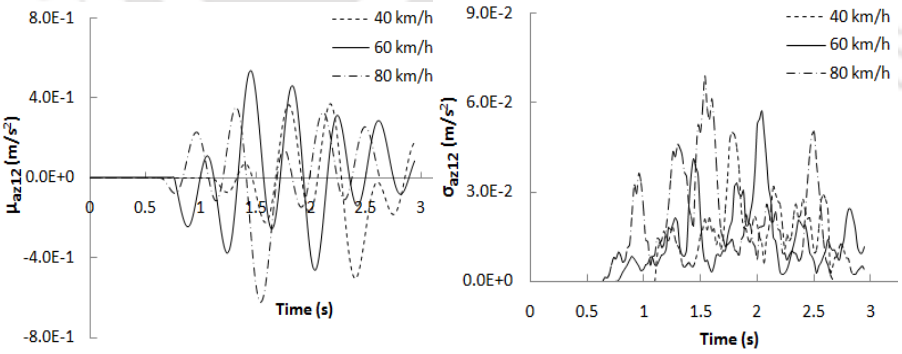

(a) Mean (b) Standard deviation

Fig.6.52. Acceleration of rear wheel in right side of the vehicle

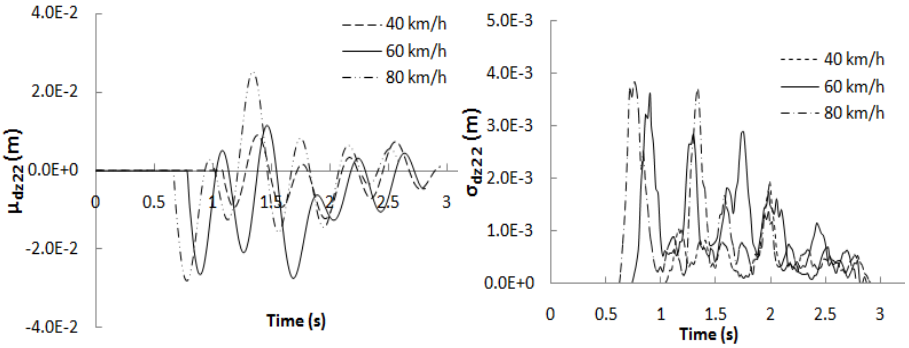

(a) Mean (b) Standard deviation

Fig.6.53. Displacement of rear wheel in left side of the vehicle

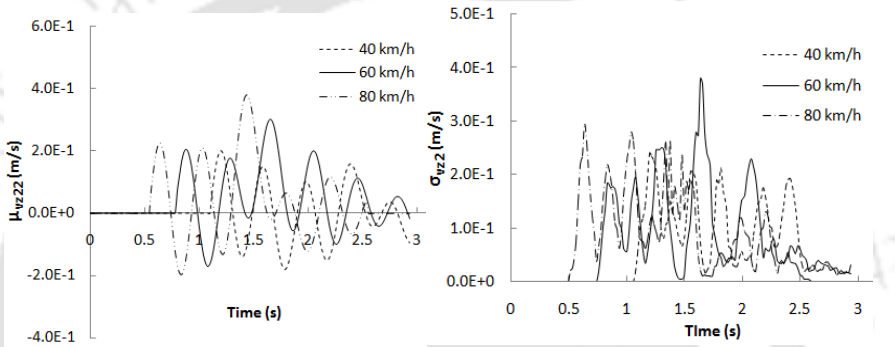

(a) Mean (b) Standard deviation

Fig.6.54. Velocity of rear wheel in left side of the vehicle

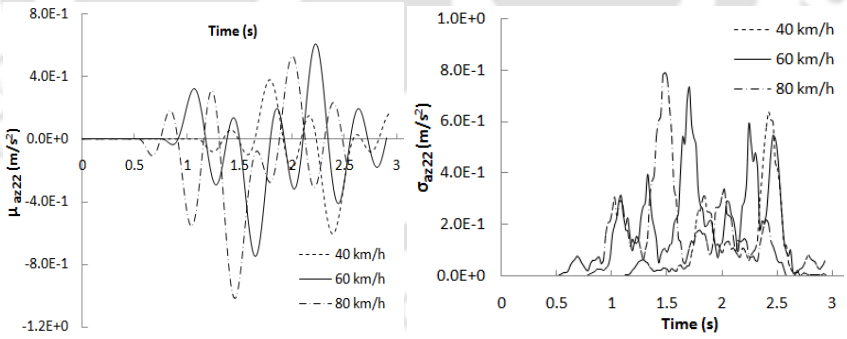

(a) Mean (b) Standard deviation

Fig.6.55. Acceleration of rear wheel in left side of the vehicle

6.7.2 Bridge Response

In this section, we present the effect of important parameters on the mean and standard deviation of mid span deflection, velocity and acceleration of the bridge due to passage of a

flexible full car body. Dynamic Amplification factors have been presented and its changes due to simultaneous variation of bridge-vehicle parameters have been discussed.

6.7.2.1 Effect of vehicle speed

In a Bridge-Full car Vehicle interaction problem, longitudinal and transverse surface roughness will play important role in transmitting dynamic force on the pavement. This has been investigated considering three different vehicle forward velocities. In this illustration, poor category of surface unevenness as per ISO classification has been considered. The mean and standard deviation of mid span deflection, velocity and acceleration have been shown in Fig.6.56- Fig.6.58. There is a systematic increase of peak magnitude of mean displacement with speed with a notable shifting of peak towards the left. This once again confirms the modification of driving frequency with increase in vehicle speed. However, in this case standard deviation does not show any definite trend. In derivatives of displacement, more number of waves appears and dependence of excitation frequency on the vehicle speed is not clearly observed. High frequency component of spatial disturbance in bridge deck has been found to appear in acceleration response. Magnitudes of standard deviation are not very significant. The coefficient of variation of peak displacement, velocity and accelerations are found to be 0.17, 0.214 and 0.113 respectively.

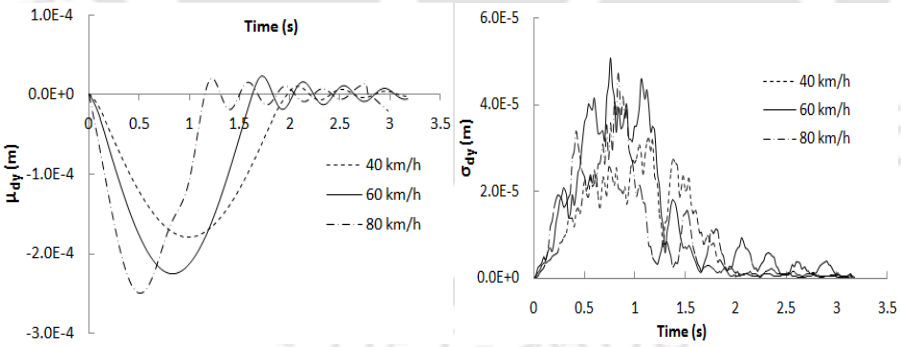

(a)Mean (b) Standard deviation

Fig.6.56. Bridge displacement at mid span

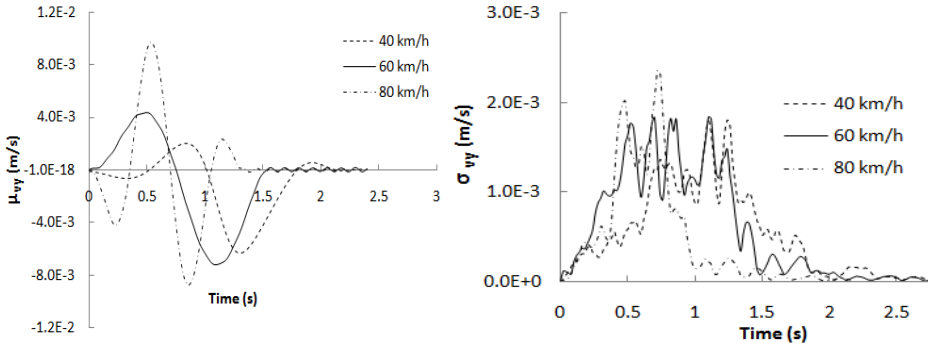

(a)Mean (b) Standard deviation

Fig.6.57. Bridge velocity at mid span

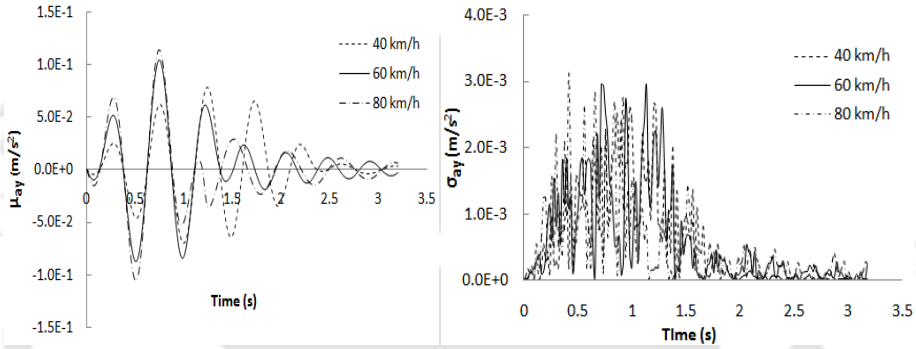

(a)Mean (b) Standard deviation

Fig.6.58. Bridge acceleration at mid span

6.7.2.2 Effect of eccentricity of vehicle path

In a Full Car Model, a distance between vehicle body longitudinal axis and the centre line of the bridge has been considered as eccentricity (e_x). In generating numerical results under this section vehicle velocity 60 km/h has been considered. The vehicle flexural and torsional stiffness are taken uniform (E_vI_v=5.3×10^6 N.m^2, G_vJ_v=9.02x10^2 N-m^2). Fig. 6.59 presents mean and standard deviation of bridge mid span vertical deflection for different eccentric position of vehicle. An increase of 6.8% to 9.1% in the bridge dynamic responses has been observed as the eccentricity varies from 0.5 m to 1.5m. It may be mentioned that bridge torsional mode is activated when load eccentricity exists. Moreover rolling of vehicle alters the pattern of vehicle loading.

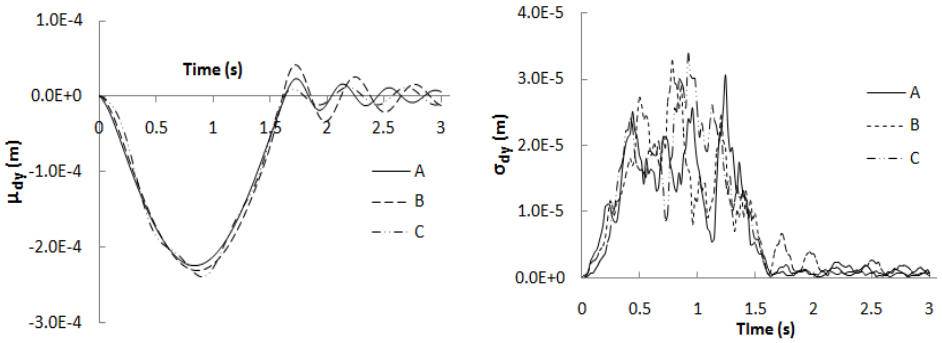

(a) Mean (b) Standard deviation

Fig.6.59. Bridge mid-span displacement due to different eccentricity of vehicle path (e_x), (A) e_x=0.5 m, (B) e_x =1 m, (C) e_x =1.5 m

6.7.2.3 Effect of approach road settlement

Bridge mid span displacements for different level of approach settlement has been shown in Fig. 6.60, by considering a full car vehicle model with 12 m vehicle axle spacing and 2 m tread width. Investigation has been performed for constant speed of 60 km/h. Result shows that approach settlement up to 15 mm has negligible effect on the bridge dynamic response. However, significant increment in the range of 13.2% to 36.2% with high fluctuation has been observed in the bridge response as settlement increases from 25 mm to 40 mm. It is apprehended that high impact effect due to sudden change of the road profile of significant amount might have triggered higher vibrational mode of bridge.

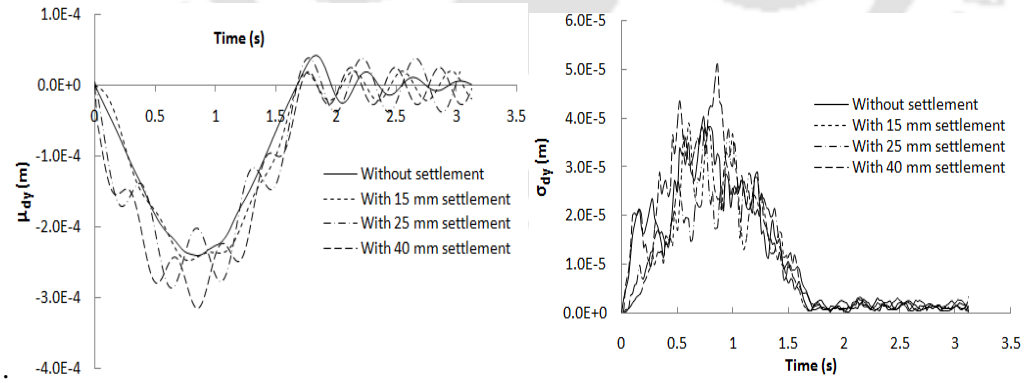

(a) Mean (b) Standard deviation

Fig.6.60. Bridge mid span deflection for different settlement

6.7.2.4 Effect of vehicle structural modes

The present vehicle model incorporates rigid as well as elastic mode in both bending and torsion. In order to investigate contribution of vehicle body structural mode on bridge response, only rigid mode has been considered first and then elastic modes are included in the analysis. The contribution of significant number of structural mode of vehicle on bridge response has been examined in a bar diagram presented in Fig 6.61 by comparing maximum mean and standard deviation of mid span deflection. Four cases have been considered. These are (A) Only rigid modes (heave, pitch and roll) of vehicle body (B) Three rigid modes along with first elastic mode in both bending and torsion (C) Three rigid modes along with first three structural modes in bending and torsion (D) Three rigid modes along with first five structural modes in bending and torsion. Bridge response magnitude has been found to be higher when only rigid body motion of the vehicle is considered in the analysis. The mid span mean displacement has been found to be 35% less when flexible vehicle loading has been considered on the bridge. From the same figure it is also seen that when flexible modes of the vehicle are considered, summation of first five modes for finding the response is adequate.

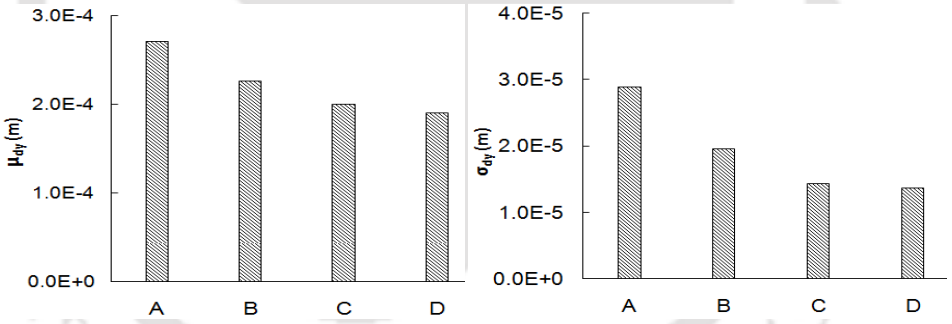

(a) Mean (b) Standard deviation

Fig.6.61. Maximum displacement of bridge at mid span (A) Only rigid modes of vehicle body, (B) Three rigid modes along with first elastic mode in both bending and torsion (C) Three rigid modes along with first three structural modes in bending and torsion (D) Three rigid modes along with first five structural modes bending and torsion

6.8. Dynamic Amplification Factor for Model-3

Amplification of bridge response due to vibratory moving load of vehicle using full car vehicle models (Model-3) has been presented in this section. More realistic trends of the

results are expected in this model since vehicle rolling due to change in pavement profile in transverse direction is considered.

6.8.1 Effect of bridge surface roughness and vehicle speed

Combined effect of surface roughness and speed of the vehicle on dynamic amplification factor has been presented in Fig.6.62. Bridge dynamic amplification factor has been found by changing bridge surface roughness coefficient for good condition to poor condition as mentioned in ISO specification (ISO 8608: 1995) with change in vehicle speed. The results show that poor condition of road induces more deflection leading to increased dynamic amplification factor on the bridge subject to moving vibratory load which can be aggravated by the increase in vehicle speed.

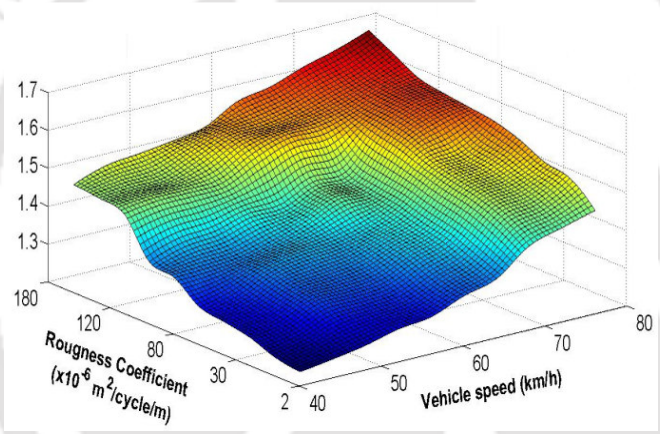

(a) Surface plot representation

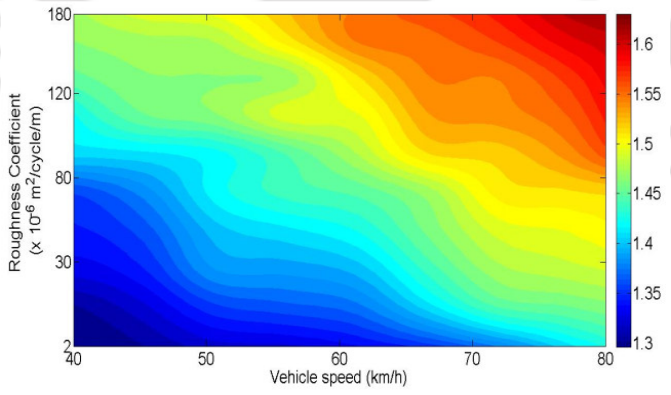

(b) Contour plot representation

Fig.6.62. Dynamic amplification factor with vehicle speed and bridge surface roughness coefficient

6.8.2 Effect of bridge span and velocity

The variation of DAF with change in bridge span and velocity is shown in Fig. 6.63. It has been found as in earlier case that bridge with a span ranging between 15 m to 35 m, dynamic amplification factor decrease by an amount of 10% to 13.2%, irrespective of increase of vehicle velocity. However, the rate of increase of DAF is slower in this model.

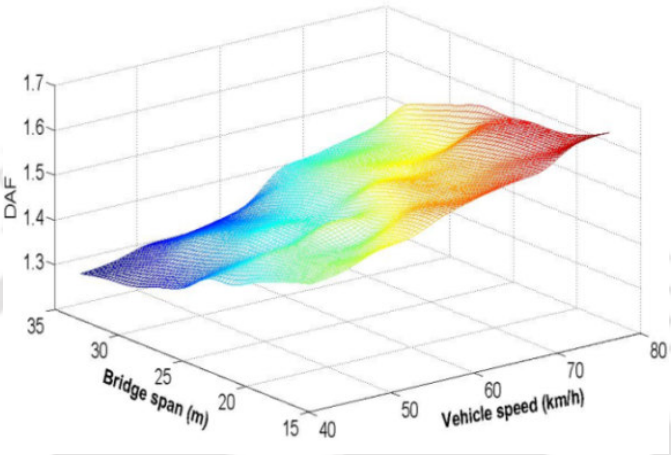

(a) Surface plot representation

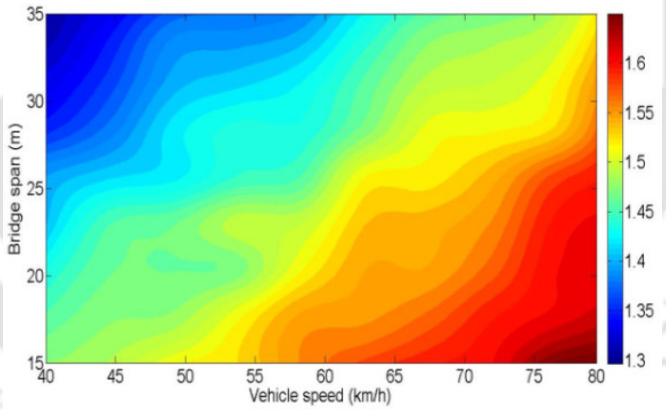

(b) Contour plot representation

Fig.6.63. Dynamic amplification factor with vehicle speed and bridge span

6.8.3 Effect of vehicle axle spacing and approach settlement on DAF

The effect of vehicle axle spacing on dynamic amplification factor (DAF) in the presence of different settlement in approach road is shown in Fig. 6.64. Case studies have been conducted for different settlement magnitude in the range of 0 mm to 40 mm and axle spacing varying from 8 m to 16 m. For the purpose of comparison, 60 km/h vehicle speed and poor pavement condition has been considered. DAF is found to be decreased with the increase in vehicle axle

spacing unless there is a significant settlement in approach road. It may be noted that increased axle spacing causes higher amount of bending moment in the vehicle body and therefore, a part of vibrational energy is utilized in bending of the beam. However, significant amount of approach settlement does not offer any further advantage of vehicle flexibility in the system model.

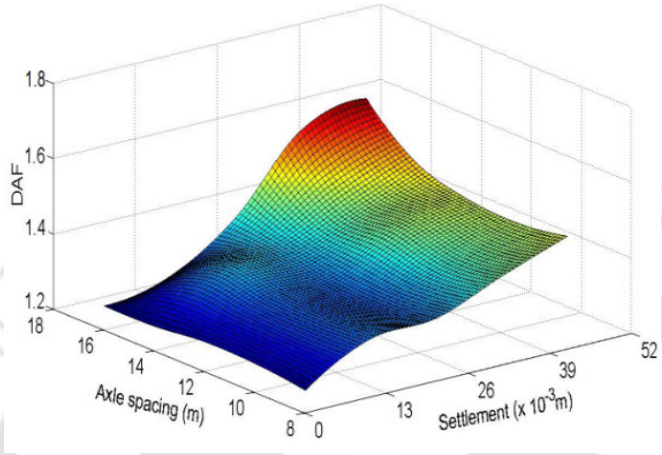

(a) Surface plot representation

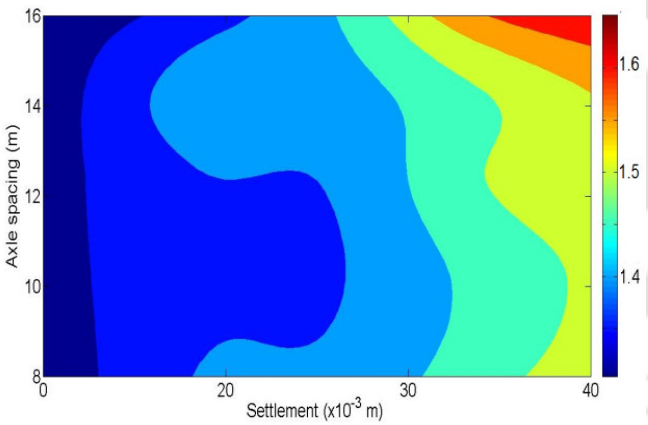

(b) Contour plot representation

Fig.6.64. Dynamic amplification factor for different axle spacing and approach settlement

6.8.4 Effect of vehicle mass and approach settlement on DAF

The contribution of distributed vehicle mass on the bridge response in presence of approach road settlement has been investigated by considering 60 km/h vehicle speed and poor bridge deck surface condition. The effect of vehicle mass as well as approach settlement on the

dynamic amplification factor (DAF) is shown in Fig. 6.65. It has been found that up to certain settlement of approach road, DAF decreases with increase of vehicle mass. However, when approach slab settlement increases from 10 mm to 40 mm, DAF is found to increase by an amount of 3.14% to 13.29% even though the static response increases with increasing weight. This is due to the fact that dynamic deflection is normalized by static deflection.

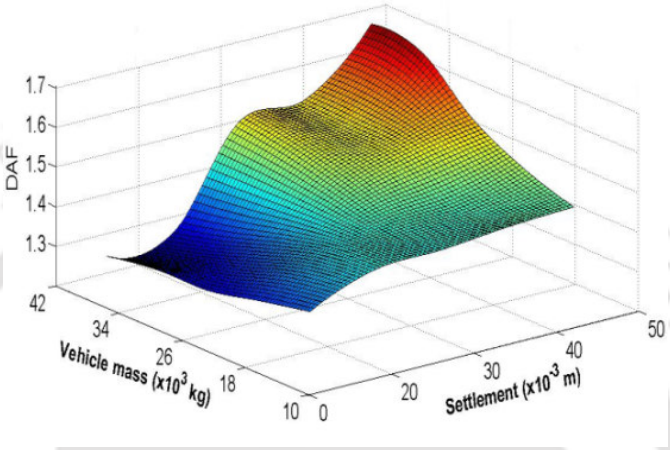

(a) Surface plot

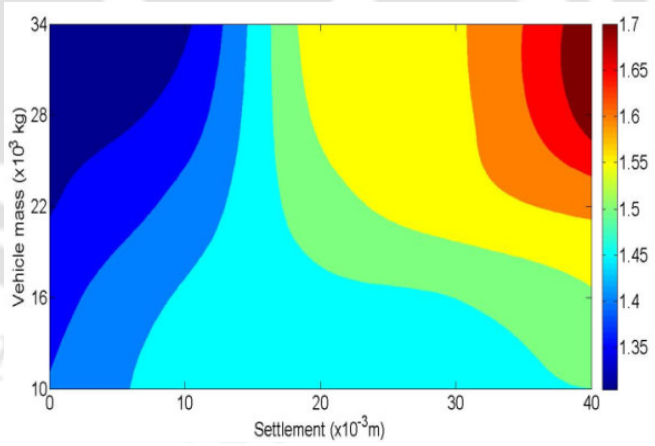

(b) Contour plot

Fig.6.65. Dynamic amplification factor for different vehicle mass and approach settlement

6.9 Comparison of Different Models Behaviour

Bridge response subjected to three different vehicle models incorporating two types of deterministic mean profile superimposed over random unevenness has been compared in the present section. Vehicle speed has been taken as 60 km/h and the deck surface roughness is assumed to be of poor category based on ISO classification (ISO 8608: 1995), unless stated otherwise.

6.9.1. Bridge response with pre-cambered profile

In the present study, bridge pre-cambering has been incorporated in the unevenness model in the form of swallow parabola. The central rise of mean parabolic surface h_0 has been taken as 0.01 m. Mean and standard deviation of bridge mid span deflection under the action of three different vehicle models has been shown in Fig 6.66. It may be seen that inclusion of vehicle body flexibility reduces the response magnitude of the bridge by an amount of 6% to 10%.

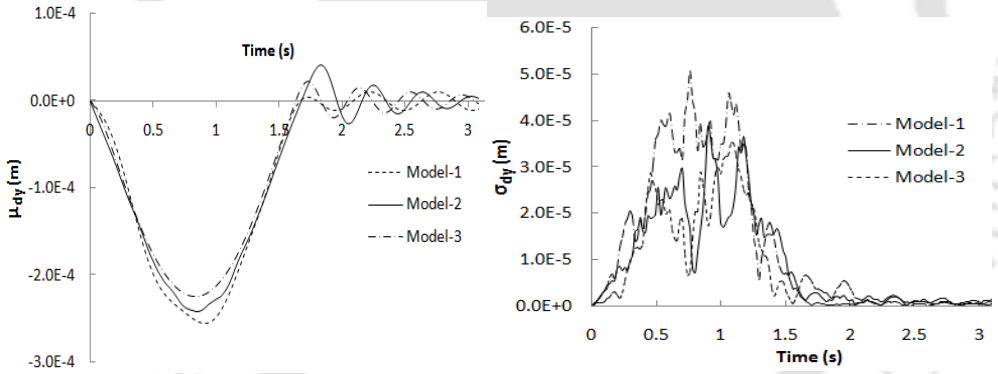

(a) Mean (b) Standard deviation

Fig.6.66. Bridge displacement at mid-span

6.9.2. Bridge Response with approach road settlement

Field observations (Shi and Cai, 2008) revealed that either faulting near the slab and the pavement joint or a sudden change in the slope grade of the approach slab causes vehicle bumping at the joint of bridge deck and approach slab. Such bump causes the initial excitation in vehicle. Therefore, vehicle initial condition is affected not only by the road roughness of the roadway that the vehicle traveled before it enters the bridge, but also by uneven approach span conditions upon entrance to the bridge (Shi and Cai, 2008).

In order to investigate the effect of different vehicle models on bridge response, an approach settlement of magnitude 40 mm has been considered. Time history of bridge mid-span deflection with different vehicle models is given in Fig. 6.67. Result shows that bridge dynamic response of Model-3 is increased by an amount of 17% in presence of approach settlement. Appearance of high frequency components in displacement mean indicates that higher modes of the bridge are excited as the flexible body passes over an abrupt change in road level. In addition to this, abrupt changes in pavement elevation also excite the higher mode of flexible vehicle which increases the frequency of the dynamic load induced in the bridge. The dynamic tyre force with higher frequency in turn excites the higher modes of bridge, which then may become significant to build up the response. This pattern, was however, not seen when there is smooth transition from road to bridge.

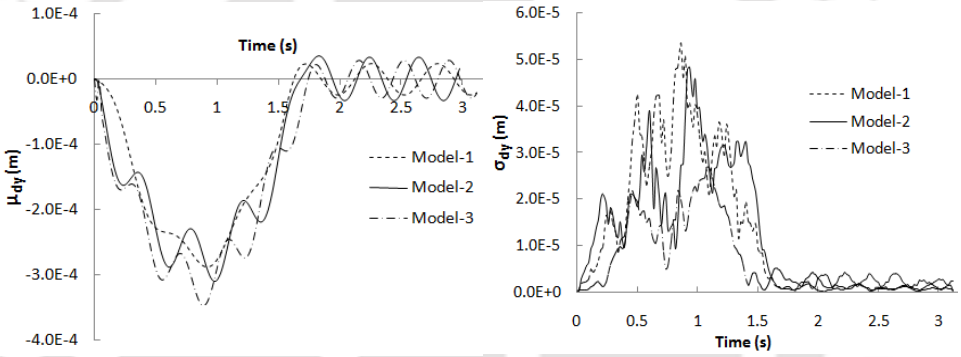

(a) Mean (b) Standard deviation

Fig.6.67. Bridge displacement at mid-span

6.10 Closure

In this chapter, the response statistics of vehicle and bridge due to passage of vehicle has been obtained using proposed semi analytical technique. The purpose of studying dynamic behavior of bridge considering vehicle models with increasing complexity is to observe the sensitivity of each model to the response statistics of the bridge. This, in fact, gives a pilot study for the subsequent parts of results and discussion when different vehicle models are used to identify moving vehicle parameters using acceleration record of the bridge. Vehicle body flexural and torsional modes are introduced in the analysis which has been ignored by the majority of past researchers on bridge-dynamics. Effect of vehicle speed, eccentricity of vehicle path, road roughness on mean and standard deviation of the bridge mid span

displacement, velocity and acceleration has been studied. Adequacy of number of flexural and torsional modes of the vehicle models has been investigated. Further, pre-cambered mean profile and approach settlement along with random unevenness have been incorporated to compare the bridge dynamic response subject to three different vehicle models.

7

RESULT AND DISCUSSION- PART-II: VEHICLE PARAMETER IDENTIFICATION FROM SIMULATED BRIDGE RESPONSE

7.1 Overview

In the present study, Bootstrap Particle Filtering Method has been applied to identify vehicle parameters based on simulated response samples. This provides one an ample scope to judge the efficiency of particle filtering method, since detail parametric study can be conducted here which are usually not be possible due to limitation of sensor data and other constraints during the field test. Earlier researchers have realized that Particle filter technique is computationally expensive as large number of samples is required to get the converged results. This problem has been overcome by utilizing the proposed method of forward solution for the generation of response samples. Different vehicle models developed in Chapter-3 have been used and results are presented separately for each model. Moving load time history over the bridge during the passage of vehicle has been reconstructed using the identified parameters.

7.2 Comparison of Vehicle Load Estimation with Published Results

Main focus of the present study is to estimate vehicle parameters from bridge dynamic response using Bootstrap Particle filtering technique. Before conducting parametric study for the vehicle parameters to be identified, a comparative study of the results obtained by Particle Filtering approach with published results obtained by different identification techniques has been performed. Efficiency of the present identification method has been judged by relative percentage error (RPE) which has been calculated as

$$RPE = \frac{|\Gamma_{identified\ \ value} - \Gamma_{reference\ value}|}{\Gamma_{reference\ value}} \times 100 \tag{7.1}$$

where, $\Gamma_{identified\ value}$ and $\Gamma_{reference\ value}$ denotes identified and true vehicle parameters value.

7.2.1Comparison with the results of numerical study

First we present a comparative study with the method proposed by Law *et. al* (2004) based on simulated data to judge the efficiency of particle filter approach for moving load identification. The loading on the bridge pavement used by them was a deterministic harmonic function composed of two different frequencies as given below

$$f_1(t) = 62680[1.0 + 0.1\sin(10\pi t) + 0.05\sin(40\pi t)] \quad \text{N} \tag{7.2}$$

$$f_2(t) = 123320\,[1.0 - 0.1\sin(10\pi t) + 0.05\sin(50\pi t)] \quad \text{N} \tag{7.3}$$

where f_1(t) and f_2(t) are the moving load function for the front and rear axle respectively. The result of the published literature (Law *et. al,* 2004) was based on Interpretive Method. The comparison is shown in Table 7.1. It may be noted that percentage error increases with the increase in vehicle speed. Besides, it has been observed that poor surface condition of the bridge produces more error in the estimation. The same patterns have been found even in the present method. However, Particle Filter method gives improved estimate of the gross axle load in all cases as compared to the interpretive method. Further, gross axle force time history has been reconstructed from the estimated vehicle parameters by considering same bridge surface condition and vehicle speed as assumed by (Law *et. al,* 2004) in their study. Comparison of reconstructed force time history with the assumed time varying axle load is presented in Fig 7.1. It may be seen that high fluctuation of moving force about the reference loading has been produced at the end of time history of front axle load and at the beginning of the rear axle load in the results obtained by (Law *et. al,* 2004). This might be due to the fact that high frequency component of random unevenness could not be properly filtered out with the sampling frequency considered in the earlier study. However, the high frequency component could not disturb the estimation of moving load when particle filter technique has been used in the present study. This resulted higher accuracy in parameter estimation in the present study.

Table 7.1 Comparison of the estimate of gross vehicle weight with published results (Law *et al.,* 2004)

Vehicle speed (m/s)	Relative Percentage Error in estimation of gross vehicle weight for different road condition					
	Class B (Good condition)		Class C (Average condition)		Class D (Poor condition)	
	Law *et al* (2004)	Present study	Law *et al* (2004)	Present study	Law *et al* (2004)	Present study
10	11.57	3.18	13.71	5.82	23.49	8.95
15	11.55	4.13	15.35	7.38	25.46	11.51
20	12.46	4.96	16.73	8.94	27.79	13.03
25	13.45	8.55	19.47	13.33	30.01	16.22

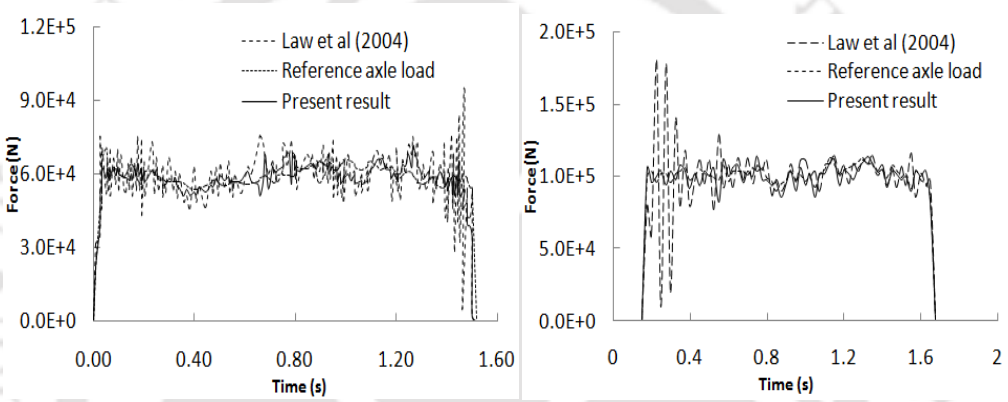

(a) Front axle load (b) Rear axle load

Fig. 7.1 Comparison of reconstructed dynamic axle load with published result (Law *et al.,* 2004)

7.2.2 Comparison with the results of experimental study

The second comparative study has been done with the help of experimental data provided by Law *et al.* (1997). They have conducted a laboratory experiment with a model car having a total mass (M_c) 7.1 kg being pulled at a speed of 3.102 m/s over a simply supported beam of span 3.376 m. The model bridge was a flat bar having cross sectional dimension of 100 mm × 25 mm. The mass and flexural rigidity of the beam were 24.12 kg/m and 63.4 kNm^2 respectively. Other details of experiments can be found in reference (Law *et al.,* 1997). Accelerometers were mounted on the beam at 1/4, 1/2 and 3/4 span. Sampling frequency was 256 Hz. Acceleration record at 3/4th of the span experimentally obtained in the reference (Law *et al*., 1997) was taken as measured data in Particle Filter Method for estimating the mass of the model car. The progress of iteration with updated estimation as obtained in the

present study has been shown in Fig. 7.2. The result shows that the filtering process converges at 57 th of iteration to a mass value of 7.26 kg. The error has been estimated as 2.25%. This demonstrates successful application of particle filter method for the estimation of moving mass when experimentally acquired data is utilized in the algorithm.

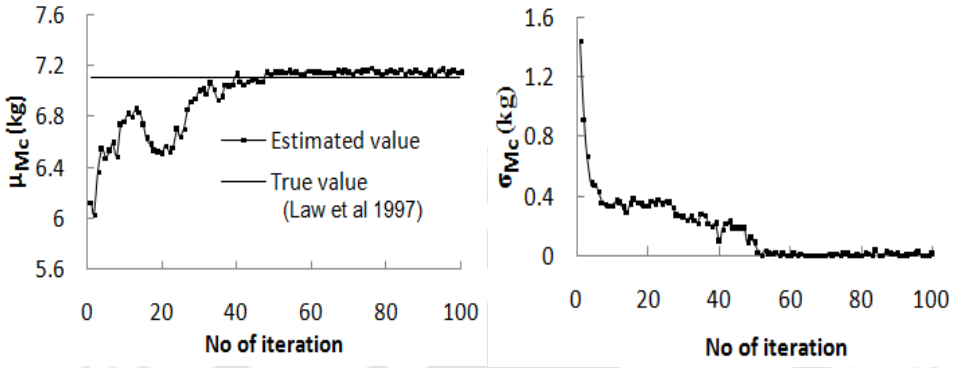

(a) Mean value (b) Standard deviation

Fig. 7.2 Progressive estimate of model car mass using experimental data (Law *et al.,* 1997) and its comparison with true value

7.3 Influence of Various Factors on Vehicle Parameters Identification in Model-1

In this section, vehicle parameters in Model-1 have been identified from simulated acceleration time history considered at different locations. Proposed semi-analytical method along with particle filtering technique has been used. For this theoretical study, measured bridge response has been mimicked by adding noise to simulated bridge acceleration using parameters given in Section 6.2.2.1.Vehicle parameters given in the Section 6.2.2.1has been used as the reference value and identified parameters are compared to determine relative percentage error (RPE). For all the case studies vehicle speed has been taken as 60 km/h and the deck surface roughness is assumed to be of average category based on ISO classification (ISO 8608:1995), unless stated otherwise. Bridge acceleration subject to moving vehicle with 60 km/h speed at different locations along the span has been shown in Fig. 7.3, which after addition of noise is utilized in particle filter algorithm in order to extract vehicle parameters.

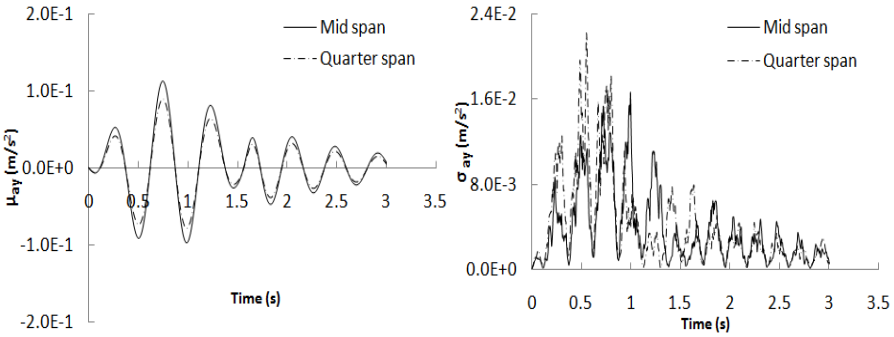

(a) Mean (b) Standard deviation

Fig.7.3. Bridge acceleration at mid-span and quarter span for vehicle speed 60 km/h

7.3.1 Effect of Bridge Response Measurement Location

The bridge acceleration measurement at different location along the span has been used as input to the particle filter algorithm. In both the cases standard deviation approaches very low value at a certain number of iteration which implies that the algorithm has achieved convergence. The progress of estimation of mean and standard deviation has been displayed in the form of graphical plot of estimated parameters vs. corresponding number of iterations (Fig. 7.4 to Fig. 7.9). Result shows that measurement taken other than the mid span takes a longer iteration to achieve convergence. Relative percentage error, given in Eq.(7.1), of each identified vehicle parameters has been calculated for different measurement input as shown in Table 7.2. Overall, the result reveals that bridge response measurement at mid span gives around 2 to 7 percent errors while measurement other than mid span leads to 4 to 7 percentage error.

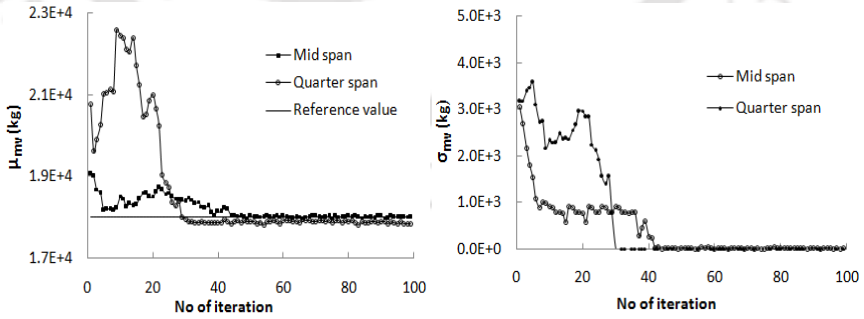

(a) Mean value (b) Standard deviation

Fig. 7.4 Progressive estimate of vehicle mass m_v from acceleration data at different locations

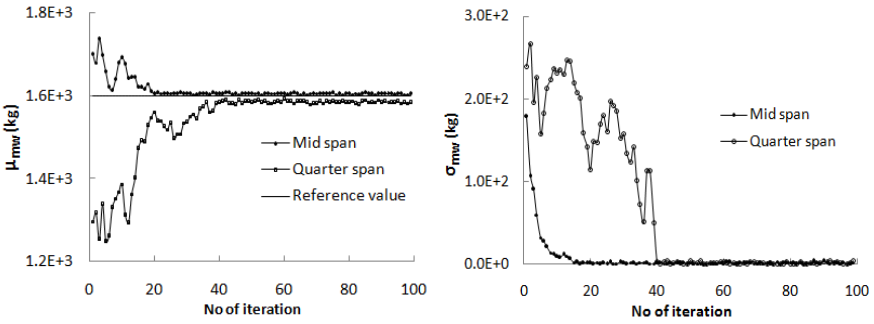

(a) Mean value (b) Standard deviation

Fig. 7.5 Progressive estimate of wheel mass m_w from acceleration data at different locations

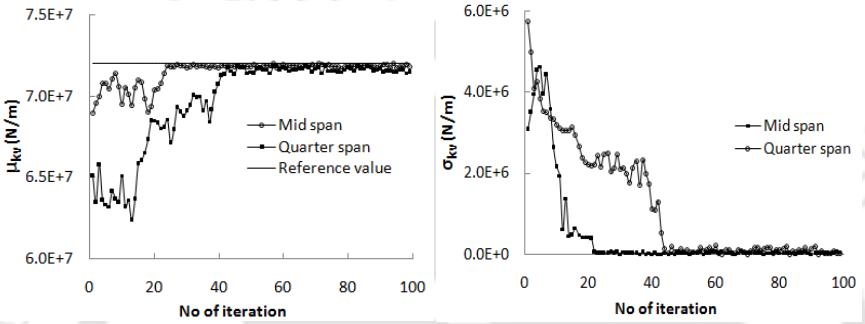

(a) Mean value (b) Standard deviation

Fig. 7.6 Progressive estimate of vehicle suspension stiffness k_v from acceleration data at different locations.

The evolution of probability density function (PDF) of all the identified parameters with the progress of iteration has been presented in Fig.7.10 to Fig.7.12. This pertains to the estimate with bridge acceleration at mid span. As the estimate approaches towards convergence, the spread of PDF decreases and finally at the end of identification process, PDF achieves a sharp peak, which corresponds to negligible amount of standard deviation of parameters. This is to be noted that peak does not necessarily occur near the expected value of initial guess.

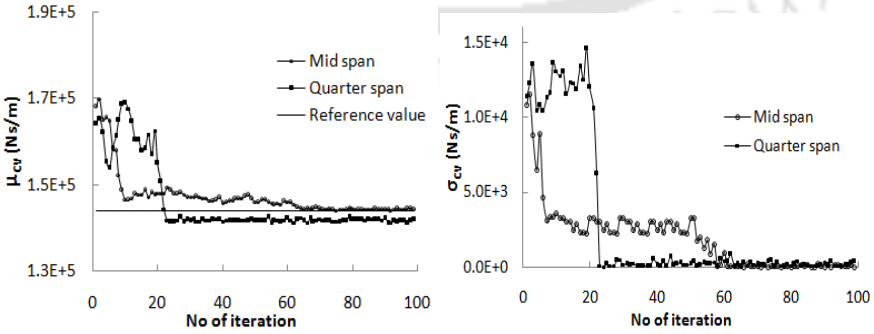

(a) Mean value (b) Standard deviation

Fig. 7.7 Progressive estimate of vehicle suspension damping c_v from acceleration data at different locations

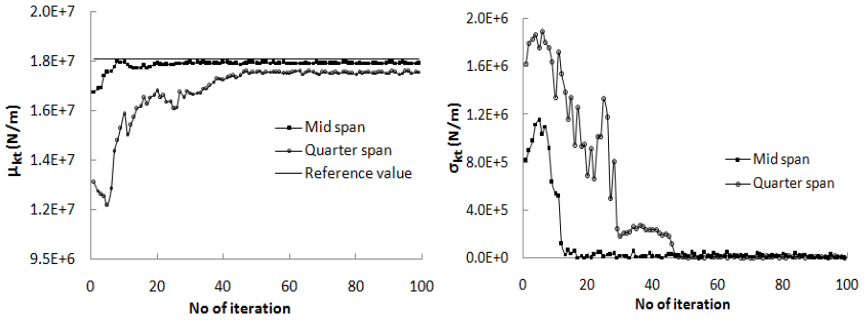

(a) Mean value (b) Standard deviation

Fig. 7.8 Progressive estimate of tyre stiffness k_t from acceleration data at different locations

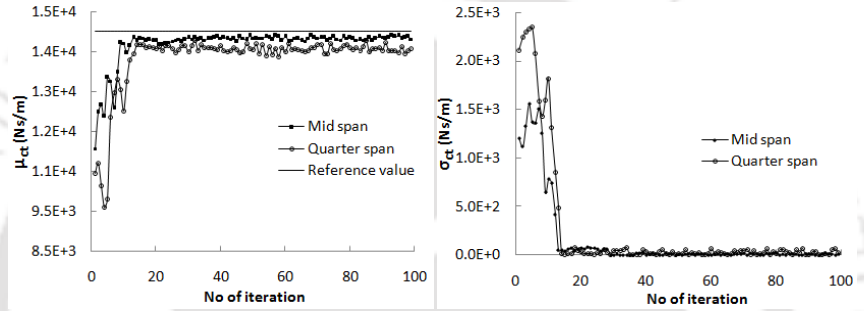

(a) Mean value (b) Standard deviation

Fig. 7.9 Progressive estimate of tyre damping c_t from acceleration data at different locations

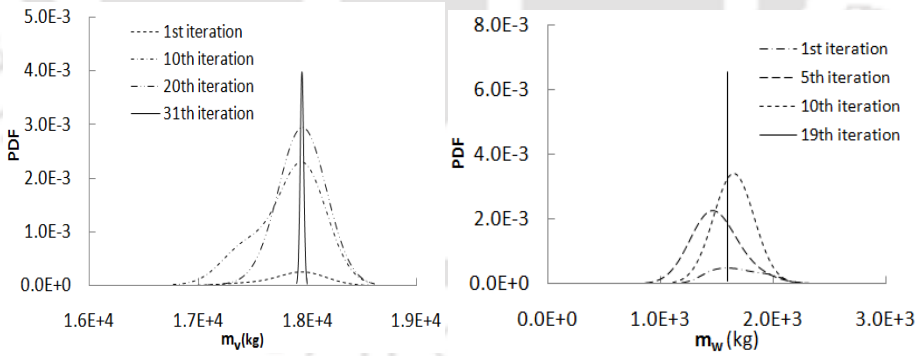

(a) (b)

Fig. 7.10 Evolution of PDF for measurement at mid span (a) mass of vehicle and (b) mass of wheel

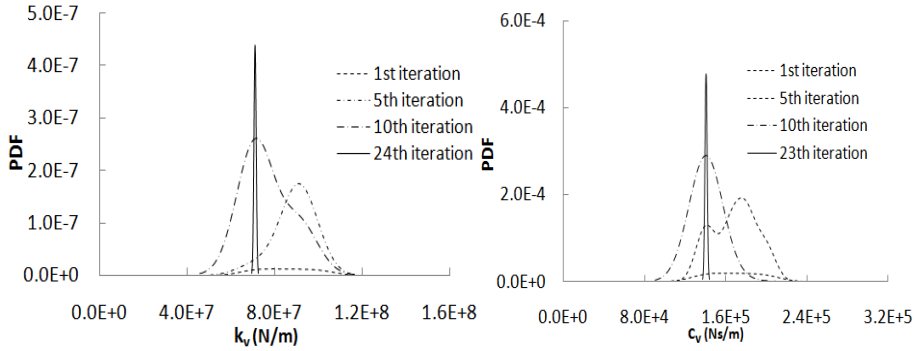

(a) (b)

Fig. 7.11 Evolution of PDF for measurement at mid span (a) suspension stiffness and (b) suspension damping

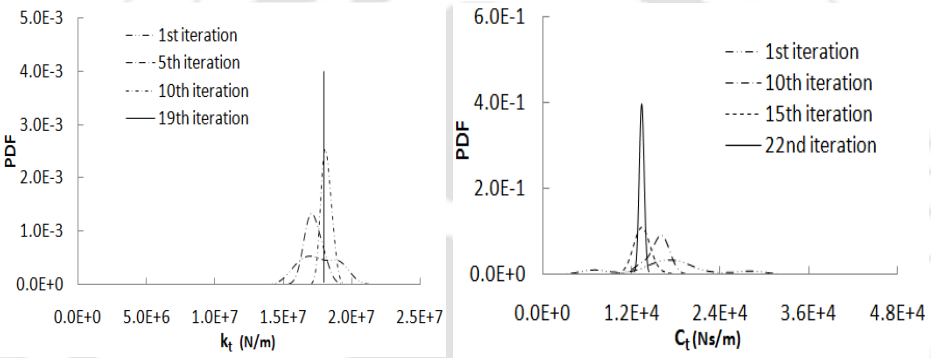

(a) (b)

Fig. 7.12 Evolution of PDF for measurement at mid span (a) tyre stiffness and (b) tyre damping

Further, moving load time history determined by solving bridge vehicle interaction model-1 using identified vehicle parameters obtained from simulated response of two different locations has been presented in Fig.7.13. The estimated moving load time history has been compared with the reference value as well as with static vehicle load. The moving load estimated using extracted parameters is very close to the reference value.

Table 7.2 Effect of response measurement location on indentified vehicle parameters

Vehicle parameters	Mid span		Quarter span	
	No of iteration	RPE (%)	No of iteration	RPE (%)
m_v	42	2.403	38	3.620
m_w	31	5.071	54	6.153
k_v	28	4.724	53	4.844
k_t	36	4.335	56	5.162
c_v	25	5.012	47	5.910
c_t	39	6.240	61	6.808

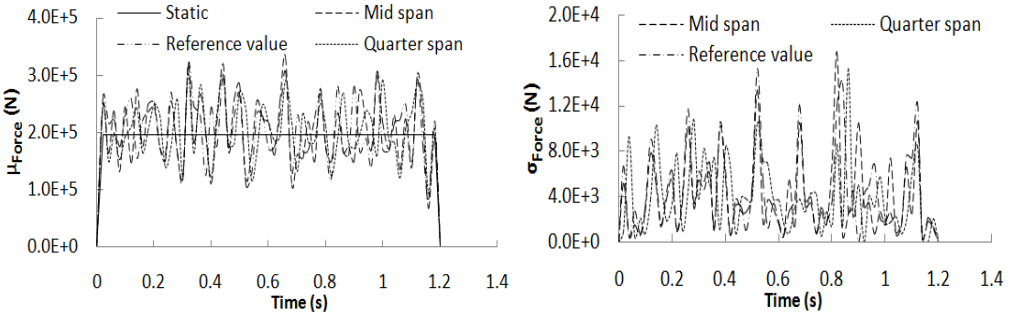

(a) Mean value (b) Standard deviation

Fig. 7.13 Comparison of interaction force based on identification from acceleration data at two locations.

7.3.2 Effect of artificial noise level

Artificial noise is added to the simulated response to reflect the contaminated measurement, since bridge responses acquired in the field usually contain measurement noise (Chan *et al,* 1999). Vehicle parameters are estimated based on this bridge response samples from analytical model contaminated by 5% and 10% noise. Table 7.3 shows the percentage error as well as number of iteration required to converge. Result shows that lower noise level give the best estimate for the vehicle parameters with less number of iteration.

Table 7.3 Effect of different noise level on the estimated vehicle parameters

Vehicle parameters	5% noise		10 % noise	
	No of iteration	RPE (%)	No of iteration	RPE (%)
m_v	42	2.403	38	6.045
m_w	31	5.071	54	8.753
k_v	28	4.724	53	6.920
k_t	36	4.335	56	9.351
c_t	25	5.012	47	7.749
c_v	39	6.240	61	10.633

7.3.3 Effect of initial range of vehicle parameters for construction of prior PDF $p(\Gamma_0)$

In the absence of any information about the unknown parameters, it is assumed that the initial prior *PDF* $p(\Phi_0)$ is uniformly distributed within a range $[\{\Phi_L\} \ \{\Phi_U\}]$. Φ is a set of unknown vehicle parameters (Γ_j). In the model-1, j=1, 2, …,6. The subscript L and U denotes upper and lower bound of the parameters. Two different cases have been considered to specify the

range within which random particles are generated assuming uniform probability density function $p(\Phi_0)$.

Case-1: When the lower and upper limits is not wide apart from the actual value

Case-2: Keeping the lower and the upper limits with large variation from the true value

The range of values of the parameters assumed for the above two cases are mentioned in Table-7.4 to 7.6. In these two cases, number of particles N_p=1000 and artificial noise is taken to be 5% of the simulated maximum acceleration of the bridge. Estimate of vehicle parameters has been shown in Table-7.7. The mean and standard deviation is observed at each stage of iteration till the entire time history of the acceleration is covered. Reconstructed vehicle bridge interaction force is shown in Fig. 7.14 simultaneously comparing with the true value of dynamic interaction force. It has been found that a wrong choice of $p(\Phi_0)$ does not necessarily lead to wrong estimates by the particle filter identification method. However, a crude assumption of the prior probability density is found to consume longer time to achieve convergence. Assumption based on the first case of prior density function leads to 2 to 6 percentage error while the second case assumption gives 4 to 9 percent error.

Table 7.4 Range of Mass of vehicle and wheel Mass to construct prior *PDF*

Range	Vehicle mass (m_v) kg		Wheel mass (m_w) kg	
	Case 1	Case 2	Case 1	Case 2
Γ_L	1.7×10^4	0.4×10^4	1.4×10^3	0.3×10^3
Γ_U	1.9×10^4	3.6×10^4	1.6×10^3	3.5×10^3

Table 7.5 Range of Suspension stiffness and Tyre stiffness to construct prior *PDF*

Range	Vehicle suspension stiffness (k_v) N/m		Tyre stiffness (k_t) N/m	
	Case 1	Case 2	Case 1	Case 2
Γ_L	2.8×10^7	0.3×10^7	0.6×10^7	5.2×10^6
Γ_U	4.0×10^7	8.5×10^7	1.1×10^8	8.5×10^7

Table 7.6 Range of Suspension damping and Tyre damping to construct prior *PDF*

Range	Vehicle suspension damping (c_v) N-s/m		Tyre damping (c_t) N-s/m	
	Case 1	Case 2	Case 1	Case 2
Γ_L	6.5×10^4	1.5×10^4	0.5×10^4	5.2×10^3
Γ_U	8.3×10^4	12.3×10^4	0.9×10^4	6.4×10^4

Table 7.7 Effect of initial range of parameters on the estimated vehicle parameters

Vehicle parameters	Case-1		Case-2	
	No of iteration	RPE (%)	No of iteration	RPE (%)
m_v	42	2.403	50	3.841
m_w	31	5.071	39	5.753
k_v	28	4.724	53	6.920
k_t	36	4.335	44	5.051
c_t	25	5.012	39	5.797
c_v	39	6.240	58	9.114

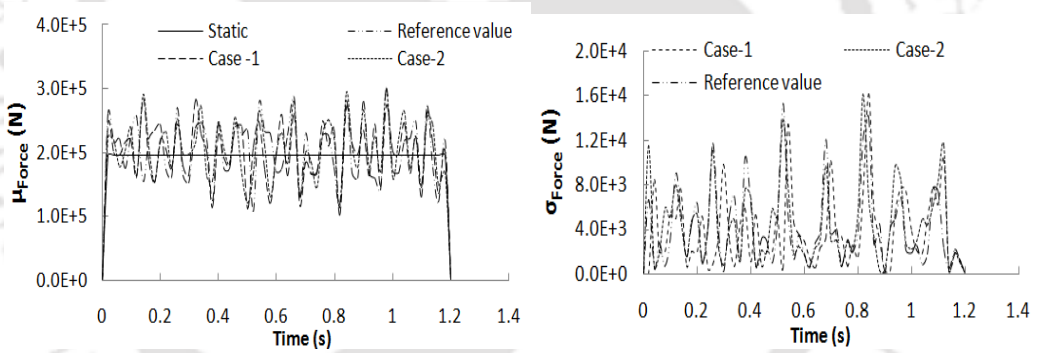

(a) Mean (b) Standard deviation

Fig. 7.14 Comparison of reconstructed interaction force based on identification from different range of values used to construct prior PDF $p(\Phi_0)$

7.3.4 Effect of Different Vehicle Velocity

The identification algorithm has been examined from the measured response for different vehicle speed over the bridge. The response samples have been generated at 40 km/h, 60 km/h and 80 km/h of vehicle speed. The sampling time interval in measured response sample (after adding 5% artificial noise) has been initially chosen as 0.01 sec. This time interval was not satisfactory in case of vehicle moving at higher speed. The reason may be that vehicle leaves the bridge in a shorter time span generating less number of data points that are

available in the working of a particle filter algorithm. Number of iteration required to get convergence and calculated relative percentage error (RPE) is tabulated in Table 7.8. It has been found that lower speed gives better estimate but it requires more number of iteration to achieve the convergence. However, this trend has not been observed in all the parameters estimated at different vehicle speed. It may be noted that relative percentage error is the best indicator to judge the performance of algorithm.

Table 7.8 Performance of the algorithm at different vehicle speed (V)

Vehicle parameters	Vehicle speed 40 km/h		Vehicle speed 60 km/h		Vehicle speed 80 km/h	
	No of iteration	RPE (%)	No of iteration	RPE (%)	No of iteration	RPE (%)
m_v	38	3.081	42	2.403	18	7.04
m_w	29	1.190	31	5.071	12	8.15
k_v	44	1.372	28	4.724	22	6.63
c_v	25	1.994	36	4.335	18	8.63
k_t	41	3.068	25	5.012	42	3.45
c_t	18	3.502	39	6.240	19	3.93

7.3.5 Effect of different deck surface roughness condition

Bridge deck surface irregularity has been considered in the identification of vehicle parameters based on ISO specification (ISO 8608:1995) for different conditions- good, average and poor. Among the three conditions, results show that good condition gives the best estimate with less number of iteration which is given in Table 7.9. This may be attributed to the reason that noise effect in dynamic input for the case of rougher pavement is amplified and thus requires more number of iterations. This is in conformity with the results obtained when artificial noise level increased from 5% to 10% as stated in Section 7.2.2.

Table 7.9 Effect of bridge deck surface condition on the estimated vehicle parameters

Parameters	No of iteration			RPE (%)		
	Good condition	Average condition	Poor condition	Good condition	Average condition	Poor condition
m_v	16	36	49	3.212	3.403	6.055
m_w	19	25	43	2.025	5.071	5.948
k_v	20	25	43	2.164	4.724	4.015
c_v	23	44	72	3.947	4.335	6.142
k_t	36	41	85	1.972	5.012	8.018
c_t	19	44	68	2.243	6.240	10.273

7.3.6 Effect of approach road settlement

In existing bridge either faulting at the road and the bridge deck joint or a sudden change in the slope grade of the approach road is often found, which may causes vehicle bumping at the joint of bridge deck and approach slab. Such bump causes the initial excitation in vehicle. This initial excitation of the vehicle, at the bridge entry causes extra impact load on the bridge and affects the performance of both the bridge and the vehicle. In the present study, bridge mid span acceleration response considering 20 mm approach settlement with vehicle speed 60 km/h has been used as input to the identification algorithm. Table-7.10 shows the number of iteration and percentage error found for each vehicle parameters. It is found that more number of iteration is required for the convergence when approach road settlement is taken into account. Moreover, relative percentage error of the estimate is also higher. Progressive statistical estimate of sprung mass and unsprung mass are plotted in Fig.7.15 and Fig.7.16.

Table 7.10 Effect of approach settlement on identified vehicle parameters

Parameters	No of iteration		RPE (%)	
	Without approach settlement	With 20 mm approach settlement	Without approach settlement	With 20 mm approach settlement
m_v	39	58	4.052	5.184
m_w	33	54	3.71	4.065
k_v	23	42	5.116	7.237
c_v	26	44	8.297	10.563
k_t	25	39	9.102	13.415
c_t	44	78	11.453	13.968

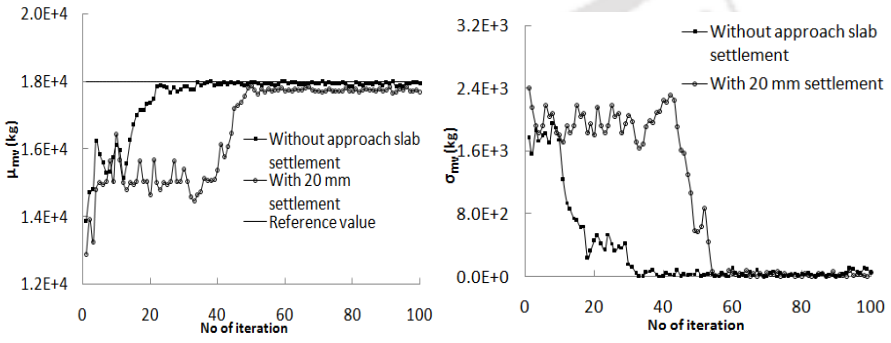

(a) Mean value (b) Standard deviation

Fig. 7.15 Progressive estimate of vehicle mass m_v from acceleration data with consideration of 20 mm approach settlement and without settlement

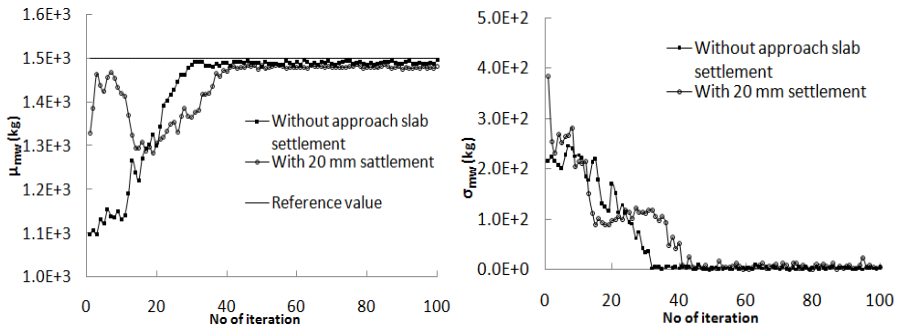

(a) Mean value (b) Standard deviation

Fig. 7.16 Progressive estimate of wheel mass m_w from acceleration data with consideration of 20 mm approach settlement and without settlement

7.4 Influence of Various Factors on Vehicle Parameter Identification in Model-2

In the present section, parameters of Half Car flexible model have been identified based on simulated bridge acceleration. For the purpose of parametric studies, number of particles N_p has been taken as 1000. The sampling time interval 0.01 s and vehicle speed 60 km/h along with average deck surface condition have been assumed. Bridge acceleration at mid span and quarter span due to flexible moving vehicle at 60 km/h speed is shown in Fig. 7.17. As stated earlier, the simulated response is used in particle filter approach after addition of model noise.

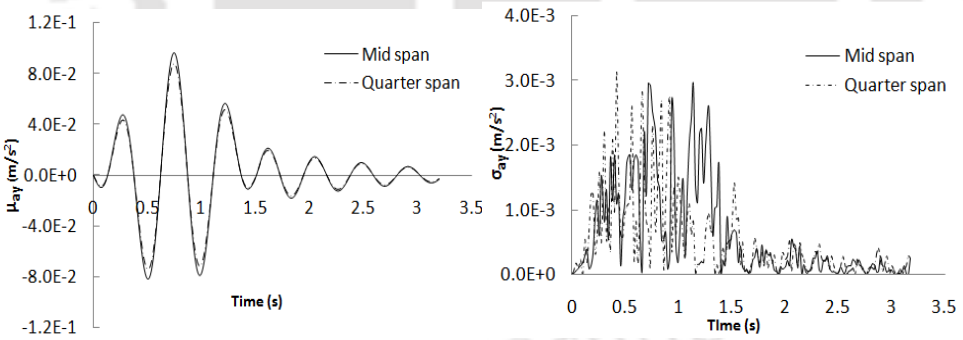

(a) Mean (b) Standard deviation

Fig. 7.17 Bridge acceleration at mid-span and quarter span for vehicle speed 60 km/h

7.4.1 Effect of Bridge Response Measurement Location

The vehicle parameters in Model-2, having two axles and with flexible body have been identified based on bridge acceleration simulated at different locations along the span. Mean estimate of the vehicle parameters and the corresponding standard deviations are shown in Fig. 7.18 to 7.29. Evolution PDF of vehicle parameters at different stage of iteration is shown

in Fig. 7.30 to Fig. 7.36. Table 7.11 displays the percentage error as well as number of iteration required to converge, for different location of bridge acceleration record. Result shows that mid span response gives the best estimate for vehicle parameters. The comparison of error in identified parameters from response data at two locations reveals that the use of mid-span time history yields around 1.5% to 17% RPE while that for quarter span leads to 2% to 21% RPE. Although, present identification method does not directly identify axle load time history induced in the bridge, still it can be reconstructed using identified vehicle parameters and solving for the states using proposed semi-analytical method. Fig. 7.37 and Fig. 7.38 show the comparison of reconstructed moving load time history for both front and rear axle using identified parameters and true vehicle parameters. Moving load in rear wheel is time delayed process and is reflected in the result presented herein.

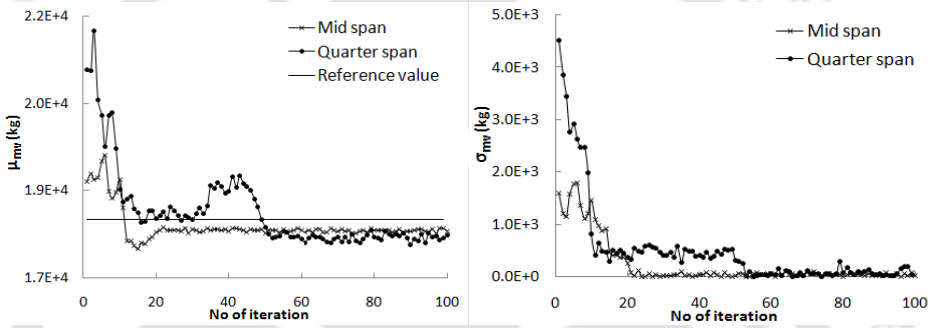

(a) Mean value (b) Standard deviation

Fig 7.18 Progressive estimate of vehicle mass m_v from acceleration data at different locations

In this model, one can get information about the flexural rigidity of the vehicle body from the dynamic response of the bridge used in particle filtering. It may be noted that flexible vehicle body induces less dynamic force over the pavement. This has been demonstrated in Chapter-2 while discussing the dynamic behavior of Model-2.

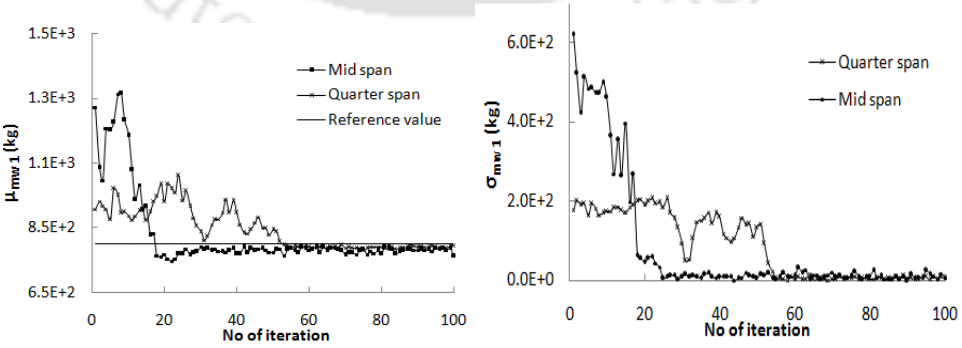

(a) Mean value (b) Standard deviation

Fig 7.19 Progressive estimate of front wheel mass m_{w1} from acceleration data at different locations

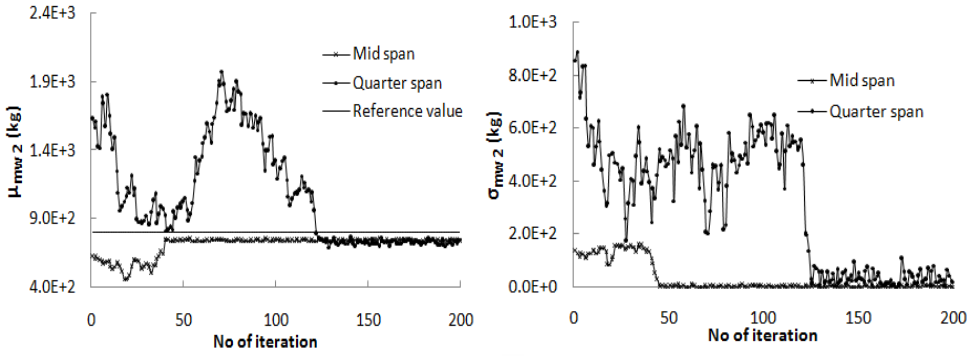

(a) Mean value (b) Standard deviation

Fig 7.20 Progressive estimate of rear wheel mass m_{w2} from acceleration data at different locations

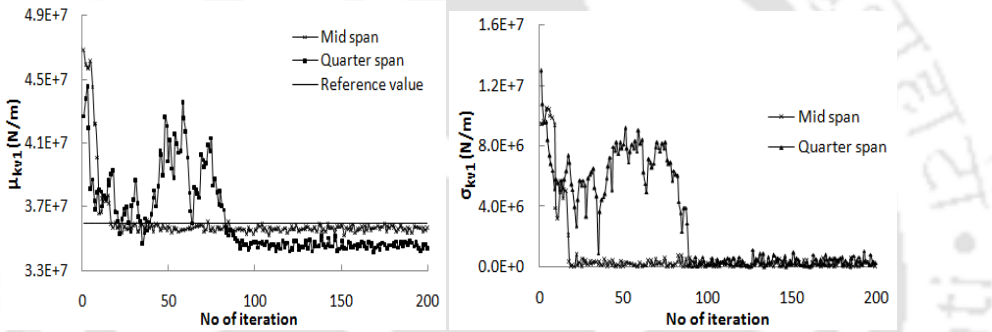

(a) Mean value (b) Standard deviation

Fig 7.21 Progressive estimate of front vehicle suspension stiffness k_{v1} from acceleration data at different locations

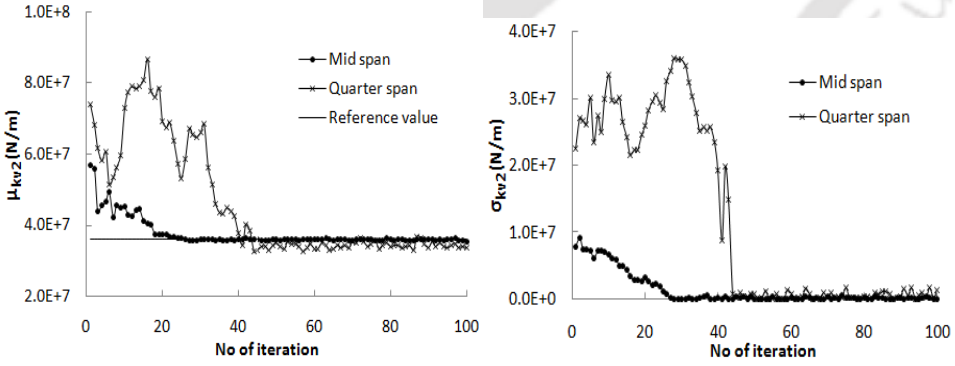

(a) Mean value (b) Standard deviation

Fig 7.22 Progressive estimate of rear vehicle suspension stiffness k_{v2} from acceleration data at different locations

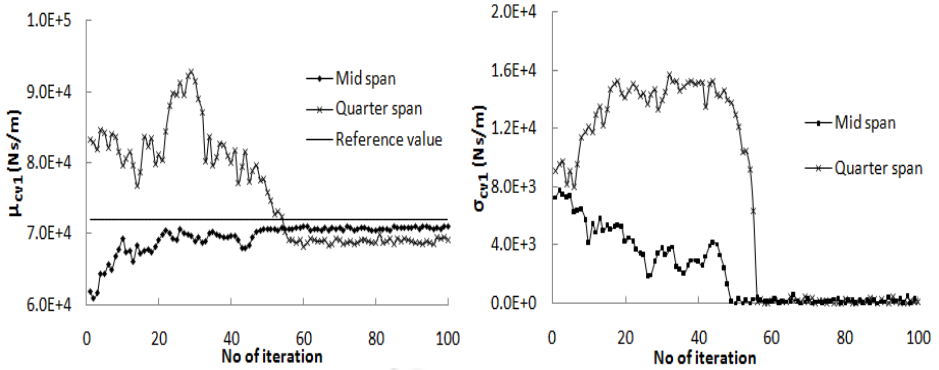

(a) Mean value (b) Standard deviation

Fig 7.23 Progressive estimate of front vehicle suspension damping c_{v1} from acceleration data at different locations

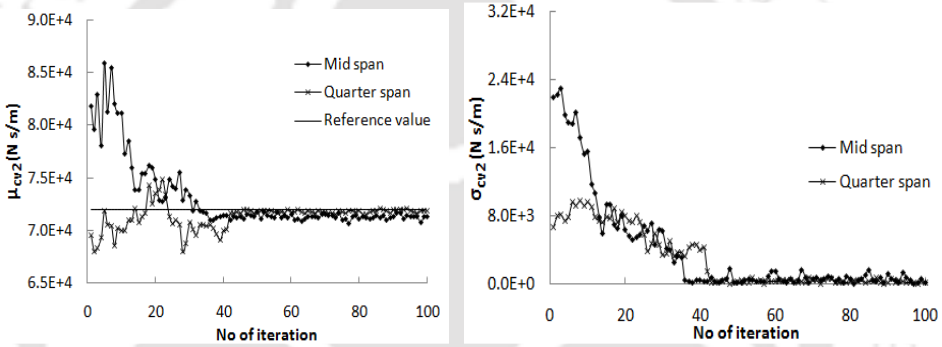

(a) Mean value (b) Standard deviation

Fig 7.24 Progressive estimate of rear vehicle suspension damping c_{v2} from acceleration data at different locations

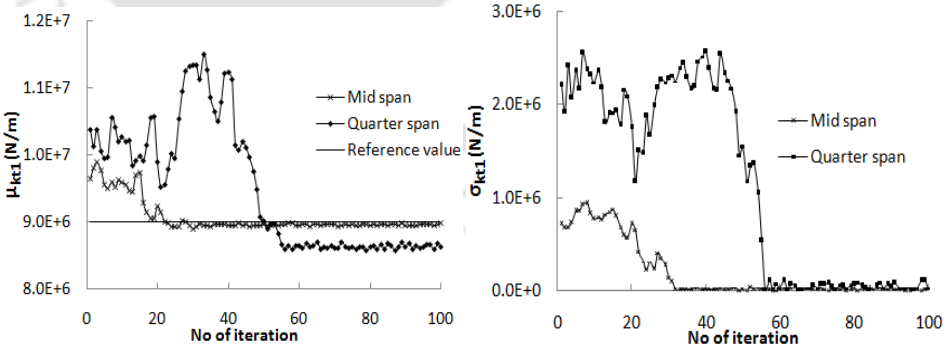

(a) Mean value (b) Standard deviation

Fig 7.25 Progressive estimate of front tyre stiffness k_{t1} from acceleration data at different locations

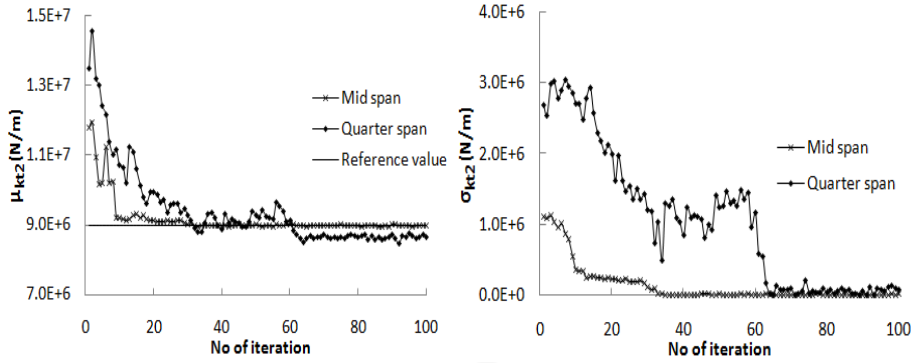

(a) Mean value (b) Standard deviation

Fig 7.26 Progressive estimate of rear tyre stiffness k_{t2} acceleration data at different locations

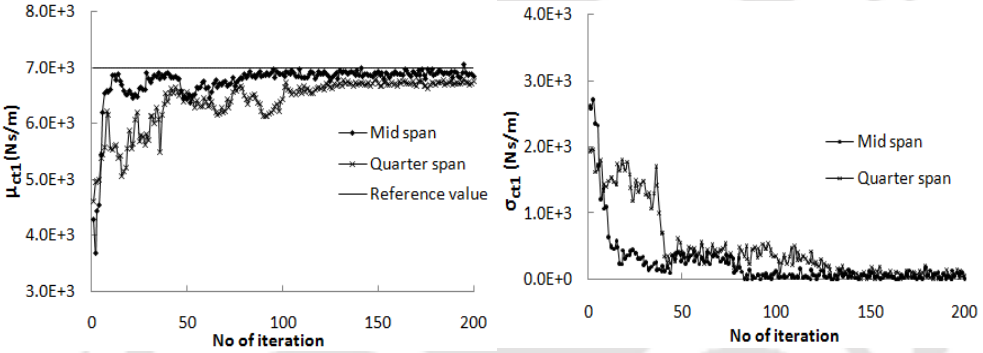

(a) Mean value (b) Standard deviation

Fig 7.27 Progressive estimate of front tyre damping c_{t1} from acceleration data at different Locations

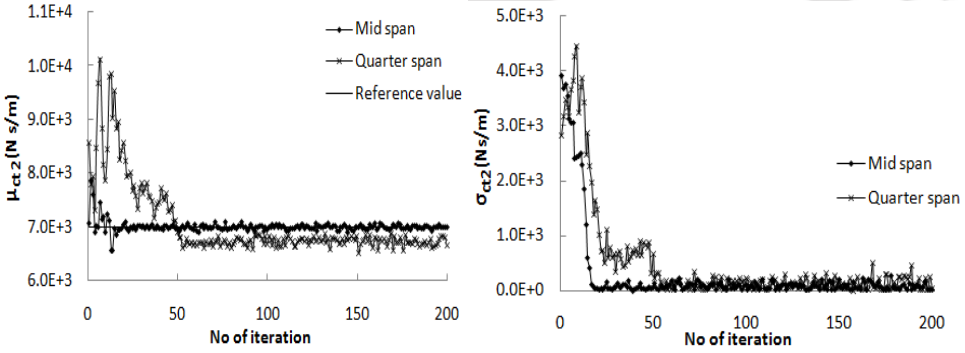

(a) Mean value (b) Standard deviation

Fig 7.28 Progressive estimate of rear tyre damping c_{t2} from acceleration data at different locations

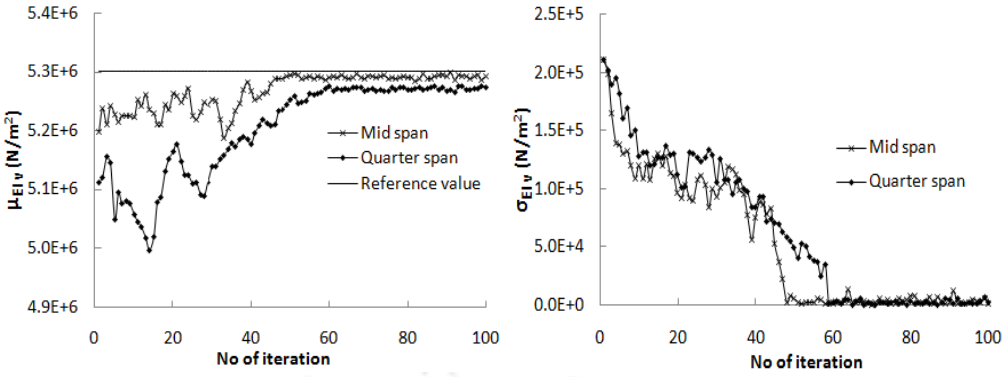

(a) Mean value (b) Standard deviation

Fig 7.29 Progressive estimate of vehicle flexural rigidity EI_v from acceleration data at different locations

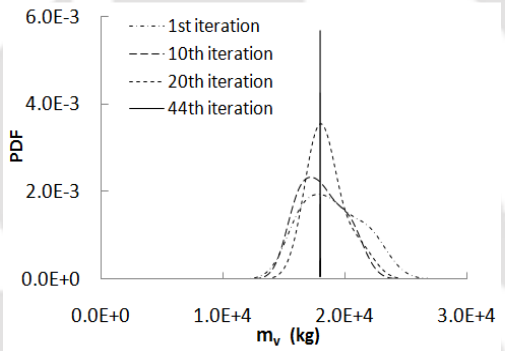

Fig. 7.30 Evolution vehicle mass PDF for measurement at mid span

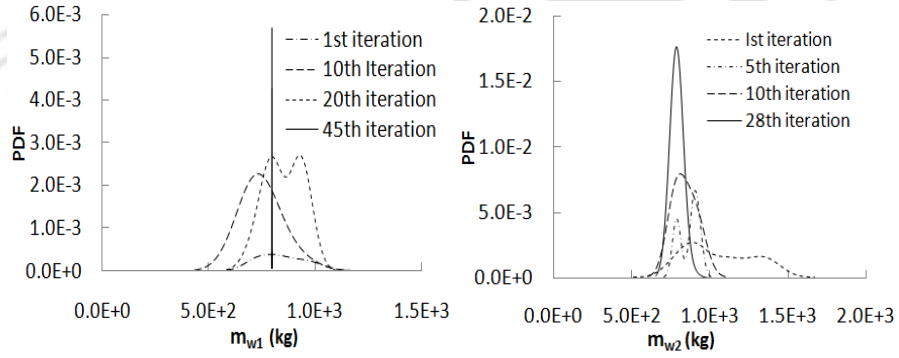

(a) (b)

Fig. 7.31 Evolution of PDF for measurement at mid span (a) mass of front wheel and (b) mass of rear wheel

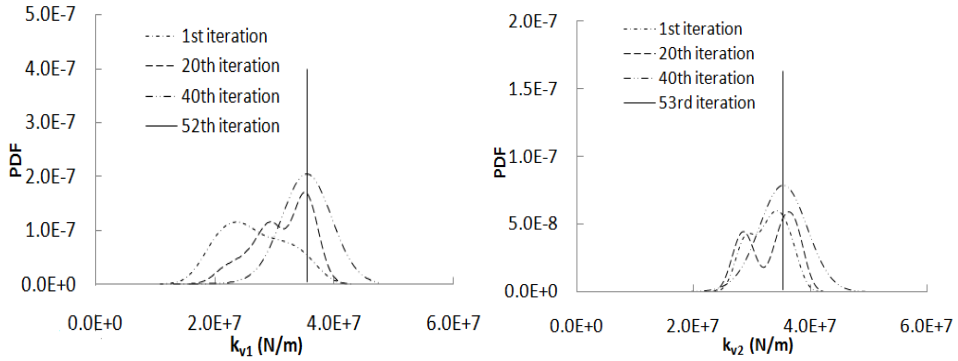

(a) (b)

Fig. 7.32 Evolution of PDF for measurement at mid span (a) front suspension stiffness and (b) rear suspension stiffness

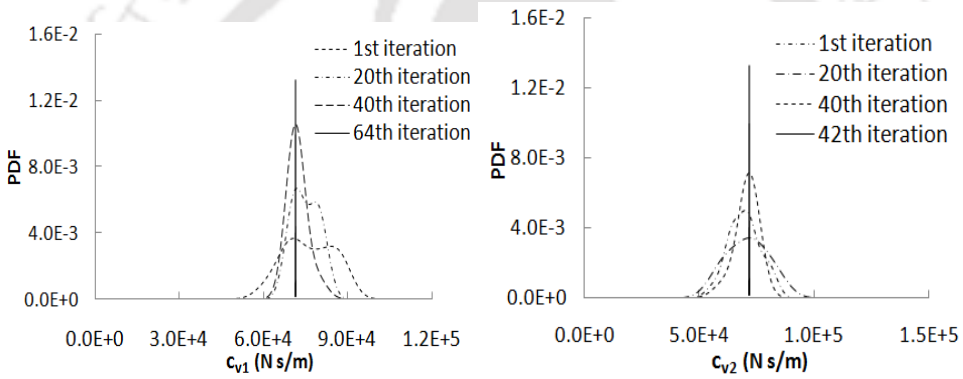

(a) (b)

Fig. 7.33 Evolution of PDF for measurement at mid span (a) front suspension damping and (b) rear suspension damping

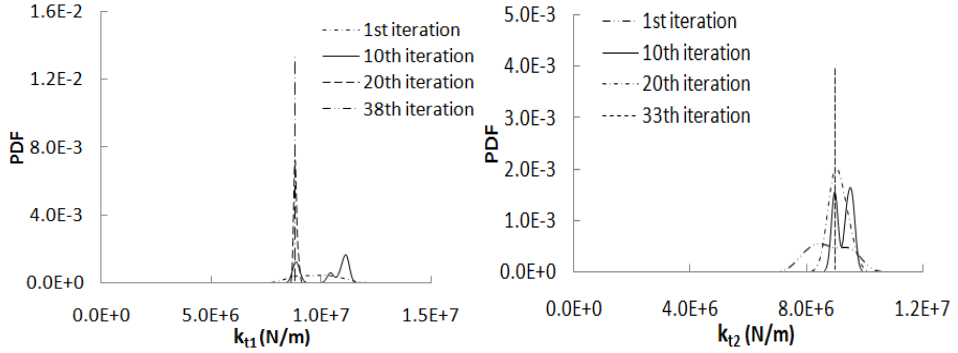

(a) (b)

Fig. 7.34 Evolution of PDF for measurement at mid span (a) front tyre stiffness and (b) rear tyre stiffness

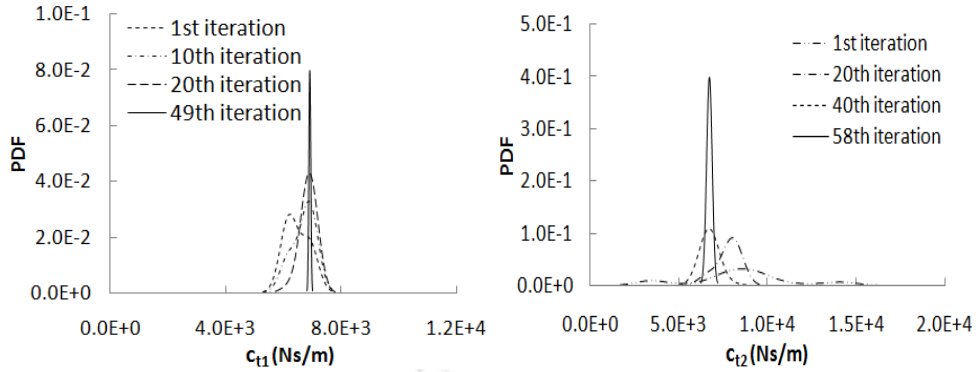

(a) (b)

Fig. 7.35 Evolution of PDF for measurement at mid span (a) front tyre damping and (b) rear tyre damping

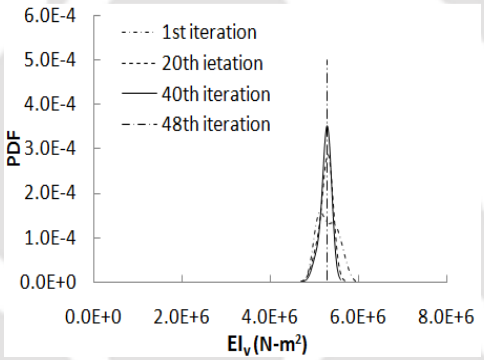

Fig. 7.36 Evolution of PDF of vehicle flexural rigidity for measurement at mid span

Table 7.11 Identification of parameters with different bridge response measurement location

Parameters	Mid span		Quarter span	
	No of iteration	RPE (%)	No of iteration	RPE (%)
m_v	44	2.164	53	2.511
m_{w1}	45	2.760	64	2.960
m_{w2}	28	2.343	115	3.370
k_{v1}	52	11.822	103	20.05
k_{v2}	53	1.670	57	2.080
c_{v1}	64	8.187	66	11.73
c_{v2}	42	3.130	43	3.270
k_{t1}	38	7.531	58	16.24
k_{t2}	33	5.016	60	10.370
c_{t1}	49	14.490	102	20.960
c_{t2}	58	1.667	61	13.810
EI_v	48	3.185	59	7.530

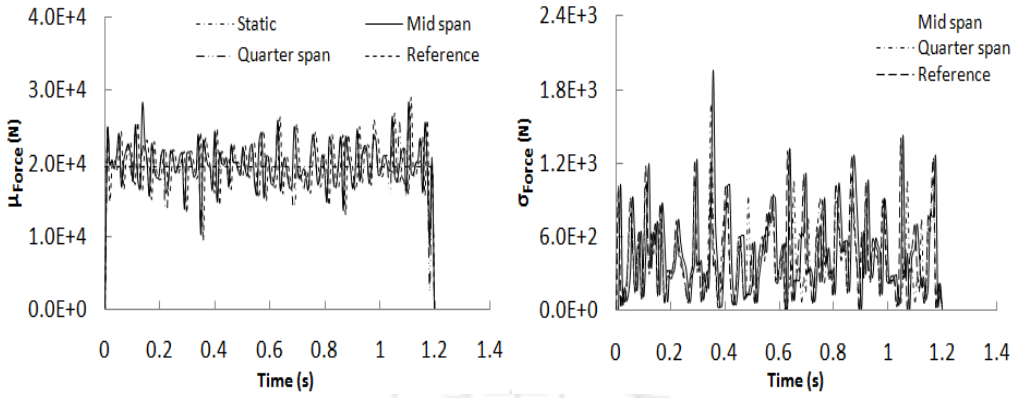

(a) Mean value (b) Standard deviation

Fig. 7.37 Comparison of reconstructed front wheel interaction force based on identification from measured bridge acceleration data at different bridge span location

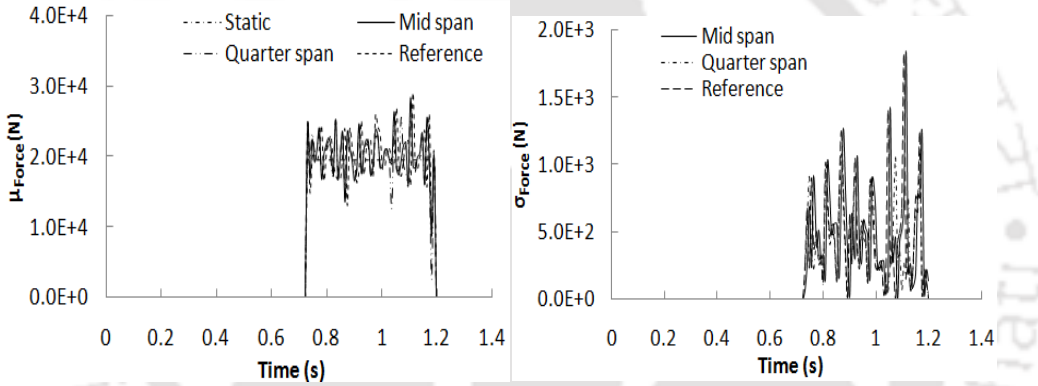

(a) Mean value (b) Standard deviation

Fig. 7.38 Comparison of reconstructed rear wheel interaction force based on identification from measured bridge acceleration data at different bridge span location

7.4.2 Effect of artificial noise level

Efficiency of the proposed identification method to estimate hidden parameters from the noisy measured data has been studied. However, in the present theoretical study measured data is to be realized after adding artificial noise of different level to the simulated bridge response. Two level of noise 5% and 10 % has been considered in the present case study. Table 7.12 show the percentage error as well as number of iteration required to converge. Result shows that, in general more number of iterations is required when higher level of noise is added to the simulated bridge response. Accuracy is also lowered when noise level is higher. In the present example, it is found that even a polluted measurement with 10% noise

can lead to maximum of 16% difference between the true value and estimated value. This shows the robustness of particle filter method in solving inverse problem.

Table 7.12 Identification of parameters with different percentage of noise

Parameters	5% noise		10% noise	
	No of iteration	RPE (%)	No of iteration	RPE (%)
m_v	44	2.164	51	2.60
m_{w1}	45	2.760	112	6.44
m_{w2}	28	2.343	51	2.84
k_{v1}	52	11.822	69	13.45
k_{v2}	53	1.670	48	3.95
c_{v1}	64	8.187	59	15.95
c_{v2}	42	3.130	47	4.26
k_{t1}	38	7.531	63	10.01
k_{t2}	33	5.016	98	8.23
c_{t1}	49	14.490	63	15.05
c_{t2}	58	1.667	52	2.08
EI_v	48	3.185	72	2.17

7.4.3 Effect of initial vehicle parameters for construction of prior PDF

Identification based on Particle Filter Method requires initial guess for the unknown parameters which is assumed to be uniformly distributed within a range [{Φ_L} {Φ_U}]. The subscript L and U denotes upper and lower bound of the parameters. {Φ}=Γ_j where j=1, 2, 3,….,12. Effect of this assumption on the parameters estimation has been judged by number of iteration required and accuracy achieved in terms of relative percentage error. Similar to Model-1, two different cases have been considered in this present model also. The range of values of the parameters assumed for the two cases are mentioned in Table-7.13 to 7.15.

For the purpose of comparison, number of particles N_p=1000 and vehicle speed 60 km/h. Artificial noise is taken as 5% of the simulated maximum bridge dynamic response. Performance of the proposed identification algorithm has been judged by number of iteration require and deviation of the identified vehicle parameters from the reference values. Table 7.16 show the percentage error as well as number of iteration required to converge. Result shows that incorrect choice of prior density does not necessarily lead to wrong estimates, but a crude assumption of the prior probability density is found to take longer time to achieve convergence. Reconstructed vehicle bridge interaction force is shown in Fig 7.39 and Fig 7.40, simultaneously comparing with the true value of dynamic interaction force. Assumption

based on the first case of prior density function leads to 2 to 14 percent error while the second case assumption gives 1 to 19 percent error.

Table 7.13 Range of vehicle mass, flexural rigidity and wheel mass to construct prior *PDF*

Range	Vehicle mass/length (m_v) kg/m		Vehicle flexural rigidity (EI_v) N-m^2		Front and rear wheel mass (m_{w1}, m_{w2}) kg	
	Case 1	Case 2	Case 1	Case 2	Case 1	Case 2
Γ_L	1.3×10^3	0.5×10^3	3.4×10^6	1.5×10^6	5.2×10^2	0.5×10^2
Γ_U	1.9×10^3	4.5×10^3	8.5×10^6	1.3×10^7	1.3×10^3	8.5×10^3

Table 7.14 Range of Suspension stiffness and Tyre stiffness to construct prior *PDF*

Range	Front and rear vehicle suspension stiffness (k_{v1}, k_{v2}) N/m		Front and rear wheel stiffness (k_{t1},k_{t2}) N/m	
	Case 1	Case 2	Case 1	Case 2
Γ_L	2.8×10^7	0.3×10^7	0.6×10^7	5.2×10^6
Γ_U	4.0×10^7	8.5×10^7	1.1×10^8	8.5×10^7

Table 7.15 Range of Suspension damping and Tyre damping to construct prior *PDF*

Range	Front and rear vehicle suspension damping (c_{v1}, c_{v2}) N-s/m		Front and rear wheel damping (c_{t1}, c_{t2}) N-s/m	
	Case 1	Case 2	Case 1	Case 2
Γ_L	6.5×10^4	1.5×10^4	0.5×10^4	5.2×10^3
Γ_U	8.3×10^4	12.3×10^4	0.9×10^4	6.4×10^4

Table 7.16 Effect of initial range of parameters on the estimated vehicle parameters

Parameters	Case-1		Case-2	
	No of iteration	RPE (%)	No of iteration	RPE (%)
m_v	44	2.164	53	2.075
m_{w1}	45	2.760	55	2.971
m_{w2}	28	2.343	104	7.852
k_{v1}	52	11.822	89	13.896
k_{v2}	61	11.754	58	14.853
c_{v1}	64	8.187	85	18.375
c_{v2}	42	3.130	36	3.0454
k_{t1}	38	7.531	56	15.20
k_{t2}	33	5.016	63	11.721
c_{t1}	49	14.490	82	14.601
c_{t2}	58	1.667	39	2.090
EI_v	48	3.185	91	5.932

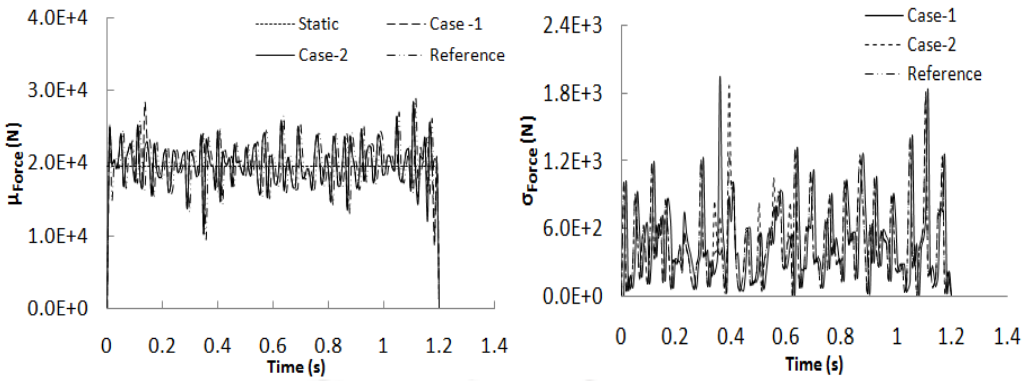

(a) Mean value (b) Standard deviation

Fig. 7.39 Comparison of reconstructed front axle interaction force based on identification from different range of values used to construct prior PDF $p(\Phi_0)$

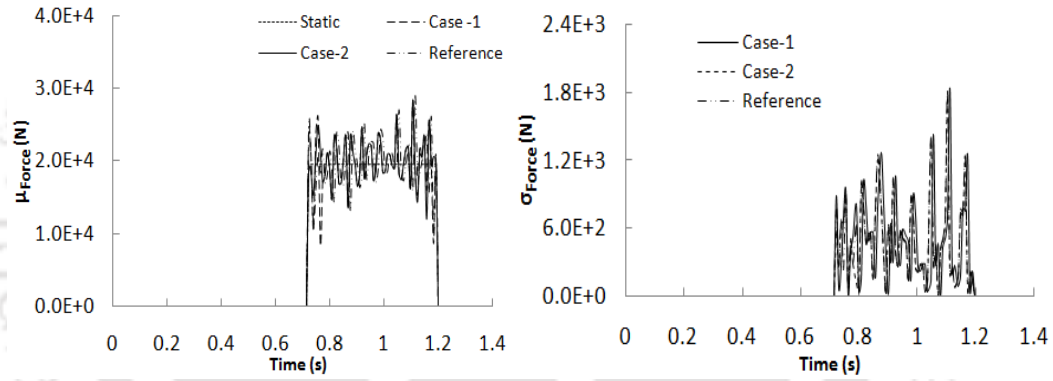

(a) Mean value (b) Standard deviation

Fig. 7.40 Comparison of reconstructed rear axle interaction force based on identification from different range of values used to construct prior PDF $p(\Phi_0)$

7.4.4 Effect of Different Vehicle Velocity

Parametric study has been conducted for Model-2 to examine performance of particle filtering algorithm in identifying vehicle parameters. Simulated bridge responses for vehicle speed 40 km/h, 60 km/h and 80 km/h, contaminated by 5% artificial noise have been considered as input to the identification algorithm. Vehicle parameters identification result in terms of iteration required and relative percentage error (RPE) are given in Table 7.17. It has been found that lower speed gives better estimate but sometimes it requires more number of iteration to achieve the convergence. In addition to this, it has been observed while carrying out computational work that a sampling time interval 0.01 sec (sampling frequency 100 Hz)

for vehicle speed 40 km/h is satisfactory to achieve convergence while sampling time interval 0.005 sec (sampling frequency 200 Hz) is adequate for vehicle speed 80 km/h. The reason for increasing sampling frequency in high speed movement of vehicle is that time duration of vehicle imposed loading on the bridge is less.

Table 7.17 Effect of vehicle speed on the estimated vehicle parameters

Parameters	No of iteration			RPE (%)		
	40km/h	60 km/h	80 km/h	40 km/h	60 km/h	80 km/h
m_v	57	44	31	2.404	2.164	1.974
m_{w1}	21	45	63	1.226	2.760	7.581
m_{w2}	18	28	65	1.782	2.343	9.413
k_{v1}	34	52	46	10.611	11.822	12.751
k_{v2}	77	46	19	5.604	9.167	10.865
c_{v1}	41	64	93	2.732	8.187	8.507
c_{v2}	22	42	48	1.237	3.130	1.693
k_{t1}	59	38	51	1.372	7.531	8.057
k_{t2}	62	33	106	1.90	5.016	6.667
c_{t1}	56	49	32	11.732	14.490	15.60
c_{t2}	81	62	93	2.068	3.907	4.586
EI_v	26	48	94	2.185	3.185	3.428

7.4.5 Effect of different deck surface roughness condition

Bridge deck surface irregularity always plays important role in Bridge-Vehicle interaction. In the present study, vehicle parameters of Model-2 has been identified in the presence of deck surface roughness based on ISO specification (ISO 8608:1995) for different conditions- good, average and poor. Parameters estimation results are given in Table 7.18. It has been found that good bridge deck surface condition gives estimate with less number of iteration. This is invariably due to increased noise level in wheel input which results in noisy record of response.

Table 7.18 Effect of bridge deck surface condition on the estimated vehicle parameters

Parameters	No of iteration			RPE (%)		
	Good condition	Average condition	Poor condition	Good condition	Average condition	Poor condition
m_v	24	44	47	1.304	2.164	2.209
m_{w1}	33	51	167	4.988	8.760	9.864
m_{w2}	23	37	127	3.785	7.241	8.552
k_{v1}	30	52	69	11.277	11.822	12.407
k_{v2}	19	50	49	3.949	9.670	10.705
c_{v1}	59	64	138	7.885	8.187	11.976
c_{v2}	38	42	92	2.125	3.130	8.695
k_{t1}	29	38	62	6.592	7.531	9.331
k_{t2}	31	33	55	3.276	5.016	11.829
c_{t1}	44	49	137	11.201	14.490	15.279
c_{t2}	47	64	110	2.857	3.561	4.552
EI_v	52	53	108	3.866	4.170	5.709

7.4.7 Effect of approach road settlement

The presence of approach settlement in a bridge greatly affects its dynamic behavior. Therefore, it is necessary to examine such condition in moving load identification using bridge response data. This has been investigated here for 20 mm settlement magnitude. Fig. 7.41 to Fig. 7.43 shows the progressive estimates of vehicle body and wheels masses based on simulated acceleration at mid span of the bridge. Both conditions (i,e with approach settlement and without approach settlement) are considered in presenting the result. Number of iteration required and error in parameters estimates are given in Table 7.19. Although improvement in accuracy is small for the case of smooth entry of vehicle to the bridge, number of iteration required to achieve converged result is very high when magnitude of settlement in approach slab is significant. This trend has been observed for almost all parameters of the model; however, for certain parameters the result does not indicate much detrimental effect of approach settlement on the identified parameters.

Table 7.19 Effect of approach settlement on identified vehicle parameters

Vehicle parameters	No of iteration		RPE (%)	
	Without approach settlement	With 20 mm approach settlement	Without approach settlement	With 20 mm approach settlement
m_v	44	55	2.164	3.08
m_{w1}	60	82	2.509	3.112
m_{w2}	102	115	4.720	8.992
k_{v1}	51	72	9.795	11.961
k_{v2}	53	71	11.671	12.048
c_{v1}	42	64	3.130	3.989
c_{v2}	61	89	7.996	8.187
k_{t1}	33	57	7.290	8.232
k_{t2}	65	70	5.098	8.016
c_{t1}	47	59	12.772	14.490
c_{t2}	63	77	4.067	5.098
EI_v	48	81	3.185	5.114

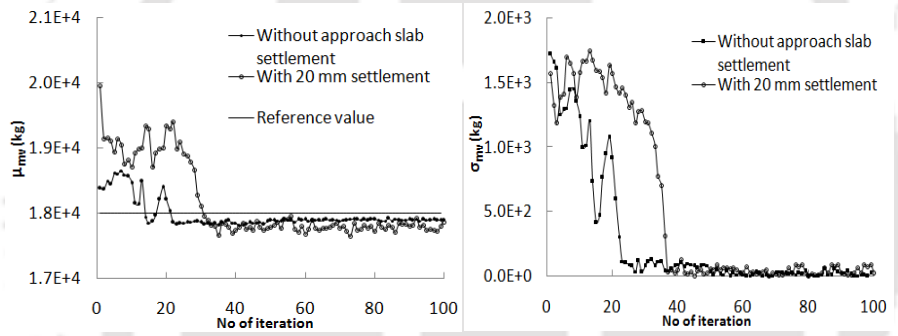

(a) Mean value (b) Standard deviation

Fig. 7.41 Progressive estimate of vehicle mass m_v from bridge acceleration with and without approach settlement

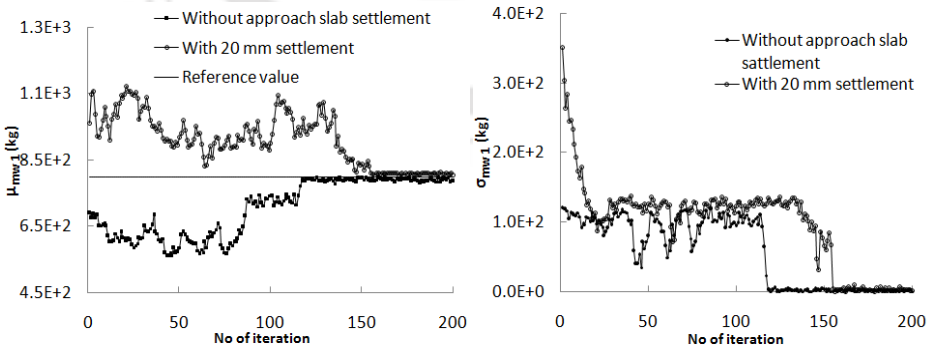

(a) Mean value (b) Standard deviation

Fig. 7.42 Progressive estimate of front wheel mass m_{w1} from bridge acceleration with and without approach settlement

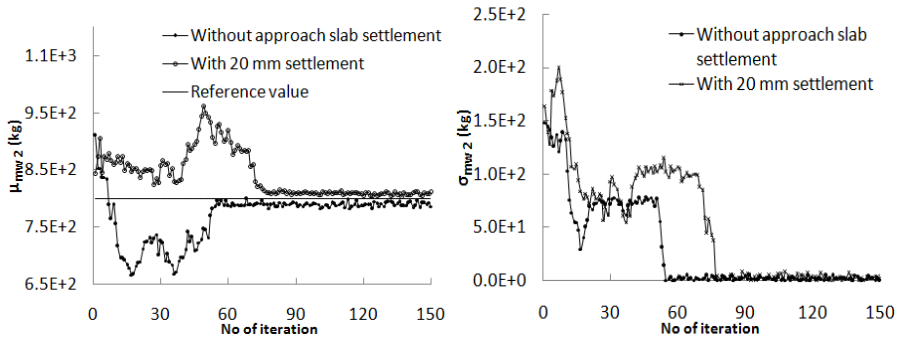

(a) Mean value (b) Standard deviation

Fig. 7.43 Progressive estimate of rear wheel mass m_{w2} from bridge acceleration with and without approach road settlement

7.5 Influence of Various Factors on Vehicle Parameter Identification Using Model-3

In Model-3, all possible degrees of freedom of vehicle model including vehicle body elastic bending and torsion has been included. Several parametric studies have been conducted to investigate efficiency of the proposed identification technique. Studies has been performed under consideration of vehicle speed 60 km/h; average bridge deck surface condition and 5% noise level, unless mentioned otherwise. Bridge acceleration has been simulated using coupled system models with physical parameters given in Section 6.2.2.3; these vehicle parameters are taken as a reference value to check the identification accuracy. Bridge acceleration at different span location for vehicle speed 60 km/h is shown in Fig. 7.44.

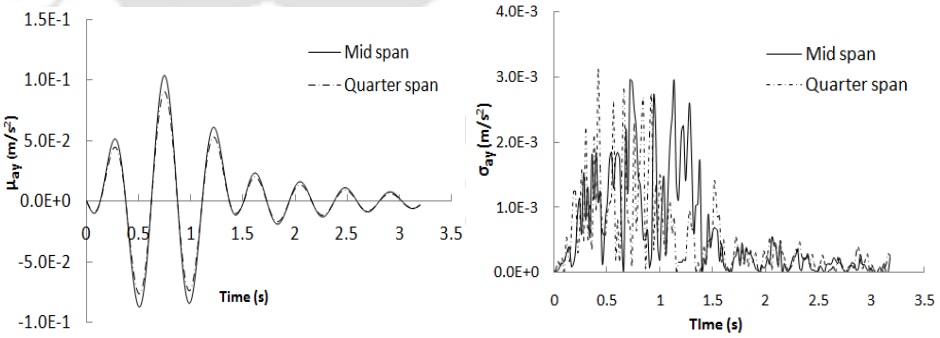

(a) Mean (b) Standard deviation

Fig. 7.44 Bridge acceleration at mid span and quarter span

7.5.1 Effect of Bridge Response Measurement Location

In actual bridge dynamic test, maintaining the pre-decided location of a sensor is often difficult due to local degradation of surface and other inconvenience for assessing a particular bridge element. In view of this, effect of response measurement location on vehicle parameters estimation has been investigated. In the present case study, bridge acceleration at mid span and quarter span of the bridge has been considered as input to the identification algorithm. Identification results are given in Table 7.20. Progress of mean and standard deviations with number of iterations till convergence are shown in Fig. 7.45 to Fig. 7.68. Evolution of PDF of identified vehicle parameters at different stage of iterations are presented in Fig. 7.69 to Fig. 7.76. Overall performance of the identification work shows that vehicle parameters estimated based on bridge acceleration at mid span gives better estimate with minimal number of iteration. The interaction forces have been obtained and compared with those obtained by using reference vehicle parameters. This is shown in Fig. 7.77 to Fig. 7.80. It may be noted that interaction forces considerably fluctuates about the static force which necessitates bridge-vehicle dynamic modeling. The closeness of interaction force reconstructed from identified parameters with that of reference force time history also reflects the reasonable accuracy of identification method applied in the present study.

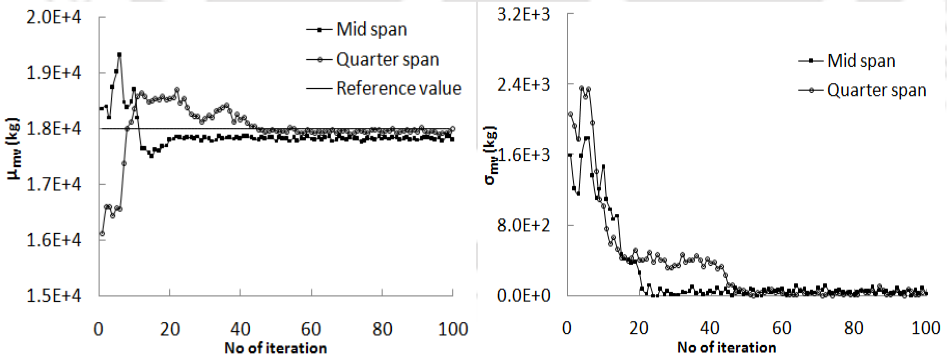

(a) Mean value (b) Standard deviation

Fig 7.45 Progressive estimate of vehicle mass m_v from acceleration data at different locations

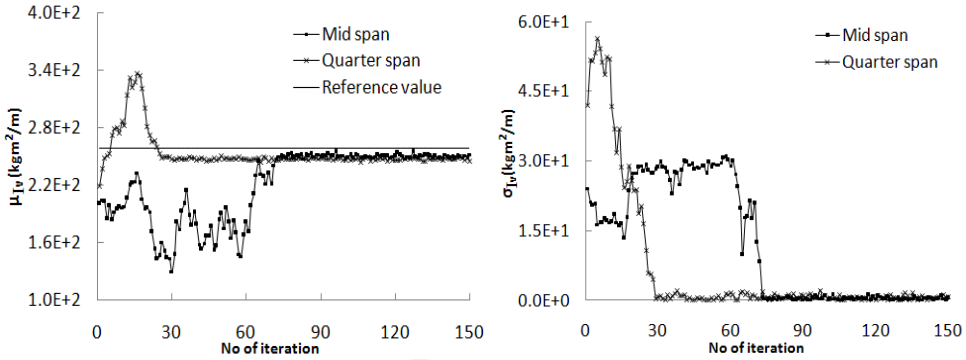

(a) Mean value (b) Standard deviation

Fig 7.46 Progressive estimate of mass moment of inertia I_v from acceleration data at different locations.

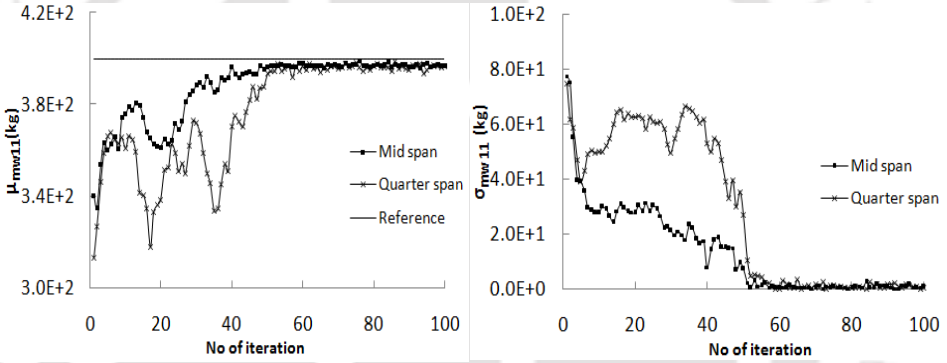

(a) Mean value (b) Standard deviation

Fig 7.47 Progressive estimate of front-right side wheel mass m_{w11} from acceleration data at different locations

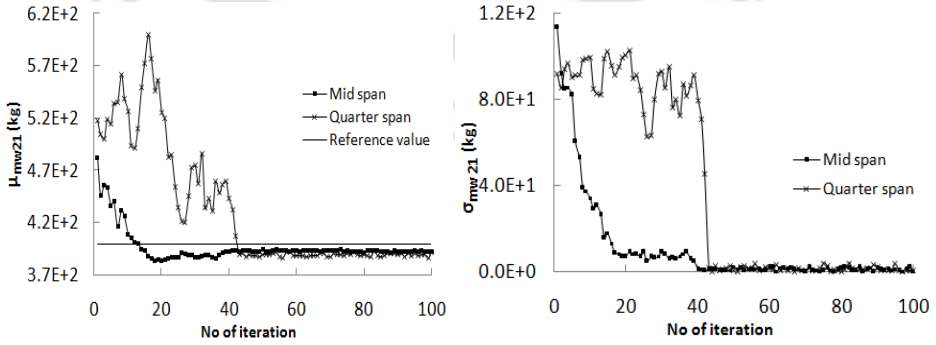

(a) Mean value (b) Standard deviation

Fig 7.48 Progressive estimate of front-left wheel mass m_{w21} from acceleration data at different locations

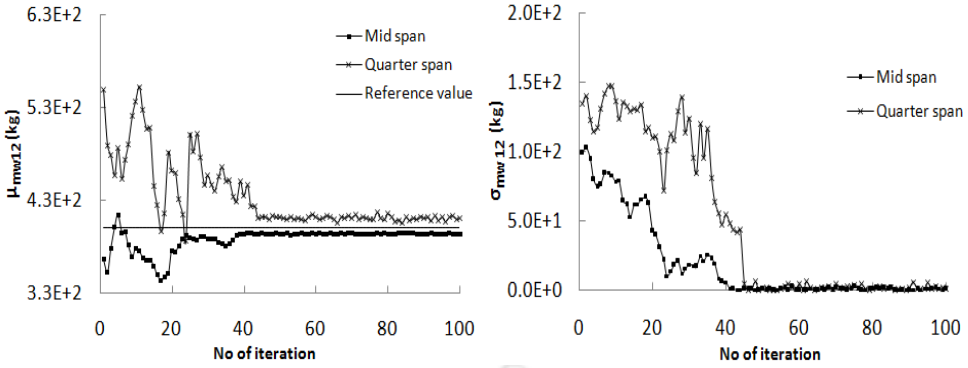

(a) Mean value (b) Standard deviation

Fig 7.49 Progressive estimate of rear-right wheel mass m_{w12} from acceleration data at different locations

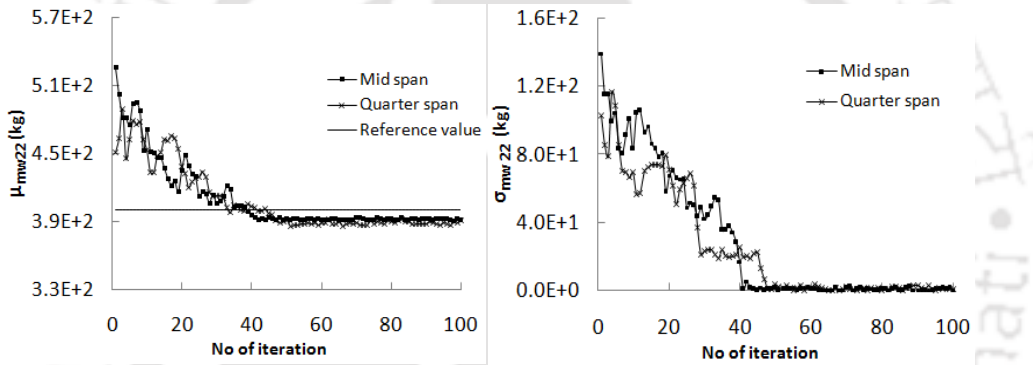

(a) Mean value (b) Standard deviation

Fig 7.50 Progressive estimate of rear-left wheel mass m_{w22} from acceleration data at different locations

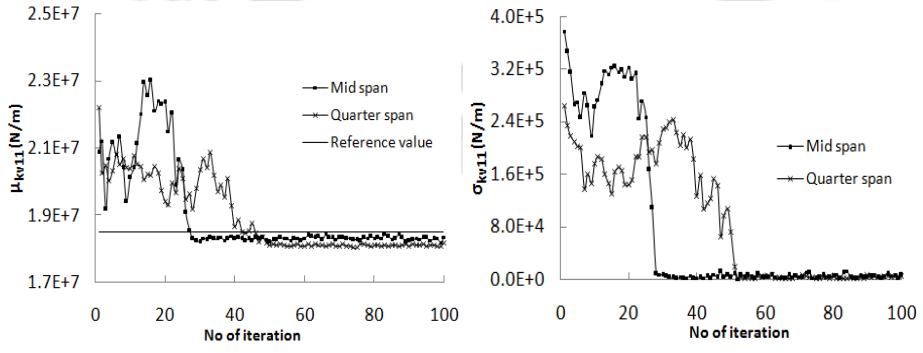

(a) Mean value (b) Standard deviation

Fig.7.51 Progressive estimate of front-right vehicle suspension stiffness k_{v11} from acceleration data at different locations

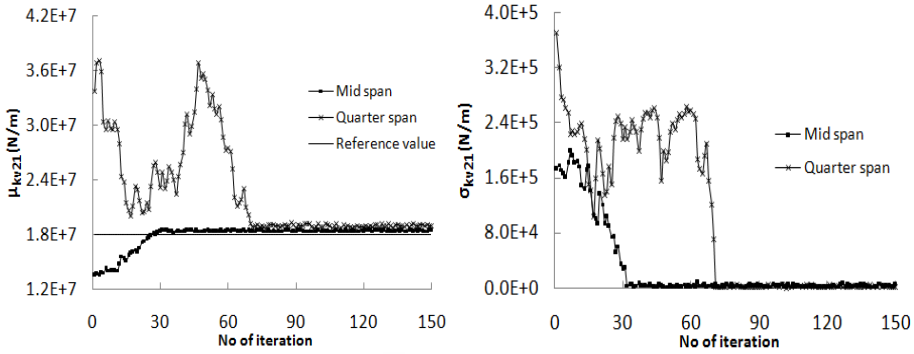

(a) Mean value (b) Standard deviation

Fig.7.52 Progressive estimate of front-left vehicle suspension stiffness k_{v21} from acceleration data at different locations

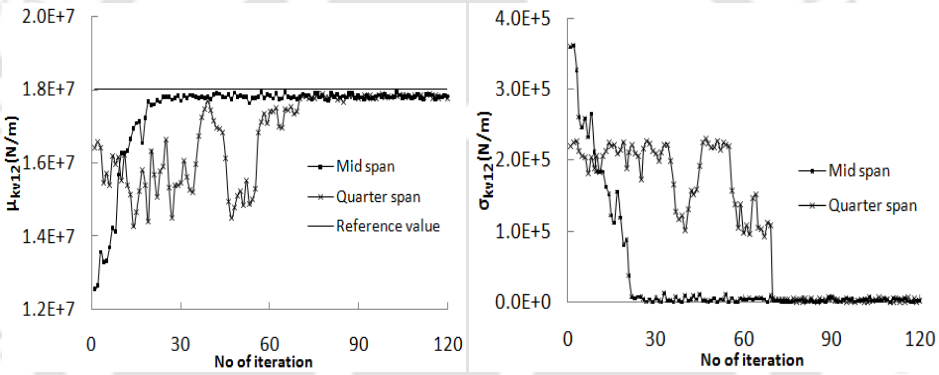

(a) Mean value (b) Standard deviation

Fig.7.53 Progressive estimate of rear-right vehicle suspension stiffness k_{v12} from acceleration data at different locations

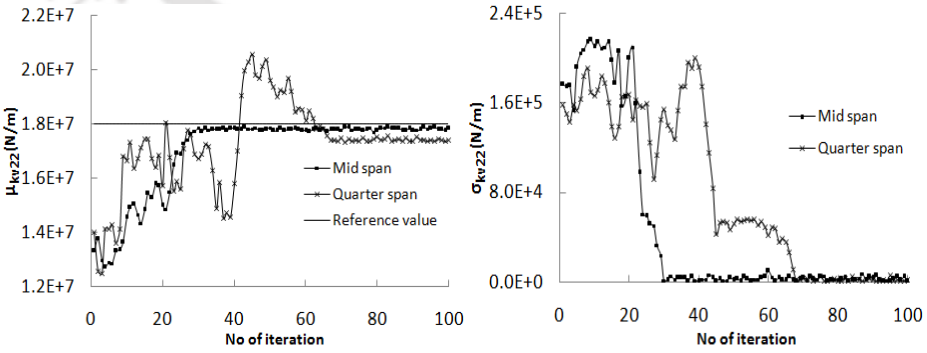

(a) Mean value (b) Standard deviation

Fig. 7.54 Progressive estimate of rear-left vehicle suspension stiffness k_{v22} from acceleration data at different locations

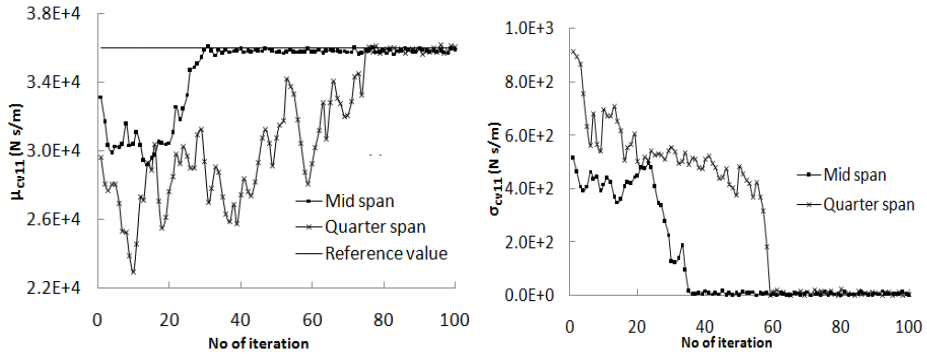

(a) Mean value (b) Standard deviation

Fig. 7.55 Progressive estimate of front-right vehicle suspension damping c_{v11} from acceleration data at different locations

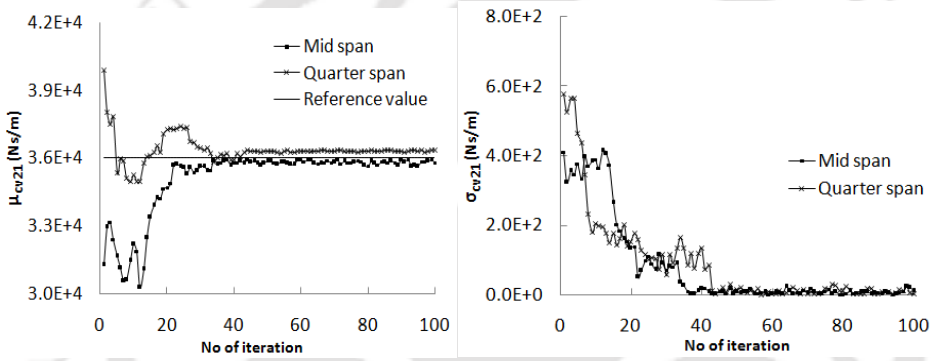

(a) Mean value (b) Standard deviation

Fig. 7.56 Progressive estimate of front-left vehicle suspension damping c_{v21} from acceleration data at different locations

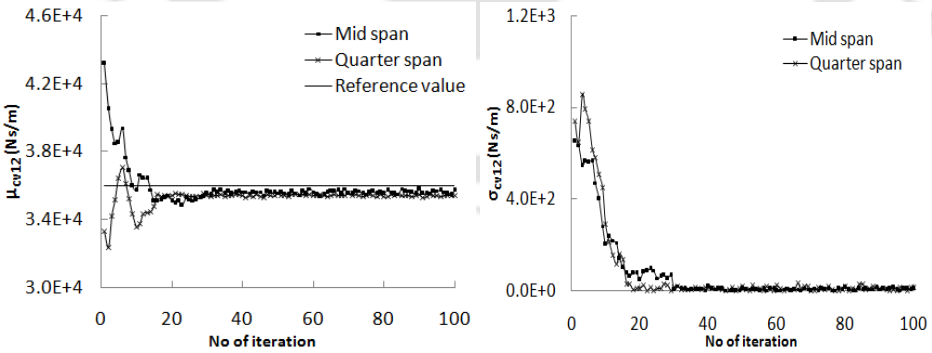

(a) Mean value (b) Standard deviation

Fig. 7.57 Progressive estimate of rear-right vehicle suspension damping c_{v12} from acceleration data at different locations

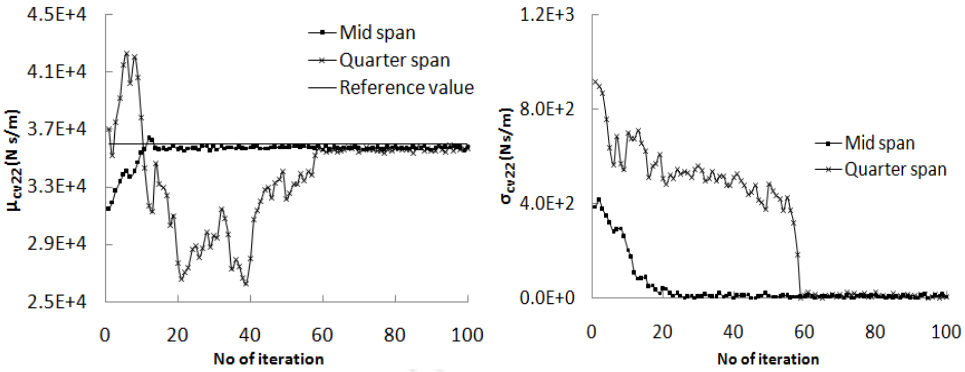

(a) Mean value (b) Standard deviation

Fig. 7.58 Progressive estimate of rear-left vehicle suspension damping c_{v22} from acceleration data at different locations

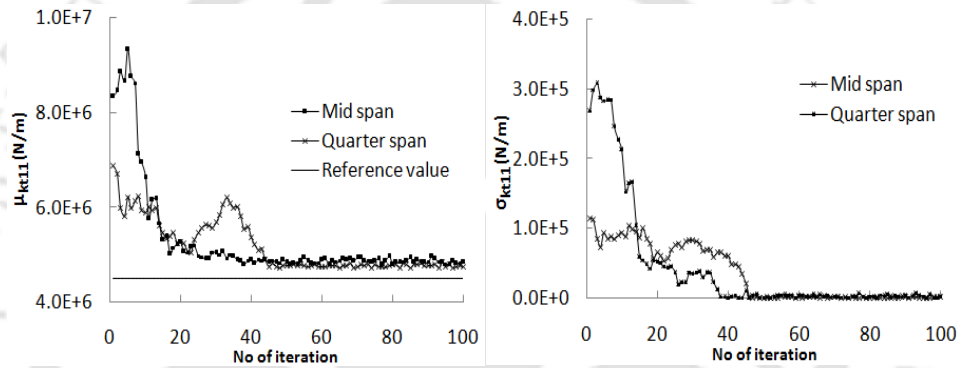

(a) Mean value (b) Standard deviation

Fig. 7.59 Progressive estimate of front-right tyre stiffness k_{t11} from acceleration data at different locations

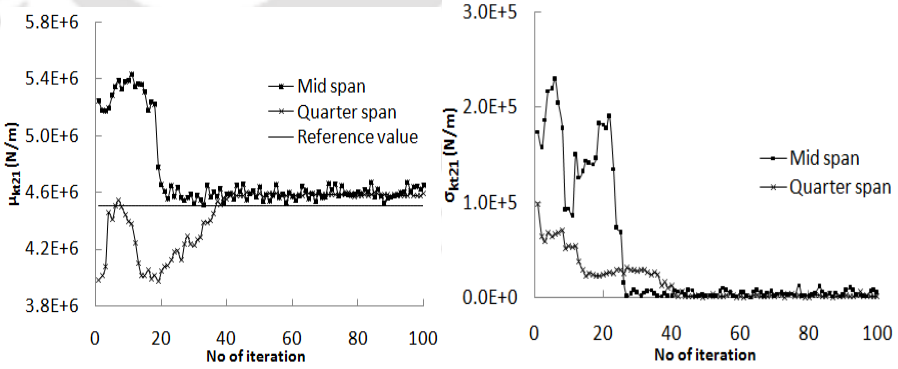

(a) Mean value (b) Standard deviation

Fig. 7.60 Progressive estimate of front-left tyre stiffness k_{t21} from acceleration data at different locations

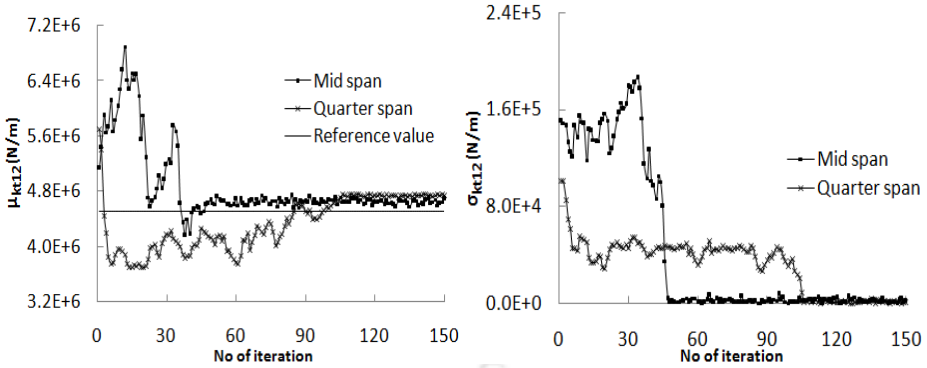

(a) Mean value (b) Standard deviation

Fig. 7.61 Progressive estimate of rear-right side tyre stiffness k_{t12} from acceleration data at different locations

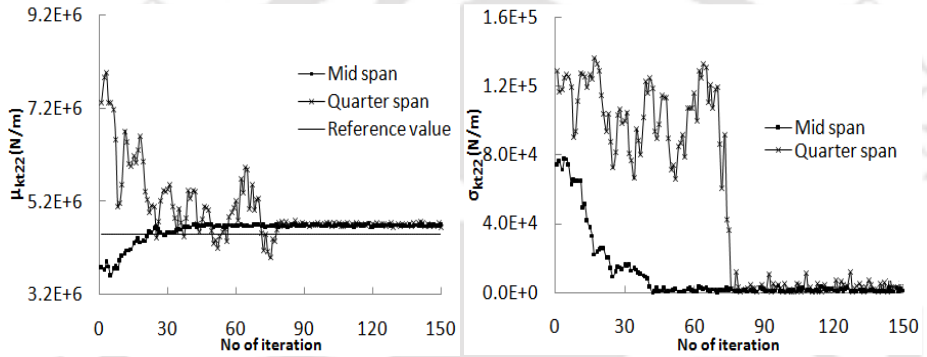

(a) Mean value (b) Standard deviation

Fig. 7.62 Progressive estimate of rear-left side tyre stiffness k_{t22} from acceleration data at different locations

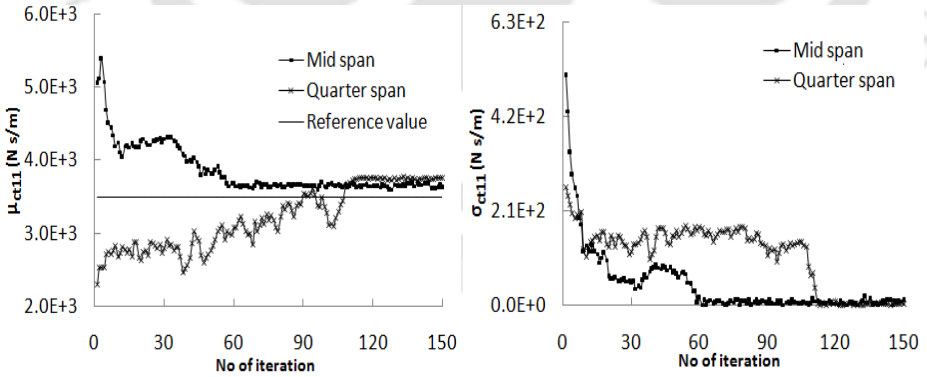

(a) Mean value (b) Standard deviation

Fig. 7.63 Progressive estimate of front-right side tyre damping c_{t11} from acceleration data at different locations

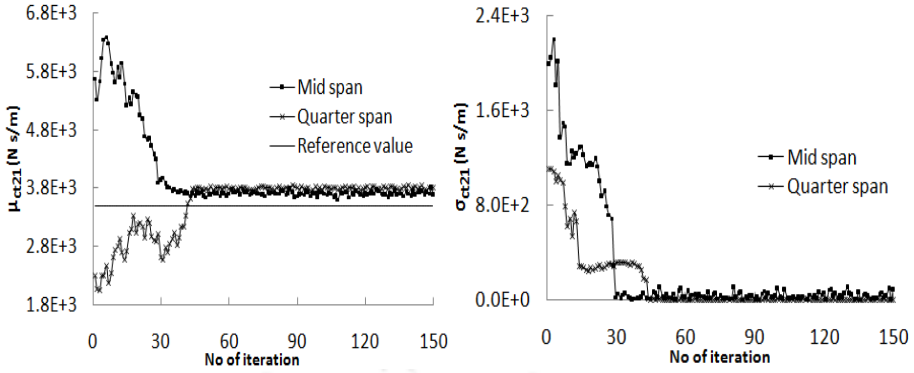

(a) Mean value (b) Standard deviation

Fig. 7.64 Progressive estimate of front-left side tyre damping c_{t21} from acceleration data at different locations

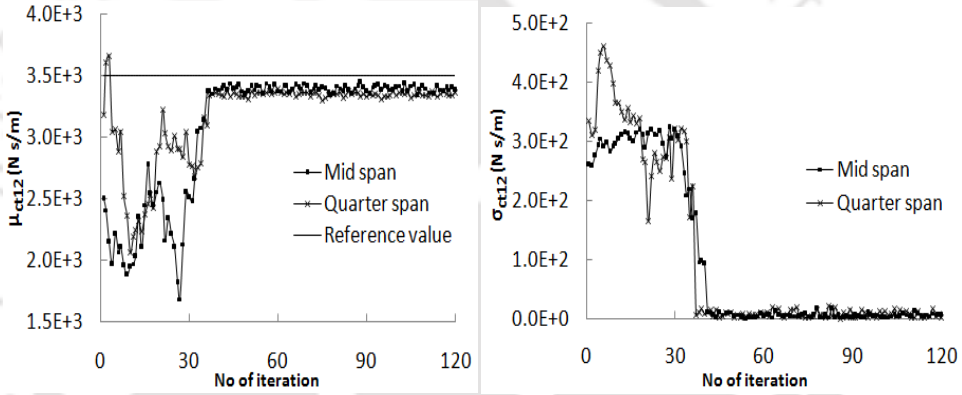

(a) Mean value (b) Standard deviation

Fig. 7.65 Progressive estimate of rear-right side tyre damping c_{t12} from acceleration data at different locations

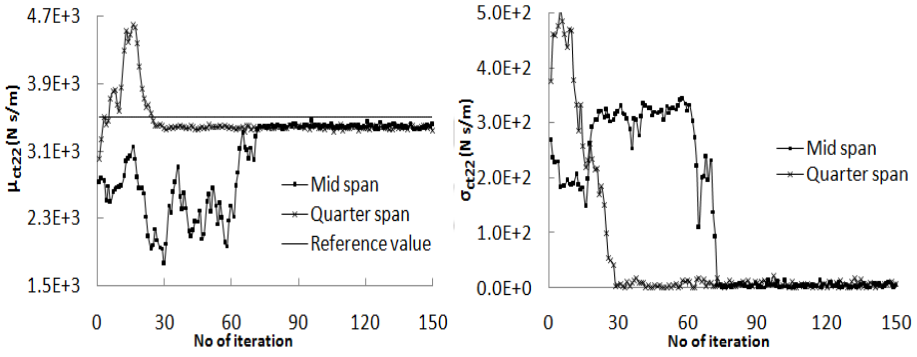

(a) Mean value (b) Standard deviation

Fig. 7.66 Progressive estimate of rear-left side tyre damping c_{t22} from acceleration data at different locations

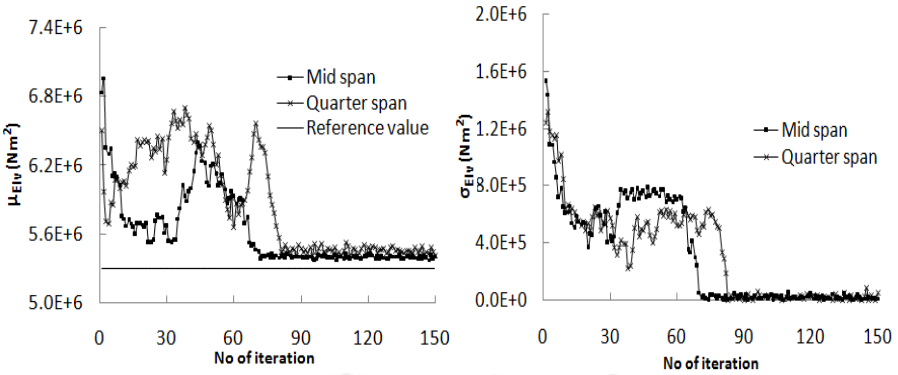

(a) Mean value (b) Standard deviation

Fig. 7.67 Progressive estimate of vehicle body flexural rigidity EI_v from acceleration data at different locations

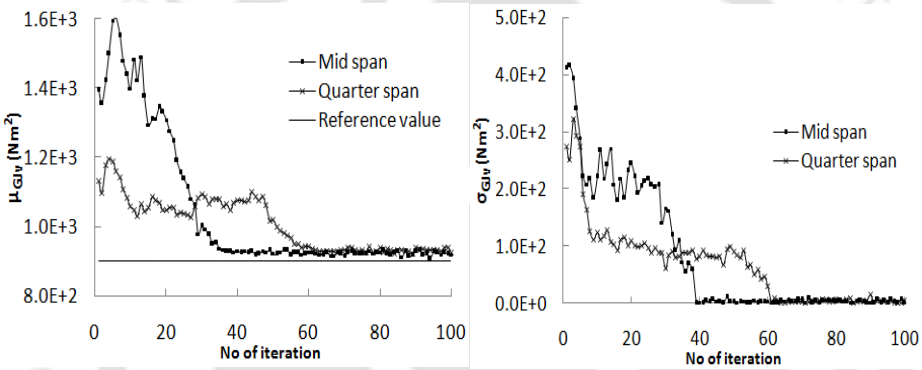

(a) Mean value (b) Standard deviation

Fig. 7.68 Progressive estimate of vehicle body torsional rigidity GJ_v from acceleration data at different locations

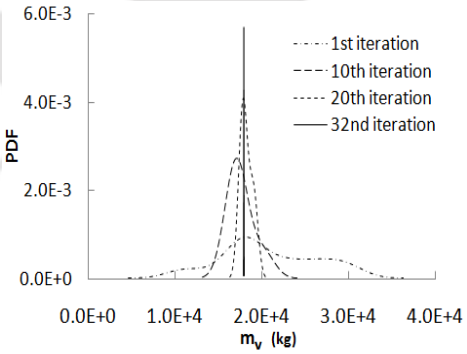

Fig. 7.69 Evolution of PDF of vehicle mass for measurement at mid span

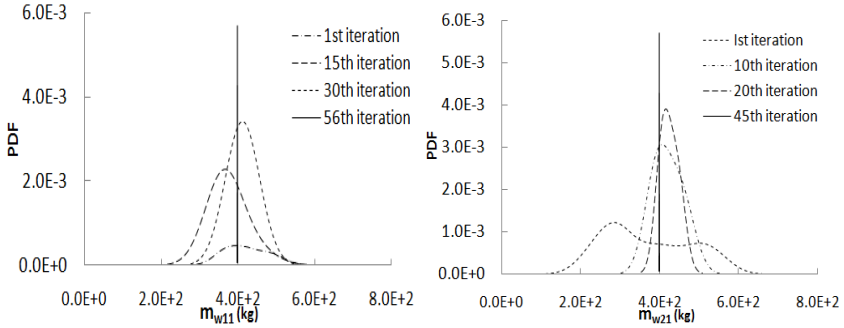

(a) (b)

Fig. 7.70 Evolution of PDF for measurement at mid span (a) front-right (b) front-left wheel mass

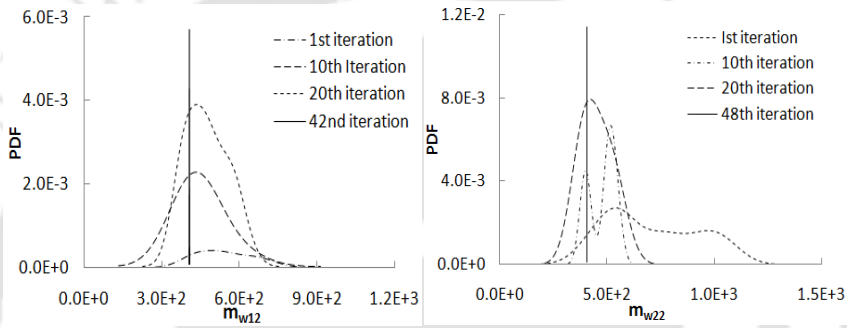

(a) (b)

Fig. 7.71 Evolution of PDF for measurement at mid span (a) rear-right (a) rear-left wheel mass

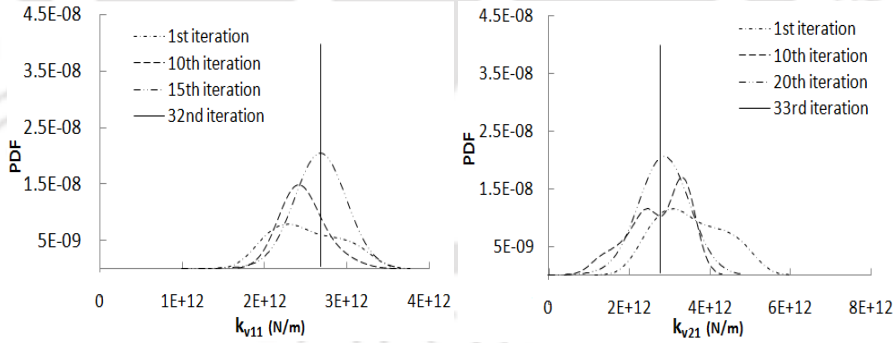

(a) (b)

Fig. 7.72 Evolution of PDF for measurement at mid span (a) front-right (b) front-left suspension stiffness

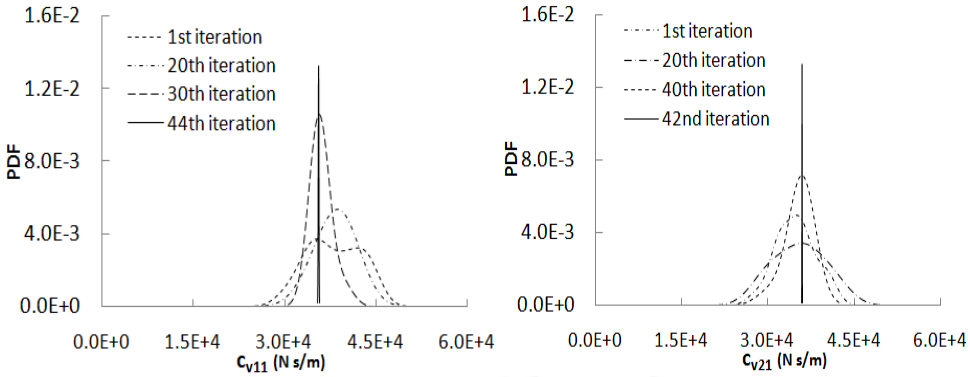

(a) (b)

Fig. 7.73 Evolution of PDF for measurement at mid span (a) front-right (b) front-left suspension damping

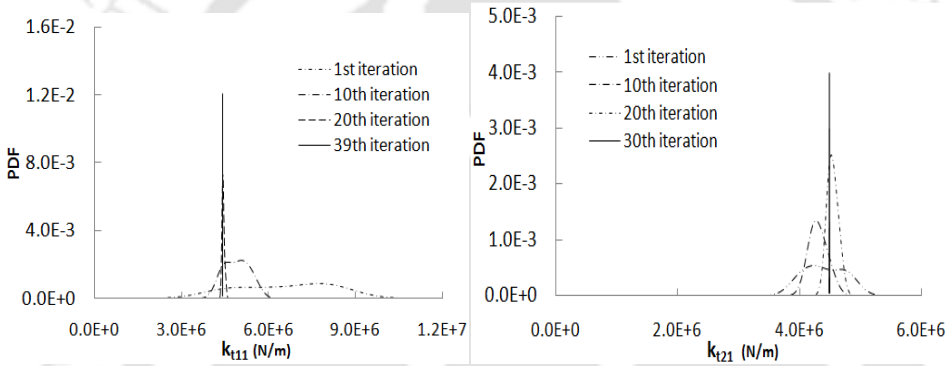

(a) (b)

Fig. 7.74 Evolution of PDF for (a) front-right (b) front-left side of vehicle tyre stiffness

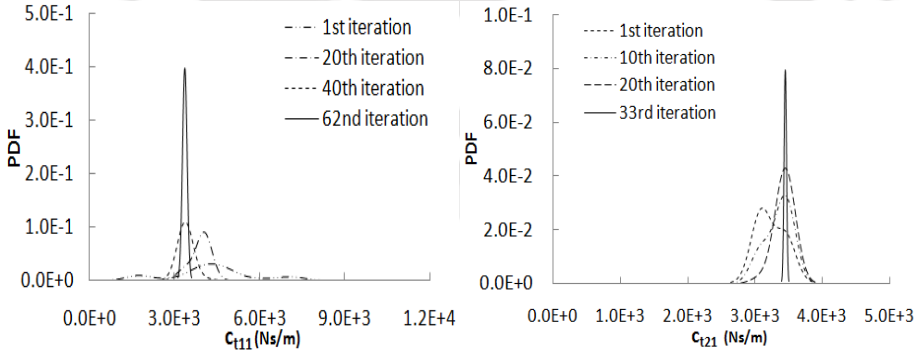

(a) (b)

Fig. 7.75 Evolution of PDF for (a) front-right (b) front-left tyre damping

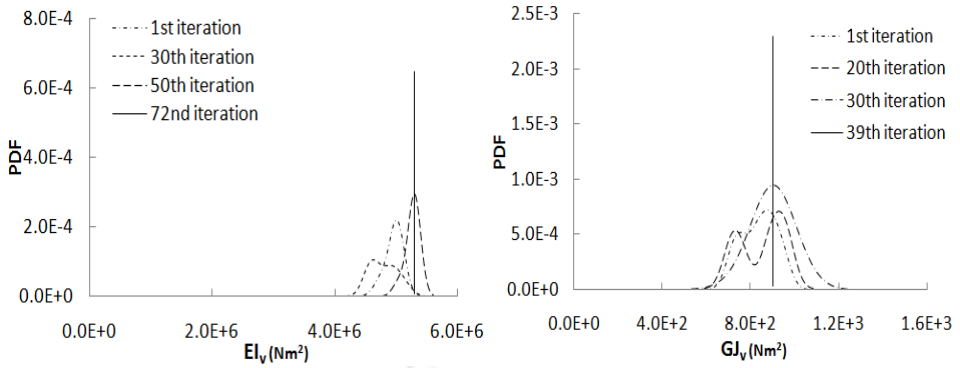

(a) (b)

Fig. 7.76 Evolution of PDF for (a) vehicle body flexural rigidity and (b) vehicle body torsional rigidity

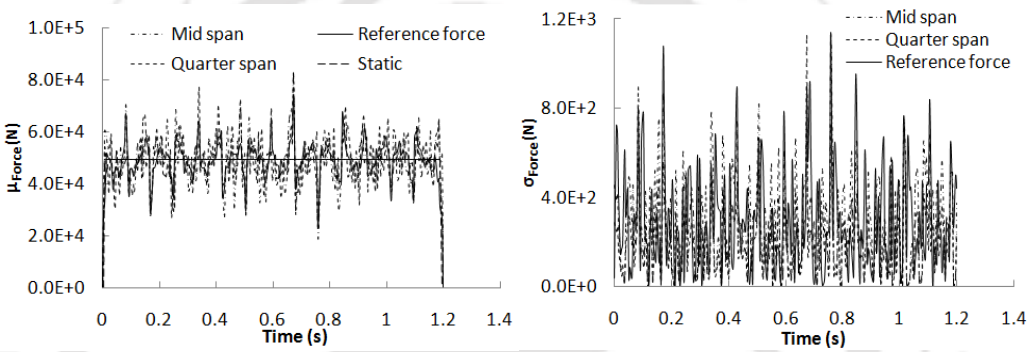

(a) Mean (b) Standard deviation

Fig. 7.77 Comparison of reconstructed interaction force imposed by front-right wheel with reference force

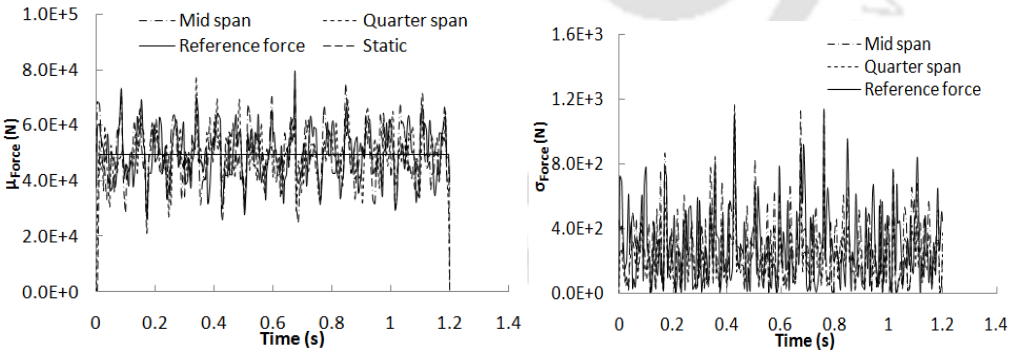

(a) Mean (b) Standard deviation

Fig. 7.78 Comparison of reconstructed interaction force imposed by front-left wheel with reference force

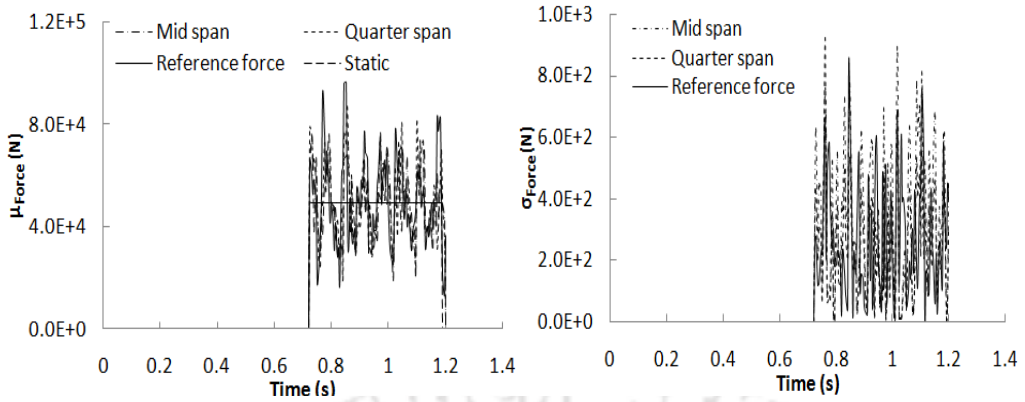

(a) Mean (b) Standard deviation

Fig. 7.79 Comparison of reconstructed interaction force imposed by rear-right wheel with Reference force

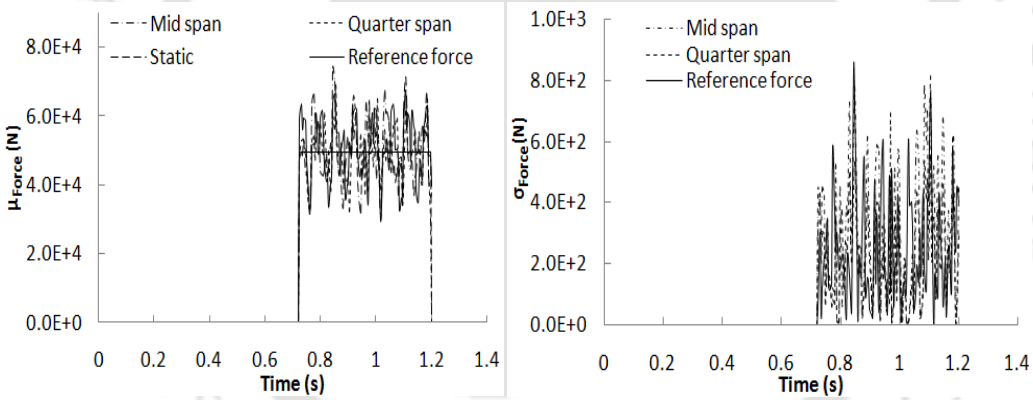

(a) Mean (b) Standard deviation

Fig. 7.80 Comparison of reconstructed interaction force imposed by rear-left wheel with Reference force

Table 7.20 Effect of response measurement location on identified vehicle parameters

Parameters	Mid-span		Quarter span	
	No. of Iterations	RPE	No. of Iterations	RPE
m_v	32	2.114	58	2.528
m_{w11}	56	3.681	67	4.096
m_{w21}	45	2.173	49	4.387
m_{w12}	42	6.052	48	7.182
m_{w22}	48	4.530	53	5.931
k_{v11}	32	4.294	73	7.507
k_{v21}	33	5. 516	69	8.374
k_{v12}	36	7.384	77	9.115
k_{v22}	34	6.982	68	10.210
c_{v11}	44	5.287	62	7.293
c_{v21}	42	3.130	43	3.278
c_{v12}	41	7.224	52	8.710
c_{v22}	35	4.912	65	6.050
k_{t11}	39	10.13	51	13.412
k_{t21}	30	11.512	49	14.223
k_{t12}	50	9.167	106	11.083
k_{t22}	43	10.607	82	12.162
c_{t11}	62	15.490	112	17.965
c_{t21}	33	17.267	51	19.610
c_{t12}	34	16.112	33	18.520
c_{t22}	33	9.815	76	11.043
I_{mv}	32	2.862	80	4.013
EI_v	72	7.182	89	9.021
GJ_v	39	5.263	62	7.811

7.5.2 Effect of artificial noise level

Noise present in the field response measurement cannot be avoided. This sometimes leads to erroneous estimation of hidden parameters from the signal. Hence we present the identification of vehicle parameters by adding noise to the simulated response to maximum level of 10%. Table 7.21 shows the number of iteration required to converge and corresponding percentage error. The relative percent error is higher in case of noisy data with noise level of 10%. Although, number of iterations is far greater in case of higher level of noise, difference in accuracy is not much. This once again proves the robustness of the particle filtering technique in identifying vehicle parameters.

Table 7.21 Effect of artificial noise level on identified vehicle parameters

Parameters	5% noise		10% noise	
	No of iteration	RPE (%)	No of iteration	RPE (%)
m_v	32	2.114	57	2.821
m_{w11}	56	3.681	78	5.091
m_{w21}	45	2.173	82	4.117
m_{w12}	42	6.052	61	8.102
m_{w22}	48	4.53	86	7.122
k_{v11}	32	4.294	71	5.117
k_{v21}	33	5. 516	62	6.072
k_{v12}	36	7.384	78	8.064
k_{v22}	34	6.982	59	9.122
c_{v11}	44	5.287	68	7.358
c_{v21}	42	3.13	59	3.635
c_{v12}	41	7.224	63	8.427
c_{v22}	35	4.912	65	5.961
k_{t11}	39	10.13	58	11.701
k_{t21}	30	11.512	79	13.832
k_{t12}	50	9.167	94	10.935
k_{t22}	43	10.607	103	13.642
c_{t11}	62	15.49	99	16.901
c_{t21}	33	17.267	59	18.866
c_{t12}	34	16.112	48	17.110
c_{t22}	33	9.815	79	12.012
I_{mv}	48	2.862	61	3.667
EI_v	72	7.182	102	10.151
GJ_v	39	5.263	95	8.614

7.5.3 Effect of initial range of vehicle parameters for construction of prior PDF $p(\Gamma_0)$

In the present section with deployment of full car flexible vehicle model, the performance of identification method has been checked by considering two different assumptions of prior PDF. Case-1 is for the parameters initially chosen having narrow range while Case-2 is for the parameters having wide range in initial choice. The range of values of the parameters assumed for the above two cases are mentioned in Table-7.22 to 7.24. In these two cases, number of particles N_p=1000 and artificial noise is taken as 5% of the simulated maximum bridge dynamic response. The estimate of all important parameters of the full car flexible vehicle model has been shown in Table 7.25. Similar to case studies of previous models, once again results demonstrate that initially incorrect choice of parameters for probability density function does not necessarily end up with incorrect estimate. This effect is only

reflected in the increased number of iterations in particle filter method, as depicted in Table 7.25. Number of iterations where range of parameters assumed large, requires generally more number of iterations. Mean of the reconstructed vehicle bridge interaction force is shown in Fig 7.81 and Fig.7.82 for each wheel in four-point input model where standard deviation of the imposed force under each wheel has been presented in Fig.7.83 and Fig.7.84. Assumption based on the first case of prior density function leads to 2 to 16 percent error while the second case assumption gives 3 to 19 percent error.

Table 7.22 Range of mass of vehicle, flexural rigidity and torsional rigidity to construct prior *PDF*

Range	Vehicle mass/length (m_v) kg/m		Vehicle flexural rigidity (EI_v) N-m^2		Vehicle torsional rigidity (GJ_v) N-m^2	
	Case 1	Case 2	Case 1	Case 2	Case 1	Case 2
Γ_L	1.3×10^3	0.5×10^3	$1.5\text{x}10^6$	3.4×10^6	6.1×10^2	3.5×10^2
Γ_U	1.9×10^3	4.5×10^3	1.3×10^7	8.5×10^6	11.3×10^2	14.5×10^2

Table 7.23 Range of suspension stiffness, tyre stiffness and wheel mass to construct prior *PDF*

Range	Vehicle suspension stiffness (k_{v11}, k_{v21} ,k_{v12}, k_{v22}) N/m		Wheel suspension stiffness (k_{t11}, k_{t21} ,k_{t12}, k_{t22}) N/m		Wheel mass (m_{w11}, $m_{w21,}$ m_{w12}, m_{w22}) kg	
	Case 1	Case 2	Case 1	Case 2	Case 1	Case 2
Γ_L	1.4×10^7	0.15×10^7	0.25×10^2	0.15×10^2	2.6×10^2	0.25×10^2
Γ_U	2.0×10^7	4.25×10^7	4.75×10^3	6.25×10^3	0.65×10^3	4.21×10^3

Table 7.24 Range of suspension damping and tyre damping to construct prior *PDF*

Range	Front and rear vehicle suspension damping (c_{v1}, c_{v2}) N-s/m		Front and rear wheel damping (c_{t1}, c_{t2}) N-s/m	
	Case 1	Case 2	Case 1	Case 2
Γ_L	3.25×10^4	0.75×10^4	0.25×10^4	2.6×10^3
Γ_U	4.15×10^4	6.15×10^4	0.45×10^4	3.2×10^4

Table 7.25 Effect of initial range of parameters on identified vehicle parameters

Vehicle Parameters	Case-1		Case-2	
	No of iteration	RPE (%)	No of iteration	RPE (%)
m_v	32	2.114	48	2.821
m_{w11}	56	3.681	108	4.160
m_{w21}	45	2.173	66	4.283
m_{w12}	42	6.052	58	7.945
m_{w22}	48	4.53	71	7.024
k_{v11}	32	4.294	59	6.107
k_{v21}	33	5. 516	60	5.982
k_{v12}	36	7.384	55	8.064
k_{v22}	34	6.982	72	5.122
c_{v11}	44	5.287	71	5.358
c_{v21}	42	3.13	89	4.095
c_{v12}	41	7.224	50	8.427
c_{v22}	35	4.912	65	5.961
k_{t11}	39	10.13	52	10.550
k_{t21}	30	11.512	69	13.304
k_{t12}	50	9.167	111	11.035
k_{t22}	43	10.607	70	12.678
c_{t11}	62	15.49	87	16.901
c_{t21}	33	14.267	79	19.116
c_{t12}	34	13.112	64	17.410
c_{t22}	33	9.815	79	11.087
I_{mv}	48	2.862	70	3.667
EI_v	72	7.182	95	8.915
GJ_v	39	5.263	77	6.613

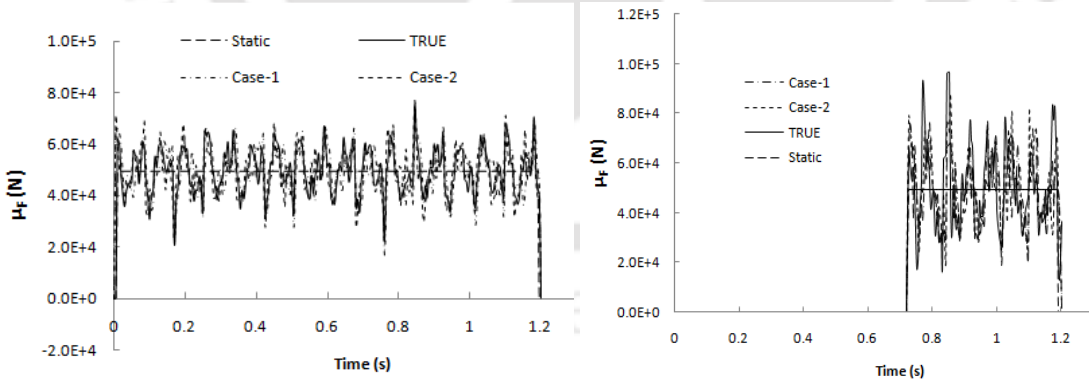

(a) (b)

Fig.7.81. Comparison of mean of identified and true dynamic interaction force (a) front-right (b) rear-right wheel using different prior distribution

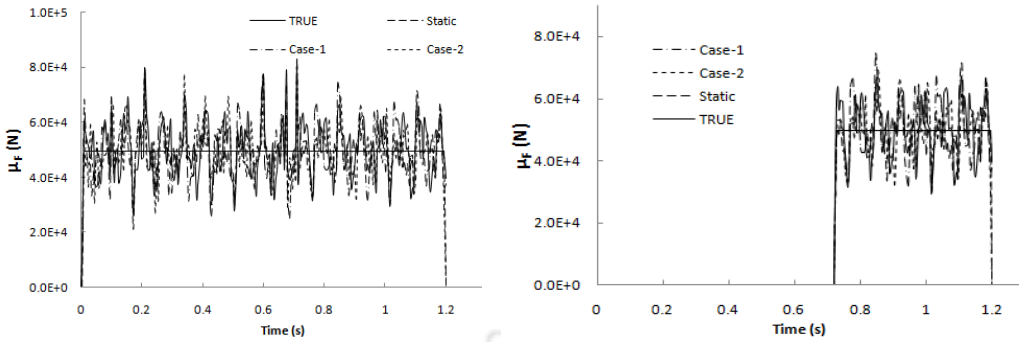

(a) (b)

Fig.7.82. Comparison of mean of identified and true dynamic interaction force (a) front-left (b) rear-left wheel using different prior distribution

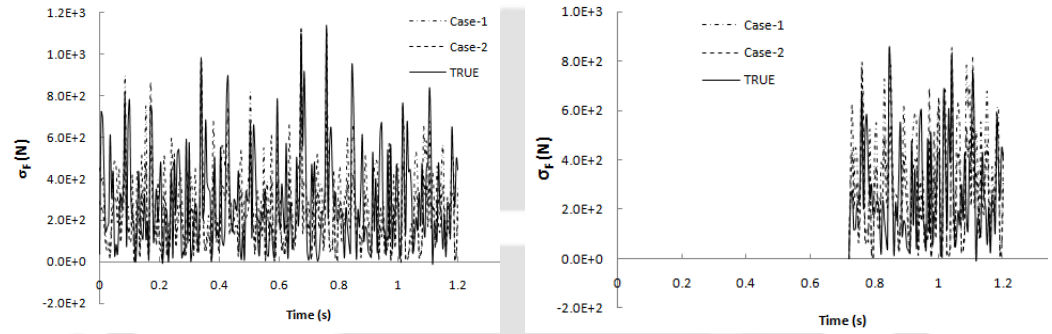

(a) (b)

Fig.7.83. Comparison of standard deviation of identified and true dynamic interaction force (a) front-right (b) rear-right wheel using different prior distribution

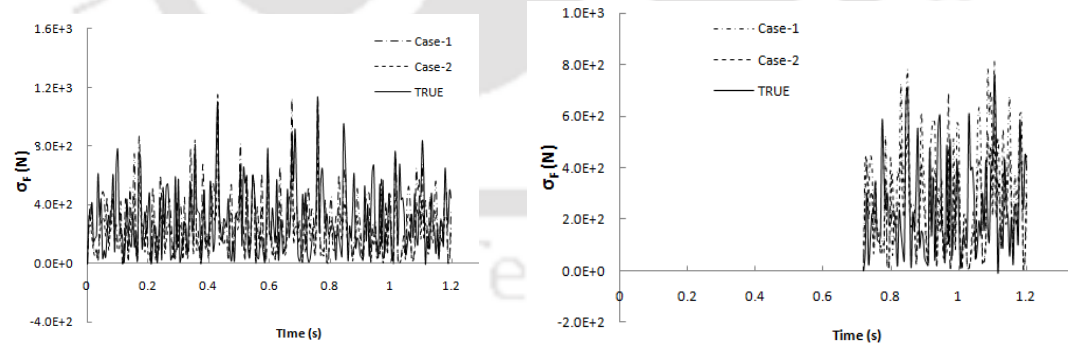

(a) (b)

Fig.7.84. Comparison of standard deviation of identified and true dynamic interaction force (a) front-left (b) rear-left wheel using different prior distribution

7.5.4 Effect of Different Vehicle Velocity

In order to investigate the effect of speed on the identification of vehicle parameters, three different speeds of the vehicle: 40 km/h, 60 km/h and 80 km/h have been considered. Similar to earlier cases on previous models, the sampling time interval in measured bridge response sample has been initially chosen as 0.01 sec. However, this requires to be decreased in order to get sufficient number of data points when vehicle movement at higher speed has been considered. Number of iteration required to get convergence and relative percentage error are tabulated in Table 7.26. As observed in other two vehicle models, performance of model is not satisfactory with smaller sampling frequency at higher speed movement. Therefore, it was necessary to increase sampling frequency in the present forward scheme. General trend of the result is that lower speed gives better estimate (in terms of lower relative percentage of error) but it requires more number of iteration to achieve the convergence. However, this observation is not consistent with all the parameters identified in this case.

7.5.5 Effect of different deck surface roughness condition

Bridge deck surface condition plays crucial role in the bridge response when vehicle moves over it especially for higher vehicle speed. Effect of this condition on vehicle parameters identification has been investigated by considering different conditions - good, average and poor based on ISO specification (ISO 8608:1995). For the purpose of comparison vehicle speed has been taken as 60 km/h with sampling time interval 0.01 sec. Number of iterations along with error in estimates is shown in Table 7.27. It has been found that poor condition of deck surface profile requires more number of iteration to achieve the converged result. From the table it has been observed that relative percentage error for different parameters ranges from 1.2%-14% in 'good' pavement condition while the error lies in the range of 2.1%-17.3% and 3.5%-18.2% for 'average' and 'poor' condition respectively.

7.5.6 Effect of approach road settlement

As observed in earlier two models, accuracy of identification decreases when there is a settlement of approach relative to deck level. Hence a study has also been made to examine the effect of approach settlement employing vehicle model-3. For this, magnitude of approach settlement is taken to be 20 mm. Progressive estimates of vehicle body and wheels masses are shown graphically in Fig 7.85 to Fig 7.89. However, all the parameters identified in presence of approach settlement are shown in Table 7.28. Number of iteration and relative

percentage error are found to be increased when approach settlement exists at bridge end. However, the error computed is found to be less compared to earlier two models.

Table 7.26 Effect of different vehicle velocity on identified vehicle parameters

Parameters	No of iteration			RPE (%)		
	40 km/h	60 km/h	80 km/h	40 km/h	60 km/h	80 km/h
m_v	61	32	31	2.057	2.114	2.752
m_{w11}	64	56	55	1.133	3.681	5.283
m_{w21}	80	45	62	3.56	2.173	3.766
m_{w12}	58	42	36	2.99	4.53	6.79
m_{w22}	85	48	30	4.673	6.052	11.109
k_{v11}	52	32	29	3.892	4.294	5.103
k_{v21}	67	33	31	5.097	5. 516	7.255
k_{v12}	55	36	34	5.813	7.384	11.440
k_{v22}	62	34	42	3.738	6.982	13.257
c_{v11}	77	44	53	1.226	5.287	6.058
c_{v21}	39	42	40	2.581	3.13	3.702
c_{v12}	80	41	47	2.773	7.224	8.411
c_{v22}	68	35	34	1.836	4.912	6.420
k_{t11}	55	39	61	8.21	10.13	9.743
k_{t21}	72	30	48	9.829	11.512	13.115
k_{t12}	79	50	43	7.563	9.167	9.924
k_{t22}	69	43	39	8.833	10.607	12.482
c_{t11}	87	62	54	11.188	15.49	16.975
c_{t21}	55	33	41	14.91	17.267	11.836
c_{t12}	60	34	48	12.08	16.112	14.17
c_{t22}	71	33	30	7.314	9.815	9.02
I_{mv}	50	48	42	1.988	2.862	3.101
EI_v	96	72	58	3.809	4.53	6.015
GJ_v	52	39	31	4.837	5.263	8.882

Table 7.27 Effect of different deck surface roughness condition on identified vehicle parameters

Parameters	No of iteration			RPE (%)		
	Good condition	Average condition	Poor condition	Good condition	Average condition	Poor condition
m_v	29	32	50	1.29	2.114	3.506
m_{w11}	47	56	102	2.273	3.681	6.199
m_{w21}	40	45	67	1.985	2.173	3.537
m_{w12}	36	42	73	3.098	6.052	8.62
m_{w22}	43	48	93	4.957	4.53	5.822
k_{v11}	30	32	48	3.638	4.294	5.182
k_{v21}	35	33	52	3.522	5. 516	5.972
k_{v12}	31	36	78	5.49	7.384	8.802
k_{v22}	28	34	47	4.121	6.982	7.283
c_{v11}	37	44	71	5.064	5.287	6.325
c_{v21}	38	42	68	2.273	3.13	3.902
c_{v12}	40	41	54	6.442	7.224	7.87
c_{v22}	29	35	65	2.866	4.912	5. 611
k_{t11}	33	39	88	8.049	10.13	12.701
k_{t21}	28	30	81	7.633	11.512	11.982
k_{t12}	42	50	115	8.781	9.167	13.957
k_{t22}	37	43	98	8.24	10.607	11.642
c_{t11}	58	62	114	13.893	15.49	16.06
c_{t21}	30	33	79	14.76	17.267	18.212
c_{t12}	28	34	66	14.135	16.112	16.917
c_{t22}	31	33	80	7.722	9.815	10.011
I_{mv}	33	48	71	2.083	2.862	4.122
EI_v	56	72	117	6.434	7.182	9.751
GJ_v	31	39	84	3.118	5.263	6.716

Table 7.28 Effect of approach slab settlement on identified vehicle parameters

Vehicle parameters	No of iteration		RPE (%)	
	Without approach road settlement	With 20 mm approach road settlement	Without approach road settlement	With 20 mm approach road settlement
m_v	32	51	2.114	2.162
m_{w11}	56	70	3.681	4.03
m_{w21}	45	39	2.173	2.917
m_{w12}	42	35	6.235	6.833
m_{w22}	48	54	4.052	4.728
k_{v11}	32	70	4.294	4.561
k_{v21}	33	45	7. 516	5.98
k_{v12}	36	37	3.384	3.679
k_{v22}	34	31	6.982	7.025
c_{v11}	44	49	1.287	1.992
c_{v21}	42	48	3.13	3.57
c_{v12}	37	41	6.224	6.361
c_{v22}	35	36	2.112	2.408
k_{t11}	19	39	9.599	10.13
k_{t21}	30	46	9.812	10.01
k_{t12}	50	90	9.167	9.982
k_{t22}	43	61	9.607	10.236
c_{t11}	62	63	7.49	7.735
c_{t21}	33	29	8.267	9.142
c_{t21}	45	92	8.112	8.853
c_{t22}	33	73	5.815	5.89
I_{mv}	55	71	6.062	7.33
EI_v	72	88	3.496	3.911
GJ_v	39	60	3.435	3.592

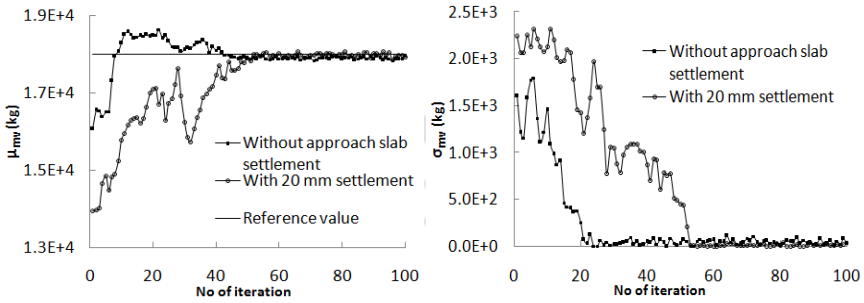

(a) Mean value (b) Standard deviation

Fig. 7.85 Progressive estimate of vehicle mass m_v from acceleration data with consideration of 20 mm approach settlement and without settlement

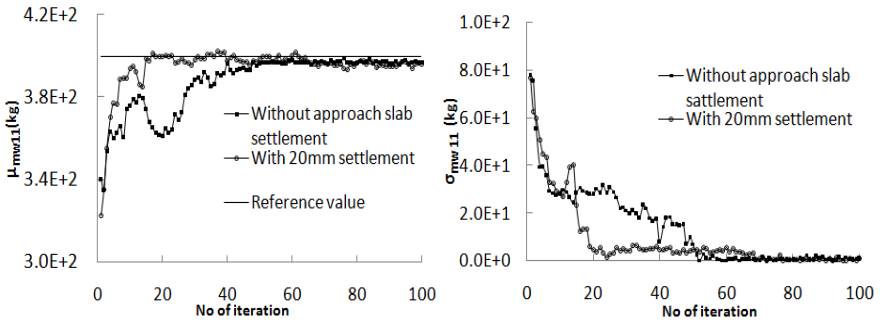

(a) Mean value (b) Standard deviation

Fig.7.86 Progressive estimate of front right wheel mass m_{w11} from acceleration data with consideration of 20 mm approach settlement and without settlement.

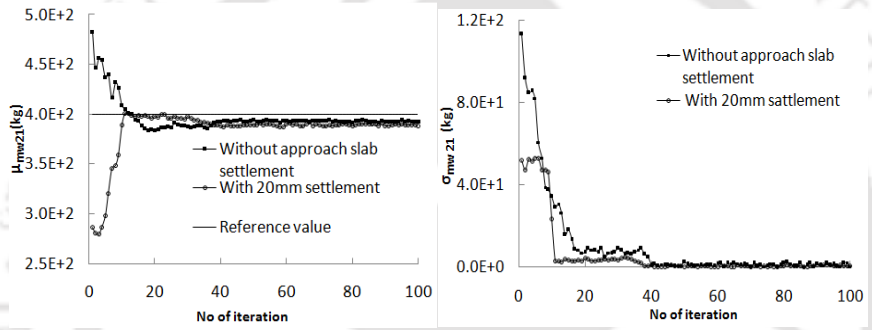

(a) Mean value (b) Standard deviation

Fig. 7.87 Progressive estimate of front left wheel mass m_{w21} from acceleration data with consideration of 20 mm approach settlement and without settlement.

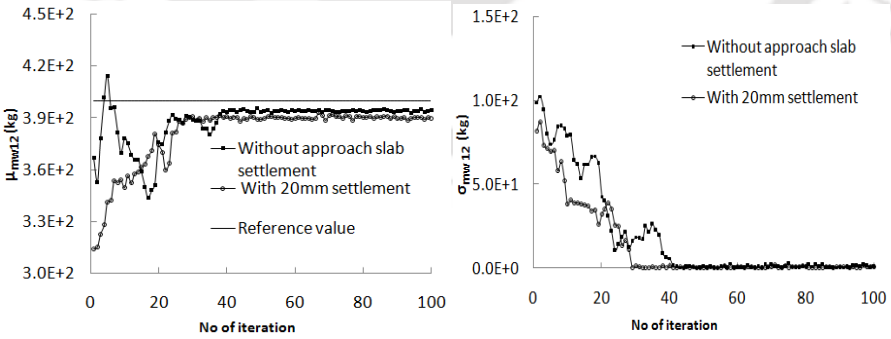

(a) Mean value (b) Standard deviation

Fig. 7.88 Progressive estimate of rear right wheel mass m_{w12} from acceleration data with consideration of 20 mm approach settlement and without settlement.

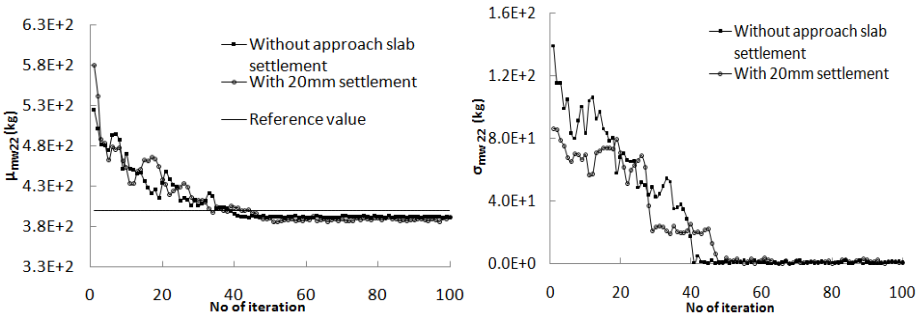

(a) Mean value (b) Standard deviation

Fig. 7.89 Progressive estimate of rear left wheel mass m_{w22} from acceleration data with consideration of 20 mm approach settlement and without settlement

7.6 Comparison of CPU processing time for estimation of vehicle parameters with numerically generated samples

The efficiency of the proposed analytical approach in the forward scheme of the identification of vehicle parameters has been judged by comparing the CPU processing time when numerically simulated samples are used. For numerical scheme, Newmark's method (Bathe, 2006) has been adopted to solve the second order coupled ordinary differential equations. The algorithm for Newmark's method is given in Appendix-D. Three different sampling frequencies 300, 500, and 700 Hz have been used to compare the convergence rate. A personal computer with Intel (R) Core (TM), i3-2120, CPU 3.3 GHz and 4.0 GB RAM has been employed for all computations. Vehicle speed 60 km/h and average bridge deck surface condition (ISO 8608: 1995) has been considered for the study. The comparisons are presented in Table 7.29 to Table 7.32. Table 7.28 and Table 7.29 are for all the parameters of Vehicle Model-1 and Model-2 respectively. Since number of parameters is very large for Model-3, the vehicle body and suspension parameters are shown in Table 7.30 while wheel masses, tyre stiffness and damping are presented in Table 7.31. It has been observed from the tables that sampling frequency affects the estimation accuracy for both the method of solutions. Higher sampling frequency leads to lower error in vehicle parameters estimation but requires more CPU time. Since several parameters are estimated simultaneously, the CPU processing time is also different for each parameter. The average time requirement for parameter estimation in the case of Model-1 has been found to be decreased by 64% while average accuracy has been increased by 24% due to use of present semi analytical method in forward scheme of Particle Filtering approach. For Model-2, it is observed that average CPU time has been decreased by 79% while for Model-3, reduction of CPU time is 88% when output

samples are generated by proposed analytical method. In Model-2 and Model-3, average accuracy is also improved by the use of analytical method in sample generations. The increase in accuracy of identification is 26% and 29% in Model-2 and Model-3 respectively. This again demonstrates the superiority of particle filter method when combined with analytical method for generations of response samples.

Table 7.29 Comparison of computer processing time for estimation of Model-1 vehicle parameters

Parameters	Sampling frequency (Hz)	Analytically generated samples		Numerically generated samples	
		Processing time (sec)	RPE (%)	Processing time (sec)	RPE (%)
m_v	300	20.21	5.98	54.37	8.811
	500	21.47	5.07	73.66	6.220
	700	26.52	3.82	102.88	5.473
m_w	300	13.47	4.09	45.65	6.502
	500	19.79	2.20	77.16	4.135
	700	22.73	1.66	117.67	3.064
k_v	300	16.00	6.21	39.22	8.391
	500	20.63	4.72	63.66	5.642
	700	23.58	2.99	167.18	3.365
c_v	300	22.31	6.54	42.44	5.990
	500	25.26	5.30	115.74	5.853
	700	32.42	5.29	158.82	5.016
k_t	300	20.63	7.51	46.30	9.304
	500	23.16	4.33	57.23	6.072
	700	25.68	4.02	83.59	5.848
c_t	300	11.79	7.25	32.15	10.11
	500	12.63	6.24	52.73	7.790
	700	13.89	2.89	91.31	5.833

Table 7.30 Comparison of computer processing time for estimation of Model-2 vehicle parameters

Parameters	Sampling frequency (Hz)	Analytically generated samples		Numerically generated samples	
		Processing time (sec)	RPE (%)	Processing time (sec)	RPE (%)
m_v	300	22.24	2.110	67.92	7.220
	500	26.44	1.690	129.23	5.408
	700	30.65	1.342	168.51	4.831
m_{w1}	300	24.04	10.084	91.78	26.210
	500	27.05	8.760	123.90	22.280
	700	37.26	7.547	199.16	21.415
m_{w2}	300	13.22	4.663	54.52	12.590
	500	16.83	2.343	79.67	7.263
	700	28.25	1.980	142.35	6.534
k_{v1}	300	28.85	13.956	105.73	25.494
	500	31.25	11.822	157.49	21.013
	700	39.67	9.504	218.07	18.214
k_{v2}	300	23.44	2.311	96.64	6.240
	500	31.85	1.670	145.93	5.010
	700	36.66	1.350	179.15	4.320
c_{v1}	300	34.26	12.132	156.94	18.396
	500	38.46	8.187	182.68	15.462
	700	45.08	8.095	247.81	11.142
c_{v2}	300	23.44	4.559	85.91	10.942
	500	25.24	3.130	107.93	8.764
	700	41.47	2.891	189.98	8.673
k_{t1}	300	18.63	8.267	85.36	29.801
	500	22.84	7.531	142.99	25.877
	700	27.65	5.822	198.43	23.363
k_{t2}	300	17.43	7.101	79.85	21.303
	500	19.83	5.016	93.89	15.550
	700	31.25	3.357	181.36	12.757
c_{t1}	300	21.64	17.005	105.73	28.416
	500	29.45	14.490	179.89	21.960
	700	37.26	12.816	284.52	18.080
c_{t2}	300	28.25	2.199	129.41	9.597
	500	34.86	1.667	159.70	7.001
	700	45.08	1.109	206.51	6.327
EI_v	300	24.64	3.142	109.13	9.112
	500	28.85	1.185	154.19	4.148
	700	37.26	1.029	233.87	4.229

Table 7.31 Comparison of computer processing time for estimation of vehicle body parameters of Model-3

Parameters	Sampling frequency (Hz)	Analytically generated samples		Numerically generated samples	
		Processing time (sec)	RPE (%)	Processing time (sec)	RPE (%)
m_v	300	25.27	3.321	136.73	11.955
	500	29.95	2.114	259.28	6.764
	700	45.86	1.983	446.64	5.155
EI_v	300	58.97	9.153	462.60	26.543
	500	67.39	7.182	638.06	25.137
	700	86.11	5.585	957.40	22.954
GJ_v	300	25.27	8.002	198.26	23.205
	500	36.50	5.263	345.62	18.420
	700	41.18	4.166	457.89	17.122
I_{mv}	300	26.21	3.877	205.60	11.243
	500	29.95	2.862	283.58	10.017
	700	45.86	1.068	509.92	4.389
k_{v11}	300	27.14	5.097	176.23	17.329
	500	29.95	4.294	267.38	14.170
	700	35.57	3.610	346.38	12.996
k_{v21}	300	24.34	6.770	177.75	18.279
	500	30.89	5.516	250.67	16.548
	700	42.12	4.253	364.61	13.609
k_{v12}	300	27.14	9.095	176.23	25.466
	500	33.70	7.384	300.80	22.152
	700	43.99	6.981	428.41	18.150
k_{v22}	300	26.21	8.132	191.42	24.396
	500	31.82	6.982	258.26	20.946
	700	47.74	5.116	413.22	15.859
c_{v11}	300	29.95	7.192	243.07	21.576
	500	41.18	5.287	346.48	16.442
	700	60.84	3.079	592.49	11.084
c_{v21}	300	34.63	6.440	224.84	15.456
	500	39.31	3.130	297.76	8.764
	700	58.03	2.061	470.95	6.183
c_{v12}	300	33.70	9.903	273.46	29.709
	500	38.38	7.224	322.86	22.466
	700	55.22	6.178	537.80	22.240
c_{v22}	300	27.14	6.733	176.23	16.159
	500	32.76	4.912	248.14	13.753
	700	49.61	2.850	402.59	8.550

Table 7.32 Comparison of computer processing time for estimation of wheel parameters of Model-3

Parameters	Sampling frequency (Hz)	Analytically generated samples		Numerically generated samples	
		Processing time (sec)	RPE (%)	Processing time (sec)	RPE (%)
m_{w11}	300	38.38	5.062	259.53	12.655
	500	52.42	3.681	425.38	11.043
	700	66.46	2.45	629.20	8.575
m_{w21}	300	37.44	3.472	273.46	9.374
	500	42.12	2.173	353.21	6.736
	700	56.16	1.996	501.34	6.586
m_{w12}	300	31.82	8.313	215.22	20.782
	500	39.31	6.052	319.03	18.156
	700	47.74	5.305	451.96	18.567
m_{w22}	300	37.44	5.574	273.46	15.049
	500	44.93	4.53	376.76	14.043
	700	58.03	3.652	518.05	12.051
k_{t11}	300	26.21	13.066	212.69	28.745
	500	36.50	10.13	404.87	21.273
	700	57.10	9.52	725.92	20.944
k_{t21}	300	22.46	12.985	182.30	29.865
	500	28.08	11.512	235.48	27.628
	700	38.38	9.976	394.49	31.923
k_{t12}	300	40.25	10.899	326.63	26.157
	500	46.80	9.167	519.06	28.417
	700	64.58	7.185	821.13	26.584
k_{t22}	300	32.76	12.777	265.86	25.554
	500	40.25	10.607	337.52	21.214
	700	51.48	8.505	529.19	15.309
c_{t11}	300	47.74	16.151	413.22	29.071
	500	58.03	15.49	627.94	23.235
	700	79.56	15.028	1076.10	16.530
c_{t21}	300	24.34	18.801	197.50	26.321
	500	30.89	17.267	250.67	20.720
	700	44.93	15.259	364.61	18.310
c_{t12}	300	23.40	18.834	202.56	28.251
	500	31.82	16.112	344.35	29.356
	700	46.80	15.909	633.00	23.863
c_{t22}	300	23.40	11.74	189.90	29.350
	500	30.89	9.815	250.67	23.556
	700	47.74	16.151	413.22	29.072

7.7 Closure

In this chapter, the simulated acceleration time history at different locations on the bridge has been utilized to illustrate the identification method. Three vehicle models have been considered. These are: Model-1 (Quarter Car Model), Model-2 (Half car model with vehicle flexibility in bending) and Model-3 (Full car model with vehicle flexibility both in bending and torsion). Before carrying out detail parametric study, the validation of the method has been presented by comparing the results with those found in published literatures. The results have been shown in the form of the progressive estimate of parameters in particle filtering approach. Relative percentage error in the estimation of the vehicle parameters has been stated. Effect of location of the simulated acceleration time history, vehicle velocity, surface roughness, approach settlement, artificial noise on the accuracy of identified parameters of all three models have been investigated. The effect of the range of initial guess of the parameters required to construct prior PDF in particle filtering algorithm has also been studied for all models. The efficiency of the proposed analytical approach in the forward scheme of the identification of vehicle parameters has been judged by comparing the CPU processing time when numerically simulated samples are used in identification method.

8

RESULTS AND DISCUSSION- PART-III: VEHICLE PARAMETER IDENTIFICATION FROM FIELD MEASUREMENT

8.1 Overview

In the present chapter, the results of the estimation of truck parameters from the measured acceleration of an existing bridge have been presented and discussed. The acceleration of bridge deck has been obtained by conducting dynamic field test under controlled movement of a loaded truck. The detail of the experimentation has been given in Chapter-5. The results have been presented in different subsections in this chapter. First the bridge surface profile measured by total station survey and its spectral information are given. The bridge surface unevenness has been treated as primary source of vehicle vibration. The acquired acceleration time histories at different sensor locations have been presented. The natural frequencies and damping of the bridge have been estimated from frequency response curve. Finite Element model updating by combination of response surface and GA has been shown illustrating different steps. These updated parameters are then used for different bridge models used in forward scheme of the particle filtering method. Results of the identification of mass of the loaded truck, its suspension stiffness and damping have been presented. Different options of bridge-vehicle models to be adopted in forward scheme have been studied. Performance of particle filter method with single or multi-sensor data has also been discussed.

8.2 Field test data

8.2.1 Bridge deck surface

The average relative height of three different longitudinal profiles of bridge deck surface is shown in Fig.8.1. Spectral information is necessary to classify the existing bridge profile as per ISO specification (ISO 8608: 1995). Hence, power spectral density of road profile has been obtained from the measured surface profile. This has been presented in Fig.8.2 along with the PSD curves for different categories of road according to ISO description. The result indicates that the tested bridge surface is in ‘very good condition’.

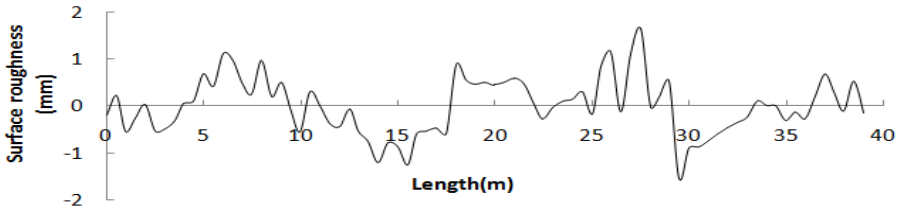

Fig. 8.1 Measured bridge deck surface profile

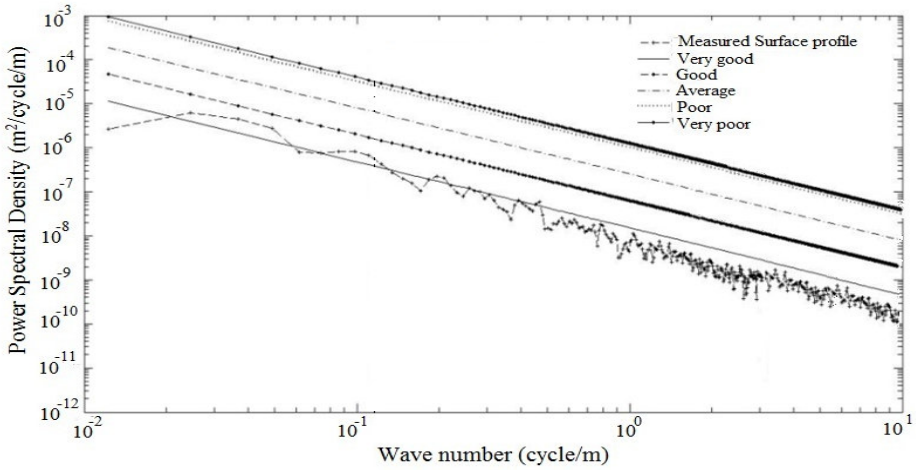

Fig. 8.2 Classification of deck surface profile based on ISO specification (ISO 8608: 1995)

8.2.2 Bridge dynamic test results

Vehicle speed has been varied in the range of 20 km/h-45 km/h. However, during running of the vehicle over the bridge, actual speed has been captured by radar gun as discussed in Chapter-5. It has been planned that experimental data can be obtained for three different speeds near 20 km/h, 30 km/h and 45 km/h by instructing the driver of the test truck. For each speed, three runs of the vehicle have been taken. However, from actual measurement, the average speed of the vehicle in three runs have been found to be 21 km/h, 29 km/h and 43 km/h. Measured accelerations were contaminated by high frequency noise. Fourth order low pass digital Butterworth filter (Haykin and Veen, 1999) has been chosen to remove high frequency noise present in the measured response.

The measured accelerations at different sensor locations have been used to estimate truck parameters using particle filter technique. It may be noted that five sensors have been used. Location of Sensor-1 is at a longitudinal distance of 19.5 m from one end of the bridge and it falls at mid span location. Sensor-2 and sensor-3 are towards left of the mid span at the distance 8.75 m and 13.1 m from sensor-1 respectively. Likewise, sensor-4 and sensor-5 have been located towards right at the distance of 8.75 m and 13.1 m from sensor-1 respectively.

Detail can be found in Fig.5.7 given in Chapter-5. The measured acceleration time histories and their corresponding FFT at some selected sensor locations (Sensor-1 and 4) for two different speeds (21 km/h and 43 km/h) have been shown in Fig.8.3 to Fig.8.10. A comparison of peak acceleration at all sensor locations for different vehicle speed has been shown in Table 8.1. The test results show that acceleration increases by an amount of 27% to 65% when vehicle speed is increased from 21 km/h to 43 km/h at different sensor locations.

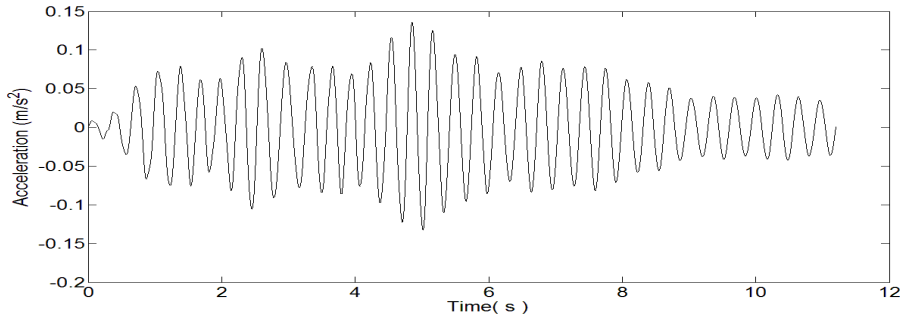

Fig. 8.3 Measured bridge acceleration at sensor-1 for vehicle speed 21 km/h

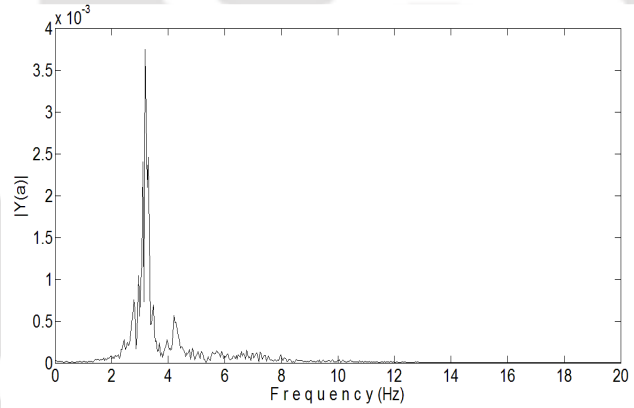

Fig. 8.4 FFT of bridge acceleration at sensor-1 for vehicle speed 21 km/h

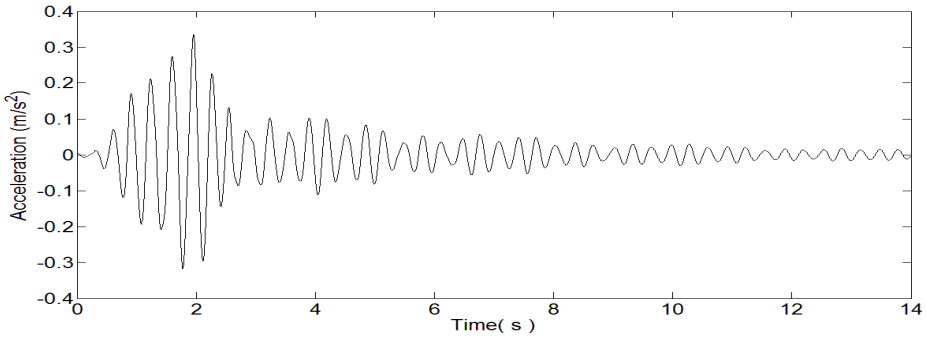

Fig. 8.5 Measured bridge acceleration at sensor-1 for vehicle speed 43 km/h

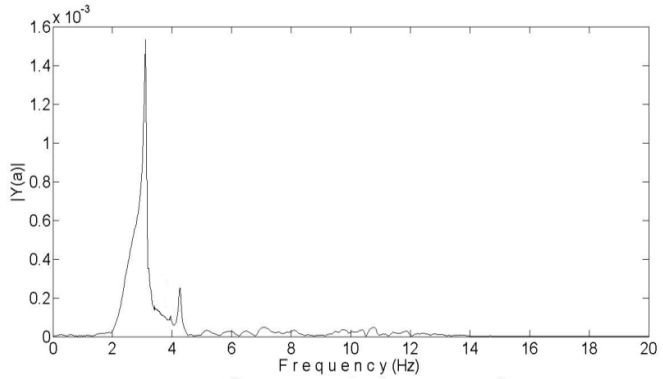

Fig. 8.6 FFT of bridge acceleration at sensor-1 for vehicle speed 43 km/h

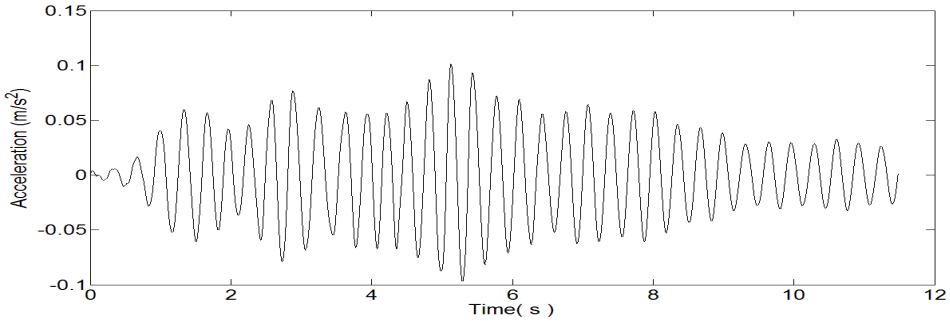

Fig. 8.7 Measured bridge acceleration at sensor-4 for vehicle speed 21 km/h

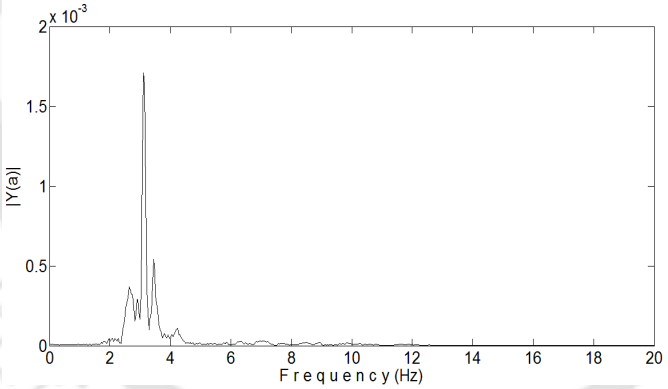

Fig. 8.8 FFT of bridge acceleration at sensor-4 for vehicle speed 21 km/h

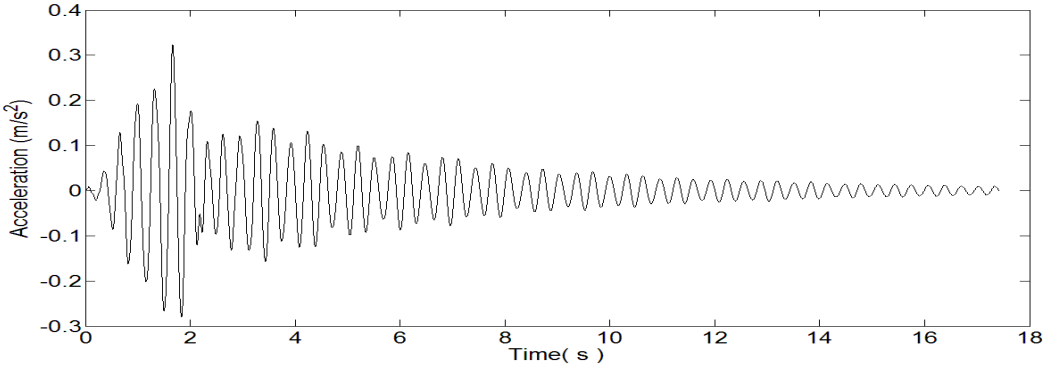

Fig. 8.9 Measured bridge acceleration at sensor-4 for vehicle speed 43 km/h

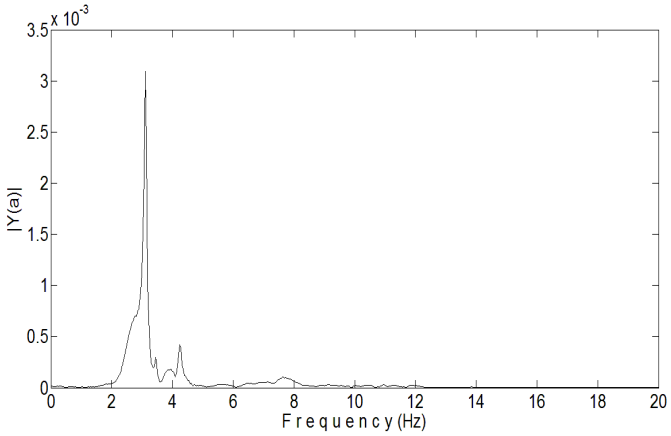

Fig. 8.10 FFT of bridge acceleration at sensor-4 for vehicle speed 43 km/h

Table 8.1 Peak acceleration at different sensors

Sensor No	Peak acceleration at different sensor for vehicle speed (m/s^2)		
	21 km/h	29 km/h	43 km/h
1	0.14	0.24	0.35
2	0.085	0.136	0.27
3	0.102	0.113	0.14
4	0.114	0.158	0.32
5	0.075	0.083	0.155

8.2.3 Estimation of bridge natural frequency and damping

Natural frequencies and damping ratio of the tested bridge have been extracted from FFT of measured bridge acceleration for different vehicle speed collected at different sensor. Mean first and second natural frequency of the bridge have been found to be 3.186 Hz and 4.21 Hz, respectively. Damping ratio has also been estimated from the frequency response using half-power bandwidth method. In this method, upper and lower cut off frequencies f_2 and f_1 at 0.707 Y_{max} on the frequency axis of the FFT has been located. Y_{max} is the peak of the frequency response curve near fundamental frequency (f_n). Let Δf = band width (Hz) which is the difference between upper and lower cut off frequencies, then for under damped system, one has damping ratio as (Chopra, 2009).

$$\xi = \frac{\Delta f}{2 f_n} \tag{8.1}$$

where ξ is damping ratio. The damping ratio of the test bridge is estimated as 4.17%.

8.3 Finite Element Updating of Bridge Parameters

The parameters of the tested bridge have been updated employing Response Surface and GA based technique, mentioned in Section 5.6. Updating of the FE bridge model has been performed based on bridge natural frequencies obtained from FFT of measured bridge response and peak acceleration responses measured at five sensor locations given in Section 8.1.3. Three parameters have been chosen for model updating which are Young's modulus, density and Poisson's ratio of concrete. These have been represented as X_1, X_2, X_3 respectively. To obtain the relationship between the responses and the selected test bridge parameters, the RSM was first used for experimental design as given in Table 5.3 in Chapter-5. In the present study, a fractional design with three factors, each with three levels has been used for experimental design. The simulated responses are denoted by Y_1, Y_2, Y_3, Y_4, Y_5, Y_6 and Y_7 which represent first and second bridge frequencies, peak bridge acceleration measured at five sensor locations respectively. The 'α' value for this three-factor experimental design has been taken to be 1.6818 (Mayer, 1971).

The base line values of bridge parameters have been chosen near the original estimates based on design drawings. Unit change of the baseline values have been assumed so that range of parameters can be defined in experimental trial. Table 8.2 presents baseline value, unit change and range of parameters. The selection of unit change values is usually based on experience (Ren and Chen, 2010). The reason why a 20% change of the base line value was taken as a unit change for Poisson's ratio and density of the concrete is because normally these two parameters will not change as much as the Young's modulus of concrete (Ren and Chen, 2010). The experimental design with designed values for whole set of bridge parameters is given in Table 8.3.

Table 8.2 Base line value, unit change and range of bridge parameters

Bridge Parameters	Base line value	Unit change of parameters	Range of parameters
Young's modulus (GPa) (X_1)	29.6	50%	14.8-44.4
Density (kg/m^3) (X_2)	2400	20%	1920-2880
Poisson's ratio (X_3)	0.15	20%	0.12-0.18

Table 8.3 Experimental design values for the three bridge parameters

Experimental trial	Factor values		
	X_1(GPa)	X_2(kg/m^3)	X_3
1	14.8	1920	0.120
2	44.0	1920	0.120
3	14.8	2880	0.120
4	44.4	2880	0.120
5	14.8	1920	0.180
6	44.0	1920	0.180
7	14.8	2880	0.180
8	44.0	2880	0.150
9	44.4	2400	0.150
10	50.3	2400	0.150
11	29.6	720	0.150
12	29.6	4080	0.045
13	29.6	2400	0.255
14	29.6	2400	0.150
15	29.6	2400	0.150
16	29.6	2400	0.150
17	29.6	2400	0.150
18	29.6	2400	0.150

Using the experimental design given in Table 8.3, Finite Element analysis has been performed in SAP2000 software to obtain the bridge natural frequencies and peak acceleration of bridge subjected to vehicle load of gross weight 192.4 kN moving at a constant speed 43 km/h at various locations. Result of the simulation for the responses is shown in Table 8.4.

Table 8.4 Results of simulation for the responses

Experi-mental trial	Bridge natural frequencies (Hz)		Simulated bridge peak acceleration (m/s^2)				
	First	Second	Sensor-1	Sensor-2	Sensor-3	Sensor-4	Sensor-5
	Y_1	Y_2	Y_3	Y_4	Y_5	Y_6	Y_7
1	1.874	2.324	0.770	0.318	0.463	0.4348	0.318
2	3.210	3.980	0.388	0.127	0.152	0.235	0.135
3	1.529	1.896	0.656	0.260	0.406	0.2448	0.206
4	2.621	3.250	0.550	0.216	0.365	0.317	0.108
5	1.873	2.323	0.523	0.319	0.465	0.276	0.285
6	3.231	4.006	0.285	0.126	0.150	0.107	0.117
7	1.530	1.897	0.649	0.258	0.403	0.145	0.213
8	2.637	3.270	0.353	0.215	0.243	0.215	0.161
9	1.297	1.608	0.997	0.402	0.617	0.326	0.317
10	3.089	3.830	0.324	0.163	0.206	0.105	0.099
11	4.327	5.365	0.215	0.119	0.203	0.1031	0.101
12	1.819	2.256	0.382	0.157	0.240	0.112	0.163
13	2.370	2.939	0.460	0.265	0.302	0.25	0.211
14	2.368	2.936	0.468	0.269	0.311	0.215	0.221
15	2.368	2.936	0.468	0.269	0.311	0.215	0.221
16	2.368	2.936	0.468	0.269	0.311	0.215	0.221
17	2.368	2.936	0.468	0.269	0.311	0.215	0.221
18	2.368	2.936	0.468	0.269	0.311	0.215	0.221

Based on the bridge parameters and their corresponding responses, regression has been performed to determine the Response Functions through the least-square method. The second order Response Functions for all the four responses are shown as below

(i) Bridge first natural frequency response function

$$Y_1 = 4.863 + 0.0506X_1 - 0.0026X_2 - 4.0277X_3 + 0.0743X_1X_3 + 0.0027X_2X_3 - 9.86X_3^2 \quad (8.2)$$

(ii) Bridge second natural frequency response function

$$Y_2 = 6.0301 + 0.0627X_1 - 0.0033X_2 - 4.9944X_3 + 0.0921X_1X_3 + 0.0033X_2X_3 - 12.226X_3^2 \quad (8.3)$$

(iii) Bridge peak acceleration response function for sensor 1

$$Y_3 = 2.794 - 0.0179X_1 - 0.0004X_2 - 16.856X_3 - 0.063X_1X_3 + 0.0037X_2X_3 + 23.201X_3^2 \quad (8.4)$$

(iv) Bridge peak acceleration response function for sensor 2

$$Y_4 = 0.3876 - 0.0176X_1 + 0.0001X_2 + 0.818X_3 + 0.0002X_1X_3 + 0.0002X_2X_3 - 1.031X_3^2 \quad (8.5)$$

(v) Bridge peak acceleration response function for sensor 3

$$Y_5 = 0.5287 - 0.0208X_1 + 0.0001X_2 + 1.6917X_3 + 0.0043X_1X_3 - 0.0002X_2X_3 - 3.3306X_3^2 \quad (8.6)$$

(vi) Bridge peak acceleration response function for sensor 4

$$Y_6 = 1.821 - 0.0242X_1 - 0.0001X_2 - 11.478X_3 + 0.021X_1X_2 + 0.0012X_2X_3 + 20.03X_3^2 \quad (8.7)$$

(vii) Bridge peak acceleration response function for sensor 5

$$Y_7 = 0.4395 - 0.0141X_1 + 0.0001X_2 - 0.7045X_3 - 0.0092X_1X_2 + 0.0003X_2X_3 + 3.924X_3^2 \quad (8.8)$$

An objective function has been built up using the residual between the measured responses and predicted responses from the Response Functions. The first and second natural frequency of the bridge and measured peak accelerations at different sensor locations for vehicle speed of 43 km/h have been selected to construct objective function. The objective function (E_{obj}) is then expressed as

$$E_{obj} = [(Y_1 - 3.186)^2 + (Y_2 - 4.21)^2 + (Y_3 - 0.35)^2 + (Y_4 - 0.13)^2 + (Y_5 - 0.16)^2 + (Y_6 - 0.22)^2 + (Y_7 - 0.15)^2]^{1/2} \quad (8.9)$$

The upper and lower bounds for each of the bridge parameters to be updated are assigned as follows

Young's modulus [25; 40] GPa; Density [1500; 3000] kg/m^3 and Poisson's ratio [0.1; 0.3]. The objective function in Eq. 8.9 obtained by RSM has been optimized using Genetic Algorithm (GA), mentioned in Section 5.6.2 in which the binary coding has been chosen to represent variable X_1, X_2 and X_3. In the calculations, 20 bits have been chosen for each variable. A roulette wheel selection, a single point crossover and a bit wise mutation operator has been chosen for Genetic Algorithm operations. The crossover and mutation probabilities are assigned to be 0.8 and 0.05, respectively (Deb, 2012). The updated results of bridge parameters and their differences from the original values are shown in Table 8.5. Young's

modulus of concrete has been found to be higher than that estimated from the grade of concrete provided in the construction drawing by an amount of 28%. Bridge natural frequencies obtained from the field test and the updated frequencies are shown in Table 8.6. The percentage differences of the first and second natural frequency of the bridge are found to be 2.5% and 3.8%, respectively. The first two mode shapes of the updated FE model are shown in Fig 8.11. It has been found that the first mode is dominated by bending while second is torsional mode. Measured peak response acceleration at different sensor locations, has been compared with the updated Finite Element Model response of bridge subjected to vehicle load of gross weight 192.4 kN moving at a constant speed 43 km/h. It is presented in Fig.8.12. Result shows that updated Finite Element model gives higher response by an amount of 6% to 13%.

Table 8.5 Updated results for bridge parameters

Parameters	Original value	Updated value	% difference
Young's modulus (GPa)	29.60	41.40	28.50
Density (kg/m^3)	2400	2150	11.63
Poisson's ratio	0.15	0.172	14.60

Table 8.6 Comparison of updated natural frequencies with experiment results

No of mode	Bridge natural frequency (Hz)		% difference
	Experiment result	Updated FEM	
First	3.186	3.105	2.5
Second	4.21	4.377	3.8

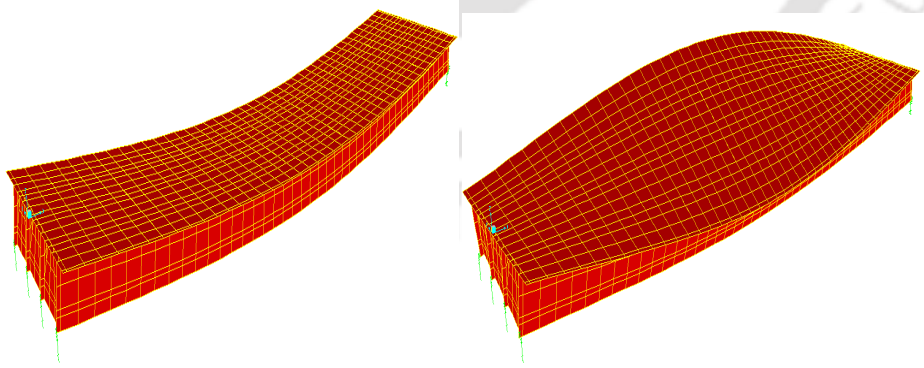

(a) First mode (3.105 Hz) (b) Second mode (4.377 Hz)

Fig. 8.11 Mode shape of updated Finite Element bridge model

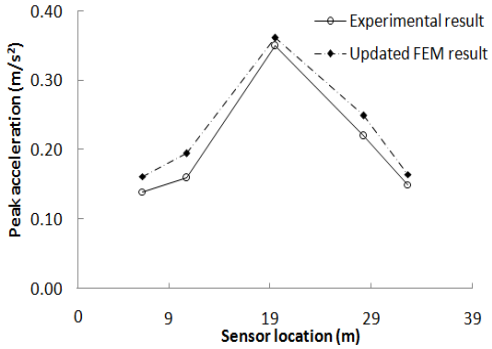

Fig. 8.12 Peak acceleration response of bridge at different sensor location (V=43 km/h)

8.4 Identification of Vehicle Parameter from Measured Response

Based on experimental data obtained from field test, the particle filter method has been applied for identification of vehicle parameters. The equivalent cross sectional properties of the updated FE bridge model has been taken in the models used in forward scheme. Four different vehicle bridge models in forward scheme of the identification algorithm have been used to examine the performance of the scheme with experimentally measured data. The models used are (i) moving mass model (ii) Quarter Car Model (Model-1) (iii) Full Car flexible model (Model-3) and (iv) Finite Element Model in SAP2000. In first three models, bridge has been idealized as a simply supported beam, in which response samples have been generated using present semi-analytical technique. In the last one, the finite element model of the test bridge created in SAP 2000 with moving vehicle has been employed in forward scheme of the inverse method used in the present study. In moving mass model, vehicle vibration and bridge surface profile has been ignored. This model is found to be attractive due to its simplicity while yielding acceptable results for engineering applications (Yang *et al*., 2004).

In Model-1 and Model-3, the measured bridge deck surface profile mentioned in Section 8.2.1 has been used as the source of vehicle excitation, thus establishing a coupled bridge-vehicle system. In Model-1, only vertical rigid body motion of the vehicle has been considered whereas Model-3 considers flexibility of vehicle body in bending and torsion. Description of the Model 1 and 3 has been given in Chapter-3. Several parametric studies have been conducted to examine the efficiency as well as the accuracy of the present identification method using experimentally measured acceleration. The sampling time interval in measured response has been chosen as 8.33×10^{-4} sec. Results have been obtained with single sensor data. Bridge acceleration time history acquired at sensor-1 for vehicle

speed 43 km/h has been used as input to the identification algorithm and 1000 number of particle (N_p) is considered for each unknown parameters, unless stated otherwise.

8.4.1 Identification of vehicle gross mass

The particle filter method has been applied for identification of vehicle mass for different dynamic models based on dynamic field test data. Progressive estimate of vehicle mass and the corresponding standard deviations are given in Fig. 8.13. PDF of vehicle mass estimate at different stage of iteration are shown in Fig.8.14 (a)-(d). Performance of different model has been judged by the number of iteration and deviation of estimated value from true value of vehicle parameter after calculating relative percentage error. True value of vehicle load including self weight is taken from the report of weigh-bridge. Number of iteration required for achieving convergence and percentage error is shown in Table 8.7. In respect of number iterations required for convergence, it is seen that moving mass model provides more rapid estimate of vehicle gross weight within reasonable accuracy. Model-2 and Model-3 requires more number of iteration to achieve convergence as compared to moving mass model. However, a reduction in percentage error has been noticed. This may be due to the fact that consideration of coupling between the two dynamic sub-systems (bridge and vehicle) incorporating bridge deck surface roughness in the modeling reflects true dynamic behaviour. Further, it has been observed that estimation of error and number of iteration are significantly increased in FE model. It may be noted that when longitudinal bending modes are dominating in the bridge responses, idealization of bridge as an equivalent beam model is good enough for parameters estimation in regard to accuracy as well as computational time involved (Zhu and Law 2003a).

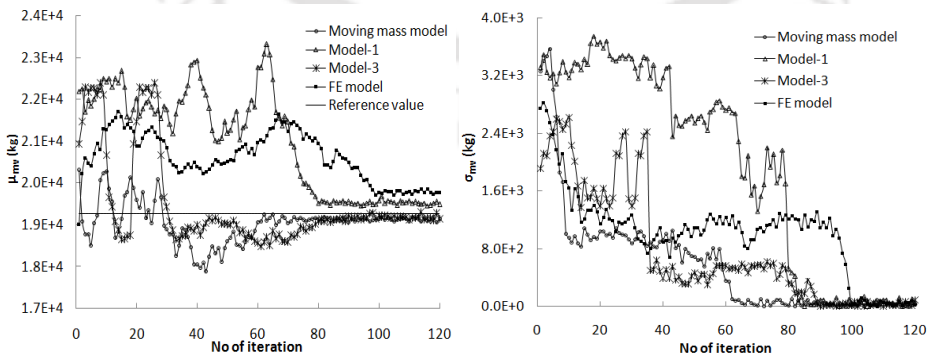

(a) Mean value (b) Standard deviation

Fig. 8.13 Progressive estimate of vehicle mass based on bridge acceleration from sensor-1

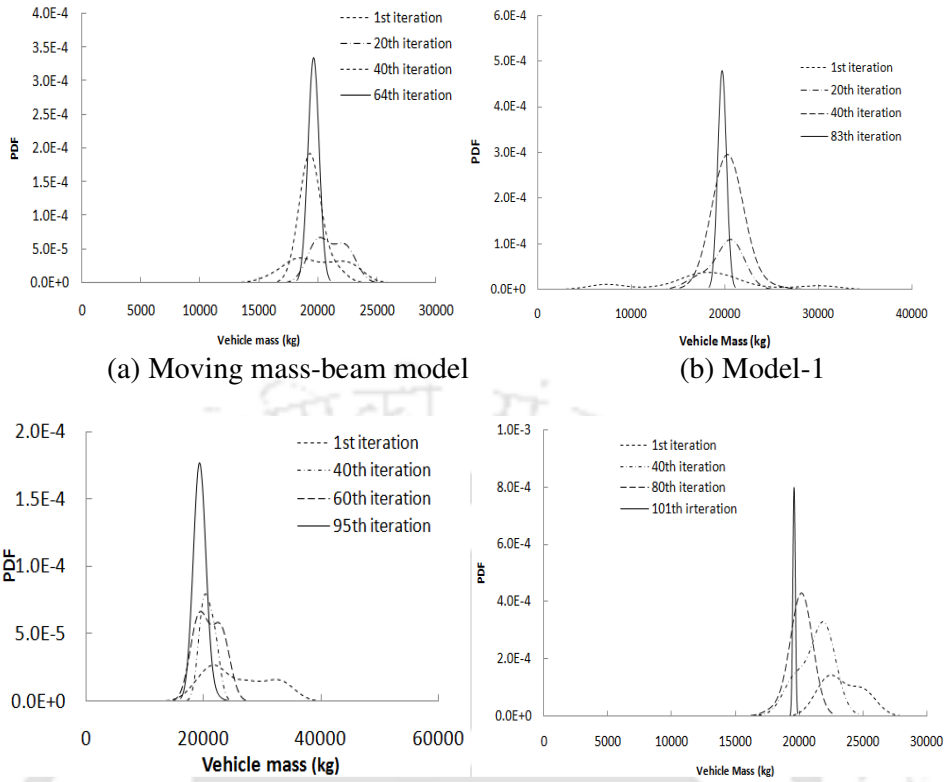

(a) Moving mass-beam model (b) Model-1

(c) Model-3 (d) Finite Element Model

Fig. 8.14 PDF of vehicle mass estimate at different stage of iterations

Table 8.7 Identification of vehicle mass with different model

Model	No of iteration	RPE (%)
Moving mass model	64	8.69
Model-1	75	7.13
Model-3	95	5.98
Finite Element (SAP 2000)	101	10.05

8.4.2 Identification of vehicle suspension stiffness and damping

In addition to vehicle gross mass, suspension stiffness and damping of the test truck have also been extracted from the bridge acceleration record using Model-1 and Model-3. Due to lack of information about the exact value of suspension stiffness and damping of the test truck, it has not become possible to find out the accuracy of identified values with reference to the true value. However, in order to utilize the models in forward solution, equivalent linear suspension stiffness has been calculated from the number and dimensions of leafs in the springs of the test truck suspension (Jadon and Verma, 2010) which is then treated as the reference value. The leaf material specification is 50CrlV23, for which Modulus of elasticity 205 GPa, Yield strength- 1750 MPa and Tensile strength- 2000 MPa have been taken (Jadon

and Verma, 2010). For one set of front and rear axle spring, suspension stiffness has been found as 6.57×10^4 N/m and 1.08×10^5 N/m, respectively.

Vehicle leaf spring provides damping due to interleaf friction. However, in the semi-analytical method used in the forward scheme, equivalent linear damping coefficient found in literature has been used. Wen-jun *et. al.* (2012) has given equivalent linear damping ratio of vehicle leaf spring subjected to harmonic loading at various frequencies. In order to utilize this specific information, the dominant frequency Ω=4.39 rad/m of the measured bridge deck surface roughness profile obtained by Fast Fourier Transform has been considered as excitation frequency. The dominant spatial frequency is first mapped to temporal frequency of excitation using vehicle speed and then linearized damping ratio has been decided from the results presented by Wen-jun *et. al* (2012). Table 8.8 shows damping ratio at various circular frequency corresponding to vehicle speeds that have been assumed in the computation.

Table 8.8 Vehicle suspension damping for different vehicle speed

Vehicle speed (km/h)	Circular frequency (rad/s)	Damping ratio
21	25.600	0.051
29	35.370	0.035
43	52.448	0.020

For carrying out identification, same sampling time interval 8.33×10^{-4} sec (sampling frequency 1200 Hz) chosen during the field test has been also considered in forward scheme. Only the acceleration record at 43 km/h has been used. Since the present models are capable of incorporating the deck surface unevenness, measured surface profile of the tested bridge has been considered in the forward solution. The mean estimate of vehicle suspension stiffness, damping and the corresponding standard deviations for Model-1 is given in Fig. 8.15 and Fig 8.16. Percentage difference between estimated value and the equivalent value calculated using the geometrical and material properties of leaf spring is shown in Table 8.9 along with number of iteration required for achieving convergence. Similarly, identification of tested truck suspension parameters using Model-3 is presented in Fig 8.17 to Fig 8.24. Number of iterations and percentage difference between theoretically calculated value and suspension parameters extracted from measured bridge acceleration by Particle Filter approach are shown in Table 8.10. Result shows that actual truck suspension stiffness is lower than the theoretically calculated value by an amount of 3% to 6% while suspension

damping is found to be higher than that by an amount of 5% to 7.5%. It is worth mentioning that the suspension parameters of the vehicle in service cannot be determined by direct measurement. The extraction of suspension parameters from the bridge dynamic response is very useful finding from vehicle maintenance point of view as well as bridge structural health monitoring, since road friendly vehicles always impose less dynamic load over the bridge.

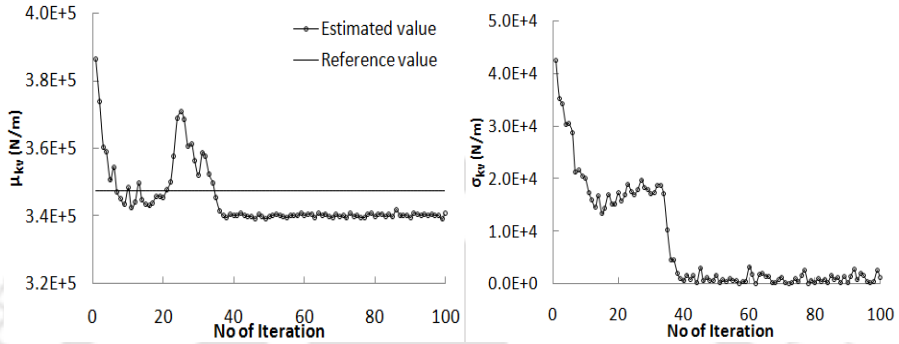

(a) Mean value (b) Standard deviation

Fig.8.15 Progressive estimate of vehicle suspension stiffness k_v from measured acceleration data considering Model-1

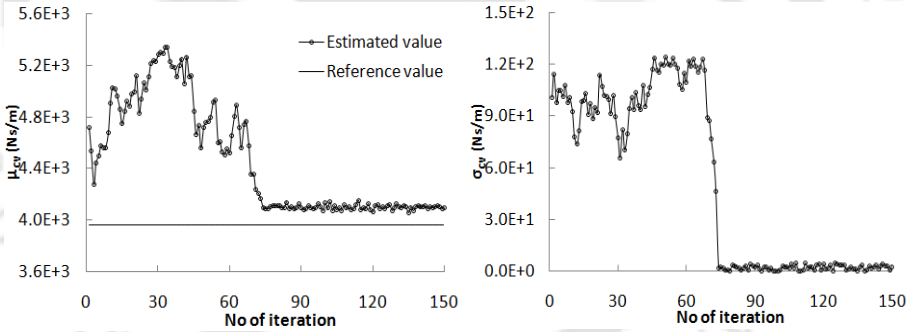

(a) Mean value (b) Standard deviation

Fig.8.16 Progressive estimate of vehicle suspension damping c_v from measured acceleration data considering Model-1

Table 8.9 Identification of vehicle suspension parameters using Model-1

Parameters	No of iteration	Percentage difference from assumed value
k_v	43	5.95
c_v	82	7.73

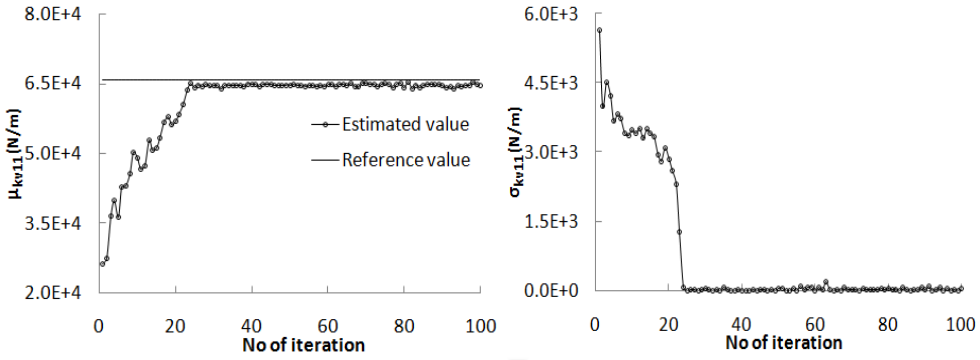

(a) Mean value (b) Standard deviation

Fig. 8.17 Progressive estimate of front-right suspension stiffness k_{v11} from measured acceleration data considering Model-3

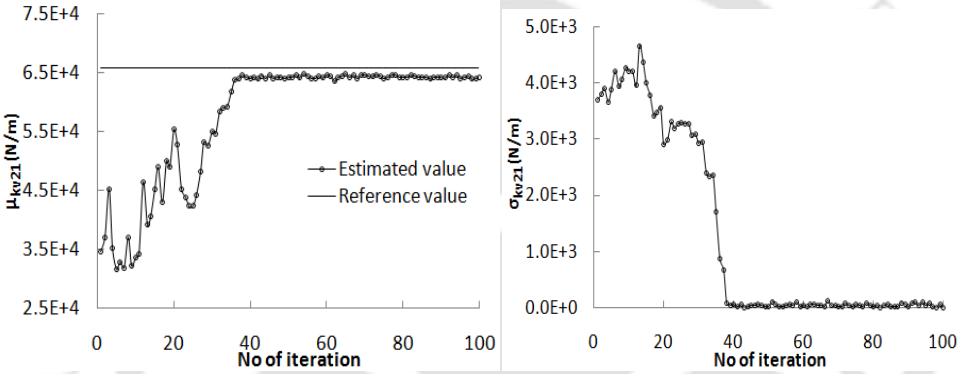

(a) Mean value (b) Standard deviation

Fig. 8.18 Progressive estimate of front-left suspension stiffness k_{v21} from measured acceleration data considering Model-3

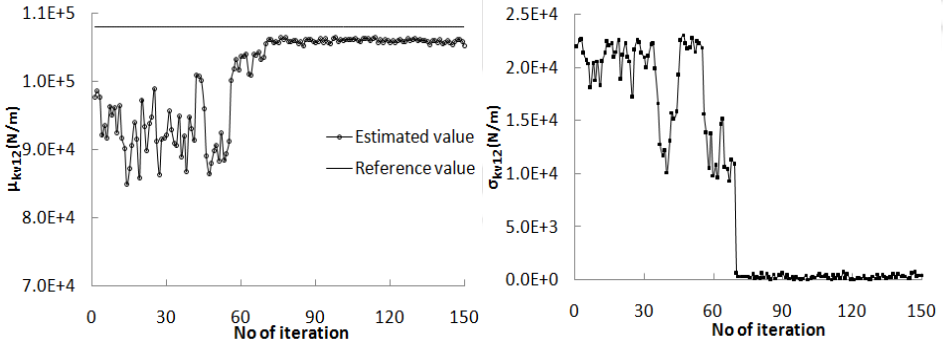

(a) Mean value (b) Standard deviation

Fig. 8.19 Progressive estimate of rear-right side suspension stiffness k_{v12} from measured acceleration data considering Model-3

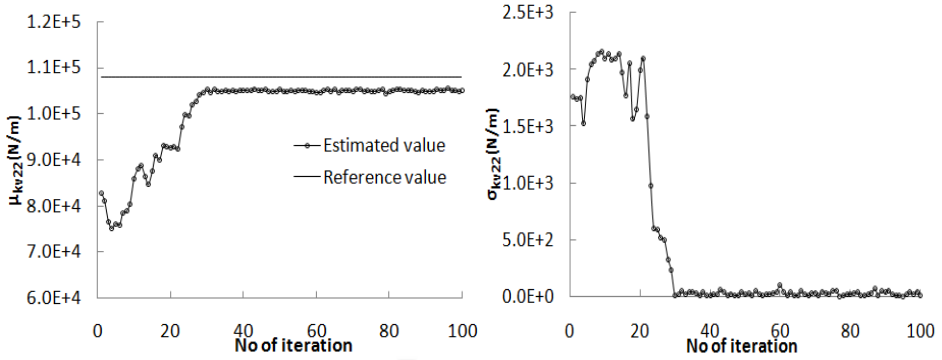

(a) Mean value (b) Standard deviation

Fig. 8.20 Progressive estimate of rear-left side suspension stiffness k_{v22} from measured acceleration data considering Model-3

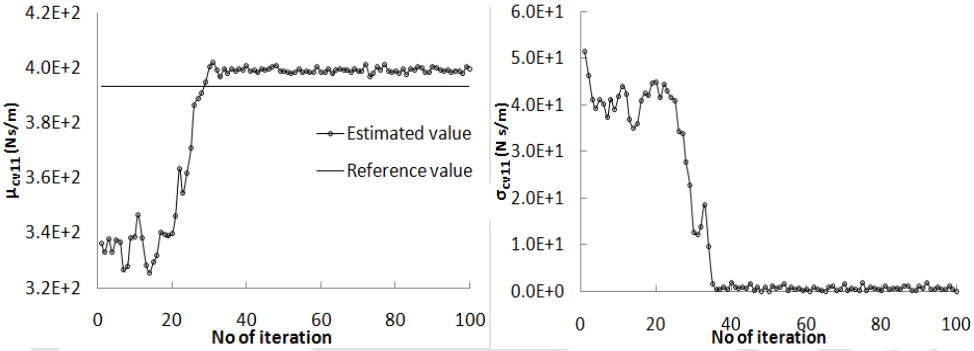

(a) Mean value (b) Standard deviation

Fig. 8.21 Progressive estimate of front-right vehicle suspension damping c_{v11} from measured acceleration data considering Model-3

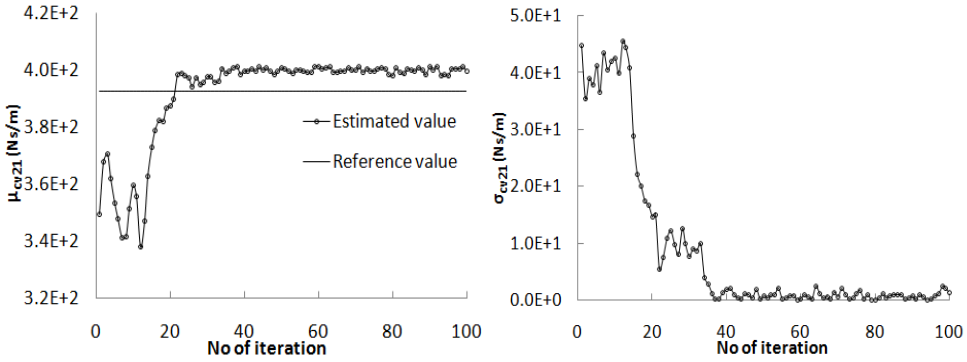

(a) Mean value (b) Standard deviation

Fig. 8.22 Progressive estimate of front-left vehicle suspension damping c_{v21} from measured acceleration data considering Model-3

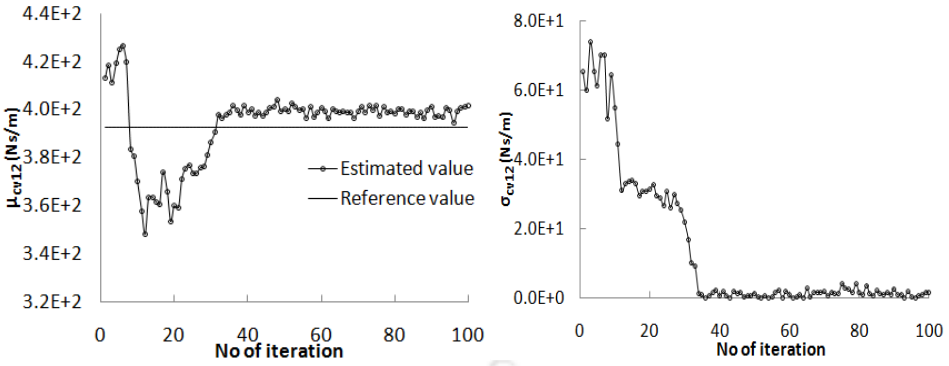

(a) Mean value (b) Standard deviation

Fig. 8.23 Progressive estimate of rear-right vehicle suspension damping c_{v12} from measured acceleration data considering Model-3

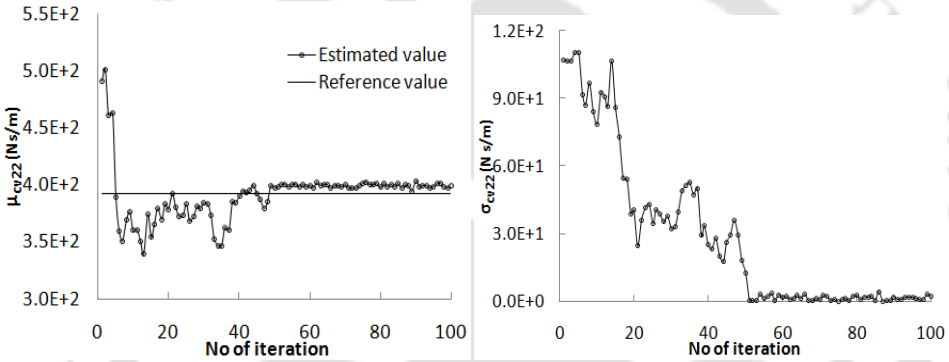

(a) Mean value (b) Standard deviation

Fig. 8.24 Progressive estimate of rear-left vehicle suspension damping c_{v22} from measured acceleration data considering Model-3

Table 8.10 Identification of vehicle suspension parameters using Model-3

Parameters	No of iteration	Percentage difference from assumed value
k_{v11}	32	3.78
k_{v21}	39	4.01
k_{v12}	78	5.81
k_{v22}	36	6.53
c_{v11}	42	5.82
c_{v21}	49	6.90
c_{v12}	44	7.86
cv_{22}	59	3.92

8.4.3 Identification of vehicle body flexural and torsional rigidity

Effect of vehicle body flexibility on bridge dynamic response as well as structural mode on parameters identification has been explored and investigated in the theoretical study presented in Chapter 6 and 7. Although, present test truck axle spacing is small, still performance of flexible vehicle model in identification algorithm needs to be judged when the field test data are available. Since the actual truck body flexural and torsional rigidity is not known, the value has been determined using SAP2000 section modeler based on geometry of the test truck frame physically measured at the site by a steel tape and a digital vernier caliper. Standard value of material constants for structural steel has been assumed. The flexural and torsional rigidity of the test truck has been calculated as 5.18×10^8 $Nm^2$and 1.77×10^8 Nm^2, which are taken as reference value for the comparison of extracted values. Progressive estimate of vehicle body's flexural and torsional rigidity from measured acceleration data is shown in Fig. 8.25 and Fig 8.26. Number of iteration required and deviation of estimated value from the calculated value is given in Table 8.11. The present identification algorithm for extracting flexible vehicle body parameters from the measured bridge response is found to be satisfactory in regard to number of iterations required for convergence and the achieved accuracy. The percentage difference from the assumed value is 6% to 9%. One can now opine that Bootstrap Particle Filter method is very appropriate method for estimating all vehicle parameters from the actual field test results within reasonable accuracy.

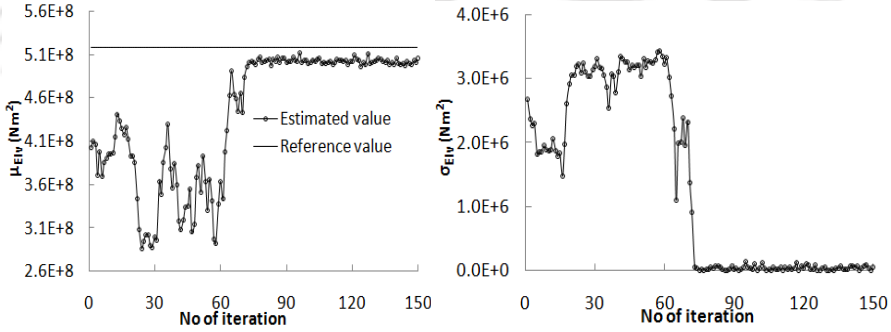

(a) Mean value (b) Standard deviation

Fig. 8.25 Progressive estimate of vehicle body flexural rigidity EI_v from measured acceleration data

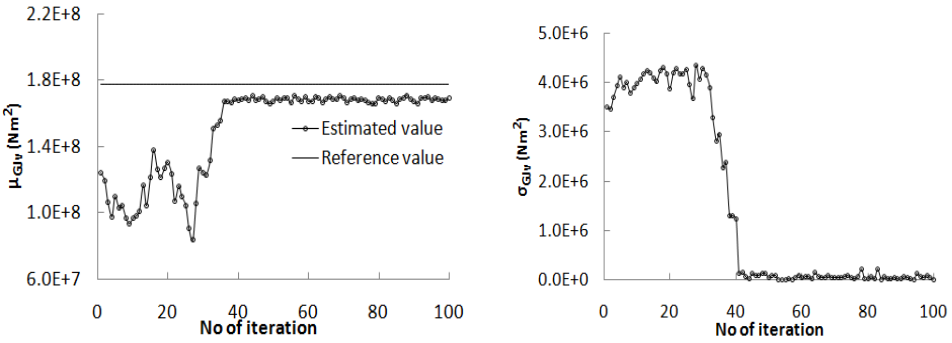

(a) Mean value (b) Standard deviation

Fig. 8.26 Progressive estimate of vehicle body torsional rigidity GJ_v from measured acceleration data

Table 8.11 Identification of vehicle body flexural and torsional rigidity

Parameters	No of iteration	Percentage difference from assumed value
EI_v	88	8.78
GJ_v	47	6.53

8.5 Comparison of Reconstructed Acceleration with Experiment Value

The reconstructed acceleration time histories with identified vehicle parameters of different models have been compared with experimentally recorded mid span acceleration at vehicle speed 43km/h in Fig. 8.27(a). Peak acceleration at different sensor locations obtained from field test is also compared with that from the reconstructed bridge response using estimated vehicle parameters. The results are shown in Fig. 8.27(b). The results indicate that Model-2 and Model-3 agree closely with the experimental values within an accuracy of 2% to 4%. Performance of other two models is also found to be satisfactory, although percentage error marginally increases in those cases. Consideration of suspension parameters and bridge surface roughness in Model-1 and Model-3 seems to depict more realistic behavior of vehicle moving on the bridge.

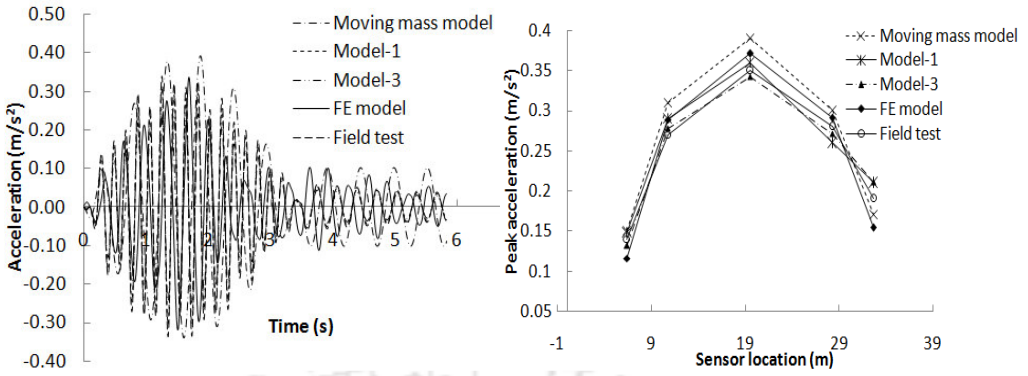

(a) (b)

Fig. 8.27 (a) Comparison of reconstructed bridge acceleration response at sensor-1 with field test result (b) Comparison of peak acceleration at different sensor locations obtained in different models with field test result

8.6 Effect of Multiple Sensor Data on Identification of Parameters

Effect of the number of sensors on the accuracy of vehicle parameters identification has been studied by considering three sets of sensor locations.

Set 1: sensor-1 placed only at the bridge mid span (Total number of sensor=1)
Set 2: sensor-1 at mid span, sensor-2 and sensor-4 placed at 10.75 m and 28.25 m from the bridge entry respectively. (Total number of sensors=3)
Set 3: sensor-1 at mid span, sensor-2 and sensor-4 at the locations as mentioned above. Sensor-3 and sensor-5 are placed at 6.40 m and 32.6 m from the bridge entry respectively. (Total number of sensors=5)

Sensor locations have been already illustrated with schematic diagram in Fig.5.8. Different models mentioned in earlier section of the present chapter have been used here in order to examine the usefulness of multi sensor data in Bootstrap Particle Filter method. Vehicle gross mass and suspension parameters have been estimated. The errors are found with reference to actually measured value or estimated from other physical parameters and dimensions.

8.6.1 Identification of vehicle gross mass

Different models mentioned in Section 8.4 have been used for identification of vehicle gross mass. Single and multiple sensor data have been utilized in the present identification algorithm. For the purpose of comparison, 43 km/h vehicle speed and the same sampling

frequency used in the field test have been considered. Mean estimate of the vehicle parameters and the corresponding standard deviations are given in Fig. 8.28 to Fig. 8.31. Table 8.12 to Table 8.15 shows the percentage error as well as number of iteration required to achieve convergence using four different models in forward solution separately. From the study of the tables, it has been found that Model-3 gives the best estimate of mass with 3.93% error when acceleration record from all sensor locations (Set-3) are simultaneously used in particle filtering process. This trend is seen in the estimated mass using all other three models also. General observation is that multiple sensor data improves the estimate of vehicle mass with reduction of number of iterations.

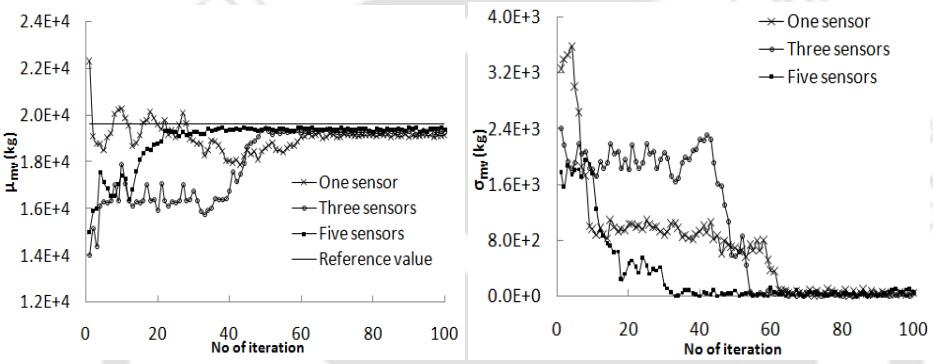

(a) Mean value (b) Standard deviation

Fig.8.28 Progressive estimate of vehicle mass for multiple sensor data using moving mass model

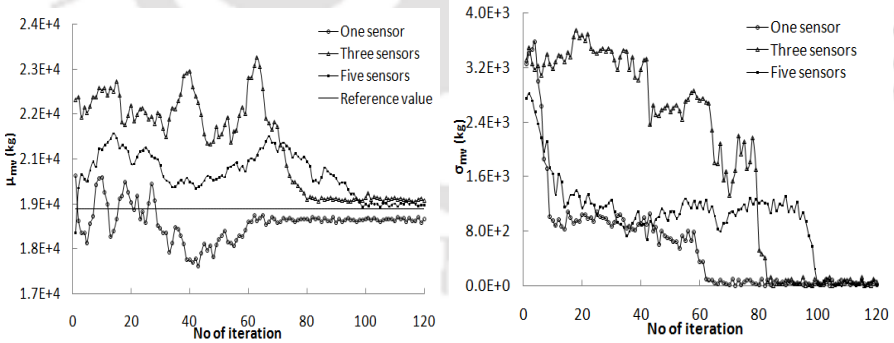

(a) Mean value (b) Standard deviation

Fig.8.29 Progressive estimate of vehicle mass for multiple sensor data using Model-1

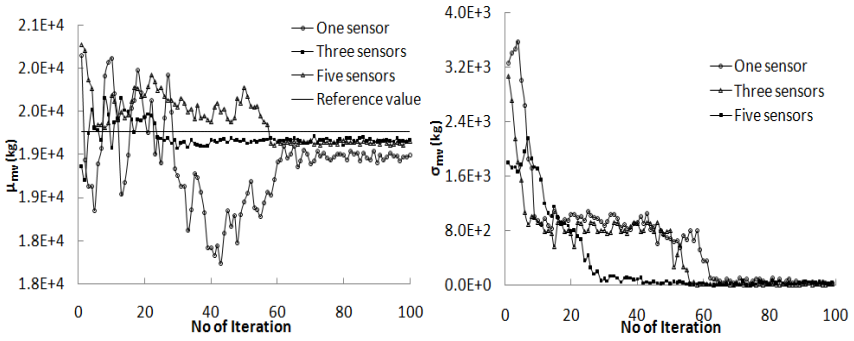

(a) Mean value (b) Standard deviation

Fig.8.30 Progressive estimate of vehicle mass for multiple sensor data using Model-3

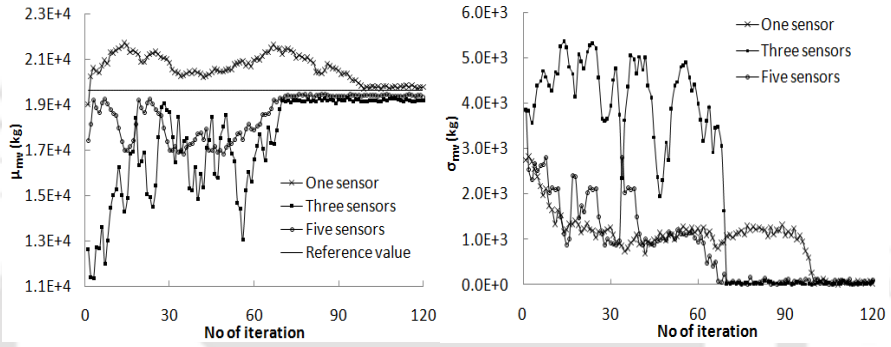

(a) Mean value (b) Standard deviation

Fig.8.31 Progressive estimate of vehicle mass for multiple sensor data using FE Model

Table 8.12 Identification of vehicle mass with different sets of sensor location using moving mass model

Set of sensor	Number of Sensor	No of iteration	RPE (%)
Set 1	1	64	8.69
Set 2	3	50	7.99
Set 3	5	42	7.23

Table 8.13 Identification of vehicle mass with different sets of sensor location using Model-1

Set of sensor	Number of Sensor	No of iteration	RPE (%)
Set 1	1	75	7.13
Set 2	3	98	6.83
Set 3	5	83	6.01

Table 8.14 Identification of vehicle mass with different sets of sensor location using Model-3

Set of sensor	Number of Sensor	No of iteration	RPE (%)
Set 1	1	59	5.81
Set 2	3	47	4.06
Set 3	5	38	3.93

Table 8.15 Identification of vehicle mass with different sets of sensor location using FE Model

Set of sensor	Number of Sensor	No of iteration	RPE (%)
Set 1	1	101	10.05
Set 2	3	72	8.83
Set 3	5	69	7.97

8.6.2 Identification of vehicle suspension stiffness and damping

Vehicle suspension parameters have been estimated by utilizing different sets of sensor data as input to the identification algorithm. Proposed semi-analytical method has been used in forward scheme with Model-1 and Model-3. Mean estimates of suspension stiffness and damping for both the models at different stage of iteration along with the corresponding standard deviations are given in Fig. 8.32 and Fig. 8.41. Identification results for different sets of sensor are given in Table 8.16 and Table 8.17. Here again one can notice that use of measured data from multiple sensors increases accuracy of the estimate of suspension parameters in Model-1 and Model-3. It may be noted that likelihood of each individual parameters which is probability density conditioned on available measurement, has been estimated at every time step based on the known information of bridge response. More number of sensor data supplied to the algorithm help to construct the unknown parameter's posterior probability density function at much faster rate. This may be the reason that rate of convergence is higher when the number of sensor is increased. However, the estimate found for the parameters of the test truck is even satisfactory when single sensor data has been used. The study thus reveals that the bootstrap particle filter technique is a very powerful tool that may be used to accurately estimate system parameters with time history of response samples from limited number of sensors.

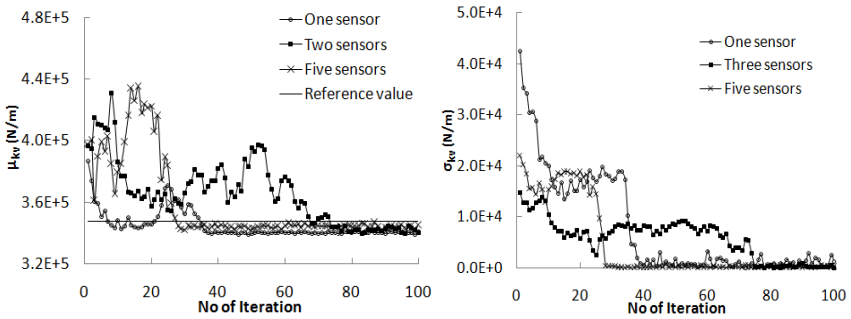

(a) Mean value (b) Standard deviation

Fig.8.32 Progressive estimate of vehicle suspension stiffness k_v for different sets of sensors considering Model-1

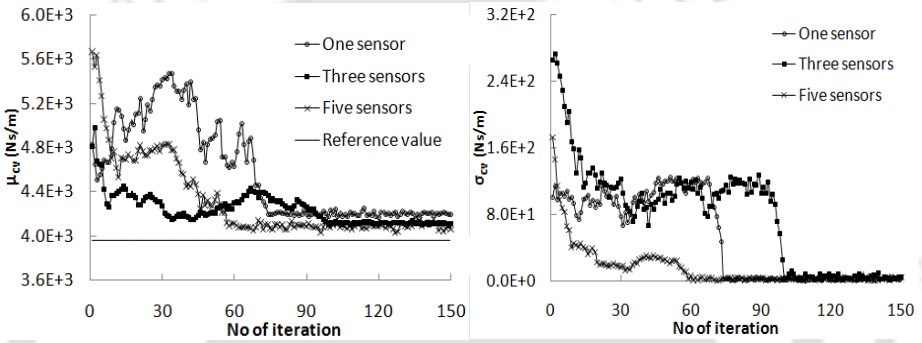

(a) Mean value (b) Standard deviation

Fig.8.33 Progressive estimate of vehicle suspension damping c_v from measured acceleration data considering Model-1

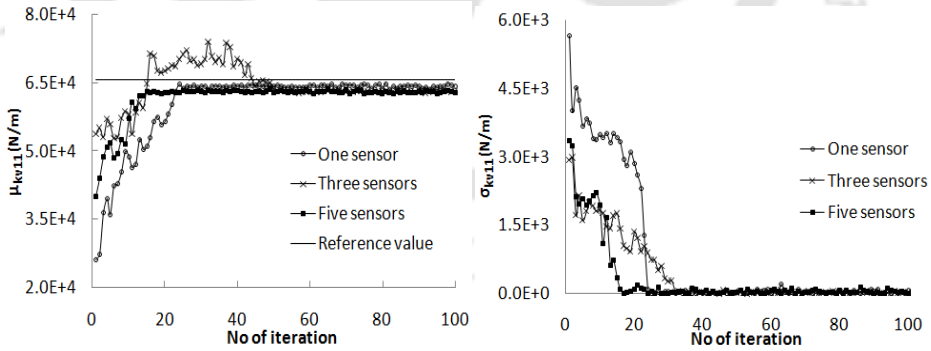

(a) Mean value (b) Standard deviation

Fig. 8.34 Progressive estimate of front-right suspension stiffness k_{v11} from measured acceleration data considering Model-3

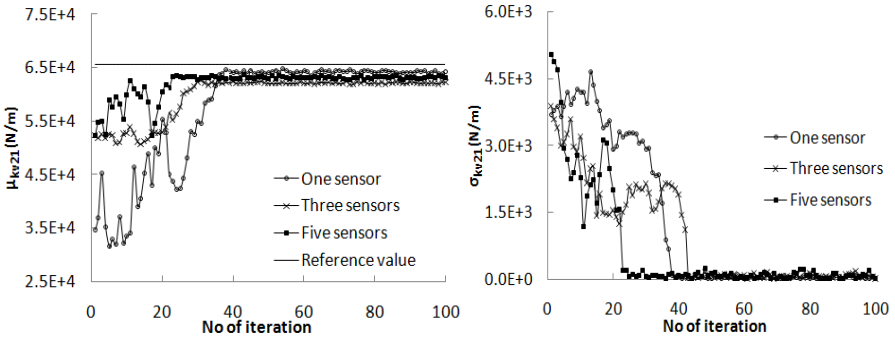

(a) Mean value (b) Standard deviation

Fig. 8.35 Progressive estimate of front-left suspension stiffness k_{v21} from measured acceleration data considering Model-3

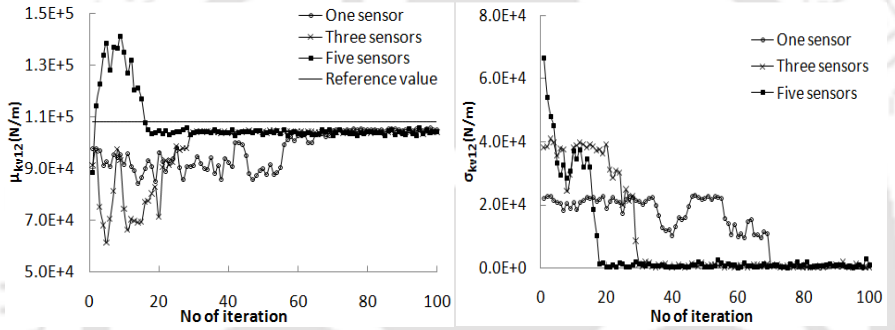

(a) Mean value (b) Standard deviation

Fig. 8.36 Progressive estimate of rear-right side suspension stiffness k_{v12} from measured acceleration data considering Model-3

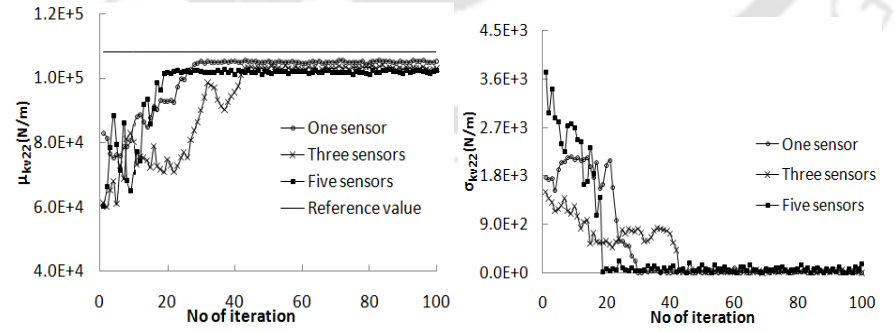

(a) Mean value (b) Standard deviation

Fig. 8.37 Progressive estimate of rear-left side suspension stiffness k_{v22} from measured acceleration data considering Model-3

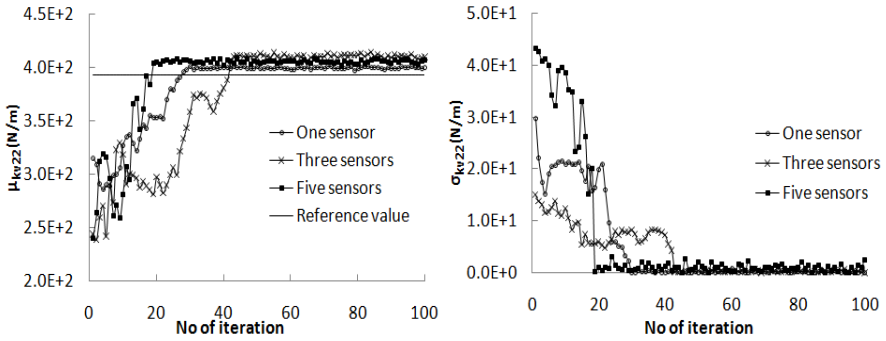

(a) Mean value (b) Standard deviation

Fig. 8.38 Progressive estimate of front-right vehicle suspension damping c_{v11} from measured acceleration data considering Model-3

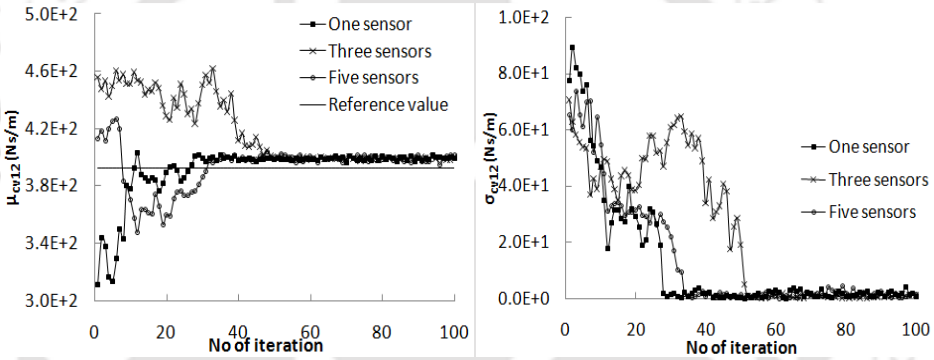

(a) Mean value (b) Standard deviation

Fig. 8.39 Progressive estimate of front-left vehicle suspension damping c_{v21} from measured acceleration data considering Model-3

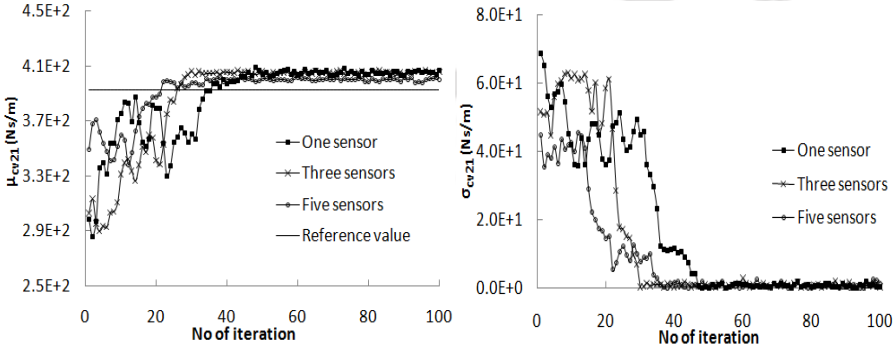

(a) Mean value (b) Standard deviation

Fig. 8.40 Progressive estimate of rear-right vehicle suspension damping c_{v12} from measured acceleration data considering Model-3

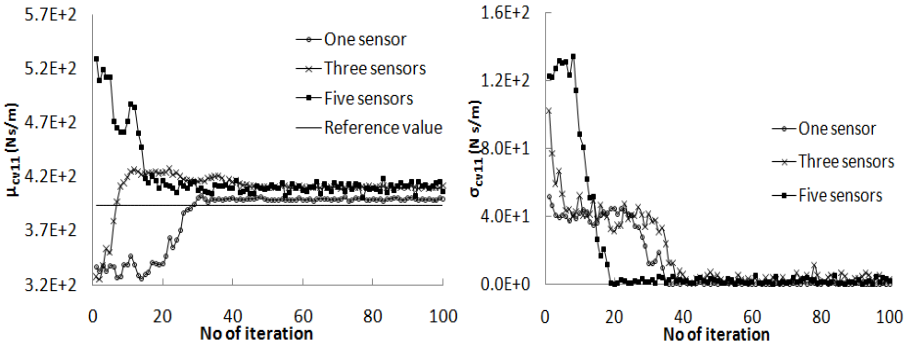

(a) Mean value (b) Standard deviation

Fig. 8.41 Progressive estimate of rear-left vehicle suspension damping c_{v22} from measured acceleration data considering Model-3

Table 8.16 Identification of vehicle suspension parameters with different sets of sensor location using Model-1

Parameters	Set of sensor	Number of sensor	Number of iteration	Percentage difference from assumed value
k_v	Set 1	1	43	5.95
	Set 2	3	76	5.14
	Set 3	5	33	4.96
c_v	Set 1	1	82	7.73
	Set 2	3	112	6.26
	Set 3	5	78	6.07

Table 8.17 Identification of vehicle suspension parameters with different sets of sensor location using Model-3

Parameters	Set of sensor	Number of sensor	No of iteration	Percentage difference from assumed value
k_{v11}	Set 1	1	32	3.78
	Set 2	3	43	3.27
	Set 3	5	25	2.96
k_{v21}	Set 1	1	39	4.01
	Set 2	3	41	5.62
	Set 3	5	26	5.05
k_{v12}	Set 1	1	78	5.63
	Set 2	3	36	2.87
	Set 3	5	29	2.39
k_{v22}	Set 1	1	36	3.78
	Set 2	3	48	3.13
	Set 3	5	31	2.99
c_{v11}	Set 1	1	42	5.82
	Set 2	3	39	4.16
	Set 3	5	24	3.97
c_{v21}	Set 1	1	49	6.90
	Set 2	3	46	5.85
	Set 3	5	31	2.70
c_{v12}	Set 1	1	44	7.86
	Set 2	3	53	4.04
	Set 3	5	39	3.83
c_{v22}	Set 1	1	35	3.99
	Set 2	3	30	4.01
	Set 3	5	27	2.98

8.7 Closure

The experimentally measured time history of bridge mid span acceleration at several sensor locations acquired by a data acquisition system under controlled movement of a loaded truck has been used in bootstrap particle filtering method to estimate the gross weight, suspension stiffness and damping of the test truck. The estimated gross weight has been checked against the report of weigh bridge station located close to the test site. Measured roughness of the test bridge and its spectral density function has been utilized in forward scheme. From the field test results, Finite Element model in SAP 2000 of tested bridge has been updated using a combination of response surface method and GA. The updated parameters are used in semi-

analytical model as well as in finite element model for implementing particle filter method in identifying vehicle parameters. First, the algorithm has been tested with single sensor data using four different models of bridge-vehicle system. Then, three different sets of sensor data have been utilized. In all the cases of identification results, numbers of iteration and percentage error have been reported.

9

CONCLUSIONS AND FUTURE SCOPE OF THE WORK

9.1 Overview

The present work has focused on the identification of vehicle parameters from dynamic response of bridge caused by the movement of the vehicle. A conditional probability based approach known as Bootstrap Particle Filter method has been implemented to perform the task. In this study, vehicle parameters are treated as hidden variables while measured bridge response as observable variable. The relationship between these variables, called as Forward scheme, has been constructed using a proposed semi-analytical solution of bridge-vehicle interaction problem. Bridge-vehicle models have been developed incorporating flexibility of the vehicle. Performance of the vehicle parameters identification technique has been first examined based on simulated bridge response. The field test has been conducted on an existing bridge under the controlled movement a loaded truck. The acceleration time history of the bridge at different locations has been thereafter utilized in Bootstrap Particle Filter algorithm to examine the performance of the identification method. The major conclusions arrived in the study and future scope of the work has been presented in this chapter.

9.2 Conclusions

Major conclusions from the theoretical and experimental study have been presented in three subsections as given below:

9.2.1 Dynamic Behaviour of Theoretical Models

In the present study, three vehicle models have been considered in bridge-vehicle interaction problem. These models are- Model-1: Bridge-Quarter Car Vehicle System, Model-2: Bridge-Half Car Vehicle System with vehicle body bending flexibility and Model-3: Bridge-Full Car Vehicle System with vehicle body bending and torsional flexibility. A semi-analytical method has been developed for obtaining response statistics of bridge-vehicle system with variation of different parameters. Detail parametric studies on the coupled dynamics have been presented in Chapter-6.

Based on results presented, some major conclusions are listed below:

- In Bridge-Quarter Car Vehicle System (Model-1), the mean responses of sprung mass and unsprung mass increase with increase of vehicle speed. Standard deviation does not show any definite trend of variation. Unsprung mass responses are found to be higher compared with the sprung mass response.

- In Bridge-Half Car Vehicle System and Bridge-Full Car Vehicle System (Model-2 and 3), where flexibility of vehicle body has been considered in the modeling, the responses found at the location of vehicle centroid are lower compared to the Bridge-Quarter Car Vehicle System. In Model-3, due to rolling of vehicle and non uniform torsion along the length, the vertical displacement of vehicle showed more fluctuating components.

- There is insignificant amount of change in output frequency of the vehicle responses due to change of vehicle speed. This trend appears in the behavior of three models studied in the present work.

- Study of the effect of vehicle speed on the dynamic response of the bridge clearly indicates that bridge mean response is higher when vehicle runs with higher velocity. This is observed on the bridge dynamic responses when all the three different vehicle models are used.

- The output frequency in bridge mean response is distinctly seen to be modified with the increase of vehicle speed with clear left shift of peak of the displacement mean. However, for the case of velocity and acceleration of bridge mid span, no such systematic change in response frequency has been noted.

- Eccentric path followed by a vehicle has an adverse affect on the bridge dynamic behavior. Study reveals that increase of eccentricity of vehicle load on the pavement increases mid span deflection of bridge by an amount of 9% for the parameters selected to illustrate the present approach. The similar features have been observed when all the three vehicle models have been used for the study.

- The mid span deflection of a bridge increases if approach road settlement occurs at bridge entry as the vehicle suddenly experiences a high transient load which is transmitted to the pavement. Numerical experiments with different values of settlement show that a settlement of 40 mm may increase defection upto 21%.

- Consideration of vehicle flexibility in the model has shown that less dynamic load is imposed on bridge pavement as compared to that produced by a rigid vehicle model.

- It is seen that as the flexural rigidity of vehicle body increases, the deflection of bridge at mid span increases.

- When flexible modes of vehicle body are considered, summation of first five modes is sufficient to obtain the response in mode superposition technique.

- The present formulation takes non homogeneity of pavement roughness into account by considering deterministic variable mean superimposed over random unevenness. Study of different model behavior with two types of deterministic mean profile along with the random unevenness reveals that vehicle in model-3, where both bending and torsional flexibility have been considered, is likely to produce less mid span deflection in the bridge having a precambered profile in addition to random uneveness. However, large approach settlement at bridge entry does not offer any benefit of flexible vehicle model considered in Model-2 and 3.

- Dynamic amplification factor (DAF) of the bridge response evaluated for the variation of vehicle speed and surface roughness reveals that these two parameters, if not kept within satisfactory limit, may produce excessive bridge response. Therefore, it becomes necessary to control speed of vehicle over the bridge and to carry out periodic maintenance of bridge surface to reduce severity of input to moving wheels.

- Study of the effect of bridge span on the DAF of the bridge response has shown that amplification decreases with the increase of bridge span. However, the conclusion is only limited to a bridge span of 15 m- 35 m with simply supported ends. The DAF in the case of 35 m span is found 12%- 15% less compared to DAF of 15 m span bridge irrespective

of increase of velocity in the range of 40 km/h to 60 km/h. Although, the same trend has been observed in case of Model-2 and 3, the magnitude of DAF is comparatively lower than that obtained using Bridge- Quarter Car Vehicle System (Model-1)

- The investigation with numerical experiment has revealed that axle spacing has some effect on the change of dynamic amplification factor. The increase of axle spacing will create increased span between the two axles, thus causing elastic bending effect in the vehicle body. Bridge- Half Car Vehicle System (Model-2) and Bridge- Full Car Vehicle System (Model-3), when used in bridge-vehicle interaction problem have shown that with increase in axle spacing DAF of bridge response decreases. However, if there is sudden change in road level due to approach settlement, DAF shows a reverse trend.

- The increase of vehicle mass has the effect of marginally reducing dynamic amplification factor. This may be attributed to the fact that increased vehicle weight lead to increase of bridge static deflection, as a result of which non dimensional DAF decreases. This is also observed if small amount of approach settlement exists, however, if the value of approach settlement is significant, DAF of bridge response increases even with the increase of vehicle mass. The behaviour of simply supported bridge studied with three different types of vehicle mode demonstrates similar facts.

9.2.2 Vehicle Parameter Identification from Simulated Results

Under this section, conclusions for the identifications of vehicle parameters from simulated acceleration of the bridge have been drawn. As mentioned earlier, the proposed semi analytical method has been used in forward scheme of the Particle Filtering method. Vehicle parameters for three models- Model-1: Bridge-Quarter Car Vehicle System, Model-2: Bridge-Half Car Vehicle System and Model-3: Bridge-Full Car Vehicle System have been estimated using time history of simulated bridge acceleration in inverse scheme. The advantage offered by semi analytical method in sample generation in forward scheme of Particle filter method has been judged by comparing CPU time with generated samples using Numerical scheme.

Major conclusions drawn from the study have been listed below:

- A comparative study with the theoretical and experimental results available in literature have shown that the particle filter technique implemented using a proposed semi-

analytical technique in forward scheme has a very good accuracy in moving force identification. The improvement of accuracy over the other method of inverse scheme has proved the efficiency of the method for moving load estimation in deteriorated pavement condition of the bridge also.

- The comparison with published literature has also revealed that high frequency component when present in poor condition of road could not disturb the moving load identification as the sampling frequency can be easily increased without any numerical instability problem in the proposed forward scheme leading to the improved estimate of moving load.

- Effect of location of the sensor is very important for the accuracy and time required for the estimation of vehicle parameters. The study has revealed that mid span time history when utilized in particle filter method gives improved estimate of the vehicle parameters by lowering the relative percentage error (RPE). However, relative error is different in each of the parameters estimated for three different vehicle models. In majority of the cases, less number of iteration is required to obtain the converged estimate of parameter for all vehicle models. It may be noted that RPE is the best indicator to comment on the efficiency of the method.

- The comparison of pavement interaction force time history obtained by using identified vehicle parameters with that obtained using the reference values of parameters show good agreement. However, the significant fluctuation of moving force about static load demands dynamic analysis of bridge subject to moving load for practical design.

- Artificial noise has been added to study its effect on the identification of parameters in particle filter method. Two levels of noise viz, 5% and 10% have been taken to perform numerical experiment. It is revealed that lower noise provides more accurate estimate. Higher noise level resulted in a maximum of 10-16% deviation of estimated parameters from the reference value in the illustrative examples. This has been noted in the present study considering all the three different vehicle models.

- Vehicle speed is another important factor which has been taken into consideration to judge the performance of the inverse scheme used in the study. The general observations from

the study of three types of vehicle model is that bridge response utilized at slower speed of the vehicle requires more number of iteration compared to that obtained at higher speed of vehicle. However, in most of the vehicle parameters estimated at lower speed give higher accuracy.

- The increase of sampling time interval becomes necessary when vehicle travels at faster speed for generation of more number of data points at discrete times as the vehicle leaves the bridge earlier compared to slower speed movement. Interestingly, the proposed forward scheme with semi analytical method could easily accommodate this increase in sampling frequency without any problem in instability of computation.

- The numerical experiment for vehicle parameter identification has considered the effect of pavement condition on the accuracy of the identified parameters in all the three models. The response of bridge obtained for rougher pavement condition and its utilization in particle filter method increases the relative percentage error. This effect is consistently observed in the estimation of all parameters in all the three models.

- The study of the effect of approach settlement of the bridge on the accuracy of different parameters of the vehicle reveals that when the bridge entry is not smooth, the particle filter technique requires more number of iteration for convergence. However study with medium amount of bridge approach settlement causes insignificant amount of percentage error in the estimate. This trend has been found with the application of three models chosen in the present study.

- Selection of the initial range of vehicle parameters for the construction of prior probability density function has an important bearing on the time required for convergence and accuracy of the parameter. Study on the effect of initial range of vehicle parameters for the construction of prior probability density function reveals that initial selection of parameters with wide range increases the number of iterations considerably, whereas final estimate does not differ significantly. This shows that incorrect choice of initial parameters does not eventually lead to wrong estimate. This is observed when vehicle parameters have been estimated using all the three vehicle models.

- The usefulness of the proposed semi-analytical method in forward scheme has been judged by comparing CPU processing time and relative accuracy with that obtained using response samples generated by existing numerical techniques. The result reveals that CPU time for the estimation of parameters remarkably decreased when samples are generated using semi-analytical method, while there is significant improvement in the accuracy of the estimate. This clearly indicates the superiority of particle filtering techniques when combined with semi analytical method of sample generations. However, sampling frequency leads to lower error in vehicle parameter estimation but requires more CPU time.

9.2.3 Vehicle Parameter Identification from Field Measurement

Dynamic Field test has been conducted on an existing bridge. The acquired acceleration time history has been utilized in particle filter method. Semi analytical method of solution proposed in the present study has been employed in forward scheme. At the same time, the test bridge has been modeled using Finite Element software and estimation has also been obtained using FE model in forward scheme. Different model options in forward scheme of particle filter method have been investigated using actually measured data.

Major conclusions drawn from the study have been listed below:

- Deck surface elevations along the bridge span has been measured and pavement classification according to ISO standard (ISO 8608:1995) has been done. From the spectral analysis, it is seen that the tested bridge surface falls under the category of very good surface.

- Acceleration records at five different locations have been obtained under the controlled movement of a loaded truck at three different velocities. Actual vehicle speed observed with the help of radar gun shows that during field test vehicle travelled at 21 km/h, 29 km/h and 43 km/h. The peak acceleration experimentally obtained shows that there is systematic increase of magnitude with the increase in vehicle speed. The same trend has been observed in the theoretical model results presented in the study. This shows that the present bridge-vehicle models predict realistic behavior of the system.

- The experimental results have also revealed that peak acceleration of bridge deck at mid span location is the highest among all sensor data. The same fact has been observed in theoretical results when effect of measurement location on identification has been studied.

- The finite element model of the test bridge has been developed in SAP2000. Model updating has been carried out based on experimentally obtained first two natural frequencies and peak acceleration at five locations. Response surface method in combination with GA has been used. The method proves to be very user friendly and reasonably accurate, while allowing heterogeneity of sensor data. The differences between the experimental first two natural frequencies and updated model frequencies were found to be 2.5% and 3.8% respectively. Measured peak acceleration at different sensor locations deviates in the range of 6% to 13% from that obtained after analyzing updated FE model subject to a moving load equal to loaded test truck weight.

- Particle filter method has been applied using experimentally measured acceleration. Four different kinds of bridge-vehicle interaction model viz. Moving Mass-Beam model, Bridge-Quarter Car Vehicle model (Model-1), Bridge-Full Car Vehicle model (Model-3) and Finite Element model have been used in forward scheme. Study reveals that a simplified moving mass model on beam gives very quick estimate of gross vehicle weight. Model-1 and Model-3 which incorporate dynamic interaction with the bridge provided better accuracy in terms of reduced relative percentage error. Model-3 which includes bending and torsional flexibility yielded the most accurate estimate of gross weight among all the four models. Overall, it can be seen that performance of all the models in the estimation of gross vehicle weight is satisfactory, although computational time in Finite Element Model is the highest among the four models.

- It may be noted that determination of vehicle suspension stiffness in practice is not straightforward like the gross vehicle weight. In the present study suspension stiffness and damping have been extracted from the bridge dynamic response, which are very useful information for the vehicle operators. The comparison of extracted suspension stiffness using Bridge-Quarter Car Vehicle model (Model-1) with that of theoretically calculated value shows that the estimated value is about 6% lower than the theoretically calculated value. Result obtained by using Model-3 shows that each of the four suspension stiffness

extracted by particle filter approach differs in the range of 4%-6% of the theoretically calculated value. Lower value of the extracted suspension stiffness may be an indication of degradation in the spring-system which may be an important finding related to the vehicle maintenance.

- Suspension damping has been extracted using Model-1 and Model-3 from the bridge acceleration obtained at 43 km/h. In the Bridge-Quarter Car Vehicle Model (Model-1), the extracted damping around is 7% higher than that assumed in the forward scheme. Full car model suspension damping extracted from the bridge acceleration show a deviation of 5%-8% in the four suspensions of the truck. Higher damping may be an indication of the increase of interleaf friction.

- Since "Road friendly Vehicles" are always desired for maintaining a good health for the bridge and vehicles, the particle filter method used in the present study can extract information about the suspension parameters from the bridge dynamic response in a cost effective way for the vehicles in service.

- The assumptions of vehicle as lumped parameter system may not be always true to reflect correct dynamic behavior. In the present study, with the use of flexible vehicle model, the flexural and torsional rigidity of the test truck body have been extracted from bridge acceleration time history and compared with the values calculated from the section geometry and material properties. The extracted value of flexural rigidity of the tested truck frame has been found to be around 9% lower than that calculated using sectional properties. Extracted torsional rigidity, on the other hand shows around 7% downward deviation from the calculated value.

- The reconstructed mid-span acceleration time history with identified vehicle parameters of different models have been compared with experimentally recorded mid span acceleration at vehicle speed of 43km/h. Very good agreement has been noted between experimental values and theoretical value. The predicted value of bridge acceleration using Model-3 differs only by 2%-4% with the field test value. Performance of other models when used in forward scheme has also been found satisfactory, although moving mass model predicts slightly higher value of peak acceleration than the experimentally obtained value.

- Use of single sensor and multiple sensor data have been separately utilized in particle filter algorithm. It has been found that use of five sensor data in the present identification method improves the accuracy of the estimation in all the four models used in forward scheme. Moreover, the number of iteration required to estimate most of the vehicle parameters reduce because of availability of more information simultaneously in particle filtering method.

9.3 Future Scope of the Study

Following are the future scope of the work:

- Multi-axles and articulated type of vehicles can be included in the study.
- Non-linear suspension characteristics of the vehicle suspension can be included in the model.
- Non-stationary excitation arising due to change in vehicle speed can be included.
- Horizontally curved bridge may be studied for moving load identification purpose.
- Study can be undertaken to estimate parameters of railway vehicles from bridge dynamic response.

9.4 Closure

In this chapter, conclusions have been drawn from the results and discussions presented in the preceding three chapters. First, conclusions by studying dynamic behavior of bridge-vehicle coupled system models obtained using proposed semi-analytical method have been discussed. Thereafter, conclusions have been drawn on the performance of particle filter method for identification of vehicle parameters in different models using simulated response time history. Lastly, the measured acceleration of an existing bridge under the movement of a loaded truck has been utilized in particle filter method and conclusions arrived using field measured data have been stated. From the detail investigation, it is now concluded that particle filter method which was not popularly used for moving load identification on bridge due to huge computational cost, can be enriched by combining a semi-analytical method for rapid generations of response sample and to avoid numerical instability due to adoption of large sampling frequency in compliance with the data acquisition in the field. The possible extension of the present research works has been also stated.

APPENDIX A

The integral I_{jk} for Model-1

Expression of the Integral I_{jk} given in Eq. (4.77) for generating response sample is given in the following equations. The vector $\{F(t)\}$ needed to perform the integration is given below:

$$F_j(t) = 0 \quad \text{For } j=1$$

$$= k_t h(Vt) + c_t V \frac{dh(x)}{dx}\Big|_{x=Vt}$$

For j=2

$$= k_t \phi_{b(t-2)}(Vt) h(Vt) + c_t \phi_{b(t-2)}(Vt) V \frac{dh(x)}{dx}\Big|_{x=Vt} - \{m_w + m_v\} g \phi_{b(t-2)}(x)\Big|_{x=Vt}$$

For j=3,4,5,….,n_b

$$= e_x \left[-k_t \phi_{t(j-3-nb)}(Vt) h(Vt) - c_t \phi_{t(j-3-nb)}(Vt) V \frac{dh(x)}{dx}\Big|_{x=Vt} + \{m_w + m_v\} g \phi_{t(j-3-nb)}(x)\Big|_{x=Vt} \right]$$

For j=1+ r, 2+ r ,…., r +n_T, where, r =n_b+2

(A-1)

Introducing the following relations

$$A_s = \sqrt{2 S_{GG}(V\Omega_s)^{-2}} \tag{A-2}$$

$$B_s = 2\pi \left\{ \Omega_L + \frac{(s-0.5)(\Omega_U - \Omega_L)}{N} \right\} \tag{A-3}$$

$$Q_s = B_s V \tag{A-4}$$

The components of I_{jk} are given below for systematic computation

For k=1,

$$I_{j1} = 0 \tag{A-5}$$

Now we write for k=2,

$$I_{j2} = \sum_{a=1}^{4} I_{j2a} \tag{A-6}$$

The components of Eq. (A-6) are obtained as

For random surface unevenness of bridge deck

For $0 \le t \le L/V$

$$I_{j21} = k_t[\sum_{s=1}^{N} A_s \frac{\exp(-\alpha_j t)}{\alpha_j^2 + (B_s V)^2}\{-\alpha_j \cos(\theta_s) - B_s V \sin(\theta_s) + \exp(\alpha_j t)[\alpha_j \cos(B_s V t + \theta_s) + B_s V \cos(B_s V t + \theta_s)]\}] \quad \text{(A-7)}$$

$$I_{j22} = c_t[\sum_{s=1}^{N} V A_s B_s \frac{\exp(-\alpha_j t)}{\alpha_j^2 + (B_s V)^2}\{-\alpha_j \sin(\theta_s) - B_s V \cos(\theta_s) + \exp(\alpha_j t)[\alpha_j \sin(B_s V t + \theta_s) - B_s V \sin(B_s V t + \theta_s)]\}] \quad \text{(A-8)}$$

For deterministic mean surface profile (parabolic pre-cambering and approach road settlement)

When $0 \le t \le L_r / V$

where, L_r represents length of ramp function.

$$I_{j23} = k_t[\frac{4h_0 V}{\alpha_j^3 L^2}\{\alpha_j L(\alpha_j t + \exp(-\alpha_j t) - 1)\} - \frac{V}{\alpha_j^3 L^2}\{\alpha_j t(\alpha_j t - 2) - 2\exp(-\alpha_j t) + 2)\}] + k_t \frac{h_1 V}{\alpha_j^2 L_r}\{\alpha_j t + \exp(-\alpha_j t) - 1\} \quad \text{(A-9)}$$

$$I_{j24} = c_t[\frac{4h_0 V \exp(-\alpha_j t)}{\alpha_j^3 L^2}\{2V[(\alpha_j t - 1)\exp(-\alpha_j t) - 1]\} + \frac{1}{\alpha_j L}\{\exp(\alpha_j t) + 2\}] + c_t \frac{h_1 V}{\alpha_j L_r}\{1 - \exp(-\alpha_j t)\} \quad \text{(A-10)}$$

If $L_r / V < t \le L/V$

$$I_{j23} = k_t[\frac{4h_0 V}{\alpha_j^3 L^2}\{\alpha_j L(\alpha_j t + \exp(-\alpha_j t) - 1)\} - \frac{V}{\alpha_j^3 L^2}\{\alpha_j t(\alpha_j t - 2) - 2\exp(-\alpha_j t) + 2)\}] + k_t \frac{h_1 V}{\alpha_j^2 L_r}\{1 - xp(-\alpha_j t)\} \quad \text{(A-11)}$$

$$I_{j24} = c_t[\frac{4h_0 V \exp(-\alpha_j t)}{\alpha_j^3 L^2}\{2V[(\alpha_j t - 1)\exp(-\alpha_j t) - 1]\} + \frac{1}{\alpha_j L}\{\exp(\alpha_j t) + 2\}] \quad \text{(A-12)}$$

For k=3,4,…, n_b, the integral is split up into five parts as follows

$$I_{jk} = \sum_{a=1}^{5} I_{jka} \tag{A-13}$$

Components of Eq. (A-13) can be expressed as

Introducing $R_k = (k-2)\pi V / L$

<u>For random surface unevenness of bridge deck</u>

If $0 \le t \le L/V$

$$I_{jk1} = \frac{1}{2} k_t \sum_{s=1}^{N} A_s \left[\frac{2R_k \exp(-\alpha_j t)\{(\alpha_j^2 - Q_s^2 + R_k{}^2)\cos(\theta_s) + 2\alpha_j Q_s \sin(\theta_s)\}}{\{\alpha_j^2 + (Q_s - R_k)^2\}\{\alpha_j^2 + (Q_s + R_k)^2\}} \right.$$
$$- \frac{\alpha_j \sin\{(Q_s - R_k)t + \theta_s\} + (R_k - Q_s)\cos\{(Q_s - R_k)t + \theta_s\}}{\{\alpha_j^2 + (Q_s - R_k)^2\}}$$
$$\left. + \frac{\alpha_j \sin\{(Q_s + R_k)t + \theta_s\} - (R_k + Q_s)\cos\{(Q_s + R_k)t + \theta_s\}}{\{\alpha_j^2 + (Q_s + R_k)^2\}} \right] \tag{A-14}$$

$$I_{jk2} = \frac{1}{2} c_t \sum_{s=1}^{N} A_s Q_s \left\{ - \frac{2R_k \exp(-\alpha_j t)\{(\alpha_j^2 - Q_s^2 + R_k{}^2)\sin(\theta_s) - 2\alpha_j Q_s \cos(\theta_s)\}}{\{\alpha_j^2 + (Q_s - R)^2\}\{\alpha_j^2 + (Q_s + R_k)^2\}} \right.$$
$$- \frac{\alpha_j \cos\{(Q_s - R_k)t + \theta_s\} + (R_k - Q_s)\sin\{(Q_s - R_k)t + \theta_s\}}{\{\alpha_j^2 + (Q_s - R_k)^2\}}$$
$$\left. + \frac{\alpha_j \cos\{(Q_s + R_k)t + \theta_s\} + (R_k + Q_s)\sin\{(Q_s + R_k)t + \theta_s\}}{\{\alpha_j^2 + (Q_s + R_k)^2\}} \right\} \tag{A-15}$$

<u>For deterministic mean surface profile (parabolic pre-cambering and approach road settlement)</u>

If $0 \le t \le L_r / V$

$$I_{jk3} = k_t \frac{2h_0 V \exp(-\alpha_j t)}{L^2(\alpha_j^2 + Q_s^2)^3} \left[\left\{ L(\alpha_j^2 + Q_s^2)[\exp(\alpha_j t)\sin(Q_s t)\{Q_s^2(\alpha_j t + 1) + \alpha_j^2(\alpha_j t - 1)\}] \right.\right.$$
$$- Q_s \exp(\alpha_j t)\cos(Q_s t)[Q_s^2 t + \alpha_j(\alpha_j t - 2)] - 2\alpha_j Q_s \Big\}$$
$$+ V(2Q_s^3 + Q_s \exp(\alpha_j t))\cos(Q_s t)\ \{ Q_s^4 t^2 + 2Q_s^2(\alpha_j^2 t^2 - 2\alpha_j t - 1) + \alpha_j^2(\alpha_j^2 t^2 - 4\alpha_j t + 6)\}$$
$$\left. - \exp(\alpha_j t)\sin(Q_s t)\{Q_s^4(\alpha_j t + 2) + \alpha_j Q_s^2(\alpha_j^2 t^2 - 3) + \alpha_j^3(\alpha_j^2 t^2 - 2\alpha_j t + 2)\} - 6\alpha_j^2 Q_s \right]$$
$$+ k_t \frac{V h_1 \exp(-\alpha_j t)}{L\, L_r (\alpha_j^2 + R_k^2)} [-2R_k \alpha_j L^3 + \exp(\alpha_j t)\{L^2 \alpha_j(\alpha_j t - 1)\cos(R_k t)\}$$
$$+ R_k^2 L^2 (1 + \alpha_j t)\cos(R_k t)] \tag{A-16}$$

$$I_{jk4} = c_t \frac{2h_0 V \exp(-\alpha_j t)}{L^2(\alpha_j^2 + V^2)^3}\{\exp(\alpha_j t)\cos(Q_s t)[Q_s^2(2\alpha_j tV - \alpha_j L + 2V) + \alpha_j^2(2\alpha_j tV - \alpha_j L - 2V)]$$
$$- Q_s \exp(\alpha_j t)\sin(Q_s t)[Q_s^2(L - Vt) + \alpha_j(\alpha_j L - 2\alpha_j tV + 4V)]\ \}$$
$$+ c_t \frac{h_1 V}{L L_r(\alpha_j^2 + R_k^2)}[\exp(-\alpha_j t) R_k L\{1 - \cos(R_k t)\} + L\alpha_j \sin(R_k t)]$$

(A-17)

For $L_r / V < t \le L/V$

$$I_{jk3} = k_t \frac{2h_0 V \exp(-\alpha_j t)}{L^2(\alpha_j^2 + Q_s^2)^3}\Big[\{L(\alpha_j^2 + Q_s^2)[\exp(\alpha_j t)\sin(Q_s t)\{Q_s^2(\alpha_j t + 1) + \alpha_j^2(\alpha_j t - 1)\}]$$
$$- Q_s \exp(\alpha_j t)\cos(Q_s t)[Q_s^2 t + \alpha_j(\alpha_j t - 2)] - 2\alpha_j Q_s\}$$
$$+ V(2Q_s^3 + Q_s \exp(\alpha_j t))\cos(Q_s t)\ \{\ Q_s^4 t^2 + 2Q_s^2(\alpha_j^2 t^2 - 2\alpha_j t - 1) + \alpha_j^2(\alpha_j^2 t^2 - 4\alpha_j t + 6)\}$$
$$- \exp(\alpha_j t)\sin(Q_s t)\{Q_s^4(\alpha_j t + 2) + \alpha_j Q_s^2(\alpha_j^2 t^2 - 3) + \alpha_j^3(\alpha_j^2 t^2 - 2\alpha_j t + 2)\} - 6\alpha_j^2 Q_s\ \Big]$$
$$+ k_t \frac{h_1 V}{L\ (\alpha_j^2 + R_k^2)}[R_k L\{\exp(-\alpha_j t) - \cos(R_k t)\} + L\alpha_j \sin(R_k t)]$$

(A-18)

$$I_{jk4} = c_t \frac{2h_0 V \exp(-\alpha_j t)}{L^2(\alpha_j^2 + V^2)^3}\{\exp(\alpha_j t)\cos(Q_s t)[Q_s^2(2\alpha_j tV - \alpha_j L + 2V) + \alpha_j^2(2\alpha_j tV - \alpha_j L - 2V)]$$
$$- Q_s \exp(\alpha_j t)\sin(Q_s t)[Q_s^2(L - Vt) + \alpha_j(\alpha_j L - 2\alpha_j tV + 4V)]\ \}$$

(A-19)

Due to static weight of vehicle ($0 \le t \le L/V$)

$$I_{jk5} = -\frac{\exp(-\alpha_j t)\, gL(m_v + m_w)}{L^2\alpha_j^2 + k^2\pi^2 V^2}\left[R_k L + \exp(-\alpha_j t)\{R_k L\cos(R_k t) + L\alpha_j \sin(R_k t)\}\right]$$

(A-20)

Again, for k=1+r,2+r,…, r +n_T , where r=2+n_b .The integral is split up into five parts as follows

$$I_{jk} = \sum_{b=1}^{5} I_{jkb} \qquad \text{(A-21)}$$

Take $R_k = (k - r)\pi V / L$

Components of I_{jk} can be expressed as

For random surface unevenness of bridge deck

If $0 \le t \le L/V$

$$I_{jk1} = -\frac{1}{2} e_x k_t \sum_{s=1}^{N} A_s \left[\frac{2R_k \exp(-\alpha_j t)\{(\alpha_j^2 - Q_s^2 + R_k^2)\cos(\theta_s) + 2\alpha_j Q_s \sin(\theta_s)\}}{\{\alpha_j^2 + (Q_s - R_k)^2\}\{\alpha_j^2 + (Q_s + R_k)^2\}} \right.$$
$$- \frac{\alpha_j \sin\{(Q_s - R_k)t + \theta_s\} + (R_k - Q_s)\cos\{(Q_s - R_k)t + \theta_s\}}{\{\alpha_j^2 + (Q_s - R_k)^2\}}$$
$$\left. + \frac{\alpha_j \sin\{(Q_s + R_k)t + \theta_s\} - (R_k + Q_s)\cos\{(Q_s + R_k)t + \theta_s\}}{\{\alpha_j^2 + (Q_s + R_k)^2\}} \right] \quad \text{(A-22)}$$

$$I_{jk2} = -e_x \frac{1}{2} c_t \sum_{s=1}^{N} A_s Q_s \left\{ - \frac{2R_k \exp(-\alpha_j t)\{(\alpha_j^2 - Q_s^2 + R_k^2)\sin(\theta_s) - 2\alpha_j Q_s \cos(\theta_s)\}}{\{\alpha_j^2 + (Q_s - R)^2\}\{\alpha_j^2 + (Q_s + R_k)^2\}} \right.$$
$$- \frac{\alpha_j \cos\{(Q_s - R_k)t + \theta_s\} + (R_k - Q_s)\sin\{(Q_s - R_k)t + \theta_s\}}{\{\alpha_j^2 + (Q_s - R_k)^2\}}$$
$$\left. + \frac{\alpha_j \cos\{(Q_s + R_k)t + \theta_s\} + (R_k + Q_s)\sin\{(Q_s + R_k)t + \theta_s\}}{\{\alpha_j^2 + (Q_s + R_k)^2\}} \right\} \quad \text{(A-23)}$$

<u>For deterministic mean surface profile (parabolic pre-cambering and approach road settlement)</u>

For $0 \le t \le L_r / V$

$$I_{jk3} = -e_x k_t \frac{2h_0 V \exp(-\alpha_j t)}{L^2(\alpha_j^2 + Q_s^2)^3} \left[\left\{ L(\alpha_j^2 + Q_s^2)[\exp(\alpha_j t)\sin(Q_s t)\{Q_s^2(\alpha_j t + 1) + \alpha_j^2(\alpha_j t - 1)\}] \right.\right.$$
$$- Q_s \exp(\alpha_j t)\cos(Q_s t)[Q_s^2 t + \alpha_j(\alpha_j t - 2)] - 2\alpha_j Q_s \Big\}$$
$$+ V(2Q_s^3 + Q_s \exp(\alpha_j t))\cos(Q_s t) \ \{ Q_s^4 t^2 + 2Q_s^2(\alpha_j^2 t^2 - 2\alpha_j t - 1) + \alpha_j^2(\alpha_j^2 t^2 - 4\alpha_j t + 6)\}$$
$$\left. - \exp(\alpha_j t)\sin(Q_s t)\{Q_s^4(\alpha_j t + 2) + \alpha_j Q_s^2(\alpha_j^2 t^2 - 3) + \alpha_j^3(\alpha_j^2 t^2 - 2\alpha_j t + 2)\} - 6\alpha_j^2 Q_s \right]$$
$$+ k_{t1} \frac{\exp(-\alpha_j t) h_1 L V}{L L_r (R_k^2 + \alpha_j^2)} e_x [2L^3 \alpha_j + \exp(-\alpha_j t)\{-R_k L[R_k^2 L^2 t + L^2 \alpha_j(\alpha_j t - 2)]\cos(R_k t)$$
$$+ L\{L^2 \alpha_j^2(\alpha_j t - 1) + R_k^2 L^2 t(\alpha_j t + 1)\}\sin(R_k t)\}] \quad \text{(A-24)}$$

$$I_{jk4} = -e_x c_t \frac{2h_0 V \exp(-\alpha_j t)}{L^2(\alpha_j^2 + V^2)^3} \{ \exp(\alpha_j t)\cos(Q_s t)[Q_s^2(2\alpha_j t V - \alpha_j L + 2V) + \alpha_j^2(2\alpha_j t V - \alpha_j L - 2V)]$$
$$- Q_s \exp(\alpha_j t)\sin(Q_s t)[Q_s^2(L - Vt) + \alpha_j(\alpha_j L - 2\alpha_j t V + 4V)] \ \}$$
$$- e_x c_t \frac{h_1 V}{L L_r (\alpha_j^2 + R_k^2)} [\exp(-\alpha_j t) R_k L\{\sin(R_k t) - 1\} + L\alpha_j \cos(R_k t)] \quad \text{(A-25)}$$

If $L_r/V < t \le L/V$

$$I_{jk3} = -e_x k_t \frac{2h_0 V \exp(-\alpha_j t)}{L^2(\alpha_j^2+Q_s^2)^3}\Big[\{L(\alpha_j^2+Q_s^2)[\exp(\alpha_j t)\sin(Q_s t)\{Q_s^2(\alpha_j t+1)+\alpha_j^2(\alpha_j t-1)\}]$$
$$-Q_s\exp(\alpha_j t)\cos(Q_s t)[Q_s^2 t+\alpha_j(\alpha_j t-2)]-2\alpha_j Q_s\}$$
$$+V(2Q_s^3+Q_s\exp(\alpha_j t))\cos(Q_s t)\ \{\ Q_s^4 t^2+2Q_s^2(\alpha_j^2 t^2-2\alpha_j t-1)+\alpha_j^2(\alpha_j^2 t^2-4\alpha_j t+6)\}$$
$$-\exp(\alpha_j t)\sin(Q_s t)\{Q_s^4(\alpha_j t+2)+\alpha_j Q_s^2(\alpha_j^2 t^2-3)+\alpha_j^3(\alpha_j^2 t^2-2\alpha_j t+2)\}-6\alpha_j^2 Q_s\ \Big]$$
$$-e_x k_t \frac{h_1 V}{L\ (\alpha_j^2+R_k^2)}[R_k L\{\exp(-\alpha_j t)+\sin(R_k t)\}-L\alpha_j\cos(R_k t)]$$

(A-26)

$$I_{jk4} = -e_x c_t \frac{2h_0 V\exp(-\alpha_j t)}{L^2(\alpha_j^2+V^2)^3}\{\exp(\alpha_j t)\cos(Q_s t)[Q_s^2(2\alpha_j tV-\alpha_j L+2V)+\alpha_j^2(2\alpha_j tV-\alpha_j L-2V)]$$
$$-Q_s\exp(\alpha_j t)\sin(Q_s t)[Q_s^2(L-Vt)+\alpha_j(\alpha_j L-2\alpha_j tV+4V)]\ \} \quad \text{(A-27)}$$

Due to static weight of vehicle $(0 \le t \le L/V)$

$$I_{jk5} = e_x \frac{\exp(-\alpha_j t)\,gL(m_v+m_w)}{L^2\alpha_j^2+k^2\pi^2V^2}\left[R_k L+\exp(-\alpha_j t)\{R_k L\cos(R_k t)+L\alpha_j\sin(R_k t)\}\right]$$

(A-28)

APPENDIX B

The integral I_{jk} for Model-2

Expression of the Integral I_{jk} given in Eq. (4.77) for generating response sample are given as follows

The vector $\{F(t)\}$ needed to perform the integration is given below:

$$F_j(t) = 0 \quad \text{For } j=1,2,3,\ldots, n_v$$

$$= k_{tj-n_v} h(x_{j-n_v}) + c_{tj-n_v} \dot{h}(x_{j-n_v})$$

For $j=n_v+1,\ n_v+2$

$$= k_{t1} h(x_1)\phi_{b(j-r)}(x_1) + k_{t2} h(x_2)\phi_{b(j-r)}(x_2) + c_{t1}\dot{h}(x_1)\phi_{b(j-r)}(x_1) + c_{t2}\dot{h}(x_2)\phi_{b(j-r)}(x_2)$$
$$- g(\frac{1}{2}m_v l_v + m_{w1})\phi_{b(j-r)}(x_1) - g(\frac{1}{2}m_v l_v + m_{w2})\phi_{b(j-r)}(x_2)$$

For $j=r+1,\ r+2,\ldots,\ r+n_b$, where $r = n_v+2$

$$= e_x\{-k_{t1} h(x_1)\phi_{t(j-p-n_b)}(x_1) - k_{t2} h(x_2)\phi_{t(j-p-n_b)}(x_2) - c_{t1}\dot{h}(x_1)\phi_{t(j-p-n_b)}(x_1)$$
$$- c_{t2}\dot{h}'(x_2)\phi_{t(j-p-n_b)}(x_2)\} + e_x g(\frac{1}{2}m_v l_v + m_{w1})\phi_{t(j-p-n_b)}(x_1)$$
$$+ e_x g(\frac{1}{2}m_v l_v + m_{w2})\phi_{t(j-p-n_b)}(x_2)$$

For $j=p+1,\ p+2,\ldots,\ p+n_T$, where $p = 2+ n_v+n_b$

(B-1)

where, $\dot{h}(x) = \frac{dh(x)}{dx} \times \frac{dx}{dt} = Vh'(x)$, $h'(x) = \frac{dh(x)}{dx}$ and V is the speed of vehicle.

If $k=1,2,3\ldots n_v$

$$I_{jk} = 0 \tag{B-2}$$

For $k = n_v+1$

Splitting the integral I_{jk} into four components, we get

$$I_{jk} = \sum_{a=1}^{4} I_{j(nv+1)_a} \tag{B-3}$$

The components of Eq. (B-3) can be written as

For random surface unevenness of bridge deck

When $0 \le t \le L/V$

$$I_{j(nv+1)_1} = k_{t1}[\sum_{s=1}^{N} A_s \frac{\exp(-\alpha_j t)}{\alpha_j^2 + (B_s V)^2}\{-\alpha_j \cos(\theta_s) - B_s V \sin(\theta_s) + \exp(\alpha_j t)[\alpha_j \cos(B_s V t + \theta_s) + B_s V \cos(B_s V t + \theta_s)]\}] \quad \text{(B-4)}$$

$$I_{j(nv+1)_2} = c_{t1}[\sum_{s=1}^{N} V A_s B_s \frac{\exp(-\alpha_j t)}{\alpha_j^2 + (B_s V)^2}\{-\alpha_j \sin(\theta_s) - B_s V \cos(\theta_s) + \exp(\alpha_j t)[\alpha_j \sin(B_s V t + \theta_s) - B_s V \sin(B_s V t + \theta_s)]\}] \quad \text{(B-5)}$$

For deterministic mean surface profile (parabolic pre-cambering and approach road settlement)

If $0 \le t \le L_r / V$

$$I_{j(nv+1)_3} = k_{t1}[\frac{4h_0 V}{\alpha_j^3 L^2}\{\alpha_j L(\alpha_j t + \exp(-\alpha_j t) - 1)\} - \frac{V}{\alpha_j^3 L^2}\{\alpha_j t(\alpha_j t - 2) - 2\exp(-\alpha_j t) + 2)\}] + k_{t1}\frac{h_1 V}{\alpha_j^2 L_r}\{\alpha_j t + \exp(-\alpha_j t) - 1\} \quad \text{(B-6)}$$

$$I_{j(nv+1)_4} = c_{t1}[\frac{4h_0 V \exp(-\alpha_j t)}{\alpha_j^3 L^2}\{2V[(\alpha_j t - 1)\exp(-\alpha_j t) - 1]\} + \frac{1}{\alpha_j L}\{\exp(\alpha_j t) + 2\}] + c_{t1}\frac{h_1 V}{\alpha_j L_r}\{1 - \exp(-\alpha_j t)\} \quad \text{(B-7)}$$

For $L_r / V < t \le L/V$

$$I_{j(nv+1)_3} = k_{t1}[\frac{4h_0 V}{\alpha_j^3 L^2}\{\alpha_j L(\alpha_j t + \exp(-\alpha_j t) - 1)\} - \frac{V}{\alpha_j^3 L^2}\{\alpha_j t(\alpha_j t - 2) - 2\exp(-\alpha_j t) + 2)\}] + k_t\frac{h_1 V}{\alpha_j^2 L_r}\{1 - \exp(-\alpha_j t)\} \quad \text{(B-8)}$$

$$I_{j(nv+1)_4} = c_{t1}[\frac{4h_0 V \exp(-\alpha_j t)}{\alpha_j^3 L^2}\{2V[(\alpha_j t - 1)\exp(-\alpha_j t) - 1]\} + \frac{1}{\alpha_j L}\{\exp(\alpha_j t) + 2\}] \quad \text{(B-9)}$$

When $k = n_v+2$

Splitting the integral I_{jk} into four components, we get

$$I_{j(nv+2)} = \sum_{a=1}^{4} I_{j(nv+2)a} \tag{B-10}$$

Components of Eq. (B-10) can be written as

For random surface unevenness of bridge deck

If $0 \le t \le L/V$

$$\begin{aligned} I_{j(nv+2)_1} = k_{t2}[\sum_{s=1}^{N} A_s \frac{\exp(-\alpha_j t)}{\alpha_j^2 + (B_s V)^2}\{-\alpha_j \cos(B_s l_v - \theta_s) - B_s V \sin(B_s l_v - \theta_s) + \\ \exp(\alpha_j t)[\alpha_j \cos(B_s (l - Vt) - \theta_s) + B_s V \sin(B_s (l_v - Vt) + \theta_s)] \\ + V^2[2 - \exp(\alpha_j t)\{\alpha_j t(\alpha_j t - 2) + 2\}]\}] \end{aligned} \tag{B-11}$$

$$\begin{aligned} I_{j(nv+2)_2} = c_{t2}[\sum_{s=1}^{N} A_s B_s V \frac{\exp(-\alpha_j t)}{\alpha_j^2 + (B_s V)^2}\{\alpha_j \sin(B_s l_v - \theta_s) + B_s V \cos(B_s l_v - \theta_s) \\ - \exp(\alpha_j t)[\alpha_j \sin(B_s (l_v - Vt) - \theta_s) + B_s V \cos(B_s (l_v - Vt) + \theta_s)] \end{aligned} \tag{B-12}$$

For deterministic mean surface profile (parabolic pre-cambering and approach road settlement)

For $0 \le t \le L_r / V$

$$\begin{aligned} I_{j(nv+2)_3} = k_{t2} \frac{4h_0 V \exp(-\alpha_j t)}{\alpha_j^3 L^2}\{2V[\exp(\alpha_j t)(\alpha_j t - 1) + 1] - \alpha_j (2l_v + L)(\exp(\alpha_j t) - 1)\} \\ + k_{t2} \frac{h_1 \exp(-\alpha_j t)}{\alpha_j^2 L_r}[V\{1 + \exp(\alpha_j t)(\alpha_j t - 1)\} - \alpha_j l_v (\exp(\alpha_j t) - 1)] \end{aligned} \tag{B-13}$$

$$\begin{aligned} I_{j(nv+2)_4} = c_{t2}[\frac{4h_0}{\alpha_j^3 L^2}\{-\alpha_j^2 l_v (l_v + L)(\exp(\alpha_j t) - 1\} \\ + \alpha_j V (2l_v + L)\{\exp(\alpha_j t)(\alpha_j t - 1) + 1\}] + c_{t2} \frac{h_1 V}{\alpha_j L_r}\{1 - \exp(\alpha_j t)\} \end{aligned} \tag{B-14}$$

If $L_r / V < t \le L/V$

$$\begin{aligned} I_{j(nv+2)_3} = k_{t2} \frac{4h_0 V \exp(-\alpha_j t)}{\alpha_j^3 L^2}\{2V[\exp(\alpha_j t)(\alpha_j t - 1) + 1] - \alpha_j (2l_v + L)(\exp(\alpha_j t) - 1)\} \\ + k_{t2} \frac{h_1}{\alpha_j}\{1 - \exp(\alpha_j t)\} \end{aligned} \tag{B-15}$$

$$I_{j(nv+2)_4} = c_{t2}[\frac{4h_0}{\alpha_j^3 L^2}\{-\alpha_j^2 l_v (l_v + L)(\exp(\alpha_j t) - 1\} + \alpha_j V(2l_v + L)\{\exp(\alpha_j t)(\alpha_j t - 1) + 1\}] \quad \text{(B-16)}$$

For k=1+r, 2+r,…., r+n_b, where r =2+n_v

$$I_{jk} = \sum_{a=1}^{5}\sum_{b=1}^{2} I_{jk\,ab} \quad \text{(B-17)}$$

Introducing the following parameters

$$R_k = (k-r)\pi V / L; S_k = (k-r)\pi / L; Z_s = l_v B_s$$

The components of the Eq. (B-17) are as follows

<u>For random surface unevenness of bridge deck</u>

For $0 \le t \le L/V$

$$I_{jk\,11} = \frac{1}{2} k_{t1} \sum_{s=1}^{N} A_s \left\{ \frac{2R_k \exp(-\alpha_j t)\{(\alpha_j^2 - Q_s^2 + R_k^{\,2})\cos(\theta_s) + 2\alpha_j Q_s \sin(\theta_s)\}}{\{\alpha_j^2 + (Q_s - R_k)^2\}\{\alpha_j^2 + (Q_s + R_k)^2\}} - \frac{\alpha_j \sin\{(Q_s - R_k)t + \theta_s\} + (R_k - Q_s)\cos\{(Q_s - R_k)t + \theta_s\}}{\{\alpha_j^2 + (Q_s - R_k)^2\}} + \frac{\alpha_j \sin\{(Q_s + R_k)t + \theta_s\} - (R_k + Q_s)\cos\{(Q_s + R_k)t + \theta_s\}}{\{\alpha_j^2 + (Q_s + R_k)^2\}} \right\} \quad \text{(B-18)}$$

$$I_{jk\,12} = \frac{1}{2} k_{t2} \sum_{s=1}^{N} A_s \left[\exp(-\alpha_j t) \left\{ \frac{(R_k + Q_s)\cos(S_s - Z_s - \theta_s) + \alpha_j \sin(S_k - Z_s - \theta_s)\}}{\{\alpha_j^2 + (Q_s - R_k)^2\}} - \frac{(R_k - Q_s)\cos(S_k - Z_s + \theta_s) + \alpha_j \sin(S_k - Z_s + \theta_s)\}}{\{\alpha_j^2 + (Q_s - R_s)^2\}} \right\} - \frac{\alpha_j \sin\{(Q_s - R_k)t + S_k - Z_s + \theta_s\} - (R_k + Q_s)\cos\{(Q_s - R_k)t + S_k - Z_s + \theta_s\}}{\{\alpha_j^2 + (Q_s - R_s)^2\}} + \frac{\alpha_j \sin\{S_k + Z_s - (Q_s + R)t - \theta_s\} + (R_k + Q_s)\cos\{S_k + Z_s + (Q_s + R_k)t - \theta_s\}}{\{\alpha_j^2 + (Q_s + R_k)^2\}} \right] \quad \text{(B-19)}$$

$$I_{jk\,21} = \frac{1}{2} c_{t1} \sum_{s=1}^{N} A_s Q_s \left\{ - \frac{2R_k \exp(-\alpha_j t)\{(\alpha_j^2 - Q_s^2 + R_k{}^2)\sin(\theta_s) - 2\alpha_j Q_s \cos(\theta_s)\}}{\{\alpha_j^2 + (Q_s - R)^2\}\{\alpha_j^2 + (Q_s + R_k)^2\}} \right.$$
$$- \frac{\alpha_j \cos\{(Q_s - R_k)t + \theta_s\} + (R_k - Q_s)\sin\{(Q_s - R_k)t + \theta_s\}}{\{\alpha_j^2 + (Q_s - R_k)^2\}} \qquad \text{(B-20)}$$
$$\left. + \frac{\alpha_j \cos\{(Q_s + R_k)t + \theta_s\} + (R_k + Q_s)\sin\{(Q_s + R_k)t + \theta_s\}}{\{\alpha_j^2 + (Q_s + R_k)^2\}} \right\}$$

$$I_{jk\,22} = \frac{1}{2} c_{t2} \sum_{s=1}^{N} A_s Q_s \left[\exp(-\alpha_j t) \left\{ \frac{(R_k + Q_s)\sin(S_k + Z_s - \theta_s) - \alpha_j \cos(S_k + Z_s - \theta_s)\}}{\{\alpha_j^2 + (Q_s - R_k)^2\}} \right. \right.$$
$$\left. + \frac{(Q_s - R_k)\sin(S_k - Z_s + \theta_s) + \alpha_j \cos(S_k - Z_s + \theta_s)\}}{\{\alpha_j^2 + (Q_s - R)^2\}} \right\} \qquad \text{(B-21)}$$
$$+ \frac{\alpha_j \cos\{S_k + Z_s - (Q_s + R_k)t - \theta_s\} - (R_k + Q_s)\sin\{S_k + Z_s - (Q_s + R_k)t - \theta_s\}}{\{\alpha_j^2 + (Q_s + R_k)^2\}}$$
$$\left. - \frac{\alpha_j \cos\{S_k - Z_s + (Q_s - R_k)t + \theta_s\} + (Q_s - R_k)\sin\{S_k - Z_s + (Q_s - R_k)t + \theta_s\}}{\{\alpha_j^2 + (Q_s - R_k)^2\}} \right]$$

<u>For deterministic mean surface profile (parabolic pre-cambering and approach road settlement)</u>

When $0 \le t \le L_r / V$

$$I_{jk\,31} = \frac{1}{2} k_{t1} \left[\frac{4h_0 V \exp(-\alpha_j t)}{L^2(\alpha_j^2 + Q_s^2)^3} \{L(\alpha_j^2 + Q_s^2)[\exp(\alpha_j t)\sin(Q_s t)\{Q_s^2(\alpha_j t + 1) + \alpha_j^2(\alpha_j t - 1)\}] \right.$$
$$- Q_s \exp(\alpha_j t)\cos(Q_s t)[Q_s^2 t + \alpha_j(\alpha_j t - 2)] - 2\alpha_j Q_s \}$$
$$+ V(2Q_s^3 + Q_s \exp(\alpha_j t))\cos(Q_s t) \ \{ Q_s^4 t^2 + 2Q_s^2(\alpha_j^2 t^2 - 2\alpha_j t - 1) + \alpha_j^2(\alpha_j^2 t^2 - 4\alpha_j t + 6)\} \qquad \text{(B-22)}$$
$$- \exp(\alpha_j t)\sin(Q_s t)\{Q_s^4(\alpha_j t + 2) + \alpha_j Q_s^2(\alpha_j^2 t^2 - 3) + \alpha_j^3(\alpha_j^2 t^2 - 2\alpha_j t + 2)\} - 6\alpha_j^2 Q_s \ ]$$
$$+ k_{t1} \frac{\exp(-\alpha_j t) h_1 L V}{L L_r (R_k^2 + \alpha_j^2)} [2L^3 \alpha_j + \exp(-\alpha_j t)\{-R_k L[R_k^2 L^2 t + L^2 \alpha_j(\alpha_j t - 2)]\cos(R_k t)$$
$$\left. + L\{L^2 \alpha_j^2(\alpha_j t - 1) + R_k^2 L^2 t(\alpha_j t + 1)\}\sin(R_k t)\}] \right]$$

$$
\begin{aligned}
I_{jk32} = -\frac{1}{2}k_{t2}\Big[\ & \frac{4h_0V}{L^2(\alpha_j^2+V^2)^3}\Big\{\sin(Vt-l_v)\{[\alpha_j l_v^2(\alpha_j^2+V^2)^2 - l_v(\alpha_j^2+V^2)\{-\alpha_j^3 L-\alpha_j LV^2 \\
& +2V^3(\alpha_j t+1)+2\alpha_j^2V(\alpha_j t-1)\}+V[V\{2\alpha_j^3+\alpha_j t(\alpha_j^2+V^2)^2+2t(\alpha_j^4-V^4)-6\alpha_j V^2\} \\
& -L(\alpha_j^2+V^2)\{\alpha_j^2(\alpha_j t-1)+V^2(\alpha_j t+1)\}\}]+V\cos(l_v-Vt)[V^4(l_v^2+l_v L+2\alpha_j^2t^2-4\alpha_j t-2) \\
& +\alpha_j^2V^2(2l_v^2+2l_v L+4\alpha_j^2t^2+6)+\alpha_j^4 l_v(l_v+L)-V^5t(2l_v+L)(\alpha_j t-1) \\
& -\alpha_j^3V(2l_v+L)(\alpha_j t-2)+l_v^2V^6]\Big\}\Big] \\
& +k_{t2}\frac{\exp(-\alpha_j t)h_1LV}{LL_r(R_k^2+\alpha_j^2)}[R_k L\exp(-\alpha_j t)\{R_k^2L^2t+L^2\alpha_j(\alpha_j t-2)\}\cos(R_k t) \\
& +2R_k L^3\alpha_j-\exp(-\alpha_j t)\{L^3\alpha_j(\alpha_j t-1)+R_k^2L^2(\alpha_j t+1)\}\sin(R_k t) \\
& -R_k L^3 l_v(R_k^2+\alpha_j^2)\{1+\exp(\alpha_j t)\cos(R_k t)+\exp(\alpha_j t)L\alpha_j\sin(R_k t)\}]
\end{aligned}
\tag{B-23}
$$

$$
\begin{aligned}
I_{jk41} = -c_{t1}\frac{2h_0V\exp(-\alpha_j t)}{L^2(\alpha_j^2+V^2)^3}\Big\{ & \exp(\alpha_j t)\cos(Q_s t)[Q_s^2(2\alpha_j tV-\alpha_j L+2V)+\alpha_j^2(2\alpha_j tV-\alpha_j L-2V)] \\
& -Q_s\exp(\alpha_j t)\sin(Q_s t)[Q_s^2(L-Vt)+\alpha_j(\alpha_j L-2\alpha_j tV+4V)]\ \Big\} \\
& +c_{t1}\frac{h_1V}{LL_r(R_k^2+\alpha_j^2)}[R_k L\{\exp(-\alpha_j t)-\cos(R_k t)\}+L\alpha_j\sin(R_k t)]
\end{aligned}
\tag{B-24}
$$

$$
\begin{aligned}
I_{jk42} = -c_{t2}\frac{2h_0V\ \exp(-\alpha_j t)}{L^2(\alpha_j^2+V^2)^3}\Big\{ & \exp(\alpha_j t)\sin(Q_s t)[Q_s^2(2\alpha_j tV-\alpha_j L+2V) \\
& +\alpha_j^2(2\alpha_j tV-\alpha_j L-2V)] \\
& -Q_s\exp(\alpha_j t)\cos(Q_s t)[Q_s^2(L-Vt)+\alpha_j(\alpha_j L-2\alpha_j tV+4V)]\ \Big\} \\
& +c_{t2}\frac{h_1V}{LL_r(R_k^2+\alpha_j^2)}[R_k L\{\exp(-\alpha_j t)-\cos(R_k t)\}+L\alpha_j\sin(R_k t)]
\end{aligned}
\tag{B-25}
$$

If $L_r/V < t \le L/V$

$$
\begin{aligned}
I_{jk31} = \frac{1}{2}k_{t1}\Big[\ & \frac{4h_0V\exp(-\alpha_j t)}{L^2(\alpha_j^2+Q_s^2)^3}\Big\{L(\alpha_j^2+Q_s^2)[\exp(\alpha_j t)\sin(Q_s t)\{Q_s^2(\alpha_j t+1)+\alpha_j^2(\alpha_j t-1)\}] \\
& -Q_s\exp(\alpha_j t)\cos(Q_s t)[Q_s^2t+\alpha_j(\alpha_j t-2)]-2\alpha_j Q_s\Big\} \\
& +V(2Q_s^3+Q_s\exp(\alpha_j t))\cos(Q_s t)\ \{\ Q_s^4t^2+2Q_s^2(\alpha_j^2t^2-2\alpha_j t-1)+\alpha_j^2(\alpha_j^2t^2-4\alpha_j t+6)\} \\
& -\exp(\alpha_j t)\sin(Q_s t)\{Q_s^4(\alpha_j t+2)+\alpha_j Q_s^2(\alpha_j^2t^2-3)+\alpha_j^3(\alpha_j^2t^2-2\alpha_j t+2)\}-6\alpha_j^2Q_s\ \Big] \\
& +k_{t1}\frac{h_1V}{L\ (\alpha_j^2+R_k^2)}[R_k L\{\exp(-\alpha_j t)-\cos(R_k t)\}+L\alpha_j\sin(R_k t)]
\end{aligned}
\tag{B-26}
$$

$$I_{jk\,32} = -\frac{1}{2}k_{t2}\Big[\ \frac{4h_0V}{L^2(\alpha_j^2+V^2)^3}\Big\{\sin(Vt-l_v)\{[\alpha_j l_v^2(\alpha_j^2+V^2)^2 - l_v(\alpha_j^2+V^2)\{-\alpha_j^3 L-\alpha_j LV^2$$
$$+2V^3(\alpha_j t+1)+2\alpha_j^2V(\alpha_j t-1)\}+V[V\{2\alpha_j^3+\alpha_j t(\alpha_j^2+V^2)^2+2t(\alpha_j^4-V^4)-6\alpha_j V^2\}$$
$$-L(\alpha_j^2+V^2)\{\alpha_j^2(\alpha_j t-1)+V^2(\alpha_j t+1)\}\}]+V\cos(l_v-Vt)[V^4(l_v^2+l_vL+2\alpha_j^2t^2-4\alpha_j t-2) \quad \text{(B-27)}$$
$$+\alpha_j^2V^2(2l_v^2+2l_vL+4\alpha_j^2t^2+6)+\alpha_j^4l_v(l_v+L)-V^5t(2l_v+L)(\alpha_j t-1)$$
$$-\alpha_j^3V(2l_v+L)(\alpha_j t-2)+l_v^2V^6]\Big\}\Big]$$
$$+k_{t2}\frac{h_1V}{L\,(\alpha_j^2+R_k^2)}[R_kL\{\exp(-\alpha_j t)-\cos(R_k t)\}+L\alpha_j\sin(R_k t)]$$

$$I_{jk\,41} = -c_{t1}\frac{2h_0V\exp(-\alpha_j t)}{L^2(\alpha_j^2+V^2)^3}\Big\{\exp(\alpha_j t)\cos(Q_s t)[Q_s^2(2\alpha_j tV-\alpha_j L+2V)+\alpha_j^2(2\alpha_j tV-\alpha_j L-2V)] \quad \text{(B-28)}$$
$$-Q_s\exp(\alpha_j t)\sin(Q_s t)[Q_s^2(L-Vt)+\alpha_j(\alpha_j L-2\alpha_j tV+4V)]\ \Big\}$$

$$I_{jk\,42} = -c_{t2}\frac{2h_0V\exp(-\alpha_j t)}{L^2(\alpha_j^2+V^2)^3}\Big\{\exp(\alpha_j t)\sin(Q_s t)[Q_s^2(2\alpha_j tV-\alpha_j L+2V)$$
$$+\alpha_j^2(2\alpha_j tV-\alpha_j L-2V)] \quad \text{(B-29)}$$
$$-Q_s\exp(\alpha_j t)\cos(Q_s t)[Q_s^2(L-Vt)+\alpha_j(\alpha_j L-2\alpha_j tV+4V)]\ \Big\}$$

<u>For static weight of vehicle</u> $(0 \le t \le L/V)$

$$I_{jk\,51} = -\frac{\exp(-\alpha_j t)gL(l_vm_v+2m_{w1})}{2(L^2\alpha_j^2+R_k^2L)}[R_kL+\exp(\alpha_j t)\{k\pi V\cos(R_k t)+L\alpha_j\sin(R_k t)\}] \quad \text{(B-30)}$$

$$I_{jk\,52} = -\frac{\exp(-\alpha_j t)gL(l_vm_v+2m_{w2})}{2(L^2\alpha_j^2+R_k^2L)}[R_kL\{\cos(S_kl_v)-\exp(\alpha_j t)\cos[S_k(l_v-Vt)]\} \quad \text{(B-31)}$$
$$-L\alpha_j\{\sin(S_kl_v)-\exp(\alpha_j t)\sin[S_k(l_v-Vt)]\}]$$

For k=1+p, 2+p…., p+n_T, where, p = 2+n_v+n_b

The integral I_{jk} is split into ten components as

$$I_{jk} = \sum_{a=1}^{5}\sum_{b=1}^{2} I_{jk\,ab} \quad \text{(B-32)}$$

Take $R_k = (k-p)\pi V/L; S_k = (k-p)\pi/L$

The components of Eq. (B-32) can be expressed as

For random surface unevenness of bridge deck

When $0 \le t \le L/V$

$$I_{jk11} = -\frac{1}{2} k_{t1} e_x \sum_{s=1}^{N} A_s \exp(-\alpha_j t) \left\{ \frac{\alpha_j \cos(\theta_s) + (Q_s - R_k)\sin(\theta_s)}{\alpha_j^2 + (Q_s - R_k)^2} + \frac{\alpha_j \cos(\theta_s) + (Q_s + R_k)\sin(\theta_s)}{\alpha_j^2 + (Q_s + R_k)^2} \right.$$
$$+ \frac{\alpha_j \cos[(Q_s - R_k)t + \theta_s] + (Q_s - R_k)\sin[(Q_s - R_k)t - \theta_s]}{\alpha_j^2 + (Q_s - R_k)^2}$$
$$\left. + \frac{\alpha_j \cos[(Q_s + R_k)t + \theta_s] + (Q_s + R_k)\sin[(Q_s + R_k)t + \theta_s]}{\alpha_j^2 + (Q_s + R_k)^2} \right\} \quad \text{(B-33)}$$

$$I_{jk12} = -\frac{1}{2} k_{t2} e_x \sum_{s=1}^{N} \left[A_s \exp(-\alpha_j t) \left\{ \frac{\alpha_j \cos(B_s l_v - S_k - \theta_s) + (R_k - Q_s)\sin(B_s l_v - S_k - \theta_s)}{\alpha_j^2 + (Q_s - R)^2} \right.\right.$$
$$\left. + \frac{\alpha_j \cos(B_s l_v + S_k - \theta_s) + (R_k + Q_s)\sin(B_s l_v + S_k - \theta_s)}{\alpha_j^2 + (Q_s + R_k)^2} \right\} \quad \text{(B-34)}$$
$$+ \frac{\alpha_j \cos[(R_k - Q_s)t + (B_s l_v - S_k - \theta_s)] + (R_k - Q_s)\sin[-(Q_s + R_k)t + (B_s l_v + S_k - \theta_s)]}{\alpha_j^2 + (Q_s - R_k)^2}$$
$$\left. + \frac{\alpha_j \cos[-(R_k + Q_s)t + (B_s l_v + S_k - \theta_s)] - (R_k + Q_s)\sin[-(Q_s + R_k)t + (B_s l_v + S_k - \theta_s)]}{\alpha_j^2 + (Q_s + R_k)^2} \right]$$

$$I_{jk21} = \frac{1}{2} c_{t1} e_x \sum_{s=1}^{N} A_s \exp(-\alpha_j t) \left\{ \frac{\alpha_j \sin(\theta_s) + (Q_s - R_k)\cos(\theta_s)}{\alpha_j^2 + (Q_s - R_k)^2} + \frac{\alpha_j \sin(\theta_s) - (Q_s + R_k)\cos(\theta_s)}{\alpha_j^2 + (Q_s + R)^2} \right.$$
$$+ \frac{\alpha_j \sin[(Q_s - R_k)t + \theta_s] + (R_k - Q_s)\cos[(Q_s - R_k)t + \theta_s]}{\alpha_j^2 + (Q_s - R)^2} \quad \text{(B-35)}$$
$$\left. + \frac{\alpha_j \sin[(Q_s + R_k)t + \theta_s] - (Q_s + R)\sin[(Q_s + R_k)t + \theta_s]}{\alpha_j^2 + (Q_s + R_k)^2} \right\}$$

$$I_{jk22} = \frac{1}{2} c_{t2} e_x \sum_{s=1}^{N} \left[A_s Q_s \exp(-\alpha_j t) \left\{ \frac{\alpha_j \cos(B_s l_v - S_k - \theta_s) + (Q_s - R_k)\sin(B_s l_v - S_k - \theta_s)}{\alpha_j^2 + (Q_s - R_k)^2} \right.\right.$$
$$\left. + \frac{\alpha_j \sin(B_s l_v + S_k - \theta_s) + (R_k + Q_s)\cos(B_s l_v + S_k - \theta_s)}{\alpha_j^2 + (Q_s + R_k)^2} \right\} \quad \text{(B-36)}$$
$$- \frac{\alpha_j \sin[(R - Q_s)t + (B_s l_v - S_k - \theta_s)] + (Q_s - R_k)\cos[(R_k - Q_s)t + (B_s l_v - S_k - \theta_s)]}{\alpha_j^2 + (Q_s - R_k)^2}$$
$$\left. - \frac{\alpha_j \sin[-(R + Q_s)t + (B_s l_v + S_k - \theta_s)] + (R_k + Q_s)\cos[-(Q_s + R_k)t + (B_s l_v + S_k - \theta_s)]}{\alpha_j^2 + (Q_s + R_k)^2} \right]$$

For deterministic mean surface profile (parabolic pre-cambering and approach road settlement)

If $0 \le t \le L_r / V$

$$
\begin{aligned}
I_{jk\,31} = {} & \frac{4k_{t1}e_x h_0 L}{V(\alpha_j^2 + R_k{}^2)^3}\Big[(\alpha_j^2 + R_k{}^2)\exp(-\alpha_j t)\Big\{\alpha_j^2 + \exp(-\alpha_j t)\cos(R_k t)[R_k{}^2(\alpha_j t + 1) + \alpha_j^2(\alpha_j t - 1)] \\
& + R_k \exp(\alpha_j t)\sin(R_k t)[R_k{}^2 t + \alpha_j(\alpha_j t - 2)] - R_k{}^2\Big\} + 2\alpha_j \exp(-\alpha_j t)(\alpha_j^2 + 3R_k{}^2) \\
& + R_k \sin(R_k t)\Big\{6\alpha_j^2 + t^2(\alpha_j^2 + R_k{}^2)^2 + 4\alpha_j t(\alpha_j^2 + R_k{}^2) - 2R_k{}^2\Big\} \\
& + \cos(R_k t)\Big\{2t(R_k{}^4 - \alpha_j^4) + 2\alpha_j(\alpha_j^2 - 3R_k{}^2)\alpha_j t^2(\alpha_j^2 + R_k{}^2)^2\Big\}\Big] \\
& + k_{t1}\frac{\exp(-\alpha_j t)h_1 LV}{L L_r(R_k^2 + \alpha_j^2)} e_x[2L^3\alpha_j + \exp(-\alpha_j t)\{R_k L[R_k^2 L^2 t + L^2\alpha_j(\alpha_j t - 2)]\sin(R_k t) \\
& - L\exp(-\alpha_j t)\{L^2\alpha_j^2(\alpha_j t - 1) + R_k^2 L^2 t(\alpha_j t + 1)\}\cos(R_k t)\}]
\end{aligned}
\tag{B-37}
$$

$$
\begin{aligned}
I_{jk\,32} = {} & \frac{4k_{t2}e_x h_0}{L^2}\Bigg[\Bigg\{\frac{l_v(l_v + L)\exp(-\alpha_j t)\{\alpha_j\cos(S_k - R_k t) - R_k\sin(S_k - R_k t)\} + R_k\sin(S_k) - \alpha_j\cos(S_k)}{\alpha_j^2 + R_k{}^2}\Bigg\} \\
& + \frac{2LV\exp(-\alpha_j t)}{(\alpha_j^2 + R_k{}^2)^2}\Big\{(\alpha_j^2 + R_k{}^2)\cos(S_k) + \exp(\alpha_j t)\cos(S_k - R_k t)[R^2(\alpha_j t + 1) + \alpha_j^2(\alpha_j t - 1)] \\
& \qquad + R_k[R_k{}^2 t + \alpha_j(\alpha_j t - 2)]\sin(S_k - R_k t) - 2\alpha_j R_k\sin(S_k)\Big\} \\
& - \frac{V^2}{(\alpha_j^2 + R_k{}^2)^3}\Big\{R_k\sin(S_k - R_k t)[6\alpha_j^2 + t^2(\alpha_j^2 + R_k{}^2)^2 - 4\alpha_j t(\alpha_j^2 + R_k{}^2) - 2R_k{}^2] \\
& \qquad + 2\exp(-\alpha_j t)[(\alpha_j^3 - 3\alpha_j R_k{}^2)\cos(S_k) + R_k(R_k{}^2 - 3\alpha_j^2)\sin(S_k)] \\
& \qquad - [2t(R_k{}^4 - \alpha_j^4) + 2\alpha_j(\alpha_j^2 - 3R_k{}^2) + \alpha_j t^2(\alpha_j^2 + R_k{}^2)^2]\cos(S_k - R_k t)\Big\}\Bigg] \\
& + k_{t2}\frac{\exp(-\alpha_j t)h_1 LV}{L L_r(R_k^2 + \alpha_j^2)} e_x[-R_k L\exp(-\alpha_j t)\{R_k^2 L^2 t + L^2\alpha_j(\alpha_j t - 2)\}\sin(R_k t) \\
& - 2R_k L^3\alpha_j - \exp(-\alpha_j t)\{L^3\alpha_j(\alpha_j t - 1) + R_k^2 L^2(\alpha_j t + 1)\}\cos(R_k t) \\
& + R_k L^3 l_v(R_k^2 + \alpha_j^2)\{1 + \exp(\alpha_j t)\cos(R_k t) + \exp(\alpha_j t)L\alpha_j\cos(R_k t)\}]
\end{aligned}
\tag{B-38}
$$

$$
\begin{aligned}
I_{jk\,41} = {} & \frac{4c_{t1}e_x h_0 L}{(\alpha_j^2 + R_k{}^2)^3}\left(\frac{V}{L}\right)^2\Big[(\alpha_j^2 + R_k{}^2)\{\alpha_j\cos(R_k t)\} + R_k\sin(R_k t) - \alpha_j\exp(-\alpha_j t)\} \\
& + 2\exp(-\alpha_j t)\Big\{\alpha_j^2 + \exp(\alpha_j t)\cos(R_k t)[R_k{}^2(\alpha_j t + 1) + \alpha_j^2(\alpha_j t - 1)] \\
& + R_k\exp(\alpha_j t)\sin(R_k t)[R_k{}^2 t + \alpha_j(\alpha_j t - 2)] - R_k{}^2\Big\}\Big] \\
& + c_{t1}\frac{h_1 V}{L L_r(R_k^2 + \alpha_j^2)} e_x[R_k L\{\exp(-\alpha_j t) + \sin(R_k t)\} - L\alpha_j\cos(R_k t)]
\end{aligned}
\tag{B-39}
$$

$$I_{jk\,42}=\frac{4c_{t2}e_x h_0}{V(\alpha_j^2+R_k{}^2)^2}\Big[-R_k\sin(S_k-R_kt)\{l_v(\alpha_j^2+R_k{}^2)+L(\alpha_j^2+R_k{}^2)-2V[R_k{}^2t+\alpha_j(\alpha_jt-2)]\}$$
$$+\cos(S_k-R_kt)\{R_k{}^2[\alpha_j(l_v+L)-2V(\alpha_jt+1)]+\alpha_j^2[\alpha_j(l_v+L)+2V(1-\alpha_jt)]\}$$
$$+\exp(-\alpha_jt)\Big\{R_k\sin(S_k)[l_v(\alpha_j^2+R_k{}^2)+L(\alpha_j^2+R_k{}^2)+4\alpha_jV]$$
$$+\cos(S_k)[R_k{}^2\{2V-\alpha_j(l_v+L)\}-\alpha_j^2\{\alpha_j(l_v+L)+2V\}]\Big\}\Big]$$
$$+c_{t2}\frac{h_1V}{LL_r(R_k^2+\alpha_j^2)}e_x[R_kL\{\exp(-\alpha_jt)+\sin(R_kt)\}-L\alpha_j\cos(R_kt)]$$

(B-40)

When $L_r/V<t\le L/V$

$$I_{jk\,31}=\frac{4k_{t1}e_x h_0L}{V(\alpha_j^2+R_k{}^2)^3}\Big[(\alpha_j^2+R_k{}^2)\exp(-\alpha_jt)\Big\{\alpha_j^2+\exp(-\alpha_jt)\cos(R_kt)[R_k{}^2(\alpha_jt+1)+\alpha_j^2(\alpha_jt-1)]$$
$$+R_k\exp(\alpha_jt)\sin(R_kt)[R_k{}^2t+\alpha_j(\alpha_jt-2)]-R_k{}^2\Big\}+2\alpha_j\exp(-\alpha_jt)(\alpha_j^2+3R_k{}^2)$$
$$+R_k\sin(R_kt)\Big\{6\alpha_j^2+t^2(\alpha_j^2+R_k{}^2)^2+4\alpha_jt(\alpha_j^2+R_k{}^2)-2R_k{}^2\Big\}$$
$$+\cos(R_kt)\Big\{2t(R_k{}^4-\alpha_j^4)+2\alpha_j(\alpha_j^2-3R_k{}^2)\alpha_jt^2(\alpha_j^2+R_k{}^2)^2\Big\}\Big]$$
$$+k_{t1}\frac{\exp(-\alpha_jt)h_1LV}{LL_r(R_k^2+\alpha_j^2)}e_x[2L^3\alpha_j-\exp(-\alpha_jt)\{-R_kL[R_k^2L^2t+L^2\alpha_j(\alpha_jt-2)]\sin(R_kt)$$
$$-L\exp(-\alpha_jt)\{L^2\alpha_j^2(\alpha_jt-1)+R_k^2L^2t(\alpha_jt+1)\}\cos(R_kt)\}]$$

(B-41)

$$I_{jk\,32}=\frac{4k_{t2}e_x h_0}{L^2}\Big[\Big\{\frac{l_v(l_v+L)\exp(-\alpha_jt)\{\alpha_j\cos(S_k-R_kt)-R_k\sin(S_k-R_kt)\}+R_k\sin(S_k)-\alpha_j\cos(S_k)}{\alpha_j^2+R_k{}^2}\Big\}$$
$$+\frac{2LV\exp(-\alpha_jt)}{(\alpha_j^2+R_k{}^2)^2}\Big\{(\alpha_j^2+R_k{}^2)\cos(S_k)+\exp(\alpha_jt)\cos(S_k-R_kt)[R^2(\alpha_jt+1)+\alpha_j^2(\alpha_jt-1)]$$
$$+R_k[R_k{}^2t+\alpha_j(\alpha_jt-2)]\sin(S_k-R_kt)-2\alpha_jR_k\sin(S_k)\Big\}$$
$$-\frac{V^2}{(\alpha_j^2+R_k{}^2)^3}\Big\{R_k\sin(S_k-R_kt)[6\alpha_j^2+t^2(\alpha_j^2+R_k{}^2)^2-4\alpha_jt(\alpha_j^2+R_k{}^2)-2R_k{}^2]$$
$$+2\exp(-\alpha_jt)[(\alpha_j^3-3\alpha_jR_k{}^2)\cos(S_k)+R_k(R_k{}^2-3\alpha_j^2)\sin(S_k)]$$
$$-[2t(R_k{}^4-\alpha_j^4)+2\alpha_j(\alpha_j^2-3R_k{}^2)+\alpha_jt^2(\alpha_j^2+R_k{}^2)^2]\cos(S_k-R_kt)\Big]$$
$$+k_{t2}\frac{\exp(-\alpha_jt)h_1LV}{LL_r(R_k^2+\alpha_j^2)}e_x[-R_kL\exp(-\alpha_jt)\{R_k^2L^2t+L^2\alpha_j(\alpha_jt-2)\}\sin(R_kt)$$
$$-2R_kL^3\alpha_j-\exp(-\alpha_jt)\{L^3\alpha_j(\alpha_jt-1)+R_k^2L^2(\alpha_jt+1)\}\cos(R_kt)$$
$$+R_kL^3l_v(R_k^2+\alpha_j^2)\{1+\exp(\alpha_jt)\cos(R_kt)+\exp(\alpha_jt)L\alpha_j\cos(R_kt)\}]$$

(B-42)

$$I_{jk\,41} = \frac{4c_{t1}e_x h_0 L}{(\alpha_j^2 + R_k{}^2)^3}\left(\frac{V}{L}\right)^2 \Big[(\alpha_j^2 + R_k{}^2)\{\alpha_j \cos(R_k t)\} + R_k \sin(R_k t) - \alpha_j \exp(-\alpha_j t)\}$$
$$+ 2\exp(-\alpha_j t)\{\alpha_j^2 + \exp(\alpha_j t)\cos(R_k t)[R_k{}^2(\alpha_j t + 1) + \alpha_j^2(\alpha_j t - 1)] \quad \text{(B-43)}$$
$$+ R_k \exp(\alpha_j t)\sin(R_k t)[R_k{}^2 t + \alpha_j(\alpha_j t - 2)] - R_k{}^2\}\Big]$$

$$I_{jk\,42} = \frac{4c_{t2}e_x h_0}{V(\alpha_j^2 + R_k{}^2)^2}\Big[-R_k \sin(S_k - R_k t)\{l_v(\alpha_j^2 + R_k{}^2) + L(\alpha_j^2 + R_k{}^2) - 2V[R_k{}^2 t + \alpha_j(\alpha_j t - 2)]\}$$
$$+ \cos(S_k - R_k t)\{R_k{}^2[\alpha_j(l_v + L) - 2V(\alpha_j t + 1)] + \alpha_j^2[\alpha_j(l_v + L) + 2V(1 - \alpha_j t)]\}$$
$$+ \exp(-\alpha_j t)\{R_k \sin(S_k)[l_v(\alpha_j^2 + R_k{}^2) + L(\alpha_j^2 + R_k{}^2) + 4\alpha_j V]$$
$$+ \cos(S_k)[R_k{}^2\{2V - \alpha_j(l_v + L)\} - \alpha_j^2\{\alpha_j(l_v + L) + 2V\}]\}\Big] \quad \text{(B-44)}$$

For static weight of vehicle ($0 \le t \le L/V$)

$$I_{jk\,51} = e_x \frac{\exp(-\alpha_j t)gL(l_v m_v + 2m_{w1})}{2(L^2\alpha_j^2 + R_k^2 L)}\left[\exp(\alpha_j t)R_k L\sin(R_k t) - L\alpha_j + \exp L\alpha_j(\alpha_j t)\cos(R_k t)\}\right] \quad \text{(B-45)}$$

$$I_{jk\,52} = e_x \frac{\exp(-\alpha_j t)gL(l_v m_v + 2m_{w2})}{2(L^2\alpha_j^2 + R_k^2 L)}\left[R_k L\{\sin(S_k l_v) - \exp(\alpha_j t)\sin[S_k(l_v - Vt)]\}\right.$$
$$\left. + e_x L\alpha_j\{\cos(S_k l_v) - \exp(\alpha_j t)\cos[S_k(l_v - Vt)]\}\right] \quad \text{(B-46)}$$

APPENDIX C

The integral I_{jk} for Model-3

Expression of the Integral I_{jk} given in Eq. (4.77) for generating response sample are given as follows

The vector $\{F(t)\}$ needed to perform the integration is given below:

$$F_j(t) = 0 \text{ For } j=1,2,3,\ldots, n_v+ n_{vT}$$

$$= k_{t11}h(x_{11}) + c_{t11}\dot{h}(x_{11}) \text{ For } j= n_v+n_{vT}+1$$

$$= k_{t21}h(x_{21}) + c_{t21}\dot{h}(x_{21}) \text{ For } j= n_v+n_{vT}+2$$

$$= k_{t12}h(x_{12}) + c_{t12}\dot{h}(x_{12}) \text{ For } j= n_v+n_{vT}+3$$

$$= k_{t22}h(x_{22}) + c_{t22}\dot{h}(x_{22}) \text{ For } j= n_v+n_{vT}+4$$

$$\begin{aligned}
&= k_{t11}h_1(x_1)\phi_{b(j-r)}(x_1) + k_{t21}h_2(x_1)\phi_{b(j-r)}(x_1) + c_{t11}\dot{h}_1(x_1)\phi_{b(j-r)}(x_1) + c_{t21}\dot{h}_2(x_1)\phi_{b(j-r)}(x_1) \\
&\quad + k_{t12}h_1(x_2)\phi_{b(j-r)}(x_2) + k_{t22}h_2(x_2)\phi_{b(j-r)}(x_2) + c_{t12}\dot{h}_1(x_2)\phi_{b(j-r)}(x_2) + c_{t22}\dot{h}_2(x_2)\phi_{b(j-r)}(x_2) \\
&\quad - g(\frac{1}{4}m_v l_v + m_{w11})\phi_{b(j-r)}(x_1) - g(\frac{1}{4}m_v l_v + m_{w21})\phi_{b(j-r)}(x_1) \\
&\quad - g(\frac{1}{4}m_v l_v + m_{w12})\phi_{b(j-r)}(x_2) - g(\frac{1}{4}m_v l_v + m_{w22})\phi_{b(j-r)}(x_2)
\end{aligned}$$

For $j= r+1, r+2,\ldots, r+n_b$, where, $r = n_v+n_{vT}+4$

$$\begin{aligned}
&= k_{t11}(b_1 - e_x)h_1(x_1)\phi_{T(j-p)}(x_1) - k_{t21}(b_2 + e_x)h_2(x_1)\phi_{T(j-p)}(x_1) \\
&\quad + c_{t11}(b_1 - e_x)\dot{h}_1(x_1)\phi_{T(j-p)}(x_1) - c_{t21}(b_2 + e_x)\dot{h}_2(x_1)\phi_{T(j-p)}(x_1) \\
&\quad + k_{t12}(b_1 - e_x)h_1(x_2)\phi_{T(j-p)}(x_2) - k_{t22}(b_2 + e_x)h_2(x_2)\phi_{T(j-p)}(x_2) \\
&\quad + c_{t12}(b_1 - e_x)\dot{h}_1(x_2)\phi_{T(j-p)}(x_2) - c_{t22}(b_2 + e_x)\dot{h}_2(x_2)\phi_{T(j-p)}(x_2) \\
&\quad - g(\frac{1}{4}m_v l_v + m_{w11})(b_1 - e_x)\phi_{T(j-p)}(x_1) + g(\frac{1}{4}m_v l_v + m_{w21})(b_2 + e_x)\phi_{T(j-p)}(x_1) \\
&\quad - g(\frac{1}{4}m_v l_v + m_{w12})(b_1 - e_x)\phi_{T(j-p)}(x_2) + g(\frac{1}{4}m_v l_v + m_{w22})(b_2 + e_x)\phi_{T(j-p)}(x_2)
\end{aligned}$$

For $j= p+1, p+2,\ldots, p+n_T$, where, $p = n_v+n_{vT}+4+n_b$

(C-1)

If $k=1,2,3,\ldots, n_v+n_{vT}$

$$I_{jk} = 0 \tag{C-2}$$

When $k= n_v+n_{vT}+1$, The integral I_{jk} is split into four components as

$$I_{jk} = \sum_{a=1}^{2}\sum_{b=1}^{2} I_{jk\,ab} \tag{C-3}$$

Taking $A_{1s} = \sqrt{2S_{GG1}(V\Omega_s)^{-2}}$ and $A_{2s} = \sqrt{2S_{GG2}(V\Omega_s)^{-2}}$, the components of Eq. (C-3) has been expressed for random unevenness and deterministic roughness separately as follows

<u>For random surface unevenness of bridge deck</u>

When $0 \le t \le L/V$

$$I_{jk\,11} = k_{t11}[\sum_{s=1}^{N} A_{1s}\frac{\exp(-\alpha_j t)}{\alpha_j^2 + (B_s V)^2}\{-\alpha_j \cos(\theta_{1s}) - B_s V \sin(\theta_{1s}) + \exp(\alpha_j t)[\alpha_j \cos(B_s V t + \theta_{1s}) + B_s V \cos(B_s V t + \theta_{1s})]\}] \tag{C-4}$$

$$I_{jk\,12} = c_{t11}[\sum_{s=1}^{N} V A_{1s} B_s \frac{\exp(-\alpha_j t)}{\alpha_j^2 + (B_s V)^2}\{-\alpha_j \sin(\theta_{1s}) - B_s V \cos(\theta_{1s}) + \exp(\alpha_j t)[\alpha_j \sin(B_s V t + \theta_{1s}) - B_s V \sin(B_s V t + \theta_{1s})]\}] \tag{C-5}$$

<u>For deterministic mean surface profile (parabolic pre-cambering and approach road settlement)</u>

If $0 \le t \le L_r/V$

$$I_{jk\,21} = k_{t11}[\frac{4h_0 V}{\alpha_j^3 L^2}\{\alpha_j L(\alpha_j t + \exp(-\alpha_j t) - 1)\} - \frac{V}{\alpha_j^3 L^2}\{\alpha_j t(\alpha_j t - 2) - 2\exp(-\alpha_j t) + 2)\}] + k_{t11}\frac{h_1 V}{\alpha_j^2 L_r}\{\alpha_j t + \exp(-\alpha_j t) - 1\} \tag{C-6}$$

$$I_{jk\,22} = c_{t11}[-\frac{4h_0 V \exp(-\alpha_j t)}{\alpha_j^3 L^2}\{2V[\exp(-\alpha_j t)(\alpha_j t - 1) + 1]\} - \frac{1}{\alpha_j L}\{\exp(\alpha_j t) - 2\}] + c_{t11}\frac{h_1 V}{\alpha_j L_r}\{1 - \exp(-\alpha_j t)\} \tag{C-7}$$

For $L_r/V < t \le L/V$

$$I_{jk\,21} = k_{t11}[\frac{4h_0 V}{\alpha_j^3 L^2}\{\alpha_j L(\alpha_j t + \exp(-\alpha_j t) - 1)\} - \frac{V}{\alpha_j^3 L^2}\{\alpha_j t(\alpha_j t - 2) - 2\exp(-\alpha_j t) + 2)\}] + k_{t11}\frac{h_1 V}{\alpha_j^2 L_r}\{1 - \exp(-\alpha_j t)\} \tag{C-8}$$

$$I_{jk\,22} = c_{t11}[-\frac{4h_0V\exp(-\alpha_j t)}{\alpha_j^3 L^2}\{2V[\exp(-\alpha_j t)(\alpha_j t-1)+1]\}-\frac{1}{\alpha_j L}\{\exp(\alpha_j t)-2\}] \quad \text{(C-9)}$$

For $k= n_v+n_{vT}+2$, The integral I_{jk} is split into four components as before

$$I_{jk} = \sum_{a=1}^{2}\sum_{b=1}^{2} I_{jk\,ab} \quad \text{(C-10)}$$

For random surface unevenness of bridge deck

When $0 \le t \le L/V$

$$I_{jk\,11} = k_{t21}[\sum_{s=1}^{N} A_{2s}\frac{\exp(-\alpha_j t)}{\alpha_j^2+(B_sV)^2}\{-\alpha_j\cos(\theta_{2s})-B_sV\sin(\theta_{2s}) + \exp(\alpha_j t)[\alpha_j\cos(B_sVt+\theta_{2s})+B_sV\cos(B_sVt+\theta_{2s})]\}] \quad \text{(C-11)}$$

$$I_{jk\,12} = c_{t21}[\sum_{s=1}^{N} VA_{2s}B_s\frac{\exp(-\alpha_j t)}{\alpha_j^2+(B_sV)^2}\{-\alpha_j\sin(\theta_{2s})-B_sV\cos(\theta_{2s}) + \exp(\alpha_j t)[\alpha_j\sin(B_sVt+\theta_{2s})-B_sV\sin(B_sVt+\theta_{2s})]\}] \quad \text{(C-12)}$$

For deterministic mean surface profile (parabolic pre-cambering and approach road settlement)

If $0 \le t \le L_r/V$

$$I_{jk\,21} = k_{t21}[\frac{4h_0V}{\alpha_j^3L^2}\{\alpha_j L(\alpha_j t+\exp(-\alpha_j t)-1)\}-\frac{V}{\alpha_j^3L^2}\{\alpha_j t(\alpha_j t-2)-2\exp(-\alpha_j t)+2)\}] + k_{t21}\frac{h_1V}{\alpha_j^2L_r}\{\alpha_j t+\exp(-\alpha_j t)-1\} \quad \text{(C-13)}$$

$$I_{jk\,22} = -c_{t21}[\frac{4h_0V\exp(-\alpha_j t)}{\alpha_j^3L^2}\{2V[\exp(-\alpha_j t)(\alpha_j t-1)+1]\}+\frac{1}{\alpha_j L}\{\exp(\alpha_j t)-2\}] + c_{t21}\frac{h_1V}{\alpha_j L_r}\{1-\exp(-\alpha_j t)\} \quad \text{(C-14)}$$

When $L_r/V < t \le L/V$

$$I_{jk\,21} = k_{t21}[\frac{4h_0V}{\alpha_j^3L^2}\{\alpha_jL(\alpha_jt+\exp(-\alpha_jt)-1)\}-\frac{V}{\alpha_j^3L^2}\{\alpha_jt(\alpha_jt-2)-2\exp(-\alpha_jt)+2)\}] + k_{t21}\frac{h_1}{\alpha_j}\{1-\exp(\alpha_jt)\} \quad \text{(C-15)}$$

$$I_{jk\,22} = -c_{t21}[\frac{4h_0V\exp(-\alpha_jt)}{\alpha_j^3L^2}\{2V[\exp(-\alpha_jt)(\alpha_jt-1)+1]\}+\frac{1}{\alpha_jL}\{\exp(\alpha_jt)-2\}] \quad \text{(C-16)}$$

For $k = n_v+n_{vT}+3$, The integral I_{jk} is split into four components as

$$I_{jk} = \sum_{a=1}^{2}\sum_{b=1}^{2} I_{jk\,ab} \quad \text{(C-17)}$$

Components of Eq. (C-17) can be expressed as

<u>For random surface unevenness of bridge deck</u>

When $0 \le t \le L/V$

$$I_{jk\,11} = k_{t12}[\sum_{s=1}^{N} A_{1s}\frac{\exp(-\alpha_jt)}{\alpha_j^2+(B_sV)^2}\{-\alpha_j\cos(B_sl_v-\theta_{1s})-B_sV\sin(B_sl_v-\theta_{1s})+ \exp(\alpha_jt)[\alpha_j\cos(B_s(l-Vt)-\theta_{1s})+B_sV\sin(B_s(l_v-Vt)+\theta_{1s})]+ +V^2[2-\exp(\alpha_jt)\{\alpha_jt(\alpha_jt-2)+2\}]\}] \quad \text{(C-18)}$$

$$I_{jk\,12} = c_{t12}[\sum_{s=1}^{N} VA_{1s}B_s\frac{\exp(-\alpha_jt)}{\alpha_j^2+(B_sV)^2}\{-\alpha_j\sin(\theta_{1s})-B_sV\cos(\theta_{1s}) + \exp(\alpha_jt)[\alpha_j\sin(B_sVt+\theta_{1s})-B_sV\sin(B_sVt+\theta_{1s})]\}] \quad \text{(C-19)}$$

For deterministic mean surface profile (parabolic pre-cambering and approach road settlement)

If $0 \le t \le L_r / V$

$$I_{jk\,21} = k_{t12}[\frac{4h_0}{\alpha_j^3 L^2}\{-\alpha_j^2 l_v (l_v + L)(\exp(\alpha_j t) - 1) + \alpha_j V(2l_v + L)[\exp(\alpha_j t)(\alpha_j t - 1) + 1]\} + k_{t12}\frac{h_1 \exp(-\alpha_j t)}{\alpha_j^2 L_r}[V\{1 + \exp(\alpha_j t)(\alpha_j t - 1)\} - \alpha_j l_v(\exp(\alpha_j t) - 1)]] \quad \text{(C-20)}$$

$$I_{jk\,22} = -c_{t12}[\frac{4h_0 V \exp(-\alpha_j t)}{\alpha_j^3 L^2}\{2V[\exp(-\alpha_j t)(\alpha_j t - 1) + 1]\} + \frac{1}{\alpha_j L}\{\exp(\alpha_j t) - 2\}] + c_{t12}\frac{h_1 V}{\alpha_j L_r}\{1 - \exp(\alpha_j t)\} \quad \text{(C-21)}$$

For $L_r / V < t \le L/V$

$$I_{jk\,21} = k_{t12}[\frac{4h_0}{\alpha_j^3 L^2}\{-\alpha_j^2 l_v (l_v + L)(\exp(\alpha_j t) - 1) + \alpha_j V(2l_v + L)[\exp(\alpha_j t)(\alpha_j t - 1) + 1]\} + k_{t12}\frac{h_1}{\alpha_j}\{1 - \exp(\alpha_j t)\} \quad \text{(C-22)}$$

$$I_{jk\,22} = -c_{t12}[\frac{4h_0 V \exp(-\alpha_j t)}{\alpha_j^3 L^2}\{2V[\exp(-\alpha_j t)(\alpha_j t - 1) + 1]\} + \frac{1}{\alpha_j L}\{\exp(\alpha_j t) - 2\}] \quad \text{(C-23)}$$

For $k = n_v + n_{vT} + 4$, The integral I_{jk} is split into four components as

$$I_{jk} = \sum_{a=1}^{2}\sum_{b=1}^{2} I_{jk\,ab} \quad \text{(C-24)}$$

Components of Eq. (C-24) can be expressed as

For random surface unevenness of bridge deck

If $0 \le t \le L/V$

$$I_{jk\,11} = k_{t22}[\sum_{s=1}^{N} A_{2s}\frac{\exp(-\alpha_j t)}{\alpha_j^2 + (B_s V)^2}\{-\alpha_j \cos(B_s l_v - \theta_{2s}) - B_s V \sin(B_s l_v - \theta_{2s}) + \exp(\alpha_j t)[\alpha_j \cos(B_s(l - Vt) - \theta_{2s}) + B_s V \sin(B_s(l_v - Vt) + \theta_{2s})] + V^2[2 - \exp(\alpha_j t)\{\alpha_j t(\alpha_j t - 2) + 2\}]\}] \quad \text{(C-25)}$$

$$I_{jk12} = c_{t22}[\sum_{s=1}^{N} A_{2s}B_sV\frac{\exp(-\alpha_j t)}{\alpha_j^2+(B_sV)^2}\{\alpha_j \sin(B_s l_v-\theta_{2s})+B_sV\cos(B_s l_v-\theta_{2s}) - \exp(\alpha_j t)\{\alpha_j \sin(B_s(l-Vt)-\theta_{2s})+B_sV\cos(B_s(l_v-Vt)+\theta_{2s})\}] \quad \text{(C-26)}$$

For deterministic mean surface profile (parabolic pre-cambering and approach road settlement)

When $0 \le t \le L_r/V$

$$I_{jk21} = k_{t22}[\frac{4h_0}{\alpha_j^3L^2}\{-\alpha_j^2 l_v(l_v+L)(\exp(\alpha_j t)-1)+\alpha_j V(2l_v+L)\{\exp(\alpha_j t)(\alpha_j t-1)+1\}] + k_{t22}\frac{h_1\exp(-\alpha_j t)}{\alpha_j^2 L_r}[V\{1+\exp(\alpha_j t)(\alpha_j t-1)\}-\alpha_j l_v(\exp(\alpha_j t)-1)] \quad \text{(C-27)}$$

$$I_{jk22} = c_{t22}[\frac{4h_0V\exp(-\alpha_j t)}{\alpha_j^2L^2}\{2V[\exp(\alpha_j t)(\alpha_j t-1)+1]-\alpha_j(2l_v+L)(\exp(\alpha_j t)-1)\}] + c_{t22}\frac{h_1V}{\alpha_j L_r}\{1-\exp(\alpha_j t)\} \quad \text{(C-28)}$$

If $L_r/V < t \le L/V$

$$I_{jk21} = k_{t22}[\frac{4h_0}{\alpha_j^3L^2}\{-\alpha_j^2 l_v(l_v+L)(\exp(\alpha_j t)-1)+\alpha_j V(2l_v+L)\{\exp(\alpha_j t)(\alpha_j t-1)+1\}] + k_{t22}\frac{h_1}{\alpha_j}\{1-\exp(\alpha_j t)\} \quad \text{(C-29)}$$

$$I_{jk22} = c_{t22}[\frac{4h_0V\exp(-\alpha_j t)}{\alpha_j^2L^2}\{2V[\exp(\alpha_j t)(\alpha_j t-1)+1]-\alpha_j(2l_v+L)(\exp(\alpha_j t)-1)\}] \quad \text{(C-30)}$$

For $k = r+1, r+2, \ldots, r+n_b$, where $r = n_v+n_{vT}+4$, the integral I_{jk} is split up into eighteen parts

$$I_{jk} = \sum_{a=1}^{9}\sum_{b=1}^{2} I_{jkab} \quad \text{(C-31)}$$

Let us take $R_k = (k-r)\pi V/L; S_k = (k-r)\pi/L$

Components of the Eq. (C-31) are as follows

For random surface unevenness of bridge deck

If $0 \le t \le L/V$

$$I_{jk\,11} = \frac{1}{2} k_{t11} \sum_{s=1}^{N} A_{1s} \left[\left\{ \frac{2R_k \exp(-\alpha_j t)\{(\alpha_j^2 - Q_s^2 + R_k^{\,2}) \cos(\theta_{1s}) + 2\alpha_j Q_s \sin(\theta_{1s})\}}{\{\alpha_j^2 + (Q_s - R_k)^2\}\{\alpha_j^2 + (Q_s + R_k)^2\}} \right.\right.$$
$$- \frac{\alpha_j \sin\{(Q_s - R_k)t + \theta_{1s}\} + (R_k - Q_s)\cos\{(Q_s - R_k)t + \theta_{1s}\}}{\{\alpha_j^2 + (Q_s - R_k)^2\}} \qquad \text{(C-32)}$$
$$\left.\left. + \frac{\alpha_j \sin\{(Q_s + R_k)t + \theta_{1s}\} - (R_k + Q_s)\cos\{(Q_s + R_k)t + \theta_{1s}\}}{\{\alpha_j^2 + (Q_s + R_k)^2\}} \right\} \right]$$

$$I_{jk\,12} = \frac{1}{2} k_{t21} \sum_{s=1}^{N} A_{2s} \left[\left\{ \frac{2R_k \exp(-\alpha_j t)\{(\alpha_j^2 - Q_s^2 + R_k^{\,2}) \cos(\theta_{2s}) + 2\alpha_j Q_s \sin(\theta_{2s})\}}{\{\alpha_j^2 + (Q_s - R_k)^2\}\{\alpha_j^2 + (Q_s + R_k)^2\}} \right.\right.$$
$$- \frac{\alpha_j \sin\{(Q_s - R_k)t + \theta_{2s}\} + (R_k - Q_s)\cos\{(Q_s - R_k)t + \theta_{2s}\}}{\{\alpha_j^2 + (Q_s - R_k)^2\}} \qquad \text{(C-33)}$$
$$\left.\left. + \frac{\alpha_j \sin\{(Q_s + R_k)t + \theta_{2s}\} - (R_k + Q_{2s})\cos\{(Q_s + R_k)t + \theta_{2s}\}}{\{\alpha_j^2 + (Q_s + R_k)^2\}} \right\} \right]$$

$$I_{jk\,21} = \frac{1}{2} k_{t12} \sum_{s=1}^{N} A_{1s} \left\{ \exp(-\alpha_j t) \left\{ \frac{(R_k + Q_s)\cos(S_s - Z_s - \theta_{1s}) + \alpha_j \sin(S_k - Z_s - \theta_{1s})\}}{\{\alpha_j^2 + (Q_s - R_k)^2\}} \right.\right.$$
$$\left. + \frac{(R_k - Q_s)\cos(S_k - Z_s + \theta_{1s}) + \alpha_j \sin(S_k - Z_s + \theta_s)\}}{\{\alpha_j^2 + (Q_s - R_s)^2\}} \right\} \qquad \text{(C-34)}$$
$$- \frac{\alpha_j \sin\{(Q_s - R_k)t + S_k - Z_s + \theta_{1s}\} - (R_k + Q_s)\cos\{(Q_s - R_k)t + S_k - Z_s + \theta_{1s}\}}{\{\alpha_j^2 + (Q_s - R_s)^2\}}$$
$$\left. + \frac{\alpha_j \sin\{S_k + Z_s - (Q_s + R)t - \theta_{1s}\} + (R_k + Q_s)\cos\{S_k + Z_s + (Q_s + R_k)t - \theta_{1s}\}}{\{\alpha_j^2 + (Q_s + R_k)^2\}} \right\}$$

$$I_{jk\,22} = \frac{1}{2} k_{t22} \sum_{s=1}^{N} A_{2s} \left\{ \exp(-\alpha_j t) \left\{ \frac{(R_k + Q_s)\cos(S_s - Z_s - \theta_{2s}) + \alpha_j \sin(S_k - Z_s - \theta_{2s})\}}{\{\alpha_j^2 + (Q_s - R_k)^2\}} \right.\right.$$
$$\left. + \frac{(R_k - Q_s)\cos(S_k - Z_s + \theta_{2s}) + \alpha_j \sin(S_k - Z_s + \theta_{2s})\}}{\{\alpha_j^2 + (Q_s - R_s)^2\}} \right\} \qquad \text{(C-35)}$$
$$- \frac{\alpha_j \sin\{(Q_s - R_k)t + S_k - Z_s + \theta_{2s}\} - (R_k + Q_s)\cos\{(Q_s - R_k)t + S_k - Z_s + \theta_{2s}\}}{\{\alpha_j^2 + (Q_s - R_s)^2\}}$$
$$\left. + \frac{\alpha_j \sin\{S_k + Z_s - (Q_s + R)t - \theta_{2s}\} + (R_k + Q_s)\cos\{S_k + Z_s + (Q_s + R_k)t - \theta_{2s}\}}{\{\alpha_j^2 + (Q_s + R_k)^2\}} \right\}$$

$$I_{jk\,31}=\frac{1}{2}c_{t11}\sum_{s=1}^{N}A_{1s}Q_s\left\{-\frac{2R_k\exp(-\alpha_j t)\{(\alpha_j^2-Q_s^2+R_k{}^2)\sin(\theta_s)-2\alpha_j Q_s\cos(\theta_{1s})\}}{\{\alpha_j^2+(Q_s-R)^2\}\{\alpha_j^2+(Q_s+R_k)^2\}}\right.$$
$$-\frac{\alpha_j\cos\{(Q_s-R_k)t+\theta_{1s}\}+(R_k-Q_s)\sin\{(Q_s-R_k)t+\theta_{1s}\}}{\{\alpha_j^2+(Q_s-R_k)^2\}}$$
$$\left.+\frac{\alpha_j\cos\{(Q_s+R_k)t+\theta_{1s}\}+(R_k+Q_s)\sin\{(Q_s+R_k)t+\theta_{1s}\}}{\{\alpha_j^2+(Q_s+R_k)^2\}}\right\} \quad \text{(C-36)}$$

$$I_{jk\,32}=\frac{1}{2}c_{t12}\sum_{s=1}^{N}A_{1s}Q_s\left[\exp(-\alpha_j t)\left\{\frac{(R_k+Q_s)\sin(S_k+Z_s-\theta_{2s})-\alpha_j\cos(S_k+Z_s-\theta_{2s})\}}{\{\alpha_j^2+(Q_s-R_k)^2\}}\right.\right.$$
$$\left.+\frac{(Q_s-R_k)\sin(S_k-Z_s+\theta_{2s})+\alpha_j\cos(S_k-Z_s+\theta_{2s})\}}{\{\alpha_j^2+(Q_s-R)^2\}}\right\}$$
$$+\frac{\alpha_j\cos\{S_k+Z_s-(Q_s+R_k)t-\theta_{2s}\}-(R_k+Q_s)\sin\{S_k+Z_s-(Q_s+R_k)t-\theta_{2s}\}}{\{\alpha_j^2+(Q_s+R_k)^2\}} \quad \text{(C-37)}$$
$$\left.-\frac{\alpha_j\cos\{S_k-Z_s+(Q_s-R_k)t+\theta_{2s}\}+(Q_s-R_k)\sin\{S_k-Z_s+(Q_s-R_k)t+\theta_{2s}\}}{\{\alpha_j^2+(Q_s-R_k)^2\}}\right]$$

$$I_{jk\,41}=\frac{1}{2}c_{t21}\sum_{s=1}^{N}A_{2s}Q_s\left\{-\frac{2R_k\exp(-\alpha_j t)\{(\alpha_j^2-Q_s^2+R_k{}^2)\sin(\theta_{2s})-2\alpha_j Q_s\cos(\theta_{2s})\}}{\{\alpha_j^2+(Q_s-R)^2\}\{\alpha_j^2+(Q_s+R_k)^2\}}\right.$$
$$-\frac{\alpha_j\cos\{(Q_s-R_k)t+\theta_{2s}\}+(R_k-Q_s)\sin\{(Q_s-R_k)t+\theta_{2s}\}}{\{\alpha_j^2+(Q_s-R_k)^2\}} \quad \text{(C-38)}$$
$$\left.+\frac{\alpha_j\cos\{(Q_s+R_k)t+\theta_{2s}\}+(R_k+Q_s)\sin\{(Q_s+R_k)t+\theta_{2s}\}}{\{\alpha_j^2+(Q_s+R_k)^2\}}\right\}$$

$$I_{jk\,42}=\frac{1}{2}c_{t22}\sum_{s=1}^{N}A_{2s}Q_s\left[\exp(-\alpha_j t)\left\{\frac{(R_k+Q_s)\sin(S_k+Z_s-\theta_{2s})-\alpha_j\cos(S_k+Z_s-\theta_{2s})\}}{\{\alpha_j^2+(Q_s-R_k)^2\}}\right.\right.$$
$$\left.+\frac{(Q_s-R_k)\sin(S_k-Z_s+\theta_{2s})+\alpha_j\cos(S_k-Z_s+\theta_{2s})\}}{\{\alpha_j^2+(Q_s-R)^2\}}\right\}$$
$$+\frac{\alpha_j\cos\{S_k+Z_s-(Q_s+R_k)t-\theta_{2s}\}-(R_k+Q_s)\sin\{S_k+Z_s-(Q_s+R_k)t-\theta_{2s}\}}{\{\alpha_j^2+(Q_s+R_k)^2\}} \quad \text{(C-39)}$$
$$\left.-\frac{\alpha_j\cos\{S_k-Z_s+(Q_s-R_k)t+\theta_{2s}\}+(Q_s-R_k)\sin\{S_k-Z_s+(Q_s-R_k)t+\theta_{2s}\}}{\{\alpha_j^2+(Q_s-R_k)^2\}}\right]$$

For deterministic mean surface profile (parabolic pre-cambering and approach road settlement)

When $0 \le t \le L_r / V$

$$
\begin{aligned}
I_{jk\,51} = \frac{1}{2} k_{t11} [\{ [& \frac{4h_0 V \exp(-\alpha_j t)}{L^2 (\alpha_j^2 + Q_s^2)^3} L(\alpha_j^2 + Q_s^2) [\exp(\alpha_j t) \sin(Q_s t) \{ Q_s^2 (\alpha_j t + 1) + \alpha_j^2 (\alpha_j t - 1) \}] \\
& - Q_s \exp(\alpha_j t) \cos(Q_s t) [Q_s^2 t + \alpha_j (\alpha_j t - 2)] - 2\alpha_j Q_s \} \\
& + V(2Q_s^3 + Q_s \exp(\alpha_j t)) \cos(Q_s t) \ \{ Q_s^4 t^2 + 2Q_s^2 (\alpha_j^2 t^2 - 2\alpha_j t - 1) + \alpha_j^2 (\alpha_j^2 t^2 - 4\alpha_j t + 6) \} \\
& - \exp(\alpha_j t) \sin(Q_s t) \{ Q_s^4 (\alpha_j t + 2) + \alpha_j Q_s^2 (\alpha_j^2 t^2 - 3) + \alpha_j^3 (\alpha_j^2 t^2 - 2\alpha_j t + 2) \} - 6\alpha_j^2 Q_s] \\
& + k_{t11} \frac{\exp(-\alpha_j t) h_1 LV}{L L_r (R_k^2 + \alpha_j^2)} [2L^3 \alpha_j + \exp(-\alpha_j t) \{ -R_k L [R_k^2 L^2 t + L^2 \alpha_j (\alpha_j t - 2)] \cos(R_k t) \\
& + L \{ L^2 \alpha_j^2 (\alpha_j t - 1) + R_k^2 L^2 t (\alpha_j t + 1) \} \sin(R_k t) \}]
\end{aligned}
\qquad \text{(C-40)}
$$

$$
\begin{aligned}
I_{jk\,52} = \frac{1}{2} k_{t21} [\{ & \frac{4h_0 V \exp(-\alpha_j t)}{L^2 (\alpha_j^2 + Q_s^2)^3} [\{ L(\alpha_j^2 + Q_s^2) [\exp(\alpha_j t) \sin(Q_s t) \{ Q_s^2 (\alpha_j t + 1) + \alpha_j^2 (\alpha_j t - 1) \}] \\
& - Q_s \exp(\alpha_j t) \cos(Q_s t) [Q_s^2 t + \alpha_j (\alpha_j t - 2)] - 2\alpha_j Q_s \} \\
& + V(2Q_s^3 + Q_s \exp(\alpha_j t)) \cos(Q_s t) \ \{ Q_s^4 t^2 + 2Q_s^2 (\alpha_j^2 t^2 - 2\alpha_j t - 1) + \alpha_j^2 (\alpha_j^2 t^2 - 4\alpha_j t + 6) \} \\
& - \exp(\alpha_j t) \sin(Q_s t) \{ Q_s^4 (\alpha_j t + 2) + \alpha_j Q_s^2 (\alpha_j^2 t^2 - 3) + \alpha_j^3 (\alpha_j^2 t^2 - 2\alpha_j t + 2) \} - 6\alpha_j^2 Q_s] \\
& + k_{t21} \frac{\exp(-\alpha_j t) h_1 LV}{L L_r (R_k^2 + \alpha_j^2)} [2L^3 \alpha_j + \exp(-\alpha_j t) \{ -R_k L [R_k^2 L^2 t + L^2 \alpha_j (\alpha_j t - 2)] \cos(R_k t) \\
& + L \{ L^2 \alpha_j^2 (\alpha_j t - 1) + R_k^2 L^2 t (\alpha_j t + 1) \} \sin(R_k t) \}]
\end{aligned}
\qquad \text{(C-41)}
$$

$$
\begin{aligned}
I_{jk\,61} = -\frac{1}{2} k_{t12} [& \frac{4h_0 V}{L^2 (\alpha_j^2 + V^2)^3} \{ \sin(Vt - l_v) \{ [\alpha_j l_v^2 (\alpha_j^2 + V^2)^2 - l_v (\alpha_j^2 + V^2) \{ -\alpha_j^3 L - \alpha_j L V^2 \\
& + 2V^3 (\alpha_j t + 1) + 2\alpha_j^2 V (\alpha_j t - 1) \} + V [V \{ 2\alpha_j^3 + \alpha_j t (\alpha_j^2 + V^2)^2 + 2t(\alpha_j^4 - V^4) - 6\alpha_j V^2 \} \\
& - L(\alpha_j^2 + V^2) \{ \alpha_j^2 (\alpha_j t - 1) + V^2 (\alpha_j t + 1) \} \}] + V \cos(l_v - Vt) [V^4 (l_v^2 + l_v L + 2\alpha_j^2 t^2 - 4\alpha_j t - 2) \\
& + \alpha_j^2 V^2 (2l_v^2 + 2l_v L + 4\alpha_j^2 t^2 + 6) + \alpha_j^4 l_v (l_v + L) - V^5 t (2l_v + L)(\alpha_j t - 1) \\
& - \alpha_j^3 V (2l_v + L)(\alpha_j t - 2) + l_v^2 V^6] \}] \\
& + k_{t12} \frac{\exp(-\alpha_j t) h_1 LV}{L L_r (R_k^2 + \alpha_j^2)} [R_k L \exp(-\alpha_j t) \{ R_k^2 L^2 t + L^2 \alpha_j (\alpha_j t - 2) \} \cos(R_k t) \\
& + 2R_k L^3 \alpha_j - \exp(-\alpha_j t) \{ L^3 \alpha_j (\alpha_j t - 1) + R_k^2 L^2 (\alpha_j t + 1) \} \sin(R_k t) \\
& - R_k L^3 l_v (R_k^2 + \alpha_j^2) \{ 1 + \exp(\alpha_j t) \cos(R_k t) + \exp(\alpha_j t) L \alpha_j \sin(R_k t) \}]
\end{aligned}
\qquad \text{(C-42)}
$$

$$I_{jk62} = -\frac{1}{2}k_{t22}\Big[\ \frac{4h_0V}{L^2(\alpha_j^2+V^2)^3}\Big\{\sin(Vt-l_v)\{[\alpha_j l_v^2(\alpha_j^2+V^2)^2 - l_v(\alpha_j^2+V^2)\{-\alpha_j^3 L-\alpha_j LV^2$$
$$+2V^3(\alpha_j t+1)+2\alpha_j^2V(\alpha_j t-1)\}+V[V\{2\alpha_j^3+\alpha_j t(\alpha_j^2+V^2)^2+2t(\alpha_j^4-V^4)-6\alpha_j V^2\}$$
$$-L(\alpha_j^2+V^2)\{\alpha_j^2(\alpha_j t-1)+V^2(\alpha_j t+1)\}\}]+V\cos(l_v-Vt)[V^4(l_v^2+l_vL+2\alpha_j^2t^2-4\alpha_j t-2)$$
$$+\alpha_j^2V^2(2l_v^2+2l_vL+4\alpha_j^2t^2+6)+\alpha_j^4l_v(l_v+L)-V^5t(2l_v+L)(\alpha_j t-1)$$
$$-\alpha_j^3V(2l_v+L)(\alpha_j t-2)+l_v^2V^6]\}\Big] \qquad \text{(C-43)}$$
$$+k_{t22}\frac{\exp(-\alpha_j t)h_1LV}{LL_r(R_k^2+\alpha_j^2)}[R_kL\exp(-\alpha_j t)\{R_k^2L^2t+L^2\alpha_j(\alpha_j t-2)\}\cos(R_k t)$$
$$+2R_kL^3\alpha_j-\exp(-\alpha_j t)\{L^3\alpha_j(\alpha_j t-1)+R_k^2L^2(\alpha_j t+1)\}\sin(R_k t)$$
$$-R_kL^3l_v(R_k^2+\alpha_j^2)\{1+\exp(\alpha_j t)\cos(R_k t)+\exp(\alpha_j t)L\alpha_j\sin(R_k t)\}]$$

$$I_{jk71} = -c_{t11}\frac{2h_0V\exp(-\alpha_j t)}{L^2(\alpha_j^2+V^2)^3}\{\exp(\alpha_j t)\cos(Q_s t)[Q_s^2(2\alpha_j tV-\alpha_j L+2V)+\alpha_j^2(2\alpha_j tV-\alpha_j L-2V)]$$
$$-Q_s\exp(\alpha_j t)\sin(Q_s t)[Q_s^2(L-Vt)+\alpha_j(\alpha_j L-2\alpha_j tV+4V)]\ \} \qquad \text{(C-44)}$$
$$+c_{t11}\frac{h_1V}{LL_r(R_k^2+\alpha_j^2)}[R_kL\{\exp(-\alpha_j t)-\cos(R_k t)\}+L\alpha_j\sin(R_k t)]$$

$$I_{jk72} = -c_{t21}\frac{2h_0V\exp(-\alpha_j t)}{L^2(\alpha_j^2+V^2)^3}\{\exp(\alpha_j t)\cos(Q_s t)[Q_s^2(2\alpha_j tV-\alpha_j L+2V)+\alpha_j^2(2\alpha_j tV-\alpha_j L-2V)]$$
$$-Q_s\exp(\alpha_j t)\sin(Q_s t)[Q_s^2(L-Vt)+\alpha_j(\alpha_j L-2\alpha_j tV+4V)]\ \} \qquad \text{(C-45)}$$
$$+c_{t21}\frac{h_1V}{LL_r(R_k^2+\alpha_j^2)}[R_kL\{\exp(-\alpha_j t)-\cos(R_k t)\}+L\alpha_j\sin(R_k t)]$$

$$I_{jk81} = -c_{t12}\frac{2h_0V\exp(-\alpha_j t)}{L^2(\alpha_j^2+V^2)^3}\{\exp(\alpha_j t)\sin(Q_s t)[Q_s^2(2\alpha_j tV-\alpha_j L+2V)$$
$$+\alpha_j^2(2\alpha_j tV-\alpha_j L-2V)]-Q_s\exp(\alpha_j t)\cos(Q_s t)[Q_s^2(L-Vt)+\alpha_j(\alpha_j L-2\alpha_j tV+4V)]\ \} \qquad \text{(C-46)}$$
$$+c_{t12}\frac{h_1V}{LL_r(R_k^2+\alpha_j^2)}[R_kL\{\exp(-\alpha_j t)-\cos(R_k t)\}+L\alpha_j\sin(R_k t)]$$

$$I_{jk82} = -c_{t22}\frac{2h_0V\exp(-\alpha_j t)}{L^2(\alpha_j^2+V^2)^3}\{\exp(\alpha_j t)\sin(Q_s t)[Q_s^2(2\alpha_j tV-\alpha_j L+2V)$$
$$+\alpha_j^2(2\alpha_j tV-\alpha_j L-2V)]-Q_s\exp(\alpha_j t)\cos(Q_s t)[Q_s^2(L-Vt)+\alpha_j(\alpha_j L-2\alpha_j tV+4V)]\ \} \qquad \text{(C-47)}$$
$$+c_{t22}\frac{h_1V}{LL_r(R_k^2+\alpha_j^2)}[R_kL\{\exp(-\alpha_j t)-\cos(R_k t)\}+L\alpha_j\sin(R_k t)]$$

For $L_r/V < t \le L/V$

$$
\begin{aligned}
I_{jk\,51} = \frac{1}{2}k_{t11}[\{[\frac{4h_0V\exp(-\alpha_j t)}{L^2(\alpha_j^2+Q_s^2)^3}L(\alpha_j^2+Q_s^2)[\exp(\alpha_j t)\sin(Q_s t)\{Q_s^2(\alpha_j t+1)+\alpha_j^2(\alpha_j t-1)\}] \\
-Q_s\exp(\alpha_j t)\cos(Q_s t)[Q_s^2 t+\alpha_j(\alpha_j t-2)]-2\alpha_j Q_s\} \\
+V(2Q_s^3+Q_s\exp(\alpha_j t))\cos(Q_s t)\ \{\ Q_s^4 t^2+2Q_s^2(\alpha_j^2t^2-2\alpha_j t-1)+\alpha_j^2(\alpha_j^2t^2-4\alpha_j t+6)\} \\
-\exp(\alpha_j t)\sin(Q_s t)\{Q_s^4(\alpha_j t+2)+\alpha_j Q_s^2(\alpha_j^2t^2-3)+\alpha_j^3(\alpha_j^2t^2-2\alpha_j t+2)\}-6\alpha_j^2Q_s] \\
+k_{t11}\frac{h_1V}{L\,(\alpha_j^2+R_k^2)}[R_kL\{\exp(-\alpha_j t)-\cos(R_k t)\}+L\alpha_j\sin(R_k t)]
\end{aligned}
\tag{C-48}
$$

$$
\begin{aligned}
I_{jk\,52} = \frac{1}{2}k_{t21}[\{\frac{4h_0V\exp(-\alpha_j t)}{L^2(\alpha_j^2+Q_s^2)^3}[\{L(\alpha_j^2+Q_s^2)[\exp(\alpha_j t)\sin(Q_s t)\{Q_s^2(\alpha_j t+1)+\alpha_j^2(\alpha_j t-1)\}] \\
-Q_s\exp(\alpha_j t)\cos(Q_s t)[Q_s^2 t+\alpha_j(\alpha_j t-2)]-2\alpha_j Q_s\} \\
+V(2Q_s^3+Q_s\exp(\alpha_j t))\cos(Q_s t)\ \{\ Q_s^4 t^2+2Q_s^2(\alpha_j^2t^2-2\alpha_j t-1)+\alpha_j^2(\alpha_j^2t^2-4\alpha_j t+6)\} \\
-\exp(\alpha_j t)\sin(Q_s t)\{Q_s^4(\alpha_j t+2)+\alpha_j Q_s^2(\alpha_j^2t^2-3)+\alpha_j^3(\alpha_j^2t^2-2\alpha_j t+2)\}-6\alpha_j^2Q_s] \\
+k_{t21}\frac{h_1V}{L\,(\alpha_j^2+R_k^2)}[R_kL\{\exp(-\alpha_j t)-\cos(R_k t)\}+L\alpha_j\sin(R_k t)]
\end{aligned}
\tag{C-49}
$$

$$
\begin{aligned}
I_{jk\,61} = -\frac{1}{2}k_{t12}[\ \frac{4h_0V}{L^2(\alpha_j^2+V^2)^3}\{\sin(Vt-l_v)\{[\alpha_j l_v^2(\alpha_j^2+V^2)^2-l_v(\alpha_j^2+V^2)\{-\alpha_j^3L-\alpha_j LV^2 \\
+2V^3(\alpha_j t+1)+2\alpha_j^2V(\alpha_j t-1)\}+V[V\{2\alpha_j^3+\alpha_j t(\alpha_j^2+V^2)^2+2t(\alpha_j^4-V^4)-6\alpha_j V^2\} \\
-L(\alpha_j^2+V^2)\{\alpha_j^2(\alpha_j t-1)+V^2(\alpha_j t+1)\}\}]+V\cos(l_v-Vt)[V^4(l_v^2+l_vL+2\alpha_j^2t^2-4\alpha_j t-2) \\
+\alpha_j^2V^2(2l_v^2+2l_vL+4\alpha_j^2t^2+6)+\alpha_j^4l_v(l_v+L)-V^5t(2l_v+L)(\alpha_j t-1) \\
-\alpha_j^3V(2l_v+L)(\alpha_j t-2)+l_v^2V^6]\}] \\
+k_{t12}\frac{h_1V}{L\,(\alpha_j^2+R_k^2)}[R_kL\{\exp(-\alpha_j t)-\cos(R_k t)\}+L\alpha_j\sin(R_k t)]
\end{aligned}
\tag{C-50}
$$

$$
\begin{aligned}
I_{jk\,62} = -\frac{1}{2}k_{t22}[\ \frac{4h_0V}{L^2(\alpha_j^2+V^2)^3}\{\sin(Vt-l_v)\{[\alpha_j l_v^2(\alpha_j^2+V^2)^2-l_v(\alpha_j^2+V^2)\{-\alpha_j^3L-\alpha_j LV^2 \\
+2V^3(\alpha_j t+1)+2\alpha_j^2V(\alpha_j t-1)\}+V[V\{2\alpha_j^3+\alpha_j t(\alpha_j^2+V^2)^2+2t(\alpha_j^4-V^4)-6\alpha_j V^2\} \\
-L(\alpha_j^2+V^2)\{\alpha_j^2(\alpha_j t-1)+V^2(\alpha_j t+1)\}\}]+V\cos(l_v-Vt)[V^4(l_v^2+l_vL+2\alpha_j^2t^2-4\alpha_j t-2) \\
+\alpha_j^2V^2(2l_v^2+2l_vL+4\alpha_j^2t^2+6)+\alpha_j^4l_v(l_v+L)-V^5t(2l_v+L)(\alpha_j t-1) \\
-\alpha_j^3V(2l_v+L)(\alpha_j t-2)+l_v^2V^6]\}] \\
+k_{t22}\frac{h_1V}{L\,(\alpha_j^2+R_k^2)}[R_kL\{\exp(-\alpha_j t)-\cos(R_k t)\}+L\alpha_j\sin(R_k t)]
\end{aligned}
\tag{C-51}
$$

$$I_{jk\,71} = -c_{t11}\frac{2h_0V\exp(-\alpha_j t)}{L^2(\alpha_j^2+V^2)^3}\{\exp(\alpha_j t)\cos(Q_s t)[Q_s^2(2\alpha_j tV-\alpha_j L+2V)+\alpha_j^2(2\alpha_j tV-\alpha_j L-2V)] - Q_s\exp(\alpha_j t)\sin(Q_s t)[Q_s^2(L-Vt)+\alpha_j(\alpha_j L-2\alpha_j tV+4V)]\} \quad \text{(C-52)}$$

$$I_{jk\,72} = -c_{t21}\frac{2h_0V\exp(-\alpha_j t)}{L^2(\alpha_j^2+V^2)^3}\{\exp(\alpha_j t)\cos(Q_s t)[Q_s^2(2\alpha_j tV-\alpha_j L+2V)+\alpha_j^2(2\alpha_j tV-\alpha_j L-2V)] - Q_s\exp(\alpha_j t)\sin(Q_s t)[Q_s^2(L-Vt)+\alpha_j(\alpha_j L-2\alpha_j tV+4V)]\} \quad \text{(C-53)}$$

$$I_{jk\,81} = -c_{t12}\frac{2h_0V\exp(-\alpha_j t)}{L^2(\alpha_j^2+V^2)^3}\{\exp(\alpha_j t)\sin(Q_s t)[Q_s^2(2\alpha_j tV-\alpha_j L+2V) + \alpha_j^2(2\alpha_j tV-\alpha_j L-2V)] - Q_s\exp(\alpha_j t)\cos(Q_s t)[Q_s^2(L-Vt)+\alpha_j(\alpha_j L-2\alpha_j tV+4V)]\} \quad \text{(C-54)}$$

$$I_{jk\,82} = -c_{t22}\frac{2h_0V\exp(-\alpha_j t)}{L^2(\alpha_j^2+V^2)^3}\{\exp(\alpha_j t)\sin(Q_s t)[Q_s^2(2\alpha_j tV-\alpha_j L+2V) + \alpha_j^2(2\alpha_j tV-\alpha_j L-2V)] - Q_s\exp(\alpha_j t)\cos(Q_s t)[Q_s^2(L-Vt)+\alpha_j(\alpha_j L-2\alpha_j tV+4V)]\} \quad \text{(C-55)}$$

For static weight of vehicle ($0 \le t \le L/V$)

$$I_{jk\,91} = -\frac{\exp(-\alpha_j t)gL(l_v m_v+4m_{w11})}{4(L^2\alpha_j^2+R_k^2L)}\left[R_kL+\exp(\alpha_j t)\{R_kL\cos(R_k t)+L\alpha_j\sin(R_k t)\}\right] - \frac{\exp(-\alpha_j t)gL(l_v m_v+4m_{w12})}{4(L^2\alpha_j^2+R_k^2L)}\left[R_kL\{\cos(S_k l_v)-\exp(\alpha_j t)\cos[S_k(l_v-Vt)]\} - L\alpha_j\{\sin(S_k l_v)-\exp(\alpha_j t)\sin[S_k(l_v-Vt)]\}\right] \quad \text{(C-56)}$$

$$I_{jk\,92} = -\frac{\exp(-\alpha_j t)gL(l_v m_v+4m_{w21})}{4(L^2\alpha_j^2+R_k^2L)}\left[R_kL+\exp(\alpha_j t)\{R_kL\cos(R_k t)+L\alpha_j\sin(R_k t)\}\right] - \frac{\exp(-\alpha_j t)gL(l_v m_v+4m_{w22})}{4(L^2\alpha_j^2+R_k^2L)}\left[R_kL\{\cos(S_k l_v)-\exp(\alpha_j t)\cos[S_k(l_v-Vt)]\} - L\alpha_j\{\sin(S_k l_v)-\exp(\alpha_j t)\sin[S_k(l_v-Vt)]\}\right] \quad \text{(C-57)}$$

For $k= p+1, p+2,\ldots,p+n_T$, where $p = n_v+n_{vT}+4+n_b$, the integral I_{jk} is split into eighteen components as

$$I_{jk} = \sum_{a=1}^{9}\sum_{b=1}^{2} I_{jk\,ab} \quad \text{(C-58)}$$

Take $R_k = (k-p)\pi V/L; S_k = (k-p)\pi/L$

Components of Eq. (C-58) can be expressed as

<u>For random surface unevenness of bridge deck</u>

If $0 \le t \le L/V$

$$I_{jk_{11}} = -\frac{1}{2} k_{t11} (e_x - b_1) \sum_{s=1}^{N} A_{1s} \exp(-\alpha_j t) \left\{ \frac{\alpha_j \cos(\theta_{1s}) + (Q_s - R_k) \sin(\theta_{1s})}{\alpha_j^2 + (Q_s - R_k)^2} + \frac{\alpha_j \cos(\theta_{1s}) + (Q_s + R_k) \sin(\theta_{1s})}{\alpha_j^2 + (Q_s + R_k)^2} \right.$$
$$+ \frac{\alpha_j \cos[(Q_s - R_k)t + \theta_s] + (Q_s - R_k) \sin[(Q_s - R_k)t - \theta_{1s}]}{\alpha_j^2 + (Q_s - R_k)^2}$$
$$\left. + \frac{\alpha_j \cos[(Q_s + R_k)t + \theta_{1s}] + (Q_s + R_k) \sin[(Q_s + R_k)t + \theta_{1s}]}{\alpha_j^2 + (Q_s + R_k)^2} \right\} \quad \text{(C-59)}$$

$$I_{jk_{12}} = -\frac{1}{2} k_{t21} (e_x + b_2) \sum_{s=1}^{N} A_{2s} \exp(-\alpha_j t) \left\{ \frac{\alpha_j \cos(\theta_{2s}) + (Q_s - R_k) \sin(\theta_{2s})}{\alpha_j^2 + (Q_s - R_k)^2} + \frac{\alpha_j \cos(\theta_{2s}) + (Q_s + R_k) \sin(\theta_{2s})}{\alpha_j^2 + (Q_s + R_k)^2} \right.$$
$$+ \frac{\alpha_j \cos[(Q_s - R_k)t + \theta_{2s}] + (Q_s - R_k) \sin[(Q_s - R_k)t - \theta_{2s}]}{\alpha_j^2 + (Q_s - R_k)^2}$$
$$\left. + \frac{\alpha_j \cos[(Q_s + R_k)t + \theta_{2s}] + (Q_s + R_k) \sin[(Q_s + R_k)t + \theta_{2s}]}{\alpha_j^2 + (Q_s + R_k)^2} \right\} \quad \text{(C-60)}$$

$$I_{jk_{21}} = -\frac{1}{2} k_{t12} (e_x - b_1) \sum_{s=1}^{N} \left[A_{1s} \exp(-\alpha_j t) \left\{ \frac{\alpha_j \cos(B_s l_v - S_k - \theta_{2s}) + (R_k - Q_s) \sin(B_s l_v - S_k - \theta_{2s})}{\alpha_j^2 + (Q_s - R)^2} \right.\right.$$
$$\left. + \frac{\alpha_j \cos(B_s l_v + S_k - \theta_{2s}) + (R_k + Q_s) \sin(B_s l_v + S_k - \theta_{2s})}{\alpha_j^2 + (Q_s + R_k)^2} \right\} \quad \text{(C-61)}$$
$$+ \frac{\alpha_j \cos[(R_k - Q_s)t + (B_s l_v - S_k - \theta_{2s})] + (R_k - Q_s) \sin[-(Q_s + R_k)t + (B_s l_v + S_k - \theta_{2s})]}{\alpha_j^2 + (Q_s - R_k)^2}$$
$$\left. + \frac{\alpha_j \cos[-(R_k + Q_s)t + (B_s l_v + S_k - \theta_{2s})] - (R_k + Q_s) \sin[-(Q_s + R_k)t + (B_s l_v + S_k - \theta_{2s})]}{\alpha_j^2 + (Q_s + R_k)^2} \right]$$

$$I_{jk_{22}} = -\frac{1}{2} k_{t22} (e_x + b_2) \sum_{s=1}^{N} \left[A_{2s} \exp(-\alpha_j t) \left\{ \frac{\alpha_j \cos(B_s l_v - S_k - \theta_{2s}) + (R_k - Q_s) \sin(B_s l_v - S_k - \theta_{2s})}{\alpha_j^2 + (Q_s - R)^2} \right.\right.$$
$$\left. + \frac{\alpha_j \cos(B_s l_v + S_k - \theta_{2s}) + (R_k + Q_s) \sin(B_s l_v + S_k - \theta_{2s})}{\alpha_j^2 + (Q_s + R_k)^2} \right\} \quad \text{(C-62)}$$
$$+ \frac{\alpha_j \cos[(R_k - Q_s)t + (B_s l_v - S_k - \theta_{2s})] + (R_k - Q_s) \sin[-(Q_s + R_k)t + (B_s l_v + S_k - \theta_{2s})]}{\alpha_j^2 + (Q_s - R_k)^2}$$
$$\left. + \frac{\alpha_j \cos[-(R_k + Q_s)t + (B_s l_v + S_k - \theta_{2s})] - (R_k + Q_s) \sin[-(Q_s + R_k)t + (B_s l_v + S_k - \theta_{2s})]}{\alpha_j^2 + (Q_s + R_k)^2} \right]$$

$$I_{jk\,31} = -\frac{1}{2} c_{t11}(e_x - b_1)\sum_{s=1}^{N} A_{1s}\exp(-\alpha_j t)\left\{\frac{\alpha_j \sin(\theta_{1s}) + (Q_s - R_k)\cos(\theta_{1s})}{\alpha_j^2 + (Q_s - R_k)^2}\right.$$
$$+\frac{\alpha_j \sin(\theta_{1s}) - (Q_s + R_k)\cos(\theta_{1s})}{\alpha_j^2 + (Q_s + R)^2}$$
$$+\frac{\alpha_j \sin[(Q_s - R_k)t + \theta_{1s}] + (R_k - Q_s)\cos[(Q_s - R_k)t + \theta_{1s}]}{\alpha_j^2 + (Q_s - R)^2}$$
$$\left.+\frac{\alpha_j \sin[(Q_s + R_k)t + \theta_{1s}] - (Q_s + R)\sin[(Q_s + R_k)t + \theta_{1s}]}{\alpha_j^2 + (Q_s + R_k)^2}\right\} \quad \text{(C-63)}$$

$$I_{jk\,32} = -\frac{1}{2} c_{t21}(e_x + b_2)\sum_{s=1}^{N} A_{2s}\exp(-\alpha_j t)\left\{\frac{\alpha_j \sin(\theta_{2s}) + (Q_s - R_k)\cos(\theta_{2s})}{\alpha_j^2 + (Q_s - R_k)^2}\right.$$
$$+\frac{\alpha_j \sin(\theta_{2s}) - (Q_s + R_k)\cos(\theta_{2s})}{\alpha_j^2 + (Q_s + R)^2}$$
$$+\frac{\alpha_j \sin[(Q_s - R_k)t + \theta_{2s}] + (R_k - Q_s)\cos[(Q_s - R_k)t + \theta_{2s}]}{\alpha_j^2 + (Q_s - R)^2}$$
$$\left.+\frac{\alpha_j \sin[(Q_s + R_k)t + \theta_{2s}] - (Q_s + R)\sin[(Q_s + R_k)t + \theta_{2s}]}{\alpha_j^2 + (Q_s + R_k)^2}\right\} \quad \text{(C-64)}$$

$$I_{jk\,41} = \frac{1}{2} c_{t12}(e_x - b_1)\sum_{s=1}^{N}\left[A_{1s}Q_s\exp(-\alpha_j t)\left\{\frac{\alpha_j \cos(B_s l_v - S_k - \theta_{1s}) + (Q_s - R_k)\sin(B_s l_v - S_k - \theta_{1s})}{\alpha_j^2 + (Q_s - R_k)^2}\right.\right.$$
$$\left.+\frac{\alpha_j \sin(B_s l_v + S_k - \theta_{1s}) + (R_k + Q_s)\cos(B_s l_v + S_k - \theta_{1s})}{\alpha_j^2 + (Q_s + R_k)^2}\right\} \quad \text{(C-65)}$$
$$-\frac{\alpha_j \sin[(R - Q_s)t + (B_s l_v - S_k - \theta_s)] + (Q_s - R_k)\cos[(R_k - Q_s)t + (B_s l_v - S_k - \theta_{1s})]}{\alpha_j^2 + (Q_s - R_k)^2}$$
$$\left.-\frac{\alpha_j \sin[-(R + Q_s)t + (B_s l_v + S_k - \theta_{1s})] + (R_k + Q_s)\cos[-(Q_s + R_k)t + (B_s l_v + S_k - \theta_{1s})]}{\alpha_j^2 + (Q_s + R_k)^2}\right]$$

$$I_{jk\,42} = \frac{1}{2} c_{t12}(e_x + b_2)\sum_{s=1}^{N}\left[A_{2s}Q_s\exp(-\alpha_j t)\left\{\frac{\alpha_j \cos(B_s l_v - S_k - \theta_{2s}) + (Q_s - R_k)\sin(B_s l_v - S_k - \theta_{2s})}{\alpha_j^2 + (Q_s - R_k)^2}\right.\right.$$
$$\left.+\frac{\alpha_j \sin(B_s l_v + S_k - \theta_{2s}) + (R_k + Q_s)\cos(B_s l_v + S_k - \theta_{2s})}{\alpha_j^2 + (Q_s + R_k)^2}\right\} \quad \text{(C-66)}$$
$$-\frac{\alpha_j \sin[(R - Q_s)t + (B_s l_v - S_k - \theta_{2s})] + (Q_s - R_k)\cos[(R_k - Q_s)t + (B_s l_v - S_k - \theta_{2s})]}{\alpha_j^2 + (Q_s - R_k)^2}$$
$$\left.-\frac{\alpha_j \sin[-(R + Q_s)t + (B_s l_v + S_k - \theta_{2s})] + (R_k + Q_s)\cos[-(Q_s + R_k)t + (B_s l_v + S_k - \theta_{2s})]}{\alpha_j^2 + (Q_s + R_k)^2}\right]$$

For deterministic mean surface profile (parabolic pre-cambering and approach road settlement)

When $0 \le t \le L_r / V$

$$
\begin{aligned}
I_{jk51} = {} & \frac{4k_{t11}h_0 L}{V(\alpha_j^2 + R_k{}^2)^3}(e_x - b_1)\Big[(\alpha_j^2 + R_k{}^2)\exp(-\alpha_j t)\{\alpha_j^2 + \exp(-\alpha_j t)\cos(R_k t) \\
& \times [R_k{}^2(\alpha_j t + 1) + \alpha_j^2(\alpha_j t - 1)] + R_k \exp(\alpha_j t)\sin(R_k t)[R_k{}^2 t + \alpha_j(\alpha_j t - 2)] - R_k{}^2\} \\
& + 2\alpha_j \exp(-\alpha_j t)(\alpha_j^2 + 3R_k{}^2) + R_k \sin(R_k t)\{6\alpha_j^2 + t^2(\alpha_j^2 + R_k{}^2)^2 + 4\alpha_j t(\alpha_j^2 + R_k{}^2) - 2R_k{}^2\} \\
& + \cos(R_k t)\{2t(R_k{}^4 - \alpha_j^4) + 2\alpha_j(\alpha_j^2 - 3R_k{}^2)\alpha_j t^2(\alpha_j^2 + R_k{}^2)^2\}\Big] \\
& + k_{t11}\frac{\exp(-\alpha_j t)h_1 LV}{L L_r(R_k^2 + \alpha_j^2)}(e_x - b_1)[2L^3\alpha_j + \exp(-\alpha_j t)\{R_k L[R_k^2 L^2 t + L^2\alpha_j(\alpha_j t - 2)]\sin(R_k t) \\
& - L\exp(-\alpha_j t)\{L^2\alpha_j^2(\alpha_j t - 1) + R_k^2 L^2 t(\alpha_j t + 1)\}\cos(R_k t)\}]
\end{aligned}
\tag{C-67}
$$

$$
\begin{aligned}
I_{jk52} = {} & \frac{4k_{t21}h_0 L}{V(\alpha_j^2 + R_k{}^2)^3}(e_x + b_2)\Big[(\alpha_j^2 + R_k{}^2)\exp(-\alpha_j t)\{\alpha_j^2 + \exp(-\alpha_j t)\cos(R_k t)[R_k{}^2(\alpha_j t + 1) + \alpha_j^2(\alpha_j t - 1)] \\
& + R_k \exp(\alpha_j t)\sin(R_k t)[R_k{}^2 t + \alpha_j(\alpha_j t - 2)] - R_k{}^2\} + 2\alpha_j \exp(-\alpha_j t)(\alpha_j^2 + 3R_k{}^2) \\
& + R_k \sin(R_k t)\{6\alpha_j^2 + t^2(\alpha_j^2 + R_k{}^2)^2 + 4\alpha_j t(\alpha_j^2 + R_k{}^2) - 2R_k{}^2\} + \cos(R_k t)\{2t(R_k{}^4 - \alpha_j^4) + 2\alpha_j(\alpha_j^2 - 3R_k{}^2) \\
& \alpha_j t^2(\alpha_j^2 + R_k{}^2)^2\}\Big] + k_{t21}\frac{\exp(-\alpha_j t)h_1 LV}{L L_r(R_k^2 + \alpha_j^2)}(e_x + b_2)[2L^3\alpha_j \\
& + \exp(-\alpha_j t)\{R_k L[R_k^2 L^2 t + L^2\alpha_j(\alpha_j t - 2)]\sin(R_k t) \\
& - L\exp(-\alpha_j t)\{L^2\alpha_j^2(\alpha_j t - 1) + R_k^2 L^2 t(\alpha_j t + 1)\}\cos(R_k t)\}]
\end{aligned}
\tag{C-68}
$$

$$
\begin{aligned}
I_{jk61} = {} & \frac{4k_{t12}h_0}{L^2}(e_x - b_1)\Bigg[\left\{\frac{l_v(l_v + L)\exp(-\alpha_j t)\{\alpha_j\cos(S_k - R_k t) - R_k\sin(S_k - R_k t)\} + R_k\sin(S) - \alpha_j\cos(S_k)}{\alpha_j^2 + R_k{}^2}\right\} \\
& + \frac{2LV\exp(-\alpha_j t)}{(\alpha_j^2 + R_k{}^2)^2}\{(\alpha_j^2 + R_k{}^2)\cos(S_k) + \exp(\alpha_j t)\cos(S_k - R_k t)[R^2(\alpha_j t + 1) + \alpha_j^2(\alpha_j t - 1)] \\
& + R_k[R_k{}^2 t + \alpha_j(\alpha_j t - 2)]\sin(S_k - R_k t) - 2\alpha_j R_k\sin(S_k)\} \\
& - \frac{V^2}{(\alpha_j^2 + R_k{}^2)^3}\{R_k\sin(S_k - R_k t)[6\alpha_j^2 + t^2(\alpha_j^2 + R_k{}^2)^2 - 4\alpha_j t(\alpha_j^2 + R_k{}^2) - 2R_k{}^2] \\
& + 2\exp(-\alpha_j t)[(\alpha_j^3 - 3\alpha_j R_k{}^2)\cos(S_k) + R_k(R_k{}^2 - 3\alpha_j^2)\sin(S_k)] \\
& - [2t(R_k{}^4 - \alpha_j^4) + 2\alpha_j(\alpha_j^2 - 3R_k{}^2) + \alpha_j t^2(\alpha_j^2 + R_k{}^2)^2]\cos(S_k - R_k t)\Bigg] \\
& + k_{t12}\frac{\exp(-\alpha_j t)h_1 LV}{L L_r(R_k^2 + \alpha_j^2)}(e_x - b_1)[-R_k L\exp(-\alpha_j t)\{R_k^2 L^2 t + L^2\alpha_j(\alpha_j t - 2)\}\sin(R_k t) \\
& - 2R_k L^3\alpha_j - \exp(-\alpha_j t)\{L^3\alpha_j(\alpha_j t - 1) + R_k^2 L^2(\alpha_j t + 1)\}\cos(R_k t) \\
& + R_k L^3 l_v(R_k^2 + \alpha_j^2)\{1 + \exp(\alpha_j t)\cos(R_k t) + \exp(\alpha_j t)L\alpha_j\cos(R_k t)\}
\end{aligned}
\tag{C-69}
$$

$$I_{jk\,62}=\frac{4k_{t22}h_0}{L^2}(e_x+b_2)\left[\left\{\frac{l_v(l_v+L)\exp(-\alpha_j t)\{\alpha_j\cos(S_k-R_kt)-R_k\sin(S_k-R_kt)\}+R_k\sin(S)-\alpha_j\cos(S_k)}{\alpha_j^2+R_k{}^2}\right\}\right.$$
$$+\frac{2LV\exp(-\alpha_j t)}{(\alpha_j^2+R_k{}^2)^2}\left\{(\alpha_j^2+R_k{}^2)\cos(S_k)+\exp(\alpha_j t)\cos(S_k-R_kt)[R^2(\alpha_j t+1)+\alpha_j^2(\alpha_j t-1)]\right.$$
$$\left.+R_k[R_k{}^2t+\alpha_j(\alpha_j t-2)]\sin(S_k-R_kt)-2\alpha_j R_k\sin(S_k)\right\}$$
$$-\frac{V^2}{(\alpha_j^2+R_k{}^2)^3}\left\{R_k\sin(S_k-R_kt)[6\alpha_j^2+t^2(\alpha_j^2+R_k{}^2)^2-4\alpha_j t(\alpha_j^2+R_k{}^2)-2R_k{}^2]\right.$$
$$+2\exp(-\alpha_j t)[(\alpha_j^3-3\alpha_j R_k{}^2)\cos(S_k)+R_k(R_k{}^2-3\alpha_j^2)\sin(S_k)]$$
$$\left.-[2t(R_k{}^4-\alpha_j^4)+2\alpha_j(\alpha_j^2-3R_k{}^2)+\alpha_j t^2(\alpha_j^2+R_k{}^2)^2]\cos(S_k-R_kt)\right]$$
$$+k_{t22}\frac{\exp(-\alpha_j t)h_1LV}{LL_r(R_k^2+\alpha_j^2)}(e_x+b_2)[-R_kL\exp(-\alpha_j t)\{R_k^2L^2t+L^2\alpha_j(\alpha_j t-2)\}\sin(R_kt)$$
$$-2R_kL^3\alpha_j-\exp(-\alpha_j t)\{L^3\alpha_j(\alpha_j t-1)+R_k^2L^2(\alpha_j t+1)\}\cos(R_kt)$$
$$+R_kL^3l_v(R_k^2+\alpha_j^2)\{1+\exp(\alpha_j t)\cos(R_kt)+\exp(\alpha_j t)L\alpha_j\cos(R_kt)\} \qquad \text{(C-70)}$$

$$I_{jk\,71}=\frac{4c_{t11}h_0L}{(\alpha_j^2+R_k{}^2)^3}(e_x-b_1)\left(\frac{V}{L}\right)^2\left[(\alpha_j^2+R_k{}^2)\{\alpha_j\cos(R_kt)\}+R_k\sin(R_kt)-\alpha_j\exp(-\alpha_j t)\right\}$$
$$+2\exp(-\alpha_j t)\left\{\alpha_j^2+\exp(\alpha_j t)\cos(R_kt)[R_k{}^2(\alpha_j t+1)+\alpha_j^2(\alpha_j t-1)]\right. \qquad \text{(C-71)}$$
$$\left.+R_k\exp(\alpha_j t)\sin(R_kt)[R_k{}^2t+\alpha_j(\alpha_j t-2)]-R_k{}^2\right\}\Big]$$
$$+c_{t11}\frac{h_1V}{LL_r(R_k^2+\alpha_j^2)}(e_x-b_1)[R_kL\{\exp(-\alpha_j t)+\sin(R_kt)\}-L\alpha_j\cos(R_kt)]$$

$$I_{jk\,72}=\frac{4c_{t21}h_0L}{(\alpha_j^2+R_k{}^2)^3}(e_x+b_2)\left(\frac{V}{L}\right)^2\left[(\alpha_j^2+R_k{}^2)\{\alpha_j\cos(R_kt)\}+R_k\sin(R_kt)-\alpha_j\exp(-\alpha_j t)\right\}$$
$$+2\exp(-\alpha_j t)\left\{\alpha_j^2+\exp(\alpha_j t)\cos(R_kt)[R_k{}^2(\alpha_j t+1)+\alpha_j^2(\alpha_j t-1)]\right. \qquad \text{(C-72)}$$
$$\left.+R_k\exp(\alpha_j t)\sin(R_kt)[R_k{}^2t+\alpha_j(\alpha_j t-2)]-R_k{}^2\right\}\Big]$$
$$+c_{t21}\frac{h_1V}{LL_r(R_k^2+\alpha_j^2)}(e_x-b_1)[R_kL\{\exp(-\alpha_j t)+\sin(R_kt)\}-L\alpha_j\cos(R_kt)]$$

$$I_{jk\,81}=\frac{4c_{t12}h_0}{V(\alpha_j^2+R_k{}^2)^2}(e_x-b_1)\left[-R_k\sin(S_k-R_kt)\{l_v(\alpha_j^2+R_k{}^2)+L(\alpha_j^2+R_k{}^2)-2V[R_k{}^2t+\alpha_j(\alpha_j t-2)]\}\right.$$
$$+\cos(S_k-R_kt)\{R_k{}^2[\alpha_j(l_v+L)-2V(\alpha_j t+1)]+\alpha_j^2[\alpha_j(l_v+L)+2V(1-\alpha_j t)]\}$$
$$+\exp(-\alpha_j t)\left\{R_k\sin(S_k)[l_v(\alpha_j^2+R_k{}^2)+L(\alpha_j^2+R_k{}^2)+4\alpha_j V]\right.$$
$$\left.\left.+\cos(S_k)[R_k{}^2\{2V-\alpha_j(l_v+L)\}-\alpha_j^2\{\alpha_j(l_v+L)+2V\}]\right\}\right]$$
$$+c_{t12}\frac{h_1V}{LL_r(R_k^2+\alpha_j^2)}(e_x-b_1)[R_kL\{\exp(-\alpha_j t)+\sin(R_kt)\}-L\alpha_j\cos(R_kt)]$$

(C-73)

$$I_{jk82}=\frac{4c_{t22}h_0}{V(\alpha_j^2+R_k{}^2)^2}(e_x+b_2)\Big[-R_k\sin(S_k-R_kt)\{l_v(\alpha_j^2+R_k{}^2)+L(\alpha_j^2+R_k{}^2))]\}$$
$$-2V[R_k{}^2t+\alpha_j(\alpha_jt-2$$
$$+\cos(S_k-R_kt)\{R_k{}^2[\alpha_j(l_v+L)-2V(\alpha_jt+1)]+\alpha_j^2[\alpha_j(l_v+L)+2V(1-\alpha_jt)]\}$$
$$+\exp(-\alpha_jt)\Big\{R_k\sin(S_k)[l_v(\alpha_j^2+R_k{}^2)+L(\alpha_j^2+R_k{}^2)+4\alpha_jV]$$
$$+\cos(S_k)[R_k{}^2\{2V-\alpha_j(l_v+L)\}-\alpha_j^2\{\alpha_j(l_v+L)+2V\}]\Big\}\Big]$$
$$+c_{t22}\frac{h_1V}{LL_r(R_k^2+\alpha_j^2)}(e_x+b_2)[R_kL\{\exp(-\alpha_jt)+\sin(R_kt)\}-L\alpha_j\cos(R_kt)] \quad \text{(C-74)}$$

If $L_r/V<t\le L/V$

$$I_{jk51}=\frac{4k_{t11}h_0L}{V(\alpha_j^2+R_k{}^2)^3}(e_x-b_1)\Big[(\alpha_j^2+R_k{}^2)\exp(-\alpha_jt)\Big\{\alpha_j^2+\exp(-\alpha_jt)\cos(R_kt)$$
$$\times[R_k{}^2(\alpha_jt+1)+\alpha_j^2(\alpha_jt-1)]+R_k\exp(\alpha_jt)\sin(R_kt)[R_k{}^2t+\alpha_j(\alpha_jt-2)]-R_k{}^2\Big\}$$
$$+2\alpha_j\exp(-\alpha_jt)(\alpha_j^2+3R_k{}^2)+R_k\sin(R_kt)\Big\{6\alpha_j^2+t^2(\alpha_j^2+R_k{}^2)^2+4\alpha_jt(\alpha_j^2+R_k{}^2)-2R_k{}^2\Big\} \quad \text{(C-75)}$$
$$+\cos(R_kt)\Big\{2t(R_k{}^4-\alpha_j^4)+2\alpha_j(\alpha_j^2-3R_k{}^2)\alpha_jt^2(\alpha_j^2+R_k{}^2)^2\Big\}\Big]$$
$$+k_{t11}\frac{\exp(-\alpha_jt)h_1LV}{LL_r(R_k^2+\alpha_j^2)}(e_x-b_1)[2L^3\alpha_j-\exp(-\alpha_jt)\{-R_kL[R_k^2L^2t+L^2\alpha_j(\alpha_jt-2)]\sin(R_kt)$$
$$-L\exp(-\alpha_jt)\{L^2\alpha_j^2(\alpha_jt-1)+R_k^2L^2t(\alpha_jt+1)\}\cos(R_kt)\}]$$

$$I_{jk52}=\frac{4k_{t21}h_0L}{V(\alpha_j^2+R_k{}^2)^3}(e_x+b_2)\Big[(\alpha_j^2+R_k{}^2)\exp(-\alpha_jt)\Big\{\alpha_j^2+\exp(-\alpha_jt)\cos(R_kt)[R_k{}^2(\alpha_jt+1)+\alpha_j^2(\alpha_jt-1)]$$
$$+R_k\exp(\alpha_jt)\sin(R_kt)[R_k{}^2t+\alpha_j(\alpha_jt-2)]-R_k{}^2\Big\}+2\alpha_j\exp(-\alpha_jt)(\alpha_j^2+3R_k{}^2)$$
$$+R_k\sin(R_kt)\Big\{6\alpha_j^2+t^2(\alpha_j^2+R_k{}^2)^2+4\alpha_jt(\alpha_j^2+R_k{}^2)-2R_k{}^2\Big\}+\cos(R_kt)\Big\{2t(R_k{}^4-\alpha_j^4)+2\alpha_j(\alpha_j^2-3R_k{}^2)$$
$$\alpha_jt^2(\alpha_j^2+R_k{}^2)^2\Big\}\Big]+k_{t21}\frac{\exp(-\alpha_jt)h_1LV}{LL_r(R_k^2+\alpha_j^2)}(e_x+b_2)[2L^3\alpha_j$$
$$+\exp(-\alpha_jt)\{R_kL[R_k^2L^2t+L^2\alpha_j(\alpha_jt-2)]\sin(R_kt)$$
$$-L\exp(-\alpha_jt)\{L^2\alpha_j^2(\alpha_jt-1)+R_k^2L^2t(\alpha_jt+1)\}\cos(R_kt)\}]$$
$$+k_{t21}\frac{\exp(-\alpha_jt)h_1LV}{LL_r(R_k^2+\alpha_j^2)}(e_x+b_2)[2L^3\alpha_j-\exp(-\alpha_jt)\{-R_kL[R_k^2L^2t+L^2\alpha_j(\alpha_jt-2)]\sin(R_kt)$$
$$-L\exp(-\alpha_jt)\{L^2\alpha_j^2(\alpha_jt-1)+R_k^2L^2t(\alpha_jt+1)\}\cos(R_kt)\}]$$

(C-76)

$$I_{jk\,61}=\frac{4k_{t12}h_0}{L^2}(e_x-b_1)\left[\left\{\frac{l_v(l_v+L)\exp(-\alpha_j t)\{\alpha_j\cos(S_k-R_kt)-R_k\sin(S_k-R_kt)\}+R_k\sin(S)-\alpha_j\cos(S_k)}{\alpha_j^2+R_k{}^2}\right\}\right.$$
$$+\frac{2LV\exp(-\alpha_j t)}{(\alpha_j^2+R_k{}^2)^2}\{(\alpha_j^2+R_k{}^2)\cos(S_k)+\exp(\alpha_j t)\cos(S_k-R_kt)[R^2(\alpha_j t+1)+\alpha_j^2(\alpha_j t-1)]$$
$$+R_k[R_k{}^2t+\alpha_j(\alpha_j t-2)]\sin(S_k-R_kt)-2\alpha_j R_k\sin(S_k)\}$$
$$-\frac{V^2}{(\alpha_j^2+R_k{}^2)^3}\{R_k\sin(S_k-R_kt)[6\alpha_j^2+t^2(\alpha_j^2+R_k{}^2)^2-4\alpha_j t(\alpha_j^2+R_k{}^2)-2R_k{}^2]$$
$$+2\exp(-\alpha_j t)[(\alpha_j^3-3\alpha_j R_k{}^2)\cos(S_k)+R_k(R_k{}^2-3\alpha_j^2)\sin(S_k)]$$
$$\left.-[2t(R_k{}^4-\alpha_j^4)+2\alpha_j(\alpha_j^2-3R_k{}^2)+\alpha_j t^2(\alpha_j^2+R_k{}^2)^2]\cos(S_k-R_kt)\right]$$
$$+k_{t12}\frac{\exp(-\alpha_j t)h_1LV}{LL_r(R_k^2+\alpha_j^2)}(e_x-b_1)[-R_kL\exp(-\alpha_j t)\{R_k^2L^2t+L^2\alpha_j(\alpha_j t-2)\}\sin(R_kt)$$
$$-2R_kL^3\alpha_j-\exp(-\alpha_j t)\{L^3\alpha_j(\alpha_j t-1)+R_k^2L^2(\alpha_j t+1)\}\cos(R_kt)$$

(C-77)

$$I_{jk\,62}=\frac{4k_{t22}h_0}{L^2}(e_x+b_2)\left[\left\{\frac{l_v(l_v+L)\exp(-\alpha_j t)\{\alpha_j\cos(S_k-R_kt)-R_k\sin(S_k-R_kt)\}+R_k\sin(S)-\alpha_j\cos(S_k)}{\alpha_j^2+R_k{}^2}\right\}\right.$$
$$+\frac{2LV\exp(-\alpha_j t)}{(\alpha_j^2+R_k{}^2)^2}\{(\alpha_j^2+R_k{}^2)\cos(S_k)+\exp(\alpha_j t)\cos(S_k-R_kt)[R^2(\alpha_j t+1)+\alpha_j^2(\alpha_j t-1)]$$
$$+R_k[R_k{}^2t+\alpha_j(\alpha_j t-2)]\sin(S_k-R_kt)-2\alpha_j R_k\sin(S_k)\}$$
$$-\frac{V^2}{(\alpha_j^2+R_k{}^2)^3}\{R_k\sin(S_k-R_kt)[6\alpha_j^2+t^2(\alpha_j^2+R_k{}^2)^2-4\alpha_j t(\alpha_j^2+R_k{}^2)-2R_k{}^2]$$
$$+2\exp(-\alpha_j t)[(\alpha_j^3-3\alpha_j R_k{}^2)\cos(S_k)+R_k(R_k{}^2-3\alpha_j^2)\sin(S_k)]$$
$$\left.-[2t(R_k{}^4-\alpha_j^4)+2\alpha_j(\alpha_j^2-3R_k{}^2)+\alpha_j t^2(\alpha_j^2+R_k{}^2)^2]\cos(S_k-R_kt)\right]$$
$$+k_{t22}\frac{\exp(-\alpha_j t)h_1LV}{LL_r(R_k^2+\alpha_j^2)}(e_x+b_2)[-R_kL\exp(-\alpha_j t)\{R_k^2L^2t+L^2\alpha_j(\alpha_j t-2)\}]\sin(R_kt)$$
$$-2R_kL^3\alpha_j-\exp(-\alpha_j t)\{L^3\alpha_j(\alpha_j t-1)+R_k^2L^2(\alpha_j t+1)\}\cos(R_kt)$$

(C-78)

$$I_{jk\,71}=\frac{4c_{t11}h_0L}{(\alpha_j^2+R_k{}^2)^3}(e_x-b_1)\left(\frac{V}{L}\right)^2\left[(\alpha_j^2+R_k{}^2)\{\alpha_j\cos(R_kt)\}+R_k\sin(R_kt)-\alpha_j\exp(-\alpha_j t)\right\}$$
$$+2\exp(-\alpha_j t)\{\alpha_j^2+\exp(\alpha_j t)\cos(R_kt)[R_k{}^2(\alpha_j t+1)+\alpha_j^2(\alpha_j t-1)]$$
$$\left.+R_k\exp(\alpha_j t)\sin(R_kt)[R_k{}^2t+\alpha_j(\alpha_j t-2)]-R_k{}^2\}\right]$$

(C-79)

$$I_{jk\,72}=\frac{4c_{t21}h_0L}{(\alpha_j^2+R_k{}^2)^3}(e_x+b_2)\left(\frac{V}{L}\right)^2\left[(\alpha_j^2+R_k{}^2)\{\alpha_j\cos(R_kt)\}+R_k\sin(R_kt)-\alpha_j\exp(-\alpha_j t)\right\}$$
$$+2\exp(-\alpha_j t)\{\alpha_j^2+\exp(\alpha_j t)\cos(R_kt)[R_k{}^2(\alpha_j t+1)+\alpha_j^2(\alpha_j t-1)]$$
$$\left.+R_k\exp(\alpha_j t)\sin(R_kt)[R_k{}^2t+\alpha_j(\alpha_j t-2)]-R_k{}^2\}\right]$$

(C-80)

$$I_{jk\,81}=\frac{4c_{t12}h_0}{V(\alpha_j^2+R_k{}^2)^2}(e_x-b_1)\Big[-R_k\sin(S_k-R_kt)\{l_v(\alpha_j^2+R_k{}^2)+L(\alpha_j^2+R_k{}^2)-2V[R_k{}^2t+\alpha_j(\alpha_jt-2)]\}$$
$$+\cos(S_k-R_kt)\{R_k{}^2[\alpha_j(l_v+L)-2V(\alpha_jt+1)]+\alpha_j^2[\alpha_j(l_v+L)+2V(1-\alpha_jt)]\}$$
$$+\exp(-\alpha_jt)\Big\{R_k\sin(S_k)[l_v(\alpha_j^2+R_k{}^2)+L(\alpha_j^2+R_k{}^2)+4\alpha_jV]$$
$$+\cos(S_k)[R_k{}^2\{2V-\alpha_j(l_v+L)\}-\alpha_j^2\{\alpha_j(l_v+L)+2V\}]\Big\}\Big] \qquad \text{(C-81)}$$

$$I_{jk\,82}=\frac{4c_{t22}h_0}{V(\alpha_j^2+R_k{}^2)^2}(e_x+b_2)\Big[-R_k\sin(S_k-R_kt)\{l_v(\alpha_j^2+R_k{}^2)+L(\alpha_j^2+R_k{}^2))]\}$$
$$-2V[R_k{}^2t+\alpha_j(\alpha_jt-2$$
$$+\cos(S_k-R_kt)\{R_k{}^2[\alpha_j(l_v+L)-2V(\alpha_jt+1)]+\alpha_j^2[\alpha_j(l_v+L)+2V(1-\alpha_jt)]\}$$
$$+\exp(-\alpha_jt)\Big\{R_k\sin(S_k)[l_v(\alpha_j^2+R_k{}^2)+L(\alpha_j^2+R_k{}^2)+4\alpha_jV]$$
$$+\cos(S_k)[R_k{}^2\{2V-\alpha_j(l_v+L)\}-\alpha_j^2\{\alpha_j(l_v+L)+2V\}]\Big\}\Big] \qquad \text{(C-82)}$$

<u>For static weight of vehicle</u> $(0\le t\le L/V)$

$$I_{jk\,91}=-e_x\frac{\exp(-\alpha_jt)gL(l_vm_v+4m_{w11})}{4(L^2\alpha_j^2+R_k^2L)}\Big[\exp(\alpha_jt)R_kL\sin(R_kt)-L\alpha_j+\exp L\alpha_j(\alpha_jt)\cos(R_kt)\}\Big]$$
$$+e_x\frac{\exp(-\alpha_jt)gL(l_vm_v+4m_{w12})}{4(L^2\alpha_j^2+R_k^2L)}\Big[R_kL\{\sin(S_kl_v)-\exp(\alpha_jt)\sin[S_k(l_v-Vt)]\}$$
$$-e_xL\alpha_j\{\cos(S_kl_v)-\exp(\alpha_jt)\cos[S_k(l_v-Vt)]\}\Big] \qquad \text{(C-83)}$$

$$I_{jk\,92}=-e_x\frac{\exp(-\alpha_jt)gL(l_vm_v+4m_{w21})}{4(L^2\alpha_j^2+R_k^2L)}\Big[\exp(\alpha_jt)R_kL\sin(R_kt)-L\alpha_j+\exp L\alpha_j(\alpha_jt)\cos(R_kt)\}\Big]$$
$$+e_x\frac{\exp(-\alpha_jt)gL(l_vm_v+4m_{w22})}{4(L^2\alpha_j^2+R_k^2L)}\Big[R_kL\{\exp(\alpha_jt)\sin[S_k(l_v-Vt)]-\sin(S_kl_v)\}$$
$$-e_xL\alpha_j\{\exp(\alpha_jt)\cos[S_k(l_v-Vt)]-\cos(S_kl_v)\}\Big] \qquad \text{(C-84)}$$

APPENDIX D

Numerical Solution of Vehicle Bridge system using Newmark Method

The following steps are carried out for numerical solution of bridge vehicle interaction problem representing generalized multi degree of freedom system (Bathe, 2006):

1. Form mass [M], damping [$C(t)$], stiffness [$K(t)$] matrices and force vector {$F(t)$} of the vehicle and bridge system.

2. Initialize displacement and velocity vectors of the bridge and the vehicle generalized coordinates

$$\{x(t)\}\,|_{t=0} = \{u_v^0; \dot{u}_v^0; u_b^0; \dot{u}_b^0\} \tag{D-1}$$

where, $\{x(t)\}\big|_{t=0}$ denotes initial response of system generalized coordinates at t=0; u_v^0 and u_b^0 represent vehicle and bridge initial response, respectively.

3. Find initial acceleration of vehicle and bridge system using the relation

$$\{\ddot{x}(t)\}\big|_{t=0} = [M]^{-1}(\{F(t)\} - [C(t)][\{\dot{x}(t)\} - [K(t)]\{x(t)\})\big|_{t=0} \tag{D-2}$$

4. Select time step size Δt and integration parameters α, β and a_j in the Newmark- β method. where j=0,1,2,…,7.

$$\alpha \geq \frac{1}{2}, \quad \beta \geq \frac{1}{4}\left(\frac{1}{2}+\alpha\right)^2 \tag{D-3}$$

$$\begin{aligned} a_0 &= \frac{1}{\beta \Delta t^2}, \; a_1 = \frac{\alpha}{\beta \Delta t}, \; a_2 = \frac{1}{\beta \Delta t}, \; a_3 = \frac{1}{2\beta} - 1 \\ a_4 &= \frac{\alpha}{\beta} - 1, \; a_5 = \frac{\Delta t}{2}\left(\frac{\alpha}{\beta} - 2\right), \; a_6 = \Delta t(1-\alpha), \; a_7 = \alpha \Delta t \end{aligned} \tag{D-4}$$

5. For $t \leq \tau$, where τ is a bridge loading time. Calculate system responses using the following expressions

(i) The displacement vector $\{x(t)\}\big|_{t=t+\Delta t}$, starting with t=0 and using the following equation

$$\begin{aligned} \{x(t)\}\big|_{t=t+\Delta t} = &\left[a_0[M] + a_1[C(t)]\big|_{t=t} + [K(t)]\big|_{t=t}\right]^{-1} \\ &\times \Big\{\{F(t)\}\big|_{t=t+\Delta t} + [M]\left(a_0\{x(t)\}\big|_{t=t} + a_1\{\dot{x}(t)\}\big|_{t=t} + a_3\{\ddot{x}(t)\}\big|_{t=t}\right) \\ &+ [C(t)]\big|_{t=t}\left(\{a_1 x(t)\}\big|_{t=t} + a_4\{\dot{x}(t)\}\big|_{t=t}\right) + \{a_5\ddot{x}(t)\}\big|_{t=t}\Big\} \end{aligned} \tag{D-5}$$

(ii) The acceleration and velocity vectors of the system's generalized coordinate at time $t=t+\Delta t$

$$\{\ddot{x}(t)\}\big|_{t=t+\Delta t} = a_0\left(\{x(t)\}\big|_{t=t+\Delta t} - \{x(t)\}\big|_{t=t}\right) - a_2\{\dot{x}(t)\}\big|_{t=t} - a_3\{\ddot{x}(t)\}\big|_{t=t} \tag{D-6}$$

$$\{\dot{x}(t)\}\big|_{t=t+\Delta t} = \{\dot{x}(t)\}\big|_{t=t} + a_6\{\ddot{x}(t)\}\big|_{t=t} - a_7\{\ddot{x}(t)\}\big|_{t=t+\Delta t} \tag{D-7}$$

6. For $\tau < t \leq T$, where T is the total time considered for system response calculation including residual response, calculate system responses using the following relations

(i) The displacement vector $\{x(t)\}\big|_{t=t+\Delta t}$, starting with $t=\tau$ and using the equation

$$\begin{aligned}\{x(t)\}\big|_{t=t+\Delta t} = &\left[a_0[M] + a_1[C(t)]\big|_{t=\tau} + [K(t)]\big|_{t=\tau}\right]^{-1} \\ &\times\Big\{\{F(t)\}\big|_{t=\tau} + [M]\left(a_0\{x(t)\}\big|_{t=t} + a_1\{\dot{x}(t)\}\big|_{t=t} + a_3\{\ddot{x}(t)\}\big|_{t=t}\right) \\ &+ [C(t)]\big|_{t=\tau}\left(\{a_1 x(t)\}\big|_{t=t} + a_4\{\dot{x}(t)\}\big|_{t=t}\right) + \{a_5\ddot{x}(t)\}\big|_{t=t}\Big\}\end{aligned} \tag{D-8}$$

(ii) The acceleration and velocity vectors of the system's generalized coordinate at time $t=t+\Delta t$

$$\{\ddot{x}(t)\}\big|_{t=t+\Delta t} = a_0\left(\{x(t)\}\big|_{t=t+\Delta t} - \{x(t)\}\big|_{t=t}\right) - a_2\{\dot{x}(t)\}\big|_{t=t} - a_3\{\ddot{x}(t)\}\big|_{t=t} \tag{D-9}$$

$$\{\dot{x}(t)\}\big|_{t=t+\Delta t} = \{\dot{x}(t)\}\big|_{t=t} + a_6\{\ddot{x}(t)\}\big|_{t=t} - a_7\{\ddot{x}(t)\}\big|_{t=t+\Delta t} \tag{D-10}$$

REFERENCES

Ahmari, S., Yang, M. and Zhong, H. (2015). "Dynamic interaction between vehicle and bridge deck subjected to support settlement." *Engineering Structures*, 84, 172–183.

Akin, J. E. and Mofid, M. (1989). "Numerical solution for response of beams with moving mass." *Journal of Structural Engineering*, 115 (1), 120-131.

Arasaratnam, I., Haykin, S., and Elliot, R. (2007)."Discrete-time nonlinear filtering algorithms using Gauss-Hermite quadrature." *Proceedings of IEEE*, 95(5), 953-977.

Arulampalam, M. S., Maskel, S., Gordon, N. and Clapp, T. (2002). "A tutorial on Particle Filters for Online Nonlinear/Non-Gaussian Bayesian Tracking." *IEEE transcation on signal processing*, 50 (2), 174-188.

Asnachinda, P., Pinkaew, T., and Laman, J.A. (2008). "Multiple vehicle axle load identification from continuous bridge bending moment response." *Engineering Structures*, 30(10), 2800–2817.

Ayre, R. S., Ford, G., and Jacobsen, L. S. (1950). "Transverse vibration of a two-span beam under action of a moving constant force." *Journal of Applied Mechanics*, 17(1), 1-12

Ayre, R. S., and Jacobsen, L. S. (1950). "Transverse vibration of a two-span beam under the action of a moving alternating force." *Journal of Applied Mechanics*, 17(3), 283–290.

Azimi, H., Galal, K., and Oscar, A. Pekau, O. A., (2013). "A numerical element for vehicle–bridge interaction analysis of vehicles experiencing sudden deceleration." *Engineering Structures,* 49,792-805

Baruch, M. and Bar Itzhack, I. Y. (1978). "Optimum weighted orthogonalization of measured modes," *The American Institute of Aeronautics and Astronautics Journal*, 16(4), 346-351.

Bayes, T. and Price, R. (1763). "An Essay Towards Solving a Problem in the Doctrine of Chances". *Philosophical Transactions of the Royal Society of London*, 53, 370-418.

Bathe, K.J., (2006). *Finite Element Procedures*, Prentice-Hall, Inc. New Jersey.

Berman, A., and Nagy, E.J. (1983). "Improvement of a Large Analytical Model Using Test Data." *The American Institute of Aeronautics and Astronautics Journal*, 21(8), 1168–1173.

Bernardo, J. M. and Smith, A. F. M. (1998), *Bayesian Theory*, 2nd Ed., New York: Wiley.

Biggs, J. M. (1964), *Introduction to Structural Dynamics,* 1st Ed., McGraw-Hill Book Co., Inc., New York, N. Y., 315-328.

Bogosjo, K., Podgorski, K., and Rychlik, I. (2012). "Models for road roughness." *Vehicle System Dynamics*, 50(5), 725-747.

Box, G. E. P., and Draper, N. R., (1987), *Empirical Model Building and Response Surfaces*, John Wiley & Sons, New York, NY.

Box, G. E. P., and Wilson, K. B., (1951). "On the Experimental Attainment of Optimum Conditions." *Journal of the Royal Statistical Society*, *Series B*, 13, 1-45.

Brady, S. P., O'Brien, E. J., and Znidaric, A. (2006). "Effect of vehicle velocity on the dynamic amplification of a vehicle crossing a simply supported bridge." *Journal of Bridge Engineering,* 11 (2), 241-249.

Brencich, A., and Sabia, D. (2007). "Tanaro Bridge: Dynamic Tests on a Couple of Spans." *Journal of Bridge Engineering*. 12(5), 662-665.

Brownjohn, J.M.W., Moyo, P., Omenzetter, P. and Lu, Y. (2003). "Assessment of Highway Bridge Updating by Dynamic Testing and Finite Element Model Updating," *Journal of Bridge Engineering*. 8(3), 162-172.

Caflisch, R. E. (1998). "Monte Carlo and quasi-Monte Carlo methods." *Acta Numerica, Cambridge University Press,* 7, 1-49.

Cai, C. S., and Chen, S. R. (2004) "Framework of vehicle-bridge-wind dynamic analysis." *Journal of Wind Engineering and Industrial Aerodynamics*, 92(7-8), 597-607.

Cai, C.S., Shi, X.M., Araujo, M., and Chen, S.R., (2009). "Effect of approach span condition on vehicle-induced dynamic response of slab-on-girder road bridges." *Engineering Structures*, 29(12), 3210-3226.

Candy, J. V. (2009), *Bayesian Signal Processing- Classical, Modern and Particle Filtering Methods*, John Wiley & Sons, Inc. New York, USA.

Cantero, D., O'Brien, E. J., and Gonzalez, A. (2010). "Modelling the vehicle in vehicle-infrastructure dynamic studies." *Journal of Multibody Dynamics*, 224 (K2), 243-248.

Cantero, D., and O'Brien, E. J, (2013). "The Non-Stationarity of Apparent Bridge Natural Frequencies during Vehicle Crossing Events." *FME Transactions,* 41, 279-284.

Captain, K.M., Boghani, A.B., and Wormley, D.N. (1979). "Analytical Tire Models for Dynamic Vehicle Simulation." *Vehicle System Dynamics*, 8(1), 1-32.

Carden, E. P., and Fanning, P. (2014). "Vibration based condition monitoring: A review." *Structural Health Monitoring*, 3(4), 355-377.

Casas, J. R., and Aparicio, C. (1994). "Structural damage identification from dynamic test data." *Journal of Structural Engineering*, 120 (8), 2437-2450.

Cebon, D. (1999). *Handbook of Vehicle-Road Interaction*. Taylor & Francis.

Chan, T. H. T., and O'Connor, C. (1990). "Vehicle model for highway bridge impact." *Journal of Structural Engineering*, 116(7), 1772-1793.

Chan, T. H. T, Law, S. S., Yung T. H., and Yuan, X. R., (1999). "An interpretive method for moving force identification." *Journal of Sound and Vibration*, 219(3), 503-524.

Chan, T. H. T, Law, S. S. and Yung, T. H., (1999). "Moving force identification using existing pre-stress concrete bridge." *Journal of Structural Engineering*, 22(10), 1261-1270.

Chan, T. H. T., Yu, L., and Law, S. S. (2000). "Comparative studies on moving force identification from bridge strains in laboratory." *Journal of Sound and Vibration*, 235(1), 87-104.

Chang, D. (1994). "Impact factor for simple span highway girder bridges." *Journal of Structural Engineering*, 120 (3), 705-715

Chang, K.C., Wu, F.B., and Yang, Y.B. (2011). "Disk model for wheels moving over highway bridges with rough surfaces." *Journal of Sound and Vibration*, 330(20), 4930-4944.

Chatterjee, P. K., Datta, T. K., and Surana, C. S. (1993). "Dynamic response of truss bridge for moving loads." *Computers and Structures,* 46(6), 1085–1093.

Chatterjee, P. K., Datta, T. K., and Surana, C. S. (1994). "Vibration of continuous bridges under moving vehicle." *Journal of Sound and Vibration*, 169(5), 619–623.

Chatterjee, P. K., Datta, T. K., and Surana, C. S. (1994). "Vibration of suspension bridges under vehicular movement." *Journal of Structural Engineering*, 120(3), 681-703.

Chatterjee, P. K., and Datta, T. K. (1995). "Dynamic analysis of arch bridges under travelling loads." *International Journal of Solids and Structures*, 32(11), 1585–1594.

Chatterjee, P, O'Brien, E., Li, Y., and Gonzalez, A (2006). "Wavelet domain analysis for identification of vehicle axles from bridge measurements." *Computers and Structures*, 84 (28), 1792-1801.

Chen, Y. H. (1978). "Dynamic analysis of continuous beams subjected to moving loads." *Journal of Civil and Hydraulic Engineering*, 5(2), 1–7.

Chen, Y. H., and Li, C. Y. (2000). "Dynamic response of elevated high-speed railway." *Journal of Bridge Engineering*, 5(2), 124–130.

Cheng, L., Zhang, H., and Li, Q. (2007). "Design of capacitive flexible weighing sensor for vehicle WIM systems." *Sensors*, 7(8), 1530-1544.

Cheung, Y. K., Au, F. T. K., Zheng, D. Y., and Cheng, Y. S. (1999). "Vibration of multi-span non-uniform bridges under moving vehicles and trains by using modified beam vibration functions." *Journals of Structural Engineering*, 228 (3), 611–628.

Chopra, A. K. (2009). *Dynamics of Structures*. 3rd Ed., Pearson Prentice Hall, New Delhi, India.

Chu, K. H., Garg, V. K., and Dhar, C. L. (1979). "Railway–bridge impact: Simplified train and bridge model." *Journals of the Structural Division*, 105(9), 1823–1844.

Chu, K. H., Garg, V. K., and Wang, T. L., (1986). "Impact in railway pre-stressed concrete bridges." *Journals of Structural Engineering,* 112 (5), 1036–1051.

Cunha, A., Caetano, E., and Delgado, R. (2001). "Dynamic test on large Cable-Stayed Bridge." *Journal of Bridge Engineering*, 6(1), 54-62.

Conte, J. P. M., He, X., Moaveni, B., Masri, S. F., Caffrey, J. P., Wanhbeh, M., Tasbihoo, F., Whang, D. H., and Elgamal, A. (2008). "Dynamic testing of Alfred Zampa Memorial Bridge". *Journal of Structural Engineering*, 134 (6), 1006-1015.

Coussy, O., Said, M., and Van Hoove, J.P., (1988). "The influence of random surface irregularities on the dynamic response of bridges under suspended moving loads." *Journal of Sound and Vibration,* 130(2), 313-320.

Costley, R.D., Diaz-Alvarez, H., Mc Kenna, M. H. and Joran, A.M., (2015). "Vibration and Acoustic Analysis of Trussed Railroad Bridge under Moving Loads." *Journal of Vibration and Acoustics*, 137(3), 1-10

Davidson ,P., Collin, J., Raquet, J., and Takala, J. (2010). "Application of Particle Filters for Vehicle Positioning Using Road Maps." 23rd International Technical Meeting of the Satellite Division of The Institute of Navigation, Portland, September 21-24, 1653-1661.

Deb, K. (2012). *Optimization for Engineering Design: Algorithm and Examples*. PHI Learning Pvt. Ltd. New Delhi, India

DeCoursey, W.J., (2003). *Statistics and Probability for Engineering Applications*. 1st Ed., Newnespress publication, United Sates of America.

Deng, L. and Cai, C.S. (2009), "Identification of parameters of vehicles moving on bridges", *Engineering Structures*, 31(10), 2474-2485

Detailed Project Report, Volume-I (2012). "Construction of Bridge on the river Yomgo at Paya Village" Public Works Department, Govt. of Arunachal Pradesh, India.

Djuric, P. M. and Bugallo, M. F. (2009). "Estimation of stochastic rate constants and tracking of species in biochemical networks with second-order reactions." 17th

European Signal Processing Conference (EUSIPCO 2009), Glasgow, Scotland, August 24-28, 2308-2311.

Doebling, S. W., Farrar, C. R., Prime, M. B., and Shevitz, D. W. (1996). "Damage identification and health monitoring of structural mechanical systems from changes in their vibration characteristics: A literature review." Rep. No. LA-13070-MS, Los Alamos National Laboratory, Los Alamos, N.M.

Dodds, C.J., and Robson, J.D., (1973). "The description of road surface roughness." *Journal of Sound and Vibration*, 31(2), 175-183.

Douglas, C. M. (2005). *Design and Analysis of Experiments: Response surface method and designs.* New Jersey: John Wiley and Sons, Inc.

Dugush, Y. A., and Eisenberger, M. (2002). "Vibrations of non-uniform continuous beams under moving loads." *Journal of Sound and Vibration*, 254(5), 911–926.

Esfandiari, A., Sanayei, M., Rahai, A., and Nejad, F.B. (2012). "Quasi-linear sensitivity-based structural model updating using experimental transfer functions." *Structural Health Monitoring An International Journal*, 11, 656-670.

Fertis, D. G. (1973). *Dynamics and Vibration of Structures*. John Wiley & Sons, New York.

Friswell, M. I., and Mottershead, J. E. (1995). *Finite element model updating in structural dynamics*. Kluwer Academic, Dordrecht, the Netherlands.

Fryba, L., (1972). *Vibration of Solids and Structures under Moving Loads.* 1st Ed., Noordhoff International Publishing, Groningen, the Netherlands.

Fryba, L., (1996). *Dynamics of Railway Bridge,* 1st Ed., Thomas Telford Ltd., London.

Fu, C. (2015). "The effect of switching cracks on the vibration of a continuous beam bridge subjected to moving vehicles." *Journal of Sound and Vibration*, 339,157–175.

Galdos, N. H., Schelling, D. R., and Sahin, M. A. (1993). "Methodology for impact factor of horizontally curved box bridges." *Journals of Structural Engineering*, 119 (6), 1917–1934.

Galdos, N. H., Schelling, D. R., and Sahin, M. A. (1993). "Methodology for impact factor of horizontally curved box bridges." *Journal of Structural Engineering*, 119(6), 1917–1934.

Gbadeyan, J. A., and Oni, S. T. (1995). "Dynamic behaviour of beams and rectangular plates under moving loads." *Journal of Sound and Vibration*, 182(5), 677–695.

Genin, J., Ginsberg, J. H., and Ting, E. C. (1975). "A complete formulation of inertial effects in the guideway–vehicle interaction problem." *Journal of Sound and Vibration*, 38(1), 15–26.

Genin, J., and Chung, Y. I. (1979). "Response of a continuous guideway on equally spaced supports traversed by a moving vehicle." *Journal of Sound and Vibration*, 67(2), 245–251.

Goldberg, D.E. (1989). *Genetic Algorithms in Search, Optimization, and Machine Learning*, Addison-Wesley, USA

Gordon, R. J.,Salmond, D. J., and Smith, A.F.M. (1993). "Novel Approach to nonlinear/non-gaussian Bayesian state estimation." In IEE Proceedings-F, April 1993, 140 (2), 107-113.

Gonzalez, A., Cantero, D., and O'Brien, E.J. (2011). "Dynamic increment for shear force due to heavy vehicles crossing a highway bridge." *Computers and Structures,* 89(23-24), 2261–2272.

Green, M.F., and Cebon, D. (1994). "Dynamic response of highway bridges to heavy vehicle loads: Theory and experimental validation." *Journal of Sound and Vibration*, 170(1), 51–78.

Green, M.F., Cebon, D., and Cole, D.J. (1995). "Effects of heavy vehicle suspension design on dynamics of highway bridges." *Journal of Structural Engineering*, 121 (2), 272-282.

Hammersley, J. M., and Morton, K. W. (1954). "Poor man's Monte Carlo." *Journal of the Royal Statistical Society, Series B (Statistical Methodology),* 16, 23-38.

Haykin, S., and Veen, B.V. (1999). *Signal and Systems*. John Wiley and Sons (Asia), Pte. Ltd.

Helmi, K., Bakht, B., and Mufti, A. (2014). "Accurate measurements of gross vehicle weight through bridge weigh-in-motion: a case study." *Journal of Civil Structural Health Monitoring*. 4(3), 195-208.

Henchi, K., Fafard, M., Talbot, M., and Dhatt, G., (1998). "An efficient algorithm for dynamic analysis of bridge under moving vehicles using a coupled and physical components approach." *Journal of Sound and Vibration*. 212 (4), 668-683.

Honda, H., Kajkawa, Y., and Kobori, T. (1982). "Spectra of road surfaces on bridges." *Journal of Structural Engineering*, 108(9), 1956-1966.

Hossain, K.A., and Amanat, K.M. (2011). "Effect of span length on the dynamic amplification factor in the deck of concrete box girder bridges." *Journal of Civil Engineering*, 39(1), 59-75.

Hou, X., Yang, X., and Huang, Q. (2005). "Using inclinometers to measure bridge deflection." *Journal of Bridge Engineering*. 10(5), 564-569.

Huang, D., (2012). "Vehicle-Induced Vibration of Steel Deck Arch Bridges and Analytical Methodology." *Journal of Bridge Engineering*, 17 (2), 241-248.

Huang, E. S., and Nowak, A. S. (1991). "Simulation of dynamic load for bridge."*Journals of Structural Engineering*. 117 (5), 1413-1434.

Huang, D., and Wang, T. L. (1992). "Impact analysis of cable stayed bridges." *Computers and Structures*, 43 (5), 897-908.

Huang, D., Wang, T. L., and Shahawy, M. (1992). "Impact analysis of continuous multi-girder bridges due to moving vehicles." *Journals of Structural Engineering*, 118 (12), 3427–3443.

Hughes, T.J.R., (1987). *The Finite Element Method: Linear Static and Dynamic Finite Element Analysis*, Prentice Hall.

Ichikawa, M., Miyakawa, M., and Matsuda, A. (2000). "Vibration analysis of the continuous beam subjected to moving mass." *Journals of Sound and Vibration*, 230(3), 493-506.

Imine, H., Delanne, Y., and M'Sird, N. K. (2005). "Road profile inputs for evaluation of the loads on the wheels." *Vehicle System Dynamics*, 43, 359-369.

Inman, D.J. (2001). *Engineering Vibration*, 1st Ed., Prentice-Hall, Inc. Upper Saddle River, New Jersey, USA.

Inglish, E.C., Sir, (1934). "A Mathematical treatise on vibration in railway bridges." 1st Ed., University Press, Cambridge.

ISO 8608:1995. Mechanical vibration-Road surface profiles-reporting measured data.

Jadon, V. K., and Verma, S. (2010). *Machine Design Data Book*, 2nd Ed., I.K. International publishing House Pvt. Ltd. New Delhi, India.

Jankowski, L. (2013), *Dynamic load identification for structural health monitoring*, IPPT Reports on Fundamental Technological Research, ISSN 2299-3657, Institute of Fundamental Technological Research Polish Academy of Sciences, Warsaw.

Jeffcott, H. H. (1929). "On the vibration of beams under the action of moving load." *Philosophical Magazine, Series 7*, 8(48), 66-97.

Jeffrey, A. (2004), *Mathematics for Engineers and Scientists*, 6th Ed., Chapman and Hall/CRC publication.

Jerath, S. and Gurav, S. (2008). "Road Surface Roughness Generation by Power Spectral Density in Bridge Design." Proceedings of the 2008 Structures Congress: Crossing Borders, held in Vancouver, British Columbia, Canada, 1-7.

Jiang, R. J. Au, F. T. K and Cheung, Y. K., (2004). "Identification of vehicles moving on continuous bridges with rough surface." *Journal of Sound and Vibration*, 274(3-5), 1045-1063.

Johannes, M. S., Polson, N. G., and Stroud, J. R. (2009). "Optimal filtering of jump diffusions: Extracting latent states from asset prices." *Review of Financial Studies*, 22(7):2759-2799.

Johansson, C., Pacoste, C., and Karoumi, R. (2013). "Closed-form solution for the mode superposition analysis of the vibration in multi-span beam bridges caused by concentrated moving loads." *Journal of Sound and Vibration*, 119, 85–94.

Ju, S.H., and Lin, H.T. (2003). "Numerical investigation of a steel arch bridge and interaction with high-speed trains." *Engineering Structures*, 25(2), 241–250.

Ju, S.H., (2011). "Vibration Analysis of 3D Timoshenko Beams Subjected to Moving Vehicles." *Journal of Engineering Mechanics*, 137(11), 713-721.

Juang, J.N. (1994). *Applied System Identification*, PRT Prentice Hall Eaglewood Cliffs, New Jersey, USA.

Kalman, R. (1960). "A new approach to linear filtering and prediction problems." *Transactions of Journal Basic Engineering*, *ASME Series D*, 82, 35-45.

Kamesh, K. M. A., and Robson, J. D. (1978). "The application of isotropy in road surface modeling." *Journal of Sound and Vibration.* 57(1), 89-100

Kawatani, M., and Kim, C. W. (2001). "Computer simulation for dynamic wheel loads of heavy vehicles," *Structural Engineering and Mechanics*, 12(4), 409–428.

Kim, S., Shephard, N., and Chib, S. (1998). "Stochastic volatility: likelihood inference and comparison with ARCH models". *The Review of Economic Studies*, 65(3):361-393.

Kishan, H., and Traill-Nash, R. W., (1997). "A model method for calculation of highway bridge response with vehicle braking." *Civil Engineering Transactions*, Institute Engineers, Australia CE 19, 1, 44-50.

Koniditsiotis, C., and Peters, B. (2008). "Heavy Vehicle on Board Mass Monitoring: Capability Review." 5th International Conference on Weigh-In-Motion HV Paris 2008, May 19-22, 159-170.

Kou, J. W., and DeWolf, J. T. (1997). "Vibrational behavior of continuous span highway bridge -Influencing variables." *Journals of Structural Engineering*, 123(3), 333–344.

Kozar, I., and Malik, N.T., (2013). "Spectral method in realistic modeling of bridges under moving vehicles." *Engineering Structures*, 50,149–157.

Kwasniewski, L., Wekezer, J., Roufa, G., Li, H., Ducher, J., and Malachowski, J. (2006). "Experimental Evaluation of Dynamic Effects for a Selected Highway Bridge." *Journal of Performance of Constructed Facilities*, 20(3), 253-260.

Lou, P. (2005). "A vehicle-track-bridge interaction element considering vehicle's pitching effect." *Journal of Finite Elements in Analysis and Design*. 41, 397-427.

Lau, P., and Au, F.T.K. (2013). "Finite element formulae for internal forces of Bernoulli-Euler beams under moving vehicles." *Journal of Sound and Vibration*. 332(6), 1533–1552.

Law, S.S, Bu, J.Q., Zhu, X.Q., and Chan, S.L. (2004). "Vehicle axle loads identification using finite element method." *Engineering Structures*, 26(8), 1143-1153.

Law, S.S., Chan, T. H. T., and Zeng, Q. H. (1997). "Moving force identification: A time domain method." *Journal of Sound and Vibration*. 201(1), 1-22.

Law, S.S., and Zhu, X. Q. (2005). "Bridge dynamic responses due to road surface roughness and braking of vehicle." *Journal of Sound and Vibration*, 282(3-5), 805-830.

Lee, P. K. K., Ho, M.D., and Chung, H. W. (1987). "Static and dynamics tests of concrete bridge." *Journal of Structural Engineering*, 113(1), 61-73.

Li, C.Y. (1996). "Bridge vibration and impact under moving vehicles." Proceedings of the 1996. 3rd Joint Conference on Engineering Systems Design and Analysis, ESDA. July 1-4 1996. Montpellier, 81(9), 17-23.

Li, J., Su, M. and Fan, L. (2003), "Natural frequency of railway girder bridges under vehicle loads." *Journal of Bridge Engineering*, 8(4), 199-203.

Li, H. and Wekezer, J. F. (2008). "Dynamic response of a highway bridge subjected to moving vehicle". *Journal of Bridge Engineering*. 13(5), 439-448.

Liljencrantz, A., Karoumi, R., and Olofsson, P. (2007). "Implementing bridge weigh-in-motion for railway traffic." *Computers and Structures*, 85 (1-2), 80-88.

Lin, C. W., and Yang, Y. B. (2009). "Use of passing vehicle to scan the bridge frequencies-an experimental verification." *Engineering Structures*, 27(13), 1865-1878.

Liu, C., Huang, D. and Wang. T.L., (2002). "Analytical dynamic impact study based on correlated road roughness." *Computers and Structures*, 80(20-21), 1639–1650.

Lu, Z.R., and Liu, J.K., (2013). "Parameters identification for a coupled bridge-vehicle system with spring-mass attachments." *Applied Mathematics and Computation,* 219(17), 9174-9186

Lu, F., Lin, J.H., Kennedy, D., and Williams, F.W. (2009). "An algorithm to study non-stationary random vibrations of vehicle-bridge systems." *Computers and Structures*, 87 (4), 177–185.

Maia, N. M. M., and Silva, J. M. M. (1997), *Theoretical and experimental modal analysis*. Research Studies Press Ltd., Somerset.

Marchesiello, S., Fasana, A., Garibaldi, L., and Piombo, B. A. D. (1999). "Dynamics of multi-span continuous straight bridges subject to multi degrees of freedom moving vehicle excitation." *Journals of Sound and Vibration,* 224 (3), 541–561.

Marcondes, J., Burgess, G.J., Harichandran, R., and Snyder., M. B., (1991). "Spectral analysis of highway pavement roughness." *Journal of Transportation Engineering.* 117(5), 540-549.

Marshall, H., and Murphy, G. (2003). "Factors affecting accuracy of weighbridge systems." *International Journal of Forest Engineering,* 14(1), 67-79.

Marwala, T. (2010), *Finite-element-model Updating Using Computional Intelligence Techniques: Applications to Structural Dynamics*, Springer.

Myers, R. H., and Montgomery, D. C., (1995). *Response Surface Methodology: Process and Product Optimization Using Designed Experiments,* John Wiley & Sons, New York, NY.

Mayers, R H. (1971), *Response Surface Methodology*. Allyn and Bacon, Inc., Boston.

Meng, X., Dodson, A.H., and Roberts, G.W. (2007). "Detecting bridge dynamics with GPS and triaxial accelerometer." *Engineering Structures*, 29(11), 3178-3184.

Michaltsos, G., Sophianopoulos, D., and Kounaids, A. N. (1996). "The effect of moving mass and other parameters on the dynamic response of highway bridge." *Journals of Sound and Vibration,* 191(3), 357-362.

Montgomery, D. C., (2000), *Design and Analysis of Experiments*, Fifth Edition, John Wiley & Sons, New York, NY.

Molina, E.C., (1930). "The theory of probability: some comments on Laplace's théorie analytique." *Bulletin of the American Mathematical Society*, 36 (6), 369-392.

Morassi, A., and Tonon, S. (2008). "Dynamic testing of structural identification of a bridge." *Journal of Bridge Engineering*. 13(6), 573-585.

Moses, F. (1979). "Weigh-in-motion system using instrumental bridges." *Transportation Engineering,* 105(TE3), 233-249.

Mottershead, J. E., and Friswell, M. I. (1993). "Model updating in structural dynamics: A survey." *Journals of Sound and Vibration*, 167(2), 347–375.

Nasrellah, H. A., and Manohar C. S., (2011). "Finite element method based Monte Carlo filters for structural system identification" *Probabilistic Engineering Mechanics*, 26(2), 294–307.

Nam, D.W., Choi, H.K., Kim, K.N. and Jung, K.S., (2008). "Resonance Characteristics of a Arch Bridge for High-Speed Railways." *Journal of Korean Society of Steel Construction* 20(4), 251-262.

National Code of Practice Vehicle Standards Bulletine, 11 (2004) Issued by Vehicle Safety standard, Australian Government, Department of Transport and Regional Services.

Newland, D.E. (1993). *An Introduction to Random Vibrations, Spectral and Wavelet Analysis*. 3 Ed., Longman Scientific & Technical, Longman House, England.

Newland, D.E. (1986). "The Effect of a Footprint on Perceived Surface Roughness." Proceedings of the Royal Society of London, Series A: Mathematical, Physical sciences & Engineering Sciences, 405,303-327.

Nielsen, J. C. O., and Abrahamsson, T. J. S. (1992). "Coupling of physical and modal components for analysis of moving non-linear dynamic systems on general beam structures." *International Journal for Numerical Methods in Engineering,* 33(9), 1843-1859.

Nigam, N.C., (1983) *Introduction to random vibrations*. The MIT Press, Cambridge, Massachusetts.

Norman, O.K., and Hopkins, R.C. (1952). "Weighing vehicle in motion." Public Road, 1952: 27(1), 1-17.

O'Connor, C. and Chan, T. H. T. (1988). "Dynamic wheel loads from bridge strains." *Journal of Structural Engineering*, 114(8), 1703–1723.

Oliva, J., Goicolea, J.M., Pablo Antolín, P., and Astiz, M. A., (2013). "Relevance of a complete road surface description in vehicle–bridge interaction dynamics." *Engineering Structures*. 56, 466-476.

Ouyang, H., (2011). "Moving-load dynamic problems: A tutorial (with a brief overview)." *Mechanical Systems and Signal Processing.* 25, 2039–2060.

Pesterev, A. V., Bergman, L. A., Tan, C. A., Tsao, T. C., and Yang, B. (2003). "On asymptotics of the solution of the moving oscillator problem." *Journal of Sound and Vibration*, 260(3), 519–536.

Paultre, P., Challal, O., and Proulx, J. (1992). "Bridge dynamics and dynamic amplification factors—a review of analytical and experimental findings."*Canadian Journal of Civil Engineering,* 19(2):260–278.

Paynter, H. M (1961), *Analysis and design of engineering systems*, MIT press, Cambridge.

Potisuk, T., and Higgins, C., (2007). "Filed testing and analysis of CRC deck girder bridge." *Journal of Bridge Engineering*. 12(5), 53-63.

Pinkaew, T., (2006). "Identification of vehicle axle loads from bridge responses using updated static component technique." *Engineering Structures*, 28(11), 1599-1608.

Qian, S.S., Stow, C. A., and Borsuk, M. E. (2003). "On Monte Carlo methods for Bayesian inference." *Ecological Modeling*, 159, 269-277.

Radley, K. G., and Traill-Nash, R. W. (1980). "Dynamic loading of highway bridges." *Journals of Engineering Mechanics*, 106(2-3), 641-658.

Ren, W.X., and Chen, H. B. (2010). "Finite element model updating in structural dynamics by using the response surface method." *Engineering Structures* 32(8), 2455-2465

Rao, G. V. (2000). "Linear dynamics of an elastic beam under moving loads." *Journal of Vibration and Acoustic*, 122(7), 281–289.

Rice, S.O. (1954), *Selected Papers on Noise and Stochastic Processes*. Dover Publications.

Ristic, B, Arulampalam, S., and Gordon, N. (2004). *Beyond the Kalman Filter: Particle Filter for Tracking Application*, Artech House Publishers, London

Robert, C. P. (2001). *The Bayesian Choice: A Decision-Theoretic Motivation,* 2nd Ed., New York: Springer.

Sadiku, S., and Leipholz, H. H. E. (1987). "On the dynamics of elastic systems with moving concentrated masses." *Ingenieur-Archiv*, 57(3), 223–242.

Salimpour, Y., and Soltanian-Zadeh, H. (2009). "Particle Filtering of point processes observation with application on the modeling of visual cortex neural spiking activity." In Neural Engineering, NER '09, 4th International IEEE/EMBS Conference on, pages 718-721.

Sayers, M.W., and Karamihas, S.M. (1996). Interpretation of Road Roughness Profile Data. Technical report, University of Michigan Transportation Research Institute (UMTRI) Report (96-19).

Schiehlen, W. (2009) "Colored Noise Excitation of Engineering Structures". Proceedings of the 2nd International Conference on Computational Methods in Structural Dynamics & Earthquake Engineering (COMPDYN 2009), Athens, Greece, 22-26.

Shi, X.M., Cai, C.S., and Chen, S.R., (2008). "Vehicle Induced Dynamic Behavior of Short-Span Slab Bridges Considering Effect of Approach Slab Condition". *Journal of Bridge Engineering*, 13(1), 83-92.

Shi, S., and Chen, D., (2011). "Enhancing particle image tracking performance with a sequential Monte Carlo method: The bootstrap filter." *Flow Measurement and Instrumentation*, 22(3), 190–200

Shi, X., and Cai, C.S. (2009). *Approach Slab and Its Effect on Vehicle Induced Bridge Vibration: 3-D FE Dynamic Analyses*, LAP LAMBERT Academic Publishing.

Shinozuka, M., (1971). "Simulation of multivariate and multidimensional random process." *Journal of Acoustical Society of America*. 49, 357-367.

Shinozuka, M. and Deodatis, G. (1991). "Simulation of Stochastic Processes by Spectral Representation." *Applied Mechanics Reviews*, 44(4),191-204.

Siringgoringo, D. M., Fujino, Y. and Nagayama, T. (2013). "Dynamic characteristics of an Overpass bridge in a Full-Scale Destructive Test." *Journal of Engineering Mechanics*, 139(6), 691-701

Smith, L. A. M. G. L., and Schmidt, S. F. (1962). "Application of statistical filter theory to the optimal estimation of position and velocity on board a circumlunar vehicle." NASA, Technical Report TR R- 135.

Sohn, H., Farrar, C. R., Hemez, F. M., Shunk, D. D., Stinemates, D. W., and Nadler, B. R. (2003). "A review of structural health monitoring literature: 1996–2001". Rep.No.LA-13976-MS, Los Alamos National Laboratory, Los Alamos, N.M.

Sokol, M. and Flesch, R. (2005). "Assessment of Soil Stiffness Properties by Dynamic Tests on Bridges." *Journal of Bridge Engineering*. 10(1), 77-86.

Sridharan, N., and Mallik, A. K. (1979). "Numerical analysis of vibration of beams subjected to moving loads." Journal of Sound and Vibration, 65(1), 147–150.

Stanisic, M. M., and Hardin, J. C. (1969) "On the response of beams to an arbitrary number of concentrated moving masses." *Journal of The Franklin Institute*, 287, 115–123.

Stanisic, M. M. (1985) "On a new theory of the dynamic behavior of the structures carrying moving masses." *Ingenieur-Archiv*, 55(3), 176–185.

Stevens, E.K. (1987) "Force identification problem–an overview." Proceedings of SEM Spring Conferrence on Experimental Mechanics, FL, USA. 838-844.

Stokes, G. G. (1849) "Discussion of a differential equation relating to the braking of railway bridges." *Transactions of the Cambridge Philosophical Society*, 8 (5) 707–735.

Sun, L., Zhang, Z. and Ruth, J. (2001). "Modeling Indirect Statistics of Surface Roughness." *Journal of Transportation Engineering*, 127(2), 105-111.

Sun, L. and Kennedy, T.W. (2002) "Spectral Analysis and Parametric Study of Stochastic Pavement Loads." *Journal of Engineering Mechanics*, 128 (3), 318-327.

Szurgott, P., Wekezer, J. P. E., Kwasniewski, L., Siervogel, J., and Ansley, M.P.E. (2011). "Experimental Assesment of Dynamic Responses Induced in Concrete Bridge by Permitted vehicles." *Journal of Bridge Engineering*. 16(1), 108-116.

Tan, G. H., Brameld, G. H., and Thambiratnam, D. P. (1998) "Development of analytical model for treating bridge vehicle interaction." *Engineering Structures*, 20(1), 54–61.

Tan, C. P. and Shore, S. (1968). "Dynamic response of a horizontally curved bridge." *Journal of Structural Division*, 94(3), 761–781.

Thite, A.N., Banvidi, S., Ibicek, T., and Bennett, L. (2011). "Suspension parameter estimation in the frequency domain using a matrix inversion approach." *Vehicle System Dynamics*, 49 (12), 1803–1822.

Tikhonov, A.N., and Arsenin, V.Y. (1977), *Solutions of Ill-posed Problems,* Winston and Sons, Washington, DC.

Timoshenko, S. P. (1922). "On the forced vibration of bridge." *Philosophical Magazine Series 6*, 43(257), 1018-1019

Ting, E. C., Genin, J., and Ginsberg, J. H. (1974). "A general algorithm for the moving mass problem." *Journal of Sound and Vibration*, 33(1), 49–58

Uhl, T. (2007), "The inverse identification problem and its technical application." *Archive of Applied Mechanics*, 77(5),325–337

Veletsos, A. S. and Huang, T. (1970). "Analysis of dynamic response of highway bridges." *Journal of Engineering Mechanics Division*, 96(5), 593–620.

Vellozzi, J. (1967). "Vibration of suspension bridges under moving loads." *Journal* of the *Structural Division*, 93(4), 123–138.

Wang, T. L. (1992). "Dynamic response of multi-girder bridge." *Journals of Structural Engineering,* 118 (8), 2222-2238.

Wang, T. L, Shahawy, M., and Huang, D. Z. (1993). "Dynamic response of highway trucks due to road surface roughness." *Computers and Structures*, 49 (6), 1055-1067.

Wang, R. T. (1997). "Vibration of multi-span Timoshenko beams to a moving force." *Journal of Sound and Vibration*, 207(5), 731–742.

Weaver, W., Timoshenko, S. P., and Young, D. H. (1990). *Vibration Problems in Engineering*. 5th Ed., John Wiley & Sons, New York, N.Y.

Wen, R. K. (1960). "Dynamic response of beams Traversed by Two Axle loads." *Journal of Engineering Mechanics Division*, 86(5), 91-115.

Wen-jun, W, Le-mei, Yu, X. Z., and Li-jun, H. (2012). "Novel method for equivalent stiffness and Coulomb's damping ratio analyses of leaf spring." *Journal of Mechanical Science and Technology* 26 (11), 3533-3538

White, D., Sritharan, S., Suleiman, M., Mekkawy, M. and Chetlur, S. (2005). "Identification of the best practices for design, construction, and repair of bridge approaches." Rep. No. CTRE Project 02-118. Ames (IA): Iowa Department of Transportation.

Willis, R. (1849), *Report of the Commissioners Appointed to Inquire into the Application of Iron to Railway Structures*, H.M. Stationary Office, London, UK.

Wiriyachai, A., Chu, K. H., and Garg, V. K. (1982). "Bridge impact due to wheel and track irregularities." *Journal of Engineering Mechanics*, 108(4), 648–666.

Wu, J. S. and Dai, C. W. (1987). "Dynamic responses of multispan nonuniform beam due to moving loads." *Journal of Structural Engineering*, 113(3), 458–474.

Wu, Y. S., Yang, Y. B., and Yau, J. D. (2001). "Three-dimensional analysis of train-rail-bridge interaction problems." *Vehicle System Dynamics*, 36 (1), 1–35.

Wu, S. Q. and Law, S. S. (2011). "Vehicle axle load identification on bridge deck with irregular road surface profile." *Engineering Structures*, 33, 591-601

Xu, D., and Yong, R. N., (1993). "Autocorrelation model of road surface roughness." *Journal of Terra mechanics*, 30 (4), 259-274

Xua, Y.L., Li, Q., Wu, D.J., and Chen, Z.W. (2010). "Stress and acceleration analysis of coupled vehicle and long-span bridge systems using the mode superposition method." *Engineering Structures*. 32(5), 1356-1368

Yadav, D., and Nigam, N. C. (1978). "Ground induced nonstationary responses of vehicles." *Journal of Sound and Vibration*, 61(1), 117–126.

Yadav, D., and Upadhyay, H. C., (1993). "Heave-Pitch-Roll dynamics of a vehicle with a variable velocity over a non-homogeneous profile flexible track." *Journal of Sound and Vibration,* 164, 337-348.

Yang, Y. B., Chang, C. H., and Yau, J. D. (1999). "An element for analyzing vehicle–bridge systems considering vehicle's pitching effect" *International Journal of Numerical Method Engineering*, 46, 1031–1047.

Yang, Y. B, Cheng, M. C., and Chang, K. C., (2013). "Frequency variation in vehicle-bridge interaction system." *International Journal of Structural Stability and Dynamics*, 13(2), 22.

Yang, Y. B., Li, Y. C., and Chang, K. C. (2012). "Using two connected vehicles to measure the frequencies of bridge with rough surface." *Acta Mechanica*, 223(8), 1851–1861.

Yang, Y. B., Liao, S. S., and Lin B. H. (1995). "Impact formulas for vehicles moving over simple and continuous beams." *Journals of Structural Engineering*, 121(11), 1644–1650.

Yang, Y. B., Wu, C. M., and Yau, J. D. (2001). "Dynamic response of a horizontally curved beam subjected to vertical and horizontal moving loads." *Journals of Sound and Vibration*, 243(3), 519–537

Yang, Y. B., Yau, J. D., and Wu, Y. S., (2004), *Vehicle bridge interaction dynamics with application to highway speed railways*, World Scientific Publishing Co. Pte. Ltd., Singapore.

Yau, J. D., Wu, Y. S., and Yang, Y. B., (1997). "Impact response of bridge with elastic bearing to moving load." *Journal of Structural Engineering*. 123 (11), 1512-1518.

Yin, X., Fang, Z., Cai, C. S. and Deng, L. (2010). "Non-stationary random vibration of bridges under vehicle with variable speed." *Engineering Structures*. 32(8), 2166-2174.

Yin, X., Fang, Z. and Cai, C. S., (2011). "Lateral Vibration of High-Pier Bridges under Moving Vehicular Loads." *Journal of Bridge Engineering*, 16 (3), 400-412.

Yu, L., Chan, T H.T (2003). "Moving force identification based on the frequency–time domain method." *Journal of Sound and Vibration*, 261(2), 329-349.

Zeng, J. and Dai, H. (1994). "The dynamic simulation of vehicle-bridge interaction using bond graph technique." *Vehicle System Dynamics*, 23(1), 591-602.

Zeng, Z.P, Zhao, Y.G, Xu, W. T, Yu, Z. W., Chen, L.K., and Lou, P., (2015). "Random vibration analysis of train-bridge under track irregularities and traveling seismic waves using train-slab track-bridge interaction model." *Journal of Sound and Vibration*, 342, 22-43.

Zhang, B., and Shepard, W.S. (2014). "Study of Moving Sinusoidal Wave Load across Simple Supported Beam for Sensor Structural Configuration." *Journal of Vibration and Acoustics*, 136(4), 1-11.

Zhang, W., Cai, C.S., Pan. F., and Zhang, Y. (2014). "Fatigue life estimation of existing bridges under vehicle and non-stationary hurricane wind." *Journal of Wind Engineering and Aerodynamics*, 133, 135–145.

Zheng, D. Y., Cheung, Y. K., Au, F. T. K., and Cheng, Y. S. (1998). "Vibration of multi-span non-uniform bridges under moving loads by using modified beam vibration functions." *Journal of Sound and Vibration*, 212(3), 455–467.

Zhibin-Jin, Z., Shiling Pei, S., Li, X., and Qiang, S. (2015). "Probabilistic evaluation approach for nonlinear vehicle-bridge dynamic performances." *Journal of Sound and Vibration* 339, 143–156.

Zhong, H., Yang, M., and Gao, Z. (2015). "Dynamic responses of prestressed bridge and vehicle through bridge–vehicle interaction analysis." *Engineering Structures* 87, 116–125.

Zhu, X. Q., and Law, S. S. (2000). "Identification of vehicle axle loads from bridge dynamic responses." *Journal of Sound and Vibration*, 236(4), 705-724.

Zhu, X. Q., and Law, S. S. (2000). "Study on different beam models in moving force identification." *Journal of Sound and Vibration*, 234(4), 661-679.

Zhu, X. Q., and Law, S. S. (2003). "Dynamic axle and wheel loads identification: laboratory studies." *Journal of Sound and Vibration*, 268(5), 855-879.

Zhu, X. Q., and Law, S. S. (2003). "Dynamic behaviour of orthotropic plate under moving loads." *Journal of Engineering Mechanics*, 129(1), 79-87.

Zhu, X. Q., and Law, S. S. (2006). "Moving load identification on multi-span continuous bridges with elastic bearings." *Mechanical System and Signal Processing*, 20(7), 1759-1782.

Zhu, X. Q., Law, S. S., and Bu, J.Q., (2009). "A State Space Formulation for Moving Loads Identification." *Journal of Vibration and Acoustics*, 128, 509-520

Ziyaeifar, M. (2005). "Interaction study of train-bridge-track systems using Maxwell model." *Vehicle System Dynamics*, 43(11), 771-794.

Znidaric, A., Kalin, J., and Lavric, I. (2002). "Bridge weigh-in-motion measurements on short slab bridges without axle detectors." 3rd International conference on weigh-in-motion (ICWIM3). (13-15 May), Orlando, Florida, USA. Accession Number: 00930072, 231-239.

LIST OF PUBLICATIONS

International Journals

- R. Lalthlamuana and S. Talukdar (2014). “Obtaining Vehicle Parameters from Bridge Dynamic Response: A combined Semi-Analytical and Particle Filtering Approach.” Journal of Modern Transportation, Springer, 23(1), 50-66.

- R. Lalthlamuana and S. Talukdar (2014). "Dynamic Response of Bridge Subjected to Eccentrically Moving Flexible Vehicle: A Semi-analytical Approach." Shock and Vibration, Article ID 546156, 24 doi:10.1155/2014/546156.

- R. Lalthlamuana and S. Talukdar (2014). “Effect of vehicle flexibility on vibratory response of bridge.” Coupled System Mechanics, 3(2), 147-170.

- R. Lalthlamuana and S. Talukdar (2014). “Identification of Flexible vehicle parameters from bridge response using particle filtering technique.” under review in Structural Engineering and Mechanics-An International Journal.

- R. Lalthlamuana and S. Talukdar (2015). “Flexible oscillator moving on beam: Monte carlo simulation using analytically derived samples.” (communicated to Journal of Sound and Vibration)

- R. Lalthlamuana and S. Talukdar (2015). “Estimation of gross weight, suspension stiffness and damping of a loaded truck from bridge measurement.” (communicated to Journal of Bridge Engineering, ASCE).

International Conference

- R. Lalthlamuana and S. Talukdar. “Model option to obtain forward solution in Particle Filter Method for identification of moving load an bridge.” Proceedings of the 5th International Congress on Computational Mechanics and Simulation, 10-13 December 2014, SERC, Chennai (India), 373-382.

- R. Lalthlamuana and S. Talukdar. “Dynamic amplification factor of concrete bridges considering flexibility of vehicle.” Proceedings of the 12th International Conference on Concrete Engineering and Technology, held during 12-14 Aug 2014, SubangJaya, Kuala lumpur (Malaysia), 111-116.

- R. Lalthlamuana and S. Talukdar. “Full scale vibration test on a concrete bridge under moving truck.” Proceedings of the 12th International Conference on Concrete Engineering and Technology, held during 12-14 August, 2014, Subang Jaya, Kuala lumpur (Malaysia), 161-166.